SANDWICH ACTION IN FOAM FILLED MASONRY CAVITY WALLS

KEVIN ANDREW WHITE

A thesis submitted in partial fulfilment of the
requirements of The Nottingham Trent University
for the degree of Doctor of Philosophy

This research programme was carried out
in collaboration with Baxenden Chemicals Ltd.

June 1998

Abstract

The objective of this project is to introduce an analysis methodology and evaluation of the flexural behaviour of masonry cavity walls treated with Isofoam Cavity Reinforcement Foam (CRF). Current masonry codes and practices do not consider composite action in masonry. As a prelude to analysing foam filled masonry cavity walls, the behaviour of plywood faced sandwich panels was modelled. Classical solutions for 'sandwich' behaviour and experimental data have been used to validate the application of finite element analysis (F.E.A) methods. The theoretical solutions have been supported by a thorough investigation of current material property evaluation methods.

Orthotropic properties of Isofoam CRF were identified as significant during uniaxial compression tests. The uniaxial compression tests were initially used to evaluate the elastic response of the Isofoam. The testing was supported by an F.E.A. study which identified experimental errors and formulated correction factors. Uniaxial tension test results aided in the formulation of these factors. F.E.A. was used to examine experimental errors arising from the test configurations and apparatus for the American and British Standard shear modulus tests. The use of control tests also identified errors inherent to the particular test equipment. A further shear modulus evaluation method used the load / displacement response of a sandwich beam at different span lengths. A ranking list has been composed to indicate the most appropriate property test method for polyurethane foamed cores. F.E.A. and experimental data showed that the length of span influenced by local bending of the facings, at load concentrations, was half that described by classical solutions.

Linear elastic F.E.A., of vertically spanning, single storey height, foam filled masonry cavity walls, utilised material properties derived from separate brick and mortar tests and representative flexural tests of masonry. For a 32 Kg/m^3 density foam F.E.A. predicted an increase in stiffness of 19, 28 and 30% according to cavity width. An F.E.A. parametric study of the efficiency of a foam filled cavity wall showed that an increase in foam density enhances this remedial system. The project concludes that the foam injection system is a valid method for short term stiffening of masonry cavity walls subject to lateral loading. The long term behaviour of the structural interaction between Isofoam CRF and masonry should be investigated further.

CONTENTS

List of tables

List of figures

Acknowledgements

I would like to thank the following for their contributions and assistance:

The Nottingham Trent University, the Department of Civil & Structural Engineering and the Research Council for allowing me the opportunity to conduct this research project.

The Laboratory Staff - Steve Goodman, Alan Freebury, Mark Flanagan, Keith Atkinson, Wayne Thomas and Roy Gregory.

The Lecturing Staff - Dr K Roodbaraky, Dr N Dixon

Baxenden Chemicals Ltd who provided specimens for the project

Special thanks and great appreciation go to **Dr David Johnson** who picked up the mantle of Director of Studies at a critical time.

Most importantly was the support offered throughout by my parents John and Pauline White to whom this thesis is dedicated.

Notation

A ..... Effective thick faced sandwich core shear area, $A = bd^2/c$

$B_1 - B_6$ ..... Constants of integration in Allen's solutions

B_{40}, B_{80}, B_{84} ..... Multiple span beam testing technique conjugate bending components of a cantilever span. 0 = support, 4 = quarter span and 8 = eighth span.

$[B]$ ..... Strain transformation matrix

$C_1 - C_6$ ..... Constants of integration in Allen's solutions

D ..... Total sandwich construction flexural stiffness

$[D]$ ..... Elastic modulus matrix

E ..... Young's or elastic modulus

E_{brick} ..... Elastic modulus of a masonry brick unit

E_{exp} ..... Experimental value of elastic modulus recorded in uniaxial compression tests

E_c ..... Isofoam CRF elastic modulus in direction of sandwich span

E_f ..... Elastic modulus of facing of a sandwich construction

$E_{masonry}$ ..... Elastic modulus for masonry as a homogeneous isotropic solid

E_{Type1} ..... Elastic modulus of Isofoam CRF evaluated from a Type 1 graphical analysis of the multiple span beam tests

E_{Type2} ..... Elastic modulus of Isofoam CRF evaluated from a Type 2 graphical analysis of the multiple span beam tests

E_y, E_z ..... Elastic modulus in the y and z directions in a sandwich

F ..... The value of a function at a location indicated by (ξ_i, η_j)

G ..... Shear modulus

G_c ..... Longitudinal shear modulus of the core of a sandwich

G_{XH} ..... Crosshead shear modulus from shear testing

G_{XP} ..... Crossplate shear modulus from shear testing

I ..... Total second moment of area of a sandwich construction

I_f ..... Total second moment of area of the two facings of a sandwich construction

$\underline{\underline{J}}$ ..... Jacobean transformation matrix

J^{-1} ..... Inverse of the Jacobean transformation matrix

[K] ..... Stiffness matrix

LVDT ..... Linearly varying differential transducer

M ..... Bending moment

M_R ..... Moment of resistance of a masonry wall

M_1 ..... Primary sandwich action bending moment

M_2 ..... Secondary sandwich action bending moment

N_N ..... Number of nodes along a sequentially noded edge

N_F ..... Number of degrees of freedom of a node

[N] ..... Shape function matrix

P ..... Point or line load normal to the contact surface

Q ..... Shear force

Q_1 ..... Primary sandwich action shear force

Q_2 ..... Secondary sandwich action shear force

R ..... Radius of curvature of a structural element bending cylindrically

U ..... Displacement in x direction for Cartesian co-ordinates

V..... Displacement in y direction for Cartesian co-ordinates

W_i, W_j ..... Weighted function describing the locations of Gauss points

Z ..... Section modulus

$a^2 = \frac{AG}{EI_f(1-I_f/I)}$ Parameter which defines the relationship between primary and

secondary shear loads in thick faced sandwich constructions

$a_{11}, a_{12}, \ldots, a_{nn}$ ..... Value and matrix position in the global stiffness matrix

{a} ..... Nodal displacement vector

b ..... Sandwich beam or panel width

c ..... Sandwich core thickness

$c_1 - c_9$ ..... Arbitrary coefficients used in shape function polynomials

d ..... Distance between neutral axes of facings in a sandwich beam

{d} ..... Displacement vector

{f} ..... Nodal load vector

h ..... Overall thickness of a sandwich construction

k_1 ..... Bending component of sandwich stiffness for cantilever spans

k_2 ..... Shearing component of sandwich stiffness for cantilever spans

f_{kx} ..... Characteristic flexural strength of masonry

l_1 ..... Simplified cantilever span length

l_2 ..... Simplified cantilever span overhang length

t ..... Sandwich beam facing thickness

u, v, w	Displacement in x, y and z directions for Cartesian co-ordinates
x, y, z	Global Cartesian co-ordinate system
$\alpha_1 - \alpha_2$ $\beta_1 - \beta_2$	Generalised parameters in Allen's solution of thick faced sandwiches
β_x	Hyperbolic function which controls secondary thick faced sandwich action bending moments
δ/δ_x δ/δ_y	Partial derivatives with respect to global co-ordinate system
$\varepsilon_x, \varepsilon_y, \varepsilon_z$	Direct strains in global Cartesian co-ordinate system
$\{\varepsilon\}$	Strain vector
$\phi = al_2$	Thick face sandwich action overhang span
γ	Shear strain
$\gamma_{xy}, \gamma_{yz}, \gamma_{zx}$	In plane shear strain
γ_m	Factor of safety for material quality
η	Natural co-ordinate
μ	Poisson's ratio
$\mu_{xy}, \mu_{yz}, \mu_{zx}$	In plane Poisson's ratio

$\theta = al_1$ ..... Thick face action cantilever span dimension

$\theta x = ax$ ..... Generalised thick face action span dimension

σ ..... Sandwich panel facing stress

$\sigma_x, \sigma_y, \sigma_z$ ..... Direct stresses in global Cartesian co-ordinate direction

$\{\sigma\}$ ..... Stress vector

τ ..... Shear stress

$\tau_{xy}, \tau_{yz}, \tau_{zx}$ ..... In plane shear stress

ω ..... Displacement in z direction

$\omega^i, \ldots, \omega^{iv}$ ..... Differential derivatives of displacement

ξ ..... Natural co-ordinate

ψ ..... A function expressing the contribution of thick facings to the overall displacement of a sandwich beam

CHAPTER 1 - PROJECT INTRODUCTION

1.1 Introduction

1.2 Methodology statement

1.3 Literature review

CHAPTER 1 - PROJECT INTRODUCTION

1.1 Introduction to the project

This research project was initiated as a result of identifying a gap in knowledge of how to assess an innovative and currently successful remedial measure to existing low rise residential housing. The work presented in this thesis advances the current knowledge of the effect of using the "foam injection system" as a remedial measure to existing masonry cavity walls. In 1989 some 124 properties on a housing estate in Newbold Verdon, Leicestershire were treated for cavity wall instability by injection of Isofoam Cavity Reinforcement Foam (CRF) into the void. This remedial measure was adopted after the observation that some buildings, their cavity walls filled with a thermally insulating foam similar to Isofoam CRF, were not distressed while those without had serious structural defects. Along with other remedial measures, the buildings have been successfully refurbished to a high quality and relatively low cost when the only other real alternative was to demolish and rebuild.

The remedial measure of injecting foam into the cavity walls, to bond the two leaves or "wythes" together, was implemented only on an 'engineering judgement' basis for enhancement to structural stiffness, stability and integrity. At the time of implementation there was no formal analysis and only a few limited site and laboratory tests had been conducted on elements of a 'specimen' building. Lock (1990), documented the stabilisation programme at Newbold Verdon. This study did not attempt any formal analysis and only presented the results of the limited testing programme and reported the apparent structural stability before and after the remedial measures. It was concluded that the stabilisation programme was successful and the buildings were again habitable. The limited range of tests did enable Baxenden Chemicals Ltd (1990) to gain a British Board of Agrement Certificate (1990) for their Isofoam CRF product when used for cavity wall stabilisation. The product currently carries a 25 year guarantee.

Evison (1991), investigated the flexural behaviour of plywood faced sandwich panels incorporating a lightweight polyurethane core, the construction of which is shown in figure 1.1. The work was intended to obtain an understanding of composite action that could then be translated to the stiffness and strength assessment of the foam injected masonry cavity walls. The study did not accomplish the original task. Experimental results comprised load versus deflection graphs and mid-span strain readings on the upper and lower plywood facings. The experimental results were compared to ordinary bending theory which was supported by a limited range of material tests. The study concluded that the mode of failure of laterally loaded panels was a diagonal tensile shearing of the core, however this occurred only at deflections too large for limiting design criterions. It was also reported that bending stresses were transferred from one face to the other, by the core, through observation of the recorded facing strains when compared to ordinary bending theory. This study did not describe the intricacies of sandwich panel behaviour well as most notably there is no account of deflection due to shear strain in the core material.

Literature relating to composite action in masonry cavity walls is scarce with only occasional mention of its occurrence or acknowledgement of its structural advantages and no formal analysis is evident. The field of sandwich construction theory has therefore been embraced in an attempt to aid in the understanding of the proposed foam injection system.

The initial objective of this project was to assess the merits of the remedial measure of injecting a rigid cellular foam into the void of a structurally defective masonry cavity wall. This was not deemed practical, as test buildings were not available and the reproduction of structurally defective walls in a laboratory was unfeasible. Therefore, the overall objective then set out for this project was to assess the flexural behaviour of purpose built cavity walls filled with Isofoam Cavity Reinforcement Foam (Isofoam CRF) while containing no metal ties.

The fundamental concept of enhancing stiffness, by injecting masonry cavity walls with Isofoam CRF, lies with the ability of the foam to transfer shear loads from the

inner load bearing leaf to the outer facing leaf thus intrinsically creating a single structural unit analogous to a steel I beam. Traditional wall ties are unable to transfer shear loads in this way and an intensive literature search uncovered no relevant information, experimental or analytical, regarding this concept in the field of masonry.

Shear load transfer between two structural elements was first described by Fairbairn (1849) as "sandwich" or composite action. Sandwich theory was first developed in the early 1940's and the first actual use of this type construction was as a wing and fuselage exterior skin in the British built Mosquito fighter aircraft. Sandwich constructions, in these applications, comprise two stiff and strong facings bonded to a thickness of weak and lightweight core material as shown in figure 1.1. Facing materials such as metal sheets, fibreglass, plywood and plastics are often used with core materials including honeycomb structures, low density woods and expanded plastics such as polyurethane. Sandwich panels are used in such diverse fields as the boat, aircraft and building industries particularly for their high strength to weight ratio, thermal and acoustic insulation and ease of manufacture, transportation and construction.

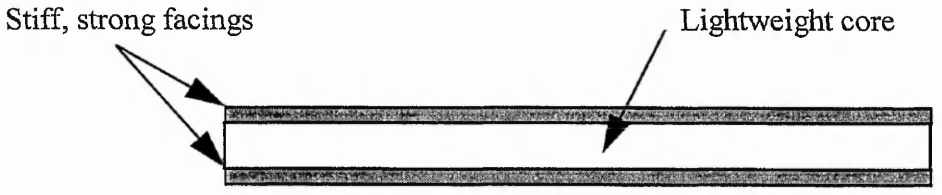

Figure 1.1 Sandwich construction components

The principal aim of this study is to analytically model the flexural behaviour of laterally loaded masonry cavity walls injected with Isofoam CRF and to critically appraise the system. Full scale experimental tests monitoring structural behaviour, under lateral loading, have been used as the control for the analytical modelling which has itself been supported by a range of material tests. Confidence in the modelling of laboratory tested specimens will allow more complex and practical situations to be evaluated in the future.

Current design standards for assessing laterally loaded masonry cavity walls using wall ties, calculate the capacity of a single thickness wall and simply double the strength. The fundamental difference in flexural strength between two masonry leaves joined by cavity wall ties and the same two leaves bonded together with Isofoam CRF is that gained by the shear load transfer from the inner load bearing leaf to the outer facing leaf.

The literature review uncovered a vast range of information on sandwich construction from various types of industry. It was evident that to understand the intricacies and application of sandwich theory to masonry cavity walls a combination of experimental and theoretical work needed to be conducted on more simple structures. Two forms of analysis were identified to predict the structural behaviour of sandwich constructions tested in this project. Firstly, the classical solutions presented by Allen (1969) and secondly, finite element analysis (F.E.A.).

Allied to the difficulties intrinsic to the understanding and prediction of masonry behaviour there were a number of practical reasons that led to the initial use in this project of plywood faced panels. To cover the wide range of experiments relevant to the theoretical concepts of sandwich theory a number of panels with various aspect ratios of core to facing thickness could be easily manufactured. Factors such as availability of materials, ease of manufacture, transportation, ability to be tested more than once (and be subsequently cut into beams) and material test specimens also affected the choice. Thus to satisfy all of these factors a number of plywood faced Isofoam CRF cored constructions have been used for an extensive programme of tests.

The experimental results of the plywood / Isofoam CRF sandwich panels were subsequently compared to the existing sandwich panel theory and finite element analysis. The theoretical modelling has been supported by a range of appropriate material tests. The material test methods have also been investigated using F.E.A modelling to establish their suitability and accuracy.

The plywood faced sandwich panel test programme incorporated pilot studies on two panels filled with an existing CFC and a new HCFC blown polyurethane foam. These panels served both to establish that the new HCFC blown polymer possessed similar properties to the old and also to establish correct testing procedures and equipment calibration for the main batch of tests.

1.2 Methodology statement

1.2.1 General

The main objective of this study is to examine the flexural behaviour of cavity walls, filled with Isofoam CRF, as vertically spanning, simply supported and laterally loaded single story height panels. The addition of the Isofoam CRF core allows shear transfer from one facing to another creating a sandwich construction. Current masonry codes and literature do not cover this type of structural behaviour and so the field of sandwich construction analysis has been investigated so that relevant concepts may be applied to the masonry cavity walls. The analysis has been restricted throughout this project to linear elastic material behaviour although recognition of the influences of non-linear behaviour have been made where necessary.

Analysis methods have been investigated by comparison to experimental data from plywood faced sandwich panel tests. The flexibility of finite element modelling method is paramount for its selection for this project, with potential analysis of larger cavity walled structures. Finite element analysis has been adopted after comparison to both the experimental data and to Allen solutions of the plywood faced panels.

The following sub-sections describe how the contents of each chapter relates to the global objectives of this project and outline the methods employed to obtain that requirement.

1.2.2 Chapter 2 - Physical properties and application of Isofoam Cavity Reinforcement Foam (CRF)

The secondary physical properties of Isofoam CRF are discussed and relevance is drawn to the inter-relationships of properties, for example density and compressive modulus. Specific material properties are evaluated, where necessary, to support the analytical modelling of sandwich constructions. Time dependant strain response, or creep, of the Isofoam CRF is identified as an important property. Two methods of limiting creep during testing are proposed.

Two unique case studies of the foam injection system are presented and discussed. The first case study reports on one of the original applications of the foam injection system as a direct remedial measure to existing masonry cavity walls. The second case study describes a different application, in itself, novel and innovative. Both case studies show that the system is a viable alternative to more expensive remedial schemes.

1.2.3 Chapter 3 - Sandwich construction analysis methods

There is a wealth of information regarding sandwich beam and panel analysis, as will be seen in the literature review, which has been derived from research in the early 1940s at the United States Forest Products Laboratories, Norris (1944) and March (1944), and in the aviation industries of England and America.

The analysis formulated by Allen (1969) as presented by O'Connor (1985) was identified for predicting the behaviour of sandwich constructions in this project. A summary of its derivation is included along with the fundamental principles of finite element theory. Finite element theory has developed exponentially since Clough (1960) first published his work described as the 'Finite Element Method'. The advent of high powered computers and their availability has sent F.E.A. to the forefront of engineering solutions with a multitude of commercial software packages being readily available. This project makes use of a number of these packages, LUSAS (1991),

ABAQUS (1995), and the Rolls-Royce Plc in-house programmes SC01 (1997) and SC03 (1997).

1.2.4 Chapter 4 - Uniaxial material testing and analysis

Uniaxial compression testing was initially used to find the elastic modulus and Poisson's ratio for the Isofoam CRF core and was originally considered to be the simplest test method available. During similar tests, O'Connor (1985) found that barrelling, in the planes parallel to the direction of loading, influenced the experimental results. O'Connor conducted an investigation using finite element analysis to establish the consequences of the barrelling effect. In addition to O'Connor's barrelling effects, other factors affecting experimental results were identified during this project's analytical modelling of the uniaxial compression testing. These factors were firstly, a geometrical shape effect that caused barrelling in the plane normal to the direction of loading and secondly, significant orthotropic material behaviour. Correction factors derived from the finite element modelling have been applied to the elastic modulus and Poisson's ratio values obtained directly from the tests. Although the uniaxial compression tests did not yield suitable results, in terms of an appropriate elastic modulus, they did point the way to a better understanding of the behaviour of the Isofoam CRF material, particularly when placed by the foam injection system. In the absence of any other suitable tests the Poisson's ratio values were adopted and used throughout all finite element analyses involving Isofoam CRF.

The further uniaxial testing used tensile specimens which were orientated to account for the orthotropic nature of the foam. The main axis of these specimens were in the direction of span for the panel flexural tests and were also configured so as to avoid the significant effects of barrelling

The uniaxial tests helped to identify the presence of orthotropic properties in the Isofoam CRF mass. Specifically the properties were directly related to the direction of foam rise. Closer visual inspection of the foam showed noticeable evidence that the

shape of the voids in the mass of the Isofoam were predominantly ovoid, with the longest axis orientated in the direction of rise thus creating the orthotropic conditions. An analogy may be made for the shape and strength of these voids to those of an egg.

1.2.5 Chapter 5 - Shear testing and analysis

Although the uniaxial testing should have provided appropriate material properties to support the theoretical analysis of the sandwich panels, doubts were raised regarding the suitability of the results. This was particularly prevalent when considering the nature of the applied direct tensile and compressive strains in the uniaxial tests and the actual nature of the shearing strains present during bending of the sandwich panels.

Two test methods, BS 4370 (1993) and ASTM C273 (1980), were identified as suitable to simulate shear strains similar to the flexural response of the Isofoam CRF in the sandwich panels. O'Connor (1985) had previously conducted a series of shear tests and had used finite element techniques to find errors in the testing configurations. Since O'Connor's investigation cast doubts on which method was most appropriate and the British Standard had recently been updated, a full and detailed finite element analysis of the test methods was completed and has been supported by various tests including control specimens. A major source of test error was discovered and corrected, through use of the control tests, which has been attributed to the displacement of the apparatus. British and American standard results still differed, although these differences were attributed to the way in which the load was applied to the specimen by the separate apparatus configurations of each method.

1.2.6 Chapter 6 - Multiple span beam testing and analysis

Multiple span beam testing was considered necessary as the two coupon tests, described above, used small specimen sizes that were particularly susceptible to variations in the quality of the Isofoam CRF core. The multiple span beam testing used larger specimens. The beams were also subject to flexure and thus the core shear strains were more closely matched to those of the panel tests.

The experimental data was analysed, to evaluate shear properties of the core, using Allen's theory, presented in a different format by O'Connor (1985) which incorporated a method to avoid experimental errors associated with sandwich behaviour. Both the experimental and finite element results in this project indicated that these errors were substantially less than O'Connor had previously predicted although the overall concept still avoided some unnecessary test error.

1.2.7 Chapter 7 - Plywood faced sandwich panel testing and analysis

The testing conducted on various configurations of plywood faced sandwich panels served two purposes. Firstly, the two types of analysis were compared to each other and against the experimental results. This was done principally to confirm confidence in the application of finite element modelling techniques to sandwich constructions. The comparisons of flexural behaviour have been made by assessing the shape of the strain profiles along the span of the outer surfaces of the facings. Secondly, the evaluation of the material properties, including the plywood facings, in the previous three chapters was inconsistent and having gained confidence in the finite element analysis, comparisons could then be made with the full scale panel tests in an attempt to identify the most appropriate property test method. The comparisons in this instance have been made by consideration of deflections at locations within the span.

1.2.8 Chapter 8 - Masonry wallette and constituent testing and analysis

This chapter describes how the properties of the masonry cavity walls were derived experimentally. Initially it was proposed to find the elastic modulus of brickwork as a homogeneous isotropic solid, for the spanning direction only, rather than the properties of the individual constituents. For this small walls, or wallettes, were tested in flexure. The results of the wallette tests proved to have a large variance and allied to the ease of testing masonry components rather than wallettes a further analysis was proposed utilising the individual component material properties. Difficulty was

experienced in evaluating the elastic properties of the masonry units and values from previous research were adopted.

1.2.9 Chapter 9 - Masonry cavity wall testing and analysis

The two types of finite element analysis, using wallette and brick / mortar properties, have been scrutinised and compared to the experimental data of three vertically spanning, simply supported, story height cavity walls, each with a different cavity thickness. The versatility and use of finite element analysis has been vindicated here and is paramount for the evaluation of the structural enhancement of cavity walls when injected with Isofoam CRF. It is recommended that the two types of analysis should be used for different situations depending on the problem size, configuration and output required.

As the leaves of cavity walls are very thick and relatively very stiff a finite element model was used to conduct a parametric study relating the density, and hence shear stiffness, of Isofoam to the overall efficiency of a foam filled cavity wall. This could assist designers to chose a particular foam density depending on the requirements of the building in question. Currently a 32 kg/m^3 density foam has been adopted as that is what the original remedial application used.

1.2.10 Chapter 10 - Conclusions

Discussions and conclusions have been included at the end of each chapter. Chapter 10 summarises these conclusions and discusses their inter-relationships. The discussions also highlight recommendations where further work is required to be able to fully vindicate the foam injection system as a remedial measure to existing masonry cavity walls for both the short and long term.

1.3 Literature review

A literature review relevant to each subject is given at the beginning of each chapter and throughout the text where appropriate. The main thrust of the literature review was directed in the fields of sandwich construction analysis, finite element concepts and laterally loaded masonry and masonry constituent behaviour.

CHAPTER 2 - PHYSICAL PROPERTIES AND APPLICATION OF ISOFOAM CAVITY REINFORCEMENT FOAM (CRF)

2.1 Introduction

2.2 Physical properties of Isofoam CRF

2.3 Remedial measures to existing masonry cavity walls

2.4 Discussion

2.5 Conclusions

CHAPTER 2 - PHYSICAL PROPERTIES AND APPLICATION OF ISOFOAM CAVITY REINFORCEMENT FOAM (CRF)

2.1 Introduction

The general physical properties of a typical isotropic homogeneous sample of 32 Kg/m^3 density Isofoam CRF are presented. Emphasis is placed on those properties that may influence the behaviour of polyurethane foams when used as a cavity wall reinforcement. Specific physical properties of the Isofoam CRF used in this project have been evaluated where required for the analytical modelling.

This project was instigated to provide an analytical model for the prediction of the flexural behaviour of masonry cavity walls when injected with Isofoam CRF and subject to lateral loading. This innovative remedial measure may be implemented for a number of reasons relating to the mechanisms of certain structural defects. The mechanisms causing the structural defects require a level of understanding so that the foam injection system is beneficial. Common types of structural defect are briefly discussed with particular relevance to the applicability of Isofoam CRF. Two case studies are described and which are of marked contrast.

2.2 Physical properties of Isofoam CRF

The principal material properties have been evaluated for the proposed linear elastic analyses in chapters 4, 5 and 6. This section briefly discusses the secondary properties associated to the Isofoam CRF product that are relevant to its application as a remedial measure to existing masonry cavity walls.

2.2.1 Specification and composition of Isofoam CRF

Isofoam Cavity Reinforcement Foam is a two component polyurethane rigid foam used as 'pour in place' in the manufacture of moulded components. A blowing agent is used to form the voids in the liquid mass during rising. The two components are a resin and an isocyanate (diphenylmethane di-isocyanate) and the blowing agent is currently HCFC gas. The HCFC gas replaces a CFC blowing agent which now meets the latest European Community environmental regulations. Table 2.1 gives the specification of the constituent proportions and specification of Isofoam CRF.

Resin Component	Poly-ol Viscosity @ 20.0 ^{0}C	460 mPa.s (cP)
	Specific gravity @ 20.0 ^{0}C	1.14
Isocyanate Component	Viscosity @ 20.0 ^{0}C	350 mPa.s (cP)
	Specific gravity @ 20.0 ^{0}C	1.24
Additives	Hydro-chloro-fluoro-carbon Surfactant (silicone oil) Water Catalysts	
Mix ratio	46% Resin 50% Isocyanate 4% Additives	by weight
Cream time	19 secs @ 20.0 ^{0}C	
Rise time	185 secs @ 20.0 ^{0}C	

Table 2.1 Specification of constituents and composition of Isofoam CRF (HCFC)

2.2.2 Typical physical properties

Table 2.2 holds the manufacturers claimed figures for the physical performance of the Isofoam CRF HCFC product. One of the fundamental properties, not specified here, to the use of Isofoam CRF its self bonding ability. The self bonding ability of the

Isofoam is obviously crucial to its application and allied to insertion as a liquid makes the product ideal for use in a cavity wall where it is able to occupy the whole volume of the void. Later it will be seen that failure in tension or shear usually occurs just inside the interface of the foam, with a thin layer of foam remaining on the facings surface. This indicates that the bond strength is greater than either the shear or direct tensile strength although there is no definition of its actual bond strength. When dry, masonry and plywood provide excellent surfaces for good bonding. BS 7457 (1991) describes a simple test method for determining the adhesion strength of Isofoam CRF to masonry. The British Standard does not account for conditions of in service masonry that may effect the adhesive ability of the foam. Wet and loose material may cause a reduction in the adhesive strength and it would therefore be prudent to apply a reduction factor to the laboratory results of the adhesive strength test method. Throughout this project the adhesive strength is not a significant factor as all surfaces bonded to Isofoam CRF are dry, free of loose material and generally in good condition.

The properties of Isofoam CRF are also influenced by ageing and exposure to the environment and in particular ultra violet light. As a general qualitative guide, unexposed Isofoam masses do not suffer from adverse effects of ageing and the integrity of the product is guaranteed for at least 25 years by the manufacturer when inserted to a cavity wall.

Free rise core density	32 Kg/m^3 @ 20.0 ^{0}C	
Compressive strength	Parallel to rise	0.216 N/mm^2
	Perpendicular to rise	0.166 N/mm^2
Thermal conductivity @ 24^{0}C		0.018 W/mK
Closed cell content	>90% = rigid cellular	92.6%

Table 2.2 Typical physical properties of Isofoam CRF (HCFC)

2.2.3 Typical physical relationships

The general physical relationships presented here are for a typical homogeneous, isotropic, rigid polyurethane foam at a density of 32 Kg/m^3. Orthotropic foam masses usually occur where there is a confined volume to fill and a direction of rise is channelled by geometrical restraints. Isotropic foam masses may be formed where free rise is allowed. In extreme cases the modulus parallel to the direction of rise may be only 40% of that normal. Graphical representations shown in the following section are diagrammatic only and specific properties have been evaluated when required throughout the project. The properties described below are of largely secondary importance to the main thrust of this investigation, but do bear some significant influence. The following graphical plots have been reproduced from Stengard (1963).

Density versus elastic modulus: As can be seen in figures 2.1 and 2.2, the compressive and tensile elastic modulii are both linear on a log / log scale with the relationship in the form log(modulus) = A + B.log(density). The linear relationship has been assumed from a tangential modulus of the stress / strain relationship curve which itself is non-linear in nature.

The density of the foam itself is controlled by the water concentration in the reaction stage, which in turn determines the amount of carbon dioxide blowing agent there is present. Therefore the less water available for the reaction the less carbon dioxide is produced and so the density increases, again according to a log(water) / log(density) relationship.

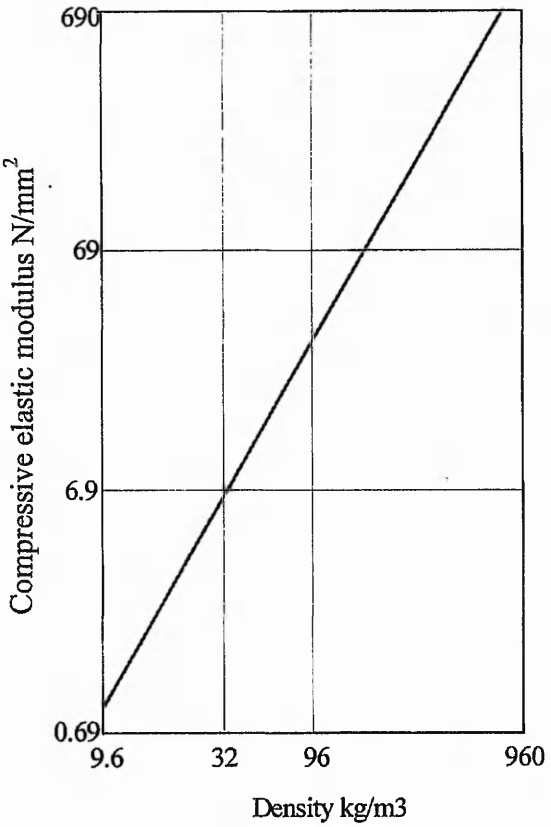

Figure 2.1 Density versus compressive elastic modulus

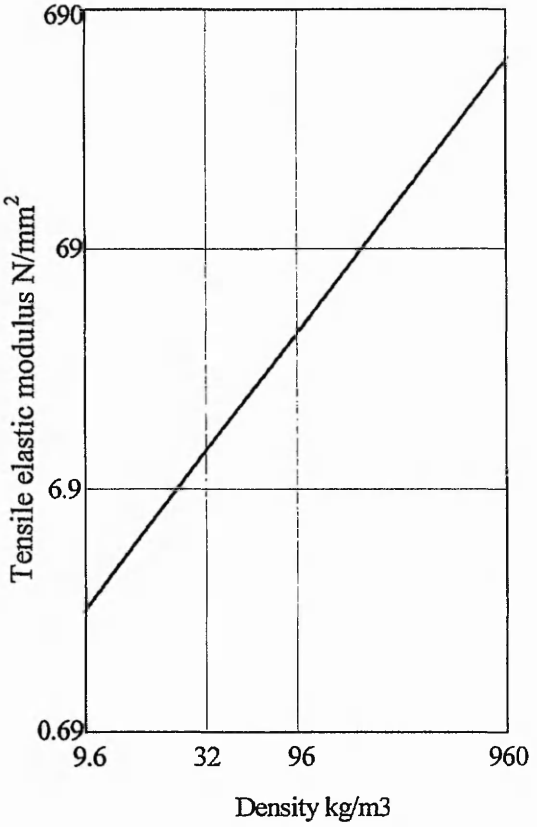

Figure 2.2 Density versus tensile elastic modulus

Density versus shear and flexural modulii: Figures 2.3 and 2.4 below illustrate the relationship between shear modulus and flexural modulus against foam density respectively. An increase in the density of the foam clearly increases both the shear and flexural modulii. This study only employs a foam density of 32 Kg/m^3 in the sandwich construction, but it is realised that the most suitable density of foam for injection into a cavity wall may be different.

The 32 Kg/m^3 Isofoam is used throughout this project as that is the density that has previously been employed and will be in the near future for cavity wall remedial measures. However, the selection of a foam density should also consider the important factors of required shear modulus, cavity thickness, what the principal aim of the application is or what the nature of the structural defect is and of course the economics.

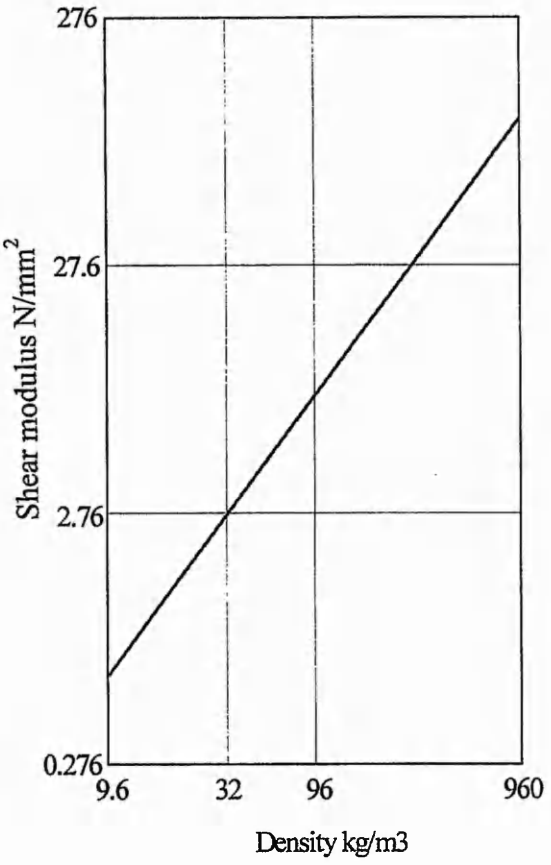

Figure 2.3 Density versus shear modulus

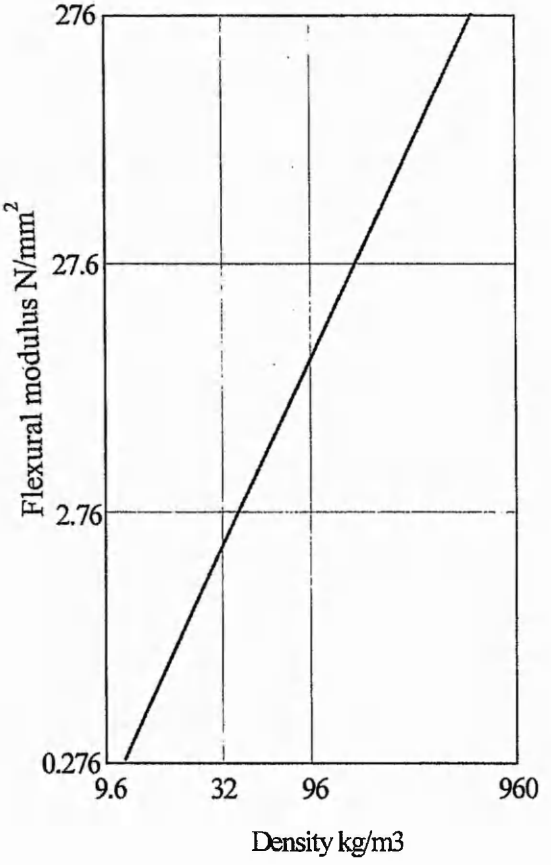

Figure 2.4 Density versus flexural modulus

Temperature versus compressive and tensile modulus: Figures 2.5 and 2.6 respectively relate the compressive and tensile modulii to changes in temperature by considering the retained percentage of the 20 ^{0}C modulii values. The behaviour of the Isofoam CRF is characteristic of a thermosetting polymer. Throughout this investigation attention to temperature has been considered important and monitoring each test environment has ensured that the temperature of all tests has been kept at 20 +/- 3 ^{0}C. It has been assumed for this project that temperatures in this range cause negligible modulii changes (where a significant change is considered to be a 1% difference).

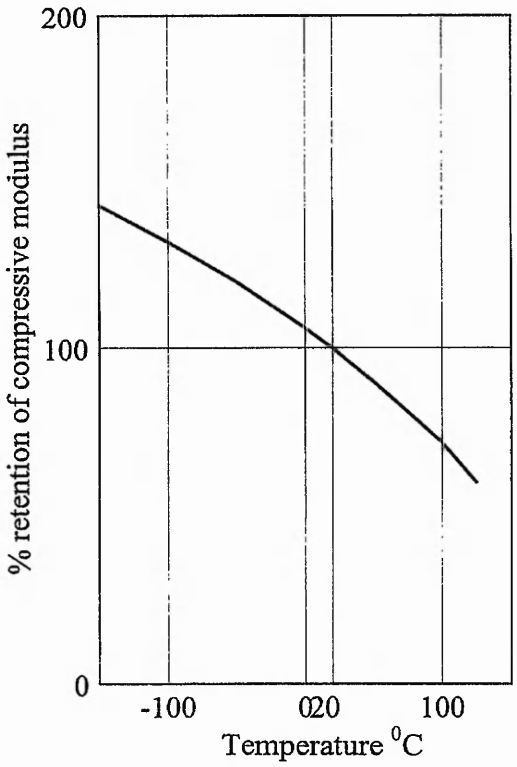

Figure 2.5 % retention of compressive modulus at 20^{0}C versus temperature

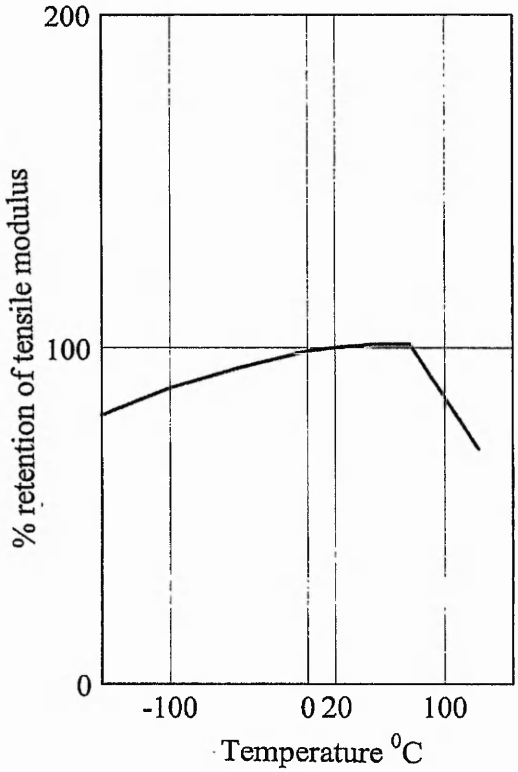

Figure 2.6 % retention of tensile modulus at 20^{0}C versus temperature

Although changes in temperature have been kept to a minimum for consistency in this project this will obviously not be the case when the foam is in situ. Extremes of temperatures that the Isofoam in a cavity wall may be subject to range from -20 to 40 ^{0}C. This range of temperatures may cause a change in modulii of approximately +8% to -6% from the modulii at 20 ^{0}C. Temperature variations may also cause an acceleration or deceleration of time dependent behaviour.

The ability of the foam to retain its compressive or tensile modulus at 20^{0}C with varying temperature is also dependant on its density. Generally the denser the Isofoam the greater its retention and thus it has more favourable thermal stability.

Time dependant behaviour: Huang and Gibson (1990) and (1991) modelled the time dependent behaviour of polymer foams when used as the core of sandwich beams and as specimens in the ASTM C 273 (1988) shear tests respectively. The modelling of

the shear test included linear and non-linear viscoelastic creep response of polymeric foam with the aim to develop a model based on the creep of the solid polymer and the initial modulii of the foam and the solid. Similarly the creep response of the deflection of beams may be modelled from knowledge of the behaviour of the solid polymer. The modelling assumes that the polyurethane masses, for both tests, is loaded below 50% of their maximum shear strength where confidence in its behaviour is good.

The time period for both shear and beam creep tests was 1200 hours of loading and the same period for unloading recovery. Figure 2.7 below is typical for the shear strain of a shear test specimen which may also be read for the deflection of a sandwich beam. The y-axis is directly interchangeable for either shear strain ($x10^{-2}$) or mid span deflection (mm). The initial loading and unloading after 1200 hours is purely an elastic response (a), with (b) representing the recovered creep strain of deflection and (c) the current level of strain or deflection at any time.

The time dependent deflection of a three point load configured sandwich beam has been modelled, by Huang and Gibson, assuming that the bending deflection remains constant while the shearing component of the deflection response increases by a factor associated with the shear creep compliance of the foam core. The modelling of the sandwich beams over a 1200 hour test was described as 'good' and when the model was applied to the 10 year creep tests of Just (1983) and Davies (1987), again 'good predictions' were found.

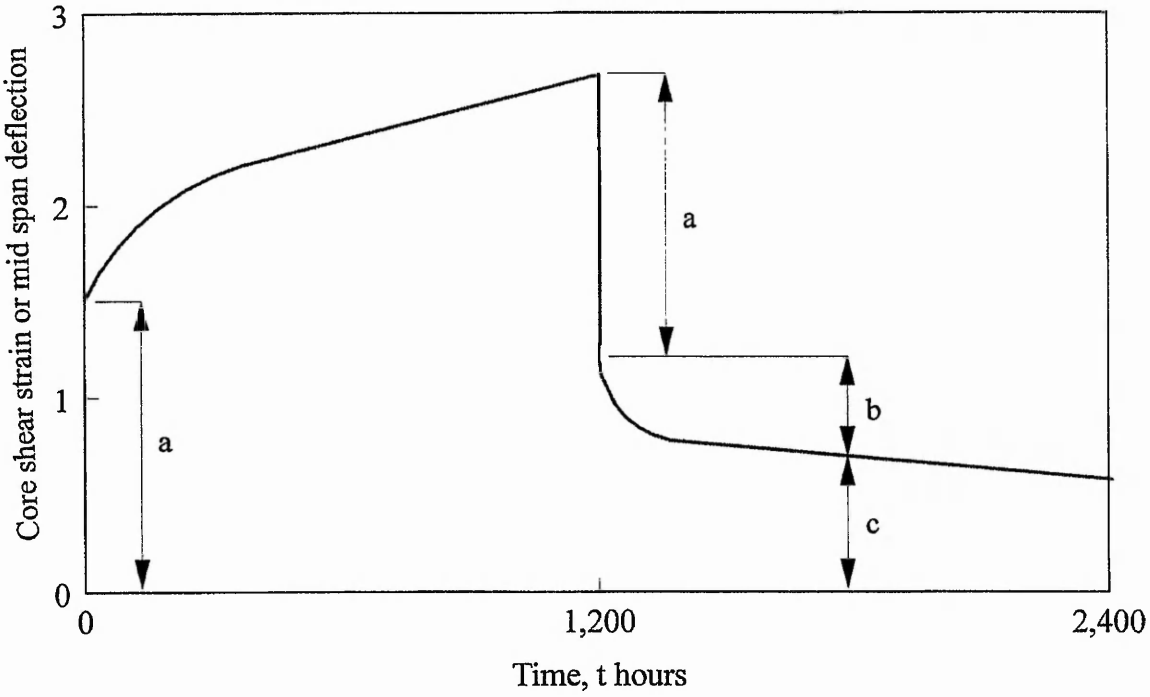

Figure 2.7 Generalised illustration of either core shear strain of a shear test specimen or mid span deflection of a sandwich beam against time under constant applied loading

During O'Connor's (1985) investigation of "The flexural behaviour of sandwich beams with thick facings and rigid plastic foam cores" experimental recordings of beam deflections were made by first applying the load and then waiting until the visual and initially rapid creep displacements had dissipated to a rate that could not be visually observed before the beam's deflection was taken. This appears to compromise the assumed elastic behaviour by over estimating the elastic displacement response. In this project, with the aid of near instantaneous data logging computer systems, beam deflections were taken immediately after the load had been placed. This technique was vindicated by the time / mid span displacement response of a simply supported beam shown in figure 2.8.

Three 80 mm wide beams of 2000 mm span, 52 mm core and 12.3 mm thick plywood facings were tested in a three point load configuration. Significant creep was deemed

to constitute 1% of the total mid span deflection. The three beams registered significant creep at approximately 30, 30 and 40 seconds.

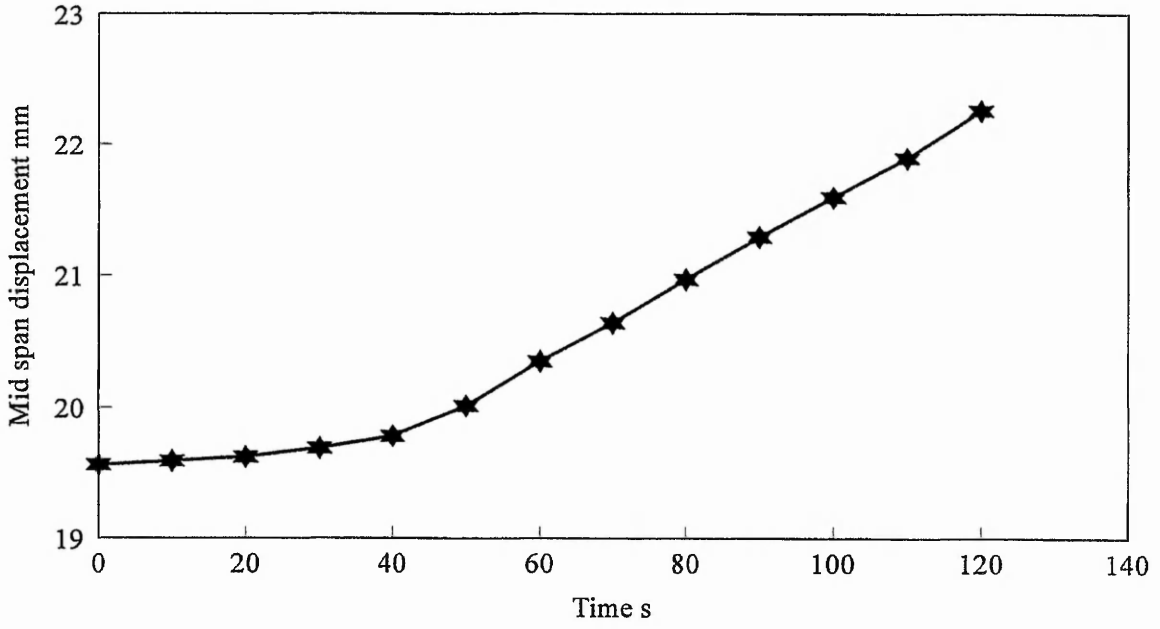

Figure 2.8 Initial creep response of a plywood faced sandwich beam

The initial rate of creep is low (up to say after 20 seconds have elapsed) as creep shear strains distribute throughout the core depth. Creep shear strains increase in the core from zero at the neutral axis to a maximum just inside each facing. Therefore it may be argued that the amount of shear strain near the facing is greater with a corresponding greater amount of creep present in that outer location. As the outer material creeps at a faster rate, stresses and strains redistribute throughout the depth of the core thus increasing the amount of shear strain in the foam immediately nearer to the neutral axis.

The experimental results of all testing of specimens that include Isofoam CRF have been, to some extent, influenced by time dependent stress / strain response. To limit the amount of creep two steps have been taken. Firstly displacements (and facing strains where required) have been recorded immediately after loading and secondly, linear relationships have been experimentally evaluated from tangential lines drawn at the beginning of the experimental response curves.

From the results displayed on figure 2.8, at 20 seconds elapsed time, there is only a 0.3% increase in total deflection and only 1.1% after 40 seconds. Where a constantly increasing rate of strain, or load ramp, has been applied to an Isofoam specimen the creep response is significantly less than seen for the three beam tests above. The duration to which time dependant shear strains in the core of beams become significant, subject to a load ramp, will be greater than the static case shown on figure 2.8. As will be seen in chapter 7, the three point load tests for panels P4-P6 and P10 are not seriously affected by creep and their experimental load / displacement relationships are reasonably linear.

Thermal conductivity: Thermal conductivity of a rigid closed cell polymer foam is not only effected by the ambient temperature of the foam itself, figure 2.9, but also its density, figure 2.10. Other factors such as the type of blowing agent, cell size and cell content also effect the thermal conductivity. As can be seen on figure 2.10, 32 kg/m^3 foam provides the optimum density for thermal insulation. Thermal movements in polyurethane foams are conveyed through the solid material and the gaseous voids. Foam denser than 32 kg/m^3 allows a greater proportion of thermal gradients to permeate throughout the skeletal structure than the voids. Less dense foams conduct thermal gradients more freely across the larger voids. The optimum density is that where the thermal currents through the solid mass and voids are balanced.

The use of 32 kg/m^3 density foam for cavity wall remedial measures was dictated by the original application of the foam as thermal insulation. In certain locations where large numbers of similar residential buildings were all subject to the same degree of subsidence (a mining wave) those with foam insulation applied to their cavity walls showed no or substantially less structural defects than those without. The properties in Newbold Verdon, Leicestershire used the 32 kg/m^3 density foam as no formal investigations of the structural benefit of injecting foam into a cavity wall had been made and the only basis for the treatment was 'engineering judgement'. This judgement was purely based on what had worked before should work again.

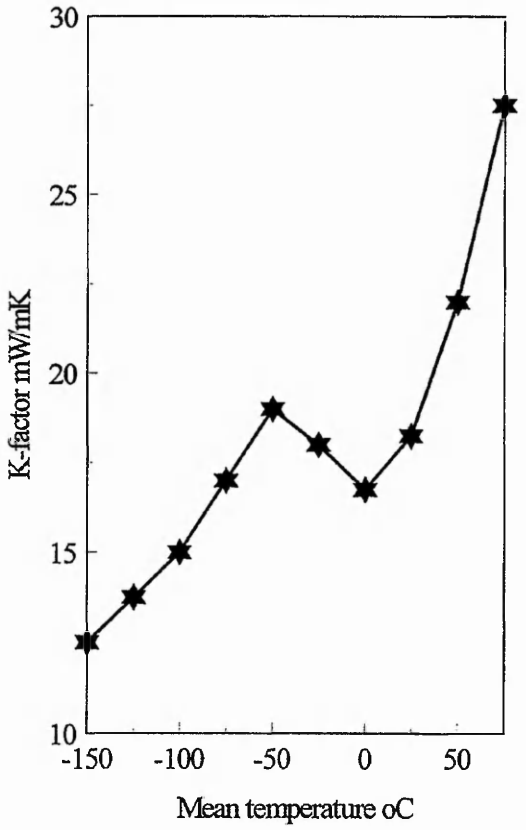

Figure 2.9 Effect of foam temperature on thermal conductivity

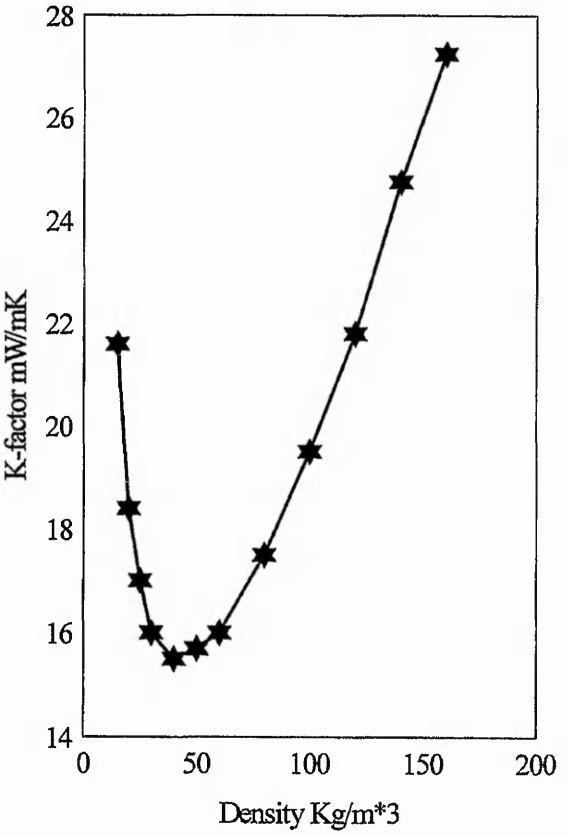

Figure 2.10 Effect of density on thermal conductivity

2.3 Remedial measures to existing masonry cavity walls

2.3.1 General application

On site installation of Isofoam CRF in to the void of cavity walls uses two large metallic drums each containing one component, a proportioning unit of two identical air driven pumps, a measuring system for the accurate supply of the resin and isocyanate components and an injection gun. The same installation system has been used for all applications of Isofoam CRF including the plywood faced panels. Pipes from each drum meet at the gun, where the components are mixed on exit and deposited through an appropriate nozzle.

2.3.2 Installation of Isofoam CRF to plywood faced panels and masonry cavity walls

2.3.2.1 Manufacture of plywood faced panels

The sandwich panels used for this project are all manufactured from various types of plywood facings and expanded polyurethane foam. The foam injection system, as used in existing masonry cavity walls, involves pumping the liquid through a series of drilled holes in the timber spacer boards. Figure 2.11 shows the basic configuration for the manufacture of the plywood faced panels. The foam is injected from both ends of the panel. The construction method of using timber spacer boards leaves a plywood overhang passed the Isofoam core, this overhang was later removed as the panels were reduced to 1000 mm wide by 2020 mm long.

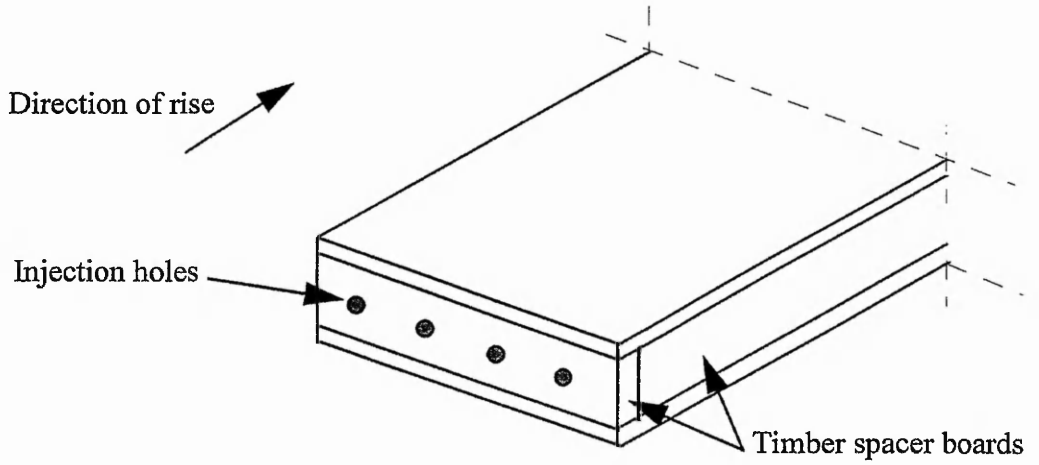

Figure 2.11 Manufacture of plywood faced panels

The method of manufacture has been instrumental in creating an orthotropic material as the foam is squeezed between the lateral containing boards along the length of the panel. The lateral pressure causes an elongation of the voids in the cellular structure as the rising liquid mass fills the required core thickness. However, this is predominantly the condition found throughout the Isofoam CRF mass when in service in cavity walls. Figure 2.12 below illustrates the shape of the voids typically found in the foam mass.

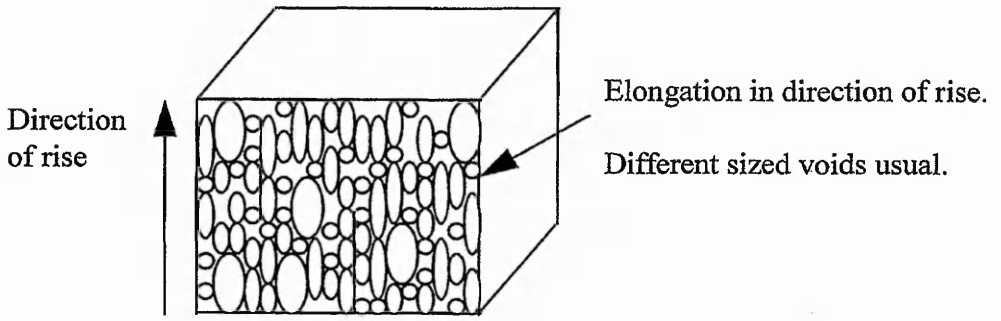

Figure 2.12 Typical cross section showing cellular structure of foam injected into a confined space

2.3.2.2 Structural defects and associated mechanisms

Cavity walls commonly comprise an exterior leaf (or wythe), usually of architectural brick connected by metal wire ties to an interior wythe usually made from concrete blocks or brick units. The inner leaf carries the majority of vertical loads from the building's self weight and imposed loads such as wind pressures. The outer leaf acts as a barrier to environmental conditions and as an architectural facing. The two wythes are separated by a void between 50 mm and 125 mm wide. Usually metal wire ties bridge the void. The functions of the ties are to transmit horizontal loads between leaves and to provide a restraint during construction.

Typical structural defects and associated mechanisms are listed in table 2.3. The table does not represent an exhaustive list of structural defects or associated structural mechanisms. A publication by The Institute of Civil Engineers (1994) discusses why structural defects occur in residential building and their implications to the structure. Forty three causal mechanisms for structural defects in traditionally built residential properties have been identified. Each mechanism may be placed in to one of three main groupings,

(i) ground movement
(ii) structural inadequacy or overloading of the superstructure
(iii) defects in the structural materials resulting from physical action, chemical or biological attack.

It is not proposed to use Isofoam CRF in all of the cases listed. Those described in table 2.3 are the most likely causes and mechanisms to benefit from foam injection as part of either preventative or remedial works. The interest and drive of this thesis is to provide an analytical model for the resistance of Isofoam CRF injected cavity walls to lateral loads. The need for cavity foam reinforcement against lateral loads usually results from the inability of the outer wall to transmit load to the inner load bearing leaf. Failure of wall ties is relatively common in housing built in the late 1940s and 1950s mainly due to the inadequate galvanising of the steel wall ties.

Structural defect	Mechanism attributed to defect	Required structural performance of Isofoam CRF
Cavity wall tie failure	(i) Bowing or buckling usually of interior load bearing leaf (ii) Reduced resistance of outer leaf to wind loads	(i) Bonds the leaves together to provide a continuous vertical support (ii) Shear transfer medium to increase stiffness of complete cavity wall by composite action and utilisation of inner wall
Differential settlements	(i) Relative settlements of corners of buildings (ii) Relative vertical settlement of cavity wall wythes	(i) Provides shear resistance between wythes and a vertical restraint connecting the corner to the rest of the building (ii) Forms a large shear resisting plane between wythes
Increase in load to the building	May accentuate any of the above defects	Increases the general integrity of the building
Excessive overall settlements	Angular distortion of complete building	Enhances the bending stiffness and strength to oppose eccentric loads

Table 2.3 Interaction of Isofoam CRF in preventing the mechanisms commonly inherent to structural defects in masonry cavity walls

2.3.2.3 Installation of Isofoam CRF to masonry cavity walls

The proposed stabilisation procedure applied to defective masonry cavity walls involves pumping a two part liquid mass into the cavity space as shown on figure 2.13, through a series of drilled holes. The liquid quickly rises (or foams) to fill the cavity and solidifies into a rigid cellular form bonding the two wythes together. The foam contains a resin compound which enhances the bonding. The ability of the foam to completely fill the void as it rises and bond to the irregular masonry surface is paramount to its use. The foam is typically inserted at a pressure of 1 psi which usually requires larger areas of external wall to be braced.

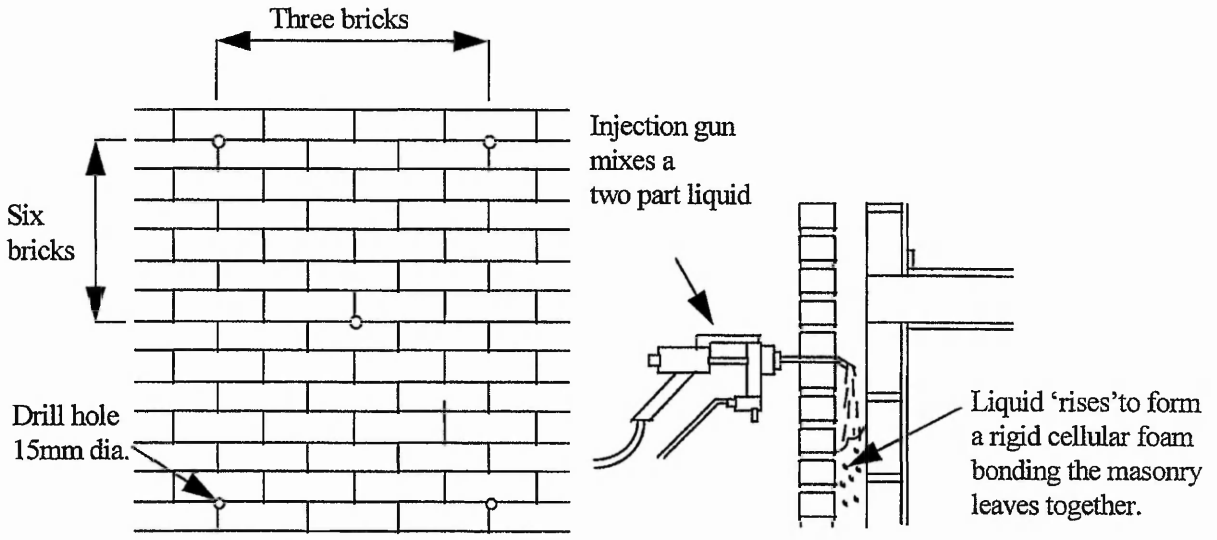

a. Typical drilling pattern for foam injection

b. Cross section through cavity wall

Figure 2.13 Injection method for cavity walls

2.3.3 Considerations for the application of Isofoam CRF to an existing cavity walled building

The problem of assessing the actual stiffness and strength of masonry in service and its need for remedial work is paramount to the effectiveness of the foam injection system. The BS 5628 flexural strength assessment of a single masonry wythe is based

on a 95% confidence limit, which is then used to formulate a total strength for a cavity wall. It is assumed that traditional remedial measures, repointing etc., refurbish the wall to an original standard.

When considering all types of remedial measures both short and long term economic aspects should be predominant in the choice. Currently Baxenden Chemicals Ltd (1986), manufacturers of the Isofoam CRF used throughout both this project and the two case studies, guarantee their product over a twenty five year period. The twenty five year life is based on observation of the foam in service throughout various applications, but most commonly as cavity wall insulation. The life of the foam may well be extended as confidence grows of the longevity of early applications.

In both case studies presented there were fundamentally two choices for the future housing of the current residents. The structural defects were such that normal refurbishments were not suitable and a complete demolition and rebuild was proposed until the foam injection system was also put forward. Use of the foam injection system is subject to the recommendations and working practices of BS 5628 (1992), BS 7456 (1991), BS 7457 (1991) and the British Board of Agrement Certificate No. 85/1567 (1986). The cost of the remedial measures incorporating the foam injection system were approximately half of the alternative demolish and rebuild program and caused far less disturbance in terms of temporary re-housing during works.

Isofoam has also been used as a cavity wall tie replacement as recommended in BS 7457 (1991) for many applications. Here the self adhesive properties of the Isofoam are mobilised in preventing the masonry wythes from bowing. The use of Isofoam CRF as a remedial measure for differential settlement and bowing is well known and particularly ideal as the large in plane surface area of the walls is utilised. A consideration not made in BS 7456 (1991) is the time dependant behaviour of the Isofoam CRF. Work carried out by Huang and Gibson (1990) and (1991) may point to the need for further investigation of the interactions of the masonry and the Isofoam since the ability to undergo strain before failure is very different.

2.3.4 Case studies

2.3.4.1 Newbold Verdon, Leicestershire, existing masonry cavity walls injected with Isofoam CRF

Background: This project was instigated by the successful application of the foam injection system to 124 residential buildings, of varying configurations, in a housing estate at Newbold Verdon, Leicestershire. Built just after the Second World War, shortages of cement, timber and skilled labour, allied to poor design created buildings that were particularly susceptible to damage from subsidence originating from old mine workings.

Structural defect mechanism: The subsidence had caused differential movement between the leaves of the cavity walls and combined with cavity wall tie failures (both from corrosive failure of the ties themselves and of them being pulled out of the highly friable mortar) had then led to some of the inner load bearing walls to bow.

Many of the structural problems were due to the inadequate design and use of gutters which were also used around the eaves as a reinforced ring to prevent spreading of the roof truss. However, as the gutter system began to fail, spreading of the roof truss occurred which in turn produced an eccentric loading to the cavity walls. The eccentric loading then caused the outer wall to bow away from the inner. This defect was accentuated by the poor quality of the mortar and the failure of wall ties.

Remedial measures: Lock (1990), documented the remedial measures carried out to the buildings and conducted preliminary structural tests on sub-elements of the residential buildings. The proposed remedial measures carried out on the buildings included providing an additional reinforced grouted ring around the outer perimeter of the spreading and spalling of the gutters. Steel plate sections were added to the roof truss to prevent further spreading. Underpinning and repointing of the cavity walls was also necessary prior to filling the void of the cavity wall with Isofoam Cavity

Reinforcement Foam. The foam was injected through holes drilled in the outer masonry leaf as described earlier.

At the time of the implementation of this innovative remedial measure there was no formal analysis or testing to validate the proposed foam injection system. A limited number of tests were conducted on elements of two trial buildings. The sub-element testing comprised creep monitoring of the relative displacement of two bricks bonded with Isofoam CRF, two shear tests of approximately 1 m^2, which displaced the two leaves in a parallel direction to one another and two laterally loaded bending tests on sections of a wall of one of the building. It was concluded from these tests that the foam injection system would provide adequate interaction to prevent differential movement and a medium to allow composite action hence strength enhancement.

Structural integrity: A few years after the remedial works were complete structural surveys of the buildings treated with Isofoam CRF established no further damage concurrent with the original problems and complete integrity had been upheld.

2.3.4.2 Bagworth, Leicestershire, existing Hawthorn-Leslie steel framed buildings bonded to a new masonry outer skin with Isofoam CRF

Background: Hawthorn Leslie construction dwellings achieved The National Building Agency appraisal certificate in 1966. In the short time the building system was in operation the original steel frameworks were reduced with some of the structural load bearing capabilities of the cladding panels being utilised. Typically, a framework of nine vertical stanchions connected by steel channels formed the skeleton of the building. Asbestos and plasterboard sheets were secured to the outer and inner faces of the channel sections with the void being coincidentally injected with polyurethane foam under high pressure. An additional outer weather proof cladding layer was then also fixed to the steel frame.

The lack, in some cases, of certain diagonal steel sections placed a high shear load into the cladding panels causing the whole building to shear. The out of plumb at

eaves level of a two story dwelling was measured at some 125 mm. This degree of structural defect would normally result in the buildings being condemned and the residents re-housed. Due to financial and logistical restraints the foam injection system was adopted. The foam injection system also allowed the residents to continue to use their properties during the repair phase.

Remedial measures: Major structural integrity required restoring and this was proposed by constructing an exterior skin of brickwork around the existing buildings. The cavity between the brickwork and the existing walls typically ranged from 25 mm to 150 mm and was injected with Isofoam CRF after the brickwork skin had been constructed. The brickwork was braced during construction with form work while the foam was injected under nominally 1 psi pressure.

Structural integrity: The structural integrity and habitability of all the treated single and two story buildings were substantially enhanced. Vastly improved levels of thermal and acoustic insulation were also achieved. The buildings are currently all in satisfactory condition.

2.4 Conclusions

(i) The long term physical properties of rigid polyurethane foam subject to constant levels of stress may cause problems of structural integrity to masonry elements. Careful appreciation of time dependant behaviour may be necessary. Applications where short term loadings are predominant are more suited to the properties of Isofoam CRF. In particular wind loading or temporary reinforcement for mining subsidence may be ideal situations for the foam injection method.

(ii) In this thesis creep response of specimens containing Isofoam CRF has been limited in two ways. Firstly, by approximating experimental result curves with a tangential line usually drawn from the origin. Secondly, by recording flexural or stress / strain response immediately the desired load level has been reached.

(iii) The two case studies have provided evidence that the foam injection system is a valid option for a wide range of structural remedial measures to existing masonry cavity walls. In particular the foam injection system appears ideal as a cavity wall tie replacement alternative as recommended in BS 7456 (1991) and BS 7457 (1991). The considerable area of most cavity walls offsets the relatively low compressive and tensile modulii and strength allowing a high degree of integrity.

(iv) Temperature of the foam plays a significant part in the behaviour of polyurethane foams. Experimental evaluation of physical properties should be conducted at a consistent temperature.

(v) There is a significant gap in the knowledge of the actual structural interaction of Isofoam CRF and masonry. The foam injection system is currently employed in an 'engineering judgmental' way with little meaningful formal analysis.

CHAPTER 3 - SANDWICH CONSTRUCTION ANALYSIS METHODS

3.1 Introduction

3.2 Sandwich beam analysis: Ordinary bending theory

3.3 Sandwich beam analysis: Allen's theory as presented by O'Connor

3.4 Finite Element Analysis

3.5 Discussion

3.6 Conclusions

CHAPTER 3 - SANDWICH CONSTRUCTION ANALYSIS METHODS

3.1 Introduction

The following sections deal specifically with literature relating to sandwich theory and the application of finite element analysis to sandwich constructions.

3.1.1 Applicable methods of analysis

Analysis of sandwich panels and beams began in the early 1940s at the United States Forest Products Laboratories and in the aviation industries of England and America. One of the first published articles, by March and Smith (1944), to present a theoretical analysis of sandwich action considered both the bending and the shear deflections as separate components which were attributed to the behaviour of the facings and the core respectively.

From this early beginning two forms of analysis developed for the flexural behaviour of thick faced sandwich beams. One was an engineering approach first developed by Norris et al (1944) and further advanced by Hartsock (1966 and 1969) and then Allen (1969). This engineering approach was formulated by examining the equilibrium of a discrete element within the sandwich and allowing for the alteration to the average stress in the core created by the self stiffness of the facings.

Hartsock and Allen derived formulae in a different manner, but the solutions were essentially the same. The other form of analysis adopted a variational method where the equilibrium statement was defined in terms of stationary energy principles. Hoff and Maunter (1948), and later Krajcinovic (1971) and (1974) both developed this method. The proposed variational solutions lead to highly complex and general equations and for this reason the engineering approach of Hartsock and Allen is preferred. Stamme and Witte (1974) also presented an alternative formulation to the engineering approach in a complete summary of sandwich panels for use as cladding to buildings.

The most appropriate and practical presentation of the flexural response of sandwich constructions in bending are the Allen solutions rewritten for specific examples by O'Connor (1985). Equations for deflections, facing stresses and shear forces may be applied to the plywood faced constructions tested in this project.

Computer generated solutions, most notably finite element analysis, have seen much development in the past 25 years partly due to the flexibility of the modelling system and partly due to the advent of powerful and widely available personal computers. Finite element methods utilise a mathematical model formulated from a pre-described group of connected discrete parts called elements, each given a specific behavioural response. The elements are defined by the positions of points, or nodes, situated at corners and along edges. The interaction of these nodes between adjacent elements gives the computational solution to the model. When analysing structural members the nodal response forms a matrix of force-displacement relationships to describe model behaviour.

Literature relating to general finite element theory is readily available, Zienkiewicz (1992), Hinton and Owen (1990) and Rao (1992) all provide excellent texts. Finite element solutions and modelling methods for sandwich constructions have been well documented by O'Connor (1985) and (1987) for thick faced elements and Davies (1986) for sandwich panels with profiled or corrugated faces. The effect of profiling thin sheets creates an inherent flexural stiffness about the facing's own centroidal axis and were therefore considered as thick faced panels. Davies also summarised the use of a 'truss analogy', but this less sophisticated form has its limitations and is time consuming in terms of data preparation.

The finite element method developed by O'Connor was specifically designed for sandwich panels and incorporated special elements for the facing / core interface as no commercially available software package could accommodate the different types of element required at that time. Today however, with the advent of high powered computers and computing engineers advancing the ability of their software products,

most modern F.E. packages have large element libraries containing appropriate element types. The commercially available software packages ABAQUS (1995) and LUSAS (1993) have been chosen to complete the finite element analysis with support from a Rolls-Royce plc in-house post-analysis processing packages SC01 and SC03. The element libraries of both analysis packages contain certain elements that have been identified as being particularly well suited for sandwich constructions.

O'Connor (1985) studied the flexural behaviour of sandwich beams with thick facings and rigid plastic foam cores. The investigation uncovered a critical span effect. This "critical span concept" describes the condition where "... under a load point there is a local distortion of stress distribution and deflections within a sandwich beam". Examination of this concept lead to the conclusion that all types of sandwich constructions were subject to some degree of thick face response near to point load concentrations.

The range of plywood faced sandwich panels tested in this study all tend towards being defined as "thick faced" constructions with one exception. The masonry cavity walls have been defined as "very thick faced". The sandwich types proposed for testing in this study, allied to O'Connor's premise that all sandwiches have some thick faced response has lead to Allen's thick faced theory being identified as most appropriate for use throughout this study.

This chapter presents Allen's solutions to sandwich panel theory with particular reference to the specific solutions derived by O'Connor for three point loading configurations. General finite element theory has been presented with reference to modelling techniques and applicability to sandwich behaviour.

3.1.2 Sandwich construction definitions

3.1.2.1 Sandwich beam dimensions

A sandwich beam, shown in figure 3.1, comprises two strong and stiff facing sheets and a lightweight, weak core material. The facings are bonded to the polyurethane core by the self-adhesive property of the foam during injection into the void. The beam is of length L, width b, with facings of thickness t, core thickness c and overall depth h. The distance between the centre lines of each facing, d, defines the effective shear depth and when multiplied by b, the effective shear area.

Axial directions are defined as positive x in the spanning direction, y across the width of the beam or panel and z the through depth direction in a positive downward direction.

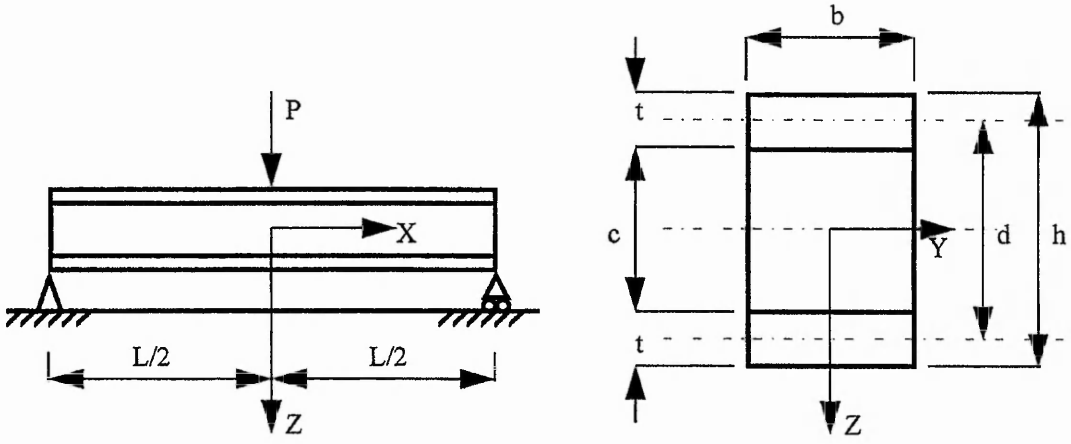

Figure 3.1 General dimensions and orientation of axes relative to a simply supported sandwich beam.

3.1.2.2 Definition of thin and thick facings

Sandwich construction analysis may be categorised essentially into two types of theory dependent upon geometric and physical properties. The two areas are described as 'thin faced' and 'thick faced' analysis. Thin faced analysis treats the facings as having relatively no stiffness about their own centroidal axis, compared to the total beam

stiffness, this is also known as membrane action. Thick faced analysis is more complex, with significant stiffness of the faces about their own centroidal axis. This has a profound effect on the bending behaviour of a beam. The assumptions of the thin faced theoretical solutions are no longer valid and the theory becomes more complex. The contribution made by the thick faces is to smooth out sharp changes in bending and shear stresses at the load and support points and to redistribute applied stresses throughout the core. This is termed 'thick face action'.

The overall bending stiffness of a sandwich beam D, is given by the following equation,

$$D = E_f \frac{bt^3}{6} + E_f \frac{btd^2}{2} + E_c \frac{bc^3}{12} \quad \text{.....(3.1)}$$

The first term on the right hand side of equation 3.1 is the contribution (total) of the facings bending about their own centroidal axis, the second term is the bending stiffness of the facings about the centroidal axis of the complete beam and the third term is the stiffness of the core about its own centroidal axis.

Definitions for the classification of sandwich type are based on the degree of contribution of stiffness from the individual components of equation 3.1 and are summarised below,

Very thin facings: The facings are assumed to have zero stiffness about their own centroidal axis and are so relatively thin that the effective core shear area is equated to A=bd.

Thin facings: The facings are assumed to have zero stiffness about their own centroidal axis, however, their thickness is such that the effective shear area is given by equation 3.2. The derivation of the effective shear area A and equation 3.2 has been given later in Section 3.2.

$$A = bd^2/c \quad \text{.....(3.2)}$$

Thick facings: The facing's geometrical thickness permits the effective shear area of the core to be as in equation 3.2. The stiffness of the facings are such that they able to significantly contribute to the overall stiffness of the sandwich. Thick faces would be described as such when their stiffness is >1% of the overall stiffness.

Very thick facings: The facings are so thick that similar magnitudes of facing self-stiffness and overall stiffness are often present. The effect of the facing's inherent stiffness to the bending characteristics is such that modifications to sandwich behaviour extends throughout much of the length of the beam. The sandwich construction is thus inefficient in nature although the composite effect produced by shear transfer through the core does still enhance the overall stiffness. In context with this project, injecting cavity walls with Isofoam CRF creates a theoretically inefficient sandwich, but the bending stiffness is significantly enhanced and it is this structural improvement that is of importance.

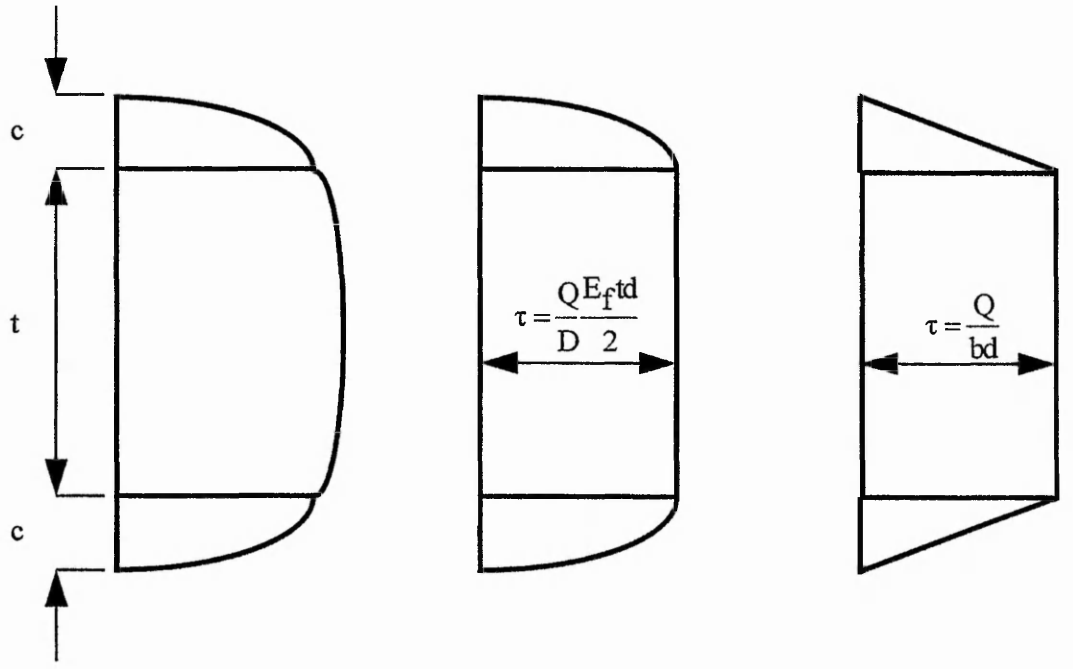

a. Stiff facings and core b. Stiff facings and weak core c. Weak facings and core

Figure 3.2 Shear stress distributions through depth of a sandwich beam

The effect of the facing's self stiffness may be examined by looking at the shear stress distribution through the depth of a sandwich. Figure 3.2 shows three conditions that relate the shear distribution through a sandwich beam with a weak core and stiff, thick facings. Figure 3.2a is the actual shear stress distribution when the beam has stiff facings and core, 3.2b shows the effect of the beam having a weak core and stiff facings. In this case it may be assumed that across the depth of the core the shear stress may be considered as uniform. Figure 3.2c shows the shear stress in the beam when the facings are also weak or are thin and do not contribute to the overall stiffness of the beam when bending about their own centroidal axis.

According to Allen (1969) a sandwich beam is considered to have thick faces when the relative elastic modulii and geometric properties of the components of the sandwich are such that,

$$3\left(\frac{d}{t}\right)^2 < 100 \quad \text{..... (3.3a),}$$

and the bending stiffness of the core may be neglected when,

$$6\frac{E_f}{E_c}\frac{t}{c}\left(\frac{d}{c}\right)^2 > 100 \quad \text{.....(3.3b),}$$

and a constant shear stress distribution may be assumed when,

$$4\frac{E_f}{E_c}\frac{t}{c}\frac{d}{c} > 100 \quad \text{.....(3.4).}$$

3.1.2.3 Displacement response of thick faced beams

Figure 3.3 a. shows an unloaded simply supported beam with thick facings. Parts b. and c. show the pure bending and pure shear displacements of the beam subject to a single point load. Part d., illustrates the effect of the thick facings on the deflection response.

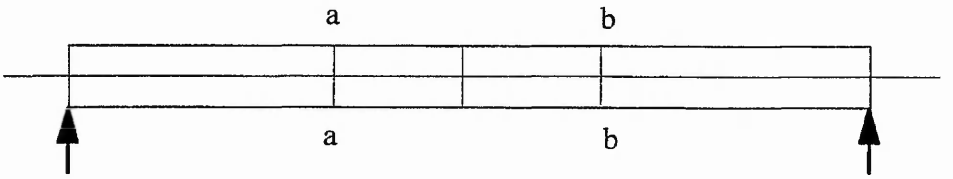

a. Unloaded beam

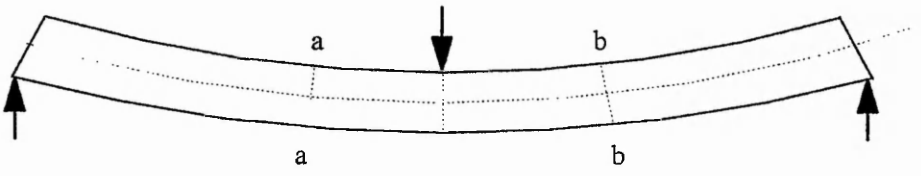

b. Pure bending

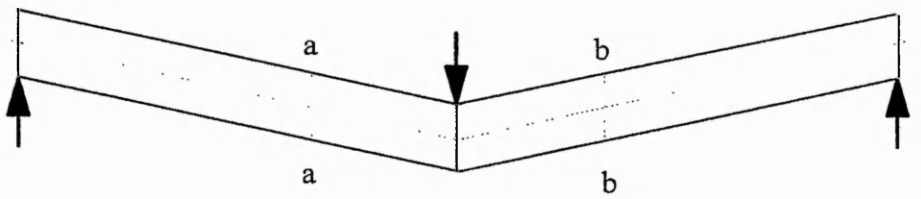

c. Pure shearing

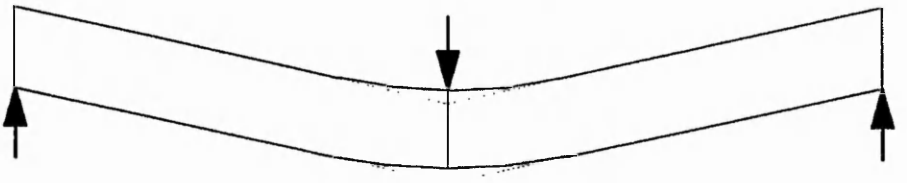

d. Shearing with local thick face response

Figure 3.3 Sandwich beam displacement characteristics

For pure bending displacement response, it is assumed that the lines **aa** and **bb** rotate, about their mid-point, but remain perpendicular to the facings and centre line of the beam. Therefore, the distance **ab** on the top face decreases, indicating compression, and the distance **ab** on the bottom facing increases, thus tension.

For pure shear displacement response the lines **aa** and **bb** are assumed to translate vertically with no lateral movement and the facings slope according to the sharp shear discontinuity of the applied load.

In thin faced sandwich response pure bending and pure shear displacement response may be superimposed to give the overall behaviour, however, for thick faced sandwich beams the contribution of overall beam stiffness from the facings creates a situation where the shear strains in the core are reduced.

The analysis of thick faced constructions is derived directly from thin faced classical methods and thus the range of plywood / Isofoam panels chosen included both types. More emphasis is placed on thick faced theory as the masonry cavity wall systems are intrinsically (very) thick faced in nature. In general, based on the assumption that the cross sections (in the yz plane) that are plane and perpendicular to the longitudinal axis remain so during bending. Positive and negative sign conventions adopted for bending moments and shear forces are shown on figure 3.4 and normal and shear stresses are shown on figure 3.5.

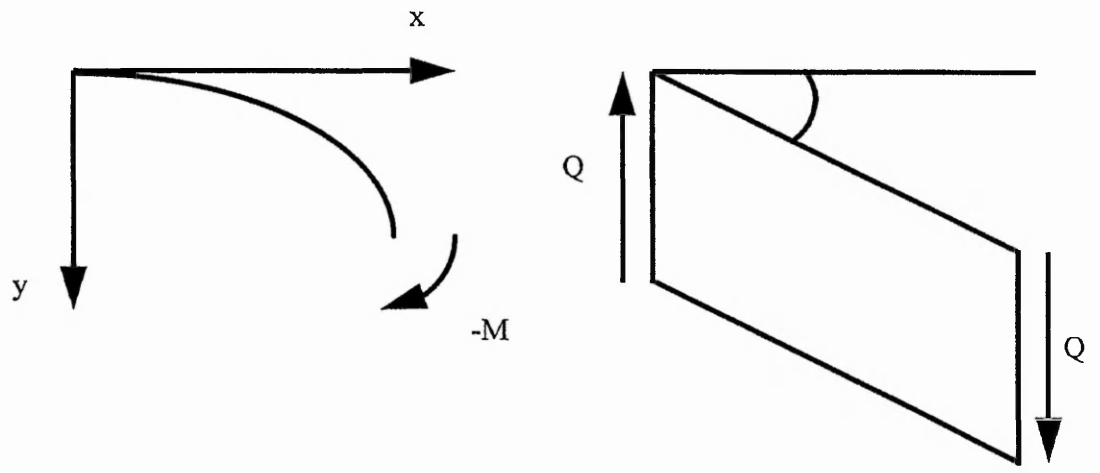

Figure 3.4 Sign convention for bending moments and shear forces.

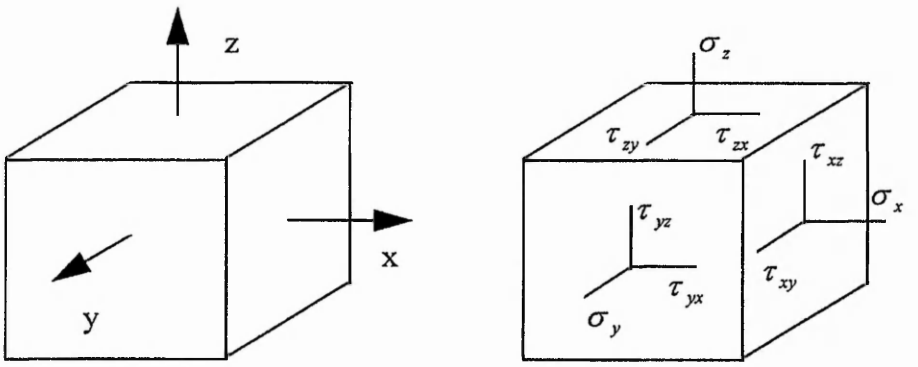

a. Axial directions b. Stresses relating to each axis

Figure 3.5 Definition of normal and shear stresses.

These definitions lead to the common load / displacement relationships for parameters in one plane which are shown in Table 3.1.

Deflection	ω	ω
Slope	$\frac{d\omega}{dx}$	ω^{i}
Curvature	$\frac{d^2\omega}{dx^2}$	ω^{ii}
Bending moment	$M = -EI\frac{d^2\omega}{dx^2}$	$-EI\,\omega^{ii}$
Shearing force	$Q = \frac{dM}{dx} = -EI\frac{d^3\omega}{dx^3}$	$-EI\,\omega^{iii}$
Loading	$w = -\frac{dQ}{dx} = -EI\frac{d^4\omega}{dx^4}$	$-EI\,\omega^{iv}$

Table 3.1 Sign convention for force / displacement of beams.....(3.3)

3.2 Sandwich beam analysis: Ordinary bending theory

Ordinary bending theory may be used as a first approximation to the solution of a loaded beam for predictions of deflection and stress assuming that cross sections remain plane

and perpendicular to the spanning or longitudinal axis if the sandwich bends cylindrically. Accuracy of this simple model is directly related to the thickness and rigidity of the facings. It may be said that the thinner the facing the more accurate the model becomes. Importantly, two further assumptions must also be satisfied: geometric uniformity and isotropic material behaviour. These assumptions then lead to the fundamental relationship for applied bending moment, stress and curvature,

$$\frac{M}{I} = \frac{E}{R} = \frac{\sigma}{y} \quad \text{.....(3.4)}$$

Deflection of a sandwich beam subject to a 3-point load configuration may be derived from considering the shear deformation of the core with thick facings, as shown in figure 3.6. For most practical situations the shear depth should be regarded as being equal to **d**, the distance between the centroidal axes of the two facings, and so there is a difference from the actual core depth **c**. Thus the core shear strain γ may be related to the overall sandwich shear slope $d\omega_2 / dx$ by geometry.

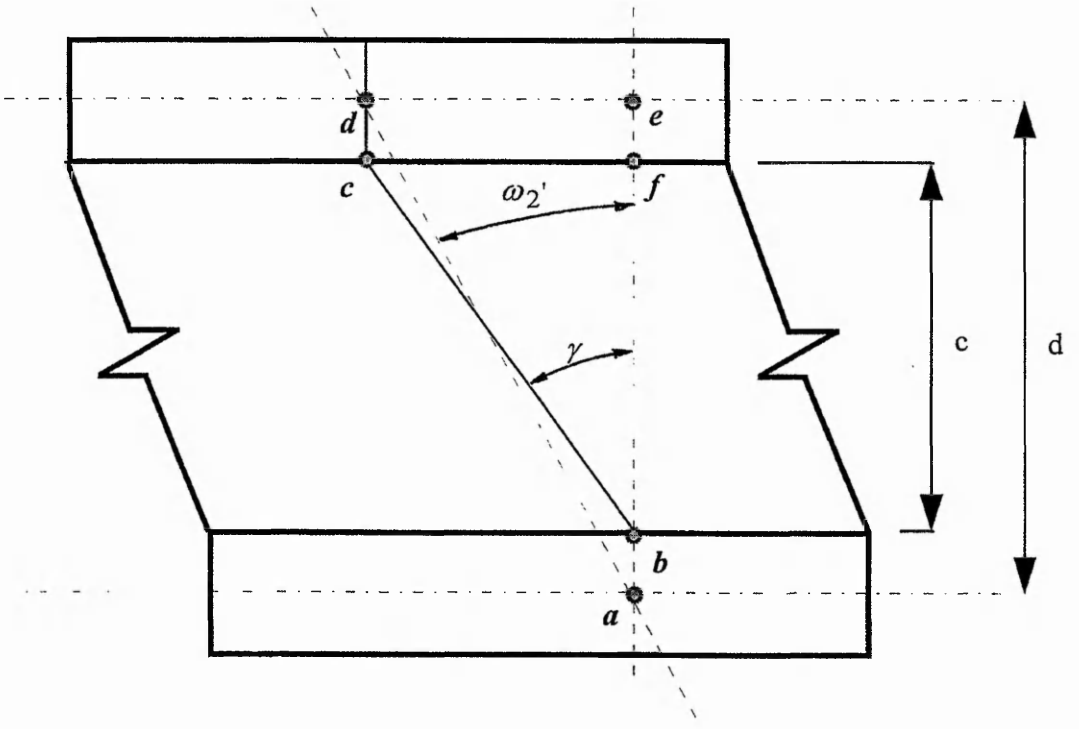

Figure 3.6 Weak core shear deformation in a beam with thick facings

If the element of beam above is considered then in the unloaded state the facings are aligned with ***abfe*** in a vertical plane. When loaded points ***e*** and ***f*** are then transposed to new positions ***c*** and ***d*** relative to ***a*** and ***b***. The transposed distance between ***d*** and ***e*** is equal to $d(d\omega_2 / dx)$, which is equal to core shear strain times the core depth, γc. This assumes that there is no shear strain in the facings themselves which is reasonable considering the difference in shear stiffnesses between the facings and core and the overall level of shear stress present throughout the depth of the beam.

The shear strains $d\omega_2 / dx$ and γ may be compared by definition with respect to shear modulus G and applied shear force Q:

By geometry

$$\frac{bf}{ae} = \frac{c}{d} = \frac{\omega_2'}{\gamma} \quad \text{.....(3.5)}$$

Stress / strain

$$\gamma = \frac{\tau}{G} = \frac{Q}{bd}\frac{1}{G} \quad \text{.....(3.6)}$$

Rearranging and substituting

$$\omega_2' = \frac{Q}{bd}\frac{1}{G}\frac{c}{d}$$

$$\omega_2' = \frac{Q}{AG} \quad \text{.....(3.7)}$$

Thus the effective shear area

$$A = \frac{bd^2}{c} \quad \text{.....(3.2)}$$

and the overall shear stiffness is AG

For the case of a simply supported beam with a central point load P, the shear force Q = P/2, thus integrating equation 3.7 and substituting for Q gives

$$\omega_2 = \frac{P}{2AG}x + C$$

The constant may then be evaluated at x = 0 where $\omega_2 = 0$ so C = 0 and therefore at the centre of the beam x = L/2 so as to give the maximum deflection due to shear deformation

$$\omega_2 = \frac{PL}{4AG} \quad \text{.....(3.8).}$$

By superposition the bending and shear deflections may be added together to give the overall deflection of a sandwich beam under symmetric 3-point loading

$$\delta = \frac{PL^3}{48E_fI} + \frac{PL}{4AG_c} \quad \text{.....(3.9)}$$

3.3 Allen solutions to thick faced sandwich theory

3.3.1 Introduction

This section presents the Allen solutions to thick faced sandwich beams assumed to have an antiplane core. Assumptions of an antiplane core are defined in the next section. General theory is described for deflections and stresses followed by the generation of specific solutions for a 3 point load configuration.

3.3.2 Assumptions for analysis

The engineering equilibrium approach of Allen incorporates simplifying assumptions which were made considering that the analysis was originated for core materials such as metal honeycombs. Allen's theory is used here for soft polyurethane cores which behave differently to honeycomb cores. There are two fundamental assumptions:

1. An antiplane core is one in which stresses in the x-, y-directions (σ_x and σ_y) and shear stress in the x-direction relative to the y- (τ_{xy}) are assumed to be zero. It is also taken that shear stresses, τ_{zx} and τ_{yz}, are independent of z-direction

influences. Figure 3.5 shows the stresses acting on an infinitely small point in the core. Effectively this means that the core acts primarily in shear and does not contribute to the overall bending stiffness of the sandwich.

2. An incompressible core where infinite stiffness in the z-direction is assumed. This assumption disregards strain in z-direction for beams that are wider than the core thickness so that at any transverse section, a single displacement may be described. It also implies that there is no relative displacement between the two faces.

3.3.3 Derivation of general deflections and stresses in a sandwich beam with thick faces and an antiplane core

The Allen analysis assumes that the antiplane core does not contribute to the bending stiffness of the whole beam and that the facings do possess significant rigidity to be considered. Thus in pure bending the facings deform firstly in compression or tension as a complete beam and secondly locally about their own axis. The contribution of the local to the overall flexural rigidity from the facings is $(E_f bt^3) / 6$. This has a knock-on effect to the shear deformation of the core and is particularly prevalent in positions of sudden changes in shear force. This can be seen in Figure 3.3d where the shear discontinuity is smoothed out. As a result, additional bending moments and shear forces are introduced to the facings. The shear stress distribution is taken as shown in Figure 3.2b, where

$$\tau = \frac{Q}{D}\frac{E_f td}{2} \qquad \text{.....(3.10)}$$

The inherent interaction between the bending stiffness of the facings and the shear stiffness of the core may be related by first considering a situation where the core has infinite shear stiffness, i.e. $G = \infty$. The primary deflection ω_1 may be attributed to the beam displacement by ordinary bending theory. Assuming the beam has a bending moment M_1 and a shear force Q_1 which are concurrent with ω_1 then

$$-Q_1 = D\omega_1''' \text{.....(3.11a).}$$

Separating the contribution of the facings to the overall stiffness, D, assuming the bending stiffness of the core is negligible,

$$-Q_1 = E(I - I_f)\omega_1^{iii} + EI_f\omega_1^{iii} \text{.....(3.11b)}$$

The term $E(I - I_f)\omega_1^{iii}$ represents the shear force carried by the beam when the facings are only subject to uniform compression or tension and without local bending. Here, it is assumed that the shear stress across the core is constant and tends towards zero over the thickness of the facings, as in Figure 3.2c,

$$\tau = \frac{Q}{bd} \text{.....(3.12)}$$

$E(I - I_f)\omega_1^{iii}$ in equation 3.11 may then be replaced by $Q = -bd\tau$ giving

$$-Q = -bd\tau + EI_f\omega_1^{iii} \text{.....(3.13)}$$

It should also be noted that $Q_1 = M_1^{i}$; $M_1 = -D\omega_2^{ii}$.

As a result of the shear stress τ, in the complete sandwich beam, the core undergoes a shear strain $\gamma = \tau/G$ and the beam is then subject to an additional deflection ω_2. The facings must share this additional deflection and are thus subject themselves to another shear force $Q_2 = M_2^{i}$ and bending moment $M_2 = -E_fI\omega_2^{ii}$. It can be said that a beam subject to a total load q has two forms of deflection ω_1 and ω_2. The primary deflection ω_1 is attributed to the ordinary bending of the beam whilst the secondary deflection is due to the shear strain of the core. The primary and secondary deflections are therefore associated to the shear forces Q_1 and Q_2 respectively and those in turn with bending moments M_1 and M_2. Thus the resultant loads, shear force, bending moments and deflection are

$$Q = Q1 + Q2 \quad \text{.....(3.14)}$$

$$M = M1 + M2 \quad \text{.....(3.15)}$$

$$\omega = \omega_1 + \omega_2 \quad \text{.....(3.16)}$$

In order to produce a general equation for the solution to deflections, core shear and facing stresses it is necessary to have a solution with only one variable. By substituting for Q_2 into equation 3.14 the total shear force may be expressed as a function of Q_1.

The primary core shear stress may be related to the secondary shearing displacement ω_2 in the same way as the primary shearing. Thus from the geometry of figure 3.6 and equation 3.5

$$\gamma = \frac{d}{c}\omega_2{}^{i} \quad \text{.....(3.17)}$$

Where the stress / strain relationship is

$$\tau = \frac{d}{c}G\omega_2{}^{i} \quad \text{.....(3.18)}$$

τ may then be substituted into 3.13 to give the primary shear force in terms of primary and secondary effects

$$-Q_1 = -\frac{bd^2}{c}G\omega_2{}^{i} + E_f I\omega_1{}^{i}$$

$$-Q_1 = -AG\omega_2{}^{i} + E_f I\omega_1{}^{i} \quad \text{.....(3.19)}$$

From the force / displacement equations 3.3 $Q_1 = -E_f I\omega_1{}^{iii}$ may be substituted into a rearranged equation 3.19 as follows

$$\omega_2{}^{i} = -\frac{E_f I\omega_1{}^{iii}}{AG}\left[1 - \frac{I_f}{I}\right]$$

$$\omega_2{}^{i} = \frac{Q_1}{AG}\left[1 - \frac{I_f}{I}\right] \text{.....(3.20)}$$

The total shear force $Q = Q_1 + Q_2$ now becomes $Q = Q_1 - E_f I \omega_2{}^{iii}$. Equation 3.20 is then differentiated twice and rearranged to give

$$-E_f I \omega_2{}^{iii} = Q_1{}^{ii} \frac{(1 - I_f/I)}{AG} \text{.....(3.21)}$$

which is substituted into $Q = Q_1 - E_f I \omega_2{}^{iii}$ to give

$$Q = Q_1 - E_f I \omega_2{}^{ii}$$

$$Q = Q_1 - Q_1{}^{ii} \frac{(1 - I_f / I)}{AG}$$

simplifying

$$Q_1{}^{ii} - a_2 Q_1 = -a_2 Q \text{.....(3.22)}$$

where

$$a^2 = \frac{AG}{(1 - I_f / I)} \text{.....(3.23)}$$

Equation 3.22 therefore is an expression for the total shear force Q and may be formulated for any specific problem, thus enabling Q_1 to be determined. M1 and ω_1 may then be found by differentiation and integration respectively. The factor a^2 is a ratio between the core shear stiffness AG and the local bending stiffness. The term $(1 - I_f / I)$ defines the degree of shear stress distributed in the core dependent on the inherent stiffness of the facings.

3.3.4 Specific solutions for a symmetrical simply supported beam under 3-point loading with an antiplane core and thick faces

The Allen solutions to three point bending theory may be simplified by the use of symmetry as shown in Figure 3.7. The solution is essentially for a cantilevered beam of span/2, l_1, and overhang l_2 with a single load P at point B. The solutions for deflection, facing stress and core shear stress are given in terms of x, the distance from the point A.

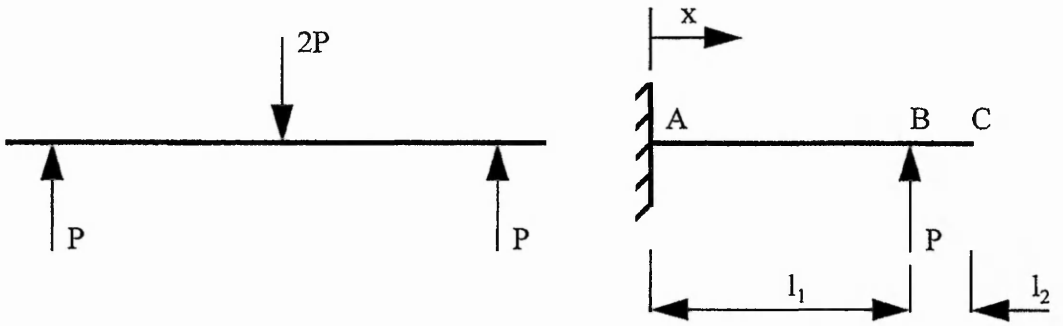

a. 3-point load test configuration b. Simplified analytical configuration

Figure 3.7 3-point load configuration

The solution begins by assuming the initial governing equation 3.22,
$Q_1^{ii} - a_2 Q_1 = -a_2 Q$ and considers the two spans AB and BC separately. Later as the primary bending slope ω_1^{i} and curvature ω_1^{ii} are continuous at B the displacement equations for each span have common governing conditions.

(i) Span AB

The shear force in span AB is -P and is the total shear force Q in equation 3.22, the solution of which is then

$$-Q_1 = C_1 \cosh ax + C_2 \sinh ax + P = EI\omega_1^{iii} \text{.....(3.23)}$$

To form the displacement equation for ω_1, 3.23 undergoes successive integration

$$EI\omega_1 = \frac{C_1}{a^3}\sinh ax + \frac{C_2}{a^3}\cosh ax + \frac{Px^3}{6} + C_3x^2 + C_4x + C_5 \text{.....(3.24)}$$

Equations 3.23 and 3.20 are then combined to give a solution for ω_2 which is then integrated,

$$-EI_f\omega_2 = \frac{C_1}{a^3}\sinh ax + \frac{C_2}{a^3}\cosh ax + \frac{Px}{a^2} + C_6 \text{.....(3.25)}$$

The six constants of integration, C_1 to C_6, may then be evaluated using boundary conditions for span AB these are:

At position A

1	Arbitrary zero deflection	$x = 0$ $\omega_1 = 0$	$\frac{C_2}{a^3} + C_5 = 0$
2	Arbitrary zero deflection	$x = 0$ $\omega_2 = 0$	$\frac{C_2}{a^3} + C_6 = 0$
3	Symmetry of primary slope criteria	$x = 0$ $\omega_1{}^i = 0$	$\frac{C_1}{a^2} + C_4 = 0$
4	Symmetry of secondary slope criteria	$x = 0$ $\omega_2{}^i = 0$	$C_1 + P = 0$
5	Applied bending moment	$x = 0$ $M = Pl_1$	$M = -EI\omega_1{}^{ii} - EI_f\omega_2{}^{ii}$ $Pl_1 = -\frac{C_2}{a} - 2C_3 + \frac{C_2}{a}$

C_1 and C_3 to C_6 may be evaluated with C_2 remaining unknown

$C_1 = -P$	$C_3 = -Pl_1/2$	$C_4 = P/a^2$	$C_5 = C_6 = -C_2/a^3$ .....(3.26)

(ii) Span BC

For the span BC, x is measured from point B and the shear force is thus zero. Again equations 3.22 is valid, however a new set of constants requires solving. To form the displacement equation for ω_1, 3.23 undergoes successive integration

$$EI\omega_1 = \frac{B_1}{a^3}\sinh ax + \frac{B_2}{a^3}\cosh ax + \frac{Px^3}{6} + B_3x^2 + B_4x + B_5 \ldots\ldots\ldots(3.27)$$

Equations 3.23 and 3.20 are then combined to give a solution for ω_2 which is then integrated,

$$-EI_f\omega_2 = \frac{B_1}{a^3}\sinh ax + \frac{B_2}{a^3}\cosh ax + \frac{Px}{a^2} + B_6 \ldots\ldots\ldots(3.28)$$

The span BC contains four boundary conditions at points B and C. At C it is assumed that the primary and secondary moments M_1 and M_2 are zero, thus there is no curvature and the ends are free to rotate.

At position B

6	Arbitrary zero deflection	$x = 0$ $\omega_1 = 0$	$\frac{B_2}{a^3} + B_5 = 0$
7	Arbitrary zero deflection	$x = 0$ $\omega_2 = 0$	$\frac{B_2}{a^3} + B_6 = 0$

At position C

8	Zero curvature at free end	$x = l_2$ $\omega_1^{ii} = 0$	$\frac{B_1}{a^3}\sinh al_2 + \frac{B_2}{a}\cosh al_2 + 2B_3 = 0$
9	Zero curvature at free end	$x = l_2$ $\omega_2^{ii} = 0$	$\frac{B_1}{a^3}\sinh al_2 + \frac{B_2}{a}\cosh al_2 = 0$

From these four boundary conditions, integration constants B_1 to B_6 may be established and are as follows

$B_2 = -B_1 \tanh al_2$	$B_3 = 0$	$B_5 = B_6 = \frac{B_1}{a^3}\tanh al_2$ .....(3.27)

Continuity must be maintained at B for both slope ($\omega_1{}^{i}$ and $\omega_2{}^{i}$) and curvature ($\omega_1{}''$ and $\omega_2{}^{ii}$). Also, it should be noted that $\omega_1{}^{iii}$ and $\omega_1{}^{iv}$ in equation 3.20 should be continuous as a result of the slope and curvature compatibility. There are three boundary conditions at point B for $\omega_1{}^{i}, \omega_2{}^{i}$ and $\omega_2{}^{ii}$, noting that in the span AB x = l_1 and in span BC x = 0:

10 $\omega_1{}^{i}$	$\frac{C_1}{a^2}\cosh al_1 + \frac{C_2}{a^2}\sinh al_1 + \frac{Pl_1{}^2}{2} + 2C_3 l_1 + C_4 = \frac{B_1}{a^2} + B_4$
11 $\omega_2{}^{i}$	$C_1 \cosh al_1 + C_2 \sinh al_1 + P = B_1$
12 $\omega_1{}^{ii}$	$C_1 \sinh al_1 + C_2 \cosh al_1 + [Pl_1 + 2C_3]a = B_2 + 2B_3 a$

Equations 3.26 and 3.27 may be used for values of the constants C_1, C_3, B_2 and B_3, while boundary conditions 1_1 and 1_2 are used to find C_2 and B_1 (B_1 is not of importance here though). Substitution for the constants C_1, C_3, B_2 and B_3 and equating 3.26 and 3.27 gives:

$$C_2 = \beta_1 P \text{ .....(3.28)}$$

$$\text{where } \beta_1 = \frac{\sinh\theta + (\cosh\theta - 1)\tanh\phi}{\sinh\theta\tanh\phi + \cosh\theta} \text{ .....(3.29)}$$

$$\text{and } \theta = al_1;\ \phi = al_2$$

The integration constants C1 to C6 and B1 to B6 may now be fully established and are summarised below;

Span AB	$C_1 = -P$	$C_2 = \beta_1 P$	$C_3 = Pl_1/2$
	$C_4 = P/a^2$	$C_5 = -\beta_1 P / a^3$	$C_6 = -\beta_1 P / a^3$

Span BC	$B_1 = \alpha^2 P$	$B_2 = -\beta_2 \alpha_2 P$	$B_3 = 0$
	$B_4 = -Pl_1^2/2$	$B_5 = -\beta_2 \alpha_2 P / a^3$	$B_6 = -\beta_2 \alpha_2 P / a^3$

$$\text{Where } \beta_2 = \tanh\phi \text{ .....(3.30)}$$

Primary and secondary effects may now be superimposed to formulate the overall sandwich behaviour response. The total deflection is expressed as a function of the distance along the beam, x, in the span AB and is given by equation 3.16.

$$\omega = \omega_1 + \omega_2 \text{ .....(3.16)}$$

From equation 3.13 the core shear stress is

$$\tau = -\frac{E(I - I_f)\omega_1^{iii}}{bd} \text{ .....(3.23)}$$

and by substituting $\omega_1^{iii} = -\frac{Q_1}{EI}$ into 3.23 the overall core shear stress becomes

$$\tau = \frac{Q_1}{bd}\left[1 - \frac{I_f}{I}\right] \text{ .....(3.31)}$$

The maximum facing stress may be found by considering the ordinary bending theory of equation 3.4 and substituting the value of $M = M_1 + M_2$,

$$\frac{M}{I} = \frac{\sigma}{y} \text{.....(3.4)}$$

$$\sigma = M_1\left[\frac{c+2t}{2I}\right] + M_2\left[\frac{t}{2I_f}\right] \text{.....(3.32)}$$

The constants C1 to C6 have all been identified and are now put into equations 3.23 and 3.24

$$-Q_1 = C_1 \cosh ax + C_2 \sinh ax + P = EI\omega_1{}^{iii} \text{.....(3.23)}$$

$$EI\omega_1 = \frac{C_1}{a^3}\sinh ax + \frac{C_2}{a^3}\cosh ax + \frac{Px^3}{6} + C_3x^2 + C_4x + C_5 \text{.....(3.24)}$$

which are then each subjected to double differentiation, giving the general equations for the solutions of deflection, core shear stress and facing stress in terms of the distance x along the beam

For span AB (x measured from A)

Deflection

$$\omega = -\frac{Px^2}{6EI}(3l_1 - x)$$
$$-\frac{Px}{AG}\left(1-\frac{I_f}{I}\right)^2\left[1-\frac{1}{ax}\left(\beta_1 - [\beta_1 \cosh ax - \sinh ax]\right)\right] \text{.....(3.33)}$$

Core shear stress

$$\tau = -\frac{P}{bd}\left(1-\frac{I_f}{I}\right)[1 - \cosh ax + \beta_1 \sinh ax] \text{.....(3.34)}$$

Facing stress

$$\sigma = \left[P(l_1 - x) - \frac{Px}{ax}(\beta_1 \cosh ax - \sinh ax)\right]\frac{c+2t}{2I} + \left[\frac{Px}{ax}(\beta_1 \cosh ax - \sinh ax)\right]\frac{t}{2I_f} \quad \text{.....(3.35)}$$

For span BC (x measured from B)

Deflection

$$\omega = -\frac{Pl_1{}^2 x}{2EI} - \frac{Px}{AG}\left(1 - \frac{I_f}{I}\right)^2 \frac{\alpha_2}{ax}(\beta_2 - [\beta_2 \cosh ax - \sinh ax]) \quad \text{.....(3.36)}$$

Core shear stress

$$\tau = -\frac{P}{bd}\left(1 - \frac{I_f}{I}\right)\alpha_2[\cosh ax + \beta_2 \sinh ax] \quad \text{.....(3.37)}$$

Facing stress

$$\sigma = -\left[Px\frac{\alpha_2}{ax}(\beta_2 \cosh ax - \sinh ax)\right]\frac{c+2t}{2I} + \left[Px\frac{\alpha_2}{ax}(\beta_2 \cosh ax - \sinh ax)\right]\frac{t}{2I_f} \quad \text{.....(3.38)}$$

3.4 Finite element methods

3.4.1 Introduction

Finite element analysis has seen a vast increase in interest for the solution of complex engineering problems, particularly where geometric and material properties do not lend themselves well to ordinary theory. Finite element modelling allows the engineer or designer to define a structural problem with many variables quickly and thus through an iterative process of analysis, formulate the most appropriate solution.

In this project finite element analysis (F.E.A.) is used to investigate the relationships between force / displacement and stress / strain for any given structure. F.E.A. has been applied to three distinct areas of analytical work. Firstly, as an aid to quantifying test errors in the uniaxial compression tests and the shear tests. Secondly, to justify its use as an analytical modelling tool for sandwich constructions by comparison with existing theory and experimental data Thirdly, to advance the understanding of the structural behaviour and interactions of a foam injected masonry cavity wall.

This section describes the fundamental theory of finite element methods, its applicability, and general modelling techniques. Specific modelling techniques have been described where there is an application of the method throughout the project. The description in this text is general and is applicable to most types of finite element theory although it is heavily biased towards this project's requirements.

Three separate finite element programs have been used in this project, LUSAS (1991) and ABAQUS (1995) both commercially available software packages and SC01/3 (1997), an in-house programme developed by Rolls-Royce Plc. The programs differ, LUSAS and ABAQUS are totally dependant on user specification for mesh generation and element type, whereas SC01/3 uses an automatic meshing system and specific associated element types. The post processing facilities of SC01/3 have been used to present results from ABAQUS analyses.

3.4.2 Basic finite element modelling concepts

The basic principle of finite element modelling is to divide a whole structural body into small discrete regions, called finite elements. The elements have nodes at corners and along sides which are common to adjacent elements. The nodes are given user defined interaction properties that dictate the overall structural behaviour. These interaction properties are in the form of nodal freedoms. Typically, each node has four degrees of freedom for a two dimensional problem and six degrees of freedom for three dimensions. The associated freedoms being two or three translational and two or three rotational degrees of freedom as appropriate. Figure 3.8 shows basic F.E.A. modelling concepts: 3.8a represents a three dimensional element with eight corner nodes, each having the freedoms shown by the arrows in 3.8b (translation in the x-, y- and z-directions and rotation about the x-, y- and z-axes). Figure 3.8c and 3.8d show how the whole structure is built up of elements, each layer (or region) may then have specified properties attributed to it.

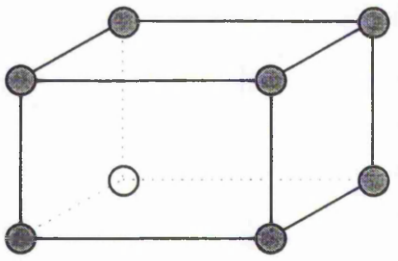

a. Typical 8-noded element

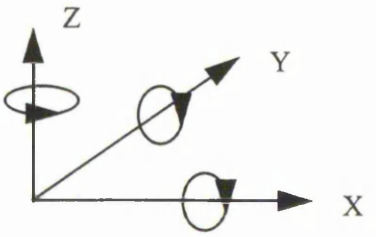

b. The six degrees of freedom possible at each node

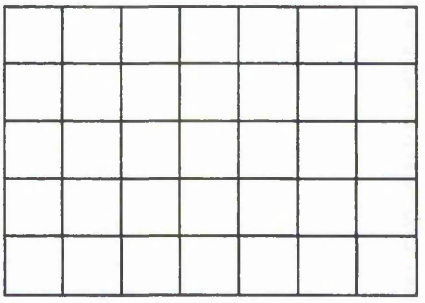

c. A 'mesh' built up from elements

d. Element layers describing different materials

Figure 3.8 Finite element concepts

When a force is applied to a body, static analysis assumes that a state of stress is developed and static equilibrium exists. The general equation (3.39) for this is:

$$[K]\{a\} = \{f\} \quad \text{.....(3.39)}$$

where $[K]$ is the stiffness matrix, $\{a\}$ is the nodal displacement vector and $\{f\}$ is the nodal load vector.

The overall stiffness matrix $[K]$ is generated by considering the equilibrium of internal and external virtual work. The external virtual work done of applying a unit displacement to nodes is equated to the sum of the internal work done of the stress / strain behaviour over the whole volume of each element. The stiffness matrix for a specific element is formed from two matrices: $[D]$, an elastic modulus matrix and $[B]$, a strain-displacement matrix. The stiffness matrix computation involves integration over the elemental volume

$$\left[K^e\right] = \int_{vol} \varepsilon^T \sigma = \int_{vol} \left[B^e\right]^T \left[D^e\right]\left[B^e\right] dV \quad \text{.....(3.40)}$$

where $\left[K^e\right]$ is the stiffness matrix of element "e" in the global co-ordinate system. Elastic constants dictate the stress / strain relationship for the elemental response

$$\{\sigma\} = [D]\{\varepsilon\} = [D][B]\{d\} \quad \text{..... (3.41)}$$

where $\{d\}$ is the elemental displacement vector.

The exact integration of the element stiffness is then replaced with an approximate numerical integration, for this instance, Gaussian, which uses a summation over the specified sampling positions. The approximate integration now becomes

$$k^e \approx \sum_{i=1}^{n} B^{eT} D^e B^e \quad \text{.....(3.42)}$$

The finite element method's discrete nature of element assemblage means that all solutions are an approximation of structural response. Thus to confirm that the model is appropriate to the structural problem it is usual to conduct a series of experimental investigations. The accuracy of each model is then improved through a convergence study. Usually an initially coarse element mesh is described, then the mesh is refined using more elements up to a point where a described physical response (e.g. a displacement) no longer changes significantly. The mesh may be refined more in certain areas of changing stress or high stress concentrations and left coarse where stresses are constant.

3.4.3 Procedure of finite element modelling

The analysis of a structure using finite element theory may be described by a number of steps. It is first necessary to divide the complete body into finite elements, which may be referred to as the discretization of the domain, then an interpolation model must be formed to approximate the behaviour of each individual element. The elements used in the analysis then require their specific matrices and vectors to be formulated so that the full assemblage of the elemental properties can be made. Finally, the solution of the overall assemblage is made and the computation of the elemental results outputted.

3.4.3.1 Discretization of the domain

The division of a domain or body into smaller regions or elements simulating the overall structure is usually user defined. In practice a structure has an infinite number of degrees of freedom, however the user chooses an appropriately small and manageable number to simulate the overall behaviour. The discretization process involves a number of steps, selection of the type of element, size and number of elements, choice of modelling in two or three dimensions, node numbering, mesh generation. The accuracy of the model is partly driven by the discretization of the domain and the user should define the mesh accordingly. Appropriate meshing of a domain has been discussed in

more detail later. Alternatively, an automatic node numbering and mesh generation system may be employed.

3.4.3.2 Interpolation model

The interpolation model is an approximate function of the solution of the nodal interactions between the finite elements in a complete structure. LUSAS, ABAQUS and SC01/3 finite element programs use a polynomial function to represent the behaviour of the solution.

(i) Polynomial displacement function. The displacement of any point within an element may be described by a typical polynomial in the form

$$u = c_1 + c_2x + c_3y + c_4xy + c_5x^2 + c_6y^2 + c_7x^2y + c_8xy^2 + c_9x^2y^2 \ldots\ldots\ldots (3.43)$$

Polynomial functions are used in preference to, say, trigonometrical functions for two reasons. Primarily, the necessary integration and differentiation is easier to perform with polynomials and secondarily, the accuracy of the solution may be enhanced by increasing the order of the polynomial. Figure 3.9 shows how the increase in the order of the polynomial interpolation model improves the accuracy of the solution for a given field variable (displacement u) in one dimension (x).

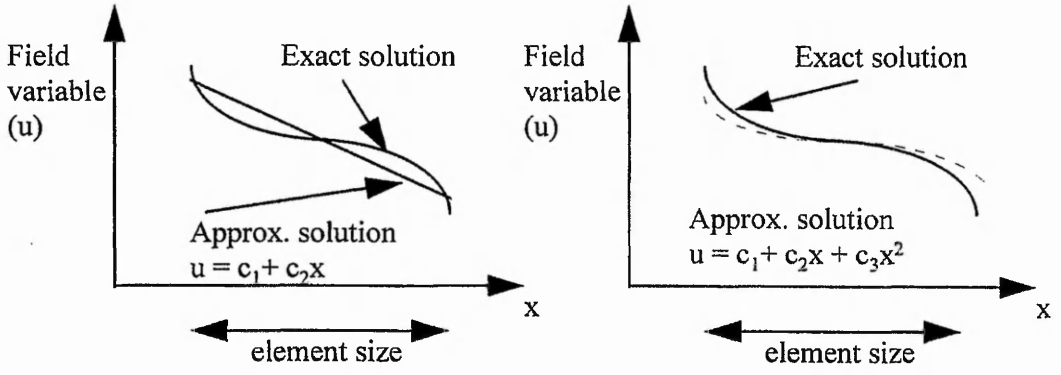

a. Linear approximation b. Quadratic approximation

Figure 3.9 Accuracy of the interpolation polynomial

Strains may be determined directly from displacements and the known original geometry. For a 2-dimensional case

$$\begin{bmatrix} \varepsilon x \\ \varepsilon y \\ \gamma xy \end{bmatrix} = \begin{bmatrix} \partial / \partial x & 0 \\ 0 & \partial / \partial y \\ \partial / \partial y & \partial / \partial x \end{bmatrix} \left\{ \frac{u}{v} \right\} \text{.....(3.44)}$$

Stresses may be related to associated strains by constitutive relationships in terms of elastic modulii and Poisson's ratio. The user may define therefore the stress / strain relationship for any given material given that;

$$\{\sigma\} = [D][\varepsilon] = [D][B]\{d\} \text{ ..... (3.41)}$$

The stress transformation matrix $[D]$ may be inputted for plane stress, plane strain, anisotropic or orthotropic material conditions. To increase the accuracy of the model it is more prudent to increase the order of the element and generally the number of nodes per element should be increased. For a four noded element only the four first terms of the polynomial are used and for an eight noded element the first eight terms are used and so on.

(ii) Local co-ordinate system. As elements may vary in shape and size a local co-ordinate system is used to define elemental response for a basic element within the range -1 to +1. The local co-ordinate system may then be mapped onto a Cartesian system by a transformation matrix. A natural local co-ordinate system is defined, for two and three dimensions, to assist in the isoparametric formulation. Figure 3.10 shows the two dimensional condition;

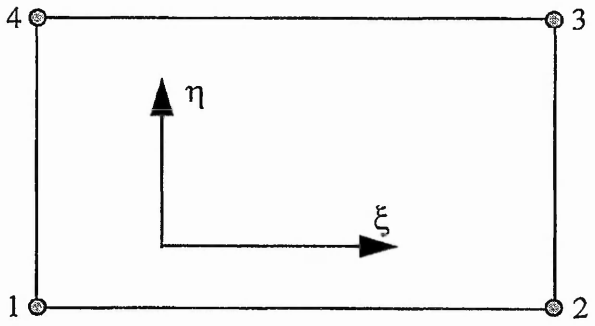

Figure 3.10 Local co-ordinate system for a two dimensional element

The element geometry is then defined as

$$X(\xi,\eta) = N(\xi,\eta)X \text{ ..... (3.45)}$$

$$Y(\xi,\eta) = N(\xi,\eta)Y \text{ ..... (3.46)}$$

and the elemental displacements

$$U(\xi,\eta) = N(\xi,\eta)U \text{ .....(3.47)}$$

$$V(\xi,\eta) = N(\xi,\eta)V \text{ .....(3.48)}$$

where X and Y are nodal co-ordinates, U and V are nodal displacements and N is the elemental shape function.

(iii) Shape function. A 'shape' function matrix $[N]$ contains a set of polynomial displacement functions which are of the appropriate order for the required solution. The elemental formulation may then be expressed, for elemental displacements, in terms of nodal displacements for the local co-ordinate system. The shape functions are required to satisfy two conditions;

$$\sum_{i=1}^{n} N_i(\xi,\eta) = 1 \text{ ..... (3.49)}$$

and

$$N_i(\xi_j,\eta_j) = \begin{Bmatrix} 1 & \text{if} & i=j \\ 0 & \text{if} & i\neq j \end{Bmatrix} \text{ ..... (3.50)}$$

The shape functions for the four noded element above are then derived from the one dimensional shape function in the ξ and η local directions. Nodes 1 to 4 may then be described as follows:

$$N_1 = \frac{1}{4}(1-\xi)(1-\eta)$$

$$N_2 = \frac{1}{4}(1+\xi)(1-\eta)$$

$$N_3 = \frac{1}{4}(1+\xi)(1+\eta) \qquad \text{..... (3.51)}$$

$$N_4 = \frac{1}{4}(1-\xi)(1+\eta)$$

(iv) Global Cartesian co-ordinates. The local co-ordinate system must then be transferred to the global Cartesian system for the determination of the strain matrix. The chain rule of partial differentiation must then be employed to convert the derivatives from one system to the other;

$$\begin{bmatrix} \partial N/\partial X \\ \partial N/\partial Y \end{bmatrix} = \begin{bmatrix} \partial \xi/\partial X & \partial \eta/\partial X \\ \partial \xi/\partial Y & \partial \eta/\partial Y \end{bmatrix} \begin{bmatrix} \partial N/\partial \xi \\ \partial N/\partial \eta \end{bmatrix} \qquad \text{.....(3.52)}$$

The terms in the first set of brackets on the right hand side of the equation are then evaluated by calculating the Jacobean matrix $\underline{\underline{J}}$

$$\underline{\underline{J}} = \begin{bmatrix} \partial X/\partial \xi & \partial Y/\partial \xi \\ \partial X/\partial \eta & \partial Y/\partial \eta \end{bmatrix} = \begin{bmatrix} (\partial N/\partial \xi)\underline{U} & (\partial N/\partial \xi)\underline{V} \\ (\partial N/\partial \eta)\underline{U} & (\partial N/\partial \eta)\underline{V} \end{bmatrix} \qquad \text{..... (3.53)}$$

and then the inverse of $\underline{\underline{J}}$, $\underline{\underline{J}}^{-1}$

$$\underline{\underline{J}}^{-1} = \begin{bmatrix} \partial \xi/\partial X & \partial \eta/\partial X \\ \partial \xi/\partial Y & \partial \eta/\partial Y \end{bmatrix}$$

The geometric data of nodal positions and the order of the generation of elements in the mesh is highly critical when considering the Jacobean matrix. Where elements may be very distorted, the Jacobean matrix can become singular.

(v) Numerical integration. All three finite element programs use the Gauss-Legrande numerical integration as below;

$$I = \int_{-1}^{+1}\int_{-1}^{+1} F(\xi,\eta)d\xi d\eta \approx \sum_{i=1}^{n}\sum_{j=1}^{n} W_i W_j F(\xi_i,\eta_j) \ldots\ldots\ldots (3.54)$$

Where Wi and Wj are the weighted functions describing the locations of the 'Gauss' points. The Gauss points are located to provide the best possible sampling of stresses within an element. $F(\xi_i,\eta_j)$ is the value of the function at location (ξ_i,η_j) and n is the order of the quadrature rule.

3.4.3.3 Assemblage of elemental matrices and vectors for the overall assemblage

When the element characteristics, matrices, and vectors have been established in terms of a global co-ordinate system the overall assemblage of system equations is made. This process is the same for any finite element analysis of any structural problem using any type of element or density of mesh.

Assemblage of the element matrices and vectors is based on the requirement of compatibility between adjacent elements with common nodes. At these nodes the values of the unknown nodal degrees of freedom, usually displacements, are the same for all the elements joining at that node. Thus for structural problems the generalised displacements are matched at common nodes with the nodal stiffnesses and loads of each joining element being added together to give overall stiffness and total nodal load.

For a typical three dimensional isoparametric eight noded, solid continuum element, as shown in Figure 3.11c, the displacements at each node may be given by

$$\underline{U} = \begin{bmatrix} U \\ V \\ W \end{bmatrix} \quad \text{..... (3.55)}$$

and the associated stress and strain vectors

$$\underline{\sigma} = \left[\sigma_x, \sigma_y, \sigma_z, \tau_{xy}, \tau_{yz}, \tau_{xz}\right]^T \quad \text{..... (3.56)}$$

$$\underline{\varepsilon} = \left[\varepsilon_x, \varepsilon_y, \varepsilon_z, \gamma_{xy}, \gamma_{yz}, \gamma_{xz}\right]^T \quad \text{..... (3.57)}$$

with the strain displacement relationship expressed as

$$\begin{bmatrix} \varepsilon x \\ \varepsilon y \\ \varepsilon z \\ \gamma xy \\ \gamma yz \\ \gamma zx \end{bmatrix} = \begin{bmatrix} \partial U / \partial X \\ \partial V / \partial Y \\ \partial W / \partial Z \\ \partial U / \partial Y + \partial V / \partial X \\ \partial V / \partial Z + \partial W / \partial Y \\ \partial W / \partial Z + \partial W / \partial X \end{bmatrix} \quad \text{..... (3.58)}$$

From the constitutive relationship for a three dimensional elastic isotropic solid,

$$\{\sigma\} = [D]\{\varepsilon\} \quad \text{..... (3.41)}$$

$$[D] = \left(\frac{E}{(1-2\upsilon)(1+\upsilon)}\right)\begin{bmatrix} 1-\upsilon & \upsilon & \upsilon & 0 & 0 & 0 \\ \upsilon & 1-\upsilon & \upsilon & 0 & 0 & 0 \\ \upsilon & \upsilon & 1-\upsilon & 0 & 0 & 0 \\ 0 & 0 & 0 & 1/(2-\upsilon) & 0 & 0 \\ 0 & 0 & 0 & 0 & 1/(2-\upsilon) & 0 \\ 0 & 0 & 0 & 0 & 0 & 1/(2-\upsilon) \end{bmatrix} \quad \text{.....}$$

(3.59)

3.4.3.4 Solution of the overall elemental assemblage for nodal values

The finite element method generates a system of matrix equations for the solution to any given structural problem. Solutions may be either linear or non-linear. Non-linear analysis may be for either material properties, where the material changes its stress-strain relationship, or structural requirements if for instance there are large deflections.

(i) Linear analysis

There are two methods for solving linear finite element analysis, direct or iterative processes. The direct method will give an exact solution for the finite element calculations although, when using computer generated solutions, will be subject to round-off errors. The direct method uses Gaussian elimination to solve equations. Alternatively, the iterative process starts with an approximate answer and refines, through a series of iterative step functions, the solution. Additionally, linear analysis systems are classified as either sparse or dense. That is to say that the matrices have relatively high or low numbers of non-zero components. The matrices generated in the applications in this project are sparsely populated and symmetrical about the leading diagonal and are thus well suited to Gaussian elimination.

The solution of equilibrium problems for linear analysis is performed using the Gaussian elimination routine for ABAQUS, LUSAS and SC01/03 F.E.A. programs.

Considering a set of equations (3.60) for the solution of a problem that has boundary conditions (supports and loads in the forms of nodal degrees of freedom) already incorporated into them;

$$
\begin{aligned}
&a_{11}x_1 + a_{12}x_2 + \ldots + a_{1n}x_n = b_1 \\
&a_{21}x_1 + a_{22}x_2 + \ldots + a_{2n}x_n = b_2 \\
&\cdot \qquad\qquad\qquad\qquad\qquad\qquad\qquad\qquad \ldots\ldots\ldots (3.60) \\
&\cdot \\
&.a_{n1}x_1 + a_{n2}x_2 + \ldots + a_{nn}x_n = b_n
\end{aligned}
$$

then the matrix notation will be for

$$[K]\{a\} = \{f\} \quad \text{.....(3.39)}$$

where $[K] = \begin{bmatrix} a_{11} & a_{12} & \cdots & a_{1n} \\ a_{21} & a_{22} & \cdots & a_{2n} \\ . & & & \\ . & & & \\ a_{n1} & a_{n2} & \cdots & a_{nn} \end{bmatrix}$, $\{a\} = \begin{bmatrix} x_1 \\ x_2 \\ . \\ . \\ x_n \end{bmatrix}$, $\{f\} = \begin{bmatrix} b_1 \\ b_2 \\ . \\ . \\ b_n \end{bmatrix}$

Gaussian elimination seeks to reduce the equation system to the following triangular form;

$$a'_{11}x_1 + a'_{12}x_2 + a'_{13}x_3 + \ldots a_{1,n-1}x_{n-1} + a'_{1n}x_n = b'_1$$
$$a'_{22}x_2 + a'_{23}x_3 + \ldots + a_{1,n-1}x_{n-1} + a'_{2n}x_n = b'_2$$
$$\vdots$$
$$a'_{1,n-1}x_{n-1} + a'_{2n}x_n = b'_{n-1}$$
$$a'_{2n}x_n = b'_n$$

The primes denote that the stiffness coefficients are not the original values and have been altered during the elimination process. The unknowns are then systematically found in reverse order as each equation introduces only one new unknown when moving up the page.

(ii) Non-linear analysis

Non-linear analysis is conducted in this project for the solution to the flexural behaviour of panels and beams where there is significant mid-span deflection causing the need for geometric re-analysis somewhere in the solution.

In this case the system of matrix equations may be solved by a number of methods, Newton-Raphson, continuation, minimisation and perturbation. LUSAS, ABAQUS and SC01/03 finite element programs use the Newton-Raphson method.

In non-linear analysis it is not possible to directly obtain internal stresses that are in equilibrium with the applied loads. The change of stiffness due to the geometric changes result in an out of balance vector. The Newton-Raphson method of solution uses an incremental-iterative step function. Incremental steps are taken and within each step there are iterative corrections as seen below in Figure 3.11;

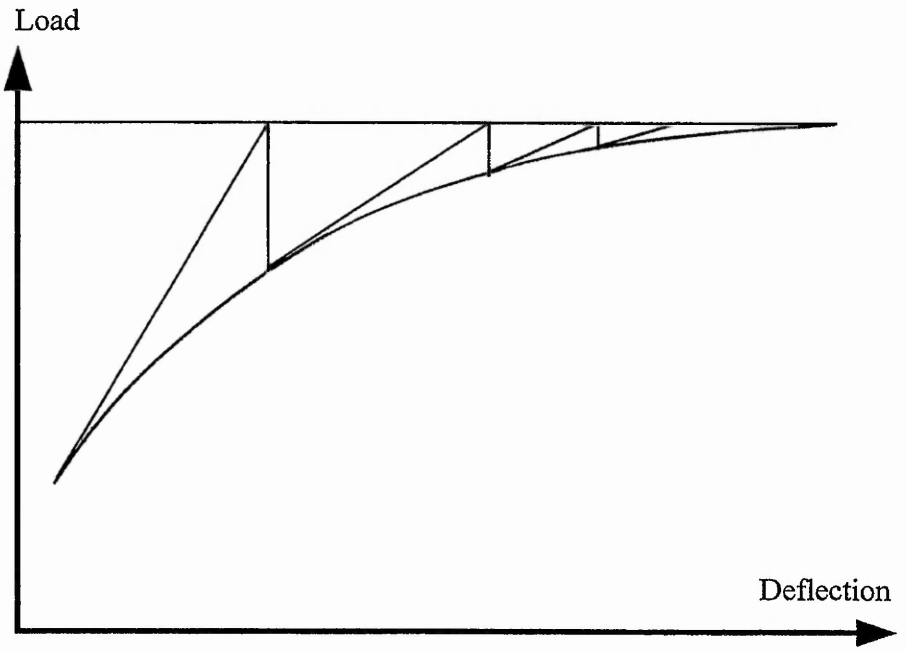

Figure 3.11 Standard Newton-Raphson incremental-iterative method for non-linear analysis.

Convergence criteria for the non-linear analysis is used to determine when a new load increment is to be applied.

3.4.4 Modelling considerations

3.4.4.1 Discretization of the structural entity

Type of element. There are five basic shapes that may be used, a one dimensional beam element, two dimensional triangular and quadrahedral and three dimensional tetrahedral and cubic. Figure 3.11 shows the typical elements available. As shown the elements have the minimum requirement of nodes. Additionally, all types of element may have a node placed at the centre point along each side or edge.

a. One dimensional beam element

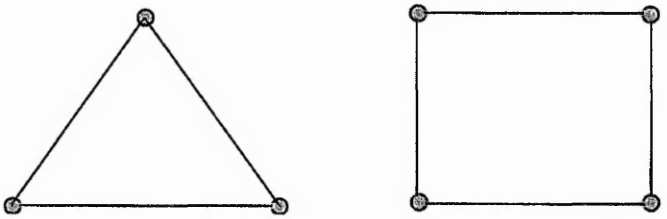

b. Two dimensional triangular and quadrilateral elements

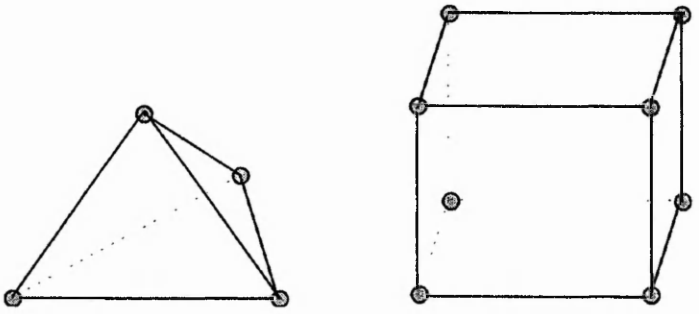

c. Three dimensional tetrahedral and cubic elements

Figure 3.11 Typical elements used in finite element modelling

The choice of element is usually dictated by the geometry of the body being modelled and the requirement to keep the original element shape as regular as possible. Regular square or near square cornered structures lend themselves to the parallelogram or cubic elements while irregular or curved shapes are best modelled with the triangular or tetrahedral elements. The parallelogram or cubic elements can geometrically fit into most spaces although this may cause large distortions within the element.

Size and number of elements. The size and therefore the number of elements used has a direct bearing on the model accuracy. In addition, the number of nodes each element has an influence on accuracy. Appreciation of structural behaviour, particularly intuitive judgement of locations where there may be stress gradients, can dictate the use of high or low density concentration of elements. Areas of limited stress gradient, whether they are in a high or low stress field, may be modelled with a coarse elemental mesh as the difference in the interaction between each node is constant. Elements are most efficient when their aspect ratio is 1:1:1 although in general aspect ratios should not exceed 20:1 in any direction and where there is a high stress gradient ratios should not exceed 3:1.

The density of an elemental mesh does not have a linear relationship to the accuracy and the time taken for the computation. For confidence in model accuracy, it is common to conduct a convergency study. Where an initially coarse mesh is first prescribed an outputted structural deflection or stress should be plotted against either element or node numbers. Subsequently, additional elements should be added to the model and the selected structural behaviour plotted against the new element or node density. This routine is continued until an appropriate accuracy is found. If a comparison to a laboratory measured deflection is made then the accuracy required would be that recorded in the practical situation. A typical convergence study plot is shown on figure 3.12.

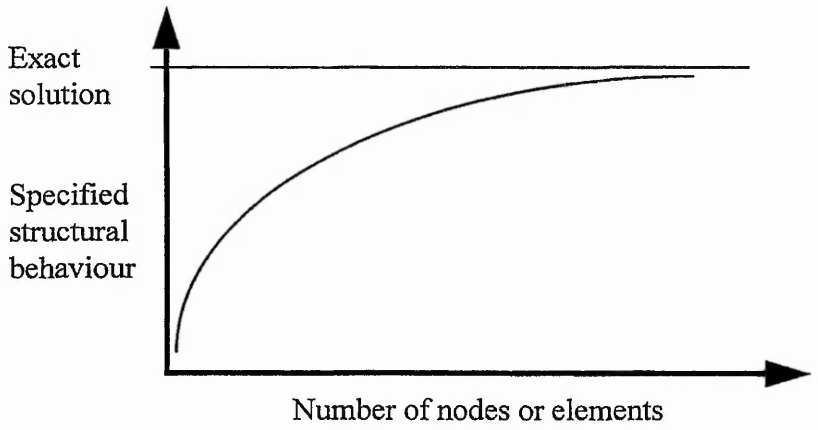

Figure 3.12 Convergence to an exact solution

The iterative process of increasing model accuracy it is more beneficial when placing any additional elements at locations of markedly changing stress fields. It should also be borne in mind that although an increase in the number of elements or nodes increases the accuracy of the finite element model the time taken to process the nodal interactions increases significantly. Figure 3.13 shows the general trend of the number of nodes or elements in a mesh against the computer processing time.

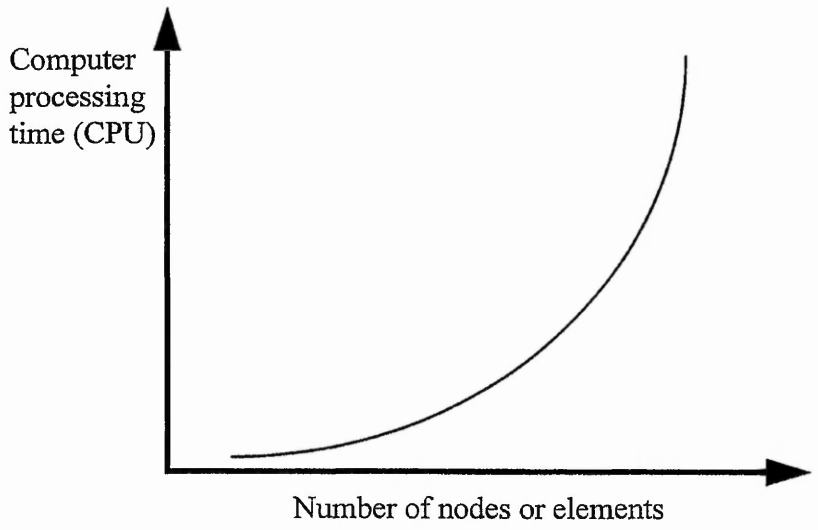

Figure 3.13 Density versus computer processing time

A satisfactory element mesh density should be related to the required accuracy of the structural component in terms of stipulated design tolerances or the degree to which its structural behaviour can be measured to. The computer processing time taken and amount of computer storage space required is also an important modelling criterion. In some cases an additional 1% increase in model accuracy could involve a disproportionate (say >10%) increase in run time and volume of computer storage space for data output.

Modelling in two or three dimensions. The selection of a two or three dimensional model should be made by considering the through depth or thickness of the simulated structure. Long, continuous bodies that contain little or no significant stress fields in one direction may use two dimensional analysis. Figure 3.14 shows how two dimensional models may represent a three dimensional structure. Irregular bodies or those subject to more than one load condition or unsymmetrical support conditions should use three dimensional analysis. Furthermore, material behaviour has a significant input for choosing two or three dimensional analysis. Orthotropic and anisotropic materials in a regular three dimensional body affect how the structure responds.

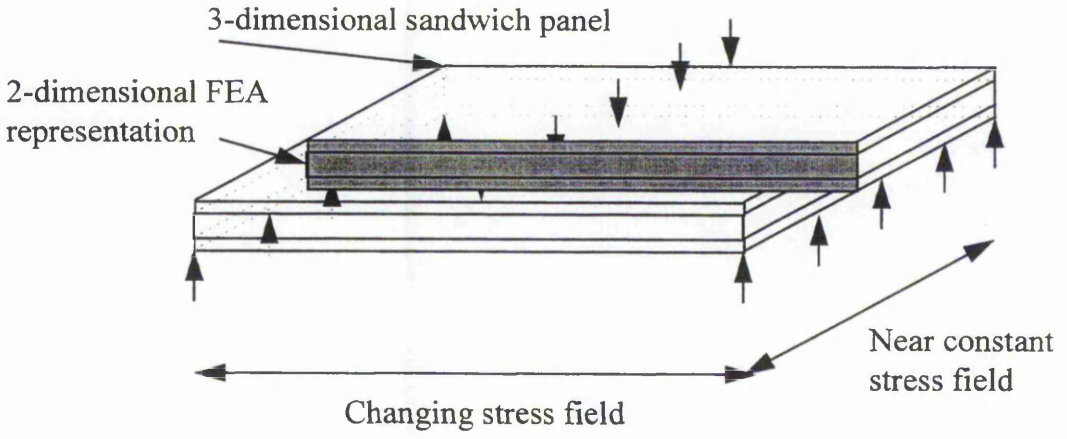

Figure 3.14 Two dimensional representation of a three dimensional body.

Where modelling of three dimensional structures is valid in two dimensions, it is assumed that there is zero strain, or effectively no strain, in the direction normal to the

sectioned plane. In this situation, the two dimensional model is defined as a plane strain condition. In Figure 3.14 the amount of lateral (y-direction) strain actually present is sufficiently small, when considering the total width, to allow a valid two dimensional plane strain approximation to be made.

Reduction of problem size using symmetry. A symmetrical structure may be reduced in size by one half, a quarter or an eighth when considering one, two and three dimensional models respectively. Using symmetry enables a smaller solution to be formulated which then requires less computer storage space and less data manipulation. Figure 3.15 shows how a simple two dimensional plate with a hole may be reduced to a one quarter sized model by using appropriately specified boundary edge conditions. For symmetry to be valid in this case the edge B-C is restrained in the x-direction for displacement while the edge D-E is restrained in the y-direction. If a three dimensional plate was analysed then the edge conditions described above would have additional rotational restraints along edge B-C and D-E.

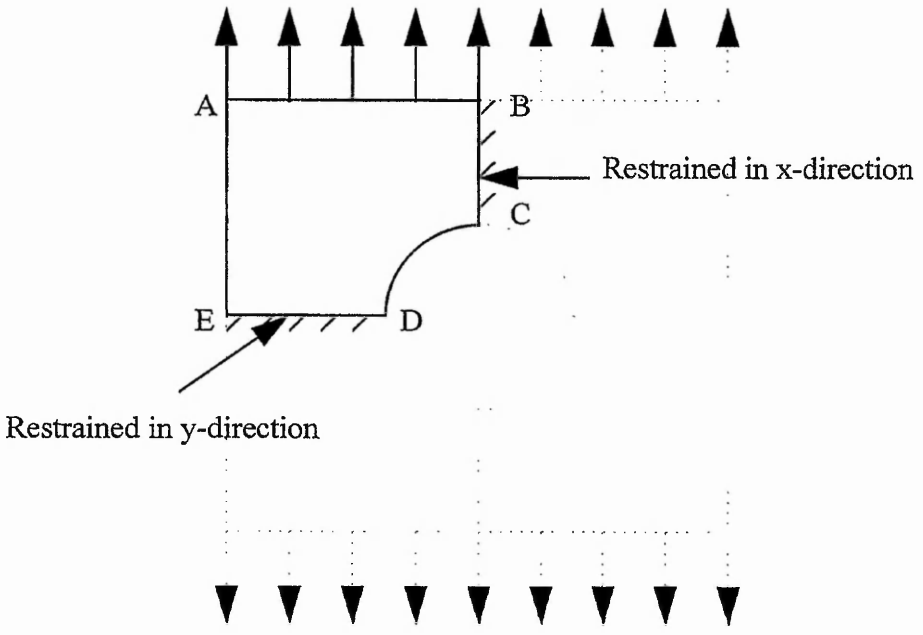

Figure 3.15 Reduction of problem using symmetry

Node numbering and mesh generation. Accuracy, for a given number of nodes or elements, of a structural problem may be enhanced by an appreciation of how the solution matrices are formed. As will be described in more detail later, the matrices are usually symmetrically banded so that the solution size may be reduced when utilising the adjacent diagonals to the leading diagonal. The solution therefore may then be described as using a 'half band width'. It is important to minimise the half band width size in the stiffness matrix so that the overall matrix does not become to expansive. This may be achieved in two ways, firstly by altering the sequence of node numbering and secondly by reducing the number of degrees of freedom per node, however this is not always appropriate.

Figure 3.16 comprises a. and b. which have identically sized meshes and elements, but each has a different node numbering system. For these two dimensional models there are three degrees of freedom for each node. If node number 1, in both cases, is given a unit displacement, then the adjacent nodes are directly influenced. This leads to the first row of the global stiffness matrix having 21 non-zero numbers for case a and 12 for case b. The bandwidths, B, in the stiffness matrix can then be equated

$$B = (N_N + 1).N_F \quad .....(3.42)$$

for case a $B = (21 + 1).3 = 66$

for case b $B = (12 + 1).3 = 39$

Where N_N is the number of nodes along sequentially numbered edge and N_F is the number of degrees of freedom. Thus for any given problem a smaller bandwidth will be more economic in terms of CPU time thus also allowing a greater number of elements to be used if a higher accuracy is required.

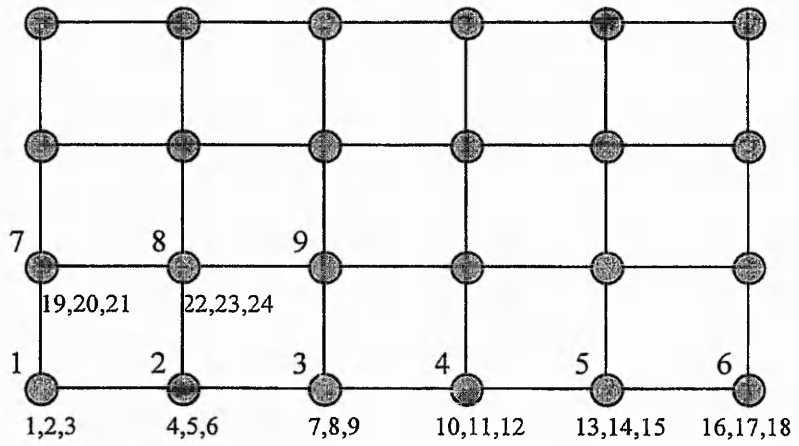

a. Node numbering along longest edge

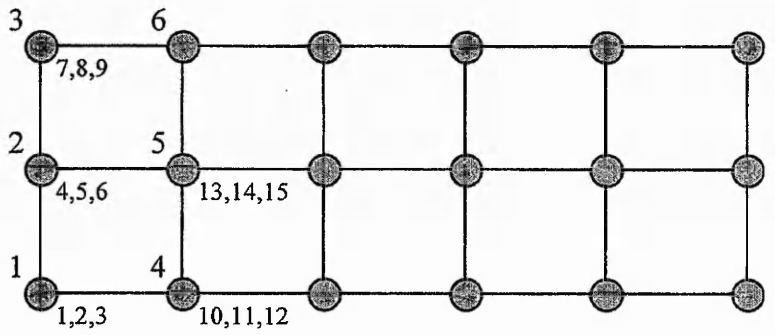

b. Node numbering along shortest edge

Figure 3.16 Node numbering systems to reduce bandwidth

Automatic node numbering and mesh generation. The finite element program SC01/3 has an automatic mesh generation system. The program has been developed for use with complex two and three dimensional structures and predominantly uses triangular and tetrahedral elements. Initially the program will select a node numbering system for a first approximation and then refine, by iterative steps, both the elemental mesh density and the node numbering order to produce the optimum overall solution to a predetermined solution accuracy. The solution accuracy is, however, governed by the user.

3.4.4.2 Solution of equations

The 'frontal solution method' has been used in all finite element analysis. The frontal solution method is a specific type of Gaussian reduction/elimination. The upper triangle of the global stiffness matrix is not used for the full Gaussian reduction method. This method assembles equations and eliminates the unknowns through substitution simultaneously. The 'front' contains only the equations currently being manipulated. The number of unknowns in the front, or frontwidth, limits the size and accuracy of the solution. However, the frontwidth may be optimised to reduce computer processing time and storage space, as described earlier.

Ill conditioning and round-off errors may occur where there is a pre-defined number of digits used for any individual number. For example,

Case 1, three significant figures

$$\begin{bmatrix} 10E-4 & 1 \\ 1 & -10E4 \end{bmatrix}\begin{bmatrix} A \\ B \end{bmatrix}=\begin{bmatrix} 1 \\ -10E4 \end{bmatrix} \therefore \begin{matrix} A=0 \\ B=1 \end{matrix}$$

Case 2, five significant figures

$$\begin{bmatrix} 10E-4 & 1 \\ 1 & -9999 \end{bmatrix}\begin{bmatrix} A \\ B \end{bmatrix}=\begin{bmatrix} 1 \\ -10E4 \end{bmatrix} \therefore \begin{matrix} A=-1.0 \\ B=1.001 \end{matrix}$$

It can thus be seen that case 1 does not provide the correct answer with particular respect to the solution of A, however, case 2 does.

Diagonal decay may occur during the reduction process which will corrupt the calculated displacements, stresses and strains. Diagonal decay is a measure of round-off that is related to the stiffness matrix.

3.4.4.3 Use of elements

Certain points have been carefully considered when selecting and using elements in order to maximise their implementation.

Node ordering is consistent and at all times taken in the anticlockwise direction.

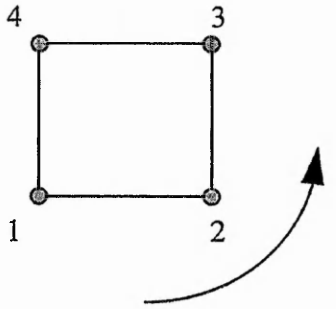

The aspect ratio A : B does not exceed 1:3 in areas of high stress and 1:20 in all other areas.

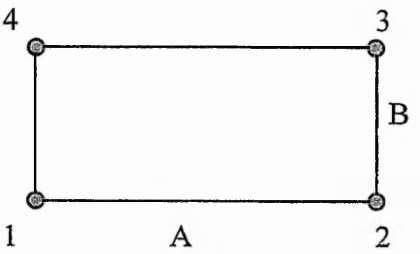

Elemental distortion has been kept to a minimum for all situations.

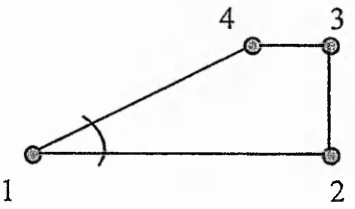

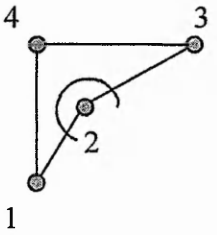

Mid-side nodes for both 2- and 3-dimensional elements as well as triangular and square elements are central and excessive curvature restricted

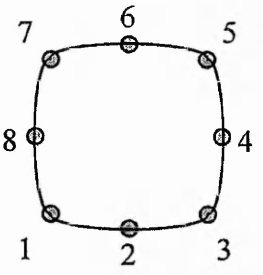

All adjacent elements are compatible and reasonably proportioned i.e. large and small elements are not sharing the same node points.

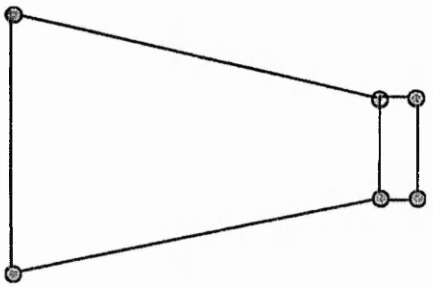

Figure 3.17 Element topology and ordering

3.4.4.4 Applied loading

Loading applied to bodies when using the LUSAS finite element package have been attributed to the nodal points. Loads applied using SC01/3 are attributed to faces and automatically distributed proportionally to nodes. Whether manually or automatically, applied loads are distributed as shown below, thus a uniform distribution is maintained.

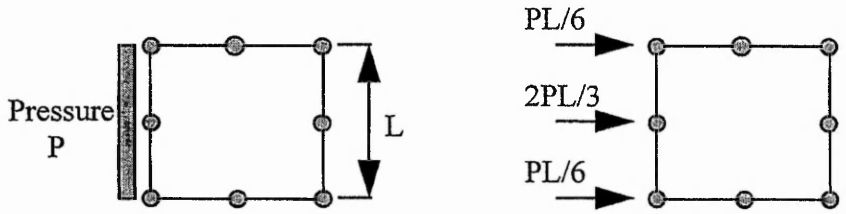

Figure 3.18 Uniform loading of nodes on a face

3.4.4.5 Symmetry conditions

Symmetry conditions have been used widely throughout this project with particular attention to mimicking the structure's behaviour correctly using appropriate boundary conditions. For instance, figure of the panel below shows how symmetry can reduce the problem size by one quarter.

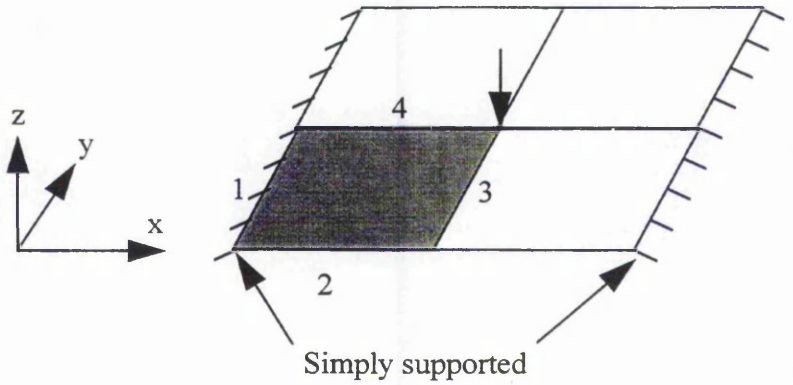

Figure 3.19 Use of symmetry and boundary conditions to reduce problem size

The nodes along the sides 1 to 4 have certain restrictions and freedoms associated to them which will allow correct model simulation of that quarter in the actual as follows.

Edge nodal freedoms

	x	y	z	θx	θy	θz
1	F	F	R	F	F	F
2	F	F	F	F	F	F
3	R	F	F	F	R	F
4	F	R	F	R	F	F

Where R = restrained and F = free.

3.4.4.6 Post processing

Displacement of nodes are accurate relative to stresses even with a coarse mesh. A displacement plot has been used as a first check for most structures as incorrect modelling considerations such as boundary conditions become easily apparent. For stresses, optimal sampling locations are based on the type of isoparametric formulations specified. For example the 2-dimensional elements shown in figure below will have different Gaussian sampling positions, which are dependent on their isoparametric formulations.

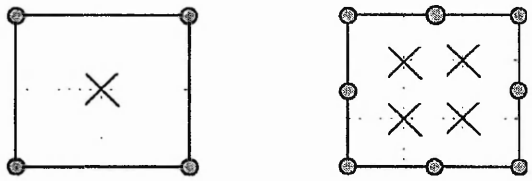

Figure 3.20 Gaussian sampling locations within different element orders

3.4.5 Verification of F.E.A. solutions with laboratory data

Computer generated finite element analysis has been used throughout this project for a number of different applications. In chapters 4 and 5, F.E.A. has been used to aid in the evaluation of correct material properties. The uniaxial and shear test methods induce experimental errors due to the configuration of the apparatus. Finite element modelling has identified these errors by simulating the actual test configurations, duplicating the test errors and then comparing the theoretical property values to the apparent values from the computer simulated test.

The F.E.A. results have been verified by two means. Initially the theoretical accuracy for each different model has been investigated with a convergence study. The convergence study, as described earlier, refines the elemental mesh (increasing both element and node numbers) until a pre-defined structural response converges. The model has then been configured to produce a theoretically perfect result, excluding test error. For instance, uniaxial compression tests are subject to the effects of having fixed edges (the facings are still attached). A uniaxial test is first modelled by allowing free and frictionless displacement at the contact surfaces with the loading platens of the compression machine. Having established that this model produces ideal results, the model is then amended to the actual test configuration by simply considering certain boundary conditions.

3.5 Discussion

3.5.1 General

This chapter has presented a theoretical background to the Allen solutions and finite element concepts for modelling the displacements and facing stresses throughout the span of sandwich constructions. Both theoretical solutions have been compared to experimental results in chapter 7. The finite element method has also been used for the analysis of the material testing methods to aid in correct material property evaluation. Further applications of the finite element method are made for predictive analysis of the wallettes and cavity walls. O'Connor (1985) has previously examined in detail the Allen analysis and has presented conclusions that are also relevant to this study. Similarly, the conclusions of O'Connor's finite element modelling of sandwich beams are summarised. This summary is therefore more wide ranging than the can be inferred from just the information described in this chapter.

3.5.2 Application of Allen's theory to multiple span beam testing

Chapter 6 presents in detail an alternative approach to evaluating the shear modulus of the core of sandwich beams from the shear testing of coupons in chapter 5. By testing the same beam at a series of different spans and graphically representing the load / displacement response, the gradient of the curve may then be found and used in an adaptation of Allen's theory to find the shear modulus of the core. Originally the multiple span beam testing method used the mid-span deflection of the three point loaded sandwich beam. In O'Connor's investigation of Allen's thick faced sandwich beam theory it was found that the central point load caused local bending of the loaded face. This local distortion was found to dissipate a certain distance away from the point load. O'Connor argued that the multiple span beam testing technique could be improved upon by considering measuring displacements at two points in the span of the beam that were not subject to the local bending of the loaded facing. O'Connor describes this revised method as the "conjugate point method".

3.5.3 Summary of the conclusions to O'Connor's examination of Allen's sandwich beam theory

(i) The assumptions of an antiplane core made in Allen's theory were verified by comparison to a finite element analysis. The finite element model was consistent with the assumptions of an incompressible core having no longitudinal stiffness. The comparison of analyses was almost exact when several different load and beam configurations were considered.

(ii) Local shear discontinuities at point loads cause a peak stress concentration which dissipate at a finite distance from the load application point. The length of span affected by the stress concentration is termed as the "critical span". The critical span length is dependent on the relative stiffnesses of the facings and the core. Not only are the stresses in the facings distorted in the zone of influence, but the displacements are also affected.

(iii) As previously mentioned Allen's theory may be used for the evaluation of the shear modulus of cores of thick faced sandwich beams, known as "multiple span beam testing". This method has been investigated thoroughly in chapter 6. Briefly, the beams are tested over a number of spans for load / displacement response and the results graphically presented. By interpretation of the experimental data a relationship of load and displacement is equated to the shear modulus. Previous use of this method was subject to displacement errors resulting from measurement at the location of the load application. The discovery of the critical span concept then led to the "conjugate point method".

3.5.4 Summary of the conclusions to O'Connor's examination of finite element modelling

O'Connor's finite element modelling included investigating uniaxial compression tests, American and British Standard shear tests and predicting the flexural behaviour of three

and four point load configuration sandwich beam tests. The conclusions to these F.E.A. applications are discussed forthwith.

(i) The finite element program was designed to be used for analysis of plane elastic continua and limited to applications within the elastic material response and small deflection. The program was not suitable for simulating material plasticity, creep or large deflection problems.

(ii) A convergence study was undertaken for all the different finite element models to verify accuracy. For each model a convergence graph of displacement versus number of nodes was plotted. Convergence was achieved when the node density reach an appropriate accuracy relative to say the measurable mid span displacement of a sandwich beam.

(iii) Although restricted by computer capacity, three dimensional models of the uniaxial compression tests were acceptably accurate. Models consisted of six elements in the xy plane and four elements in depth. The models used twenty noded three dimensional solid brick continuum elements.

(iv) The overall shear test F.E.A. model used an irregular mesh consisting of twenty eight elements in length and six in depth. The steel edge plates were modelled with two noded beam elements, one element in depth. The core used eight noded element. The elemental mesh was denser near to the ends of the model to counter the increase in stress gradient.

(v) A similar mesh structure to that of the shear tests was adopted for the analysis of the sandwich beams.

3.6 Conclusions

The conclusions presented here have been based on theoretical contents of this chapter and the findings of the literature review. The literature review identified an extensive and comprehensive detailed examination of Allen's sandwich beam theory, by O'Connor (1985). Only the theory specifically relating to the overall project requirements has been presented in this chapter. Within the scope of this project and regarding the investigation by O'Connor a complete review of Allen's theory is not necessary. The conclusions include recommendations from O'Connor's findings as summarised previously.

3.6.1 General

(i) The literature review has identified both Allen's theory and finite element methods for use in analysing the plywood faced sandwich constructions. O'Connor (1985) has shown that Allen's theory is capable of predicting facing stresses and displacements of thick faced sandwich beams and panels in a three or four point load configuration.

3.6.2 Allen solutions

(ii) Allen's assumptions of an antiplane and incompressible core were made on the basis of analysing a beam with a honeycombed, or similar, core rather than a soft and flexible core such as polyurethane. An incompressible core also enabled a single displacement value to be given at each position in the span - not so if the core were compressible. It would seem that the overall displacement and stress response of a sandwich beam could be well represented, but the local effects would not be so well modelled.

(iii) Allen's theory may also be used for the evaluation of the shear modulus of the Isofoam CRF core of sandwich panels. Allen's theory has been re-written for specific "conjugate point" solutions by O'Connor. Chapter 6 details the conjugate point method more thoroughly.

(iv) O'Connor's investigation of Allen's solutions provide evidence to suggest that a good approximation of displacement and stress profile of sandwich beams are achievable. Allen's solutions are therefore used to provide further comparison, along with experimental data, to the finite element modelling.

3.6.3 Finite element analysis

(v) F.E.A., by its discrete nature, provides an approximation of a structural system and it is therefore necessary to conduct a convergence study. Both LUSAS and ABAQUS programs have user defined element topology and therefore a convergence study is required. SC01/3 contains a sub-routine which contains an iterative process essentially carrying out a convergence study. The SC01/3 analysis has been pre-defined with a structural accuracy determining the mesh density throughout the model, but in certain situations nodal density has been increased.

(vi) To establish that finite element methods and techniques are suitable for approximating sandwich behaviour, a comparison of finite element analysis results, Allen's theory and experimental data is made in chapter 7. Stress profiles have been identified as the most appropriate way of comparing the results.

(vii) The modelling techniques and element types used by O'Connor do not appear to be as necessary with today's highly powered computers and advanced software programs. Descriptions of each F.E.A. model used is contained within each relevant chapter.

CHAPTER 4 - UNIAXIAL MATERIAL TESTING AND ANALYSIS

4.1 Introduction

4.2 Isofoam CRF uniaxial compression testing and analysis

4.3 Isofoam CRF uniaxial tension testing and analysis

4.4 Discussion

4.5 Conclusions

CHAPTER 4 - MATERIAL TESTING AND ANALYSIS

4.1 Introduction

Uniaxial testing involves subjecting a body, or coupon, of Isofoam CRF to a force in a single direction, whilst measuring certain aspects of physical behaviour. The test coupons have been machined directly from off-cuts of the panels and were therefore as representative as possible. Uniaxial testing of the Isofoam CRF core of plywood faced sandwich panels has been conducted to evaluate material properties that support theoretical analysis of the complete sandwich panels. The uniaxial test methods themselves have also been scrutinised by comparing displacement behaviour of the full scale sandwich panels with the theoretical predictions when incorporating the uniaxial test results. This examination and the subsequent conclusions are held in chapter 7.

The uniaxial tests, both compressive and tensile, have been performed to determine the elastic modulus and Poisson's ratio in the three mutually perpendicular directions. Both compression and tension tests have been conducted in accordance with relevant British Standards where applicable. Revisions to the test configurations, recommended by previous research and early pilot studies, have been incorporated to achieve greater test result accuracy. In addition there were other factors, such as the specimen thickness and the type of available test apparatus, that have meant a deviation from the British Standard.

Experimental test configurations dictated that ideal, or theoretical, material behaviour characteristics were not achieved in practice. Using the LUSAS (1991) finite element modelling package both the experimental and the theoretical configurations could be reproduced and compared. The discrepancies were identified and appropriate correction factors formulated to be applied directly to the experimental results. Conversion charts have been devised to display the correction factors graphically for ease of use.

The detailed examination of the behaviour of the Isofoam CRF revealed marked orthotropic foam properties. Prior to the uniaxial compression tests, it was originally assumed that isotropic conditions were present. The load applied during the uniaxial compression tests was in the through thickness direction and thus normal to the spanning direction. On close inspection of the foam's cellular structure it was noticeable that the cell shapes were elongated in the direction of the span. This coincided with the direction of rise. The assumption of an isotropic and homogeneous core material did not then hold. As the uniaxial compression tests did not conform to the required data output (the elastic modulus in the spanning direction) further testing was necessary. Uniaxial tensile tests were then performed. These additional tensile tests were orientated to provide experimental data according to the spanning direction of the panels and beams. The uniaxial compression tests were useful in establishing the presence of orthotropic properties and the Poisson's ratio values have been adopted in the light of no other available experimental data.

The conversion charts for the uniaxial compression tests have been based on work conducted by O'Connor (1985) for isotropic homogeneous foam, but extended to incorporate orthotropic conditions. O'Connor's conversion charts accounted only for the barrelling effects caused by the attached facings, which prevented lateral movement of the upper and lower faces that were in contact with the machine platens. Subsequent to this barrelling effect a "geometric shape effect" was also discovered. This geometric effect also created barrelling in the lateral faces, but in an axis perpendicular to and in the same plane as the through thickness barrelling effect.

The conversion charts shown in this text are based on assumptions of material behaviour and are therefore approximate in nature rather than the more exact solutions describing isotropic behaviour.

4.2 Isofoam CRF uniaxial compression testing and analysis

4.2.1 Introduction

The foremost objective of the uniaxial compression tests was to determine the appropriate elastic modulii and Poisson's ratio for the Isofoam CRF cores of all the panels in order to support the subsequent theoretical modelling of sandwich panels. Six specimens from each of the panels P1-P6 and P8-P10 were tested.

Pilot compression tests on specimens from panels P1 and P2 highlighted some of the difficulties in obtaining appropriate properties. The specimens used were rather small in comparison to the loading characteristics of the compression machine. Initially, temperature and relative humidity conditions were those of the laboratory and thus different environmental conditions existed from specimen to specimen. The applied strain rate was also difficult to maintain as the loading machine was manually operated and dial gauge displacements were recorded manually.

These initial experiments helped to develop improved methods for the main testing programme for specimens from panels P3-P6 and P8-P10. A new heating and ventilation system installed in the laboratories enabled a reasonably constant temperature and relative humidity to be maintained negating the need to construct an environmental chamber. The British Standard BS 4370 recommends a strain rate of 10% per minute of the specimen's original thickness. This was still difficult to control although a more rigid regime using a stopwatch and pre-estimated load increments was adopted. One important feature adopted for the main batch of tests was the use of very thin metal plates, and approximately 10 mm square, to prevent the dial gauge's spring loaded rods from indenting the foam when measuring lateral displacements.

During testing it was noticed that lateral barrelling occurred over the complete height of the specimen and was most apparent at mid-height. This was due to the use of Isofoam

samples still bonded to plywood facings. The barrelling phenomena has been previously reported by O'Connor (1985) where conversion factors, formulated from finite element analysis, were then applied to test results. O'Connor limited his investigation to isotropic material behaviour of the core. The uniaxial tests samples had been cut directly from sandwich beams which were manufactured from a large and pre-formed isotropic polyurethane block. Conversely, the sandwich constructions in this project have had their cores foamed-in-place. This process, as described in chapter 2, creates a foam with different properties in the three mutually perpendicular axes. This is most prevalent for the properties in the direction of rise. In all cases the direction of rise occurs in the spanning or x-direction.

The discrepancy between mid-span displacements of theoretical models and experimental sandwich panel results was initially attributed to solely the barrelling effects. Although the barrelling did effect the actual compressive strength (and the Poisson's ratios) the principal cause of the discrepancy was found to be the orthotropic nature of the Isofoam. Analytical solutions and subsequent tensile tests confirmed this condition.

During the course of the uniaxial compression test investigation, presented in this chapter, it was found necessary to perform and use the results from additional tensile tests to complete the conversion charts. This chapter first describes the compression tests and provides conversion factors, incorporating the tensile test results, to compensate for the barrelling effects. The tensile test results have then been presented and their relevance highlighted.

4.2.2 Test methods and procedure

BS 4370: Part 1: 1988 gives recommendations for compression tests of rigid cellular materials. The procedures in the standard have been noted, but in some cases not followed exactly for various reasons of convenience and practicality.

The plan area dimensions of the test specimens differed. The plan areas used were 80 x 80 mm for panels P1 and P2 and 150 x 150 mm for panels P3 - P10. The BS recommended 50 x 50 mm sizes, but these were not suitable for use with the available compression machine. Subsequently the 80 x 80 mm specimens were also found to be too small for satisfactory results and the 150 x 150 mm size was adopted. The thickness of each sample was that of the panel from which it came, varying from 21 to 104 mm.

The compression machine was not capable of applying a constant rate of strain to the specimen, and in any case the vertical compression and lateral expansion dial gauge readings required manual observation. Constant intervals between load steps throughout all testing was rigidly adhered to by means of a countdown stopwatch. A typical time step used for each load increment was 15 seconds with the load steps calculated to provide approximately 10 % strain per minute of the specimen's original thickness. Care was also taken to avoid time dependent behaviour, particularly in the linear elastic region, from influencing the results. Simple observation during preliminary tests showed that the incrementation used was sufficient to avoid compressive creep strain from corrupting the readings.

Conditioning and temperature of the Isofoam CRF samples prior to and during the tests were that of the laboratory as no ideal environmental conditioning facilities existed. All temperatures and relative humidities for each test were recorded and are included in tables A4.1a-c. Table 4.1 summarises the environmental conditions. A new heating and ventilation system that had been recently installed in the laboratory enabled a satisfactorily constant temperature and relative humidity for the duration of the tests on specimens from panels P3 - P10. The preliminary tests on panel P1 and P2 coupons were conducted at temperatures and relative humidities well below those recommended. Simple care in selecting when to test was also used to maintain consistent conditions.

Average values	P1	P2	P3	P4	P5	P6	P8	P9	P10
Temperature °C	16.0	15.2	19.9	19.6	19.8	19.6	19.9	20.4	20.0
Relative Humidity %	44	39	48	49	48	48	48	48	49

Table 4.1 Compression test environmental conditions.

The two part polyurethane foam mixture contains a resin compound that creates a naturally strong adhesion to the plywood faces when injected into the core cavity during manufacture. Foam cut for use from a large homogeneous isotropic mass and glued to the facings often have a significant glue line thickness. This reduces the effective core thickness. Close visual inspection of the foamed-in-place cellular structure, in juxtaposition to the plywood facings, found the bonding surface was consistent with the main body of foam allowing the whole thickness to be considered.

There were three reasons for leaving the specimens with the plywood facings still attached to the Isofoam as in the original complete sandwich construction. Firstly, removing the facings would reduce further the thinner samples, which were already below the British Standard recommended thickness. Secondly, the plywood facings would provide a smooth and flat surface for the machine platens to locate. Thirdly, some degree of fixity would have been present in any case, between sample surfaces and machine platens, so by leaving them fully fixed a known condition would then be applicable when considering the finite element modelling.

Six samples were tested for each of the nine panels P1 to P6 and P8 to P10 and were placed between two thick steel platens of the loading machine. The upper platen was free to rotate about the x- and y-axes (parallel to the plane of the top facing) to accommodate small variations in dimensions between specimens. Figure 4.1 shows typical specimen dimensions.

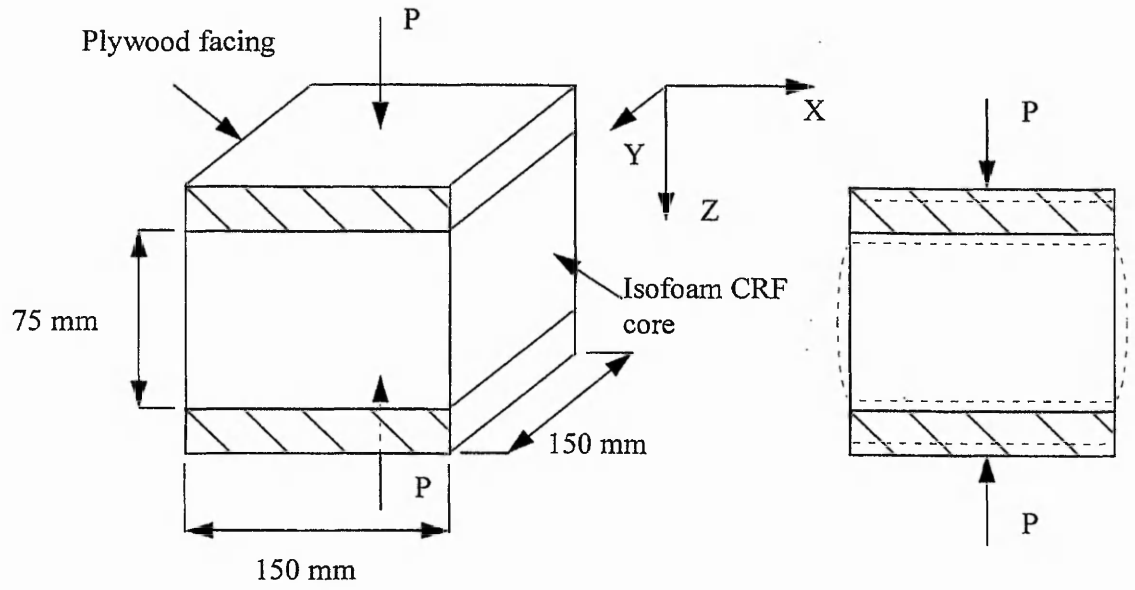

a. Typical dimensions for a uniaxial compression test

b. Line figure showing two dimensional barrelling

Figure 4.1 Uniaxial compression test.

Dial gauges were placed normal to the centre of each face and to the upper moving part of the test rig in the x-, y- and z-directions respectively. Small thin metal 'plates' were placed between the specimen and the tip of the gauge to prevent local indentations. Dial gauges were used instead of LVDTs as the spring loading of the displacement rod was significantly less for the dial gauges. The LVDT displacement rods had created slight depressions in the Isofoam CRF in the preliminary tests and it was felt that this would adversely influence the results when considering the magnitude of the lateral displacements.

The specimens were orientated such that the direction of their axes simulated that of the panel from where it came. Great care was taken with the test arrangement and in particular with placing the specimen central to the vertical axis of the test machine.

4.2.3 Compression test results and analysis

Compression testing on specimens from all nine panels was completed in two stages. Firstly, tests on samples cut from panels P1 and P2 were part of the preliminary investigation and then secondly by developing and adapting these techniques, samples from panels P3-P6 and P8-P10. Tables A4.1a, b, c, display laboratory test details and material properties for all the specimens associated with beam or panel tests. Typical stress / strain figures are plotted for panels P1 and P6 and shown on figures A4.1 and A4.2 respectively. The displacements used for calculating lateral strain were the average of the two opposite dial gauge readings. This was found to be particularly beneficial as some of the cubes had a tendency to shear slightly under loading. Thus any movement in an adverse direction could be accounted for.

'S-shaped' displacement versus load curves, as shown on figures A4.1 and A4.2 were synonymous of the polyurethane foam specimens. The initial "up take" curve is attributed to the bedding down of the test specimen and the establishment of an even distribution of applied stress over the loaded surface. The linear portion shows pure elastic behaviour and then at the higher stress levels unrecoverable plastic deformation before complete crushing and failure. The elastic modulus has been evaluated from the figures using the tangential gradient extrapolated along the linear central portion of the curve. Poisson's ratio has been calculated, in this case, by obtaining the gradients of the lateral (x- and y-directions) stress / strain curves and relating those to the gradient of the normal (z-direction) stress / strain curve for υ_{zx} and υ_{zy}.

Although, at this stage, the theoretical results, using raw compression test modulii and complete panel experimental data, appeared to underestimate flexural stiffness it was borne in mind that a major influencing factor in the panel bending behaviour was the shear strength. Initial F.E. solutions assumed isotropic conditions and calculated the shear modulus from $G_{xz} = E_z/2(1+\upsilon)$. From prior knowledge that barrelling effectively

increased the measured elastic modulus, it was evident that further investigation of the physical properties of the foam were necessary. At this point attention was drawn to an orthotropic physical state by observation of the shape of the voids in the foam mass. Rather than regular spherical voids, oval shaped voids had been created instead as the foam was squeezed between the two facings, in the direction of rise, and span.

4.2.4 Finite element modelling

The use of Isofoam specimens cut directly from sandwich panels with the facings attached leads to barrelling in the compression tests. The barrelling is caused by the restraint of lateral expansion where the foam bonds the plywood facings. It was decided to leave the facings attached as they would provide a known fixity rather than a partial restraint of unknown magnitude. Using finite element techniques, 'fixed' and 'free' conditions may be used to simulate and quantify the experimental configuration. The fixed edge models simulate the actual laboratory conditions and the free edge, allowing uniform lateral expansion, the ideal or theoretical situation.

Figure 4.2 shows the theoretical conditions of (a.) pure strain and (b.) pure stress. Part (c.) shows the experimental condition where the actual behavioural state consists of both pure stress and pure strain. Finite element analysis uses three dimensional pure stress modelling conditions with certain restraint conditions to simulate the attached plywood facings. The effect of the barrelling phenomenon creates higher values of experimentally measured elastic modulus and lower Poisson's ratio than theory suggests as it restricts lateral expansion. A general assumption for the stress / strain state of the polyurethane mass is that it behaves in a pure stress state governed in response by its inherent Poisson's ratio behaviour. Pure stress, as shown in figure 4.2, involves a volumetric change which is related to the Poisson's ratio. Pure strain, on the other hand, assumes zero Poisson's ratio and the volumetric strain is proportional to the material strength and the applied load. Most materials, including rigid cellular polyurethane foams, display a response somewhere in between pure stress and pure strain, thus some additional volumetric change occurs.

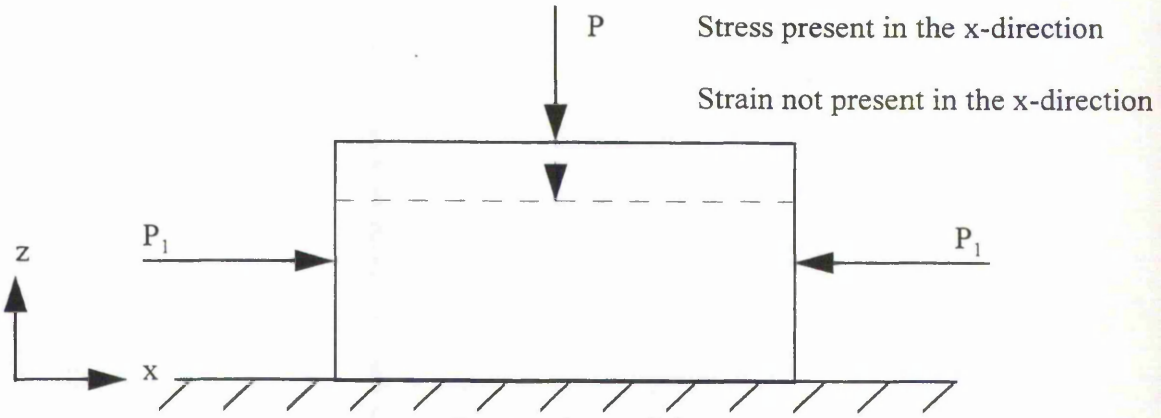

a. Pure strain condition

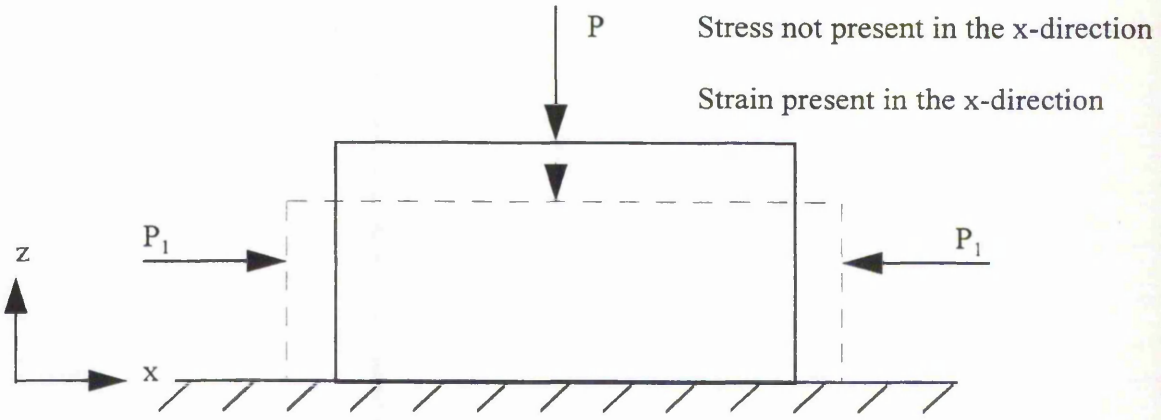

b. Pure stress condition

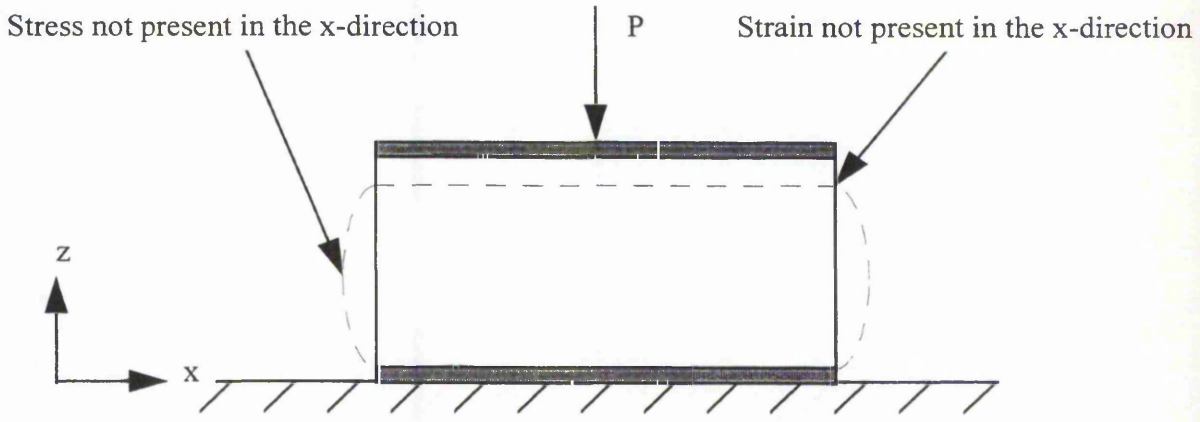

c. Fixed edge experimental condition

Figure 4.2 Stress / Strain condition of uniaxial compression tests

4.2.4.1 Element type

The two types of element considered for use in the analysis are the HX8 and HX20, both three-dimensional solid brick continuum, with eight and twenty nodes respectively. Each node has three degrees of displacement freedom in the x-, y- and z-directions. They are both suitable for isotropic, orthotropic and anisotropic linear and elasto-plastic three-dimensional continuum material properties.

The HX20 element has been chosen in preference to the HX8 as an equal degree of accuracy may be obtained more quickly from a model that contains less elements but of a higher order. For example, to run an equivalent nodal density containing the HX8 element the run time is 610 seconds and produces a lateral displacement of 0.3449 mm. The HX20 elemental mesh, see table 4.2, takes 147 seconds and produces a lateral displacement of 0.3451 mm, thus being both slightly more accurate and significantly quicker. Laboratory displacement measurement accuracy, using linearly variable differential transducers, has been recorded to 0.01 mm. The HX20 element displacement output would therefore normally be rounded to 0.35 mm, whereas the HX8 element output would be rounded to 0.34 mm. This represents approximately 3% discrepancy in accuracy as opposed to an actual discrepancy of 0.06% between the equivalent outputs. In this computer study it has been decided to keep the accuracy of the outputs reasonably high until quoting final figures.

4.2.4.2 Use of symmetry and support conditions

To significantly reduce the problem size a uniaxial compression specimen has been divided by symmetry so that only one eighth is represented by the finite element model. Figure 4.3 below shows the use of symmetry in reducing the problem size. The 'internal' sides then have their 'surface' nodes restrained in appropriate directions. In detail, the mid-height nodes in the x-y plane (internal surface) are restrained in the z-direction and its two inside edges are additionally restrained in the x and y- directions accordingly. Thus the 'inside'

face in the xz plane is free to move in the x- and z- directions, but is restrained in the y-direction. Similarly, the 'inside' face in the yz plane is free to move in the y- and z-directions, but is retrained in the x-direction.

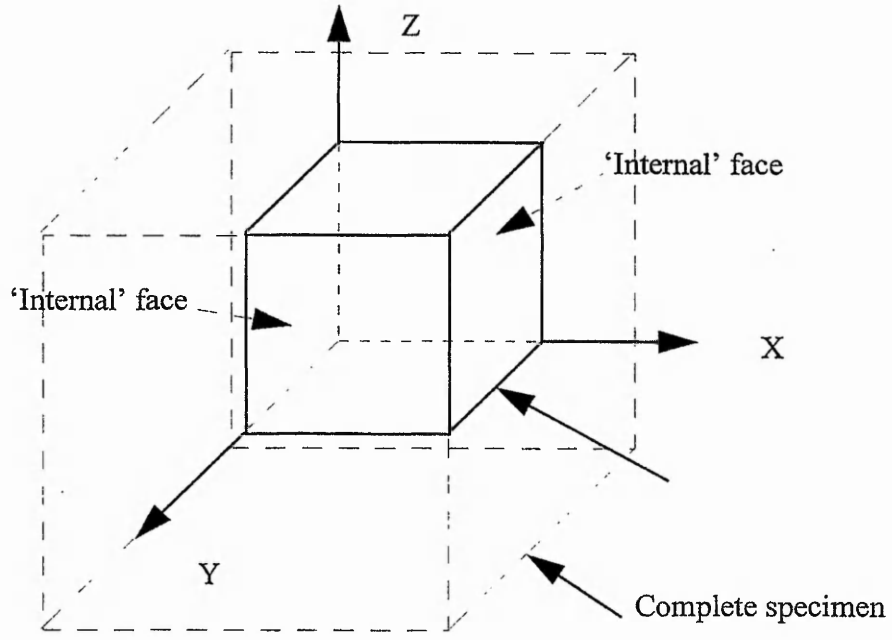

Figure 4.3 Use of symmetry to reduce problem size

The top loaded surface nodes are a special case when modelling the 'free' and 'fixed' edge uniaxial compression tests. In the 'free' edge set-up the top surface is allowed to laterally expand in the x- and y-directions except for the 'inside' top surface edges, which are restrained in the x- and y-directions accordingly. In the 'fixed' edge condition all nodes on the top surface are restrained in all directions.

4.2.4.3 Applied loading

In O'Connor's investigation of stress contours on the loaded surface of a uniaxial compression specimen it was found that an uneven stress distribution existed when a uniform load was applied. This created a situation of unequal vertical displacements on the loaded face. To overcome this inherent unequal vertical displacement distribution, which

obviously does not occur in practice, a prescribed displacement response is utilised. The method firstly restrains the top surface nodes in the 'loaded' or z-direction and then prescribes a magnitude of displacement to each node. In all cases a prescribed displacement of 1.00 mm has been used. The material was specified as fully linear-elastic and so the magnitude of the displacement does not influence the relationships of the results.

4.2.4.4 Convergence study

Before analysing the effect of barrelling on the uniaxial compression tests, a suitable element mesh was established. The factors to be considered in conducting the convergence study were run time, required accuracy, amount of data input and the size of output file. The dimensions required for the elemental mesh may be reduced by symmetry, described above, and by using appropriate loading and support conditions. The actual specimen size of 150 x 150 may then be reduced to 75 x 75 mm in plan and 10.5, 25, 39, and 52 mm in depth, depending upon the original core thickness of the panel .

Using the 52 mm thickness of specimen, for the dimensions of the model used in the convergence study, an initial mesh of one element is used. This was then followed by a 2 x 2 x 2 and so on up to a 10 x 10 x 10 mesh. This initial convergence study uses isotropic elastic material properties, which allows for cross checking of deflections and applied stresses. Material properties used for the convergence study were typical for the Isofoam core, elastic modulus = 5.0 N/mm^2 and Poisson's ratio = 0.25.

Table 4.2 shows the results of the convergence study. The convergence has been based on the maximum lateral displacement found at the specimens mid height and side position. The table lists the computer processing (units) time, in seconds, as well as the Poisson's ratio. Figures of number of nodes versus lateral displacement and number of nodes versus computer processing time are shown on figures A4.3 and A4.4 respectively.

Element mesh	No. of elements	No. of nodes	C.P.U. time (s)	Lateral disp. mm	Poisson's ratio
1 x 1 x 1	1	20	2	0.3400	0.2385
2 x 2 x 2	8	81	8	0.3416	0.2368
3 x 3 x 3	27	208	23	0.3430	0.2378
4 x 4 x 4	64	425	60	0.3449	0.2391
5 x 5 x 5	125	756	147	0.3451	0.2392
6 x 6 x 6	216	1225	533	0.3452	0.2393
8 x 8 x 8	512	2709	2118	0.3452	0.2394
10 x 10 x 10	1000	4961	8874	0.3453	0.2394

Table 4.2 Elemental mesh density convergence study for the 'fixed' edge condition

Selection of the most appropriate mesh density has been based on a suitable accuracy as well as a sensible processing time. The finite element model results shown on figure A4.3 appears to converge somewhere marginally below 0.35 mm of lateral displacement. This accuracy has been chosen to match that of the physical ability to measure the experimental displacements. To be confident of achieving this accuracy the displacement requires convergence above 0.3449. Looking at the lateral displacements the 5 x 5 x 5 gives 0.3451 mm, as opposed to the 4 x4 x 4 mesh which gives 0.3449 mm. A total processing run time of 147 seconds was by no means inconvenient and thus the 5 x 5 x 5 mesh density has been chosen.

4.2.4.5 Barrelling in 3-dimensional solid cubes subject to uniaxial compression

In figure 4.2, which displays the stress / strain conditions that were present in the uniaxial compression tests, it may be seen that in both the pure stress and pure strain states, no barrelling exists. In addition, it should also be noted that this is only a two dimensional

representation. Part c. of figure 4.2 then shows the barrelling phenomenon, caused by the top and bottom edges being restrained against lateral displacement, assuming that again the two dimensional state only applies.

For three dimensional solid continuum there was discovered to be an additional, geometrical, constraint at the intersection of two mutually perpendicular faces, point A. As discussed earlier, symmetry has been used to reduce the finite element model size. Figure 4.4a, below, shows one quarter of the complete plan area of the compression cube. The section shown is of a slice taken at the complete specimen's mid-height, normal to the direction of loading. Figure 4.4b is the finite element model output of the lateral deflection, as a result of an applied load in the z-direction, along the line A-B, depicting one half of the mid-height profile; note the exaggerated scale. The centre of the three dimensional model is located at the bottom left hand corner.

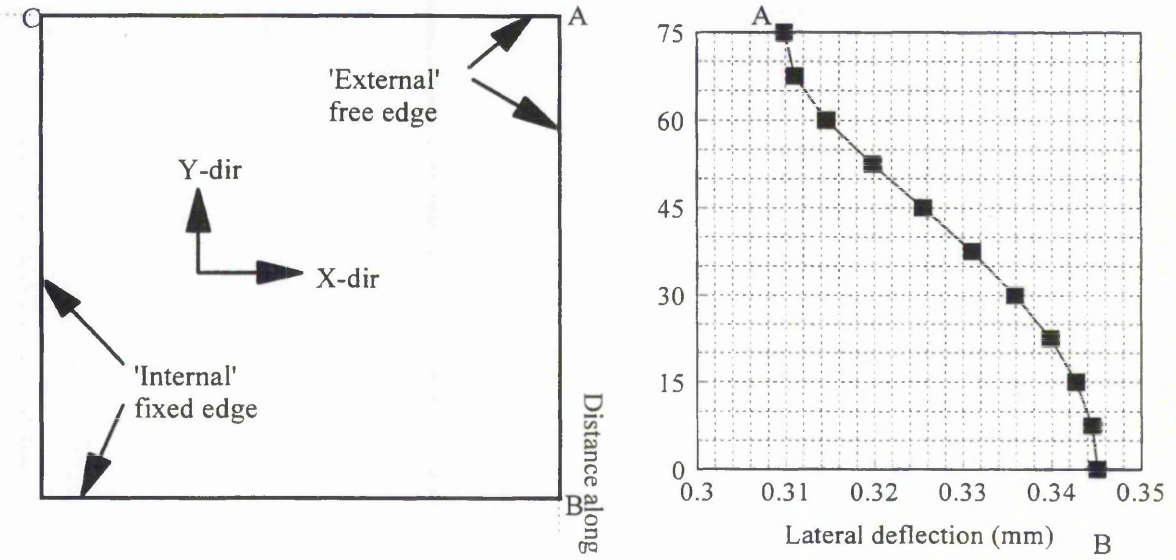

a. Plan view of one quarter of compression cube

b. Exaggerated lateral deflection in x-dir along A-B

Figure 4.4 The effect of 3-dimensional geometry on lateral expansion along one edge (A-B) for a uniaxial compression test specimen at mid height. Loading is normal to the plane shown in plan.

The F.E.A. deflection profiles show that the centre point of any face, point B in this case (0.345 mm), is subject to the greatest lateral deflection along the line A-B. Point A, at the intersection of two perpendicular faces, has the least lateral deflection (0.309 mm). This may be attributed to the Poisson's ratio effects and the subsequently incurred stress distribution throughout the x-y plane. The free corner, A, is required to translate both in the x and y directions, whereas the mid side point B is only required to translate in the x direction. The stresses dissipate radially from the mid point of the cube leaving a less stressed zone in the outer corners near to A. As the area around point A has a lower stress than at the mid position of the sides, there is subsequently less lateral displacement.

The side elevation, shown in figure 4.5, plots the lateral deflection due to an applied load in the (negative) z-direction, along the height of the finite element model. The line B-D, figure 4.5a, thus represents the original positions of both the deflected profiles of a vertical line located at mid-width and a vertical line described by the intersection between two faces. The mid-width vertical deflection profile, as also shown on figure 4.4b, shows a greater lateral displacement than the line defined by the intersection of the faces. The vertical deflection profiles differ due to the level of stress, and thus strain, that decreases towards the outer surfaces.

When looking at the deflection profile, in figures 4.4 and 4.5, it should be noted that this is for the fixed edge condition, where the deflection at the point D is zero for both vertical lines. For the ideal theoretical case of a compression cube with free edges, the deflection profiles would be of a constant displacement in the x-direction for the entire height and remaining different relative to one another. There would still be a geometric barrelling effect present for the free edge condition.

This three dimensional geometric barrelling effect does not appear to have been identified previously. The finite element analysis carried out by O'Connor primarily concentrated on the barrelling effect created by the fixed edges. Furthermore, O'Connor assumed that the polyurethane foam used was entirely isotropic and homogeneous. Although two forms of

barrelling have been identified as potentially corrupting experimental results they have been dealt with together in the three dimensional finite element modelling.

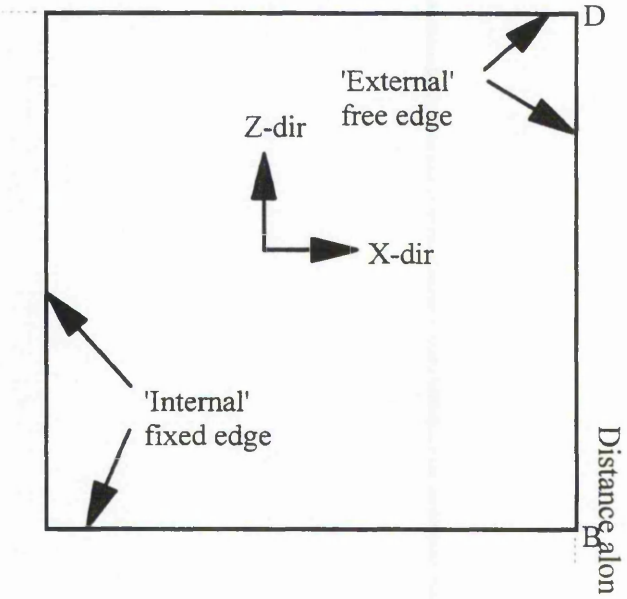

a. Side elevation of one quarter of a uniaxial compression cube.

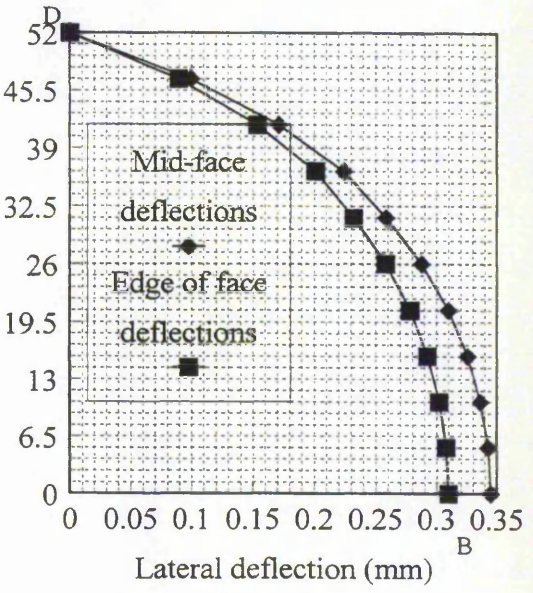

b. Exaggerated lateral deflection for side B-D at mid-face and edge-of-face locations.

Figure 4.5 The effect of 3-dimensional geometry on lateral expansion along vertical sections, mid-face and edge-of-face (B-D) for a uniaxial compression test. Loading is applied in the Z-direction.

Fixed edge barrelling reduces the lateral displacement, particularly in the case of the low aspect ratio specimens. However, this is somewhat offset by the barrelling due to the three dimensional geometry. Theoretically, considering the problem two dimensionally, it is assumed that the faces of the compression cube remain in-plane. Thus the lateral displacement, for calculating Poisson's ratio, may be taken at any point on the face. As shown above the maximum lateral displacement is at the centre point of the cube and this is where the experimental displacements were taken. Ideally, when calibrating the effects of

barrelling using finite element analysis, the change in lateral volume would be more appropriate to measure than the displacement at the face's centre point. This is impractical and is accounted for anyway in the fixed edge finite element analysis by comparison to theoretical lateral displacements.

Further evidence of the three dimensional geometric effect on the experimentally recorded lateral deflection is shown on figure A4.5, the relationship of aspect ratio to measured Poisson's ratio. As mentioned before, the fixed edges reduce the experimental Poisson's ratio, which in turn are dependent upon the aspect ratio. The greater the aspect ratio, the less influence the fixed edges have on the lateral expansion. As the aspect ratio increases, the curve on figure A4.5 rises above 0.25, which is the theoretical inputted value. Thus there is a point where the effect of the fixed edges reduces sufficiently for the three dimensional effect to be the major influencing factor.

4.2.4.6 Effect of aspect ratio on apparent Poisson's ratio

Prior to investigating the orthotropic properties of the foam cores, it was necessary to study the effect of the foam's thickness on the measured laboratory Poisson's ratio for the fixed edge tests. Material properties used in the 5 x 5 x 5 elemental mesh were: elastic modulus = 5.00 N/mm^2 and Poisson's ratio = 0.25 and by symmetry reducing the model's plan dimensions to 75 x 75 mm aspect ratios were plotted against the experimental Poisson's ratio. The aspect ratio being taken as the core thickness divided by the width of the cube. Figure A4.4 shows that the thickness of the specimen to it's side length has a significant influence on the measured Poisson's ratio.

In conducting this computer study of the effect of aspect ratio on experimental Poisson's ratios, all specimens were subjected to loading, in the negative z-direction, prescribed by a 1.0 mm displacement of the upper facing relative to the lower. In table 4.3, it may be seen in the third column, the lateral displacements decrease relative to an increase in aspect ratio. It should be noted that the prescribed displacement loading was kept at 1.0 mm and

therefore the strain in the z-direction intrinsically decreases due to the change in core thickness. The theoretical Poisson's ratio in the fourth column represents the value inputted into the finite element programme. This value was the same for all core thicknesses so that the effect of the aspect ratio was distinguishable.

Core thickness c (mm)	Aspect ratio (c/150)	Lateral displacement (mm)	Actual Poisson's ratio	Measured Poisson's ratio	Percentage difference %
21	0.140	0.4822	0.25	0.068	-72.8
50	0.333	0.4579	0.25	0.153	-38.8
78	0.520	0.4086	0.25	0.204	-18.4
104	0.693	0.3451	0.25	0.239	-4.40

Table 4.3 Effect of aspect ratio on measured Poisson'ratio

At low aspect ratios, the degree of lateral restraint provided by the facings is more marked than at high ratios and this leads to lower values of laboratory measured Poisson's ratio. Table 4.3 gives the actual specimen thicknesses used in the uniaxial tests, their aspect ratios and the F.E.A. generated fixed edge Poisson's ratio. To highlight this trend, the percentage difference from the theoretical value is calculated. The negative percentage difference indicates that the laboratory 'fixed' edge measurement was less than the theoretical 'free' edge result. At the low aspect ratio of the 21.0 mm thick cored sample, the percentage difference was approximately -73% and at the higher aspect ratio of the 104 mm thick specimen the percentage difference reduces significantly to approximately -4%.

4.2.4.7 Effect of barrelling on the measured elastic modulus

The fixed edge uniaxial tests over estimate the elastic modulus due to the stiffening effect of the lateral restraint provided by the plywood facings. When comparing the theoretical

elastic modulus (inputted to the finite element model), with the apparent experimental, this phenomenon may be highlighted.

O'Connor had formulated a conversion chart that would allow the actual, or theoretical, Poisson's ratio (and elastic modulus) to be evaluated from the experimentally determined Poisson's ratio. This was achieved by running a series of F.E. analyses with varying Poisson's ratio values whilst keeping the theoretical elastic modulus constant. From the output file it was possible to find the simulated experimental Poisson's ratio and relate it to the inputted value. Similarly, the inputted elastic modulus (kept constant for all models) could be compared to the simulated experimental elastic modulus. A ratio of the inputted to outputted elastic modulii could then be related to the simulated Poisson's ratio. Again using the 5 x 5 x 5 finite element mesh with an elastic modulus of 5.0 N/mm^2, various Poisson's ratio values were inputted to the model. Table 4.4 summarises the input and output data for an isotropic material.

E_{act} N/mm^2	υ_{act}	E_{exp} N/mm^2	υ_{exp}	E_{act}/E_{exp}
5.0	0.10	5.046	0.120	0.991
5.0	0.15	5.106	0.187	0.979
5.0	0.20	5.196	0.261	0.962
5.0	0.25	5.322	0.343	0.940
5.0	0.30	5.491	0.436	0.911

Table 4.4 Ratio of actual to measured Poisson's ratio, E_{act}/E_{exp}.

The elastic modulus used in the fixed edge finite element models is typical for the Isofoam CRF core samples. The magnitude of the elastic modulus does not have any effect on the relative behaviour of the model. Any actual elastic modulus may be found by factoring experimental result by the ratio E_{act}/E_{exp}. The finite element analysis results output in table 4.4 has been presented graphically to show how both the experimental Poisson's ratio and

the ratio E_{act}/E_{exp} change with the actual Poisson's ratio. Figure A4.6 may then be described as a calibration chart, but for isotropic elastic polyurethane foams only.

The calibration chart, figure A4.6, may be used as follows; Step 1, from experimental results of Poisson's ratio, say 0.25, a horizontal line should be drawn from the vertical scale at 0.25 to intercept the lower Poisson's ratio curve. Step 2, from this point a vertical line is then drawn down to intercept the horizontal axis. The actual Poisson's ratio may then be read off. Step 3 draws a vertical line up from the original intercept on the lower curve to the upper curve representing E_{act}/E_{exp}. Step 4 then draws a horizontal line to the vertical axis and a value for E_{act}/E_{exp} is read off.

From figure A4.6, using an experimentally obtained Poisson's ratio $PR_{exp} = 0.195$, $PR_{act} = 0.25$ and $E_{act}/E_{exp} = 0.962$. As the actual elastic modulus is that inputted ($E_{exp} = 5.0$ N/mm^2) in the finite element model, E_{exp} can be calculated;

$$E_{act} = 0.962 \times 5.0 = 4.8 \text{ N/mm}^2$$

This represents approximately a 4% reduction in the measured elastic modulus and a 23% reduction in the measured Poisson's ratio. Although only a relatively small discrepancy for the 104 mm thick panel P6 specimens the lower aspect ratios of panel P5, P4 and P3 show greater differences as displayed in table 4.3.

Initially, it was assumed that the discrepancy between experimental results from the full scale sandwich panel tests and the finite element solutions, supported by the compression tests, were due to the barrelling effects corrupting the material properties. After applying conversion factors to the raw compression test results there was still found to be a marked discrepancy. In fact, the conversion factors made the finite element solutions appear even less stiff and created a larger discrepancy than the original unfactored material properties. Analysis of British and American Standard shear tests (described in the next chapter) indicated a higher value of elastic modulus, assuming that $E = G / (1 + 2\upsilon)$.

The initial assumption that the Isofoam was isotropic began to look doubtful. When considering the other material testing results further investigation seemed appropriate. The other material tests pointed to orthotropic properties, particularly in the spanning or x-direction. Before fully investigating the shear and multiple span beam tests (chapters 5 and 6) it was felt necessary to conduct further simple uniaxial tests. In addition, it was felt that the very nature of the shear tests, loading the specimens in pure shear, was inappropriate for direct support to the uniaxial compression tests. Likewise, the multiple span flexural beam tests were also used to find the shear modulus and were therefore also deemed unsuitable. Bearing this in mind, it was felt that simple uniaxial tension tests would be most appropriate.

Other considerations for conducting uniaxial tensile tests were, firstly, that the specimens would be subjected to loading in the x-direction and, secondly, as seen in the compression tests, high aspect ratio (long and relatively thin) samples were less inclined to be influenced by edge, or support, conditions. The tension tests had the added advantage that the loading configuration would not corrupt the experimental results. Long thin samples are relatively free of fixed edge effects and three dimensional constraints.

Section 4.3 of this chapter illustrates the testing and identifies the appropriate tensile elastic modulii. It has been generally assumed that the tensile and compressive modulii are equal at all displacements. The following sub-section describes the formulation of the conversion factors for orthotropic Isofoam CRF, using finite element modelling, of the uniaxial compression tests combining data from the tensile tests with the compression tests.

4.2.4.8 Modelling the behaviour of orthotropic foam

Producing a conversion chart for orthotropic foam was not possible without making certain assumptions. For instance, specifying different modulii in the x-,y- and z-directions influences the Poisson's ratio effect, thus leading to three unknown parameters. Therefore,

the simulated experimental outputted Poisson's ratios will not be in relative proportion to one another or those inputted in the original model. In the case of foamed-in-place masses, where the direction of rise has a direct influence on the orthotropy, some assumptions have been made. The principal assumption is essentially that properties in the y- and z-directions are equal, but those in the x-direction (i.e. in the direction of rise) are different.

Assumptions:

- that $E_x > E_y$ and $E_y = E_z$
- that $\upsilon_{zx} = \upsilon_{xz} = \upsilon_{xy} = \upsilon_{yx}$; and $\upsilon_{zy} = \upsilon_{yz}$; but υ_{zy} and υ_{xz} are not equal hence the orthotropic nature of the polyurethane
- The direct strains ε_x, ε_y and ε_z are related to the applied direct stress σ_z by the following equations:

$$\varepsilon_z = \sigma_z / E_z ; \quad \varepsilon_x = -\upsilon_{zx}\varepsilon_z ; \quad \varepsilon_y = -\upsilon_{zy}\varepsilon_z$$

- It is also assumed that the elastic modulus $E_x = E_z(\upsilon_{zy} / \upsilon_{zx})$. As no uniaxial compression tests have been performed with direct stress in the x direction, this assumption has been made from comparison with the relevant tensile tests.

Finite element analysis of the uniaxial compression cube uses the 5 x 5 x 5 element density mesh. Material property data input for the HX20 orthotropic element for specimens from panels P4-P6 and P8-P10 would therefore now be as shown in table 4.5. Tensile tests were not conducted for panel P3 for two reasons. Firstly, the dimensions of the test apparatus required a 140 x 25 x 25 mm sample size and this was not appropriate due to the 21.0 mm thick core of panel P3. Secondly, in the relatively thin gap, between the two plywood facings, it appeared that mixing of the two constituent had not been accomplished as successfully as for the other panels and on inspection of the foam's quality, significant areas of hard and soft foam mixes were present. These areas were likely to have been formed by an imbalance between the masses of resin and Isocyanate compounds. This was

also interspersed with areas where excessive blowing agent had caused an increase of void size in the cellular structure, thus leading to lower density masses.

The calibration charts for orthotropic conditions were similar to the isotropic charts. As mentioned before, the shear modulus does not influence the model behaviour and an arbitrary value is used. Formulation of the charts started with a range of theoretical Poisson's ratios being inputted to the F.E.A. model, with a constant actual elastic modulus, the model analysis completed and the output scrutinised and presented in the form of figures A4.7 to A4.11. The elastic modulus, in the x-direction (E_x), has been taken directly from the tensile tests whereas E_y and E_z were arbitrarily set at 5.00 N/mm^2. Panel P3 specimens were also given an arbitrary E_x = 5.00 N/mm^2 as no data was otherwise available.

Panel No.	Cube size mm	E_x N/mm^2	E_y, E_z N/mm^2	G_{xy}, G_{yz}, G_{xz} N/mm^2	υ_{xy}, υ_{yz}, υ_{xz}
P3	75 x 75 x 21	5.00	5.0	2.0	vary
P4	75 x 75 x 51	5.00	5.0	2.0	vary
P5	75 x 75 x 72	6.24	5.0	2.0	vary
P6	75 x 75 x 104	6.71	5.0	2.0	vary
P10	75 x 75 x 50	6.20	5.0	2.0	vary

Table 4.5 Properties used in the F.E.A. for orthotropic conditions

Formulation of the conversion factor charts, figures A4.7 to A4.11, have been made by inputting the data from the above table 4.5 into the finite element model. For each chart (one chart represents one set of samples from one panel) the third, fourth and fifth columns of data were kept constant, at the values shown, while the Poisson's ratio is modified for each model run. The inputted Poisson's ratio was that of the actual theoretical value of the foam and so the outputted displacements can then be used to calculate the experimental Poisson's ratio. A range of theoretical Poisson's ratios were inputted to cover the range of experimental Poisson's ratios. Thus, as described for the isotropic condition displayed on

figure A4.6, the known experimental Poisson's ratio may be used to find the theoretical. For all the panels P3-P6 and P10 there are two plotted theoretical versus experimental curves. These represent the Poisson's ratios in the x- and y-directions, which in most cases were different due to the different elastic modulii in those respective directions.

Table 4.6 summarises the conversion factors, E_{act}/E_{exp}, from the figures A4.7 to A4.11 and the actual material properties E_{act} obtained from the uniaxial compression tests. These actual material properties have been used in chapter 7, both to support the finite element analysis and the Allen solutions when compared to the related panel tests. The E_{act}/E_{exp} conversion factor values in this table are not as large as those found in O'Connor's (1985) investigation as they include the geometric shape effect factor and the specimen size was significantly different.

Panel No.	Measured υ_{yz}	Actual υ_{yz}	E_{exp} N/mm^2	E_{act}/E_{exp}	E_{act} N/mm^2
P3	0.25	0.15	2.3	0.95	2.2
P4	0.20	0.18	4.3	0.97	4.2
P5	0.24	0.18	6.5	0.96	6.2
P6	0.24	0.19	6.0	0.96	5.8
P10	0.19	0.13	6.4	0.98	6.3

Table 4.6 Conversion table for uniaxial compression tests.

4.3 Isofoam CRF uniaxial tension testing and analysis

4.3.1 Introduction

The uniaxial tension testing has been partly conducted to support the finite element modelling of the orthotropic behaviour of the Isofoam found in the compression tests. The

results will also be used in the comparison of material testing techniques when finite element analysis predicted displacements are compared to experimental sandwich panel results. The initial assumption that the Isofoam CRF was isotropic was inappropriate especially in the light of the shear and multiple span beam tests. The applied stresses in both the shear and multiple span tests are in contrast to the uniaxial nature of the compression tests. Thus it was decided that a more appropriate supporting test method would be a uniaxial tensile test, where the principal strains could be directly applied in the spanning, or x-direction. The chosen test configuration also prevented any edge or three dimensional geometry effects from corrupting the laboratory results.

Tensile tests have been conducted on panel P4 - P6 and P10 specimens. The thickness of the core of panel P3, 21.0 mm, was deemed unsuitable for use in the tensile tests as the head grips were designed for 25 mm thick specimens. Specimens from panels P1 and P2 were also unsuitable for use as they had been exposed to natural sunlight for a long period and their condition had deteriorated.

4.3.2 Test methods

British Standard BS4370 Part 2 for Rigid cellular material gives a detailed description of the appropriate methods for tensile testing. These methods have been adopted to a large extent, but the exact specification tailored to suit this application and availability of equipment. As no appropriately sensitive loading equipment was available dead weights were used. Figure 4.6 shows outline details of the test configuration.

A dial gauge, attached to each side of the upper aluminium plates with its displacement rod braced against a bracket on the lower plate, was used to measure the deflection. The recorded displacements were then averaged. Load was applied by dead weights stacked on a hanger attached centrally to the bottom fixture. To achieve a reasonably consistent strain rate to the compression tests a 5N weight was added every 15 seconds. This produced a strain of approximately 0.35% per load increment for the 25 x 25 mm cross sectional area.

The cross sectional area deviated from the recommended standard of 12.5 x 12.5 mm due to the relatively delicate nature of the Isofoam. Stiffer foams would normally use the smaller dimensions.

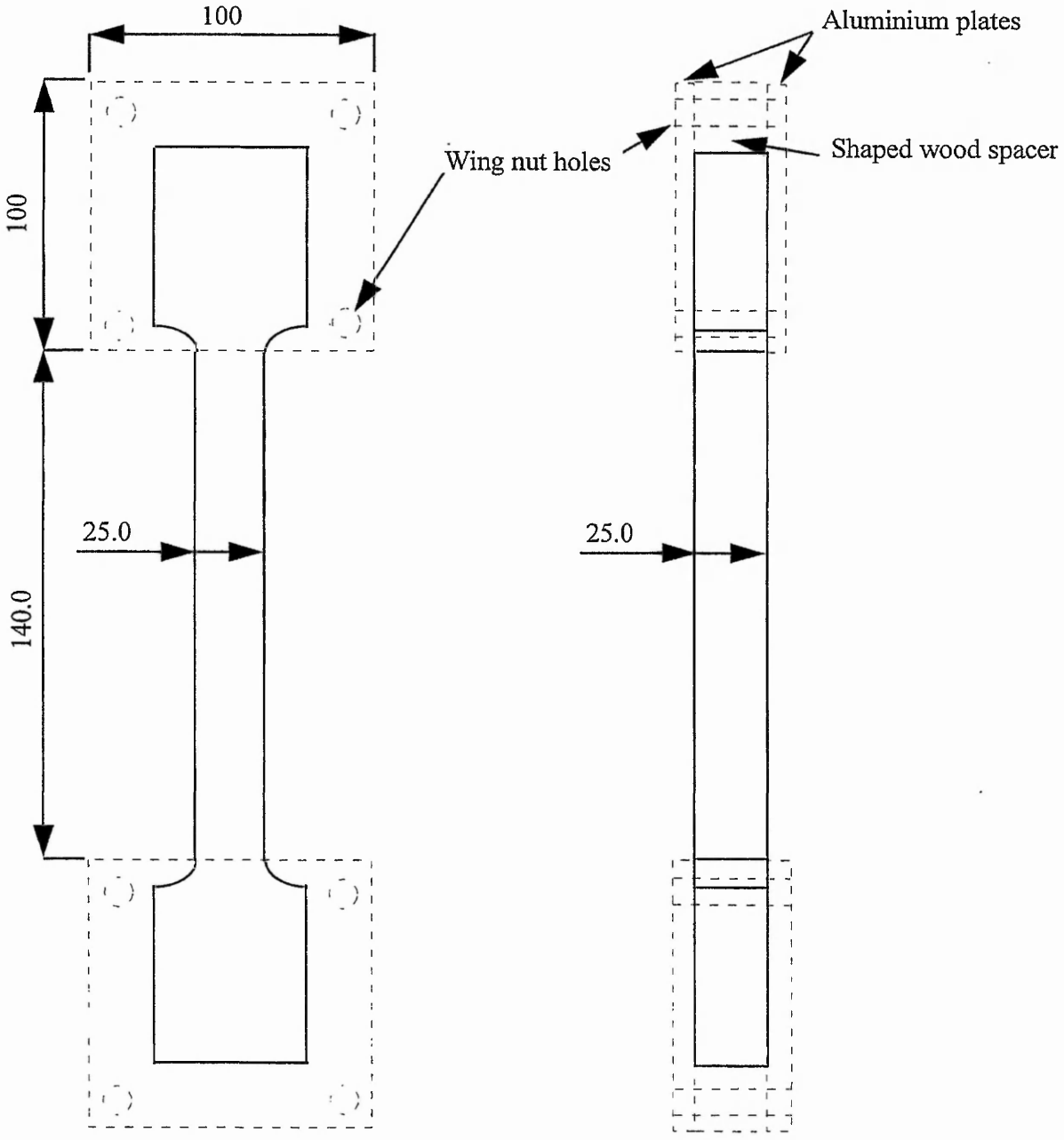

a. Front elevation b. Side elevation

Figure 4.6 Uniaxial tensile test configuration

Test conditions, shown in table 4.7, were similar to those of the compression tests, however they were again that of the ambient laboratory temperatures and humidities rather than the standard specification.

Average values	P4	P5	P6	P10
Temperature ^{o}C	18.7	19.6	19.6	18.8
Relative Humidity %	48	49	49	48

Table 4.7 Tensile test environmental conditions.

4.3.3 Test results

The tensile tests were specifically aimed at obtaining the elastic modulus in the spanning, or x-direction relative to the main sandwich panels. Figures A4.12 - A4.15 display experimental stress / strain relationship curves for all coupons of panels P4 - P6 and P10 respectively. The elastic modulii have been calculated using a tangential line extrapolated from the linear portion of each 'S-shaped' curve. Table 4.8 summarises the averaged tangential elastic modulii for each panel:

Average values	P4	P5	P6	P10
Elastic modulus N/mm^2	5.00	6.24	6.71	6.20

Table 4.8 Tensile test elastic modulus summary.

The following section describes a short finite element modelling programme to identify any similar experimental error to the uniaxial compression tests. As will be seen the finite element analysis provided evidence that the experimental results did not require modification. The elastic modulii in table 4.8 were used directly in the finite element

analysis for the orthotropic Isofoam conditions as no conversion factors needed to be applied. The following section gives brief details of the finite element study used to establish the validity of using the raw experimental data from the tensile tests.

4.3.4 Finite element modelling

A brief finite element study was conducted to investigate any restraining edge effects that the tensile specimens may have been subjected to. Similar modelling techniques were employed for the tensile test pieces as were used for the compression tests.

4.3.4.1 Element type and mesh density

The HX20 three dimensional solid continuum brick element was used for all the F.E. modelling of the tensile tests. The HX20 element proved to be the most suitable for the application to the uniaxial compression tests and so was adopted for the tensile tests. A convergence study was not considered appropriate for this application as only a few models were run. The mesh density was comparative, using a 14 x 5 x 5 density. As an approximate guide to accuracy the elemental dimension aspect ratio for this mesh density is 5 x 2.5 x 2.5 mm, and this compares to the compression cube models which were up to 10.4 x 2.5 x 2.5 mm. Thus it may be reasonably concluded that the chosen mesh density was able to produce sufficient accuracy.

4.3.4.2 Use of symmetry and support conditions

The geometry of the finite element model employed was a simplified and reduced form of the test configuration. It was assumed that the coupon was strictly 140 x 25 x 25 mm and that there would be no appreciable strain from the chamfered section that lead into the head grips. The use of symmetry allowed one eighth of the overall dimensions to be analysed, ie. 70 x 12.5 x 12.5 mm. Similar face restraints and freedoms were used for the tensile test model as to the compressive test model.

4.3.4.3 Applied loading

A displacement was applied to the whole of the loaded face so that an even stress distribution was maintained. To do this it was necessary to restrain the face in the direction of loading and then prescribe a magnitude of displacement. A loading displacement of 1.00 mm in the positive z-direction was used for all models. Although this displacement does not appear to fully represent the complete range of displacements throughout the tests, the finite element model assumes elastic material properties, even for large strains, and so the magnitude of displacement and its response was always proportional.

4.3.4.4 Properties used in the finite element models

Table 4.9 contains the properties used for the finite element modelling of both the fixed and free edge tensile tests. Orthotropic conditions were again considered in this application. It was assumed that the elastic modulii in the y- and z-directions were equal and that those in the x-direction were greater. A full range of models, considering all material properties of each panel, was not necessary after inspection of the initial results using panel P6 properties. In total, only two models, one a fixed edge and the other a free edge, were used.

Panel No.	Model size mm	E_x N/mm^2	E_y, E_z N/mm^2	G_{xy}, G_{yz}, G_{xz} N/mm^2	υ_{xy}, υ_{yz}, υ_{xz}
P6	70 x 12.5 x 12.5	6.5	5.0	2.0	0.25

Table 4.9 Tensile properties used in the F.E. analysis for orthotropic conditions

4.3.4.5 Results and discussion of the finite element modelling

Lateral displacement at the mid-height point of the complete test piece was taken as the basis for identifying the accuracy of the two models. The free edge model produced an actual Poisson's ratio of 0.2591, while the fixed edge 0.2594, a discrepancy of some 0.1%. Similarly, the elastic modulii obtained were 6.50 and 6.5013 N/mm^2 for the free and fixed edge models respectively.

It was noted as unlikely that a fully restrained condition would be present where the specimen was held in the head grips. The short finite element study concluded that the difference between the free and fixed edge models was negligible and thus the results of the tests could be used directly.

4.3 Discussion

BS4370: Part1: 1988 gives guidance for testing rigid polyurethane samples in uniaxial compression. Although a recommended specimen cube of side 50 mm should be used, where possible, the actual specimen size in plan was of side 150 mm with the original panel core thickness being used for the main batch of testing. Pilot tests, conducted prior to the main batch of tests, on samples from panels P1 and P2, used plan dimensions of 80 x 80 mm. This plan area, combined with the relatively weak Isofoam, was found to be still insufficient yielding too few readings for a reasonable graphical output. It was noticed that the crushing mode of failure for the 80 x 80 mm plan area cubes tended to be concentrated on one side, which then led to the upper platen tilting causing the loading distribution to deteriorate further. It was felt that the larger plan size would also be more stable.

Temperature and humidity levels, specified by the British Standard, could not be controlled and those of the laboratory had to be accepted. During the pilot experiments, on specimens cut from panels P1 and P2, temperature variations ranged from 15.2 to 16.0 °C and relative

humidity from 39 to 44%. These environmental conditions were some 5 °C and 6% relative humidity below the minimum recommended and were not consistent with either the British Standard or the testing on the relevant sandwich panels. As the uniaxial compression test results were to be used to support the analytical models of the complete sandwich panels, it was felt necessary to conduct further tests in more suitable environmental conditions.

The method of testing the main batch of specimens would therefore require improved techniques. Initially it was envisaged that an environmental chamber would need to be built as the compression, beam and panel tests required a reasonable degree of consistency. Fortunately, the stability of the temperature and as an indirect result the relative humidity, were greatly helped by the installation of a controlled heating and ventilation system. The temperature varied between 19.6 and 20.4 °C and relative humidity levels were kept between 48 and 49%. Although not quite within the British Standard recommendations of 23 °C +/- 2 °C and 50% +/- 5% relative humidity, the conditions were consistent with the beam and panel tests.

Having acceptably standardised the environmental conditioning of the samples there were still marked differences in the stiffness of samples taken from any one particular panel. These differences were likely to have been associated with the fact that the specimens were taken from a large panel which contained variations in the quality of the foam. These variations arose from the manner in which the foam was mixed and injected through a series of holes around the perimeter of the panel and its subsequent 'rising' pattern between the faces.

Noticeably softer and harder regions existed in the foam's mass where the components have either not been mixed fully or contain disproportionate amounts of one constituent or other. This is inevitable due to the type of mixing system employed, where separate pumps are used for each of the storage tanks holding the two Isofoam CRF compounds. This was particularly evident on close visual inspection of the foam's cellular structure throughout the 21.0 mm thick core of panel P3. The quality of the foam in the thicker cored panels

tended to be more consistent in colour (denser foam being darker) and more resistant to indentation.

The barrelling phenomenon noticed during uniaxial compression of cubes of Isofoam CRF appeared to be more complex than had been previously described by O'Connor. Not only were there barrelling effects rising from the fixed edges, but also from the inherent nature of the three dimensional geometry of the cubes. O'Connor's investigation into barrelling only accounted for the stiffening effects of the fixed edges. It was found that the three dimensional geometric effect reduced the adverse influence of the fixed edges.

Initially, isotropic material properties were assumed, but it was obvious from preliminary analysis of the complete sandwich panels, using the raw experimental compression data, that the results were underestimating the elastic modulus. Subsequently, the shear and the multiple span tests also pointed to higher modulii values and with the visual observation of the orientation of voids in the foam's mass, it was necessary to establish the possibility of orthotropic behaviour. This was successfully established by conducting uniaxial tension tests. The uniaxial tension tests results have also been used both to support the analysis of the compression tests and the comparison of theoretical solutions to the flexural behaviour of sandwich panels.

The solution to the barrelling problem then became more complex. Simple finite element models simulating free and fixed edge restraints were valid for establishing the effect of barrelling for isotropic conditions, but now there was the addition of orthotropy.

Bearing in mind the inherent variability of the quality of the foam throughout a panel, a sensibly simplified method was utilised. After many attempts to quantify exactly the problem of the relationship between elastic modulus and Poisson's ratio in the three mutually perpendicular directions two assumptions were made. Firstly, that the elastic modulus in the y- and z-directions were equal and secondly that the Poisson's ratio was equal in all three directions. Although this second assumption may seem rather arbitrary,

the effect on the stiffness was small in comparison to the effect of introducing a different x-direction elastic modulus. In addition to this was the fact that the experimental Poisson's ratio from the computer output model, when using orthotropic elastic modulus properties, were different in the x- and y-directions. It was therefore accepted that the actual Poisson's ratio in the x- and y-directions were different in proportion to the stiffness in the respective directions.

It has been noted that strain rates may also influence the accuracy of experimentally determining the apparent elastic properties of Isofoam CRF. Certainly, during the pilot studies, no attempt was made to correlate the strain rate to the complete sandwich panel tests. This would have been difficult in any circumstance as the core acts primarily as a shear stiffener between the facings whereas these tests have been applying a uniaxial strain. However, simple estimation of the rate of strain for the shear tests and multiple span beam tests have been correlated to the full scale sandwich beam tests. This was done by relating the uniaxial test strain rate to the rate of core shear strain of the two panel tests to failure (panels P8 and P9).

4.4 Conclusions

Although the shear and multiple span testing may be more applicable to sandwich response behaviour, this chapter has proved that good correlation with simple uniaxial tests is possible. The important aspects of this chapter are concluded below:

(i) The elastic modulus and Poisson's ratio for panels P3, P4, P5, P6 and P10 have been determined and are contained in Table A4.2a, b and c. Correction factors formulated from finite element analysis have been established to counter experimental error due to test configuration.

(ii) The experimental error was attributed to the barrelling phenomenon which has two components. Firstly, the effect of the fixed edges, caused by the facings, creates an underestimation of the lateral displacement response. Secondly, the three dimensional geometry effect causes each lateral face to bow between vertical face edges thus over estimating the lateral displacement response. For the 150 x 150 mm plan specimens (figure A4.5), the two opposing effects offset each other at an aspect ratio of approximately 0.8 (ie. a core thickness of 120 mm).

(iii) Orthotropic properties exist when the foam injection system is used to fill a void or cavity and may be reasonably assessed using uniaxial testing techniques and finite element analysis. The final orthotropic material properties for all panels are given in table 4.4.

CHAPTER 5 - SHEAR TESTING AND ANALYSIS

5.1 Introduction

5.2 British and American Standard Test Methods

5.3 Results and Analysis

5.4 Finite Element Analysis

5.5 Discussion

5.6 Conclusions

CHAPTER 5 - SHEAR TESTING AND ANALYSIS

5.1 Introduction

5.1.1 Shear strains in flexure

The shear modulus, or shear stiffness, when considering the composite action of a sandwich panel, is the ability of the core material to transmit opposing bending forces between the two facings. An analogy may be made between sandwich beams and steel I-sections: for weight and cost purposes material is placed where it has the greatest structural benefit. For the steel I-section, the web separates the two flanges that carry the bending stresses while the web carries the shear load generated between the two flanges. For a sandwich beam, the web is essentially replaced by a relatively weak, but full width, lightweight core. The core thus acts like the web of the steel I-section in keeping the two facings a constant distance apart and transfers the shearing forces. However, unlike the steel web the lightweight and weak Isofoam core undergoes significant shear strains and contributes to the overall flexural displacement.

Shear response, in both thin and thick faced flexural sandwich panels and beams, is a major influence on bending behaviour. It is thus essential to correctly specify the core shear modulus for the analytical methods used to model the flexural behaviour of sandwich panels. Shear strains may account for 20% to 50% of the total elastic deflection of a thin faced, simply supported, sandwich panel subject to a single mid-span load and some 50% to 80% for typical thick faced panels.

The shear tests performed and described in this chapter attempt to evaluate the corresponding shear modulus for the seven panels tested in three point loading configuration. The shear modulus, G_{xz}, is tested for and evaluated only in the spanning, or x-direction, as all comparative panel and beam tests are simply supported and loaded to create bending, and thus shear strain in the core, in that direction. Figure 5.1 shows an element of sandwich core under shear by opposing forces P and complementary

forces P_1 . The forces are mobilised by the relative movement of originally adjacent positions on the compressive and tensile facings under flexural bending of the overall sandwich beam. The shear modulus, in this case the xy plane, G_{xy}, is derived as - the shear stress, τ, divided by the shear strain, γ .

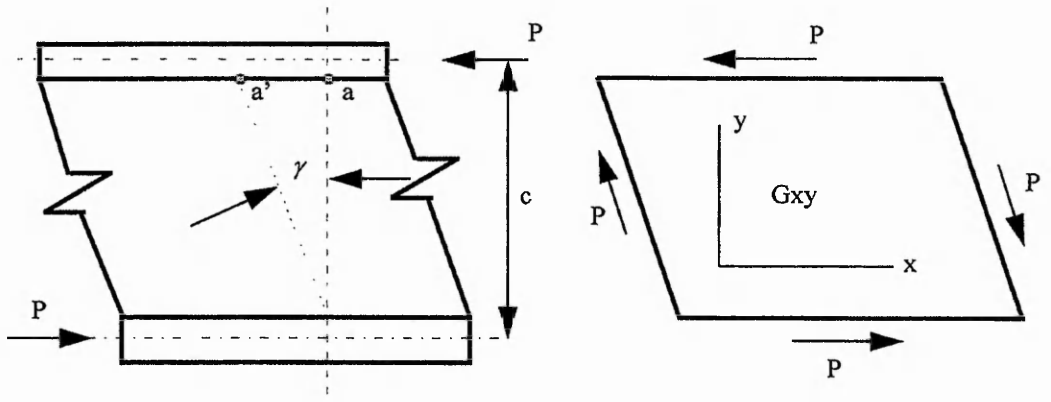

a. Section of sandwich beam b. An element of core under shear force P

Figure 5.1 Shearing of a sandwich beam core during flexure

5.1.2 Applicable Standards and relevant literature

Both British and American Standards, BS4370: Pt 2: 1993: Method 6 and ASTM C273-61 respectively, describe and recommend test configurations and methods for the laboratory evaluation of shear modulus and shear strength of rigid cellular materials. The German Standard DIN 53 427 also describes a test method for the shear modulus, however, as it is very similar to the British Standard it is not examined in this investigation.

Other literature relating to the testing of rigid cellular foams for shear stiffness properties has been identified and is useful to the fulfilment of the aims of this section of the project. Allen (1967) reviewed the then current methods of shear stiffness measurement of cores of sandwich beams. Methods included direct shear testing, of core material coupons, and also shear modulus evaluation using a multiple span beam testing technique. This latter technique is described in chapter 5 and further work carried out and presented in assessing its applicability.

Figure 5.2 shows four possible techniques that may be used to evaluate the shear properties of relatively weak rigid polyurethane core materials. Shown are the (a.) double block shear test (b.) single shear block test (c.) compressive panel shear test and (d.) tensile panel shear block test. The panel shear tests are not suited to this project as the required size dictates large core thickness not available or applicable to this project. The panel shear test method is also difficult to set up correctly particularly where the edge plates meet at the corners. The double block shear test method has advantages over the single block when considering the direction of the applied shear force since the applied load is transmitted through the specimen without the edge plates pulling away from the specimen corners. However, this method requires two identical samples which was deemed unlikely for the foam used in this application and thus the single block method has been used.

Further work has been conducted by O'Connor (1989), which compares single block test methods for shear properties of the cores of sandwich constructions. O'Connor's investigation compared and appraised British and American Standards using finite element modelling, but were only supported by a limited number of laboratory tests which were not vindicated by modelling full scale sandwich panels using the shear test results. O'Connor's investigation identified the discrepancies found between the two methods with the results pointing to the importance of how the apparatus configuration applied load to the specimen and the displacement measuring techniques.

This chapter describes the British and American Standard shear tests that have been conducted to determine the shear modulus of the Isofoam CRF cores of the seven, main, plywood faced panel tests. The previous research, described above, on these methods has been studied and in some cases revisions to the test configurations have been made from the concluding recommendations.

This chapter concentrates on the evaluation of shear modulii by the single shear block methods of British Standard BS4370: Pt 2: 1993: Method 6 and American Standard ASTM C273-61.

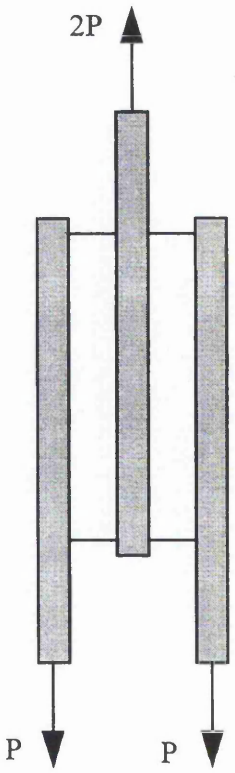

a. Double block shear test

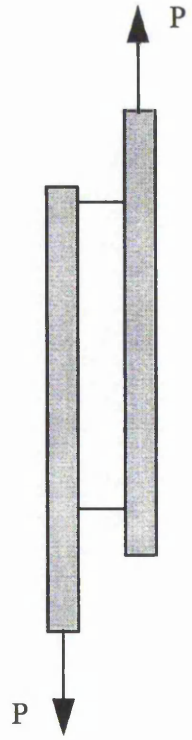

b. Single block shear test

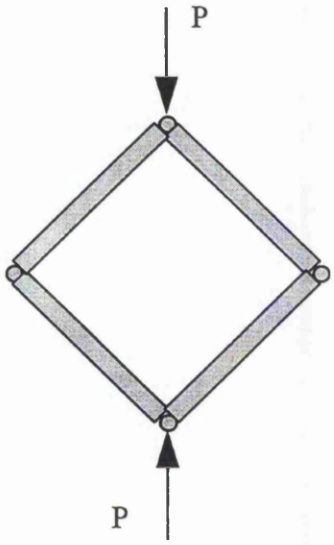

c. Compressive panel shear test

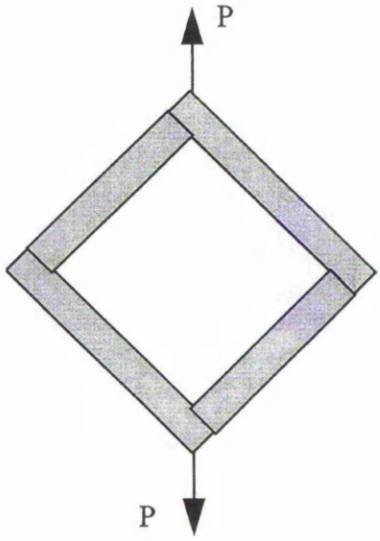

d. Tensile panel shear test

Figure 5.2 Alternative shear tests on core material coupons

5.2 British and American Standard Test Methods

5.2.1 Introduction

This section describes the testing apparatus including the shear test assemblies, specimen preparation, conditioning, environmental control, loading procedure and the experimental shear modulus results. In particular the differences and similarities between the British and American Standards are highlighted and discussed.

In principle, both Standards apply a shear stress to a sized coupon of material through two very stiff metal edge plates. These in turn are attached to the loading machine through head grips. The line of action of the applied load through the specimens is dictated by the configuration of the apparatus. As can be seen on figure 5.3 the line of action of the American Standard is applied through opposite corners of the test sample whereas the British Standard configuration applies the load through the centre line of the specimen. Differences are therefore apparent, between shear modulii results of each test method. These are attributed to the direction of the applied load to the specimen and the effects this has on the behaviour of the apparatus.

5.2.2 Specimen dimensions

The British Standard test specimen should have nominal dimensions of length 250 mm, width 50 mm and thickness 25 mm. There is an allowable tolerance of 2% in all dimensions. The specimen should also be a parallelepiped with no two opposite sides varying more than 1%. The American Standard has a different specification for the dimensions of the shear test specimen, the length and width being related to the thickness. The original total core thickness of the sandwich construction should be used and the width should be not less than twice the thickness with the length not less than twelve times. This would mean that although the width used was 50 mm the length should have been 300 mm. The British Standard dimensions have been adopted for all tests, including the American Standard tests. It was felt that the most significant

difference between the two test methods lay in the way the load was applied and so to obtain direct comparisons for the two methods the same core samples should be used. The British Standard recommends a specimen length of 250 mm, width 50 mm and thickness 25 mm. This gives the British Standard an aspect ratio of 10:1 compared to the American Standard of 12:1. It will be shown later that there is only a nominal difference between the two aspect ratios.

5.2.3 Test apparatus

The test apparatus may be dealt with by considering three separate aspects. Firstly, the configuration of the edge plates and head grips, secondly the loading machine specification and thirdly the additional displacement measuring equipment.

5.2.3.1 Edge plates and head grips

For both simplicity and to complete a comparative study the edge plates were manufactured so that they would be compatible for both the British and American Standard head grips. The geometry of the head grips was different however, as figure 5.4 shows.

Edge plates and head grips were manufactured from mild steel with a nominal elastic modulus of 200 kN/mm^2. The thickness of the edge plates was nominally 16.0 mm as specified in the British Standard. The American Standard requires a plate thickness that relates the stiffness of the plate to the core thickness; the plate stiffness should not be less than 267 x 10^6 N.mm^2/ 10 mm of width per 10 millimetres of core thickness. Therefore using the specified 16.0 mm plate thickness of the British Standard, the plate stiffness was 683 N.mm^2/ 10 mm of width. This was satisfactory with the American Standard's recommended plate stiffness of 273 x 10^6 N.mm^2/ 10 mm of width per 10 millimetres of core thickness.

Figure 5.4 illustrates in detail the head grip arrangements for the American and British Standards. The head grips were attached to universal joints, one manufactured as part of

the lower head grip and the other integral with the loading machine, both providing free rotational movement. As well as the tongue and groove slot, the British Standard specifies two diagonally opposite location bolts, however O'Connor recommended the use of four bolts in a symmetrical square pattern for the plate / head grip joint and this has been adopted. The location blots hold the head grips rigidly to the edge plates preventing separation during loading and their positions are denoted by the dashed lines. O'Connor had concluded from bending tests on the head grips that when using only two bolts some degree of movement and rotation occurred, which accounted for some of the loss of accuracy encountered. It was thus felt four bolts rather than just two were a reasonable and simple addition to the specification.

5.2.3.2 Loading machine

The loading machine used was an Instron 8514 C, which was capable of applying a constant crosshead displacement rate of 1 mm per minute which was subsequently adopted for all shear tests. A continuous graphical readout of applied load versus time was recorded for the crosshead displacement. The time taken for a test, or a portion of the figure, could then be calibrated to give a displacement. The specimens were all tested in a vertical plane.

5.2.3.3 Additional displacement measuring equipment

One source of error identified in O'Connor's study was the method of recording shear displacements. The British Standard requires the crosshead displacements to be recorded, while the American Standard recommends a crossplate displacement measurement. The loading machine provides a continuous graphical output of the relative vertical movement of the machine grips and additional measuring equipment was attached so that the relative parallel movement of the edge plates could be monitored. Two linearly varying differential transducers (LVDT) were attached to each flank of the edge plates. For direct comparison between the two standards both crossplate and crosshead displacements were recorded for each test. The displacements from the LVDTs were recorded on a Schlummberger 9914 datalogger

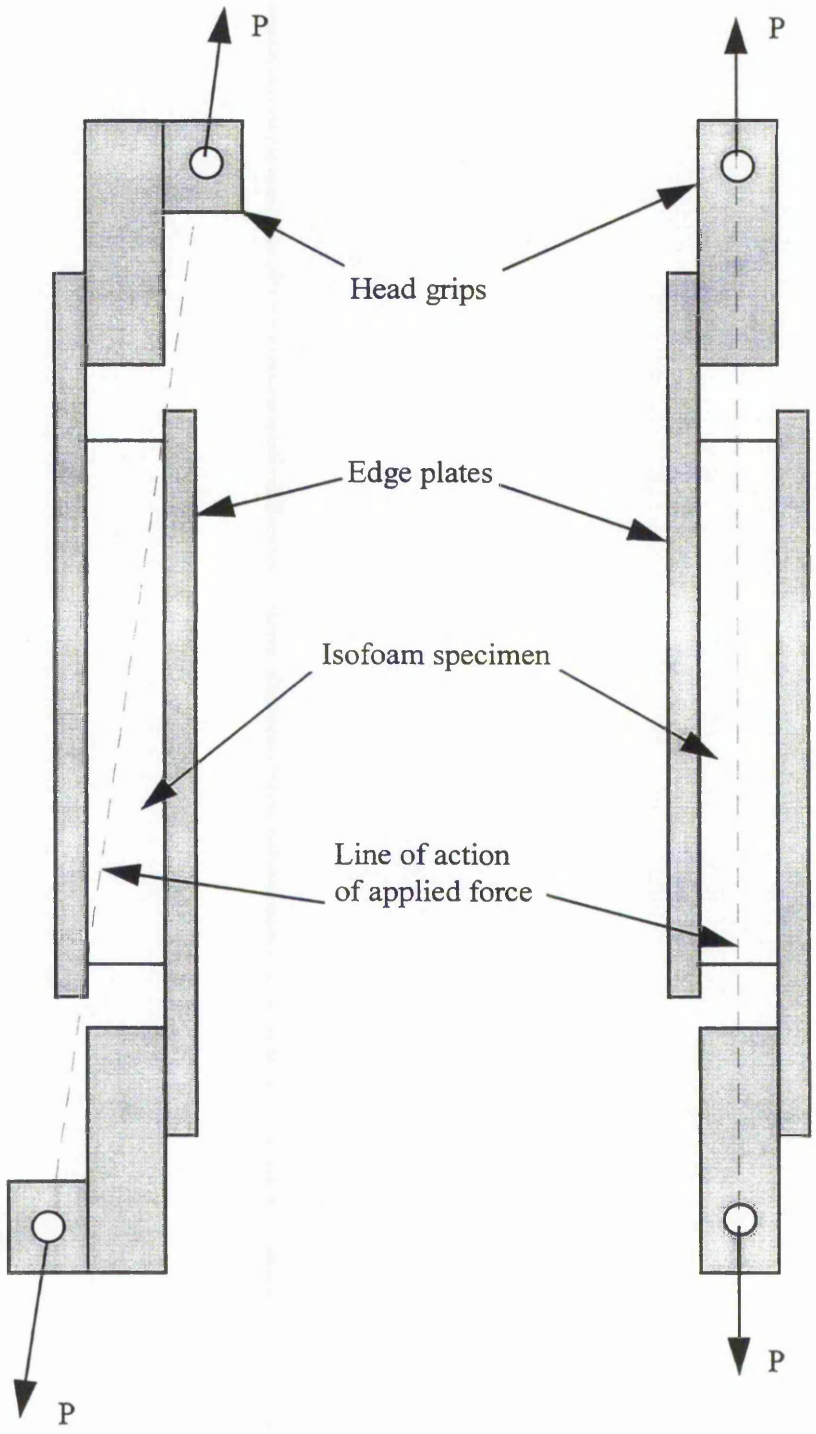

a. ASTM C273-61 b BS 4370

Figure 5.3 American and British Standard shear tests

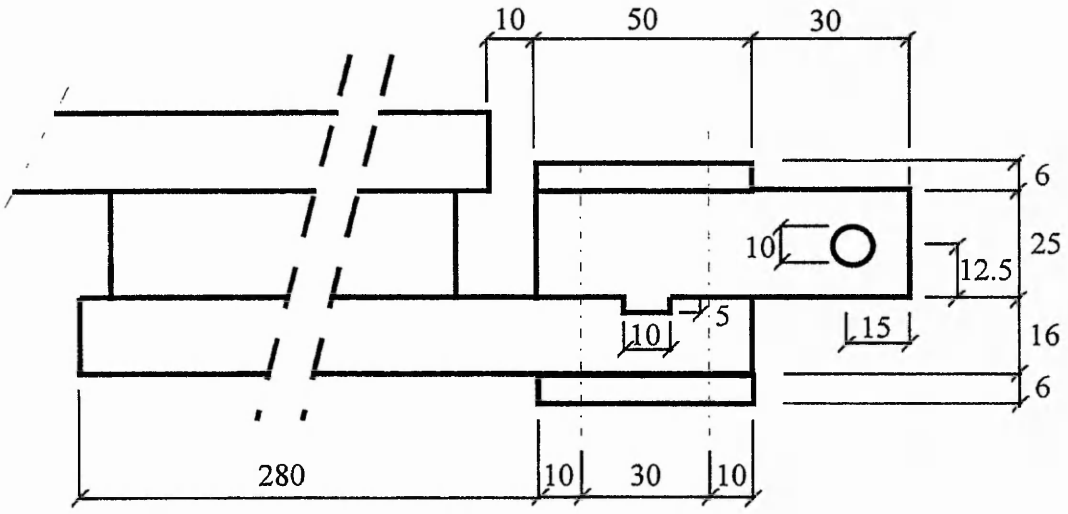

a. British Standard BS 4370

N.B. The dashed lines indicate the position of the centre line of the bolt holes.

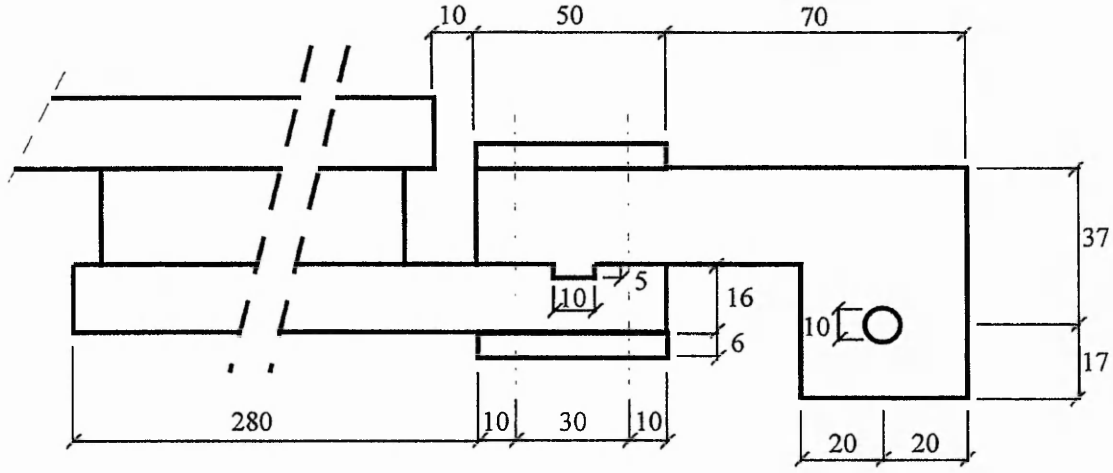

b. American Standard ASTM C273-61

Figure 5.4 Shear test head grip configuration

5.2.4 Conditioning and preparation of test samples

5.2.4.1 Environmental conditioning

The British and American Standards are very similar in the specification of the required environmental conditions. Both specify a base temperature of 23 °C with a discrepancy of +/- 2 °C and +/- 1.1 °C and a relative humidity of 50% with a discrepancy of 5% and 2% respectively. The test machine was located in the Textile Testing Laboratory which had full environmental control facilities. All specimens were placed in the laboratory for approximately 24 hours prior to their testing. The temperature of the laboratory ranged between 20.6 and 23.1 °C with a mean value of 22.0 °C, while the relative humidity varied from 53 to 67 % with an average of 58%. Although, the temperature was within acceptable limits the relative humidity varied more than the acceptable tolerances.

5.2.4.2 Dimensional control of the specimens

Specimens were cut using a fixed circular saw, which gave smooth and particularly parallel surfaces. All samples were measured, using a micrometer, prior to attachment to the edge plates. Allowable tolerances for the British Standard specimens were, length 250 +0 / -5 mm, width 50 +0 / -1 mm and thickness 25 +/- 0.5 mm. The American Standard specified tolerances of not greater than 1% for the length and width and 0.5% for the thickness. This relates to a maximum allowable 2.5 mm discrepancy in length, 0.5 mm in width and 0.125 mm in thickness. The thickness control for the American Standard appears very stringent but it must be remembered that it also covers all core thicknesses that may be used which may be significantly thicker in certain circumstances.

It was therefore decided that for dimensional tolerance acceptance the length of each specimen should be in the range of 247.5 - 250.0 mm, the width 49.5 - 50.0 mm and the thickness 24.5 - 25.5 mm. All specimens used in the shear test experiments were within

these dimensions. Specimens were first cut slightly larger than necessary, measured for dimensional tolerances and then re-cut to within tolerance.

5.2.4.3 Bonding of Isofoam CRF core samples to metal edge plates

It was felt that bonding of Isofoam CRF to metal edge plates was of an underestimated importance. The adhesive selected for use was a two part epoxy araldite, with a complete curing time of sixteen hours. Of particular concern was the thickness and effectiveness of the adhesive line. An adhesive line of 1mm thickness could constitute to a reduction in the effective thickness of the Isofoam specimen by some 8% causing a higher than expected shear modulus. It was felt that this was significant and so a series of pilot tests were conducted to find a suitable method of applying the thinnest possible adhesive line. Conversely, too thin an adhesive line applied and the effective shear surface between the specimen and the metal edge plate might be reduced leading to a lower than expected shear modulus.

The short series of trial runs, to check the testing equipment and the loading machine, was utilised for investigating a suitable adhesive line thickness. Two methods of controlling adhesive 'thicknesses' were investigated. Firstly, a metal plate with a 0.25 mm recess was slid manually up and down each edge plate with the excess adhesive being removed. However, the viscosity of the adhesive was too great, leaving irregular depths of adhesive. Attempts with a larger recess were also somewhat unsuccessful and another method was therefore required. It was found that by weighing out a fixed quantity of adhesive and using 'honed manual spreading techniques' with a smooth straight edged spatula, a reasonably even thickness could be achieved. Five weights of adhesive were tried; 2, 3, 4, 5 and 6 grams, 2 grams being the least mass that could reasonably be spread over the entire surface.

The five samples were tested to failure and the modes of failure noted. For the 2g adhesive mass failure occurred through debonding along one entire surface. The 3g adhesive mass had a similar failure although a shear plane at one end of the specimen had left a small piece of core on one edge plate while the remainder had debonded. The

4, 5 and 6g adhesive masses had similar failure modes. There was a shear failure across the specimen in the central third portion with roughly one half of the specimen remaining bonded to each edge plate. In addition, significant areas of foam were left on the edge plate where the main body of the specimen had come away. These areas ranged from 1 - 5 mm in thickness. This indicated that the adhesive line was sufficient for transferring shear stresses up to shear failure.

From this short evaluation of required adhesive 'thickness' it was decided to use a 4g mass, however, as only one of each were tested the adhesive mass would come under close inspection during the initial tests on samples from panels P1 and P2. Subsequently, it was found for all cases that this adhesive mass proved to be adequate in preventing debonding before some mode of shear failure had occurred. Occasionally, probably due to the manual application, there were small patches where debonding would occur between the edge plate and the sample.

Once the adhesive had been applied to the metal edge plates and the foam test piece located the sample was then placed on its side and two 'G' - cramps applied at approximately one quarter of the length from each end. The applied pressure from the 'G' - cramps was again manually administered to a point where, as a rule of thumb, a small amount of adhesive seeped from between the foam and edge plates.

Special care was taken to prepare both the metal and the Isofoam bonding surfaces as this could result in a poor bond. Dust and grease were removed from the edge plates using a soft cotton cloth dampened with trichloroethelene. The Isofoam samples were cleared of dust and cutting debris using a compressed air brush. An electronic balance was used to weigh the two adhesive constituents for exact quantity to give regular mix consistency.

5.2.5 Testing procedures

The test apparatus was placed vertically in the tensile loading machine, using the universal joint of the machine as the upper head grip and the lower universal joint

manufactured as part of the test apparatus. To reduce crosshead displacement errors caused by take-up in the head grips and loading machine an initial 5 Kg load was applied to all specimens before the full prescribed load ramp. The initial position of the head grips was considered to be standardised when a 5kg load was recorded. At this point the force-deflection plotter was 'zeroed' and the moveable machine head grips set to a speed of 1 mm/min. The scale of the graph plotter had been previously calibrated to accommodate the force-deflection curve.

All the specimens were subjected to British and American Standards configurations with damage during the first test being avoided by keeping the applied load well within the elastic range of the Isofoam core. The data from the pilot studies, on the adhesive line thickness, gave good estimates of the elastic modulus and shear strength for a load limit. A 'recovery' period of approximately 24 hours was allowed before re-testing.

The force-deflection output graph was controlled by a 'chart speed', plotted along the chart for deflection and the load range across the chart for the applied force. The load range used for the British Standard test was 500 kg with a chart speed of 20 mm/min and for the American Standard a chart speed of 50 mm/min.

5.3 Results and Analysis

5.3.1 Presentation of the results

The design of the shear test apparatus was such that each specimen could be tested under British and American configurations. Five specimens were tested from each of the panels P1-P6 and P8-P10. The shear modulii derived from crosshead displacements have been calculated directly from the loading machine graph plotter for both the American and British shear tests. The ASTM C273-61 test was carried out first and only up to a shear strain that was well within the elastic region.

The shear modulii have been calculated by defining the tangent to the curve, beginning where the initial 'play' in the apparatus and Isofoam assembly has noticeably been taken up. It is noted at this time that the method of manually drawing a tangent to the force/deflection curve is somewhat subjective. The task is made harder, and therefore potentially less accurate, by the influences of time dependant strains which create the curved plot. An increase in strain rate may have reduced the amount of creep, however, the increase could also have increased the stiffness of the Isofoam. It was felt necessary for the applied strain rate to be consistent to the experimental work throughout the project so 1 mm per minute was adopted for all shear tests.

To evaluate the shear modulus from the machine output chart, the gradient is first calculated. The chart strictly plots the force applied across the chart and the progress along the chart is the test duration (seconds), although this may then be directly related to deflection knowing that the speed of the machine's moving head was 1 mm/min with the chart plotted at 20 mm/min.

The crossplate deflections were measured by two LVDTs situated at mid height on either flank of the edge plates, with their deflections averaged. The LVDTs were programmed to record displacements at 8 second intervals and were activated a few intervals before the load ramp began. By comparing the point at which displacement began and the start times at the beginning of the of the crosshead graph with the crossplate readings it was possible to relate them to the applied load. Figures B5.1 and B5.2 show, for American and British Standard test configurations respectively, the crossplate displacement versus time relationship of sample from panel P8. The figures only show the elastic portion of the load displacement relationship of the foam core as the LVDTs were removed before the sudden nature of shear failure endangered them.

5.3.2 Presentation of the laboratory data analysis

The following equation 5.1 has been used to calculate the shear modulii for both crosshead and crossplate displacement measuring configurations.

$$G = \frac{c}{lw} \cdot \frac{P}{\delta} \quad \text{..... (5.1)}$$

In all cases, except panel P3 specimens, the dimensions were c = 25.0 mm, w =50.0 mm and l = 250.0 mm. The core thickness of panel P3, 21.0 mm, could not be used in the American Standard as the direction of load application would be different from the rest of the tests. Therefore, the core was cut out with 2.0 mm of facing remaining on each face of the sample. The shear modulus is then calculated using c = 21.0 mm. Table 5.1 summarises the laboratory results. Tables B5.1 and B5.2 hold the full test result details.

	ASTM C273-61 (1980)		BS 4370 Pt:2 (1992)	
Panel No.	G_{XH} N/mm^2	G_{XP} N/mm^2	G_{XH} N/mm^2	G_{XP} N/mm^2
P1	1.89	2.37	1.87	2.37
P2	1.39	1.52	1.30	1.45
P3	2.94	3.92	2.72	3.29
P4	2.61	3.31	2.39	3.13
P5	2.55	3.31	2.29	2.99
P6	2.41	3.15	2.24	2.80
P8	3.10	3.82	2.72	3.17
P9	2.13	2.64	1.90	2.23
P10	2.04	2.41	1.94	2.30

Table 5.1 Summary of American and British Standard shear test results

5.3.3. Discussion of testing and analysis

From initial observation of the results in table 5.1, it may be seen that for one particular sample, or averaged group of samples from one panel, there is a trend relating to the shear modulii values obtained for each of the four separate force / deflection methods. For all related American and British Standard tests the crossplate shear modulii are greater than the crosshead. Additionally, all related crosshead and crossplate modulii

are greater when subject to the American Standard test configuration than to the British Standard. The explanations for these results are discussed later.

Temperature and relative humidity variations were small (although the humidity levels were higher than standard recommendations) and it has been assumed that they have not had any influence on the discrepancies between the test methods. These discrepancies must therefore be attributed to the configurations of the two standards and to the two different methods of measuring the shear strains.

The suitability of using the raw test results directly as material property data in the finite element analysis and classical sandwich panel theory is discussed in chapter 7. As the variations in the laboratory results indicate, further investigation into these apparent discrepancies is warranted. The following section 5.4 describes the finite element modelling of the two methods and highlights the most appropriate one to use as material property data.

To complete the laboratory work control tests were conducted to evaluate any 'unseen' errors in the testing and subsequently a control test for each Standard was employed. The control tests were completed before any formal analysis had been made of the shear test configurations. Subsequently the control tests have proved to be fundamental in helping to identify the discrepancies between crosshead and crossplate displacement measurements as not all the differences could be explained by the inherent errors in the two measurement techniques uncovered in the finite element analysis and also reported on by O'Connor.

5.3.4 Control tests

As mentioned above, a control test to the range of shear tests conducted it was felt necessary to calibrate the loading machine and the two different test apparatus configurations. This investigation comprised bonding the two mild steel edge plates to a substitute block of aluminium. The object of this test was to have a zero shear strain present in the specimen, therefore isolating the displacement experienced by the

apparatus. As with the Isofoam coupons, the aluminium block was bonded using the two part epoxy araldite, although a very thin and evenly distributed adhesive line was more readily possible by a tighter clamping pressure. The results of the force / displacement plots are shown on figures 5.5 and 5.6.

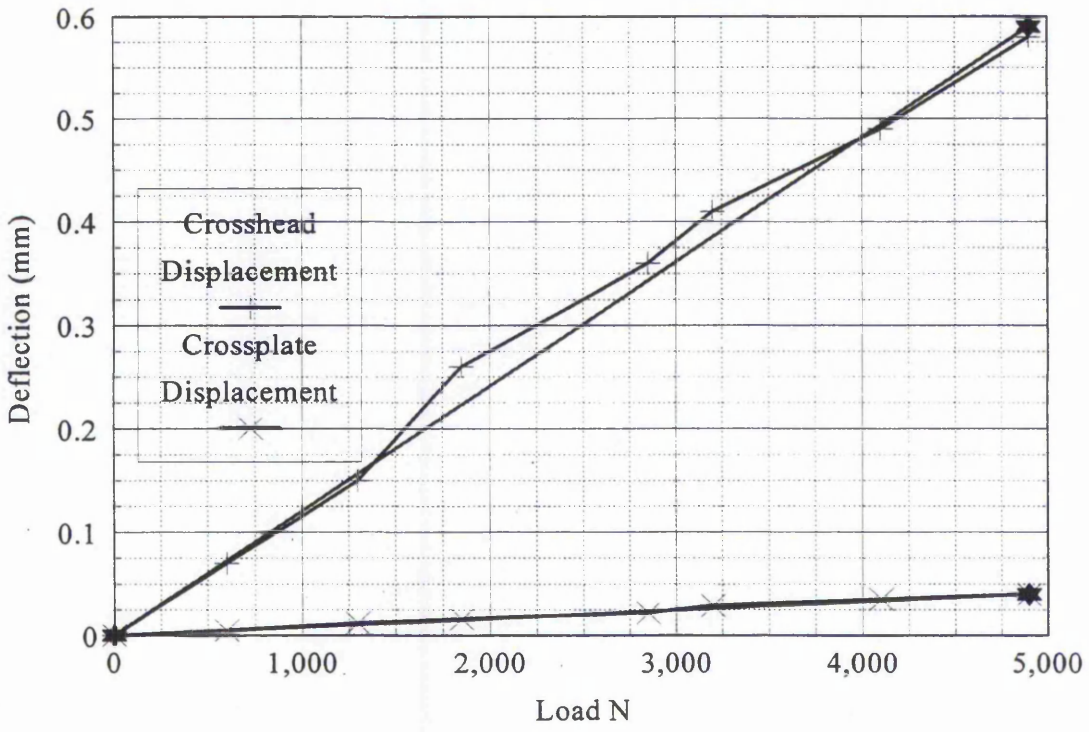

Figure 5.5 British Standard control shear test
load versus displacement relationship

The graphical displacement plots for the two shear tests show similar trends in that the crosshead displacement is significantly greater than the crossplate. This directly indicates that crosshead displacements are subject to additional influences to the shear strain of an Isofoam core sample from plate bending, edge effects and machine 'take-up'. The machine 'take-up' will have probably been due to the flexibility of the universal grips, bedding of the holding dowels and compression of machine components.

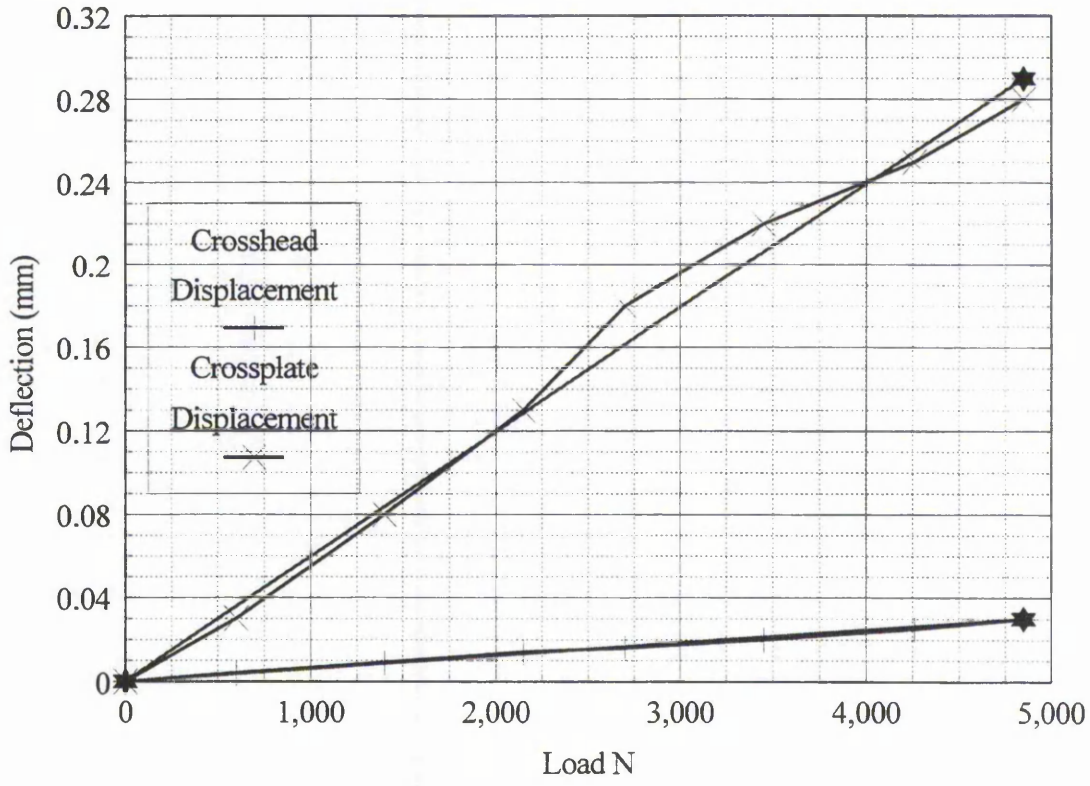

Figure 5.6 American Standard control shear test
load versus displacement relationship

Shear displacement of the aluminium block and two adhesive lines will also contribute to the overall shear displacement. If it is assumed that the shear modulus of aluminium is 26500 N/mm^2 and the adhesive is 385 N/mm^2 and the thicknesses are 25 mm and say 1 mm respectively, then the resulting shear strain due to the aluminium specimen will be

$$\delta_{al} = \frac{25 \times 500g}{250 \times 50 \times 26500} = 0.0004mm$$

$$\delta_{glue} = \frac{1 \times 500g}{250 \times 50 \times 385} = 0.001mm$$

from equation 5.1 allowing for a 500 kg load to be applied.

It would therefore be viable to assume that the crossplate displacement measurements would be negligible, however the actual displacements recorded were 0.05 and 0.04 for

British and American Standards respectively. These recorded displacements may in part be attributed to stress relief by fractures in the adhesive as audible cracking noises were present throughout the test. The significance of the control tests will be dealt with in the following sections.

5.4 Finite Element Analysis

5.4.1 Introduction

The objective of this finite element study is to identify and quantify the errors associated to the shear tests which are intrinsic to the apparatus configurations and displacement measurement methods. Throughout this F.E.A. investigation the software package SC01 has been used. The F.E.A. modelling consists of six noded, two dimensional, plane stress, triangular elements. O'Connor (1984) conducted an extensive finite element study of the then current American and British Standard shear test methods. Three error mechanisms common to both shear test methods were identified. The first was due to 'free' edge effects, incurred by the lack of continuity of the shear stresses at the free ends of the sample. These are mostly offset by using a long thin sample and are limited to approximately 3 to 4% of the theoretical value when using a sample with an aspect ratio of 10:1. Secondly, errors are derived from edge plate bending and which in turn were caused by the inherent eccentric load application. This error was minimised by specifying the use of a relatively stiff edge plate. Thirdly, rotation of the edge plates relative to one another was the cause of significant errors in the crosshead displacement measurements.

O'Connor concluded that errors inherent with crosshead displacement measurements were significantly greater than the associated crossplate measurement, with the errors being magnified when using thinner edge plates. Similarly an increase in specimen stiffness was also related to an increase in the magnitude of this error. The then British Standard was particularly sensitive to these error mechanisms as crosshead displacement and 5 mm 'thin' edge plates were specified in the standard. Additionally, the configuration of the head grips/edge plates caused high stress concentrations in the

corners of the specimen. The ASTM test configuration, with measurement of crossplate displacements, was found to be the most accurate method of shear modulus evaluation provided that the recommended plate stiffnesses were adhered to.

5.4.2 Finite element modelling of end effects

This section describes the finite element modelling techniques used and highlights how the modelling has been used to identify the test errors and how real shear modulus values have been obtained from the test results. The finite element modelling takes two forms, firstly a study to identify end effects and rotation of edge plates and secondly the modelling of the test configurations to enable a comparison of test methods.

End effects contribute to errors in shear response due to the absence of complementary shear forces acting on the ends of the shear test specimens. The degree of error is governed by the aspect ratio of the specimen. This finite element study is conducted to find the amount of error and to also justify the use of a specimen aspect ratio of 10:1 as opposed to 12:1 as specified for the American Standard.

The F.E.A. models consist of an Isofoam block and two edge plates, 50 mm wide, which are displaced 2.00 mm relative to one another, in a parallel direction but the plates have been allowed to rotate. Holding the plates parallel to one another induces a force in the y-direction which significantly alters the F.E. calculated shear modulus. Instead, allowing the plates to rotate provokes a bending moment throughout the plate, as in the actual apparatus, adding to test errors. The ends of the Isofoam block have no restraint. A plane stress and a plane strain analysis have been specified for the finite element modelling partly to show the difference. The plane stress analysis uses the thickness property of the shear test specimen, 50 mm. A number of models of varying aspect ratio have been analysed with a theoretical shear modulus of 2.5 N/mm^2 (elastic modulus = 6.00 N/mm^2 and Poisson's ratio = 0.2), the results have been plotted on figure 5.7.

For the plane stress model, it may be concluded that the error induced by using an aspect ratio of 10:1 and 12:1 is 3.6% and 3.0% respectively. The plane strain model has end

effect errors of 3.5% and 2.9% for the same aspect ratios. The difference of the two analyses coming from allowing a non-zero strain in the z-direction in the plane stress model. All further analysis is plane stress as this is strictly a truer representation.

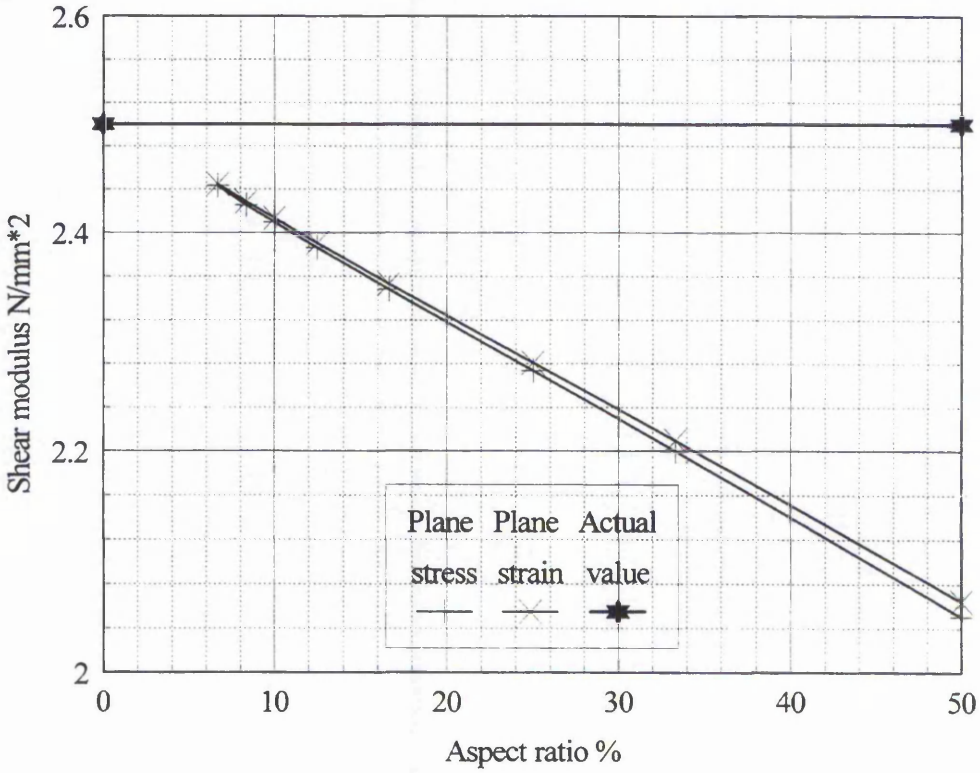

Figure 5.7 End effects: Effect of aspect ratio on plane stress and plane strain finite element models.

The finite element analysis investigation of the aspect ratios of the shear tests leads to the assumption that, although the American Standard is not quite followed exactly when using a 10:1 aspect ratio rather than 12:1, sensibly close comparisons may be made with little difference in shear modulus results between the aspect ratios.

5.4.3 Edge plate behaviour

O'Connor (1985) identified plate bending and plate rotation as important sources for errors in the evaluation of shear modulus values. It is principally the effect on the measured shear displacements of these two plate mechanisms that gives rise to the errors. The two mechanisms are difficult to distinguish as plate bending gives rise to the

relative plate rotation as well as the direction of the applied load path. A simplification may be assumed in order to provide a discrete dissociation of the two errors. Plate rotation may be defined as the whole shear test assembly turning around an axis and plate bending defined as the curvature of the plate along its own axis. It should be noted that the applied loading causes both of these mechanisms and without one there would not be the other in this instance.

5.4.3.1 Edge plate bending

The ASTM and BS shear test methods both have similar plate bending characteristics in that the plates bend in a convex manner (i.e. the plates curve into the specimen from the outer ends). Figures B5.3a and B5.3b show the y displacements of the two plates for the ASTM C273 and BS 4370 shear test methods respectively. The resultant displacement (x and y) has not been included as incorporation of the x component would dilute the scale of the graphs showing the plate bending effect.

Plate bending as mentioned before is the displacement along the plate relative to the original linear profile. The plot of y displacements along the outer face of the plates in Figures B5.3 a. and b. include both plate bending and plate rotation effects. Plate bending may be defined graphically by drawing a line between the points 1-1 and 2-2. It appears that the effect on measured displacements would be to reduce the recorded value for a given load. It may also be seen that the plate bending has the effect of 'shortening' the plate along its original axis. Shear modulus values would therefore be larger than otherwise expected. The trend of plate bending increases with specimen stiffness, as can be seen on figures B5.3 b., c. and d which have core elastic modulii values of 2, 6 and 10 N/mm^2 respectively. A Poisson ratio of 0.2 has been used for all three analyses. Both plates bend to the same degree as the test configuration is symmetrical.

5.4.3.2 Edge plate rotation

It should be noted that plate rotation is not the relative differential rotation of the two plates from each other, they remain essentially parallel, but the rotation of the whole test assembly. As the plates bend about their own axes the apparatus re-orientates itself so that the furthest possible distance between load points exists. Thus the degree of plate bending has a profound effect on the orientation of the apparatus. Importantly, the plate rotation re-directs the load path through the specimen from its originally intended line and this is where the error mechanism manifests itself. Figures B5.3 b., c. and d. show not only how the increase in stiffness of the specimen influences the amount of plate bending but also the degree of plate rotation. Plate rotation in the ASTM shear test is subject to the eccentric load path application from one corner of the specimen to the diagonally opposite, so this must be taken into consideration.

5.4.3.3 Overall effects of plate bending and rotation

The rotation of the assembly is particularly applicable to errors associated with the crosshead displacement measurement rather than the crossplate. The crossplate measurements will obviously be unaffected by the overall rotation of the apparatus as just the differential movement of the plates is recorded. Plate bending, at the mid-specimen position, causes the plates to separate by some 0.1mm (figure B5.3a and B5.3c), which is itself in the y-direction. It is therefore assumed that neither plate bending nor rotation has a significant effect on the actual measurement of the crossplate displacement. However, the recorded applied load may be influenced by both mechanisms. If the apparatus realigns itself to allow the load path of 'least resistance' and conversely the plate bending accounts for some of the applied strain energy in the overall system, then the actual applied load may be more than the necessary amount to just shear the specimen by the recorded displacement.

Evaluation of the effects of plate bending and plate rotation are difficult to assess due to the nature of available modelling techniques, although if the plates were given an artificially high elastic modulus then plate bending may be eliminated. This model

would then also require errors from end effect to be isolated before a satisfactory quantitative value is obtained. It is not envisaged that this will bring any further understanding to the identification of errors as the main thrust of the finite element modelling investigation has all the three error mechanisms built into it anyway. This section is merely an introduction to two of the error mechanisms.

5.4.4 Finite element modelling of test configurations

It was felt appropriate that a finite element modelling investigation was worthwhile as the British Standard specification had changed and more sophisticated modelling techniques were attainable since O'Connor's study was conducted. The main objectives were to establish the more accurate method of shear displacement measurement and the more accurate test method. The experimental results, shown in summary table 5.1, clearly indicate sizeable discrepancies between crossplate and crosshead modulii and smaller discrepancies between the British and American Standard test methods.

5.4.4.1 Model configuration

A two dimensional plane stress finite element model with a 50 mm thickness property was utilised for the investigation. The model simulated the exact physical dimensions as described in figure 5.3. It was assumed that the head brackets were secured so rigidly to the edge plates that no movement was present and a single solid mass could therefore be used for representation. A solid circular dowel was used as the support and load application points. A non-linear joint around the circumference of the dowel was given an initial clearance gap of 0.0001 mm which allowed the dowel and the head fixing to rotate freely. The clearance gap was assumed so small as not to influence the overall displacements. Figure B5.4a and B5.4b show the final mesh density and stress contours around the dowel used in for British and American Standards respectively.

The dowel joints are depicted on figures B5.4a and B5.4b with each stress contour plot showing three distinct circles. The inner circle gives an internal geometrical line to which support conditions were attributed, the middle circle represents the non-linear

joint between the external and internal faces of the dowel and head bracket respectively, and the external circle was present to complete the required mesh density in that location.

5.4.4.2 Element type

The shear test modelling has been completed using the SC01/3 finite element program and thus incorporates six noded parabolic two dimensional triangular elements. The automatic mesh generation may be governed by a specified structural accuracy or by forcing positions of node points by introducing breaks in the geometry. Forcing breaks in the geometry was more appropriately used for areas of highly changing stress gradients to increase local mesh densities. For instance, on figure B5.4a, each of the three geometric circles has been broken 32 times inducing 64 elements in the outer and middle portions while the inner area is divided into 32 elements.

5.4.4.3 Applied loading

The finite element model simulated the tests in the horizontal direction rather than the actual vertical direction with no effects of self weight accounted for. Additionally, the initial 5kg load applied at the start of each test was approximately the weight of the upper edge plate and head bracket hence negating the need to model self weight of the test apparatus. A prescribed displacement was given to one dowel while the other was fixed in the x- and y-directions. The prescribed displacement response was a more suitable loading condition, rather than an actual applied load, as the exact direction of the load path could then be maintained. The British standard test model displacement was a single translation in the positive x-direction of 2.00 mm, while the American loading displacement was 2.00 mm in the positive x-direction and 0.20 mm in the negative y-direction.

The loading for the F.E. analysis was prescribed as a single displacement controlled load ramp and as such did not account for the duration of the experimental load ramp of the actual shear test. Thus no time dependant creep effects were accounted for in the

analysis. However, the graphically represented experimental load / displacement response curve was approximated to with a linear tangential relationship hence negating the creep effects.

5.4.4.4 Model accuracy

Model accuracy has been determined by a convergence study based on obtaining a suitable structural accuracy to time ratio whilst not generating too large data and result files. The accuracy as mentioned above may be increased using a higher prescribed structural accuracy or more specifically by forcing the positions of nodes. Higher mesh densities have been forced around the dowels and over areas in the core material where there is a high stress gradient at the edges and corners, while using a structural accuracy of 1%. This percentage related to the continuity of stress gradient between elements at node points. The model has then been specified for structural non-linearity so that as the dowel and head bracket rotate new contact locations are mobilised throughout the iterative procedure.

The required output from the finite element models were the total force applied and relative crossplate displacements, the crosshead displacement being an inputted parameter. It was therefore appropriate to examine the accuracy of the model by looking at the convergence of the crossplate displacements. The total force, given by the reaction of a non-linear joint, does not converge with the value remaining constant throughout the increase in element numbers. A figure of element number against relative plate displacements has not been completed as only three elemental meshes were necessary to confirm model accuracy. The convergence study used the American Standard test configuration with an elastic modulus of 6.00 N/mm^2 and Poisson's ratio = 0.25. Table 5.2 gives the results of the convergence study.

Model #2 was selected as being the most appropriate, the final mesh for the British and American Standards may be seen on figures B5.5a and B5.5b, together with stress contour plots as described later. The final elemental mesh for the British Standard

configuration is obviously different around the head grip geometry, using fewer elements, however the mesh is comparably dense with some 1733 elements used.

	No. of elements	Relative crossplate displacement (mm)	CPU time (seconds)
Model #1	1024	1.9917	46
Model #2	1752	1.9942	63
Model #3	2245	1.9943	189

Table 5.2 Convergence study

Model #2 was selected as being the most appropriate, the final mesh for the British and American Standards may be seen on figures B5.5a and B5.5b, together with stress contour plots as described later. The final elemental mesh for the British Standard configuration is obviously different around the head grip geometry, using fewer elements, however the mesh is comparably dense with some 1733 elements used.

5.4.5 Results of modelling the behaviour of the shear tests with isotropic foam properties

5.4.5.1 Introduction to F.E.A results

A two dimensional finite element analysis, specifying isotropic material properties was used throughout this investigation. A range of orthotropic properties, for a three dimensional analysis, was considered but the advantage of this type modelling was far outweighed by the practicalities and significance of the overall thrust of the investigation.

As mentioned previously the aim of the finite element modelling is to establish the discrepancy between the actual shear modulus of the Isofoam coupons and those obtained experimentally. The finite element models simulate the test configurations and how they respond during testing so that known material properties may be compared to

those outputted from the computer simulated tests. The finite element modelling of the shear tests may be separated into two distinct parts. Firstly, the difference between crosshead and crossplate displacement measurements is examined and, secondly, the differences between the ASTM and BS methods are evaluated.

5.4.5.2 Examination of crosshead and crossplate measurements

A finite element model has been used to simulate, as accurately as possible, the exact laboratory conditions and apparatus configurations. In doing so, known material property values of the Isofoam core samples have been inputted and their associated computer generated laboratory output results compared. The outputted computer generated results will therefore be subject to the inherent test conditions and so the laboratory recorded test results may be corrected to real values. In this part of the finite element study, because the actual material properties of the specimen are not known and therefore cannot be inputted into the model, it is impossible to make a direct comparison between the finite element analysis and laboratory results so another comparative method must be used. However, to make the comparison as good as possible similar properties, from the uniaxial compression tests, are inputted into the computer analysis.

The investigation of crosshead and crossplate displacement measurements attempts a comparison of computer analysis and laboratory data by expressing the difference in displacement measurements in terms of the ratio of crosshead/crossplate shear modulii. Table 5.3 shows the comparison for samples taken from all panels; all values in the table are a percentage given by equation 5.3,

$$G_{XH/XP}\% = \frac{G_{XH} - G_{XP}}{G_{XH}} \quad \text{.....(5.3)}$$

The results in table 5.3 show the general trend, all values negative, that crosshead shear modulii are less than those derived from the crossplate modulii for both experimental and computer predicted analysis, i.e. the measured crosshead displacement is greater than the crossplate. It can also be seen that the F.E. modelling produces significantly different results to the experimental findings. This discrepancy is related to the 'ideal'

modelling output of the crosshead displacement as opposed to the actual laboratory conditions where there are significant errors related to measurement of crosshead response. The values in table 5.2 appear to have little significance until the findings from section 5.3.4, control tests, are incorporated into the results.

P1	F.E.A	Exp	P2	F.E.A	Exp	P3	F.E.A	Exp
BS	-0.6	-18.4		-0.4	-11.5		-0.5	-44.1
ASTM	-0.4	-25.4		-0.2	-9.4		-0.2	-33.3
P4			P5			P6		
BS	-0.8	-31.0		-1.1	-30.6		-1.1	-25.0
ASTM	-0.7	-26.8		-0.8	-29.8		-0.8	-30.7
P8			P9			P10		
BS	-1.2	-16.5		-0.9	-17.4		-1.1	-18.6
ASTM	-0.7	-23.2		-0.7	-23.9		-0.8	-18.1

Table 5.3 Percentage discrepancies between crosshead and crossplate displacements

Correction values, from the aluminium block control tests, have been applied to the measured displacements and then the shear modulii are re-calculated. Table 5.4 gives the values obtained from the control tests, represented on the figures 5.6 and 5.7 above, and are based on a 500 kg applied load,

	Crosshead displacement	Crossplate displacement
British Standard	0.59	0.04
American Standard	0.29	0.03

Table 5.4 Correction displacement values.

Superposition of the control tests directly on to the Isofoam shear test results reduces the recorded displacements for both the crosshead and crossplate measurements with the values in table 5.1 now becoming:

	ASTM C273-61 (1980)		BS 4370 Pt:2 (1992)	
Panel No.	G_{XH} N/mm^2	G_{XP} N/mm^2	G_{XH} N/mm^2	G_{XP} N/mm^2
P1	2.19	2.41	2.11	2.39
P2	1.54	1.54	1.41	1.46
P3	3.76	4.04	3.25	3.33
P4	3.23	3.40	2.79	3.14
P5	3.14	3.40	2.66	3.00
P6	2.93	3.23	2.58	2.83
P8	4.02	3.94	3.25	3.21
P9	2.53	2.69	2.15	2.25
P10	2.40	2.46	2.33	2.43

Table 5.5 Corrected American and British Standard shear test results by superposition of control tests

The corrected American and British Standard shear test results, by superposition of control test values, may again be scrutinised by examining the percentage difference between crossplate and crosshead measurement techniques in accordance with equation 5.3. The amended percentages are represented in table 5.6.

P1	F.E.A	Exp	P2	F.E.A	Exp	P3	F.E.A	Exp
BS	-0.6	-11.7		-0.4	-3.4		-0.5	-2.4
ASTM	-0.4	-9.1		-0.2	0.0		-0.2	-6.9
P4			P5			P6		
BS	-0.8	-11.1		-1.1	-11.3		-1.1	-8.8
ASTM	-0.7	-5.0		-0.8	-7.6		-0.8	-9.3
P8			P9			P10		
BS	-1.2	1.2		-0.9	-4.4		-1.1	-4.1
ASTM	-0.7	2.0		-0.7	-5.9		-0.8	-2.4

Table 5.6 Percentage discrepancies between crosshead and crossplate displacements

The same general trend for table 5.3 appears in table 5.6 in that the percentages are negative, indicating that the crossplate shear modulus is greater than the crosshead. This is true in all cases except for P8 specimens where the correction values have made the crosshead shear modulii greater. The percentage differences however, are markedly smaller indicating that the control tests have been useful in determining some of the difference between crossplate and crosshead results.

5.4.5.3 Comparison of actual modulii values to the outputted values from the finite element modelling

Much of the difference between crosshead and crossplate shear modulii values has been identified. It remains the task of relating test values to actual shear modulii and this may be done by considering the finite element modelling in terms of theoretical to calculated shear modulii. The theoretical material property data, actual theoretical values, are obviously known and therefore may be compared directly to the calculated data from the computer simulated laboratory test configuration. In doing so the errors of plate rotation, plate bending and free ends should be made apparent.

Figure 5.8 plots the relationship of Poisson's ratio against shear modulus for actual theoretical values used in the F.E. analysis of crossplate shear modulus values for the British and American Standards. The figure is generated by holding the elastic modulus constant while specifying varying values of Poisson's ratio. The computer model assumes that linear elastic theory is valid and thus an inputted elastic modulus of 6.00 N/mm^2 relates to a shear modulus according to $G = E / 2(1 + \nu)$. To quantify the errors shown in figure 5.8, from theoretical to test result, a percentage difference is calculated by the following equation;

$$G\% = \frac{(G_{FE} - G_T)}{G_T} \times 100 \quad \text{..... (5.4)}$$

Where $G\% =$ percentage error in shear modulus measurement

$G_{FE} =$ shear modulus from finite element model simulating test configurations

$G_T =$ linear stress/strain relation shear modulus for a uniform shear stress distribution

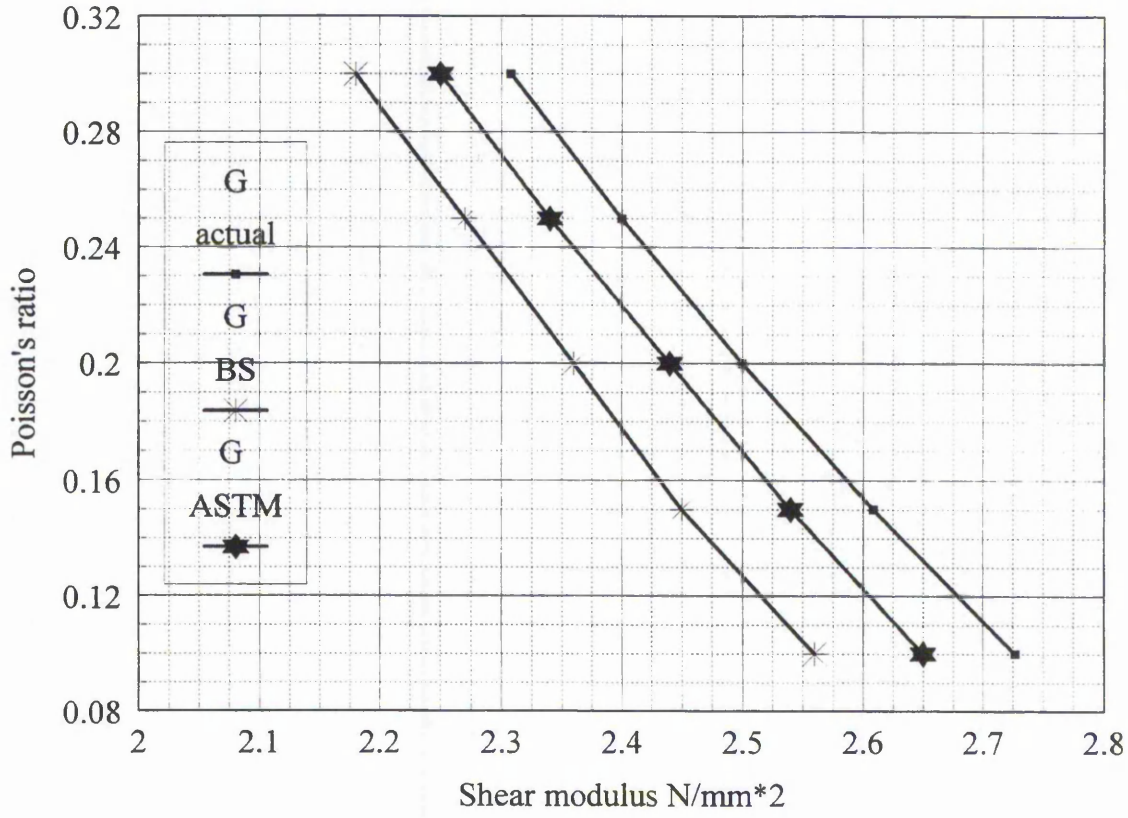

Figure 5.8 Relationship between Poisson's ratio and shear modulus for crossplate displacements

Percentage differences as described by the above equation are held in table B5.3 with a typical graphical representation shown below. Table B5.3 holds the inputted physical parameters of Poisson's ratio and elastic modulii and the percentages are derived assuming the actual shear modulus is derived from $G = E / 2(1 + \nu)$.

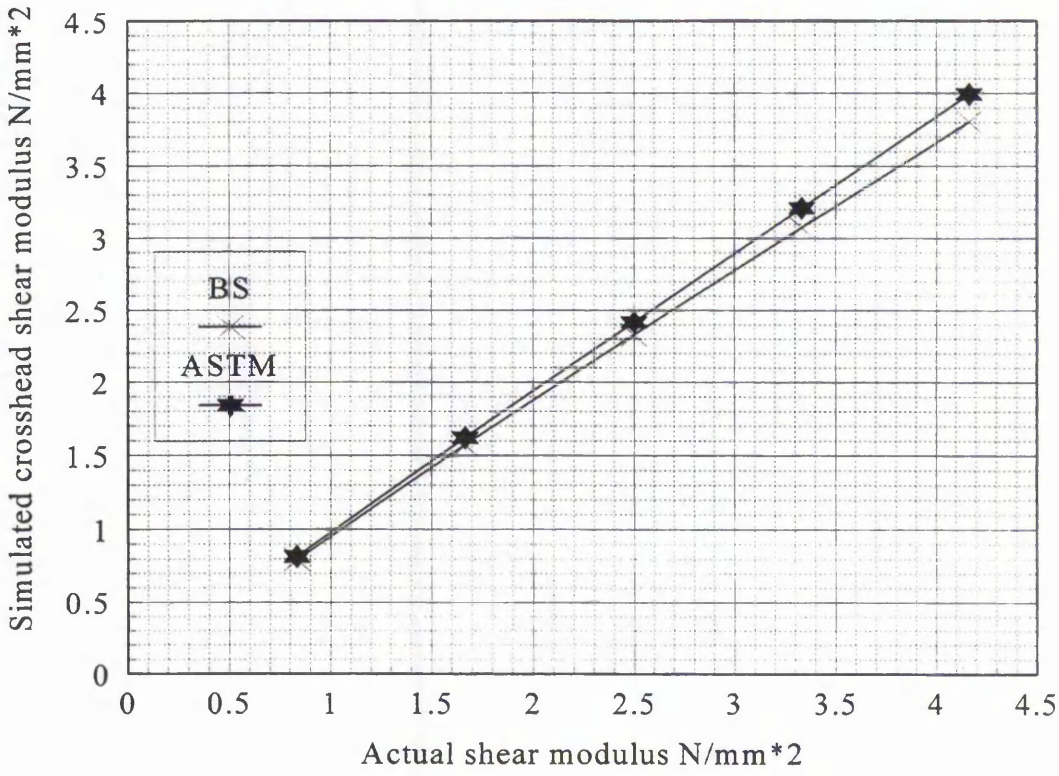

Figure 5.9 Relationship between actual shear modulus and F.E. modelled BS and ASTM shear tests

Table B5.3 contains the computer results for a range of Isofoam samples with various inputted elastic modulii and Poisson's ratios. Percentage differences for crosshead and crossplate measurements, from the theoretical values, for both British and American are also given. General trends in behaviour of the interaction between shear test assembly and the Isofoam specimen identified in the finite element study are:

(i) the stiffer the specimen the greater the percentage error

(ii) an increase in Poisson's ratio gives a smaller percentage error

(iii) the British Standard test configuration produces higher percentage errors than the American Standard for all specimen stiffnesses

(iv) crossplate displacement measurement errors are smaller than crosshead.

Corrected values may be extrapolated from table B5.3, but those specific to the samples in this project are set out in table 5.7.

		ASTM C273-61 (1980)		BS 4370 Pt:2 (1992)	
Panel No.	Poisson's ratio	G_{XH} N/mm^2	G_{XP} N/mm^2	G_{XH} N/mm^2	G_{XP} N/mm^2
P1	0.21	2.12	2.35	1.98	2.26
P2	0.22	1.50	1.51	1.33	1.39
P3	0.25	3.61	3.88	3.00	3.11
P4	0.20	3.11	3.30	2.58	2.94
P5	0.24	3.03	3.31	2.47	2.81
P6	0.24	2.83	3.14	2.40	2.66
P8	0.19	3.86	3.82	2.99	3.00
P9	0.17	2.44	2.62	2.01	2.12
P10	0.19	2.32	2.39	2.17	2.36

Table 5.7 Corrected American and British Standard shear test results by superposition of control tests and comparison to finite element analysis

5.4.5.4 General discussion of F.E.A. results

The test errors highlighted and discussed above are viewed as mechanisms arising from the apparatus and configurations used. The effects that the test apparatus had directly on the Isofoam sample is now discussed. It should be borne in mind that the object of the test apparatus is to impart an ideal uniform stress distribution throughout the sample. This section is not intended to evaluate any parameters involved only to add weight and understanding of the influences of the error mechanisms. The separate error mechanisms have already been discussed and they will not be cited for causing a particular anomaly in the core.

Figures B5.6 a. and b. show the stress contour plots of one end of the Isofoam core sample for the British and American Standards respectively. Stress concentrations are generated at each of the four corners of the sample in a reasonably symmetric pattern. The discontinuity of uniform stress near the ends covers approximately 25 mm which accounts for 20% of the overall length. Stress concentrates at these points due to the lack of complementary shear forces along the free ends.

Figures B5.7 a. and b. show the displacement response at the free ends for the British and American Standards respectively. The displacement contours clearly show bowing along the free edge and how therefore the stress concentrations are generated.

5.5 Discussion

Finite element analysis has identified, and as far as possible quantified, some of the errors inherent to the British and American Standard shear tests. Those errors are attributed to end effects, plate bending and plate rotation. Most significantly, however, is the identification of the crosshead displacement measurement error due to 'slack' or 'take-up' in the machine and test apparatus head grips as well as deflection of the test machine itself. This error was identified and corrected for the particular test apparatus by control tests. In practice, the crosshead displacement is widely used for the evaluation of the shear modulus as the results may be obtained directly from the test machine output. It is recommended that the crosshead displacements be calibrated against a control test similar to that described in this chapter.

There are however, outstanding inconsistencies between recorded values for the same sample when comparing British and American Standards. The American standard tests were conducted on the specimens first, prior to the British Standard, but as there was usually a 24 hour recovery period, this is not thought to have any great bearing on the results as a whole. The inconsistency of the two standards is further supported by the percentage differences 15% and 13% for crosshead and crossplate shear modulii respectively. The fact that the percentages are very similar indicates that there is

common discrepancy between the two standards rather than a difference between the two displacement measurement techniques. Temperature and relative humidity levels were kept well within acceptable tolerances so differences between tests should be insignificant.

It is tentatively suggested that one possible source for errors is damage to the specimens during the course of the American Standard testing. Although the tests were stopped within the elastic range there remained a degree of inelasticity with the displacement recorder not returning to the origin. The shear modulus was derived from a tangent drawn on the curved load/deflection plot. It has been assumed that the curve represents the influences of time dependant effects and so there would be a residual deflection that would then be recoverable between tests. However, this hysterisis may have some bearing on the following British Standard tests.

The only other discrepancy between the two methods not highlighted previously is the direction of load application through the specimen. The American Standard's 'corner to corner' load line shears the specimen over a length of 0.5% greater than that of the British Standard. This further discrepancy is again of only a small significance and does not finally resolve the discrepancies between the results. The finite element analysis models the ideal test configurations and has been instrumental in pinpointing and evaluating the test errors. Table 5.7, corrected American and British Standard shear test results by superposition of control tests and comparison to finite element analysis, gives the final shear modulii values.

The three error mechanisms identified by O'Connor are all borne out in this finite element study. The F.E.A. results in table B5.3 only show a 0.4% to 1.7% error difference between crosshead and crossplate shear modulus values. This discrepancy probably describes the difference of influences of edge plate bending and rotation between the crossplate and crosshead displacement measurements. Although both edge plate bending and rotation affect crosshead and crossplate displacements, it is assumed that the percentage differences given above quantify the two error mechanisms. The errors due to end effects have been evaluated, in section 5.4.2, to be approximately 3%

to 4%, depending on specimen stiffness, which would then lead to the assumption that the errors due to plate bending and plate rotation are approximately 2% to 5%.

Although there are remaining discrepancies between the American and British Standards that are not clearly definable, it is not suggested at this stage which is the more accurate method. The ultimate comparison of shear test results will be conducted in chapter 7.

5.6 Conclusions

The finite element study has verified the occurrence of error mechanisms and has been used to correct the laboratory results. These error mechanisms are derived from the way in which the apparatus configurations transfer and apply the shear load to the specimen. The following conclusions may be made;

(i) Shear modulii values derived from crosshead displacements incorporate large errors and the raw laboratory data should be treated with caution. This is true for both American and British Standard test methods. A major source of crosshead error is attributed to the 'slack' or 'take up' in both the loading machine and the test apparatus assembly. Evaluation of this additional crosshead displacement, through an aluminium substitute shear block control test, may be used to find a more accurate shear modulus value. The control tests implemented in this investigation are specific for the apparatus used. It is recommended that this procedure be adopted for particular apparatus if crosshead displacements are used for shear modulus evaluation.

(ii) Finite element analysis has quantified the error due to test configurations. Aspect ratio errors are found to be between 3% and 4% depending on specimen properties, increasing with stiffness. Plate bending and rotation errors were inherent with each other and evaluated to be 2% to 5% again increasing with an increase in specimen stiffness.

(iii) The difference between American and British Standard shear modulus evaluations are 15% and 13% for the crosshead and crossplate measurement techniques respectively.

(iv) The difference between crosshead and crossplate shear modulii are 5.6% and 7.5% for the American and British Standards respectively.

(v) The finite element analysis investigation of the aspect ratios of the shear tests leads to the assumption that, although the American Standard is not quite followed exactly when using a 10:1 aspect ratio rather than 12:1, sensibly close comparisons may be made with little difference in shear modulus results between the aspect ratios.

(vi) General trends in the interaction of test apparatus and shear specimen concluded from the finite element study are:

a. the stiffer the specimen the greater the percentage error
b. an increase in Poisson's ratio gives a smaller percentage error
c. the British Standard test configuration produces higher percentage errors than the American Standard for all specimen stiffnesses
d. crossplate displacement measurement errors are smaller than crosshead.

(vii) The importance of the bond between sample and edge plate is of an underestimated importance. The pilots studies were wholly vindicated in identifying a suitable adhesive thickness (in fact an adhesive mass) so that the thinnest possible adhesive line could be applied. A 1mm thick adhesive line could influence the results by some 10% and too thin an adhesive line could result in a much larger error.

CHAPTER 6 - MULTIPLE SPAN BEAM TESTING AND ANALYSIS

6.1 Introduction

6.2 Theoretical development

6.3 The conjugate point method

6.4 Test Methods

6.5 Results and Analysis

6.6 Plywood bending tests

6.7 Discussion

6.8 Conclusions

CHAPTER 6 - MULTIPLE SPAN BEAM TESTING AND ANALYSIS

6.1 Introduction

6.1.1 General

This section of work focuses on the multiple span beam testing (MSBT) technique which has been employed here to evaluate material property data of principally the Isofoam CRF cores and in part the plywood facings. The properties have been assessed to provide appropriate support for the analytical modelling of the full scale sandwich panel tests discussed in chapter 7. The MSBT technique has been chosen as an additional material property evaluation method for two reasons. Firstly, the MSBT technique appears to be a more appropriate method than small coupon tests as it produces similar flexural characteristics in the Isofoam CRF core as is found in the panel bending tests. Secondly, during the uniaxial and shear test programmes, relatively small specimens sizes were used. These were subject to the variations in the quality of the Isofoam masses as the variation of results highlights.

As will be seen the MSBT method takes several forms, one of which requires the elastic modulus of the plywood facings to be independently assessed prior to analysis. Section 6.6 contains the evaluation of plywood properties, by four point load beam testing, which has been referred to in the earlier sections of this chapter.

6.1.2 Multiple beam span testing literature

Multiple span beam testing has been conducted to evaluate the shear modulus of the Isofoam CRF core directly from flexural bending tests on beams cut from the complete sandwich panels. In addition, the technique may also be used to find the elastic modulus of the facings. The multiple span beam testing method involves obtaining the load / deflection characteristics of a single, simply supported, beam over a sufficient range of different span lengths. The beams may either be cut to a new length for each change in

span or left with an overhang. From the experimentally determined load / deflection relationship and length of span, a graphical representation may be made to isolate the influences of shear stiffness of the core and elastic modulus of the facings.

The multiple span beam testing technique was first proposed and investigated by Doherty, Ball and Walker (1965) when considering the physical properties of rigid urethane foam sandwich panels. The technique involved the original March (1944) equation for the mid-span displacement of a sandwich beam. Norris, Ericksen and Kommers (1962) contributed amendments to the theory which accounted for thick faced sandwich response. Allen (1967) then applied his thick faced theory to the multiple span testing method.

Although Allen's theory had been developed for overall thick faced response, it did not allow consideration of localised point concentrations (load and support contact locations) that caused displacements of the facing separate to the overall beam deflections. O'Connor (1988) later proposed the 'conjugate point method'. This method utilises recorded displacements at positions outside the zones of influence of the point effects. In addition, as relative displacement positions were used, the effects of local bending of the facings and compression of the core at the support points was negated.

The principal of the multiple span beam testing method stems from the fact that the original March equation (6.1), for the deflection for a three point loaded sandwich beam, includes two unknowns, the shear modulus of the core, G_c, and the elastic modulus of the facings E_f. However, when the equation is re-written in the linear form y=mx + c, equation 6.2, and graphically represented using the laboratory results for the load / displacement relationship for each different span, the two unknowns, E_f and G_c, may be evaluated from the gradient and the intercept respectively. Further development of the multiple span testing method is discussed in section 6.2.

$$\delta = \frac{PL^3}{48E_fI} + \frac{PL}{4AG_c} \quad \text{..... (6.1)}$$

$$\frac{\delta}{PL} = \frac{1}{48E_f I}.L^2 + \frac{1}{4AG_c} \quad \text{..... (6.2)}$$

where $y = \frac{\delta}{PL}$, $m = \frac{1}{48E_f I}$, $x = L^2$ and $c = \frac{1}{4AG_c}$.

6.2 Theoretical development

6.2.1 Doherty et al (1965): ordinary bending theory

The multiple span beam testing technique was first examined, through a series of tests on sandwich panels containing a rigid urethane foam core with various facing materials, by Doherty et al (1965). This method uses the original March (1944) equation, but in a rearranged form, for the mid-span deflection of a beam under a symmetric 3-point load configuration. The rearrangement of the original March equation may be made in two ways, and hence two different graphical outputs are possible, as will be described later. For further reference the two methods are described as type 1 and type 2 and have been described below.

For both method types, the technique starts by testing a single beam at a number of different spans using a series of equal load increments at each span. The mid-span deflection is recorded at each increment and span to find the load / displacement relationship, typically shown in figure 6.1. Throughout the work described in this text all beams were cut to the appropriate span length. An overhang may be used although its inclusion merely adds to further thick faced response in the beam and a more complex solution is required.

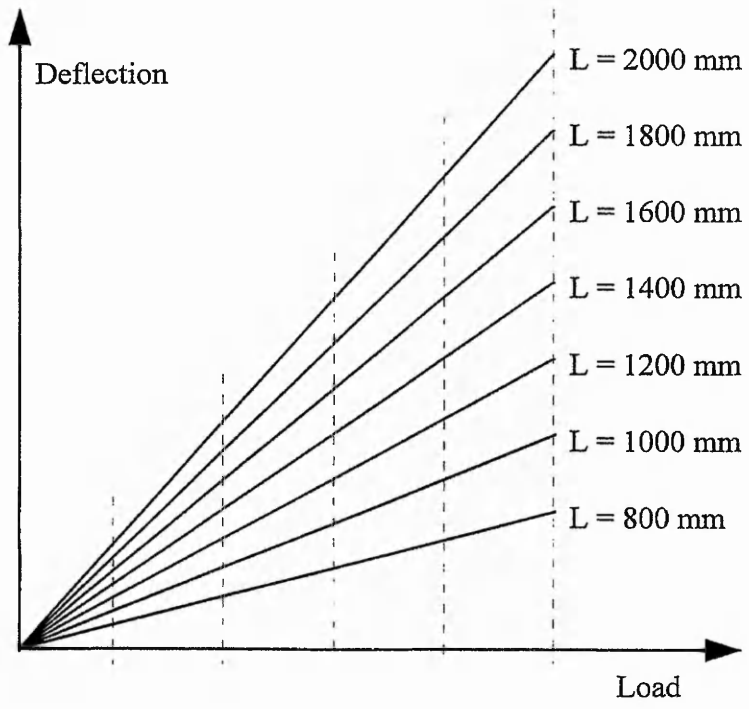

Figure 6.1 Load displacement plots for varying spans of the same beam

The gradient of each line represents a single beam span and yields the deflection per unit load for each beam. This may then be used in equation 6.1 to find the elastic modulus of the facings and the shear modulus of the core. To do this, equation 6.1 must be rewritten in the form of $y = mx + c$ as in equation 6.2a, δ/PL is then plotted against L^2 as shown on figure 6.2.

$$\text{Type 1} \qquad \frac{\delta}{PL} = \frac{L^2}{48EI} + \frac{1}{4AG} \quad \ldots\ldots\ldots \text{(6.2a)}$$

A tangential line drawn on the upper linear portion of the curve and extended to the vertical axis is used to isolate the shear modulus of the core and the elastic modulus of the facings. The intercept value on the vertical axis is therefore equated to 1/4AG and the slope of the line equated to $1/48E_fI$, thus the shear modulus of the core and the elastic modulus of the facings may be found.

Alternatively, equation 6.1 may be written in the form, where δ/PL^3 versus $1/L^2$ is plotted for each span length on figure 6.3.

Type 2 $$\frac{\delta}{PL^3} = \frac{1}{48EI} + \frac{1}{4AG}.\frac{1}{L^2} \quad \text{.....(6.2b)}$$

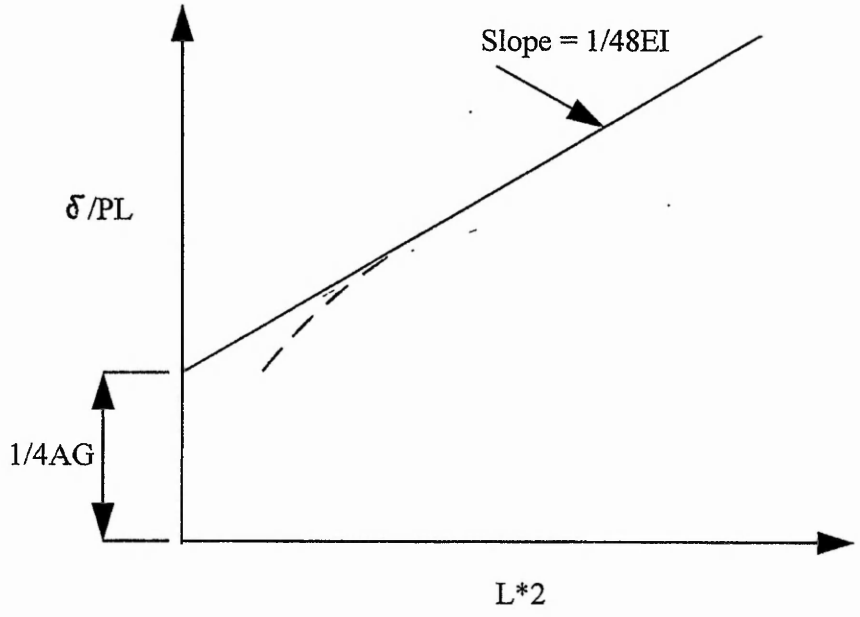

Figure 6.2 (Type 1) Representation of δ/PL versus L^2

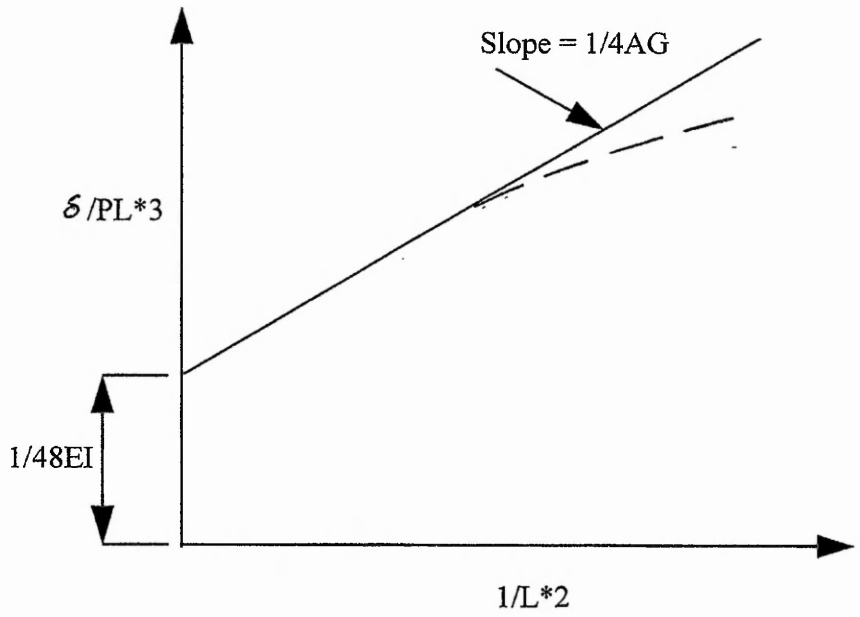

Figure 6.3 (Type 2) Representation of δ/PL versus L^2

Similarly, a tangential line drawn on the lower linear portion of the curve and extended to the vertical axis is used to isolate the elastic modulus of the facings and the gradient of the line yields the shear modulus. The intercept value on the vertical axis is therefore equated to $1/48E_fI$ and the slope of the line equated to $1/4AG$, thus the shear modulus of the core and the elastic modulus of the facings may be found.

The method as presented by Doherty et al (1965), described above, is more appropriate to applications with thin faced sandwich beams. When considering thick faced sandwich beams there are two influencing factors which have not been accounted for. Firstly, local compression at the support positions contribute to overall displacement at the mid point and should therefore be taken into consideration during experimental investigation of the load / displacement response. Secondly, thick faced beams are subject to local bending effects caused by the inherent stiffness of the facings themselves near point concentrations. These thick faced effects cause both graphical plots, figures 6.2 and 6.3, to be non-linear in nature. This can be identified by observation of the range of beams tested by Doherty et al which included various types and thicknesses of facings. Doherty et al point out that whereas one set of beams gives good agreement to the proposed theory another set does not. This phenomenon may be traced to the different types of facings used and whether each facing may have had a significant degree of self-stiffness. From simple four point bending tests conducted on the facing material, the stiffness of the two types of facing used in the experiments were some eight times different. This suggests that thick faced effects were more significant for one beam type than the other, hence the discrepancy of experimental and theoretical results encountered.

6.2.2 Allen (1967): inclusion of thick faced effects to Doherty et al

Allen (1967) revised the ordinary bending theory of March (1944) by adding a term to the shear displacement component of the overall mid-span deflection equation which accounted for the thick faced effects. This more comprehensive theory is described in detail in chapter 3, and shown as equation 6.4;

$$\delta = \frac{PL^3}{48E_f I} + \frac{PL}{4AG}\left(1 - \frac{I_s}{I}\right)^2 \psi \quad \text{..... (6.4)}$$

The method proposed by Allen (1967, 1969), differs from that of Doherty et al (1965) by the additional factor applied to the shear deflection (the right hand term of equation 6.4) accounting for thick faced effects. The squared bracket term is a geometrical shape factor based on the relative values of the second moment of area of the facings to the overall second moment of area of the complete sandwich panel. Usually this geometrical shape factor accounts for less than 1% of the total deflection. More significant is ψ which governs the non-linearity, shown by the dashed lines in figures 6.2 and 6.3, attributed to thick faced response.

$$\psi = 1 + \left[\frac{2\sinh(aL_1)(1 - \cosh aL/2) - \sinh(aL/2)\cosh(aL_1)}{(aL/2)\cosh(aL/2 + aL_1)}\right] \quad \text{..... (6.5)}$$

where

$$a^2 = \frac{AG}{E_f I}\left(1 - \frac{I_f}{I}\right)^{-1} \quad \text{..... (6.6)}$$

Thus the slope of the experimental plot on figure 6.2 is now factored as follows:

$$\text{Slope} = \frac{1}{4AG}.\left\{1 - \frac{I_f}{I}\right\}^2 \psi \quad \text{..... (6.7)}$$

This revised method, described by Allen (1967), accounts for the thick faced effects encountered during bending tests, however, in practice the deflections are recorded at the mid-span, under the central load point. Allen recommend that the deflections directly over the supports, due to local bending of the facings and compression of the core, be experimentally measured and superimposed on the overall recorded deflection of the beam at mid-span.

Allen went on to make a further recommendation to enhance the accuracy of laboratory results by plotting several curves, from equation 6.4, around the approximate value of the initial experimental shear modulus. Allen then commented that where the experimental curve intersects a theoretical curve, the shear modulus may be obtained. Furthermore, a greater emphasis should be placed on the results at longer spans as these are subject to proportionally less point effects. For a given load applied to a sandwich beam with thick facings a local distortion will occur under the load point. This distortion will be identical for that beam at any span length. The mid-span displacement, on the other hand, will increase as the span increases. Thus at longer span lengths the significance of the local distortions diminishes when compared to the overall beam displacements.

6.2.3 O'Connor (1985): the conjugate point method

O'Connor (1985) investigated the displacement analysis of thick faced beams. Here a different approach to the multiple span testing technique led to the proposal of a 'conjugate point method'. Theoretically, this method suggests that more appropriate shear modulii could be found during the experimental determination of sandwich stiffness properties by the MSBT method. Fundamentally, it was proposed that deflections were recorded at positions on the beam at a suitable distance away from the influences of load points. O'Connor proposed that two associated displacement positions within the span would give a better result of flexural response than the mid-span position. In effect O'Connor replaces the assumed datum position, the support point, for the mid-span response with another away from point effects.

6.3 Conjugate point method

6.3.1 Background

O'Connor's (1985) study of thick faced response of sandwich beams using Allen's thick faced theory, included the investigation of longitudinal stress distribution throughout the beam. A finite element analysis of the stress field near point loads and experimental

data confirmed Allen's theory. The study identified that the stress concentrations present under load points were an important aspect of the thick faced response. These localised stress concentrations were found to diminish to zero at a specific distance from the point load when considering a continuous beam. Similarly, the displacements near to the load concentrations were found to be significantly distorted due to the localised bending of the facings about their own centroidal axis. The distance either side of the load position, influenced by the point effects, was proven to be a distance of $\theta x = 5$, where $\theta = al_1$ and

$$a = \sqrt{\frac{AG}{E_f I_f (1 - I_f / I)}} \quad \text{..... (3.23)}$$

It can be seen from the above equation that the function 'a' is dependent on the shear stiffness of the core, AG, the relative stiffnesses of the facings, $E_f I_f$, and the overall beam stiffness and will obviously vary according to the geometric properties of the beam.

Point concentrations, for instance support locations, at a discontinuous part of the beam are not subject to the same peak stresses as a continuous span and are therefore not similarly considered. The peak stresses at discontinuities are not as marked as those at continuous sections of sandwich beams as the stresses quickly dissipate to zero at the end of the beam. Figures D7.4 to D7.8 show the worst two dimensional stress contour profiles from the finite element analyses of panels P3 to P6 and P10. As can be seen at the support end, the stresses dissipate to values close to zero. The small residual values are attributed to through thickness stresses and Poisson's ratio effects. It can also be seen that peak stresses around the support locations are significantly less than those at the load point, even considering the difference in magnitude of loads. The reaction load being half the applied mid-span load.

O'Connor's conjugate point theory for the determination of material property values from multiple span beam testing was based on the displacement measurement of two relative locations in the span, both away from the influences of point concentrations.

Multiple span testing techniques and theory have been put forward for three, four and five point loads, however, in the light of O'Connor's investigations it is apparent that it would be most appropriate to use a three point load technique. This would then limit the number and thus length of span that would be subject to thick faced effects around point concentrations. Furthermore, beams with no overhang are more suitable as this configuration prevents the peak stresses from arising at support points.

The proposal for the conjugate point method is supported by the fact that previous evaluation of material properties employing the multiple span testing technique, Doherty et al (1965) and Allen (1967), have taken deflection measurements at the position of the load concentration, further corrupting accurate displacement measurement. The inaccuracies encountered in the investigation of the multiple span beam testing method by Doherty et al are related to the use of the mid-span displacement. The divergence of experimental and theoretical curves shown on Type 1 and 2 graphical representations, using the method of Doherty et al, increases as the span length decreases. This suggests, as described earlier, that the local distortions begin to have a greater proportion of the overall displacement response recorded.

6.3.2 Critical span concept

O'Connor's investigation of localised point concentrations and their effect on deflections, shear stresses in the core and principal facing stresses uncovered the phenomenon of the critical span concept. The critical span concept may be summarised as the distance over which either side of a point load, the facing is influenced by a stress concentration. O'Connor defines the distance as $\theta x = \pm 5$. It was found that $\theta x = ax$, where 'a' is a non-dimensional term that relates the stiffness of the facings to the shear stiffness of the core and is given by equation 3.23. The definition of 'a' may be found in chapter 3. The local bending of the facing about its own centroidal axis under a point load smoothes out the discontinuity of shear displacement in a finite distance from the contact point. The local bending gives rise to secondary facing moment M_2 which is the principal cause of the elevated facing stresses. In turn there are changes to the local displacements and core shear stress response. O'Connor showed that the distribution of

secondary moments were directly related to point concentrations and that each equation for secondary moments at any point concentration may be reduced to;

$$\beta x = [\beta \cosh \theta x - \sinh \theta x] \ldots\ldots\ldots (6.8)$$

The function βx dissipates exponentially, reducing to an assumed zero value at a longitudinal distance $\theta x = 5$ from the point concentration. It was then argued that any sandwich panel with any type or form of facing experienced some degree of thick faced action. Sandwich beam definitions relating to thin, thick or very thick constructions may then be discussed with regard to the critical span concept when considering load points.

6.3.3 Conjugate point theory

Conjugate point theory uses Allen's thick faced theory for displacements in a simply supported span with a central load and no overhang as detailed in chapter 3. In practice an overhang of 10 mm or less was present so that the beams would not slip off their supports during loading. It is assumed that this overhang is not significant to the bending stiffness of the beams. Equation 3.33 is formulated for the solution to above configuration when considering half the beam as a cantilever span as shown in figure 6.4;

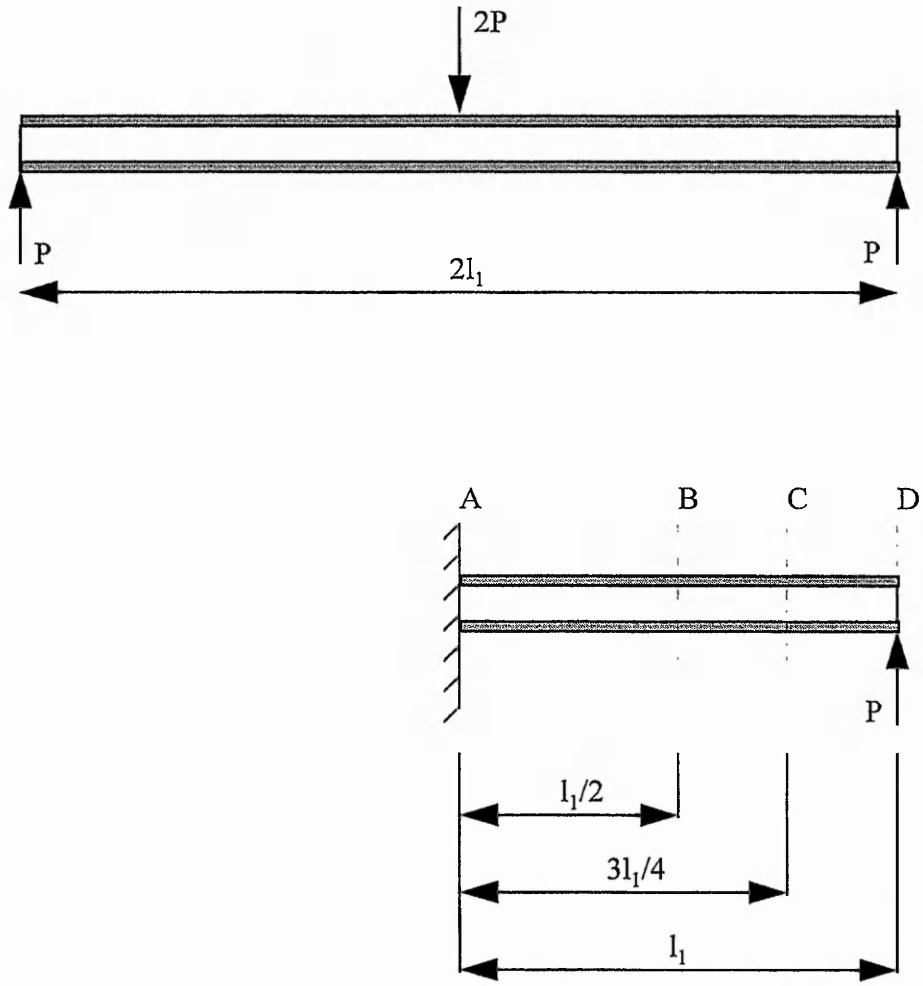

Figure 6.4 Position of conjugate points on a cantilever span

for span AB (x measured from A), positive deflection upward

$$\omega = \frac{Px^2}{6EI}(3l_1 - x) + \frac{Px}{AG}\left(1 - \frac{I_f}{I}\right)^2\left[1 - \frac{1}{ax}\left(\beta_1 - [\beta_1 \cosh ax - \sinh ax]\right)\right] \text{.....(3.33)}$$

The general displacement equation 3.33 may then be described in a different format for ease of manipulation,

$$\omega = k_1x^3 + k_2x\left(1 - \frac{1}{\theta x}[\beta_1 - \beta x]\right) \text{ ..... (6.9)}$$

where

$$k_1 = \frac{P}{3EI} \quad \text{..... (6.10)}$$

and

$$k_2 = \frac{P}{AG}\left(1 - \frac{I_f}{I}\right)^2 \quad \text{..... (6.11)}$$

and where $\theta = a$; $\beta_1 = \tanh\theta$ with no overhang; and

$$\beta x = [\beta \cosh\theta x - \sinh\theta x] \quad \text{..... (6.8)}$$

so that now

$$\omega = k_1 x^3 + k_2\left(x - \frac{1}{a}[\beta_1 - \beta x]\right) \quad \text{..... (6.12)}$$

Additionally, when $\theta > 5$ $\beta_1 = \tanh\theta$ tends to unity and $\beta x = 0$.

The above conditions therefore imply that outside the critical span, or $\theta x > 5$, thin faced sandwich action is precedent and only in the critical span does thick faced action exist. The proposal for the determination of material properties in the multiple span testing technique, employing the conjugate point method, thus indicates that displacements recorded outside the critical span concept are now given by reducing equation 6.12 to;

$$\omega = k_1 x^3 + k_2\left(x - \frac{1}{a}\right) \quad \text{..... (6.13)}$$

The theory developed in chapter 3 is given for a cantilever beam with a single point load which is positioned at the outermost point on the span. Deflections are therefore relative to the stationary encastre support with positive displacements in a positive y-direction (or upwards). Deflections deemed most suitable for use in the conjugate point method are at the support, eighth and quarter span. These three locations may be used

in any pairing to provide conjugate displacement points. The three point load configuration has been simplified by symmetry as shown in figure 6.4.

The original mid-span position is now assumed to be an encastre support with the original support point becoming the load point. The displacements at the original support, eighth and quarter span positions, are therefore relative to the new encastre support position for a unit cantilever load, and are given as follows in accordance with equations 3.33 and 6.14 to 6.16 and shown on figure 6.5. These equations are presented in accordance with those set out by O'Connor (1985). Equations 6.17 to 6.19 give the conjugate displacements for relative span positions $(\delta_0 - \delta_8)$, $(\delta_0 - \delta_4)$ and $(\delta_8 - \delta_4)$ respectively.

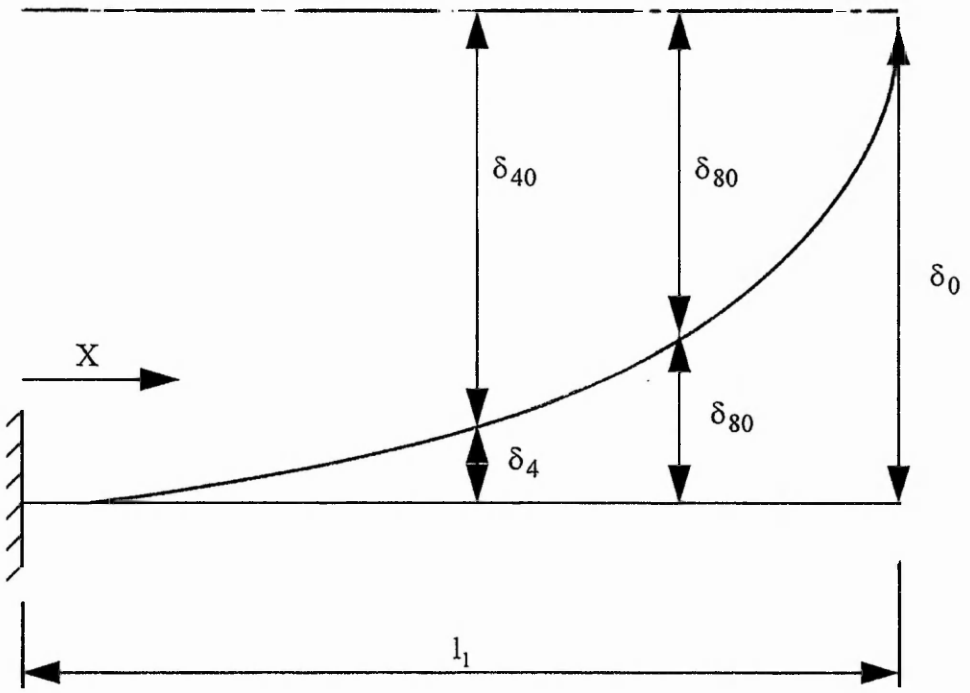

Figure 6.5 Relative displacements on a cantilever span

Displacements relative to the encastre support at centre span of the complete beam with the distance x measured from the original mid-span position.

For $x = l_1$

Support

$$\delta_0 = \frac{128}{384}\frac{l_1^3}{EI} + k_2 l_1 - \frac{k_2}{a} \quad \text{.....(6.14)}$$

For $x = 3l_1/4$

Eighth span

$$\delta_8 = \frac{81}{384}\frac{l_1^3}{EI} + k_2\frac{3l_1}{4} - \frac{k_2}{a} \quad \text{.....(6.15)}$$

For $x = l_1/2$

Quarter span

$$\delta_4 = \frac{40}{384}\frac{l_1^3}{EI} + k_2\frac{l_1}{2} - \frac{k_2}{a} \quad \text{.....(6.16)}$$

Conjugate displacements:

$\delta_0 - \delta_8$

$$\delta_{80} = \frac{88}{384}\frac{l_1^3}{EI} + \frac{k_2}{2}l_1 \quad \text{.....(6.16)}$$

$\delta_0 - \delta_4$

$$\delta_{40} = \frac{41}{384}\frac{l_1^3}{EI} + \frac{k_2}{4}l_1 \quad \text{.....(6.17)}$$

$\delta_8 - \delta_4$

$$\delta_{84} = \frac{47}{384}\frac{l_1^3}{EI} + \frac{k_2}{4}l_1 \quad \text{.....(6.18)}$$

Equations 6.16, 6.17 and 6.18 give the deflections of a complete, simply supported sandwich beam under three point loading at eighth and quarter span and for the relative displacement between eighth and quarter span respectively. Additionally, compression of the core at the support points may be included for the true displacements at quarter span and eighth span. The relative displacements of eighth and quarter span do not require the inclusion of support compression. Equations 6.17 and 6.18 now become;

$\delta_0 - \delta_8$

$$\delta_{80} = \frac{88}{384}\frac{l_1^3}{EI} + \frac{k_2}{2}l_1 + C_s \quad \text{.....(6.19)}$$

$\delta_0 - \delta_4$

$$\delta_{40} = \frac{41}{384}\frac{l_1^3}{EI} + \frac{k_2}{4}l_1 + C_s \quad \text{.....(6.20)}$$

6.4 Test methods

6.4.1 Introduction

Initially, the two sandwich panels P1 and P2 were cut into beams and tested in accordance with the multiple span technique proposed by Doherty et al with consideration of Allen's thick faced effects. Primarily the testing was to establish the material properties of the two different foams used in the panels. The second batch of multiple span beam tests was conducted on a wide range of panels with different facings and core thicknesses so that thin and thick facings could be investigated and the relevant theory applied and compared. The results obtained in this chapter have been compared relative to each other. In chapter 7 the results are compared to the other forms of material test by inputting them into a finite element model of the full scale sandwich panels and assessing the F.E.A. results against the experimental panel results.

6.4.2 Specimen dimensions

Table 6.1 gives the dimensional specification of all the beams used in the multiple span testing including the elastic modulus of the facings and an 'initial' shear modulus taken from the laboratory results for the ASTM C273 crossplate test. An initial shear modulus value has been given to aid in the calculation of the critical span length x. All of the beams are assessed for their critical span so that the appropriate conjugate points may be chosen. In practice the shear modulus of all of the beams in the main group of multiple span beam tests have been assessed by all three conjugate point relative displacements techniques.

The thick facing effect dimension $\theta x = 5$ is now calculated to show the extent of the influence due to local bending. These thick face effect lengths, x, are given in table 6.2.

Panel No.	Facing Thickness (mm)	Core Thickness (mm)	Foam Type	Elastic mod E_f N/mm^2	Initial shear mod G N/mm^2
P1	12.7	52	CFC	11200	2.37
P2	12.7	52	HCFC	11200	1.52
P3	12.2	21	HCFC	9400	3.92
P4	12.2	51	HCFC	9400	3.31
P5	12.2	72	HCFC	9400	3.31
P6	12.2	105	HCFC	9400	3.15
P8	12.2	51	HCFC	9400	3.82
P9	12.2	51	HCFC	9400	2.64
P10	3.91	50	HCFC	14000	2.30

Table 6.1 Beam specifications

Panel No.	d (mm)	A= bd^2/c (mm^2)	I_f (mm^4)	I (mm^4)	a	Length x (mm)
P1	64.7	6038	25605	1987467	0.0078	640
P2	64.7	6038	25605	1987467	0.0062	640
P3	33.2	3937	22698	526973	0.0087	580
P4	63.3	5892	22698	1855850	0.0096	520
P5	84.2	7385	22698	3266208	0.0107	470
P6	127.2	11557	22698	7424975	0.0131	380
P8	63.2	5874	22698	1850063	0.0103	490
P9	63.2	5874	22698	1850063	0.0086	580
P10	53.9	4358	747	426723	0.0310	161

Table 6.2 Local distortion length , x.

The local distortion lengths in the last column of table 6.2 are based essentially on the ratio of core shear depth and stiffness to the self stiffness of the facings. As the core shear stiffness tends towards zero, i.e. no core, the local distortion length increases towards infinity. In practice this would indicate the condition of the facings bending

about their own centroidal axis. Alternatively, a greater thickness of the plywood facings (for panels other than P10) provide a relatively high self stiffness and the critical span length is extended.

It was originally intended that the plywood facing of the panels were to be seven plies thick, approximately 9.5 mm, and thus the critical spans would have been less, however availability for the manufacturer of suitable plywood dictated nine ply thick facings. The nine ply facings have resulted in the effective thick face distortion lengths being greater than would have otherwise been preferred in order to examine the conjugate point method ideally. Beams cut from panels P10 and P6 have a relatively short critical span so that comparisons between various types of thin and thick faced sandwich beams may still be made over a wide range of spans. The remaining beams have critical spans which are really only suitable for a small number of the longer span lengths when considering the conjugate points of quarter span and support. The objective of this chapter is to identify the correct material properties for the core, specifically the shear modulus, to then support the theoretical comparisons when considering the complete panels. Therefore, the most appropriate way forward is to consider the conjugate points at eighth span and the support.

The critical span lengths given in this chapter, in table 6.2, have been based on Allen's (1969) theory as adapted by O'Connor (1985). In this case the critical span lengths have been established by classical analysis. The critical span lengths have been reassessed in chapter 7 by examining the experimental facing stress profiles and finite element models of the sandwich constructions. The conclusions drawn at the end of this chapter reflect the findings directly associated to the work conducted here. Conclusions presented for chapter 7 relate both to the direct comparison of F.E.A. results with the displacement response of the sandwich panels and to the finite element facing stress profiles.

6.4.3 Test apparatus

The testing was completed in two distinct groups, panels P1 and P2 were used in the pilot study whereas panels P3 to P6 and P10 formed the main batch of tests.

6.4.3.1 Beam configuration

In both sets of tests the three point load method was used with the supports originally 10 mm from each end and the load point located centrally. The supports were each a 15 mm diameter cylindrical solid steel length and the load was applied through a 10 mm diameter solid steel cylindrical length welded to a loaded hanger. Dial gauges were placed on the upper surface of the beam, one above each support and one at quarter, eighth and centre span.

6.4.3.2 Applied loading

For the pilot study, load increments were used and a load / displacement graph drawn for all spans and for each of the two beams P1 and P2. The load / displacement relationship was then obtained from the gradient of the experimental relationship. This proved to be rather onerous and it was felt that an equally good load / displacement relationship could be found by using a single load as there was little variation from linearity of points on the experimental line. The single load was adopted for each beam throughout the shortening of its spanning length. Suitable loads for beams P3, P4, P5, P6 and P10 for use, on a lever arm, were determined beforehand and are summarised in tables C6.3 to C6.5.

6.4.3.3 Displacement measuring equipment

Manually read dial gauges were used for the pilot study, but later LVDTs combined with a datalogger were during the main group of tests. The LVDTs proved to be invaluable principally for their rapid data gathering which prevented creep effects of the foam from corrupting the elastic displacement response results.

6.4.4 Conditioning and preparation of test samples

It was found that even small changes in temperature (and to some extent humidity) altered the physical properties of the foam. The pilot tests were conducted at the ambient temperatures and humidities of the laboratory. These varied markedly and the effects can be seen on figures C6.2 and C6.3. The effect of temperature has been discussed in general terms in chapter 2 and the relevant consequences are highlighted in section 7.6. An environmental chamber was built after observation of the MSB test results of P1 and P2 beams. All subsequent full scale panel and the multiple span beam tests were conducted in the chamber. Fortuitously, an electronically controlled heating system was also installed at the same time as the environmental chamber and the combination of the two ensured a constant temperature throughout the remaining test programme.

6.4.4.1 Environmental conditioning

All samples for the main batch of multiple span beam tests were kept in the environmental chamber for the entire testing sequence and were held at approximately the same temperature and relative humidity as the associated panel tests. The temperature range for the beam tests was 19.0 to 20.2 ^{0}C while the relative humidity ranged from 50% to 56%.

6.4.4.2 Dimensional control of the specimens

The beams were cut directly from panels using a fixed circular saw. This gave excellent accuracy for the specified width and lengths. A self-designated tolerance for the widths and lengths for all the beams was imposed. A width of 75 mm was chosen with a tolerance of +/- 0.5 mm and a length, dependant on required span, with a tolerance of +/- 1.0 mm. These tolerances were achieved in all cases for all beams.

6.4.5 Testing procedures

Throughout the entire project it was felt absolutely necessary to be able to relate the applied rate of strain on samples during the material property tests to that of the complete sandwich panel tests. In addition, required loading rates were kept at levels such that creep effects were kept to a minimum so that purely elastic behaviour was predominant. This brought the proposed technique of applying a single load to the beams into a distinct advantage over a series of manually applied dead weights as no creep effects were minimised. The single load applied to the beams equated to approximately 25% of their ultimate flexural capacity and was placed over a period of 40 seconds. The simulation of loading rates was maintained quite simply by gradually applying the single load to the beams over the equivalent period encountered in the panels tests. The panels were loaded to approximately 75% of their ultimate flexural capacity in a period of approximately 120 seconds.

Verticality of the LVDTs was checked with a small spirit level each new span and the two LVDTs over the supports were lined up prior to the beam being placed. Positions where the LVDTs were placed were lightly sanded and free from dust. Some beams had a slight twist over their length. The twist was combated by firstly levelling the supports before each load application and secondly by the levelling effect of the initial dead weight of the lever arm and hanger. An initial displacement was recorded with the lever arm and hanger in place and a further single reading immediately after the full applied load. The supports had been checked for movement prior to any testing and it was found that there was no discernible displacement. As the tests were of a limited duration each beam was given a minimum of six hours recovery time before the next span length was tested.

6.5 Results and Analysis

6.5.1 Introduction

As shown above, in table 6.2, the panels vary in their critical span length and therefore some of the panels were, for O'Connor's proposed theory, not ideally suited to the conjugate point method. For completeness and as a basis for comparison all the beams from panels P3-P6 and P10 tested have been analysed for the conjugate point method and the original method of Doherty et al with the addition of thick faced theory as developed by Allen (1973). Panels P1 and P2 were tested and are analysed using solely the method of Doherty et al. It was felt that further analysis of these experimental results was not worthwhile due to the inaccuracies caused by the differential temperatures and relative humidities present during the sequence of testing.

Both type 1 and type 2 graphical representations have been made for the main batch of beam tests. The elastic modulus of the facings has been evaluated from the type 1 analysis and compared to the modulii values from the four point load test on plywood coupons. The modulii from the coupon tests, presented in section 6.6, have been used in type 2 analysis.

6.5.2 Presentation of laboratory data, graphical output and analysis

6.5.2.1 Results of beams from panels P1 and P2

As mentioned before the beams from panels P1 and P2 were tested in accordance with the multiple span method presented by Doherty et al (1965). Thick faced effects have been incorporated into the analysis in accordance with the method for treatment of beams with thick facings as proposed by Allen (1973). Both type 1 and type 2 graphical analyses have been used and examined. The main aspects of work carried out on beams from panels P1 and P2 is described below.

- Figure C6.1 shows a typical plot of load versus deflection at centre span for varying lengths of span. For clarity not all of the different spans have been shown. The mid-span deflections have been reduced by the recorded compression above the support points. From the experimental load / displacement relationship the gradient is calculated to provide a displacement for a unit load which is then carried forward to the graphical evaluation for type 1 or type 2 analyses.

- Figures C6.2 and C6.3 both show the same plot of δ/PL versus L^2 for beams from panel P1. The treatment of each graph is different for the evaluation of elastic modulus of the facings and shear modulus of the Isofoam CRF core material properties. Figure C6.2 has tangential lines drawn on the upper part of the plot, with the intercept value equal to $1/4AG$ and the gradient of the line equal to $1/48E_fI$. Figure C6.3 has the gradient of the tangential lines fixed, E_f being predetermined.

- Figures C6.4 and C6.5 both show the same plot of δ/PL^3 versus $1/L^2$ for beams from panel P1. The treatment of each graph is different for the evaluation of material properties. Figure C6.4 has tangential lines drawn on the lower part of the plot, with the intercept value equal to $1/48E_fI$ and the gradient of the line equal to $1/4AG$. Figure C6.5 has the intercept of the tangential lines fixed, E_f being predetermined.

- Tables C6.1 and C6.2 hold the elastic modulii of the facings and the shear modulii of the core from the multiple span testing figures C6.2 and C6.4 for beams from panels P1, similar figures for P2 are similar and have not been shown. Where a figure reference number is placed in brackets indicates that that value has been derived from a graph of similar type, but which is not held in the appendix. Table 6.3 summarises the values in tables C6.1 and C6.2,

Beam	Figure Type 1	Elastic modulus, E_f N/mm^2	Shear modulus, G N/mm^2	Figure Type 2	Elastic modulus, E_f N/mm^2	Shear modulus, G N/mm^2
P1	C6.2	7300	2.3	C6.4	7400	2.3
P1	C6.3	11000	2.2	C6.5	11000	2.2
P2	(C6.2)	6400	3.1	(C6.4)	10400	2.8
P2	(C6.3)	11000	2.5	(C6.5)	11000	2.6

Table 6.3 MSBT Doherty et al / Allen method panels P1 and P2 specimens.

6.5.2.2 Results of beams from panels P3 to P6 and P10

O'Connor's conjugate point method has been used to find the shear modulus of the core by theoretically comparing the deflection of two points situated away from the localised load concentrations. O'Connor proves the method by comparing three sets of two displacements, those being at the support and quarter span, support and eighth span and finally at quarter span and eighth spans. For a complete evaluation of the conjugate point theory this investigation has concentrated on finding the shear modulii derived from all three sets of relative displacements. The pilot study identified the most appropriate method of experimental and analytical technique for the main batch of beam tests. The conjugate point method has used type 2 graphical representations in all cases. A fixed intercept value has been predetermined from the four point load tests on coupons of the plywood facings. Type 2 graphical plots have been chosen, in preference to type 1, as the gradient of the line drawn to the experimental curve is tangential where the spans of the beam are longest.

- Figure C6.6 is typical for all beams from all panels. Figure C6.6 represents one beam with the three conjugate point sets of displacement, those being at the support and quarter span, support and eighth span and finally at quarter span and eighth spans.

- Tables C6.3, C6.4 and C6.5 give the test data, physical properties used for the construction of the graphs and the shear modulii for beams P3 to P6 and P10.

- Table 6.4 below summarises the results from tables C6.3, C6.4 and C6.5. The shear modulii given are for the support and quarter span, G_{40}, support and eighth span, G_{80}, and finally at quarter span and eighth spans, G_{84}.

Beam	G_{84} N/mm^2	G_{40} N/mm^2	G_{80} N/mm^2
P3	2.9	2.8	2.7
P4	3.1	3.0	2.8
P5	3.6	3.2	3.0
P6	3.5	3.3	3.2
P10	2.0	2.0	1.8

Table 6.4 Shear modulii based on the conjugate point method.

6.6 Plywood bending tests

To enhance the accuracy of the multiple span beam testing technique the intercept may be first identified to give a start point for the gradient of the tangent to the test results plot on graph type 2. The intercept value incorporates the elastic modulus parameter for the facings which may be determined by a four point bending test as described below.

The four point load test has been used in order to eliminate any displacements caused by shear strains in the plywood veneers or adhesive. Figure 6.6 shows the test configuration;

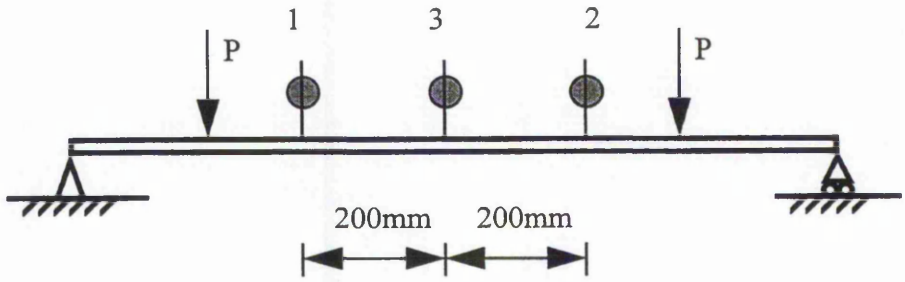

Figure 6.6 Plywood - four point bending test

All beams were 50 mm wide and overhung the span by approximately 5 mm to prevent the ends from slipping off the supports. Deflection were taken at positions 1, 2 and 3 with the relative deflection of 3 taken from the average of 1 and 2 and then being used for the elastic modulus calculation. Table 6.7 summarises the results of the beam tests and plywood thicknesses. The figures highlighted are those carried forward into further analysis throughout this chapter and the rest of the project. Values for panels P1 and P2 have been averaged together as their variation is small and they used the same plywood grade. This is similarly true for panels P3-P6.

Beam designation	No. of samples	Width, mm	Thickness, mm	Elastic modulus E N/mm^2
P1	10	50	12.2	11200
P2	10	50	12.2	11000
		Average	12.2	11100
P3	4	50	12.2	9500
P4	4	50	12.3	9100
P5	4	50	12.3	9300
P6	4	50	12.2	9300
P8	4	50	12.3	9800
P9	4	50	12.3	9400
		Average	12.3	9400
P10	10	50	3.9	14100

Table 6.5 Results of the plywood bending tests

The plywood coupon bending test results for panels P3 to P9 were supported by the material properties given in the 'Handbook of Finish plywood' (1991) for nine ply birch veneer, grade IV/IV. The elastic modulus perpendicular and parallel to the direction of span are given as 5860 and 9320 N/mm^2 respectively. This shows good agreement with the four point test results in table 6.5, 9400 N/mm^2.

6.7 Discussion

The main thrust of this section of work was to evaluate the shear modulus of the core of sandwich constructions when in flexure as opposed to the shear or uniaxial coupon tests. The multiple span beam testing technique has encompassed the method proposed by Doherty et al (1965) (incorporating amendments for thick faced effects by Allen) and the conjugate point method of O'Connor. By investigating the development of the MSBT technique through the pilot experiments the best method has been exposed for use with the main batch of tests.

The shear modulii of the Isofoam CRF core of beams from panels P1 and P2 are displayed in table 6.3. It is evident that the elastic modulus of the facings have not been evaluated well by either type 1 or type 2 graphical analyses, assuming the four point bending tests on the plywood facings provided good results. Consequently the shear modulii values of the cores were not consistent within the same type of graphical representation. For beams from panel P2 the shear modulii values were only 4% different when the predetermined elastic modulus of the facings was used. Not using the facing's elastic modulus incurred a difference of 11%. Although the shear modulii of panel P1 were very consistent it was felt that using the predetermined elastic modulus of the facings was more appropriate.

The results held in table 6.4 indicate a distinct trend. The shear modulii were consistently greater in value for the quarter and eighth span conjugate points and descending in value for those of quarter and support and then eighth and support. This trend is associated to the fact that the relative displacements of the conjugate points

were less for quarter and eighth span positions etc. It would be difficult to attribute this trend to a particular cause although the two most probable reasons could be either the local bending and compression at the support or whether the beam is bending cylindrically or anticlastically.

Although there has been development of the theoretical work, laboratory accuracy and interpretation of results must still be considered as fundamentally one of the most important features in obtaining the appropriate shear modulus of the Isofoam CRF core.

Four features of testing and treatment of results important to the accuracy, additional to the theoretical approach of data representation, are temperature and relative humidity, truly representative facing modulii, method of obtaining load / deflection relationships and interpretation of figure types 1 and 2. Each of these four points are discussed, however, within the context of this investigation their influence is not quantified and the original results in tables 6.3 and 6.4 remain.

Temperature and relative humidity play an important part to the accuracy of the results. It is essential to maintain constant environmental conditions. Figures C6.2 and C6.3 highlight this condition particularly well as can be seen at the upper part of the figure. Table 6.6a and b gives the temperature and relative humidity readings for each test.

During the pilot study, a day of testing usually comprised morning and afternoon sessions with approximately six hours recovery time for each beam. The temperature and relative humidity levels followed a pattern of cool mornings and warmer afternoons, hence the variations seen in table 6.6a. Figure C6.3 clearly shows the effect of temperature differences of the beam tests. As an example, at a span of 1900 mm the temperature was 25.4 ^{o}C, a difference of at least 6 ^{o}C from the adjacent span lengths. This caused an anomalous result and an irregular plots for type 1 and 2 graphical analyses. The tests on beams from panels P3-P6 and P10 were all conducted inside the environmental chamber which was kept between 19.0 to 20.2 ^{0}C, while the relative humidity ranged from 50% to 56%. Having established better environmental control it potentially enabled a more accurate method of establishing load / deflection relations.

Span mm	2000	1900	1800	1700	1600	1500	1400	1300	1200	1100	1000	900	800
Temp °C	19.5	19.4	19.9	20.2	20.0	19.1	19.5	19.0	19.1	19.8	20.2	19.3	19.7
Rel Hum%	56	55	50	51	51	51	53	54	55	55	56	56	54

Table 6.6a Temperature and relative humidity levels
for tests on beams P3 to P6 and P10.

Span mm	1980	1900	1800	1700	1600	1500	1400	1300	1200	1100	1000	900	800
Temp °C	17.3	25.4	19.0	23.6	17.5	24.1	18.6	23.9	17.1	22.0	25.9	21.0	20.3
Rel Hum%	42	55	48	54	41	56	44	53	43	49	57	46	47

Table 6.6b Temperature and relative humidity levels
for tests on beams P1 and P2.

Load / deflection relationships for beams from panels P1 and P2 were obtained by using a series of manually applied load increments to each beam. This was not only an onerous task but the time taken allowed creep effects to begin to develop at the end of the loading sequence. The load / displacement response was initially "very linear" for each individual beam. This led to confidence that a single applied load would give a representative load / displacement response and reduce the handling process.

The concept of applying a single load for the load / displacement relationship was valid, however, it is believed to have been one of the main sources of errors producing "saw-toothed" plots on type 1 and 2 graphs. The total load used in the main batch of tests was approximately the same to that of the total of the load increments used in the first set of tests. Whereas in the pilot tests the load increments allowed initial "take up" in the apparatus and beam configuration to be isolated the single load for the main batch of beam tests did not to the same extent. The main batch of tests did have a small pre-load of a lever arm, but retrospectively it is believed that this would not have provided enough load to remove all the "take up" in the system.

The single load was applied gradually over a period of approximately 40 seconds and the displacements recorded immediately after the total load was released. Although great care was taken to apply the load, it was noticeable that there were occasions when a residual oscillation remained. Close observation of the effect of this dynamic load indicated that the displacements slightly increased after fully releasing the single load and before a displacement reading was taken a few seconds later. It was estimated that this slight increase in displacement accounted for less than 2% of the total displacement. As the effect of the dynamic loading on displacements was different from beam to beam and its magnitude difficult to assess the effect was not considered.

Representative facing modulii were essential for evaluating the initial intercept and gradient for the tangent to the curve in type 1 and intercept in type 2 graphs respectively. Throughout the testing it has been assumed that the elastic modulus for all of the plywood facings were very similar and that testing a reasonable number of coupons tests would lead to a representative material property being obtained. This must be put into some doubt as the variation in values shown in tables C6.1, C6.2 and 6.1 depict. There is a clear discrepancy between elastic modulii obtained from the multiple span testing and those from the plywood four point flexural tests. The averaged elastic modulii value derived from the four point load coupon tests was 9400 N/mm^2. This value was found for two coupons from each of the relevant sandwich panels with the results averaged. It was then assumed that this was representative of all plywood facings. This assumption was supported by the manufacturers claimed values. In retrospect a larger sample size should have been used from each panel and that elastic modulus used only for that set of beams.

Interpretation of graph types 1 and 2 was completed by manually applied 'lines of best fit' which had some potential for error. Difficulty was encountered in applying a tangential line without a predetermined intercept point. Even with the intercept point or the gradient defined the exact tangential line to the curve was still subjectively placed.

The results of the multiple span testing methods will be further examined in the following chapter when they are considered and compared in the theoretical modelling of the full scale panel tests.

6.8 Conclusions

The ultimate validation of the multiple span beam testing methods will be made when the results are used as property data in the finite element analysis comparison with the associated full scale panel tests. This separate analysis is contained in chapter 7. In particular the critical span concept is reviewed. Conclusions are made here regarding only the methodology and procedures carried out in obtaining the shear modulii values by the multiple span beam testing methods.

(i) The load / deflection relationship should only be obtained by a series of load increments rather than one load step application procedure. This will eliminate errors due to "take up" in the system and also prevent any significant dynamic loading effects. The rate of application of load increments should be tailored to that of the full scale tests.

(ii) The scatter of the facing's elastic modulii values in the four point load tests suggests that each plywood facing may in fact have significantly different properties. The elastic modulii values obtained in the multiple span beam tests indicate this may well be the case. The elastic modulii of the facings from the MSBT should not be used rather the modulii should be obtained from separate four point load tests on suitably representative coupons. Predetermining the elastic modulii of the facings greatly assists the insertion of an appropriate tangent to the experimental curves.

(iii) Manually fitting a tangent to the experimental multiple span beam testing result curves (graphical analysis types 1 and 2) was found to be subject to misfit error. The degree of error depended on how linear the curve was at the tangent point. The error

was not quantified as it was found to be subjective. Over a suitable number of experimental curves it could be argued that the error averages out.

(iv) Theoretically the conjugate point method is the most accurate means of shear modulus evaluation as it is not influenced by local distortion around point concentration. The significance of the conjugate point method diminishes as the facings become stiffer, the core weaker relative to the stiffness of the overall sandwich beam and the length of span becomes greater.

(v) Control of constant environmental conditions was seen to be essential for accurate evaluation of load / displacement relationships. The results of the multiple span beam tests from panels P1 and P2 showed that a total variation of 8.8°C gave the experimental type 1 and 2 analyses graphs a distinct "saw toothed" appearance. Difficulty then arose when the tangent to the curves was drawn.

CHAPTER 7 - SANDWICH PANEL TESTING AND ANALYSIS

7.1 Introduction

7.2 Full scale sandwich panel tests

7.3 Theoretical modelling

7.4 Material property evaluation

7.5 Conclusions

CHAPTER 7 - SANDWICH PANEL TESTING AND ANALYSIS

7.1 Introduction

In many texts on sandwich panel analysis, the theory, when supported with material property data, is not directly compared to full scale experimental data. In addition, a rigorous comparison of the various current material property test methods does not seem apparently obvious and again it remains for a numerical argument to validate each method's merits or shortcomings. This chapter has been dedicated to the direct validation of theoretical models and ascertains the most appropriate material property test method for rigid polyurethane cores placed by the foam injection system.

Classical solutions have been developed by Allen (1969), who provides an excellent text on thick faced sandwich panel analysis, derived using a similar engineering equilibrium approach to Norris (1948). Allen's text also and includes material property test methods. Hartsock (1968) also used the engineering equilibrium method pioneered by Norris (1948) to derive solutions for thin and thick faced sandwich constructions. In a later text, Allen (1973) further developed the original multiple span beam testing technique of Doherty et al (1965) to incorporate thick face effects. A continuation of the development of the multiple span beam testing was made by O'Connor (1985). O'Connor proposed the "critical span concept" which was derived from Allen's sandwich beam theory. The critical span concept avoided local stress concentrations that would normally cause errors in experimental data. However, for most cases there was seemingly no direct comparison of sandwich panel theory, when supported by the proposed material testing methods, to full scale sandwich beams or panels.

In this chapter two fundamental aspects, which have already been presented in this project, are addressed in a more perspective way. Firstly, the finite element and Allen theoretical solutions are compared and validated and secondly the identification of the most appropriate method of material property evaluation is made. Both aspects are

compared directly to the experimental data of flexural behaviour from the series of full scale sandwich panel tests.

The theoretical methods, finite element analysis and Allen's analytical solutions, are compared to experimental results by examining stress profiles along the outer surfaces of facings in the spanning direction of plywood faced sandwich panels. In chapters 4, 5, and 6 material properties of Isofoam CRF core and plywood facings have been experimentally established. However, the physical properties of the Isofoam CRF core evaluated from three distinct test methods produce significantly varying values. Therefore the second part of this chapter is devoted to a direct comparison, between the material test property data from the evaluation methods, using a proven theoretical solution against the deflection response of the sandwich panels.

7.2 Full scale sandwich panel tests

7.2.1 Test configuration

All panels were subject to a three point load configuration. The test configuration is similar to the multiple span beam testing in that a small overhang is allowed (approximately 10 mm) at the supports. The supports used were the same solid steel circular sections, with one support allowed to translate in the x-direction. The load however, is now applied across the full panel width through a steel I-section from a single, centrally located load actuator ram, bearing on a 'soft' (MDF) 20 mm thick shim. The shim is present to ensure an even contact and pressure across the width of the panel and to allow a smooth rounded bearing surface.

7.2.2 Monitoring of flexural behaviour

Flexural behaviour, used for the validation of theoretical models, is described, in this text, by strain profiles in one half of the span of the sandwich panels. Comparisons of material property test methods are made by observing deflections at prescribed points,

again in one half of the span. A Schlumberger SI 3535D Data logger was used to record all information from the strain gauges and LVDTs. It was felt necessary to record all data over the least possible time whilst still maintaining a good accuracy. Consultation with the datalogger's manufacturer indicated that 40 channels per second would be the optimum acquisition speed which relates to a total time of 1.5 seconds. A single continuously increasing load ramp was applied to each specimen. At this stage it is noted that over the duration of the logging scan there would have been a slight increase in applied load. However, not only would the difference in load be small over the time step, 0.12 kN, but the difference in load between each strain gauge would be the same at logging intervals, hence negating much of the discrepancy.

Two equally spaced lines of twelve strain gauges were placed over one half of each panel on the outside surfaces of both the upper and lower facings. A gauge length of 20 mm was used for the main batch of testing after the pilot tests on panels P1 and P2 used 60 mm gauges. The 60 mm gauge lengths were deemed too long when considering the rate of change of strain in areas of local distortion near load points. A 10 mm gauge length was considered but discounted due to the rather rough finish of the plywood surface and other irregularities such as knots.

Two LVDTs were positioned at quarter and eighth span and were complemented by two directly over each support to measure displacements on the upper facing. Similar to the two lines of strain gauges, each pair of LVDTs were positioned at 'third widths' and their readings averaged. It was felt necessary to do this as the panels in the pilot tests tended to twist slightly despite each roller support being parallel with the panel.

7.2.3 Test conditions

To draw conclusions to the most appropriate property test method, the environmental conditions of temperature and relative humidity have been highlighted. The conditions of the uniaxial compression and tension, the shear tests and the multiple span testing together with those of the full scale sandwich panel tests. Table 7.1a and 7.1b hold all the relevant environmental conditions for the material and panel tests respectively;

Test method	Mean temperature ^{O}C	Standard deviation	Mean relative humidity %	Standard deviation
Uniaxial compression	19.9	0.2	48	0.3
Uniaxial tension	19.1	0.3	48	0.5
BS shear test	22.0	0.2	61	1.9
ASTM shear test	21.8	0.4	61	2.7
Multiple span testing	19.6	0.3	54	1.7

Table 7.1a Temperature and relative humidity levels for sub-element testing

	Panel 1	Panel 2	Panel 3	Panel 4	Panel 5	Panel 6	Panel 10
Temperature ^{O}C	17.9	18.6	20.0	19.6	19.5	20.0	20.5
Relative humidity %	45	46	45	50	49	47	55

Table 7.1b Environmental conditions for three point load panel test

The temperature and relative humidity values for the material property testing methods in table 7.1a compare favourably to the full scale tests of panels P3 to P6 and P10 given in table 7.1b. Panels P1 and P2 however were tested at significantly lower temperatures to their associated material property tests. To put these temperature and humidity differences into context, for the Isofoam CRF (at a density of 32 Kg/m^3) as used throughout the project, a difference of 1 ^{O}C relates to a loss of approximately 0.4% in elastic modulus from the 'control' value at 22 ^{O}C. The actual relationship between modulii and temperature (given in chapter 2) is not linear although for 20 ^{O}C +/- 10 ^{O}C a linear variation is a reasonable approximation.

For panels P3-P6 and P10, it is assumed that the environmental differences between material property tests and panel tests are not significant. Although there may be some significant difference for panels P1 and P2, the associated panel tests are not part of the main thrust of the investigation.

7.2.4 Test procedure

7.2.4.1 Loading configuration and loading rates

A single continuous load ramp was used for all the 3-point load tests. In order to set a limit for an applied load a reserve panel was tested to failure. Panel P8, 50 mm Isofoam core and 12.3 mm thick plywood facings, recorded an ultimate load of 14.6 kN. Failure occurred in the Isofoam core, with a sudden 45^{O} shear crack forming at approximately quarter span. Once the shear crack had formed, debonding of the Isofoam CRF core from the facings propagated until complete failure of the panel. For panels P4, P5 and P6 a load limit of 10 kN was imposed and for P3 and P10 a load limit of 6 kN.

The rate of applied loading for the panels was based on matching strain rates in the Isofoam to those of the sub-element tests. The test to failure of panel P8 produced a similar tensile shear failure that was predominant in the failure mechanism of the shear test specimens. The duration of loading to failure of panel P8 was approximately the same as the related shear tests, 120 seconds and 128 seconds respectively. To an extent this was followed in the uniaxial compression and tensile tests with the applied loading to the elastic / plastic yield point being in the region of 100 to 140 seconds. The multiple span beam testing however, did not load to failure and used both a substantially less and a singly applied load. The single load was equivalent to approximately 30% of the failure load for a panel, but was applied gradually, by hand, with any slight residual oscillations being allowed to damp out, with the whole process taking roughly 35 to 40 seconds.

A rigorous examination of the loading rates, for universal synchronisation across all tests, was not warranted as the Isofoam core, during flexure in a sandwich panel, varies in its rates of strain throughout the length of span and depth of core. The rate of loading has been noted as a possible factor in the evaluation of appropriate material properties and has been, to a certain extent, kept constant. Additionally when other factors such as the variability of Isofoam core quality probably bear more influence on result

differences, the rate of loading is considered less important. It should also be noted that the rates of loading used in testing are such that significant creep effects do not begin to influence the elastic behaviour.

7.2.4.2 Significance of creep on sandwich panel flexural behaviour

Part of the initial series of pilot tests included observations on the behaviour of secondary displacements of sandwich beams. Section 2.2 describes the short and long term displacement effects associated with time dependent loading. The work of Huang and Gibson (1990 and 1991) addressed the modelling of 1200 hour long creep tests of shear specimens and sandwich beams with polymer cores. The sandwich beam creep model was then extrapolated for tests lasting 10 years and good predictions were made. More significant to the flexural behaviour of the plywood faced panels in this study were the short term creep effects. Three beams were loaded, in three point configuration, to approximately 30% of their ultimate load capacity. A typical mid span displacement versus time plot is shown on figure 2.7. All three beams showed insignificant creep after 20 seconds. At 40 seconds approximately 1% of the total deflection was due to creep.

There were a number of factors, attributed to creep effects, that were important when considering the load / displacement response of the sandwich panels subject to the imposed load ramp. It was assumed that significant creep displacements represented 1% of the total displacement of a beam or panel. For the beam tests creep strains, although mobilised immediately the load was applied, were small enough up to approximately 30 seconds from load application to be ignored. However, the sandwich panel flexural tests for panels P3 - P6 and P10 comprise approximately 120 second load ramps indicating that some degree of creep would have been present. Typically the load ramp was halted at maximum load which related to approximately 65% of the panel's ultimate capacity. It could therefore be assumed that over the first 30 seconds creep effects were not significant and probably even longer than that. Observation of the experimental results for panels P3 - P6 and P10 show that indeed significant secondary displacements only became apparent some way into the loading ramp. Table 7.2

summarises the characteristics of time dependent displacements for each panel. The time to onset of creep has been determined from the experimental quarter span deflection. Significant divergence of the experimental displacements from a tangential line drawn at the start of the load / displacement plot is taken as being the onset of creep.

Panel	Facing thickness (mm)	Core thickness (mm)	Maximum load (kN)	Duration of load ramp (s)	Time to onset of creep (s)
P1	12.2	52	10.0	240	150
P2	12.2	52	10.0	240	140
P3	12.3	21	6.0	120	90
P4	12.3	51	10.0	120	110
P5	12.3	78	10.0	120	110
P6	12.3	102	10.0	120	120
P10	3.9	50	6.0	120	120

Table 7.2 Time to onset of significant creep during the flexural testing of sandwich panels

The time to the onset of creep clearly indicates that for panels P4 - P6 and P10, linear elastic response over the 120 second load ramp was predominant and no significant time dependent behaviour was exhibited. The load / displacement relationships for panels P1 and P2 were effected by the duration of the load ramp. Using a tangential approximation at the start of the load application was valid as more than half the response is not influenced by creep effects. The core and facing thickness also has an effect on the rate of creep in that the shear strain in the core is dependent on the configuration of the sandwich panel

7.2.5 Experimental Results

The results of the flexural testing have been placed in two sections. Firstly, stress profiles are plotted along the outside surfaces of the upper and lower facings, figures

D7.4, D7.5, D7.6, D7.7 and D7.8, together with the finite element analysis and Allen solution stress profiles. Section 7.3.4.2 and tables 7.4 a-e, contain a summary of the important flexural response values for all panels measured from the stress profile plots. Stress profiles for panels P4 to P6 are shown for a single load level of 10.0 kN and panels P3 and P10 for a load level of 6.0 kN. Secondly, the material property values from the sub-element testing are used in the theoretical models in order for a direct comparison and in this case displacement response is compared to experimental results. Displacement response comparisons are shown on figures D7.9 a-b, D7.10 a-b, D7.11 a-c, D7.12 a-c, D7.13 a-c, D7.14 a-c and D7.15 a-c for panels P1, P2, P3, P4, P5, P6 and P10 respectively.

7.3 Validation of the theoretical modelling of the plywood faced sandwich panels with experimental stress profiles

7.3.1 Introduction

Theoretical modelling of the flexural behaviour of sandwich panels is made by the use of finite element analysis and Allen's classical solutions. The principal objective of this part of the investigation is to validate the use of finite element concepts for the application to sandwich panel behaviour. The Allen solutions are well documented, Allen (1973) and O'Connor (1985), and have been proven to produce appropriately accurate models of facing stresses and displacements for simple loading configurations. However, the ultimate use of any modelling tool in this project is its application to masonry cavity walls. Finite element analysis has distinct advantages over the Allen solutions when considering additional secondary effects of self weight, boundary conditions and easy manipulation of geometrical features and results presentation. Potential analysis of more complex, in service, structural cavity walls could not realistically be made using Allen's analysis and thus finite element analysis must be the way forward. It therefore remains the task to verify finite element theory and modelling techniques by comparison to experimental results and Allen's solutions for the simple plywood faced panels.

7.3.2 Finite element analysis

7.3.2.1 Finite element analysis program and solution method

The F.E.A. package used in all analysis models of the sandwich panels was ABAQUS (1995) with the graphical outputs manipulated by the, Rolls-Royce in-house, post processing package SC03 (1997). As reasonably large deflections, 40 mm central deflection in a two metre span, were encountered a geometrical non-linear analysis was compared to a linear static analysis. A total applied load of 10 kN for both analyses was used which produced a difference in mid-span deflection of less than 1% when considering panel P6. It could therefore be concluded that there was not a sufficient discrepancy between the two types of analysis to justify the additional C.P.U. time, manipulation and interpretation of non-linear results and only linear static analysis has been used hereafter. The ABAQUS F.E.A. package uses a half bandwidth in the frontal solution method for the global stiffness matrix. The frontwidth is automatically optimised.

7.3.2.2 Model definition and considerations

The use of two dimensional plane strain models throughout the finite element analysis of the panels was subject to a short investigation of the three dimensional flexural response. The displacement profile across the width of the three dimensional finite element model of a sandwich panel had been scrutinised for three dimensional effects. The displacement at the centre width of the panel, table 7.3, was -13.76 mm and varied in a near parabolic shape to the outside edge which had displaced -13.88 mm, a difference of 0.9%. The three dimensional effects encountered are attributed to the Poisson's ratio effects of both facing and core. Essentially a state of anticlastic bending was described by the finite element analysis.

Considering plane sections in the spanning direction, at the mid-width of the panel, a near plane strain condition was predominant, with little or no lateral expansion allowed

due to constraint by the surrounding material. A plane stress state would be more apparent at the very edge of the panel where freer and unconstrained lateral expansion occurred. Therefore the stiffness of the panel increases slightly towards the centre of the panel and hence the slight difference in displacement across the width is experienced. An additional modelling consideration was the applied load. For the test, the load was assumed to be constant across the width of the panel, which would probably not be the actual situation as the I section spreader beam would deflect along its length giving a slightly uneven load distribution.

The three dimensional mid span displacements were compared to plane strain and plane stress two dimensional values in the table below. From these results it was therefore decided that there would be little to gain from three dimensional analysis over a two dimensional plane strain model with the inherent assumptions made and the negligible difference in deflection results.

Type of F.E.A. analysis	Centre deflection (mm)	Edge deflection (mm)
3-dimensional	-13.76	-13.88
2-dimensional plane strain	-13.74	
2-dimensional plane stress	-13.92	

Table 7.3 Mid span deflections for different analysis types

7.3.2.3 Element type and mesh density

The element chosen was a plane strain continuum, quadrilateral two dimensional isoparametric element containing eight nodes. A short convergence study was conducted to validate model accuracy. The model is based on linear elastic, orthotropic material properties for the core and facings which are contained in table 7.4. The shear modulus value used is based on the elastic modulii in the x- direction, calculated from the ordinary linear elastic relationship, $G = E / 2(1 + \upsilon)$.

	Ex N/mm^2	Ey N/mm^2	Gxy N/mm^2	υxy
Isofoam CRF core	6.5	5.0	2.3	0.25
Plywood Facing	9400	2000	3920	0.20

Table 7.4 Orthotropic two dimensional material properties for plywood facings and Isofoam CRF core used in the convergence study

Table 7.5, shows the convergence for panel P6, with all other finite element models of panels containing the same number of elements. Model number 5 was chosen as the final mesh density as the displacement response appeared to converge on -13.74 mm, to two decimal places.

Model no.	No. of elements	C.P.U time (s)	Displacement (mm)
1	303	22	13.654
2	404	35	13.702
3	505	57	13.729
4	606	92	13.738
5	707	149	13.740

Table 7.5 Convergence study output data

7.3.2.4 Use of symmetry, boundary conditions and load configuration

The use of symmetry has been used to half the model size by applying appropriate boundary conditions. The finite element analysis, like the Allen solutions presented by O'Connor (1985), models the panels with a single point load as the actual point support and an encastre support as the mid span position. Essentially the F.E. model simulates the full length beam by restraining a half length beam at the full beam's centre span. All the nodes along the mid-span vertical edge of the half beam are restrained in the x-direction with the top right hand outside node on the upper facing also restrained in the y- direction. This would normally represent the position of the load point. A single

static imposed point load is now applied to the F.E. model half beam at the original support point.

7.3.2.5 Final finite element model and properties used for the comparison of stress profiles and displacement response.

The final mesh density used, panel P6 and P10 only shown, may be seen on figures D7.1 and D7.2, with each rectangle depicting one eight noded element. The upper and lower two element layers represent the facings with the core being modelled by a seven element deep mesh. The mesh could have been reduced in density away from regions of changing stress, but the additional C.P.U. time would be far outweighed by the additional time taken to create the irregular input data cards. The colour contour plot shown is for the maximum principal two dimensional stress.

The comparison of theoretical and experimental results is directed at the shape of the overall stress profile and in particular the local distortion effects originating from the load and support points. In particular the length of span influenced by the "critical span concept" of O'Connor has been compared to the finite element results. Displacement response is used in the direct comparative study of the material property evaluation methods. In this part of the chapter only finite element analysis is used to provide the means of theoretical measure of the material properties when compared to the full scale panel tests. As the finite element analysis is further used for the direct comparison of material property evaluation methods against the full scale panel experimental tests the material properties used were orthotropic in nature to be as realistic as possible.

7.3.3 Allen solutions

The Allen solutions for a three point load configuration are derived in chapter 3 (equations 3.33 and 3.35) and are summarised below. It has been assumed that a 10 mm overhang is present for all panels, however, the stress profiles shown in Figures D7.4, D7.5, D7.6, D7.7 and D7.8 are only shown in the span AB. A Microsoft Excel (1994) spreadsheet was used to calculate both the stress profiles and displacement values

throughout the span. Material property values used were identical to the finite element analysis solutions assuming that $E = 2G(1 + \upsilon)$. It should be noted that the material properties for elastic and shear modulus are those in the spanning or x-direction and that Poisson's ratio effects are taken into consideration in the finite element analysis but are not directly considered for the Allen solutions.

Allen (1969) does allow for plane strain or plane stress conditions, depending on the width of the sandwich, by factoring the elastic modulus. Allen recommends that where infinitely wide panels are modelled, strains in the y- direction are taken as zero. In this case the ratio of stress to strain in the x- direction is $E/(1-\upsilon^2)$ which should be used instead of E. Where anticlastic bending is permitted then the value E should be used. Essentially the elastic modulus value chosen for the Allen solutions accounts for the Poisson's ratio effect most likely to occur in practice (wide or narrow beams). The Allen solutions, therefore, may be applied in an analogous manner to plane strain or plane stress problems. Cylindrical bending being similar to plane stress conditions and should be used for the analysis of narrow beams. Anticlastic bending, where freely permitted, models the conditions of plane strain and should be used for wide beams or panels.

The configuration of the panel tests conducted in this study allows anticlastic bending at each of the supports. At the supports, the panel was only constrained in z- direction for displacement. The anticlastic bending effect manifests itself, in this situation, with a varying reaction force (per unit width) across the width of the support. Proportionally there would be a greater reaction at the centre of the panel, dissipating toward the edges of the panel. At the mid width position the core and facings behave in a pure strain state as at that point any section is laterally constrained by the material next to it. Nearer to the sides of the panel the material is freer to expand laterally and a plane stress state is more prevalent. The finite element modelling, in the previous section, of the three dimensional panel confirms this when considering the displacement response across the width of the panel at centre span. An equal load was applied to all the nodes across the width of the panel. The displacements were greater at the edges of the panel than at the

centre. Thus for the same displacement across the entire width of the panel, less support reaction would have been required at the edges compared to the centre.

The mid span load application for the tests contradicted the anticlastic flexural response of a wide sandwich beam. The transverse displacement curvature was reversed as the load spreader I beam deflected. The anticlastic flexural behaviour of the panel remained consistent but actual displacements would not be modelled exactly by the Allen solutions assuming the use of $E^* = E/(1-\upsilon^2)$. This was also the case with the finite element modelling and it was therefore assumed that a plane strain condition was predominant. The anticlastic behavioural response has been adopted in all Allen solutions for modelling of the sandwich panels. Elastic and shear modulii values for the facings and the Isofoam CRF core have been factored by $1/(1-\upsilon^2)$ and are represented as E* and G* respectively.

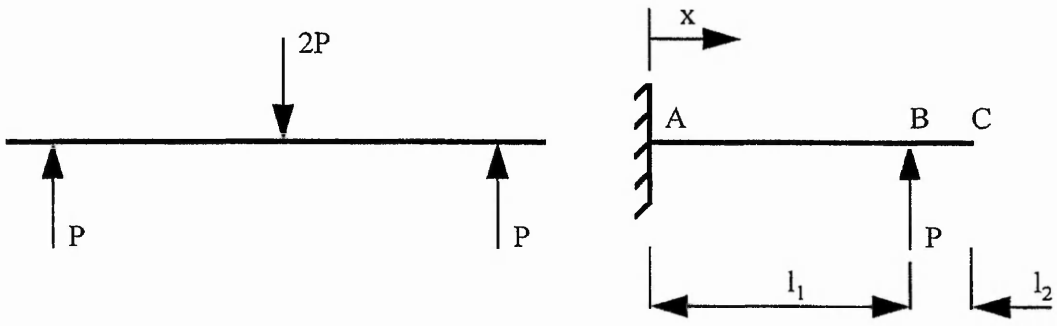

a. 3-point load test configuration b. Simplified analytical configuration

Figure 7.1 Use of symmetry for Allen solutions

For span AB (x measured from A)

Deflection

$$\omega = -\frac{Px^2}{6E^*I}(3l_1 - x) - \qquad \text{..... (3.33)}$$

$$\frac{Px}{AG^*}\left(1-\frac{I_f}{I}\right)^2\left[1-\frac{1}{ax}\left(\beta_1-\left[\beta_1\cosh ax-\sinh ax\right]\right)\right]$$

Facing stress

$$\sigma = \left[P(l_1 - x) - \frac{Px}{ax}(\beta_1 \cosh ax - \sinh ax)\right]\frac{c+2t}{2I} \quad \text{.....(3.35)}$$

$$+\left[\frac{Px}{ax}(\beta_1 \cosh ax - \sinh ax)\right]\frac{t}{2I_f}$$

7.3.4 Verification of theoretical solutions with experimental results of the full scale sandwich panels

7.3.4.1 General

One of the two objectives of this chapter is the verification of theoretical solutions by comparison with experimental results. In particular both the finite element analysis package and its application are examined against Allen's solutions, which have previously been well documented and scrutinised by O'Connor (1985). This section discusses the direct comparison of finite element analysis, Allen solutions and experimental results by means of stress profiles long the outer surface of the upper and lower facings.

Each of the stress profiles sets for the five plywood faced panels are discussed and a summary of the important aspects of sandwich panel behaviour made. The most significant aspect, other than the overall matching of profile shape, is the critical span length. The critical span length being defined as the distance along the span, from a load point, that the stress profile is influenced by the local point effects. This part of the chapter also has a direct bearing on the previous chapter which examined the multiple span beam testing technique.

7.3.4.2 Discussion of stress profiles

The set of five tables D7.2 a-e summarise the local distortion lengths of the each of the panels P3, P4, P5, P6 and P10. The values held in the tables are distances along the span from a point contact to where local distortion effects subside to a negligible

amount. Stress profiles have been used in this instance as local displacement profiles are impractical to obtain experimentally. Additionally, as can be seen on figure D7.3, the critical span distance is difficult to estimate from a finite element analysis displacement profile output due to the small local displacement distortions.

The experimental stress profiles have been calculated directly from the raw data strain values during testing according to $\sigma = \varepsilon E$ where E = elastic modulus of plywood. Material and geometric properties used for the Allen and finite element solutions are identical and are as representative as possible to the panel's properties.

The values in the tables D7.2 a-e have all been obtained from direct manual estimates from the graphical representations, except in the case of O'Connor's critical span lengths. The values are therefore approximate to within 10%. It should be noted that the evaluation of the experimental critical span lengths are compromised to some extent by the location and number of strain gauges used. From practical experience it may be estimated that the critical span lengths obtained from the experimental plots are to within an accuracy of 15 mm, or 10 - 20 % of a typical recorded value. In addition, the 20 mm length of the gauges may also have an effect on the recorded strain especially at positions of changing strain gradients as the strain gauge 'averages' the reading over its length and assumes this value to be at its longitudinal mid-point. This situation would be valid if the stress profiles were linear.

It is immediately apparent that Allen's theory only models a single stress profile of one facing. This is not suggested in Allen's own text, but is shown in the work on Allen's theory by O'Connor (1987). It is not immediately apparent, from the stress profile figures, which facing the theory actually applies to. Certainly Allen's theory models the facing stresses on both outer surfaces, away from point effects, reasonably well. The theory then appears to assume that there is only the load point concentration on the upper facing at mid span. The absence of a further peak stress concentration at the support point is attributed to the discontinuity of the panel at the support with the stress assumed to dissipate to zero at the free end.

The small value of the peak stress concentration above the support is intrinsically determined by the relative stiffnesses of the facing and core. Panels P3-P6 may all be described as 'thick faced', however, panel P10 is described as 'thin faced'. The peak stress concentration, calculated by Allen's theory, at the support, is proportionally greater than the other panels and has a more pronounced peak. This is supported by the critical span lengths, for experimental, F.E.A. and Allen's solutions being substantially less than for panels P3-P6.

Simple observation of the shape of each of the five stress profile plots suggests that the F.E. analysis more closely models the panels flexural behaviour than the Allen solution, particularly near the support. This in part may be helped by the finite element analysis being freely able to yield realistic stresses in the region of the load contact points and at the same time incorporating the small overhang. The most appropriate way of evaluating the merits of the two theoretical solutions is to compare their critical span lengths to those of the experimental data. Tables D7.4 a-e contain all the critical span lengths for the five panels. The 'load point' described in the tables D7.2 a-e is the actual load point on the complete panel, not the half-panel as modelled, and similarly the support point is the actual rather than modelled support point. Table 7.6 provides a summary list for the percentage discrepancies of the theoretical solutions to the experimental according to:

$$\% = \frac{\text{Experimental} - \text{theoretical}}{\text{Experimental}} \times 100$$

The percentage differences in table 7.6 clearly show that the finite element method models the local distortion critical span length more accurately than the Allen solutions. The local distortions on the facing opposite the load or support point is not strictly modelled by the Allen solutions and is therefore not scrutinised further. The finite element model local distortion lengths on the opposite facing to the load or support points are again modelled fairly accurately when the previously discussed approximations are taken into consideration.

Panel	Theoretical	Upper facing		Lower facing	
		Support point	Load point	Support point	Load point
P3	O'Connor		205		
	Allen	111	74	111	74
	F.E.A.	16	26	5	5
P4	O'Connor		189		
	Allen	111	58	54	66
	F.E.A.	5	11	8	9
P5	O'Connor		135		
	Allen	111	50	43	50
	F.E.A.	5	0	7	20
P6	O'Connor		100		
	Allen	111	5	43	0
	F.E.A.	0	0	14	10
P10	O'Connor		78		
	Allen	22	22	42	22
	F.E.A.	11	11	11	17

Table 7.6 Percentage differences of theoretical from experimental critical span lengths

The implication of the percentage differences of O'Connor's critical span concept is that the theory greatly over estimates the critical span. This suggests that the multiple span beam testing techniques investigated in the previous chapter may be regarded in a different light. The locations, quarter and eighth span, of the LVDTs are sufficiently far away from the influences of the local distortions not to be corrupted. Local distortion at the support point is relevant as it does have a direct influence on the displacements recorded.

In the case of no overhang, the hyperbolic function controlling thick faced effects in equations 3.33 to 3.38,

$$\beta_1 = \frac{\sinh\theta + (\cosh\theta - 1)\tanh\phi}{\sinh\theta\tanh\phi + \cosh\theta} \quad \text{.....(3.29)}$$

reduces to

$$\beta_{1x} = [\cosh(ax) - \sinh(ax)] \quad \text{..... (7.1)}$$

where $\theta_x = ax$ and x is the distance along the beam as shown on figure 3.7. The critical span concept derived from Allen's (1969) theory, by O'Connor (1985), for the length of beam influenced by the local distortion of the facings sets the length at ax = 5. O'Connor assumed that the local effects dissipated with an exponential decay function given by

$$\beta_{1x} = e^{-ax} \quad \text{..... (7.2)}$$

and when $\beta_1 = 1$, $\beta_{1x} = 0$ when ax = 5. It should be noted that this mathematical model was based on antiplane cored (usually honeycombed) sandwich beam.

Both the F.E.A. and experimental data presented in this chapter indicate that the local distortion length of a transversely soft cored sandwich panel is approximately half that assumed by the antiplane cored condition. It is proposed that the critical span length may be modelled by equation 7.3,

$$\beta_{1x} = e^{-2ax} \quad \text{..... (7.3)}$$

It should be considered that this investigation was not originally directed at finding the critical span length of transversely soft cored sandwiches and a more intensive study should be conducted to verify this proposal.

7.4 Investigation of the material property tests methods by comparison of F.E.A. modelling with the experimental results of the plywood faced sandwich panels

7.4.1 Introduction

The previous section of work compared the facing stress profiles produced from the finite element modelling, Allen's solutions and experimental data. It was concluded that the finite element modelling correlated well with the flexural behaviour of the sandwich panels by comparison to the experimental stress profiles. The Allen solutions did not model the experimental stress profiles as convincingly as the F.E.A. Allied to the flexibility and potential of finite element methods the analysis has been carried forward to this section of the investigation. In this section it is intended to identify the most appropriate method of material property evaluation. The properties of Isofoam CRF have supported finite element analysis displacement predictions which have been directly compared to the experimental displacement of the sandwich panels. The elastic modulii and Poisson's ratio of the plywood facings has been found from independent four point load tests, the results agreeing well with the plywood manufacturer's claimed values. This section includes discussions regarding both facing material properties and those of the Isofoam CRF core.

7.4.2 Plywood facing material properties used for the F.E.A modelling

Four point bending tests have been used to determine the elastic modulus for the plywood facings as described in chapter 5. The result for the 9 ply Finish birch grade IV/IV, E = 9400 N/mm^2, has been supported by the manufacturers claimed figure of 9320 N/mm^2. The modulus of elasticity for the 3 ply thick plywood facing used for panel P10 was evaluated as 14000 N/mm^2, but no value has been published by the manufacturer. The confirmation with the manufacturers claimed figures suggests that the elastic modulus evaluated and adopted is appropriate. Discussion with the manufacturer indicated a Poisson's ratio of 0.20 and this has been adopted in all modelling cases. Difficulty in evaluating the Poisson's ratio was also expressed by the manufacturer, with the problems related to the orientation of the ply layers and the

interaction of the adhesive used. Panels P1 and P2 used a different type of plywood facing, a 9 ply Russian birch grade IV/IV, where the elastic modulus was evaluated as E = 11200 N/mm^2. Again this was supported by the manufacturer's value of elastic modulus, E = 11100 N/mm^2.

7.4.3 Isofoam CRF core material properties used for the F.E.A modelling

Linear elastic Isofoam CRF properties have been evaluated from uniaxial compression, uniaxial tension, shear, and multiple span beam tests. Chapter 4 investigates and discusses the uniaxial compression and tension testing where it was established that the Isofoam core mass exhibited distinct orthotropic material properties. It was assumed that the direction of rise was predominantly in the direction of the span. The lateral pressure exerted on the rising foam mass by the edge containment created ovoid shaped cells orientated in the spanning direction. The elastic modulus was found to be greater in the spanning, or x-direction, than in either the transverse or through thickness directions (x-, y- and z-directions respectively). The elastic modulus was assumed to be equal in the y- and z- directions.

The shear and multiple span beam tests evaluated the shear modulus of the core in flexure as opposed to the direct compressive and tensile nature of the uniaxial tests. The type, direction and orientation of the applied strain in each test and the material property evaluated have been considered. The material properties used for the comparative finite element analysis were orthotropic. The principal property in the x-direction has come directly from each individual test method, but through thickness properties (in 2-dimensional analysis this is the y-direction) have been taken from the uniaxial compressive testing. It was felt that this procedure was more representative than assuming isotropic homogeneous properties. Where the shear modulus was evaluated from testing, ordinary stress / strain relationships have been used to derive an elastic modulus and vice versa where the elastic modulus is found from a test. The finite element analysis concurs with this assumption. Poisson's ratio values have also been taken from the uniaxial compression tests as no other test incorporates the necessary

evaluation. Poisson's ratio values used in the finite element analysis for Isofoam CRF sample from any one panel have all assumed equal.

7.4.4 Presentation and discussion of the F.E.A. and experimental results

7.4.4.1 General discussion and summary of F.E.A. and experimental displacement result percentage discrepancies

Tables 7.7a and 7.7b summarise the percentage differences between finite element analysis displacements of panels, using the various material properties derived from the sub-element testing, from the experimental full scale panel test displacements. The displacements have been compared at both quarter and eighth span. The quarter and eighth span displacements have been adjusted by the local compression of the core and bending of the lower facing. Table 7.7a contain the percentage difference values for panels P1 and P2 and table 7.7b those values for panels P3-P6 and P10. The percentage differences have been in the tables have been generated from the load / displacement figures D7.9 a-b, D7.10 a-b, D7.11 a-c, D7.12 a-c, D7.13 a-c, D7.14 a-c and D7.15 a-c for panels P1, P2, P3, P4, P5, P6 and P10 respectively.

The finite element analysis displacements have been calculated by subtracting the compression of the core above the support from the total recorded displacement at both quarter and eighth span. This has been necessary for a more accurate comparison as the experimentally recorded displacements at quarter and eighth span have been also reduced by the displacement at the supports. The experimental support displacements comprise core compression, local bending of the lower facing and any support movement during loading. In addition, the experimental displacements at either support were rarely identical and a weighted average has been incorporated when subtracting from the eighth and quarter span displacement locations.

		Panel no.			
Test method	Description	P1		P2	
		δ_4	δ_8	δ_4	δ_8
UC	Uniaxial compression	N/A	N/A	N/A	N/A
UT	Uniaxial tension	N/A	N/A	N/A	N/A
ST BS XH	Shear test British Std. crosshead	19	23	2	1
ST BS XP	Shear test British Std. crossplate	15	18	-8	-9
ST ASTM XH	Shear test American Std. crosshead	8	12	-4	-5
ST ASTM XP	Shear test American Std. crossplate	7	11	-11	-12
MSBT Type 1A	Multiple span beam test, Type 1A	-5	-2	-3	-1
MSBT Type 1B	Multiple span beam test, Type 1B	-16	-14	-11	-10
MSBT Type 2A	Multiple span beam test, Type 2A	-6	-3	12	11
MSBT Type 2B	Multiple span beam test, Type 2B	-16	-14	14	13

Table 7.7a Summary of percentage discrepancies from experimental to F.E.A. displacements with material properties generated from the described test methods

	Panel no.									
Test method	P3		P4		P5		P6		P10	
	δ_4	δ_8	δ_4	δ_8	δ_4	δ_8	δ_4	δ_8	δ_4	δ_8
UC	61	56	28	21	5	2	17	12	-26	-21
UT	N/A	N/A	12	7	5	2	4	0	-19	-20
ST BS XH	-17	-19	-3	-8	11	7	18	13	-6	-7
ST BS XP	-18	-20	-11	-16	0	-3	9	5	-10	-11
ST ASTM XH	-23	-25	-15	-19	10	-10	4	0	-9	-11
ST ASTM XP	-18	-27	-19	-23	-12	3	-5	-10	-11	-13
MSBT G_{84}	-16	-18	-15	-19	-17	-20	-13	-15	0	-3
MSBT G_{40}	-14	-16	-13	-17	-13	-14	-9	-13	0	-3
MSBT G_{80}	-13	-15	-9	-12	-9	-16	-7	-13	6	4

Table 7.7b Summary of percentage discrepancies from experimental to F.E.A. displacements with material properties generated from the described test methods

It has been possible to identify certain trends in the values held in tables 7.7a and 7.7b intrinsic to the methods of material property evaluation and also to the behaviour of

each individual panel. It has been appreciated that in all cases of material property test methods a relatively small number of samples have been used for each panel. This would probably have been significant, in a study such as this, if only one panel were tested. However, if there were general trends apparent across the whole range of panels the total number of samples then represents a reasonably large sample size.

7.4.4.2 Errors common to all panels

Finite element analysis. Previously it was established that the accuracy of finite element analysis for modelling the intricacies of sandwich panel flexural behaviour was to within a theoretical approximate maximum of 2% (for linear elastic materials) the remaining errors in tables 7.7a and 7.7b must be attributed to the apparent physical properties used in the analysis and experimental practices. The errors related to F.E.A. were common for all panels and therefore should not affect the relative discrepancies from one test method to another, but only their relation to the experimental results.

Experimental equipment. LVDTs were calibrated prior to both the multiple span beam testing and again before the full scale sandwich panel test programme. There appeared to be no measurable discrepancy between the two calibrations and it was assumed that very little inaccuracy could be attributed to LVDT displacements. The location of each LVDT was carefully made and verticality manually checked with a square and spirit level. Loading rates were kept constant and similar for all panels used in the main batch of tests. Load application was made by a manually operated hydraulic jack in panels P1 and P2 tests while the remaining tests used an electronically controlled load actuator ram.

Manufacturer's quoted tolerances for strain gauge resistance was +/- 0.25%. It was therefore assumed that the gauges themselves did not contribute to experimental error. The thickness and behaviour of the adhesive was of some concern. Analogous to the bonding of the Isofoam CRF specimens to the edge plate, the adhesive line and surface preparation was considered very important. Each gauge was placed manually with the adhesive being squeezed to a thin film. A small load was then applied for 24 hours

during the completion of the curing process. The surface of the plywood was prepared by sanding the wood grain smooth and carefully removing remaining dust particles first. Two parallel lines of gauges were attached to one half of each panel. The results at each span distance were averaged. It was not obvious from the stress profiles that there were any anomalous reading and therefore it was assumed the gauges were operating normally and producing good results.

Interpretation of experimental results. The linear elastic analysis finite element and Allen solutions employed to model the displacement (and facing stress response) required the experimental results to be approximated by a linear load / displacement relationship. The linear approximations shown on figures D7.9 to D7.15 are drawn along the initial linear portion or tangential to the curve usually from the origin. It is difficult to attempt to identify what discrepancies may exist with a linear approximation of this nature, but it has been accepted that some inaccuracy does exist.

7.4.4.3 Differences between quarter and eighth span displacement percentage discrepancies

The percentage discrepancies in tables 7.7a and 7.7b show that in all cases there was some difference between quarter and eighth span values. For panels P3 to P6 and P10 the eighth span has a slightly lower numerical value of percentage discrepancy to the quarter span. Over the complete range of panels this indicates the presence of a consistent trend between the finite element modelling and the experimental results. A similar trend was observed during the multiple span beam testing analysis, where the conjugate point method clearly showed a discrepancy between quarter / support and eighth / support span shear modulii. At first some of this difference was attributed to the local distortion effects causing a slightly greater displacement at the quarter span than eighth span position. However, in the light of the finite element and experimental strain profiles showing the critical span lengths (held in table D7.2 a-e) to actually be quite short and not influencing the displacements at quarter or eighth span, this argument does not seem valid.

7.4.4.4 Physical properties of the plywood facings

One assumption that was made early on in the project that the plywood facings for panels P3 to P6 were all identical in material properties. Certainly this was indicated by the manufacturer's claimed figures and with no 'range' for a specific modulus value given it seemed a reasonable assumption to make. However, as the four point load plywood beam tests indicated, there were significant differences in elastic modulii encountered. Values ranged from 9100 to 9800 N/mm^2, an 8% difference, which approximately might relate to an approximate 4% displacement difference. This possible source of error may only be related to the difference between F.E.A. and experimental results for one particular panel.

The percentage discrepancies for panel P10 are nearly all negative which would indicate that the facings are stiffer than had been evaluated in the four point bending tests.

It has also been assumed that the shear stiffness of the facings is proportional to the elastic modulus derived from the bending tests. This was thought to be a reasonable assumption as the main structural involvement of the facings is in the bending stiffness rather than shear stiffness. As the plywood is intrinsically a laminate structure, with the adhesive line being subject to in plane shear forces, it is likely that the shear stiffness is not proportional to the elastic modulus. What it actually is has not been determined and was not available from the manufacturer. However, the difference in shear stiffness between the plywood and Isofoam and the relevant cross sectional areas points to the conclusion that the shear stiffness of the plywood, probably somewhere above 1000 N/mm^2, is not a significant factor in the overall displacement response.

7.4.4.5 Differences between the material property evaluation methods

Special mention of panel P3 should be made before attempting to assess the most appropriate material property test method. There are two issues to consider, firstly that, in terms of sandwich definition, panel P3 is the least economic construction having *very thick* facings. Secondly, the quality of the Isofoam is poor in comparison to the other

panels. This is probably due, in part, to the core thickness, 21 mm, not being conducive to the foaming and rising process. Certainly all the samples taken from the core for coupon testing uncovered volumes of highly varying stiffness and size of cellular formation.

The discussions below for each of the testing methods do not relate to panels P3 or P10 as there are obvious adverse influences from poor Isofoam quality or other inappropriate material property evaluation other than the Isofoam core.

Uniaxial compression testing under estimates the elastic modulus of the core although the results generally improve with increased core thickness. The uniaxial compression tests are fundamentally flawed as the axial load is applied in the z-direction and not the x-direction as required. The uniaxial test results improve with increased core thickness as the quality of the foam is better and its orthotropic nature becomes less.

Uniaxial tension testing also predominantly under estimates the elastic modulus of the core although the percentage discrepancies are small. The uniaxial tension testing elastic properties provide numerically the best displacement results of all across the range of panels. This is partly explained by the fact that the tension tests are freer from test anomalies and partly from the fact that the tests are conducted on coupons orientated in the direction of the span and therefore more representative.

Despite the apparent success of the uniaxial tension tests the results, and those of the compression tests, should be used with caution as the foam core is principally subject to shear strains in the zx-plane.

Shear modulus testing produces results that for each panel are reasonably consistent although from panel to panel the displacement results both over and under estimate the panel displacements. It would be inadvisable to choose one shear test method from the comparative study to the be the most appropriate as other factors such as F.E. modelling, testing and facing properties all contribute to the inaccuracies incurred.

The *multiple span beam testing method* in all cases except panel P2 produces an over estimation of the elastic modulus. The graphical evaluation method 'type 1' gave the closest results for panels P1 and P2 and this type was thus adopted for remaining panels. For panels P3 to P6 a general trend that is apparent from the testing results is that the three conjugate point shear modulii produce smaller, and therefore better, absolute displacement discrepancies in the following order, worse to better, G_{84}, G_{40} and G_{80}.

Tests on beams to identify material properties of the component parts of the panels they were cut from intrinsically points to the evaluation of potentially accurate material properties. The three types of conjugate point method for panels P4 to P6 all over estimate the elastic modulus of the Isofoam. This suggests that there is either a common error throughout the testing procedure or graphical and theoretical analysis of the multiple span technique or the properties of the facings are inappropriate.

7.5 Conclusions

These conclusions have been made subject to the findings and methods detailed throughout this thesis so far. It should be noted that the Isofoam CRF used in this study has been placed by the foam injection system. This system inherently creates an orthotropic foam mass with local variabilities in foam quality. It is recommended that these conclusions be verified by a more intensive and specific study with a greater number of tests specimens. In evaluating the material tests in this way it would be preferable to use an isotropic and homogeneous foam. The foam specified for the plywood faced sandwich panels was designed to represent that which would be commonly found in applications of the foam injection system to masonry cavity walls.

7.5.1 Conclusions to the theoretical modelling of sandwich panel behaviour

These conclusions are based on the direct comparisons of proven and well understood theory to reasonably well controlled experimental data. It should be remembered that the critical span lengths have been measured manually from the graphically represented

stress profiles and not from a theoretical stand point except in the case of O'Connor's lengths. This potentially disregards some of the very small displacements and strains at the further most positions of the critical span lengths, which may have been theoretically present, but as such does provide a more practical justification to measured displacement response within the span.

(i) Finite element analysis has been proven to give good agreement with experimental data both for the overall shape of the stress profile and to the critical span lengths. It is recommended that two dimensional plane strain finite element analysis is used for modelling wide and uniform sandwich panels. The finite element models have used eight noded two dimensional continuum elements. The facings have been modelled using two element deep mesh and the core a seven elemental deep mesh.

(ii) Allen solutions approximate the stress profiles only for one facing. The solution tends to under estimate the magnitude of stresses away from the local distortions and over estimate the stresses near the point load positions. In practice Allen's theory, developed by O'Connor, for the critical span lengths over estimate the experimental critical spans, although this may be due to the ability to visually detect very small stresses and displacements.

(iii) O'Connor's critical span concept seriously over estimates the experimental critical span lengths by up to 200 %. However, the use of conjugate points for the multiple span testing method was still necessary due to the local displacement distortions at the centre span load point.

(iv) The displacement measurements in the multiple span beam testing of chapter 6 have not been adversely influenced by the local point effects as first anticipated by O'Connor's critical span concept.

(v) Tables D7.2a-e give the local distortion lengths derived from O'Connor's critical span concept, finite element analysis and experimental results. From the values held in the tables it is possible to conclude that the critical span length is different for

transversely soft cored sandwiches than as suggested by the critical span equation $ax = \pm 5$, where $a^2 = \frac{AG}{E_f I(1 - E_f/E)}$ and $A = bd^2/c$. Instead both the finite element analysis and experimental data point to the critical span of $ax = \pm 2.5$, at which value $\beta_{1x} = 0$, assuming exponential dissipation of thick faced effects according to $\beta_{1x} = e^{-2ax}$, equation 7.3.

7.5.2 Conclusions to the material property evaluation method comparison

(i) The multiple span beam testing results for the three conjugate points showed a consistent trend of the evaluated shear modulus of the core. The difference between quarter / support, eighth / support and quarter / eighth span conjugate points may be explained by considering the finite element displacements. For any given shear modulii used in the finite element analysis the displacement predictions at quarter and eighth spans were found to consistently have the same discrepancy when compared to the experimental displacements. The finite element modelling took into consideration the compression of the core and the local bending of the lower facing at the supports. It may therefore be argued that the assumptions used in the Allen solutions were not valid for polyurethane cores. However, it should also be remembered that the Allen solutions were based on honeycombed cores where the assumptions of an antiplane and incompressible ($E_y = \infty$) core were more appropriate.

(ii) The plywood facings elastic modulii for panels P1 and P2 and P3-P6, 11100 and 9400 N/mm^2 respectively, were supported by manufacturer's claimed values. These values were adopted for the all facings in their respective groups. Retrospectively a greater number of four point load tests on coupons from individual plywood sheets to determine the modulii for that facing would have been preferable. The variation in the four point load tests on all coupons represented an 8% difference in modulus value.

(iii) Orthotropic material properties for the plywood facings and Isofoam CRF core have been used in the finite element analysis of the sandwich panels. A degree of judgement and assumptions were required to implement orthotropic properties of the

core. Uniaxial compression results provided the Poisson's ratio and y- direction elastic modulii.

(iv) Attention should be brought to the relative strain rates of the material testing methods and those of the full scale panel tests. Inherent difficulty was encountered simulating both the strain rates, particularly of the Isofoam CRF, as the applied loads between test methods was different. Discrepancies of this nature have probably contributed to some differences between experimental panel displacements and F.E.A. results using material property data. However, it may be argued that this is built into the ranking list for the most suitable material property test method.

(v) Identification of the most appropriate material property evaluation method has been made by considering the percentage discrepancies from experimental displacement results to F.E.A. displacements supported with material properties generated from the various test methods. Identification has been made by averaging the magnitudes of the percentage discrepancies to obtain a numerical ranking value for each test type. Table 7.6 displays the a ranking list for each test type .

Panel	Test method	Average value	Ranking for test type	Overall ranking
P3-P8 & P10	UC	25	2	13
P3-P8 & P10	UT	8.6	1	4
All	ST BS XH	8.6	2	4
All	ST BS XP	10.3	3	6
All	ST ASTM XH	8.2	1	3
All	ST ASTM XP	13.1	4	10
P1 & P2	MSBT Type 1A	2.8	1	1
P1 & P2	MSBT Type 1B	12.8	3	9
P1 & P2	MSBT Type 2A	8.0	2	2
P1 & P2	MSBT Type 2B	14.3	4	12
P3-P6 & P10	MSBT G_{84}	13.6	3	11
P3-P6 & P10	MSBT G_{40}	10.9	2	8
P3-P6 & P10	MSBT G_{80}	10.4	1	7

Table 7.8 Rankings for the material property evaluation methods

From table 7.8 the rankings suggest the following:

- that the multiple span beam tests type 1A and 2A give the best evaluation of elastic modulii. Type 1A and 2A do not utilise the predetermined elastic modulus of the facings. In fact the modulii of the facings found from the MSBT varied markedly from those determined from the four point loading of facing coupons.

- the ASTM C273-61 crosshead displacement test method produces the best shear test results with the BS 4370 crosshead displacement results also producing reasonable agreement. For applications where the multiple span beam testing method is inappropriate shear testing would be the most suitable method.

- the uniaxial compression testing appears to be quite wide of the mark and is not advisable as a test method for the evaluation of the elastic modulus. The uniaxial tensile testing does provide reasonable results and could be used as an economic alternative to the other test methods.

- the revised multiple span beam testing using the conjugate point method produced consistent results, but also proved to have significant variation from the actual properties of the Isofoam CRF core. These results were particularly disappointing as the beam tests were so similar in their flexural testing nature to the panel tests. This may point to the some of the error being derived form the assumptions made in Allen's solutions, where honeycombed cores were considered rather than expanded plastic used here.

CHAPTER 8 - MASONRY WALLETTE AND CONSTITUENT TESTING AND ANALYSIS

8.1 Introduction

8.2 Masonry component testing and analysis

8.3 Wallette test methods

8.4 Results and analysis

8.5 Finite element analysis

8.6 Discussion

8.7 Conclusions

CHAPTER 8 - MASONRY WALLETTE AND CONSTITUENT TESTING AND ANALYSIS

8.1 Introduction

8.1.1 Objectives of masonry wallette testing

The principal aim of the masonry wallette testing is to determine an elastic modulus for bending stiffness in the spanning (vertical) direction. It was also intended to evaluate an ultimate strain criterion that could be used for predictive strength analysis. Strain readings were recorded across each mortar joint at equal load and time intervals. However, it is unlikely that the exact strain value at failure has been recorded as failure may occur between reading intervals.

In characterising the elastic and ultimate flexural behaviour of the wallettes, the behaviour of the full scale masonry cavity walls subject to a lateral load may then be modelled. Due consideration of experience and technique gained from the previous testing and analysis of the plywood faced sandwich panels has also been incorporated.

All masonry elements were built and tested in the Nottingham Trent University heavy structures laboratories.

8.1.2 Review of relevant literature

Relevant literature was deemed to comprise not only direct wallette testing but also any lateral load testing and analysis regarding masonry structures. In addition, sources of information relating to other contributory factors that effect the flexural behaviour and strength of masonry have been discussed. Important to both the flexural behaviour and ultimate strength of a masonry structure is the quality of the bond between mortar and brick unit. Literature relating to factors influencing the bond characteristics have assisted in the designation of complementary materials to achieve a good bond.

8.1.2.1 Laterally loaded brickwork

Flexural bond strength. ASTM C 1072-93 covers the method for the determination of flexural bond strength of mortar to masonry unit. Although this interaction drives the ultimate strength of a masonry structure in flexure it does not provide for the assessment of elastic modulus and, as such, the actual bond strength is not required in this investigation.

Wallette testing. Satti and Hendry (1975) conducted flexural tests on wallettes to find the modulus of rupture of brickwork. Various brick types were used together with two designations of mortar. The findings concluded that the modulii of rupture do not correlate well with other properties except the initial absorption rate of the masonry units. It was recommended that a mortar specification 1 : 1/4 : 3 produced an improved bond strength over 1 : 1 : 6 mortar in flexure.

West and Beech (1979), at the then British Ceramic Research Association, collated a considerable number of wallette tests to provide statistically proven information on the influence of water absorption of the bricks and the grade of mortar on the flexural strength of masonry. The results, based on a 95% confidence limit, have formed the basis for the characteristic flexural strengths of brickwork in BS 5628: Part 1: 1978.

BS 5628 recommends the use of wallette testing to determine the ultimate strength of a specified brick / mortar combination. However, to obtain the elastic modulus of the masonry specified using the BS 5628 method, additional flexural monitoring is required. Mid-span deflection, with careful monitoring of any support movement, may be plotted against applied load and from ordinary bending theory, the elastic modulus is found.

Anderson (1982) observed that when using the two bricks long, ten course high wallettes, recommended in BS5628, failure almost always occurred along the mortar/brick interface where there was only one header joint. He recommended that an equal number of header joints should be present in each bed joint and makes further observations on the testing of wallettes. This appears to be a valid point although each

mortar joint will have one header joint on one side and two header joints on the other. In this project the wallettes have been specified as four masonry units wide by ten courses high.

de Vekey et al (1982) reported on the BS5628 flexural test of wallettes from four separate laboratory programmes. It was found that there was a larger than expected variation in the results despite the use of common materials and workmanship and it was concluded that improved test specifications should be adopted in BS 5628. These measures have been incorporated into the current BS 5628 methods used in this project.

The elastic properties of masonry are not well researched with only limited references as described below. Most masonry analysis and design is concerned with the ultimate load capacity from which empirical strength formulae are based. Powell and Hodgkinson (1977) describe the stress-strain relationship of masonry under uniaxial compressive load and found the curve to be parabolic in shape suggesting a non-linear relationship. Dhanasekar et al (1982) presented a study of the elastic behaviour of brickwork under biaxial stress. Values of elastic modulus parallel and perpendicular to the bed joint in the plane of the wall are given although no values were derived for bending normal to the plane of the masonry.

When investigating the effect of thickness and bond pattern on the lateral strength of brickwork in wallette tests, Lovegrove (1988) found that the lateral strength of brickwork depends on the strength of the mortar in the bed joints. Using finite element analysis to investigate the tensile stresses in the brickwork, it was concluded that it was not necessarily those stresses which determined the structure's strength but in fact the bond stresses.

The elastic modulus in compression has been evaluated using different statistical analyses depending upon the type of application. Two standard tests are currently available, the NORDTEST uses tangent modulii from the stress-strain curve whilst the RITTER curves approximate the stress-strain relationship with parabolic and logarithmic curves. Knutsson and Neilson (1995) investigated both of these methods. It

is proposed, however, to use a simple tangential evaluation for the load / deflection relationship throughout this study.

Laterally loaded masonry walls. Single wythe brickwork walls of single, or greater, storey height subjected to horizontal lateral loads are also of importance as the methods and techniques of testing and analysis may be applied both to the wallettes and cavity walls in this project.

In an overview of the lateral strength of brickwork, Baker (1977), states that "A complete understanding of the behaviour of brickwork when subjected to lateral loads has largely eluded researchers despite concentrated efforts ...", and this still appears to hold today. The overview considers various ways of testing the lateral resistance of brickwork and examines secondary effects associated with load application, support details, testing frame stiffness and self weight. Conclusions drawn from the study indicate that, at an extreme, secondary effects, present in the test methods of many different establishments, may increase the ultimate strength by 60% although 33% would be more usual.

Currently there are four methods of predicting the lateral load behaviour and capacity of a masonry wall panel in flexure. These are elastic plate theory, finite elements analysis, yield line theory and the strip method. The former two methods calculate the elastic behaviour up to the formation of the first crack. The latter two forms of analysis predict the ultimate capacity.

The BS 5628 design recommendations for laterally loaded walls is based on a yield line theory proposed by West et al (1977) after an extensive testing programme conducted by Haseltine et al (1977), as there was found to be good correlation and a simple method of application. Lawrence (1979) at the Experimental Building Station in Sidney, Australia also conducted an investigation into the lateral load resistance of masonry infill panels with the aim of supplying designers with suitable guidance. Additional testing of small walls to monitor the bond strengths and flexural properties were carried out.

Anderson (1985) reported on the partial fixity at the base of test walls subject to lateral loads due to self weight giving some degree of stabilisation when considering the strength of the masonry cavity walls. Mullins et al (1991) studied the magnitude of base restraint and its dependence on elastic modulii of the masonry elements, top support stiffness, surcharge loads and damp proof course thickness with the use of finite element analysis methods. It is expected that self weight will have some effect when regarding the full scale masonry cavity walls although no account of self weight will be considered for the wallette testing.

Fried et al (1988) pointed out that the chosen method of predictive analysis should relate to the type of material test used. Thus a full understanding of how the tests are performed, all material specifications, curing and test dates are essential to be able to justify one type of analysis.

Lawrence (1988) presented an analysis based on the elastic plate theory for the prediction of loads to cause the first crack but concluded that accurate predictions were difficult due to the random variability of masonry.

8.1.2.2 Factors effecting flexural strength of masonry

It is well known that two masonry specimens, seemingly identical in preparation and constituents, may have markedly different ultimate strengths. Baker (1979) investigated the age of the specimen, curing conditions, the flow of the mortar and the composition of the mortar. He concluded that all these factors were significant in the strength test results, but it was difficult to quantify each of these factors precisely. The most significant factor to influence the flexural strength and stiffness of masonry was the flow of the mortar. In general the greater the flow the stronger the bond. Drysdale et al (1985) reported on a parametric study of the influence of the constituents on mortar properties. In addition to the parameters studied by Baker, sand gradation of the mortar and water absorption and strength of the brick unit were examined. Again certain trends were apparent but only qualitative guidelines were given.

Experimental investigations on the flexural bond strength of masonry by Ghosh (1990) indicate that it is not only the mortar properties that influence the bond but that it is the combination of the types of mortar and masonry unit chosen. de Vekey et al (1993) observed various joint finishes along bedding planes, by testing the masonry in flexure, and found that joint type had no significant effect on strength. de Vekey found that unfilled header joints did influence the strength markedly.

The 'Handbook to BS5628' (1988) clearly shows that flexural strength parallel to the bedding joints is directly related to both water absorption and water / cement ratio. The relationship between water absorption and strength shows that the lower the absorption the stronger the bond. Absorption of water by the brick units deprives the cement of its water of hydration and it is therefore essential to choose a suitable mortar to be used with the brick units supplied. Similarly, the higher the cement content the stronger the bond in flexure.

de Vekey (1985), also reporting on aspects of the influence of mortar type on the flexural strength of masonry, found that there was an increase in wallette flexural strength with an increase in mortar compressive cube strength. Additionally, mortar with a lime content also produced an increased flexural bond strength. However, the introduction of lime was found to cause a small number of very low and anomalous results whereas mortars without lime did not and were more consistent.

8.2 Masonry component testing and analysis

As the wallette testing supports the analysis of the cavity walls it is obviously essential for there to be continuity of material types, construction and curing methods used. A single, experienced and skilled brick layer was employed for all masonry constructions and briefed to provide the most consistent workmanship possible. Butterley Brick Ltd supplied 'end of line' grade B engineering bricks so a suitable mortar designation was chosen accordingly. It was therefore necessary to test the initial suction rate of the brick units supplied and the water absorption.

Structural testing of the components comprises mortar cube and brick unit uniaxial compressive tests. This short study was intended to identify the elastic modulii of both the mortar and brick components, while at the same time provide some form of quality assessment for the mortar batches.

8.2.1 Initial suction rate and water absorption of masonry units

Yorkdale (1982) concentrated an investigation on the initial rate of absorption and mortar bond concluding that there appeared to be no obvious relationship and that further study should examine such factors as roughness and pore structure of the masonry units. Gazzola et al (1985), investigating the influence of mortar materials on the flexural tensile bond strength of block and brick masonry, concluded that there did not seem to be any correlation between tensile bond strength and initial rates of absorption of the masonry units.

However, for the record, twenty brick units were tested in accordance with BS 3921 methods determining the initial suction rate and water absorption. The initial rate of absorption was found to be 0.92 kg/m^2 per minute, and the water absorption, A = 5%. These figures were confirmed by Butterley Brick LTD's (1993) 'A complete guide to Butterley Brick products' manual.

8.2.2 Component material selection

The mortar designation has reflected the previous research findings and subsequently the specification used was 1 : 1/4 : 3 (cement: lime: sand) which should complement the strength of the brick units. The outstanding factor remaining was the water / cement ratio. Taking account of the suggestion that an increase in compressive cube strength is related to an increase in flexural bond strength, the water / cement ratio was chosen for that mixture which has the strongest axial compression value. Allied to the water / cement ratio is the increase in bond strength due to mortar flow and workability.

Six samples of five different water / cement ratios were selected and plotted against their averaged compressive strengths. Figure 8.1 shows the relationship with the choice of the final water / cement ratio being 0.52. This ratio would be later vindicated by the compressive strength of the cubes from the working mixes to be, on average, 14.0 N/mm^2. In order to maintain the consistency of the water / cement ratio, all mortar batches used pre-dried sand.

Figure 8.1 shows an increase in compressive strength with an increase in water / cement ratio up to the peak of the graph. The increase in strength is related to providing enough water to react with all the cement present to produce the optimum mortar matrix. A decrease in strength after the peak occurs as the excess water in the matrix evaporates leaving voids in the matrix.

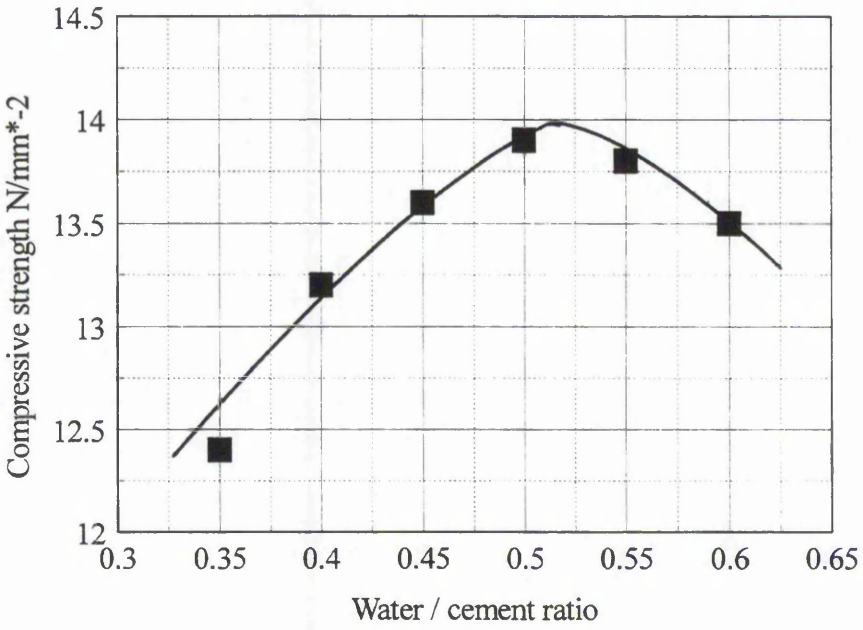

Figure 8.1 Water / cement ratio versus compressive strength

8.2.3 Elastic modulus and compressive strength of masonry units

The brick unit tests were unsuccessful in that they did not yield reasonably realistic elastic modulii values. Problems were encountered with both methods of displacement

measurements, strain gauges and LVDTs. In both cases strain in the bricks, before failure, was almost negligible and those which were recorded were corrupted by the inaccuracy of each method at such low levels of displacement. Additionally, spalling and cracking of the outer faces of the brick units early in the loading ramp immediately gave erroneous results.

Consultation with Butterley Brick Ltd indicated similar occurrences during testing, however, it was suggested that an elastic modulus of 16 000 N/mm^2 could be tentatively used. This value has been adopted for the finite element analysis presented later. The elastic modulus for brick units value has essentially be chosen to give good agreement of F.E. modelling to experimental. A number of models were run with varying elastic modulii until a good match between F.E. analysis predictions and experimental data was achieved. Additionally, Poisson's ratio effects would have been distorted by the perforations through the thickness and the intrinsic void content of the clay bricks. It has been assumed that Poisson's ratio is 0.20 for the masonry units.

8.2.4 Elastic modulus and compressive strength of mortar cubes

The mortar cubes were manufactured and cured according to BS 5628 and used standard 100 x 100 x 100 mm square steel moulds. Each mould was placed on a vibrating table and continuously filled until a positive meniscus formed when a smooth edge trowel skimmed any excess material off. A slight convex meniscus remained that would later level to the horizontal due to shrinkage effects.

The mortar cube uniaxial compression tests were successful in that they produced an elastic modulus, Poisson's ratio values and an ultimate strength. For each construction day, comprising one wallette and one half of one cavity wall leaf, six batches of mortar were made. Initially, six cubes were taken from a trial batch of mortar and tested. Their compressive strengths were found to be close enough to assume a uniform mix quality. From the results of the trial batch tests only one cube was taken from each of the six batches throughout the daily construction phase of the wallettes and cavity walls.

In all seventy-two cubes were tested for ultimate compressive strength, elastic modulus and Poisson's ratio values. However, as the mortar cubes proved to be reasonably uniform in strength and elastic modulus only twelve cubes were evaluated for elastic modulii and Poisson's ratio. Figure E8.1 illustrates a cube test load versus displacement relationship. Values of elastic modulus and Poisson's ratio were evaluated from the central linear portion of the experimental plot. Unlike the Isofoam uniaxial compression tests there were only small displacements present and it was assumed that barrelling and three dimensional effects caused an insignificant influence over the readings. Table E8.1 a and b give the details of the mortar cube uniaxial compressive tests. Table 8.1 below gives averaged values.

As can be seen there is a marked difference between Poisson's ratio values in the x-direction and y-direction. The x-direction and y-direction are arbitrary, mutually perpendicular axes that only relate the orientation of each cube. The y-direction Poisson's ratio was taken from the lateral displacement of the open face of the cubes, when in their moulds. The irregularity of this face may contribute to the disproportionate Poisson's ratio values in the x- and y-directions although another explanation may relate to particle orientation in the mortar and separation of the constituents. As a vibrating table was used to remove voids from the mortar and allow compaction there would certainly be enough energy put into the system to allow rotation of particles into a certain orientation relating to their least potential energy. In addition, any voids remaining in the matrix may also contribute to the different Poisson's ratio values by either forming ovoid shapes or there being more voids near to the free surface.

Ultimate compressive strength	14 N/mm^2
Elastic modulus	2500 N/mm^2
Poisson's ratio x-dir	0.20
Poisson's ratio y-dir	0.28

Table 8.1 Uniaxial compressive mortar cube averaged test results.

During compression it was noticed that there was a tendency for the free face to spall prior to the cube failing. This may indicate further that the material near to the free face varies from the rest of the mortar cube. For this reason the Poisson's ratio in the x-direction has been adopted throughout the finite element analysis of masonry structures containing mortar.

8.3 Wallette test methods

8.3.1 Environmental conditions and conditioning of component materials and wallettes during and after construction

Ambient environmental conditions had to be accepted throughout the manufacture of the masonry elements. The automatically controlled heating and ventilation system enabled a reasonably constant temperature and relative humidity to be present throughout the build and test programme. Temperatures were recorded throughout each day and varied from 19.0 to 21.4 ^{0}C with relative humidity variations from 48 to 57%. The temperature and relative humidity levels tended to increase during each day but kept within the limits given above.

Brick units were not wetted before mortar application. The mortar was mixed in small batches to prevent drying or hardening before application and kept under a damp covering. All masonry rises for the cavity walls were sixteen courses high whereas the wallettes were complete with ten courses. Each were immediately covered with damp hessian and plastic sheeting and had three additional dry courses laid on top to provide a compressive load. The compressive load was then present for at least 48 hours and the curing measures were in place for a minimum of seven days.

During one day, construction comprised one wallette and one sixteen course high rise for a cavity wall. This represented one half of one leaf of each of the three cavity walls. Thus the wallettes and the cavity walls could be more suitably compared.

8.3.2 Four point load test configuration

A four point line load configuration was chosen in accordance with the recommended method in BS 5628. Uniformly distributed loading was considered but the additional difficulty in test set up and pressure/load calibration meant that it was unnecessarily impractical. A single point load was also thought of but the concentrated shear force and bending moment under the load may create premature failure of the wallette. Figure 8.2 shows the four point line load used. The supports, shown on the right hand side of the figure, were positioned at the outermost edge of the brickwork while the load application points were positioned at the centre of a brick unit. Load was applied through a single hydraulic jack and evenly distributed through I-beams to the two solid steel cylindrical bars. The wallettes were placed on a solid steel cylinder to allow free rotation during flexure.

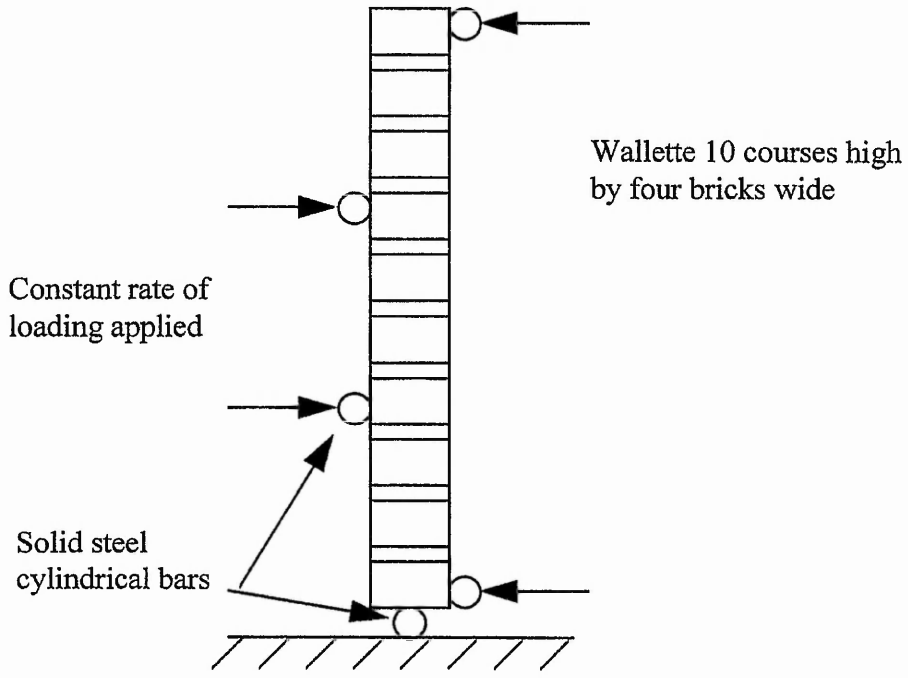

Figure 8.2 BS 5628 Wallette Test

Contact between the steel bars and the brickwork was of concern as the masonry face was slightly uneven causing possible single contact points rather than a continuous line contact. To resolve this problem a rapid setting plaster was used to fill an approximately 6 mm gap between a metal strip and the brickwork, thus allowing even contact. Figure 8.3 shows the system as employed. This system also enabled the contact between solid cylinders and wallette to be parallel to one another as the metal strip could be chocked out appropriately.

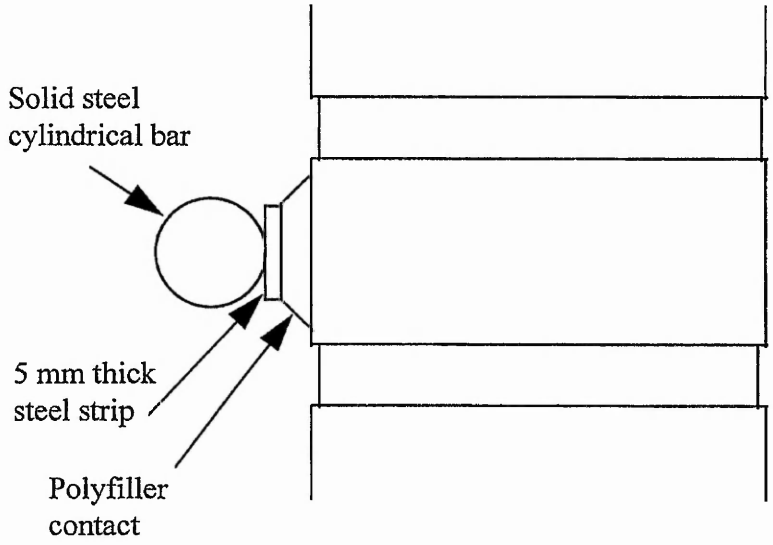

Figure 8.3 Method used to provide an even load distribution

8.3.3 Testing procedure and flexural monitoring

Two wallettes were tested the day before and two the day after each related cavity wall test sequence. All masonry elements were tested at a minimum age of 28 days. For the purposes of this study it has been assumed that all the masonry specimens had reached relatively equal strength and modulus of rupture values in terms of age relations.

Displacement measurement and positioning. Load was applied through a single hydraulic ram in increments of 0.4 kN at which LVDTs and strain gauges were read. Two transducers were placed at mid height and two on the opposite side to each upper and lower support. The failure load was recorded for each wallette.

Strain gauging and positioning. A single column of strain gauges were placed on both sides of the wallettes, a gauge over each joint. With failure and significantly most flexural response expected at the mortar / brick unit interface and in the mortar a 30 mm gauge length was used to adequately cover the average joint thickness of approximately 10 mm. Although a flush mortar joint was specified slight shrinkage had recessed the mortar from the brick face. Application of strain gauges is discussed in more detail below.

After conducting uniaxial compressive tests on mortar cubes and the engineering brick units it has been concluded that the difference between modulii values is greater than an order of magnitude. Allied to previous research experience indicating bond failure as the most likely governing factor of strength, it was therefore felt reasonable to assume that the vast majority of the elastic flexural behaviour of the wallettes must be derived from the stress / strain behaviour across the mortar joint.

8.3.4 Application of strain gauges to mortar joints and brickwork

Discussions with strain gauge manufacturers, Measurements Group Inc. and Techni Measure, indicated that a polyester backed wire strain gauge and a two part quick curing araldite adhesive. However, surface preparation was essential as a good and representative contact was paramount. Although a flush joint was prescribed, and made, the small amount of shrinkage of the mortar caused each joint to have a slightly concave surface. This hollow required filling in and reducing to a smooth and flush surface with the brickwork. A ceramic self bonding putty was used to fill the hollow which could be left proud and later reduced to a smooth finish. The araldite adhesive was then applied directly to the putty. For the vast majority of joints the putty was reduced completely back to leave the original mortar / brick interface. It was felt that contact of the two mortar / brick interfaces with the strain gauges would provide a reasonable measurement of strain across the mortar and interface. Additionally, as failure was expected at the interfaces, the strain gauges would need to overlap the joint and 30 mm long strain gauges were therefore used.

The 30 mm gauges were also used on the brick units of some of the wallettes. Here application was more straightforward with the surface of the brick unit being sanded smooth and the strain gauges then attached directly with the araldite adhesive.

It is appreciated that the solution used for strain gauge placement was not an ideal situation and that the resultant readings may be influenced to some degree. However, it seemed a good initial starting point to measuring strain profiles of laterally loaded masonry. Great care was taken in all strain gauge applications with regard to the adhesive thickness. An area of adhesive was first administered and the gauge offered in a 'rolling' action squeezing all excess araldite out. Repeated pressure applications over a period of 30 minutes resulted in an acceptable bond.

8.4 Results and analysis

8.4.1 Elastic modulus and ultimate failure load

The modulus of elasticity of the wallettes or modulus of rupture has been calculated from the following equation derived from ordinary bending theory;

$$E_R = \frac{P}{\delta}\frac{3L^3}{144I_{xx}} \quad \text{..... (8.1)}$$

The relationship of P/δ is evaluated from the figures E8.2, E8.3 and E8.4 using a tangential line fitted by hand to the experimental curves. Testing and analysis data is held in table E8.2. The averaged elastic modulus assumed from these tests has been taken as 5500 N/mm^2. As a comparison previous research, Anderson (1982) and Dodia et al (1988) assumed the elastic modulus of masonry in flexure to be 4000-12000 N/mm^2 (over a range of similar brickwork wallettes) and 8500 N/mm^2 respectively. Lovegrove used an elastic modulus for masonry units of 11 000 N/mm^2 and 5000 N/mm^2 for the mortar.

Stiffness of masonry is influenced by rate of loading to an extent. Although a controlled loading machine has not been used the rate of loading applied to the wallettes has been matched to that of the full scale masonry cavity walls. The rate at which load has been applied to the wallettes was 0.4 kN per 8 second. This is compared to the rate of 0.5 kN per 10 seconds for the cavity walls. Additionally, the time taken for the datalogger and checks to be made was 8 and 10 seconds for the wallettes and cavity walls respectively.

8.4.2 Strain profiles and ultimate strain values at failure

It has previously been assumed, in this project, that the flexural behaviour of the masonry wallettes is governed by the behaviour of the mortar and the interface between the mortar joint and the brickwork. Additionally, there will be some influence from the header joint and this is borne out by the failure pattern that will be described later. To verify this hypothesis, wallettes 1 and 3 had strain gauges placed on both faces covering all joints and on all brick units. The experimental results of wallettes 1 and 3 will first be scrutinised followed by the ultimate strain values at failure of all wallettes.
For identification purposes the brick units are numbered 1 to 10 from top to bottom and the joints are numbered 1 to 9 similarly. Support positions are therefore on the brick units 1 and 10 with load points on units 3 and 7.

8.4.2.1 Comparison of strain profiles in the mortar and in the brick units during flexural tests of wallettes

Figures E8.5 and E8.6 plot the strain profiles on both faces of wallettes 1 and 3 respectively. The strain profiles are recorded from gauges across each mortar joint and on each brick unit. The failure plane is shown on each figure and is typified by the high peak strain value recorded just before failure.

Figure E8.5 indicates that a large proportion of the strain energy is focused at the failure joint. The peak tensile value on the 5th joint is accompanied by a compressive peak. In all cases the tensile strains are greater than their accompanying compressive strains on

the opposite side of the wallette. There is only negligible strain in the upper four brick units and three mortar joints. This is similar to the lower courses although strain does increase immediately below the lower load point. Figure E8.6 shows two marked differences from figure E8.5. Firstly there are significant strain values in five of the mortar joints both in compression and tension. Secondly, strain in the brick units represents a more significant proportion of the overall strain in the wallette.

A failure plane in masonry would normally be expected to form in a certain location depending upon maximum applied bending stress, axial load, geometry and strength of joint. It is clear from figure E8.6 that although the failure plane is not in the region of highest stress or axial load (self weight) the governing factor is the bond strength. It may also be ventured that the bonding for wallette 3 is more uniform as there are five joints with significant strain associated to them. Wallette 1 on the other hand is dominated by the behaviour of just one joint.

There appears to be no ordinary bending theory stress / strain relationship which might expose intrinsic flexural behaviour of wallettes. This is most probably associated to the different materials used and their interaction at the mortar / unit interface bond. The nature of this bond has been subject to much investigation, but a definitive understanding not yet fully apparent and therefore the stress / strain relationship remains uncertain. Table E8.2 gives all the relevant experimental data from which a relationship could be formed. The only possible exception to this is the location of the failure joint and the failure pattern. Seven of the wallette failure planes are located at the 5th joint with the others on joints 4 and 6 and only one on the 3rd joint outside the load points. This does indicate that the failure position is dominated by the area of highest bending stress rather than merely the weakest joint. Shear stress does not appear to be a limiting criterion for any of the wallettes tested.

8.4.2.2 Ultimate strain values across the failure joint

Table E8.2 holds the maximum compressive and tensile strain values just before failure for the failure joint. In all cases these maximum strain values always occur at the failure

joint. In all cases the tensile strain value is significantly greater than the opposing compressive strain. This indicates that the flexural behaviour of brickwork is dominated by tensile strength, in particular the bond strength between mortar and brick unit, as would be expected. The ultimate tensile strain values themselves vary enormously, 110 to 895 με with no relation to either deflection or applied load. This again highlights the considerable differences of bond strength when it is considered the quality control of materials, manufacture and curing techniques employed in this study.

8.4.3 Comments and visual observation of failure modes of the wallettes in flexure

All wallettes failed along a mortar / brick interface with a sudden and complete debonding across the entire width. All wallettes were positioned so that the smooth face was loaded. Debonding took two forms. Firstly a complete debond along either the top or bottom of a mortar joint through each header joint was most prevalent. Secondly, a 'zig zag' pattern with debonding occurring away from each header joint and indeed on the opposite side to the header joint. Inspection of the failure surface revealed a thin layer of mortar retained on the brick units. Some of this mortar comprised small particles of matrix which could easily be removed with a gentle puff of air. Roughly half of the mortar then remained bonded to the brick units.

8.5 Finite element modelling of masonry wallettes

8.5.1 Finite element modelling considerations

It was originally intended that this chapter would provide the modulus of elasticity of brickwork from the wallette tests that could then be used to support the simplistic finite element modelling proposed for the Isofoam injected cavity walls. It was envisaged that each wythe would be modelled as a single homogeneous material, however, it was felt that with the difference in modulus of the masonry units and mortar warranted a more refined analysis. The advantage of the using separate mortar and masonry unit material

properties is that the preparation and testing is more straight forward and the variations in the test result less.

Finite element analysis is used in this chapter to provide a comparison of the two proposed methods of analysis which use separately obtained and applied material properties. Type 1 F.E.A. describes the use of the modulus of elasticity of the wallettes while Type 2 uses the separate properties of the masonry units and mortar from the compressive tests.

A four point model configuration with identical geometric properties as shown on figure 8.1 has been assumed. Support positions were placed at the centre of the top and bottom brick courses, while the load points are centred on the 4th and 7th courses (from the base). The wallette is assumed to be free to rotate about the base although self weight effects have been accounted for.

The Rolls-Royce Plc "in house" finite element package SC01 has been used for the linear elastic material, geometrically non-linear plane strain analysis. Six noded triangular elements are in the elemental mesh, which is controlled partly by a specified structural accuracy of 5% and partly induced by the placement of 'redundant' geometry. The mortar bedding joints are three element layers thick and the brick units are represented by at least three layers. The elemental layers in the mortar are governed by the use of additional geometry whereas the brick units are controlled by the structural accuracy.

8.5.2 Displacement response and elastic modulus of brickwork

Both type 1 and type 2 models were identical in terms of geometrical configuration and elemental mesh density. A total lateral load of 6600 N was applied with the mid height displacement being of primary interest. Table 8.2 below gives details of the finite element analyses. Figures E8.7 and E8.8 give the SC01 outputs for the type 1 and type 2 analyses.

F.E.A	Material properties (N/mm^2 where appropriate)			Load N	Mid height displacement	Equiv. modulus
Type 1	E_{masry}=5500	υ = 0.20		6600	0.0966 mm	E_{T1}=5480
Type 2	E_{brick}=16000	υ = 0.20	E_{mortar}=2500	6600	0.0968 mm	E_{T2}=5470

Table 8.2 Finite element data for wallette tests

The two types of analyses produce very similar mid height displacements. To put this in to perspective an equivalent modulus for an assumed isotropic homogeneous material may be calculated from equation 8.1. For type 1 modelling this should produce an identical modulus to that inputted, which it essentially it does. The small discrepancy between $E_{masonry}$ and E_{Type1} may explained by the finite element analysis including some proportion of shear deflection. The ordinary bending theory (equation 8.1) assumed, does not include shear response. It could also be considered that the difference may be partly attributed to various modelling approximations such as the small overhangs, inclusion of self weight and finite element solution techniques. Similar differences and approximations will lead to slight inaccuracies for the Type 2 equivalent modulus. The discrepancy between $E_{masonry}$ and E_{Type2} is again small which infers that the assumed elastic modulus for brick unit is appropriate.

8.6 Discussion

Defining material property values for masonry is difficult to establish as not only are there two constituents present, mortar and brick unit, but also their interaction requires evaluation. The properties of the brick units and mortar matrix are themselves reasonably well understood so it remains the determination of their combination in the form of masonry that is necessary. As has been described in the available literature this has been attempted many times with no consistent results. The component and wallette testing has once again pointed towards a lack of understanding with regard to the mechanism of flexural bonding. This chapter has not attempted to quantify and reason the factors that effect bond strength as those are well documented previously. However,

in gaining an understanding of them, measures have then been taken to produce the strongest and most consistent flexural bond possible. It should be noted that although there were many rigid procedures carried through both the manufacturing and testing the results still produced highly variable behaviour.

The principal objective of this chapter has been to identify an elastic modulus of one type of masonry combination in order to support elastic theoretical analysis of the full scale masonry cavity walls. The results of this investigation have led to a mean elastic modulus of 5500 N/mm^2 with a standard deviation of 2000 N/mm^2, and it should be also be remembered that the values obtained ranged from 1100 to 8400 N/mm^2. The failure load had a mean of 6.6 kN and a standard deviation of 1.8 kN, ranging from 3.0 kN to 8.8 kN.

Failure will always occur at a compromise point where greatest bending moment and weakest joint coincide. As has already been discussed there are many factors effecting the bond strength, however, workmanship has not yet been addressed. Having observed the construction of all masonry specimens in this project two issues of note on workmanship seem apparent. Firstly, the amount and distribution of mortar between courses, which includes the type of joint finish, and secondly the out of plane any individual masonry unit is. The general plane of the masonry was very good, however individual units were occasionally out of line or at a slightly rotated angle. These observations are not quantifiable but are worth mentioning for future investigations or adoption in quality control procedures.

It may be considered that the type 1 finite element modelling technique verifies the ability of the model to accurately represent the wallette testing configuration and the experimental elastic modulus value of brickwork. The type 2 analysis method then provides evidence that the modulus of the brick units used is appropriate. Within the limits of the approximations of modelling in two dimensions it may be further proposed that either method could be used and extrapolated to three dimensional analysis of more complex structures. For a three dimensional or where support conditions other than

vertically spanning, simply supported type 1 analysis is proposed, further wallette testing would be required to evaluate the y-direction elastic modulus.

8.7 Conclusions

(i) It may be generally concluded from the literature review that quantifying the influences of certain factors involved in the flexural bond strength and modulus of masonry is difficult. This has also been found for this investigation as seen in the results for the elastic modulus and the ultimate failure load. Both having a significant standard deviation from their respective mean value when seemingly identical materials and practices were rigorously adhered to.

(ii) The modulus of elasticity carried forward to be used in the analysis of the cavity walls is 5500 N/mm^2 with a standard deviation of 2000 N/mm^2. It has been impractical to attempt to evaluate the Poisson's ratio of masonry and a similar value of 0.20 has been adopted from the work of Lovegrove (1988).

(iii) The total ultimate lateral flexure load for the four point (at equal third points) load configuration is a mean of 6.6 kN with a standard deviation of 1.8 kN.

(iv) The modulus of elasticity of mortar designation (i) in compression, water / cement ratio 0.52, is 2500 N/mm^2.

(v) Either type 1or type 2 analysis may be used for masonry structures that can be modelled by simplifying the problem into two dimensional vertically spanning members. Choice of which method should be based on the availability and ease of sub element testing. The use of type 1 and 2 F.E.A. modelling is discussed further in chapter 9.

(vi) Further investigation of the elastic properties of masonry units is strongly recommended.

CHAPTER 9 - MASONRY CAVITY WALL TESTING AND ANALYSIS

9.1 Introduction

9.2 Masonry cavity wall testing procedures

9.3 Analysis methods

9.4 Discussion of cavity wall testing and analysis

9.5 Discussion

9.7 Conclusions

CHAPTER 9 - MASONRY CAVITY WALL TESTING AND ANALYSIS

9.1 Introduction

9.1.1 General

Within the scope of this project it is intended to examine the validity of the innovative concept of the foam injection system as a remedial measure to existing masonry cavity walls. This chapter investigates the influence to the structural stiffness of filling the void of a masonry cavity wall with Isofoam CRF in an attempt to further existing knowledge of composite action in masonry. As will be seen in the review of relevant literature, there is very little information and research regarding composite action, in particular shear transfer, between cavity wall members or "wythes". Composite action is noted in many texts as a partial explanation to a strength and stiffness being greater than the sum of the two individual walls. In most cases the enhancement is attributed to the mechanical interaction and type of the metal wall ties used in the construction.

Throughout this investigation shear transfer between facings of sandwich constructions has been induced by bending, with one face predominantly in tension and the other in compression, forming an overall cylindrically deflected shape at small displacements. Intrinsically, cavity walls have additional structural interactions which are influenced by factors such as axially applied vertical loads, thermal gradients and structural defects which may result from poor material and design specification or ground bearing changes. Chapter 2 considered potential structural defects, their mechanisms and how the implementation of Isofoam CRF could arrest the problems. These additional factors are difficult, if not impossible, to quantify by attempting to reproduce conditions in a laboratory whilst at the same time modelling their behaviour.

Therefore, in this project the cavity walls tested have been built to standard and injected with Isofoam CRF in the most controlled and ideal manner possible, so that factors other than those stated above have been minimised and a good approximation of solely the bending behaviour made.

The foam injection system is complemented by other benefits besides increasing bending stiffness such as a cavity wall tie replacement alternative, providing a thermal and acoustic barrier. The foam's ability to transfer direct shear resulting from differential movement of the two wythes in a parallel direction is also highly beneficial. Essentially, a straightforward assessment of the Isofoam's shear stiffness may be made directly from the results of the British or American Standard shear tests and knowledge of the magnitude of loading conditions and resisting area of Isofoam CRF.

9.1.2 Objectives of masonry cavity wall testing

The principal aim of this part of the project is to evaluate the overall concept of injecting masonry cavity walls with Isofoam CRF to enhance their structural stiffness and strength to withstand lateral loads. It is proposed to validate this by comparison of experimental testing to the finite element methods developed here and in the previous chapters. It is tentatively argued that the gain in strength from two individual wythes to a single sandwich panel comprising two wythes and an Isofoam CRF core is entirely due to the introduction of a shear transfer medium. Shear transfer increases the total second moment of area of the cavity wall from the sum of the stiffnesses of the two individual wythes to that analogous to a steel I section. Unlike the steel section the web, or core in this case, undergoes a significant shear strain resulting in an additional displacements to that of bending. However, the net effect is always beneficial considering remedial measures to existing masonry cavity walls.

The three cavity walls tested act as a control to provide a direct comparison to the finite element model. The finite element modelling techniques developed earlier have been then used to assess the increase in stiffness of the cavity walls when injected with Isofoam CRF. This is discussed in more detail in section 9.3.1.

9.1.3 Review of relevant literature

When investigating the lateral resistance of cavity walls with different types of wall ties, West et al (1979) reported that when using a 'truss type' wall tie there was an additional gain in strength and stiffness above that of the combined strength of each individual leaf. Similarly when using four times the normal number of wire wall ties there was a further enhancement in strength above the normally expected levels of strength of the addition of two single wythes. There was no indication given that the strength enhancement was attributed to shear transfer. Later West et al (1982) examined the lateral resistance of cavity walls with dissimilar leaves and found, by experimentation, that the all the cavity walls tested possessed at least the combined strength of the two individual walls. West et al conclude that "the cavity walls having vertical twist ties generally exhibited greater strengths than the simple addition of the strength of the two leaves; this suggests that some composite action which might permit the design strength of such walls to be enhanced". Analysis of the cavity walls was made by "yield line" theory which had no inclusion of composite action and it appears that there was no follow up investigation.

According to Brown et al (1979), for cavity walls with metal wire ties, the distribution of lateral load between each wythe is dependent on the wythe's relative stiffnesses and boundary conditions provided that a sufficient number of wall ties are used. Two similar types of analysis were proposed and both used a discrete number of 'springs' connecting the two wythes and employed a displacement method for solution. It was stated that although this does not necessarily indicate full sandwich action the increased number of wall ties allows both wythes to resist the lateral load more evenly and keeps them a constant distance apart.

Further indications of the presence of shear load transfer was given in a parametric study of laterally load cavity walls by Dodia et al (1988) based on elastic theory. It was again noted that selective positioning of wall ties contributed to an improvement in structural performance. Analysis of the cavity walls was conducted using F.E.A with linear elastic material properties of the brickwork coming from the earlier work on the wallette tests

of Anderson (1982). The elastic modulus of the 'commonly used type and thickness masonry' was found to be 8000 N/mm^2. The F.E.A. model used for the investigation was fairly basic, assuming brickwork to be isotropic and homogeneous in nature.

Rashwan (1991) found that stiff metal connectors contributed to composite action between the two wythes and through an extensive testing and analysis programme it was concluded that a more economical cavity wall assembly could designed with this in mind. Analysis of this system employed a planar frame analogy and the results were used to form a design load / deflection table to enable the selection of a more economical cavity wall.

Two British Standards that deal with the use of polyurethane foam systems for use in cavity walls, BS 7456 (1991) and BS 7457 (1991). BS 7456 is a code of practice for the 'Stabilisation of cavity walls...by filling with polyurethane foam systems' but does not present any quantitative evaluation of additional strength or stiffness. The standard advises that "because the strength of the rigid polyurethane foam is significant the system has been widely used for the restoration of the integrity of cavity walls in which the wall ties have become ineffective due to corrosion". The standard goes on to recommend the methods of injection and suitability of masonry structures to the system.

BS 7457 is the specification for 'Polyurethane (PUR) foam systems suitable for stabilisation and thermal insulation of cavity walls with masonry or concrete inner and outer leaves'. The standard gives the property, composition and the production parameters of suitable rigid urethane foam systems, which are dispensed on site, to fill the cavities of maximum width 150 mm and maximum continuous cavity height 12 m.

The literature review has been instrument in identifying the existence of composite action, leading to a structural performance increase, in flexural behaviour of masonry cavity walls with various shear connections. The review has also shown that there is currently no formal analysis that evaluates this structural enhancement. This thesis therefore attempts to examine the additional stiffness achieved by having a shear connection between the wythes of a cavity wall.

9.2 Masonry cavity wall testing procedures

9.2.1 General

The focal point of the overall project is based on the laboratory testing of the masonry cavity wall Isofoam injection system and the analysis thereof. Three types of lateral load test should be performed on each of the three cavity walls. A four point load test configuration was used for all tests on masonry cavity walls. Firstly, an equivalent wind load was applied to the cavity walls. The maximum wind load bending moment was calculated which was then adapted for the maximum four point loading configuration. This equivalent loading regime was employed to find the corresponding deflection and strains present in extreme 'working' circumstances. No vertical pre-load was applied to represent the load bearing characteristics of an in-service wall. Secondly, a 'hysteresis' load and unload test to evaluate if there may be any residual or permanent displacement after loading and thirdly an ultimate load test to failure. After the hysteresis test on cavity wall 2, no measurable residual strain remained and the two other cavity walls were not subjected to this test.

9.2.2 Cavity wall construction methods, practices and dimensions

The cavity walls were constructed in an identical manner to the wallettes although a single rise constituted fifteen or sixteen courses. The cavity walls were all 31 courses high allowing 10 courses between each load or support point. Each rise was post loaded with three dry courses of bricks and covered with damp hessian cloth and plastic sheeting for at least three days. All mortar joints were finished smooth with the brick units. Butterfly wall ties were used during construction for safety reasons, but were cut just prior to the foam injection. Table 9.1 below gives the dimensions of all three cavity walls together with the maximum and minimum variations taken from twelve measurements of each dimension.

Wall	Length, mm	Height, mm	Total thickness, mm	Cavity width, mm
1	1365 +/-3	2360 +/-3	263 +/-4	59 +/-3
2	1365 +/-4	2340 +/-3	281 +/-3	75 +/-3
3	1360 +/-4	2340 +/-4	310 +/-3	104 +/-2

Table 9.1 Cavity wall dimensions

9.2.3 Environmental conditions and conditioning of component materials and cavity walls during and after construction

The cavity walls and their component materials have been treated in the exactly the same way as the wallettes. All cavity wall and wallette constructions and tests were conducted in the Heavy Structures Laboratory at the Nottingham Trent University. The laboratory was conditioned by an automatically controlled heating and ventilation system and provided a reasonably stable environment. In addition to the build and testing dates, the temperature and relative humidity at the time of each test is also set out in table 9.2. As each cavity wall was built over a four day period there are four construction dates given.

Cavity wall	Date built	Test date	Test type	Temperature ^{o}C	Relative humidity %
1	31.07.95 01.08.95	22.02.96	wind load	19.3	49
	07.08.95 08.08.95	22.02.96	ultimate	19.3	49
2	02.08.95 03.08.95	05.12.95	wind load	18.5	45
	09.08.95 10.08.95	05.12.95	hysteresis	19.0	46
		0512.95	ultimate	19.0	46
3	04.08.95 05.08.95	11.12.95	wind load	19.2	47
	16.08.95 18.08.95	11.12.95	ultimate	19.2	47

Table 9.2 Cavity wall testing general data

9.2.4 Four point load test configuration

A four point load configuration was used in all tests on the cavity walls. A uniformly distributed load was considered, particularly as a lateral wind load could then be simulated, but the additional set up problems, equipment calibration and interference with instrumentation, weighed in favour of point loads. The point loads were in fact continuous line loads across the entire width of the walls.

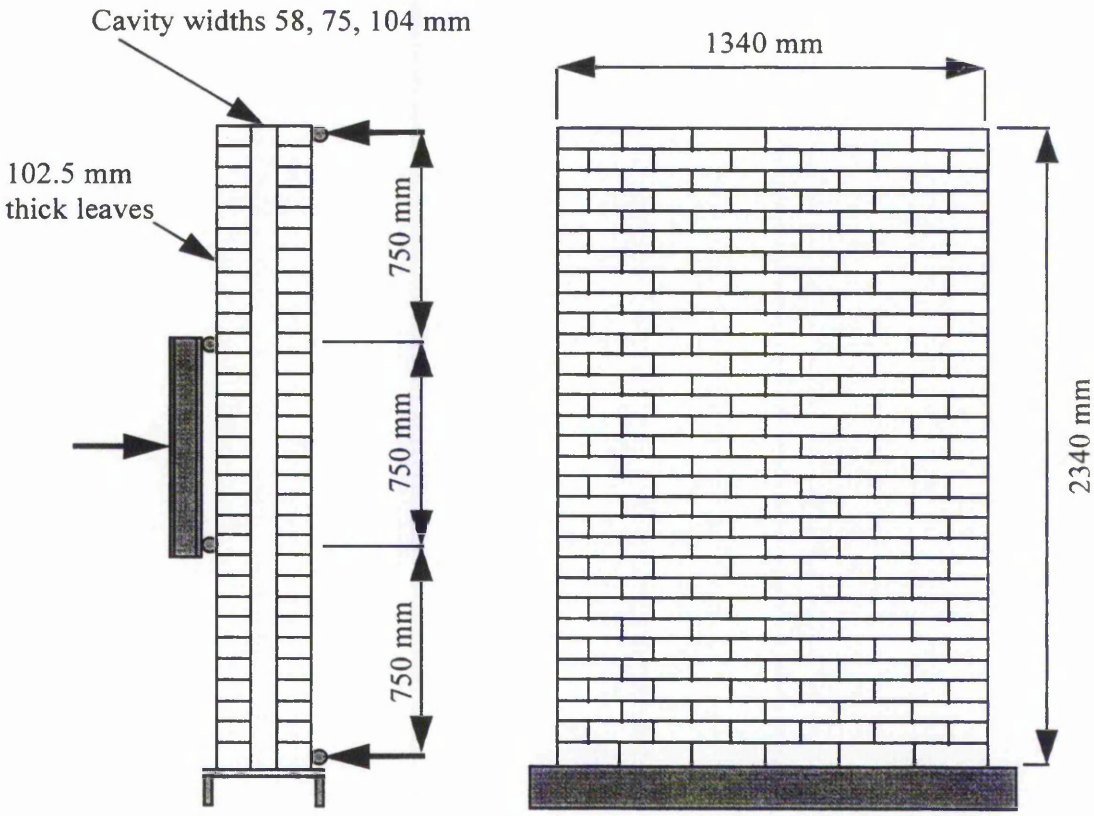

a Side elevation showing position of support and load points

b. Front elevation showing wall dimensions

Figure 9.1 Cavity wall testing configuration

To eliminate potential inaccuracies caused by test frame displacements and settlement the frame was pre-loaded with similar support reactions present in the ultimate load test and displacements taken. The test frame was somewhat 'heavy' and 'over designed' as

sections were chosen for geometric compatibility and economy. Displacements at the mid point of the supports being less than 0.05 mm at 10 kN in a near linear relationship. The frame displacements had already been minimised by a series of load and unload cycles with the bolts being tightened at each stage prior to the final load / displacement calibration test being taken.

9.2.5 Testing procedure and flexural monitoring

9.2.5.1 Flexural monitoring equipment used and positioning

Displacement response was recorded by LVDTs on the loaded face opposite each support, at mid height on the loaded face and on the unloaded face at mid height. Two LVDTs at third width positions were placed at each location. Additional dial gauges were placed on the steel support frame so that frame displacements would be visible during the tests. The LVDTs were placed approximately at the centre of masonry units which were firstly prepared to a smooth contact surface with the LVDTs displacement spindle. A single line of strain gauges were placed over mortar joints in the same fashion as for the wallette testing and on both the loaded and support faces. All mid height displacements used have been reduced by the averaged support movements.

9.2.5.2 Equivalent wind load test

The three walls were all tested for an equivalent wind load condition. A wind pressure, based on BS 6399 Part 2 (1997) Loading for buildings, code of practice for wind loads, was used to find the maximum applied bending moment to the cavity walls. Assumptions made to find the applied wind load were, for a building in the outskirts of Nottingham, less than 3m height, with class A cladding and a period of 50 years exposure. A worst case combination of internal and external pressure coefficients were used in the wind load calculation. The total lateral load for a four point configuration was then calculated to produce the same maximum wind load bending moment at mid height.

Figures F9.1a-c show the load / displacement relationship for cavity walls, CW1, CW2 and CW3 respectively, subject to the four point equivalent wind load. The load was applied in increments of 0.2 kN up to 1.65 kN and down to zero with displacements recorded at each stage. Each figure displays load / displacement relationships for the loaded face and the supported face both at mid height. Descriptions of characteristics have been given for each of the three figures below.

In the first instance it should be noted that the maximum mid span displacements are small (less than 0.14 mm) and that the accuracy of the LVDTs, mainly restricted by small fluctuations in the power supply, may have some influence on the results. The accuracy of the LVDTs was limited to approximately 0.01 mm.

All three figures display the similar trend of a 'loop' with the increasing load ramp recording a lesser displacement than the return decreasing load ramp. In fact four of the displacement plots show that the recorded mid span deflections increase shortly after the load begins to decrease. This may be caused by the time dependent strain response of the Isofoam. As the load is increased the strain imparted on the foam nearest to the facings takes time to distribute throughout the body of Isofoam, thus an initially stiffer core is immediately apparent than after a certain elapsed time. This is in keeping with the explanation of the pilot test for the initial creep response of a plywood faced sandwich beam described in chapter 2.

The mid span loaded face displacements were all greater than the support face displacements. There are two possible explanations for this. Firstly, for the loaded face, the load is applied through two line loads at third span creating a maximum bending moment of PL/3. For the support face, the self stiffness of the loaded facing combined with its thickness, were such that effectively the load applied to the supported wythe could be assumed to be a near uniformly distributed load. This would create a bending moment of PL/4. Thus the difference of applied loads to each wythe suggests that there would be a difference in the distribution of total applied load and hence maximum bending moment. In addition, the load is also required to be transmitted through the Isofoam CRF, which is compressible. This allows the loaded face to deflect slightly

more. Secondly, as seen in the high variance of wallette modulii, the variation of stiffness of each wythe may be substantial and may add to the uneven distribution of loads described above.

Further trends have been difficult to attribute to any particular behavioural response as the deflections were so small they may be subject to experimental errors such as the smoothness of the brick unit bearing surface with the LVDT's spindle.

The displacement plots for cavity walls CW1 and CW2 suggest that there may be some degree of hysteresis in that the original mid span position does not return to parity. Again this is difficult to determine from these relatively low levels of load applied and a further direct test for hysteresis has been conducted and is described below.

9.2.5.3 Hysteresis evaluation

An evaluation of hysteresis in the cavity walls was made to check for the possible effects of lag between releasing of applied stress and the cessation of strain to help understand the interaction of Isofoam and brickwork. Both deflections and strain readings have been used in the evaluation. Figure F9.2a shows the load and unload ramp against deflection and figure F9.2b gives the relationship of displacement and duration of the load ramp. The load ramp used 1.0 kN load increments up to 9.0 kN while the displacement versus time relationship spanned approximately 20 second intervals.

The load versus displacement relationship for the loaded face, figure F9.2a, shows a similar 'loop' characteristic to the wind load tests previously discussed. The time taken to reach the maximum applied load, which was the same as the load ramp back to zero, was approximately 180 seconds. There remained a mid height displacement of 0.16 mm which dissipated to 0.05 mm after a further period of 120 seconds. No further recovery was evident thereafter.

The hysteresis test has indicated that, like the plywood faced panels tests, the time dependent properties of the Isofoam CRF have some influence on the load / displacement relationship when recorded over a series of time related load increments. If the worst case is considered for time dependent displacement response to influence the assumed elastic load / displacement relationship, it may be argued that in this test the maximum elastic displacement may be approximately 10% greater than expected. The 10% influence is calculated from the maximum displacement to the residual when the load has been removed.

In addition, unknown time dependent strain response of the brickwork may influence the hysteresis results further. Although outside the scope of this project, the strain rates of the various masonry element testing has been maintained reasonably consistent throughout. As an approximation of strain rates between wallette and cavity wall tests ordinary bending theory has been used to find the rate of applied bending stress. The cavity walls are subject to a rate of 0.008 N/mm^2/second compared to 0.010 N/mm^2/second for the wallettes. It is thus taken that the rates of strain are approximately the same and any difference in strain rate related stiffness differences of masonry is negligible.

9.2.5.4 Ultimate lateral load test

The ultimate lateral load test has been conducted to establish both the elastic flexural behaviour of the cavity walls up to failure and to find the ultimate strain values across the mortar joints for a comparison to the wallette testing data and finite element analysis strain profiles. The cavity walls are loaded with 1.0 kN increments up to failure.

Positioning of the strain gauges on the masonry was cause for some deliberation and a compromise was reached. The problem was that gauges solely placed on brick units would be subject to substantially less strain than across the mortar joints and would not be subject to the potential failure plane at the interface. Gauges placed over the mortar joints would record some strain in the brick units and some in the mortar joint. The wallette testing used two specimens with gauges both on the brick units and over each

bedding mortar joint and it was concluded there that the more meaningful strain measurements could be taken over the joint. This, however, was still not ideal as the gauges used were 30 mm long and were bonded to both the 10 mm thick bedding joints and the brick units either side. Therefore the actual strain values are of less interest than the characteristic shape of the strain profiles in determining the presence of sandwich behaviour. The experimental strain profiles have been compared to the finite element stress plots on this basis in order to verify sandwich action. The identification of the presence of sandwich action itself is an indication of an increase in flexural strength and stiffness. Finite element modelling is also be used to identify the theoretical stiffness enhancement. The displacement measurements taken alongside the strain readings will be used to directly assess the structural performance of the foam injected masonry cavity walls.

Strain profiles, just before failure, have been plotted on figures F9.3 a-c for cavity walls CW1-3 respectively. Mid height displacement versus load plots have been shown on figures F9.4 and F9.5 a-c along with finite element analysis and BS 5628 displacements. The mid height displacements versus load plots are given for both the loaded and unloaded faces for experimental and finite element models. Figure F9.4 contains complete load / displacement plots to failure, however, due to distinct non linear flexural response of all the cavity walls after approximately 6 kN, figures F9.5 a-c have been limited to below this load to show predominantly the linear portion of the curves.

9.3 Analysis methods

9.3.1 Finite element analysis

The finite element modelling in this chapter has exclusively utilised the Roll-Royce Plc., SC01 package. F.E.A. has been chosen in preference to Allen's solutions as effects of self weight and support conditions may be applied readily. In addition, future modelling of more complex geometrical configurations of cavity walled buildings, such as returns and openings, may be easily accounted for when using finite element analysis. The

work presented in chapter 7 has verified the use of finite element analysis methods employed for the plywood faced sandwich panels in terms of overall flexural response and it is now assumed that the same methods and practices may be used for analysis of the cavity walls. It is appreciated that the masonry cavity walls with an Isofoam CRF core constructed for this study constitute very thick sandwich constructions and as such are inefficient. However, it should be remembered that firstly it is a gain in structural performance that is sought and secondly the stiffness of the wythes in service may be significantly less stiff.

Lovegrove (1988), when investigating the effect of thickness and bond pattern on the lateral strength of brickwork, used finite element analysis to determine stress distributions in the bed joints. The method of analysis presented, modelled each individual brick unit and mortar joint. The isotropic properties used in the two dimensional analysis were, for the elastic modulus, 11 000 N/mm^2 and 5000 N/mm^2 for the masonry units and mortar respectively and Poisson's ratio was 0.15 for both materials. Lovegrove stated that as brickwork was brittle, with a distinct failure point, linear elastic analysis was most suitable as it was difficult to predict when the limited plastic response occurred before failure. The short finite element analysis study in chapter 8 of the wallettes indicated the appropriate material properties to use for the cavity wall analysis and these will be assumed satisfactory for the analysis of the cavity walls.

In this project finite element methods used for the sandwich panels has been largely duplicated for the cavity wall analysis. Linear elastic material properties have been employed in the geometrically non linear plane strain two dimensional analysis. Material properties, given in tables 9.3 and 9.4, have been derived from the wallette tests, mortar compressive cube tests and Butterley Brick Ltd (1993) for the masonry units and from Baxenden Chemicals Ltd proprietary data for the Isofoam CRF. Two types of finite element analysis have been presented here and designated as type 1 and type 2. The two types of analysis originate from the sub-element testing of the wallettes, brick units and mortar cube compressive tests and in particular the F.E.A. of the wallettes.

Cavity wall no.	Material	Elastic mod. E N/mm^2	Poisson ratio, υ_{xy}	Density, ρ kg/m^3
All	Brickwork	5500	0.2	2400
All	Isofoam	5.0	0.2	32

Table 9.3 Material properties used in the F.E.A. type 1 of the cavity walls

Cavity wall no.	Material	Elastic mod. E N/mm^2	Poisson ratio, υ_{xy}	Density, ρ kg/m^3
All	Brick units	16000	0.2	2400
All	Mortar	2500	0.2	2400
All	Isofoam	5.0	0.2	32

Table 9.4 Material properties used in the F.E.A. type 2 of the cavity walls

The two types of finite element analysis have been proposed and they are intended to be applicable to two different aspects of modelling masonry. Type 1 analysis assumes an isotropic homogeneous material for the brickwork in the spanning direction only, as opposed to type 2's solution of independent properties for the bricks and mortar. It is proposed that type 1 analysis may be used for large masonry structures, whereas type 2 analysis should be used where stress / strain response is required particularly in smaller masonry applications. Correct use of type 1 analysis should also be subject to the mode of support or boundary conditions. This may lead to a requirement to evaluate the elastic modulus of wallettes in the orthogonal direction.

9.3.1.1 General finite element modelling considerations

All models were two dimensional plane strain simulations and used six noded triangular elements. The automatic elemental mesh generation of the Rolls-Royce in house program SC01 (1997) was driven partly by the geometry describing the problem. A

tight structural accuracy of 5% was also prescribed to refine the overall mesh density. To further enhance the elemental mesh each mortar joint was split into two areas creating at least a two element deep bedding joint.

Self weight was included for all finite element models with the average density of brickwork assumed to be 2400 Kg/m^3. The inclusion of self weight had a direct influence on the support conditions prescribed. A fully restrained base (as seen on the right hand side of figure F9.6) provided the reaction to the self weight. A compromise was required when considering the modelling of the contact between the bottom of the wythes and the base as there is clearly some friction present in the actual testing. The contact was neither a simple support nor an encastre fixture. The compromise reached was to model a 10 mm thick joint, between the bottom brick course and the base, and assume that a weak material was present between the wythes and base. Both conveniently and coincidentally the material properties chosen were that of the Isofoam CRF. A rigorous examination of this interface was not conducted as the global stress profile does not indicate significant influence from its behaviour. The Isofoam connection allowed both rotation and some y- direction displacement.

Both types of F.E. analysis are described below and use the same geometry and thus elemental mesh densities. Full colour contour plots of both stresses and displacements are included in appendix F as they illustrate the flexural response more vividly. It should be noted that the direct displacement outputs shown on the colour contour plots give the total displacement which must then be reduced by the average movement at the support points. The F.E.A. calculated mid span displacements only are also shown on figures F9.5 a-c as a direct comparison to the experimental results.

9.3.1.2 Type 1 F.E.A.

Type 1 F.E.A. utilises the modulus of elasticity evaluated from the wallette tests and applies this modulus globally to the brickwork which is then modelled as a solid homogeneous body. Therefore, both the mortar joints and masonry units are assumed to

have the same modulus and Poisson's ratio values, with the solution now being similar to the plywood / Isofoam CRF panels analysed in chapter 6.

Figures F9.6 and F9.7 give the worst principal stress and y- displacement colour contour plots of cavity wall CW3 subject to a 6.0 kN total lateral load. Type 1 analysis method has only been used for cavity wall CW3 as an illustrative example to compare to the type 2 analysis. Type 1 analysis is not applied to all three cavity walls as Lovegrove (1988) recommended that where stress distributions are required the non homogeneity of masonry should be accounted for. Also the relatively small size and more detailed complexity of the problem lend themselves to a higher level of modelling segregation.

9.3.1.3 Type 2 F.E.A.

Type 2 F.E.A. employs the material properties derived from sub element testing of the masonry units and mortar compression cube tests and have been applied to the separate material masses for the cavity wall analysis. The properties and modelling techniques are identical to those used in the wallette testing analysis where appropriate. Figures F9.8 a-c, F9.9 a-c give the worst principal stress and y- displacement colour contour plots of cavity walls CW1-3 respectively.

Both type 1 and type 2 F.E. models have incorporated self weight. The stabilising effect of self weight has been removed from the F.E.A. plot of stress and displacement profiles for cavity wall CW3, shown on figures F9.10 and F9.11 respectively. The stabilising effect of self weight is discussed in section 9.3.1.5.

9.3.1.4 F.E.A. of a single wythe

Assessment of the stiffness enhancement of a cavity wall by the foam injection system may be made either by a significantly large number of test results to an acceptable variance or by F.E. modelling techniques where sufficient confidence exists. The former method was not possible for logistical reasons as tests for cavity walls with and without Isofoam CRF, of single storey height, would be numerous and highly laborious.

However, the latter method has been used to clearly identify the increase in stiffness by using the same modelling techniques and material properties for an analysis of a single wythe, doubling the stiffness and comparing that directly to an F.E. analysis of a cavity wall with Isofoam CRF. Currently, BS 5628 recommends that for cavity walls the overall strength is the addition of the strengths of the two individual wythes where there are sufficient cavity wall ties and this has been adopted in the case of the finite element modelling simulation.

Figures F9.11 and F9.12 show the y- displacement and worst 2D stress profile plots respectively for a single wythe. The single wythe has been identically modelled to the cavity wall type 2 analysis and subject to the same four point load configuration as the cavity walls. The total load applied for this model was 3.0 kN. For the comparison with the foam injected cavity walls it is assumed that two individual wythes loaded with a total load of 6.0 kN each behave in the same way as a single wythe with a 3.0 kN total load.

9.3.1.5 Summary and discussion of F.E.A. results

Table 9.5 below gives a summary of the mid span displacements for the loaded face of all the finite element models described and presented above. The mid span deflections have been corrected for the loaded face by the displacement encountered between wythes adjacent to the supports.

The type 1 analysis of cavity wall CW3 the total applied load was 12.0 kN, whereas the type 2 analyses used a total applied load of 6.0 kN. As both analyses used linear elastic material properties the load / displacement is also linear in response thus for comparative reasons the a 6.0 kN total load creates a 0.62 mm mid span displacement. Similarly, the single wythe is subject to a total load of 6.0 kN, but for a direct comparison to the type 2 analysis this should be halved to 3.0 kN giving a mid span displacement of 0.95 mm.

Type 2 analysis: From the results presented in chapter 7 it may be reasonably assumed that an increase in core thickness, for one given facing material, the overall stiffness of the sandwich panel increases itself. However, in this sandwich application the facings are very thick with the stiffness being largely driven by the self stiffness of the individual facings. As can be seen in the above table of F.E.A. results the displacement of CW2 and CW3 are very close suggesting that the increase in bending stiffness is nearly outweighed by the additional shear related deflection of the core.

Analysis type	Wall no.	Applied load kN	Cavity width mm	Ave. support disp. mm	Mid span disp. mm	Corrected mid span disp. mm
Type 1	CW 3	6.0	104	0.15	0.69	0.54
Type 2	CW 1	6.0	57	0.10	0.87	0.77
Type 2	CW 2	6.0	75	0.12	0.81	0.69
Type 2	CW 3	6.0	104	0.14	0.81	0.67
Type 2	CW 3*	6.0	104	0.15	0.87	0.72
Type 2	Single wythe	6.0	N/A	0.0	0.95	0.95

*No self weight

Table 9.5 Summary of F.E.A. mid span displacements for cavity walls

Type 1 versus type 2 analysis: The type 1 analysis of CW3 displays a lesser mid span displacement than the type 2 analysis. The two types of analysis were first presented in chapter 7 for the wallette tests, and it was concluded there that the material properties were reasonably appropriate in that situation. It has been assumed that those properties were also appropriate for the cavity wall F.E.A. As can be seen there is a theoretical discrepancy of 7% from type 2 analysis. This suggests that the properties used here may require further verification for the more complex analysis of the foam filled cavity walls. The 7 % discrepancy between analysis types should be put into context however, when considering the inconsistent nature of masonry specimens.

Single wythe versus cavity walls: An experimental evaluation of the bending behaviour of a single wythe to compare with a cavity wall was not appropriate as the number of

specimens to be confident of a good result would be both time consuming and costly. Hence a comparison using finite element models is ideal for this application. The comparison is made specifically to determine the increase structural performance of a cavity wall by introducing a shear transfer medium.

The single wythe F.E.A. results represent the total stiffness of a cavity wall when no composite action is present, but an equal load is applied to both leaves. From the F.E.A. results in table 9.5 above the percentage increase in stiffness by introducing the Isofoam CRF to the void may be expressed by the following equation;

$$\text{Percentage increase} = \left(\frac{\delta sw - \delta cw}{\delta sw}\right) \times 100\% \ldots\ldots\ldots (9.1)$$

Therefore the percentage increases in overall flexural stiffness are 19%, 27% and 30% for cavity walls CW1-3 respectively.

Self weight: Inclusion in the F.E.A modelling of self weight of the cavity walls shows a significant stabilising effect over a model without self weight. Figure F9.10 and F9.11 show the F.E.A. stress contours and load versus mid span displacement plots for cavity wall CW3 with no self weight. These plots have been compared to F9.9c and F9.8c for cavity wall CW3 with self weight.

The effect of self weight may be partly explained by examination of the stress contour plots, figures F8.8c and F8.10, with and without self weight respectively, for cavity wall CW3. The graphical output for the outer surface profiles, for the no self weight case shows a symmetrical stress profile. With self weight the stress profiles become unsymmetrical. In particular at the base of the wall (at the right hand side) the compressive stress profile (1-1) becomes positive indicating that there is a degree of fixity at the support. Similarly, the tensile (loaded face) profile stress plot (2-2) become negative indicating compressive stresses.

The stress contour plots of figure F9.8c provide evidence to suggest that the effect of self weight produces a support condition somewhere between a simple support and an

encastre support. It is then argued that the reduction of displacement response of the model incorporating self weight, manifests itself with the partial encastre support condition.

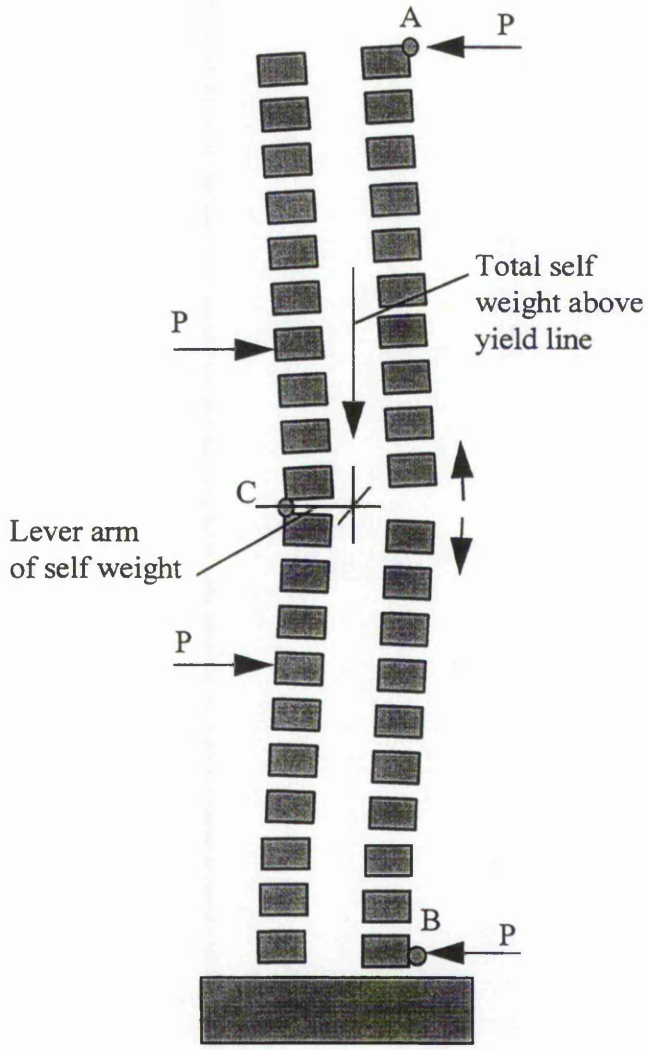

Figure 9.2 Illustration of the effect of self weight on mid span displacement and bending stresses

The percentage discrepancy of stiffness of the model with no self weight from one with self weight was found to be 7.4%. The tensile stress decreased by 12% and the compressive stress decreased by 3%. Self weight is therefore significant when considering the modelling of masonry structures. In service cavity walls have additional axial compressive loads from the structure they are supporting providing a further reduction in stresses and lateral displacement.

9.3.2 Existing BS 5628 (1992) strength assessment

Table 3 in BS 5628 : Part 1 : 1992 gives the characteristic flexural strength of masonry. The ultimate flexural strength assessment assumes that the clay bricks used have a water absorption less than 7% and mortar designation grade (i). This combination of masonry has a flexural strength, $f_{kx} = 0.7$ N/mm^2, from which a maximum moment of resistance may be calculated. Therefore for one wythe the moment of resistance is given by:

$$M_R = \frac{f_{kx(perp)} \cdot Z}{\gamma_m} \quad \ldots\ldots\ldots (9.1)$$

where $Z = bd^2/6$ and the material factor of safety, $\gamma_m = 3.5$, therefore $M_R = 0.473$ kNm or 0.95 kNm for two wythes. The moment of resistance may be translated to a total applied load of 2.5 kN, in four point configuration. Alternatively, to be consistent with the finite element modelling, utilising unfactored wallette test results, the material factor of safety, γ_m, does not need to be applied, thus $M_R = 1.66$ kn. per wythe. This unfactored approach leads to a total applied four point load capacity of a cavity wall with each wythe loaded equally of 8.75 kN. Comparison to the masonry cavity wall ultimate load test results shows that the BS 5628 unfactored total load underestimates the failure test loads. The total ultimate failure loads of the three foam injected cavity walls CW1-3 were 11.4, 11.8 and 12.0 kN respectively.

The BS 5628 flexural strength assessment does not take into account the pre-stressing effect of the wall's self weight. An additional shortfall of the BS 5628 assessment method, when assessing foam injected cavity walls, is the assumption that there is no composite action between the two wythes and thus the lateral load resistance is entirely due to the self stiffness of the sum of the two individual wythes.

The Handbook to BS 5628 (1981) code of practice states that design charts and formulae were based on a "partial safety factor format". These partial safety factors were adopted due to the uncertainty of the possible difference in strength of masonry

elements and the difference in the assumed from the actual loading conditions. The safety factors are then applied to the characteristic ultimate strengths which were derived from statistical interpretation of experimental data.

The finite element work in this thesis has provided evidence that there is a distinct enhancement to the stiffness of a masonry cavity wall injected with Isofoam CRF and indicates that there is also an increase in the lateral ultimate strength. A similar approach to the flexural capacity assessment laid out in BS 5628 would need to be adopted where the cavity wall has been treated with the foam injection system. Finite element modelling could then be utilised to extrapolate design data for different cavity wall parameters.

9.4 Discussion of cavity wall testing and analysis

9.4.1 General discussion

There is no existing methodology or theory in the field of masonry that incorporates the structural interactions of a cavity wall with a shear transfer medium introduced to the void. At the onset of this project it was envisaged that sandwich panel concepts and theory could be used for the analysis of the masonry cavity walls and that has largely been adhered to in this chapter. Finite element concepts have been proven to model sandwich action when compared alongside the existing sandwich panel theory of Allen (1969) and experimental work on simpler plywood faced sandwich panels as presented in chapter 7. Allen's theory has not been applied directly to the masonry as finite element concepts prove more versatile for the purposes of this investigation and will certainly have more potential if further studies on more complex masonry structures are attempted.

Having proved that finite element analysis is appropriate for modelling the plywood faced sandwich panels the same modelling techniques have been translated to, and built upon, the more complex interactions of single story height cavity walls. The F.E.A. has

firstly treating the masonry as a homogeneous isotropic mass, designated as type 1 analysis, and then by taking the mortar and brick units as separate materials, type 2 analysis.

The two sections below attempt to identify the presence of sandwich action by way of strain profiles and displacement response. The analyses presented in this part of the investigation are entirely restricted to linear elastic behaviour. Failure predictions and non linear behaviour of masonry are inherently difficult to quantify due to the intrinsic nature of the bond strength between the mortar and masonry unit and have not been attempted at this stage.

9.4.2 Stress profiles

The experimental stress profiles are presented on figures F9.3a-c and the F.E.A. type 2 stress profiles are shown on figures F9.8a-c for cavity walls CW1-3 respectively, with analysis type 1 stress profile on figure F9.6 for cavity wall CW3 only.

9.4.2.1 Experimental stress profiles

For direct comparison to the F.E.A. stress outputs, the experimental stress profiles have been formulated from the raw strain data by multiplication with a "compound" elastic modulus. This compound elastic modulus has been derived as each strain gauges was placed over both the mortar joint and brick units. It has been assumed that the mortar joint is 10 mm thick and so compound modulus has been derived from a third of the mortar and two thirds of the brick unit.

The three experimental stress profiles all follow similar trends in that only a few joints undergo significantly large strains with failure usually occurring at one of those locations. Tensile bond failure of the supported face has occurred outside the load points in all three cavity walls. Failure of the loaded face has occurred near to the upper load point and in all cases below the failure plane in the support face.

It can be seen that general trends relating to sandwich theory also exist, however, the large peak values have diluted the overall stress profiles. Additionally, it should be borne in mind that the intrinsic variability of the behaviour of masonry components and their interaction has led to an irregular stress profile. Ignoring the peak stress concentrations, the shape of the stress plots for both the loaded and supported faces follows approximately the outline of the applied bending moment figure. It is difficult to draw further definitive conclusions to the existence of sandwich action from the experimental results for the reasons given beforehand and the additional effects of self weight stabilisation.

The differences in experimental mid span displacements of the loaded and support faces was earlier attributed the compression of the core and the applied loading to each facing. It was argued that whereas the loaded face underwent bending from point loading, the support face was subject to near uniformly distributed loading. The loaded face had such self stiffness that it effectively spread the two point loads out uniformly. This phenomena is clearly shown on figure F9.8c. The loaded face (line 2 on the graphical output part) has two peak stress concentrations around the point loads. These point stress effects have completely dissipated for the support face. This indicates that the loaded face deflects more than the support face incurring higher stresses, as shown in the graph on figure F9.8c.

9.4.2.2 Finite element analysis stress profiles

The decision to use type 2 analysis, rather than type 1, was based partly on the results of the stress profiles. The type 2 analysis is shown for all three walls on figures F9.8 a-c. The F.E.A. colour contour stress plots clearly show the effects of self weight as the compressive stress reduces the tensile stress nearer to the base of the walls. Effects of self weight can be easily determined from a visual comparison of stress contour profile graphs on figures F9.8c and F9.10 for cavity walls with and without self weight respectively. Essentially self weight has the effect of making the base support of the wall behave as a partial encastre fixture, figure 9.2 and stress plot 9.8c, reducing the flexural displacement response and in turn the bending stresses. The overall worst 2D

principal stresses also include the compressive pre-stressing of self weight accounting for the difference in the reduction of tensile and compressive bending stresses. The effect of self weight has been discussed in more detail in section 9.3.1.5.

Previously it was suggested that the masonry wythes are designated, in sandwich theory terms, as 'very thick' facings and certainly this is evident in all F.E.A. stress plots. The peak stress concentrations, at the load points, are small when compared to the plywood faced panels. Similarly the local bending of the faces at the supports, as again seen on the plywood faced panels, is negligible indicating the disproportionate self stiffness of the masonry facings to the sandwich as a whole. The self stiffness of the wythes is also responsible for the stress profile of the supported face. Clearly the peak stresses under the load points are not translated to the support face with the resultant stress plot indicating a uniformly distributed load being applied to the support face.

9.4.3 Displacement response

9.4.3.1 Experimental displacements

Experimental load versus mid span displacements have been plotted on figure F9.4 to failure for all cavity walls. Only the loaded face deflections, after account of compression at the supports has been taken, have been shown. Beyond a load of approximately 6.0 kN the load / displacement relationship becomes distinctly non-linear. Figures F9.5 a-c show experimental and finite element load versus displacement plots which are limited to 6.0 kN so that a meaningful comparison of the linear elastic behaviour may be made.

9.4.3.2 Finite element modelling displacements

The finite element analysis displacements have been presented as both colour contour plots and boundary profiles along the outer surface of the loaded and supported faces on figures F9.7 for type 1 analysis of cavity wall CW3, F9.9 a-c for type 2 analysis of cavity walls CW 1-3 and F9.10 for wall CW3 with no self weight. The F.E.A. plots all

show only the lateral displacements rather than a resultant in order to be consistent with the experimental data.

All the finite element boundary plots show the loaded face to be displaced to a greater extent than the supported face indicating that the whole of the Isofoam core is in compression. The magnitude of the core compression is dependent on the thickness of the core. This can be easily seen by the difference between boundary displacements on the three figures F9.9 a-c comprising core thicknesses of 58, 75 and 104 mm. Local bending of the support face and compression of the core near the support points is shown by the divergence of the boundary displacements. The positive displacement shown on the supported face is attributed to the slight rotation of the small overhang past the support points.

9.4.3.3 Comparison of experimental and F.E. modelling displacements

The comparison of experimental and F.E.A. displacements is made with regard to figures F9.5 a-c for cavity walls CW 1-3. A quantitative comparison has incorporated the load versus displacement gradient rather than actual displacements. This is so that the initial 'up-take' seen on the experimental curves may be ignored and the linear elastic response behaviour of the walls isolated. Table 9.6 summarises the load / displacements gradients for the loaded face, experimental and F.E.A. analysis, results and presents the discrepancy as a percentage difference from the experimental result.

It should be noted that although trends and conclusions have been drawn from this study they are tentative and subject to further confirmation through a wider range of specimens tests as only three experimental cavity walls have been tested and each is subject to the variabilities intrinsic to masonry. The percentage differences shown in the last column are calculated from:

$$\%.\text{difference} = \frac{\delta_{exp} - \delta_{F.E.A.}}{\delta_{exp}} \quad \ldots\ldots\ldots (9.2)$$

A negative percentage difference indicates that the finite element modelling predicts a more flexible response than the experimental results.

The foremost trend is the increase in percentage difference of the displacements for a single wythe from the experimental cavity wall mid span displacements. The percentage differences increase as the cavity widths increase, -3.9, -49 and -78 for walls CW1-3 respectively. This clearly indicates the enhancement of flexural stiffness against lateral loads as the cavity walls become increasingly more efficient sandwich constructions with the increase of cavity width. The efficiency and optimisation of the foam injection system to masonry cavity walls is discussed in the next section. Considering the variations in strength and modulii values obtained from the wallette testing, the F.E. analysis of the cavity walls appears to show good correlation with percentage differences of 4.6, -8.5 and -26. It would be difficult to attribute a specific trend to these percentage differences as there was only one specimen for each difference.

Wall no.	Analysis / Experimental	Applied load, kN	Displacement/load gradient, mm/kN	Percentage difference from exp.
CW1	Experimental	6.0	0.152	
Single wythe	Type 2	6.0	0.158	-3.9
CW1	Type 2	6.0	0.145	4.6
CW2	Experimental	6.0	0.106	
Single wythe	Type 2	6.0	0.158	-49
CW2	Type 2	6.0	0.115	-8.5
CW3	Experimental	6.0	0.089	
Single wythe	Type 2	6.0	0.158	-78
CW3	Type 1	6.0	0.103	-16
CW3	Type 2	6.0	0.112	-26

Table 9.6 Load / displacement gradients for the loaded face of experimental and F.E.A. analysis.

9.4.4 Optimisation of the cavity wall foam injection system

Sandwich theory has been introduced to masonry cavity walls to aid in the analysis and understanding of composite action present after Isofoam CRF has been applied to the void. In sandwich terms the masonry cavity walls are termed as very thick faced and inefficient. The self stiffness of the facings mean that they carry a significant proportion of the overall stiffness and the wythes are merely acting as individual beams with the core simply transmitting lateral load. A balanced sandwich construction is dependent on a number of factors. Usually the facing and foam types have been predetermined. For any given facing and foam type the optimal core thickness may be then obtained. Allen (1969) identified three factors to formulate the optimal core thickness. These were based on not exceeding the facing stress criteria, face wrinkling stress and shear stress of the core. Alternatively, a displacement criteria may be imposed.

For cavity walls the facings stiffness and core thickness are as existing. This leaves the specification of the foam the only changeable parameter. The current British Standards BS 7456 and BS 7457 recommend the use of 32 kg/m^3 density foam. The use of this density foam does not produce a particularly effective sandwich construction although a stiffness enhancement is still achieved. Figure F9.8c shows the stress plot for cavity wall CW3. The colour contour stress plot clearly shows that the each wythe is bending predominantly about its own centroidal axis with compressive and tensile stresses present in each facing. The Isofoam CRF core does provide some shear transfer but is acting mainly to distribute lateral loads between the facings.

A parametric study, looking at the mid span displacement when increasing the density (and effectively the elastic and shear modulii), for the finite element analysis of cavity wall CW3 is shown in table 9.7. The identical type 2 finite element model has been used to predict mid span displacements against Isofoam CRF density for a constant applied load. The analysis results have been presented graphically on figure 9.3.

It is suggested that the this type of figure (F9.3) may be formulated for any brick unit / mortar designation to aid in the selection of a more appropriate density foam. If the

geometry of the cavity wall is known along with the type of mortar and brick unit then the choice of foam density can then be controlled by a maximum allowable deflection criteria or a required stiffness. Other criteria, set by economic aspects, would play a part in the specification of foam density.

		Maximum mid span displacement		
Core density kg/m^3	G_c N/mm^2	Loaded face mm	Support face mm	Difference mm
32	2.5	-0.752	-0.718	0.034
64	5.2	-0.582	-0.565	0.017
96	8.1	-0.481	-0.470	0.011
128	11.1	-0.411	-0.404	0.007
160	14.1	-0.361	-0.355	0.006
320	29.8	-0.232	-0.230	0.002
640	63.1	-0.148	-0.148	0.0

Table 9.7 F.E.A. mid span displacements of the loaded and support faces

The mid span displacements of the loaded and support facings effectively converge as the density of the foam increase. The increase in density also increases the physical properties of the foam which compresses less and transfers a greater amount of shear forces between facings during bending. As the density of the foam increases the cavity wall becomes a more efficient sandwich structure. The corresponding stress profiles of the cavity wall to the displacement versus core density plots have been shown on figures F9.14 a-h. Each stress profile has a line section at centre span. The line section does not necessarily slice the maximum and minimum stress points as those are found nearer the load point concentrations. The line sections are indicative of the trend of the cavity wall becoming a more efficient sandwich. The graph on each figure shows that the increase in core density begins to balance the stresses for each wythe into either tensile or compressive only. The results of the stress profile plots have been summarised in table 9.8 and shown in graphical form on figure 9.3.

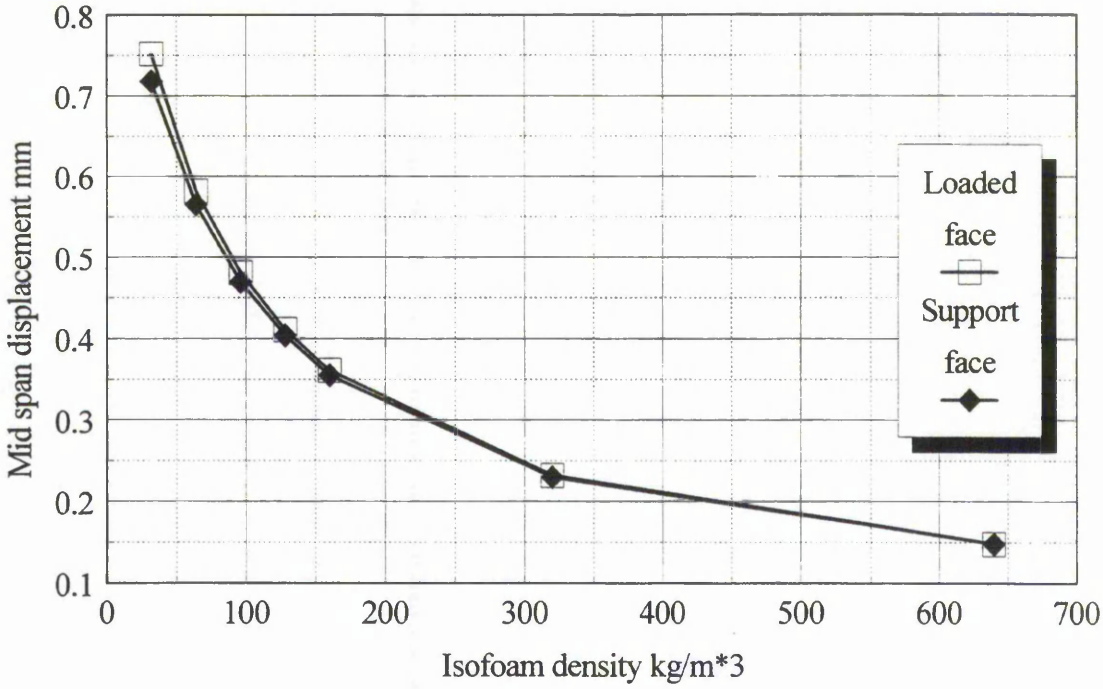

Figure 9.3 Mid span displacement versus Isofoam CRF density

		Facing stress N/mm^2			
		Loaded face		Support face	
Core density kg/m^3	G_c N/mm^2	Outside of wythe	Inside of wythe	Outside of wythe	Inside of wythe
32	2.5	-0.703	0.554	0.698	-0.685
64	5.2	-0.567	0.422	0.577	-0.533
96	8.1	-0.493	0.356	0.498	-0.430
128	11.1	-0.438	0.243	0.443	-0.345
160	14.1	-0.398	0.195	0.402	-0.300
320	29.8	-0.294	0.053	0.291	-0.160
640	63.1	-0.226	-0.022	0.209	-0.065
1280	133.4	-0.199	-0.066	0.167	-0.009

Table 9.8 Summary of stress profiles against core density

Figure 9.4 shows how the increase in core density changes the behaviour of the cavity wall acting as a sandwich construction. At a low core density the wythes respond more as individual members than as a composite structure. In this case the wythes are bending predominantly about their own axis with compressive and tensile stresses present in each and approximately equal in magnitude. At higher densities the core transfers more shear force between the members and the wythes begin to act more in only tension or compression. The convergent lines for each wythe indicate this behaviour.

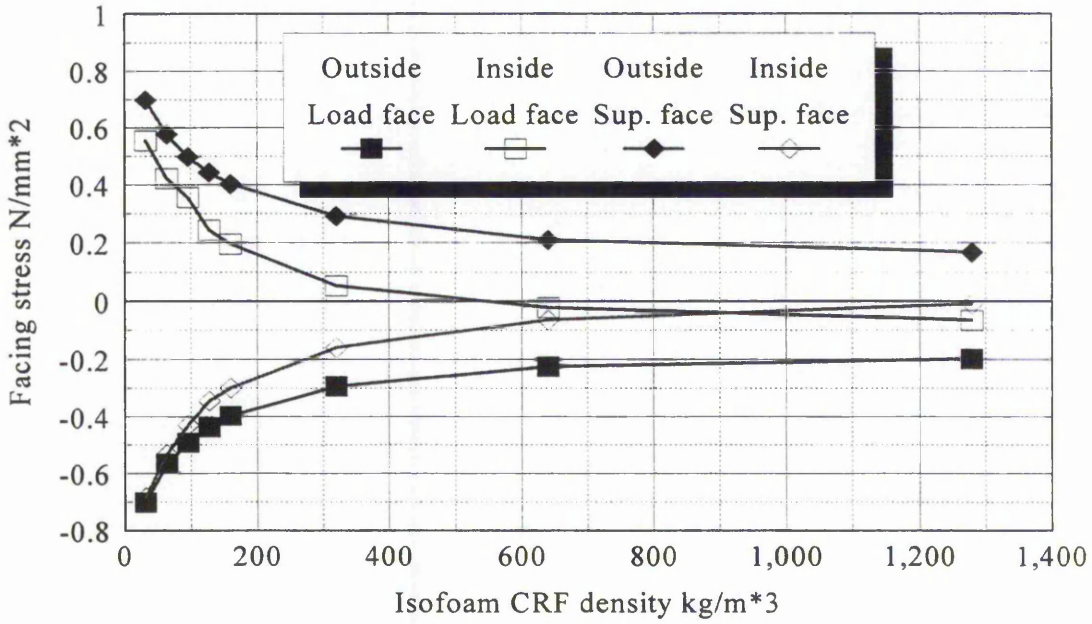

Figure 9.4 Facing stresses against Isofoam CRF density

It should be remembered that the choice of Isofoam CRF density is dependent on many factors such as cost, structural defect mechanism, required performance and time dependent behaviour. Secondary factors, including thermal, acoustic and moisture insulation may also be significant.

9.7 Conclusions

The foam injection system has been investigated by good correlation of finite element modelling techniques with experimental data. The innovative technique of masonry cavity wall stabilisation with Isofoam CRF has been proven to enhance the structural performance of simple supported, vertically spanning cavity walls. The following conclusions have been drawn from this section.

(i) The literature review has been instrument in identifying the existence of composite action, leading to a structural performance increase, in the flexural behaviour of masonry cavity walls with various shear connections. The review has also shown that there is currently no formal analysis that evaluates this structural enhancement. This thesis has attempted to subjectively verify the additional stiffness of a shear connected cavity wall.

(ii) An applied worst case equivalent wind loading test to all three cavity walls showed no evidence of distress in the masonry. The ultimate failure load of all the cavity walls was at least seven times that of the applied wind load. Additional pre-stressing from the structure, not included in this investigation, would further enhance this factor.

(iii) The hysteresis test on cavity wall CW2 showed no obvious signs of significant permanent deformation. There remained a mid height displacement of 0.16 mm which dissipated to 0.05 mm after a further period of 120 seconds. No further recovery was evident thereafter. The hysteresis test has also indicated that, like the plywood faced panels tests, the time dependent properties of the Isofoam CRF have some influence on the load / displacement relationship when recorded over a series of time related load increments.

(iv) Using finite element modelling it was possible to identify the effect of self weight on the lateral stiffness of the cavity walls. The increase in stiffness of the model of cavity wall CW3 with no self weight from one with self weight was 7.4%. The tensile stress decreased by 12% and the compressive stress decreased by 3%. Self weight was

therefore significant when considering masonry structures. In service cavity walls have additional axial compressive loads from the structure they are supporting providing a further reduction in tensile stresses and lateral displacement.

(v) The foremost trend associated to the foam injection system was the increase in flexural stiffness. Finite element modelling enabled the stiffness response of a single wythe (when doubled) to be compared to the F.E. models of the foam injected cavity walls. The percentage increases in overall flexural stiffness are 19%, 27% and 30% for cavity walls CW1-3 respectively.

(vi) Considering the variations in strength and modulus of the wallette testing programme, the F.E. analysis of the cavity walls appears to model the experimental mid span displacements reasonably well with percentage differences of 4.6, 8.5 and 26 for cavity walls CW1-3 respectively.

(vii) Two, two dimensional F.E. analysis types were proposed. Type 1 assumed an overall isotropic homogeneous material for the brickwork. Type 2 segregated the brick units and mortar joints. It is recommended that the use of either analysis type is dependent on the availability of material properties and the size and complexity of the problem.

(viii) Current British Standards recommend the use of 32 kg/m^3 density Isofoam CRF for the injection system. However, the method described in this chapter should provide the user with a more appropriate selection of foam density for a stiffer and more economic resulting structure.

(ix) The finite element work in this thesis has provided evidence that there is a distinct enhancement to the stiffness of a masonry cavity wall injected with Isofoam CRF, but the analysis does not imply that there is an increase in the lateral ultimate strength. A similar approach to the flexural capacity assessment laid out in BS 5628 would need to be adopted where the cavity wall has been treated with the foam injection system. Finite

element modelling could then be utilised to extrapolate design data for different cavity wall parameters.

(x) It should be noted that although trends and conclusions have been drawn from this study they are tentative and subject to further confirmation through a wider range of specimen testing as only three experimental cavity walls have been tested and each is subject to the variabilities intrinsic to masonry.

CHAPTER 10 - CONCLUSIONS

10.1 Summary

10.2 Final Conclusions

10.3 Recommendations

CHAPTER 10 - CONCLUSIONS

10.1 Summary

10.1.1 General

This research project was undertaken to provide a more advanced understanding of the foam injection system when used as a remedial measure to existing masonry cavity walls. The review of masonry cavity wall literature uncovered little information regarding composite action between cavity wall wythes. Moreover, the current masonry codes and analysis techniques do not account for the stiffness or strength enhancement of a shear transfer medium between the inner and outer masonry leaves. Sandwich theory was identified as a means to analyse the structural interaction of the masonry and Isofoam CRF.

10.1.2 Chapter 2 - Physical properties and application of Isofoam Cavity Reinforcement Foam

The importance of the secondary physical properties of Isofoam CRF have been discussed in this section and relevance has been drawn to the inter-relationships of the properties. Specific material properties have been evaluated in chapters 4, 5 and 6. The two most significant secondary properties are time dependant strain response and the effect of temperature as they both directly influence the primary properties.

The long term physical properties of rigid polyurethane foam subject to constant levels of stress may cause future problems of structural integrity of a masonry cavity wall. Situations where short term loadings are predominant are more suited to the properties and use of Isofoam CRF. In particular wind loading or temporary reinforcement against mining subsidence may be ideal for applications of the foam injection method.

Two unique case studies of the foam injection system have been briefly presented and discussed. The first case study reports on one of the original applications of the foam injection system as a direct remedial measure to existing masonry cavity walls. The second describes a different application, in itself, novel and innovative. The case studies have provided practical evidence that the foam injection system is a valid option for a wide range of structural remedial measures to existing masonry cavity walls.

The literature search regarding laterally loaded masonry cavity walls highlights a significant gap in the knowledge of the structural interaction of the foam injection system as a remedial measure to existing masonry cavity walls. The system is currently employed in an 'engineering judgmental' way with little meaningful formal analysis.

10.1.3 Chapter 3 - Sandwich construction analysis methods

The finite element analysis and the classical solutions formulated by Allen (1969), as presented by O'Connor (1985), were identified for predicting the behaviour of sandwich constructions. A summary of the Allen's theory has been included along with the fundamental principals of finite element theory. This project makes use of a number of F.E.A. commercial and proprietary software packages.

O'Connor's investigation of Allen's solutions provide evidence to suggest that a good approximation of displacements and stress profiles of sandwich beams are achievable, but the local effects near point loads are not so well modelled. Allen's assumptions of an antiplane and incompressible core were made on the basis of analysing a beam with a honeycombed, or similar, core rather than a soft and flexible core such as polyurethane. Allen's solutions provide further comparison, along with experimental data, to the verification of finite element modelling techniques.

The vast amount of literature regarding finite element analysis indicates that the method is ideally suited to the requirements of this project. By its discrete solution method F.E.A. provides an approximation of a structural system. Correct modelling techniques to achieve the best prediction have been discussed and adopted throughout the project.

10.1.4 Chapter 4 - Uniaxial material testing and analysis

Uniaxial compression tests were originally used to find the elastic modulus and Poisson's ratio for the Isofoam CRF core and were considered to be the simplest test method available. During similar tests, O'Connor (1985) found that barrelling, of the four free vertical faces, was caused by the top and bottom faces being restrained and the experimental results were adversely affected. This thesis presents an additional test error to O'Connor's fixed edge barrelling, described here as a three dimensional geometrical shape effect. Correction factors, including both types of barrelling, were derived from finite element modelling and were applied to the elastic modulus and Poisson's ratio values obtained directly from the tests.

The effect of the fixed edges, caused by testing with the facings still bonded, creates an under estimation of the lateral displacement response and hence Poisson's ratio values. As a consequence the experimental elastic modulus is higher than expected. The three dimensional geometry effect causes each lateral face to bow between vertical face edges thus overestimating the lateral displacement response. Similarly this increases the Poisson's ratio and creates an apparently less stiff specimen. The overall effect was found to depend on the aspect ratio of the uniaxial test specimen. It was shown that for a 150 x 150 mm plan area an aspect ratio of 0.8 (120 mm thickness) the two types of barrelling cancelled each other.

Although the uniaxial compression tests did not yield what was first anticipated they did point the way to a better understanding of Isofoam CRF, particularly when placed by the foam injection system. In the absence of any other suitable tests the Poisson's ratio values were adopted for all finite element analysis involving Isofoam CRF. Specifically the properties were related to the direction of foam rise. Closer visual inspection of the foam showed noticeable evidence that the shape of the voids in the mass of the Isofoam were predominantly ovoid, with the main axis orientated in the direction of rise thus creating the orthotropic conditions.

10.1.5 Chapter 5 - Shear testing and analysis

Two shear modulii test methods, BS 4370 (1993) and ASTM C273 (1980), were identified as suitable to simulate shear strains similar to the flexural response of the Isofoam CRF in the sandwich panels. O'Connor (1985) had previously conducted a series of shear tests and had used finite element techniques to find errors in both the testing apparatus and configurations. Since O'Connor's investigation did not draw a positive conclusion to which method was most appropriate and the British Standard had recently been updated, a full and detailed finite element analysis of the test methods was completed. A major source of test error was discovered and corrected, through the implementation of control tests and was attributed to the displacement of the test rig and apparatus. British and American standard results still differed, although these differences were common with their respective apparatus configurations.

Aspect ratio errors (errors relating to the free specimen ends) were found to be between 3% and 4%, depending on specimen properties, and increased in magnitude with stiffness. Plate bending and rotation errors were inherent with each other and evaluated to be between 2% to 5% again increasing with an increase in specimen stiffness. The difference between American and British Standard shear modulus evaluations were 15% and 13% for the crosshead and crossplate measurement techniques respectively. The difference between crosshead and crossplate shear modulii were 5.6% and 7.5% for the American and British Standards respectively.

The importance of the adhesive bond between sample and edge plate was found to be of an under estimated importance. The pilot studies were wholly vindicated in identifying a suitable adhesive thickness (in fact a total mass used) so that the thinnest possible adhesive line could be applied. A 1mm thick bond line could influence the results by some 8% and too thin an adhesive line could result in a much larger error as the specimen might not be bonded over its entire length.

10.1.6 Chapter 6 - Multiple span beam testing and analysis

Multiple span beam testing was considered necessary as the two coupon tests used small specimen sizes to evaluate core properties that were particularly susceptible to variations in the quality of the Isofoam CRF core. The beams were subject to flexure and thus the core shear strains were closely matched to those of the panel tests.

The experimental data was analysed using Allen's theory, presented in a different format by O'Connor (1985) which incorporated the conjugate point method that avoided experimental errors associated with local point effects. In chapter 7 the experimental and finite element results indicated that these errors were substantially less than O'Connor had predicted although the overall concept still avoids unnecessary test error.

The load / deflection relationship should only be obtained by a series of load increments rather than one load step application procedure. This will eliminate errors due to "take up" in the system and also prevent any significant dynamic loading. The rate of application of load increments should be tailored to that of the full scale tests.

Pre-determining the elastic modulii of the facings greatly assisted in fitting a tangent to the experimental curves. Manually fitting a tangent to the experimental multiple span beam testing result curves (graphical analysis types 1 and 2) was subject to misfit error. The degree of error depended on how "linear" the curve was at the tangent point. The error was not quantified as it was found to be too subjective.

Theoretically the conjugate point method is the most accurate means of shear modulus evaluation as it is not influenced by local distortion around point concentrations. The effectiveness of the conjugate point method diminishes as the facings become stiffer or the core weaker relative to the stiffness of the overall sandwich beam.

10.1.7 Chapter 7 - Sandwich panel testing and analysis

The testing conducted on various configurations of plywood faced sandwich panels served two purposes. Firstly, the Allen and F.E.A solutions were compared to each other alongside experimental results. This was done principally to confirm confidence in the application of finite element modelling techniques to sandwich constructions. The comparisons of flexural behaviour have been made by assessing the shape of the strain profiles along the span of the outer surfaces of the facings. Secondly, the evaluation of the material properties, including the plywood facings, in the previous three chapters was inconsistent. Having gained confidence in the finite element analysis, comparisons could then be made, with the full scale panel tests, in an attempt to identify the most appropriate property test method. The comparisons in this instance have been made by consideration of deflections within the span. Finite element analysis has been proven to give good agreement with experimental data both for the overall shape of the stress profile and to the critical span lengths.

The critical span lengths have been assessed from the graphically represented stress profiles and not from a theoretical stand point except in the case of O'Connor's. This potentially disregards some of the very small displacements and strains at the extremes of the critical span lengths, which may have been theoretically present, but as such does provide a more practical justification to measured displacement response within the span. This study has shown O'Connor's critical span concept to over- estimate the experimental critical span lengths by up to 200 %. However, the use of conjugate points for the multiple span testing method was still necessary due to the local displacement distortions at the centre span load point. The displacement measurements in the multiple span beam testing of chapter 6 have not been adversely influenced by the local point effects as first anticipated by O'Connor's critical span concept.

From the values held in the tables D7.2a-e for the finite element analysis and experimental data it is possible to conclude that the critical span length does not appear to be influenced by the depth of the core as suggested by the critical span equation

$\theta a = \pm 5$. Instead both the finite element analysis and the experimental results point to the fact that the critical span of a sandwich beam is influenced purely by the modulus of the core and the self stiffness of the facing. For transversely soft cored sandwiches it is proposed that $\theta a = \pm 2.5$.

The difference between quarter / support, eighth / support and quarter / eighth span conjugate points may be explained by considering F.E.A. displacement results. The F.E. modelling took into consideration the compression of the core and the local bending of the lower facing at the supports, whereas the assumptions used in the Allen solutions did not. However, it should also be remembered that the Allen solutions were based on honeycombed cores where the assumptions of an antiplane and incompressible ($E_y = \infty$) core were appropriate.

The plywood facings elastic modulii were supported by the manufacturer's claimed values and were adopted for all the respective groups. Retrospectively a greater number of coupons tests from individual plywood sheets to determine the modulii for that facing would have been preferable. The variation in the four point load tests on all coupons represented a possible 8% difference in modulus value from facing to facing

Identification of the most appropriate material property evaluation method has been made by considering the percentage discrepancies from experimental displacement results to F.E.A. displacements supported with material properties generated from the various test methods. Table 7.6 displays the a ranking list for all test methods and for each test type .

10.1.8 Chapter 8 - Masonry wallette and constituent testing and analysis

This chapter describes how the properties of the masonry cavity walls were derived experimentally. Initially it was proposed to find the elastic modulus of brickwork as a homogeneous isotropic solid, for the spanning direction only, rather than the properties of the individual constituents. For this wallettes were tested in flexure. The results of the wallette tests proved to have a large variance and allied to the ease of testing the

individual masonry components a further analysis was proposed utilising the component material properties. Difficulty was experienced in evaluating the elastic properties of the perforated brick units and values from previous research were adopted.

It may be generally concluded from the literature review that quantifying the influences of certain factors involved in the flexural bond strength and modulus of masonry is difficult. This has also been found for this investigation as seen in the results for the elastic modulus and the ultimate failure loads of the wallettes. Both having a significant standard deviation from their respective mean value when seemingly identical materials and practices were rigorously adhered to.

The modulus of elasticity carried forward to be used in the analysis of the cavity walls was 5500 N/mm^2 with a standard deviation of 2000 N/mm^2. It has been impractical to attempt to evaluate the Poisson's ratio of masonry and a similar value of 0.20 has been adopted from the work of Lovegrove (1988). The modulus of elasticity of mortar designation (i) in compression, water / cement ratio 0.52, is 2500 N/mm^2.

10.1.9 Chapter 9 - Masonry cavity wall testing and analysis

The literature review has been instrumental in identifying the existence of composite action, leading to a structural performance increase, in the flexural behaviour of masonry cavity walls with various shear connections. The review has also shown that there is currently no formal analysis that evaluates this structural enhancement. The work in this thesis has attempted to subjectively verify the additional stiffness of a shear connected cavity wall.

The two types of finite element analysis, Type 1 using wallette and Type 2 brick / mortar properties, have been scrutinised and compared to the experimental data of three vertically spanning, simply supported, story height cavity walls, each with a different cavity thickness. The versatility and use of finite element analysis has been vindicated for use here and is paramount for the evaluation of the structural enhancement of cavity walls when injected with Isofoam CRF.

The validity of using foam injected in to masonry cavity walls as a system to enhance stiffness has been investigated and a good correlation between finite element modelling techniques and experimental data has been established. The innovative technique of masonry cavity wall stabilisation with Isofoam CRF has been proven to enhance the structural performance of simply supported, vertically spanning cavity walls.

An applied worst case equivalent wind loading test to all three cavity walls showed no evidence of distress in the masonry. The ultimate failure load of all the cavity walls was at least seven times that of the applied wind load. The hysteresis test showed no obvious signs of significant permanent deformation. The hysteresis test has also indicated that, like the plywood faced panels tests, the time dependent properties of the Isofoam CRF have some influence on the load / displacement relationship when recorded over a series of time related load increments.

Using finite element modelling it was possible to identify and isolate the effect of self weight on the lateral stiffness of the cavity walls. Self weight was found to be significant when considering the masonry structures. In service cavity walls have additional axial compressive loads from the structure they are supporting, thus providing a further reduction in tensile stresses and lateral displacement.

The foremost trend associated to the foam injection system was the increase in overall flexural stiffness. Finite element modelling enabled the stiffness response of a single wythe (when doubled) to be compared to the F.E. models of the foam injected cavity walls. The percentage increases in overall flexural stiffness are 19%, 28% and 30% for cavity walls CW1-3 respectively. Considering the variations in strength and modulus of the wallette testing programme, the F.E. analysis of the cavity walls appears to model the experimental mid span displacements reasonably well with percentage differences of 4.6%, -8.5% and -26% for cavity walls CW1-3 respectively.

Current British Standards recommend the use of 32 kg/m^3 density Isofoam CRF for the injection system. However, the method described in section 9.4.4 for the optimisation

of the cavity wall foam injection system, should provide the user with a more appropriate selection of foam density for a stiffer and more economic resulting structure if and as required.

10.2 Final Conclusions

(i) Only the linear elastic response of all specimens has been modelled. At all times strain rates have been kept constant and uniform for related tests. Time dependant strain response has been largely eliminated from test results.

(ii) In addition to O'Connor's barrelling effect in uniaxial compression tests, a three dimensional geometrical shape effect was discovered that also caused barrelling.

(iii) A major source of British and American shear test error was discovered and corrected, through the implementation of control tests and was attributed to the displacement of the test rig and apparatus.

(iv) The importance of the adhesive thickness between sample and edge plate of shear tests was found to be of an under estimated importance.

(v) O'Connor's critical span concept for sandwich beams over estimates the experimental and F.E.A. critical span lengths by up to 200 %. However, the use of conjugate points for the multiple span testing method was still necessary due to the local displacement distortions at the centre span load point. The displacement measurements in the multiple span beam testing of chapter 6 have not been adversely influenced by the local point effects as first anticipated by O'Connor's critical span concept.

(vi) The finite element analysis and the experimental results, presented in this thesis, point to the fact that the critical span of a sandwich beam is influenced purely by the modulus of the core and the self stiffness of the facing.

(vii) The percentage increases in overall flexural stiffness of cavity walls with void thicknesses of 50, 78 and 104 mm were 19%, 28% and 30% respectively when injected with 32 kg/m^3 density Isofoam CRF.

10.3 Recommendations

(i) It should be noted that the Isofoam CRF used in this study has been placed by the foam injection system. This system inherently creates an orthotropic foam mass with local variabilities in foam quality. It is recommended that these conclusions be verified by a more intensive and specific study with a greater number of test specimens. In evaluating the material tests in this way it would be preferable to use an isotropic and homogeneous foam. The foam specified for the plywood faced sandwich panels was designed to represent that which would be commonly found in applications of the foam injection system to masonry cavity walls.

(ii) Current British Standards recommend the use of 32 kg/m^3 density Isofoam CRF for the injection system. However, the method described in section 9.4.4 for the optimisation of the cavity wall foam injection system, should provide the user with a more appropriate selection of foam density for a stiffer and more economic resulting structure if and as required.

(iii) The finite element work in this thesis has provided evidence that there is a distinct enhancement to the stiffness of a masonry cavity wall injected with Isofoam CRF, but the analysis does not imply that there is an increase in the ultimate strength to lateral loads. A similar approach to the flexural capacity assessment laid out in BS 5628 would need to be adopted where the cavity wall has been treated with the foam injection system. Finite element modelling could then be utilised to extrapolate design data for different cavity wall parameters.

(iv) Two separate, two dimensional F.E. analysis types were proposed. Type 1 assumed an overall isotropic homogeneous material for the brickwork. Type 2

segregated and used the individual properties of the brick units and mortar joints. It is recommended that the use of either analysis type is dependant on the availability of material properties and the size and complexity of the problem. Type 1 analysis should be used where large and complex structures, including openings and returns, are to be modelled. Type 2 analysis should be used where detailed stress / strain interaction of the mortar and bricks is required. Type 2 analysis could readily be adapted to three dimensional work using the individual mortar and brick properties. Type 1 analysis would require properties of masonry in the orthogonal direction to the wallette testing described in chapter 8.

(v) The long term physical properties of rigid polyurethane foam subject to constant levels of stress may cause future problems of structural integrity of a masonry cavity wall. Situations where short term loadings are predominant are more suited to the properties and use of Isofoam CRF. In particular wind loading or temporary reinforcement against mining subsidence may be ideal for applications of the foam injection method.

(vi) Further investigation of the elastic properties of masonry units is strongly recommended.

Appendix A

CHAPTER 4

UNIAXIAL MATERIAL TESTING AND ANALYSIS

	Plan Size (mm)	Thick. (mm)	Temp ^{0}C	Rel. Hum. %	Elastic Mod E N/mm^2	Poisson's Ratio υ_{xz}	Poisson's Ratio υ_{yz}	Average values
P1a	80x80	52.0	16.2	45	4.4	0.14	0.16	t = 52mm
P1b	80x80	52.0	15.6	41	6.1	0.17	0.12	T = 16.0^{0}C
P1c	80x80	52.0	16.0	42	6.0	0.22	0.15	RH = 44%
P1d	80x80	52.0	15.9	46	5.8	0.20	0.18	E = 5.5
P1e	80x80	52.0	16.0	44	5.5	0.21	0.19	υ_{xz} = 0.19
P1f	80x80	52.0	16.1	45	5.0	0.17	0.15	υ_{yz} = 0.16
P2a	80x80	52.0	15.0	41	3.3	0.14	0.10	t = 52mm
P2b	80x80	52.0	15.0	38	4.2	0.23	0.20	T = 15.2^{0}C
P2c	80x80	52.0	14.8	37	4.3	0.25	0.22	RH = 39%
P2d	80x80	52.0	15.5	40	4.8	0.24	0.21	E = 4.4
P2e	80x80	52.0	14.6	42	5.0	0.20	0.19	υ_{xz} = 0.21
P2f	80x80	52.0	15.4	38	4.7	0.17	0.15	υ_{yz} = 0.18

Table A4.1a Compression Test Results

	Plan Size (mm)	Thick. t (mm)	Temp. ^{0}C	Rel. Hum. %	Elastic Mod E N/mm^2	Poisson's Ratio υ_{xz}	Poisson's Ratio υ_{yz}	Average values
P8aa	150x150	50.1	20.1	49	5.9	0.21	0.20	t = 50mm
P8b	150x150	50.1	19.5	48	5.3	0.26	0.16	T = 19.9^{0}C
P8c	150x150	50.0	20.4	48	4.4	0.18	0.15	RH=48%
P8d	150x150	49.8	19.6	49	4.8	0.25	0.19	E = 4.9
P8e	150x150	49.9	19.8	47	5.0	0.23	0.23	υ_{xz} = 0.22
P8f	150x150	49.9	19.9	46	4.2	0.17	0.20	υ_{yz} = 0.19
P9a	150x150	50.5	20.6	49	4.5	0.19	0.18	t = 50mm
P9b	150x150	49.9	20.5	48	3.7	0.15	0.14	T = 20.4^{0}C
P9c	150x150	50.1	20.7	47	3.7	0.16	0.16	RH=48%
P9d	150x150	49.5	20.2	48	3.1	0.19	0.13	E = 3.8
P9e	150x150	49.8	20.3	46	4.2	0.23	0.21	υ_{xz} = 0.19
P9f	150x150	49.9	20.2	48	3.8	0.20	0.17	υ_{yz} = 0.17

Table A4.1c Compression Test Results

	Plan Size (mm)	Thick. t (mm)	Temp. ^{0}C	Rel. Hum. %	Elastic mod E N/mm^2	Poisson's Ratio υ_{xz}	Poisson's Ratio υ_{yz}	Average values
P3a	150x150	21.1	20.6	48	2.23	0.29	0.21	t = 21mm
P3b	150x150	21.0	20.7	49	1.94	0.21	0.15	T = 19.9^{0}C
P3c	150x150	20.9	20.3	47	1.98	0.23	0.23	RH=48%
P3d	150x150	20.8	19.6	47	2.03	0.18	0.08	E = 2.3
P3e	150x150	21.2	19.4	48	2.94	0.37	0.31	υ_{xz} = 0.021
P3f	150x150	21.0	18.9	48	2.58	0.44	0.28	υ_{yz} = 0.025
P4a	150x150	50.7	19.8	49	3.79	0.09	0.09	t = 51mm
P4b	150x150	50.9	19.6	48	4.43	0.10	0.14	T = 19.6^{0}C
P4c	150x150	51.2	19.6	49	4.02	0.09	0.09	RH = 49%
P4d	150x150	51.0	19.8	48	5.11	0.10	0.14	E = 4.3
P4e	150x150	51.1	19.4	47	4.14	0.06	0.08	υ_{xz} = 0.11
P4f	150x150	51.1	19.4	50	4.34	0.07	0.09	υ_{yz} = 0.10
P5a	150x150	71.9	19.9	47	6.90	0.26	0.30	t = 72mm
P5b	150x150	71.8	19.5	47	6.10	0.26	0.26	T = 19.8^{0}C
P5c	150x150	71.9	20.1	48	5.71	0.25	0.27	RH=48%
P5d	150x150	72.0	19.6	47	6.72	0.23	0.26	E = 6.5
P5e	150x150	72.2	19.6	49	6.99	0.24	0.29	υ_{xz} = 0.25
P5f	150x150	72.2	20.0	48	6.72	0.27	0.28	υ_{yz} = 0.24
P6a	150x150	104.6	19.5	48	6.25	0.27	0.25	t = 105mm
P6b	150x150	104.2	19.9	47	5.56	0.22	0.22	T = 19.6^{0}C
P6c	150x150	104.9	19.4	49	6.37	0.24	0.23	RH=48%
P6d	150x150	104.5	19.6	49	5.49	0.26	0.24	E = 6.02
P6e	150x150	104.7	19.7	48	5.84	0.25	0.25	υ_{xz} = 0.25
P6f	150x150	104.7	19.7	48	6.62	0.26	0.24	υ_{yz} = 0.24
P10a	150x150	49.7	19.7	48	7.48	0.19	0.18	t = 50mm
P10b	150x150	49.8	20.0	48	5.86	0.24	0.20	T = 20.0 ^{0}C
P10c	150x150	49.7	20.0	49	5.00	0.19	0.17	RH=49%
P10d	150x150	49.6	19.9	49	6.76	0.23	0.17	E = 6.4
P10e	150x150	49.5	19.8	48	6.22	0.24	0.21	υ_{xz} = 0.21
P10f	150x150	49.8	20.4	49	7.19	0.18	0.16	υ_{yz} = 0.19

Table A4.1b Compression test results

	Specimen size (mm)	Temperature °C	Relative Humidity %	Tensile elastic modulus N/mm^2
P4a	25 x 25 x 140	18.7	48	5.25
P4b	25 x 25 x 140	18.7	48	5.45
P4c	25 x 25 x 140	18.7	48	4.45
P4d	25 x 25 x 140	18.7	48	5.24
P4e	25 x 25 x 140	18.7	48	4.59
P4f	25 x 25 x 140	18.7	48	4.99
			Average =	5.00
P5a	25 x 25 x 140	19.6	49	6.53
P5b	25 x 25 x 140	19.6	49	6.81
P5c	25 x 25 x 140	19.6	49	5.39
P5d	25 x 25 x 140	19.6	49	6.87
P5e	25 x 25 x 140	19.6	49	6.13
P5f	25 x 25 x 140	19.6	49	5.70
			Average =	6.24
P6a	25 x 25 x 140	19.6	49	7.50
P6b	25 x 25 x 140	19.6	49	6.62
P6c	25 x 25 x 140	19.6	49	5.53
P6d	25 x 25 x 140	19.6	49	7.16
P6e	25 x 25 x 140	19.6	49	6.93
P6f	25 x 25 x 140	19.6	49	6.50
			Average =	6.71
P8a	25 x 25 x 140	19.1	48	5.01
P8b	25 x 25 x 140	19.1	48	5.65
P8c	25 x 25 x 140	19.1	48	4.84
P8d	25 x 25 x 140	19.1	48	5.39
P8e	25 x 25 x 140	19.1	48	4.52
P8f	25 x 25 x 140	19.1	48	5.43
			Average =	5.14
P9a	25 x 25 x 140	18.8	47	4.21
P9b	25 x 25 x 140	18.8	47	4.09
P9c	25 x 25 x 140	18.8	47	4.00
P9d	25 x 25 x 140	18.8	47	5.37
P9e	25 x 25 x 140	18.8	47	4.06
P9f	25 x 25 x 140	18.8	47	4.01
			Average =	4.29
P10a	25 x 25 x 140	18.8	48	6.00
P10b	25 x 25 x 140	18.8	48	6.18
P10c	25 x 25 x 140	18.8	48	5.90
P10d	25 x 25 x 140	18.8	48	6.46
P10e	25 x 25 x 140	18.8	48	6.03
P10f	25 x 25 x 140	18.8	48	6.60
			Average =	6.20

Table A4.2 Tensile test results

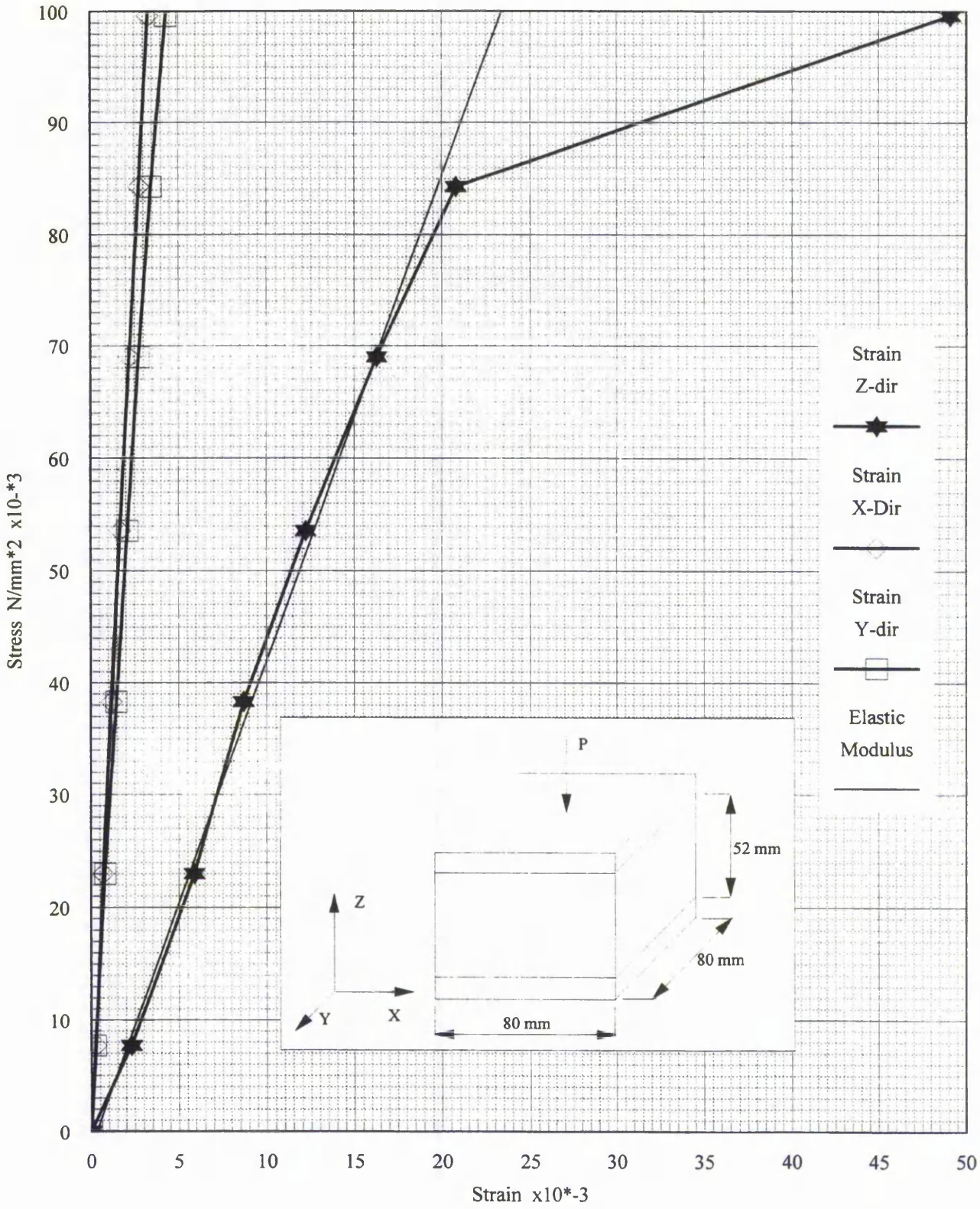

Figure A4.1 Experimental load versus displacement plot
for a specimen from panel P1

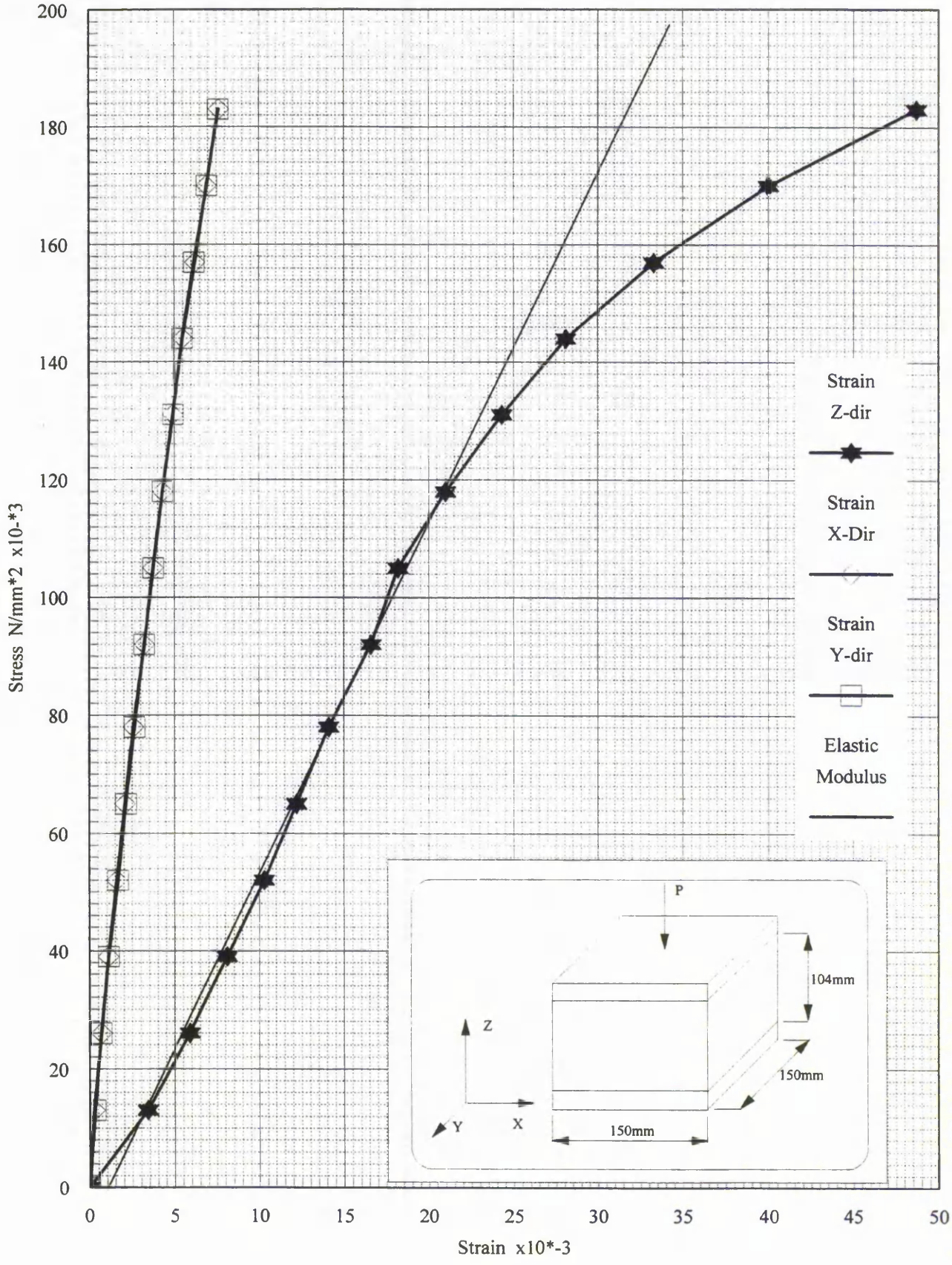

Figure A4.2 Experimental load versus displacement plot
for a specimen from panel P6

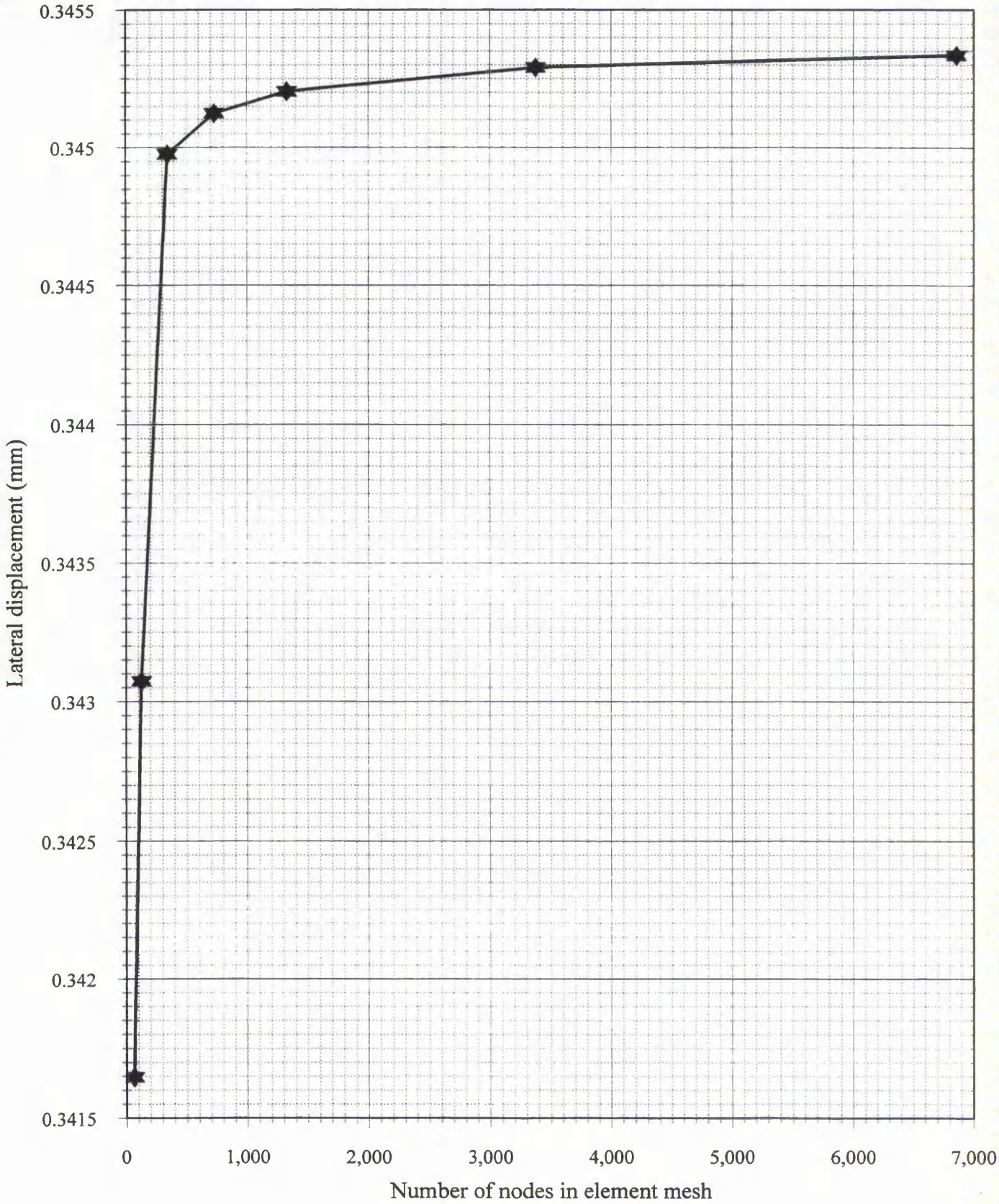

Figure A4.3 Finite element convergence study for lateral displacement versus number of nodes uniaxial compression specimen from panel P6

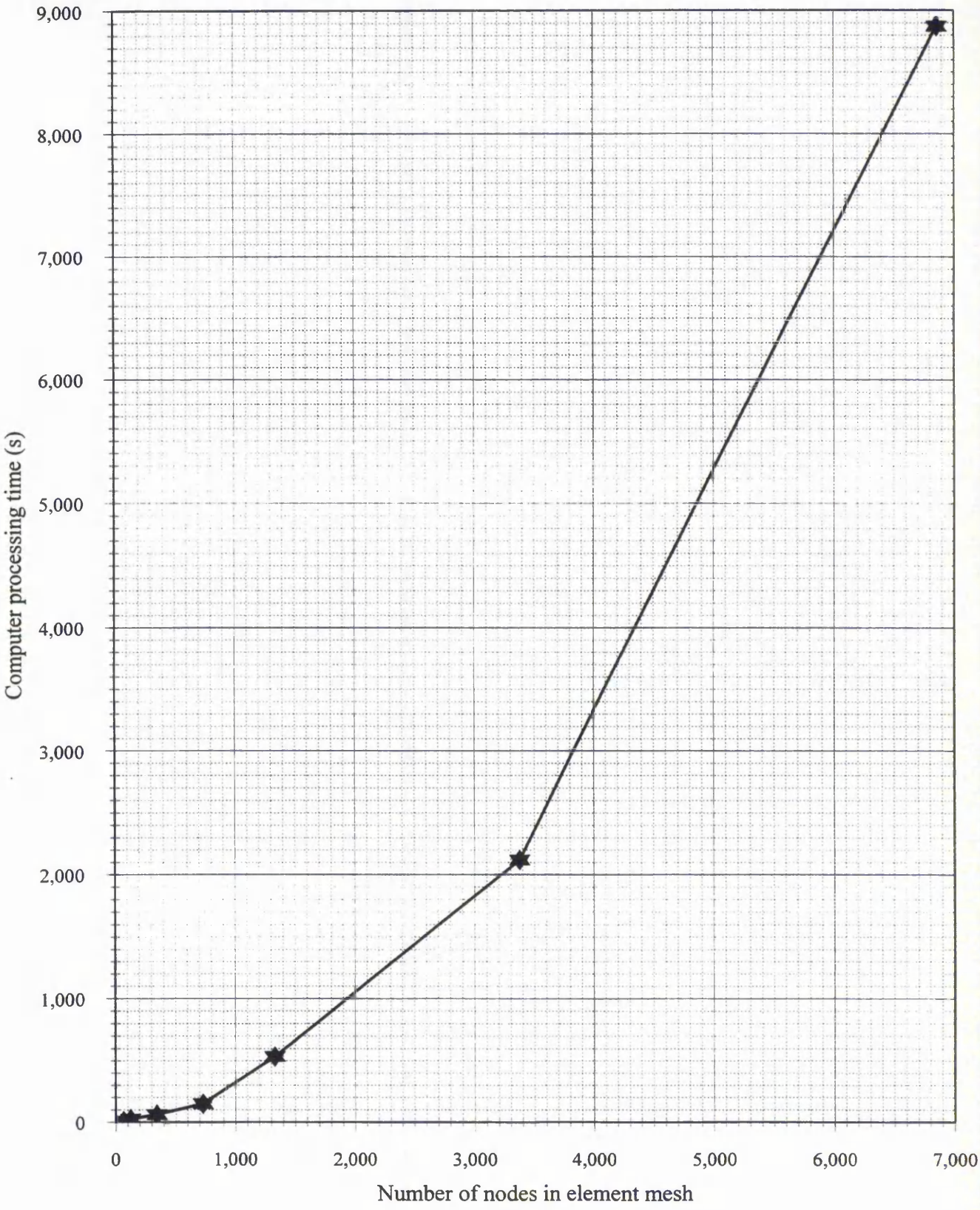

Figure A4.4 Finite element convergence study for computer processing time versus number of nodes uniaxial compression specimen from panel P6

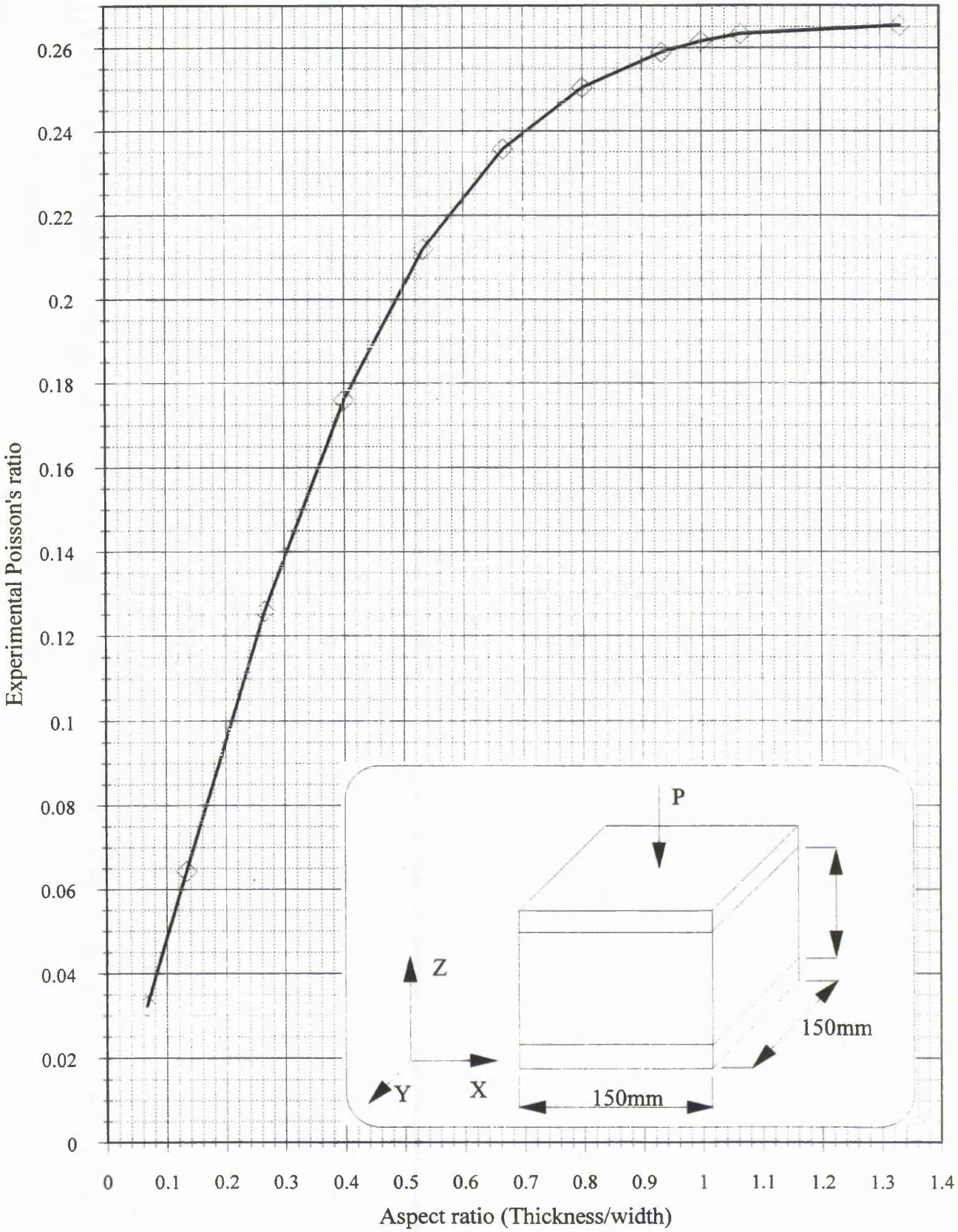

Figure A4.5 The effect of aspect ratio on Poisson's ratio

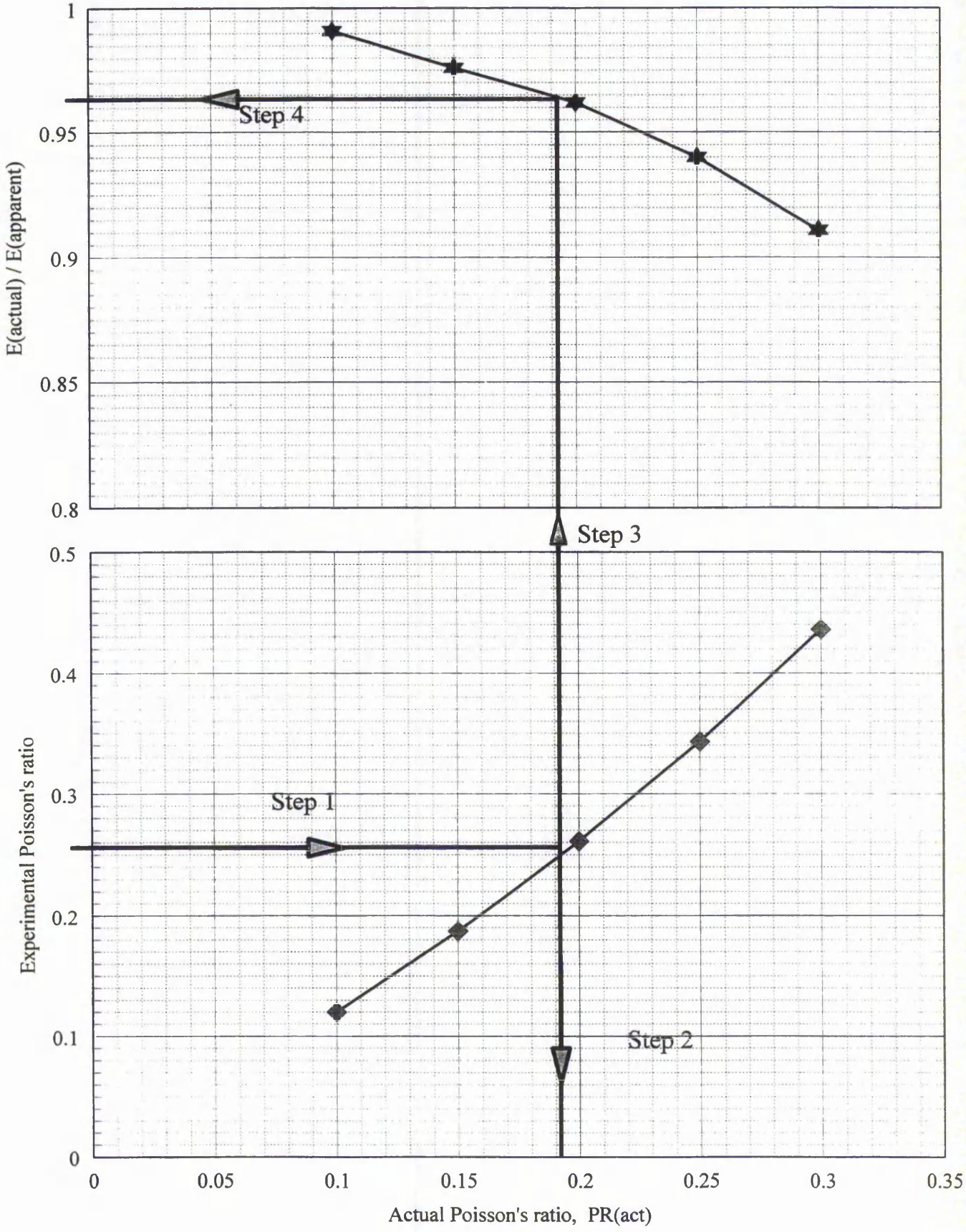

Figure A4.6 Calibration chart to find actual elastic modulus and Poisson's ratio values from experimental results for isotropic polyurethane foams

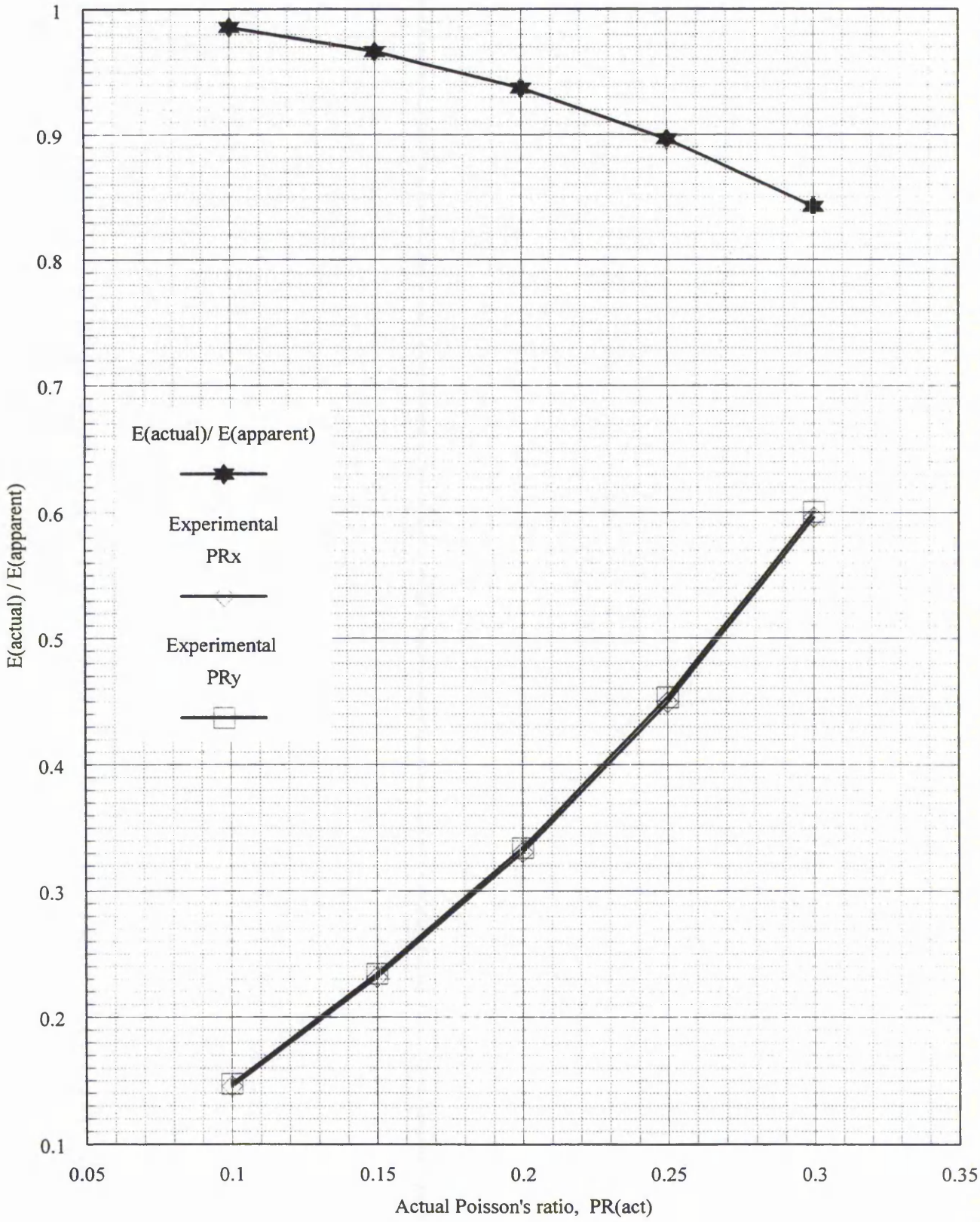

Figure A4.7 Calibration chart to find actual elastic modulus and Poisson's ratio values from experimental results for panel P3

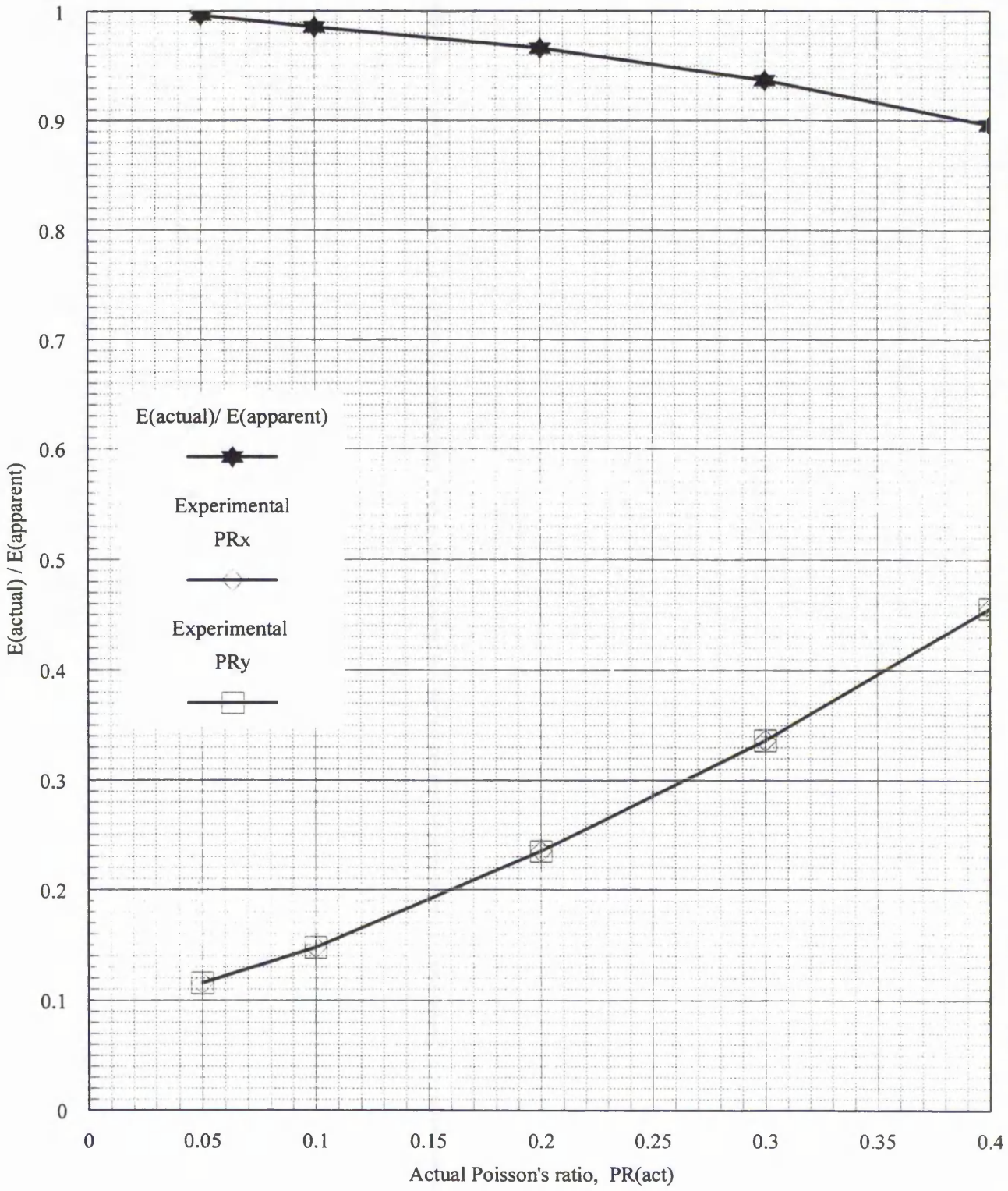

Figure A4.8 Calibration chart to find actual elastic modulus and Poisson's ratio values from experimental results for panel P4

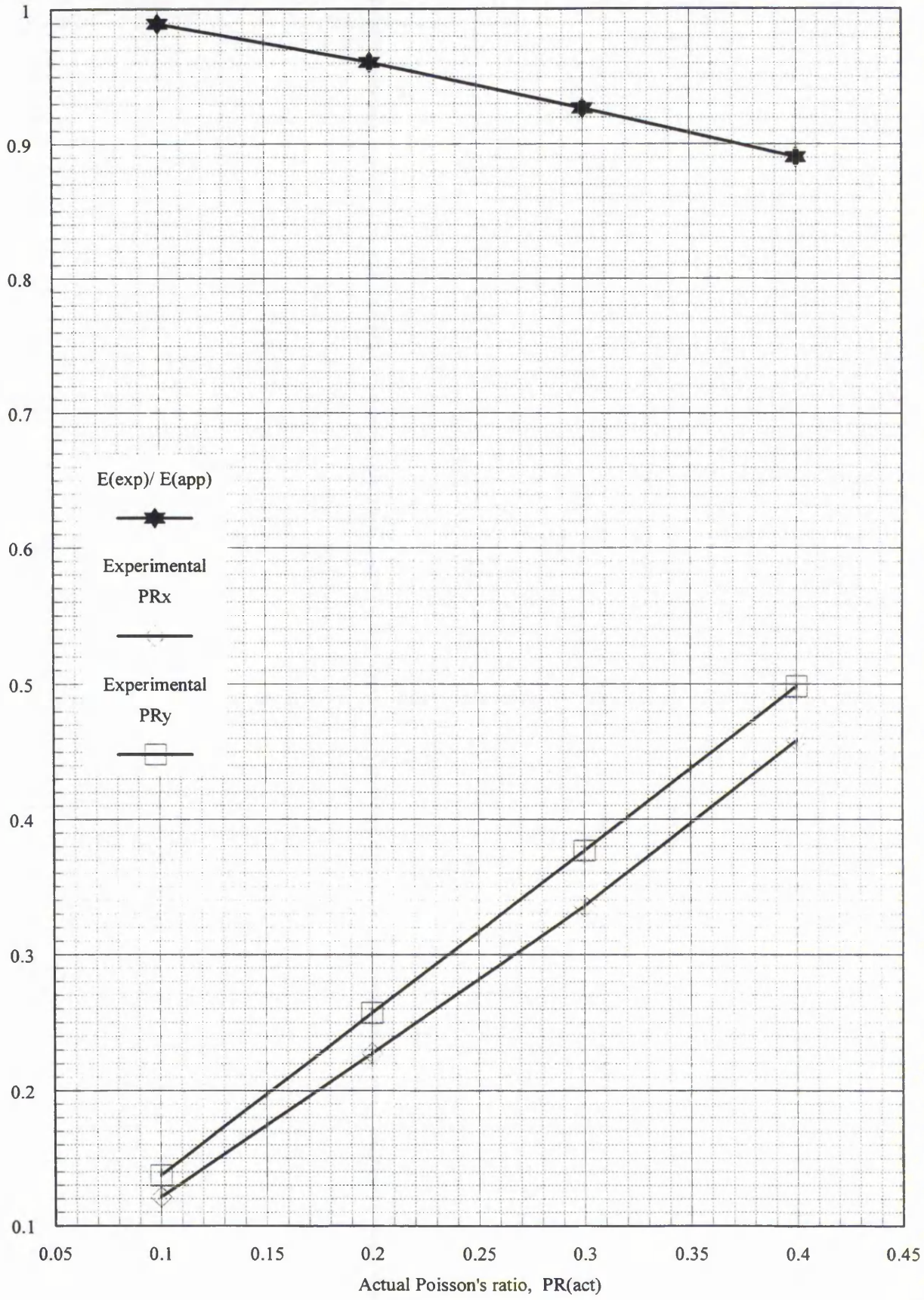

Figure A4.9 Calibration chart to find actual elastic modulus and Poisson's ratio values from experimental results for panel P5

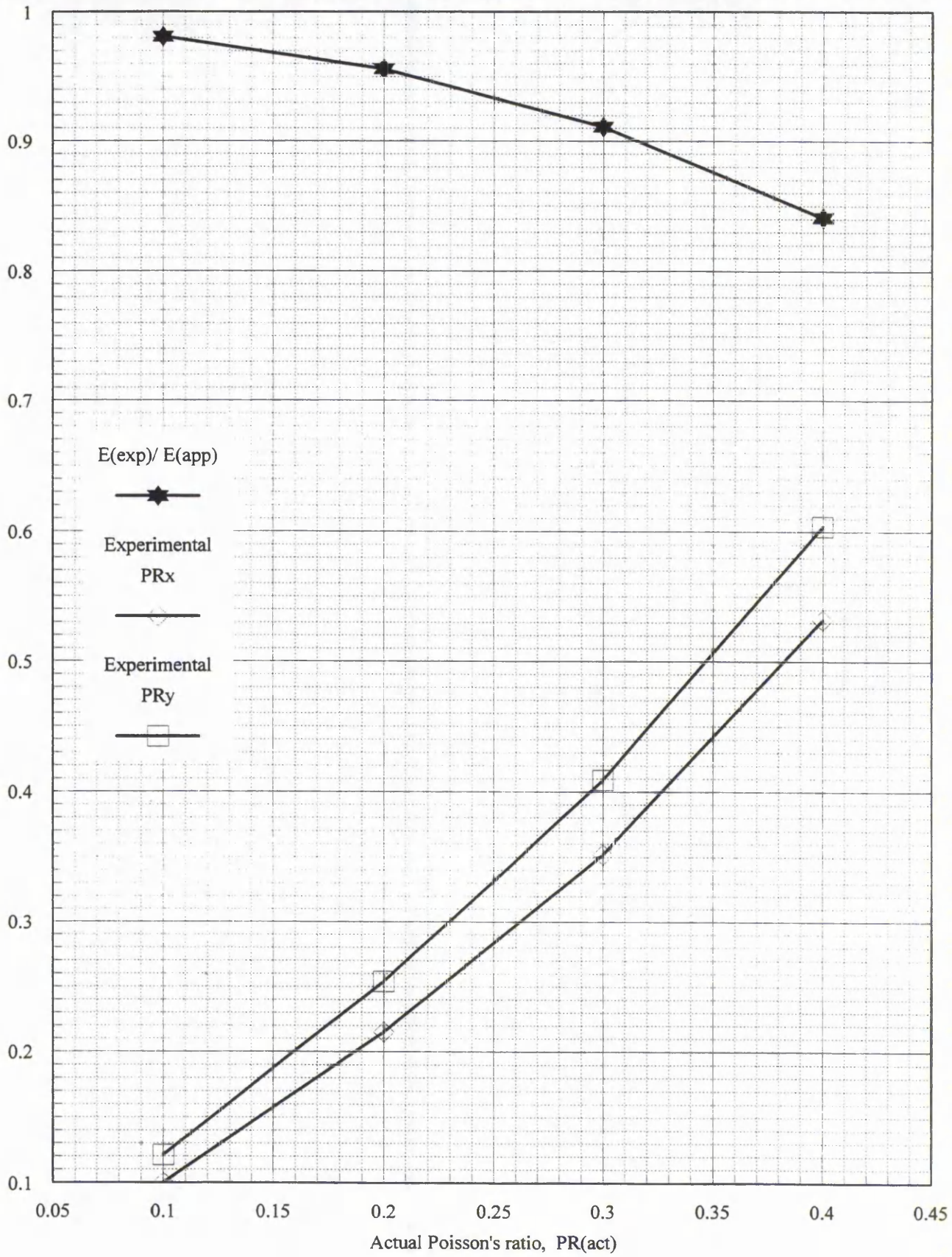

Figure A4.10 Calibration chart to find actual elastic modulus and Poisson's ratio values from experimental results for panel P6

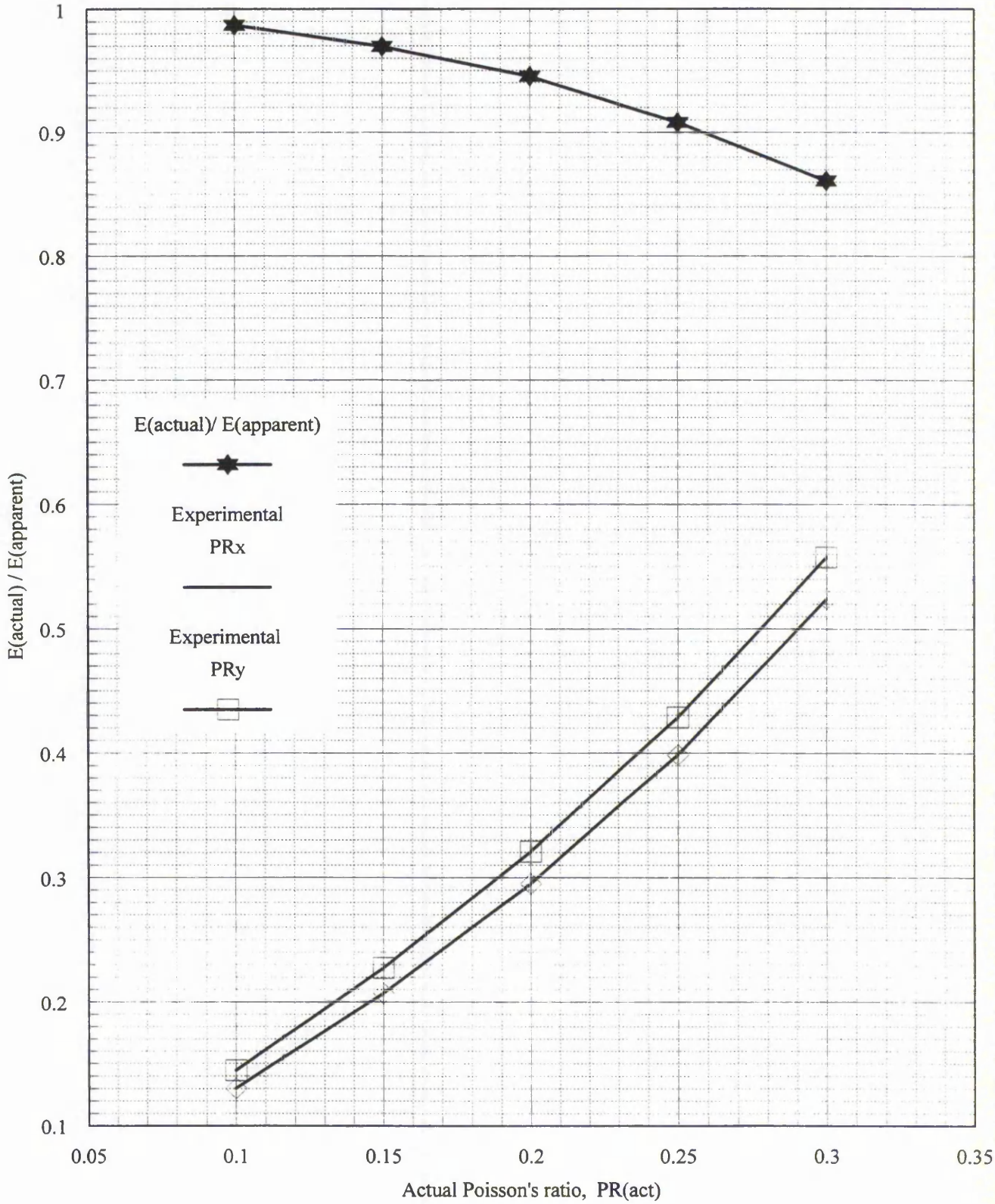

Figure A4.11 Calibration chart to find actual elastic modulus and Poisson's ratio values from experimental results for panel P10

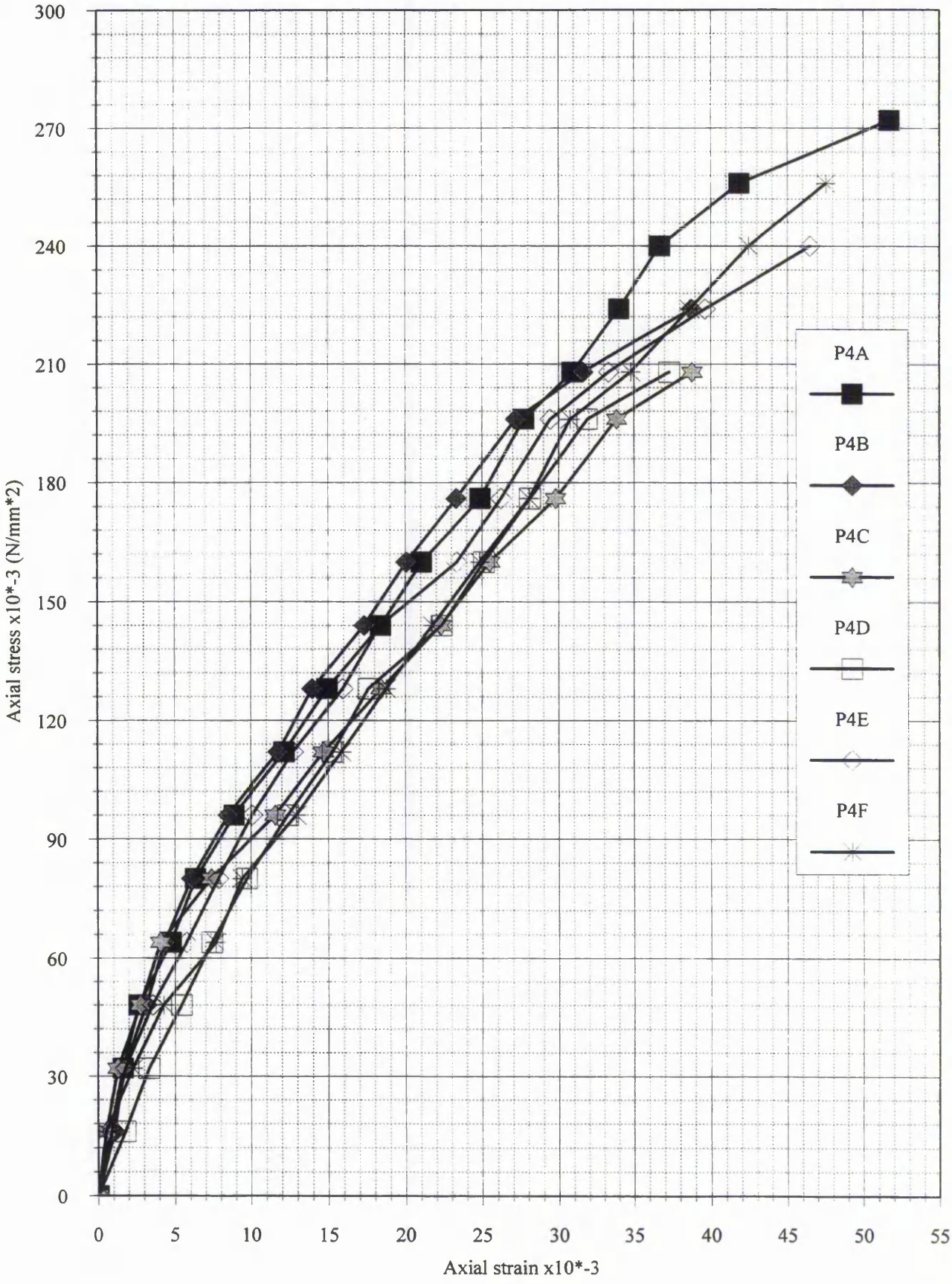

Figure A4.12 Uniaxial tension tests results for panel P4

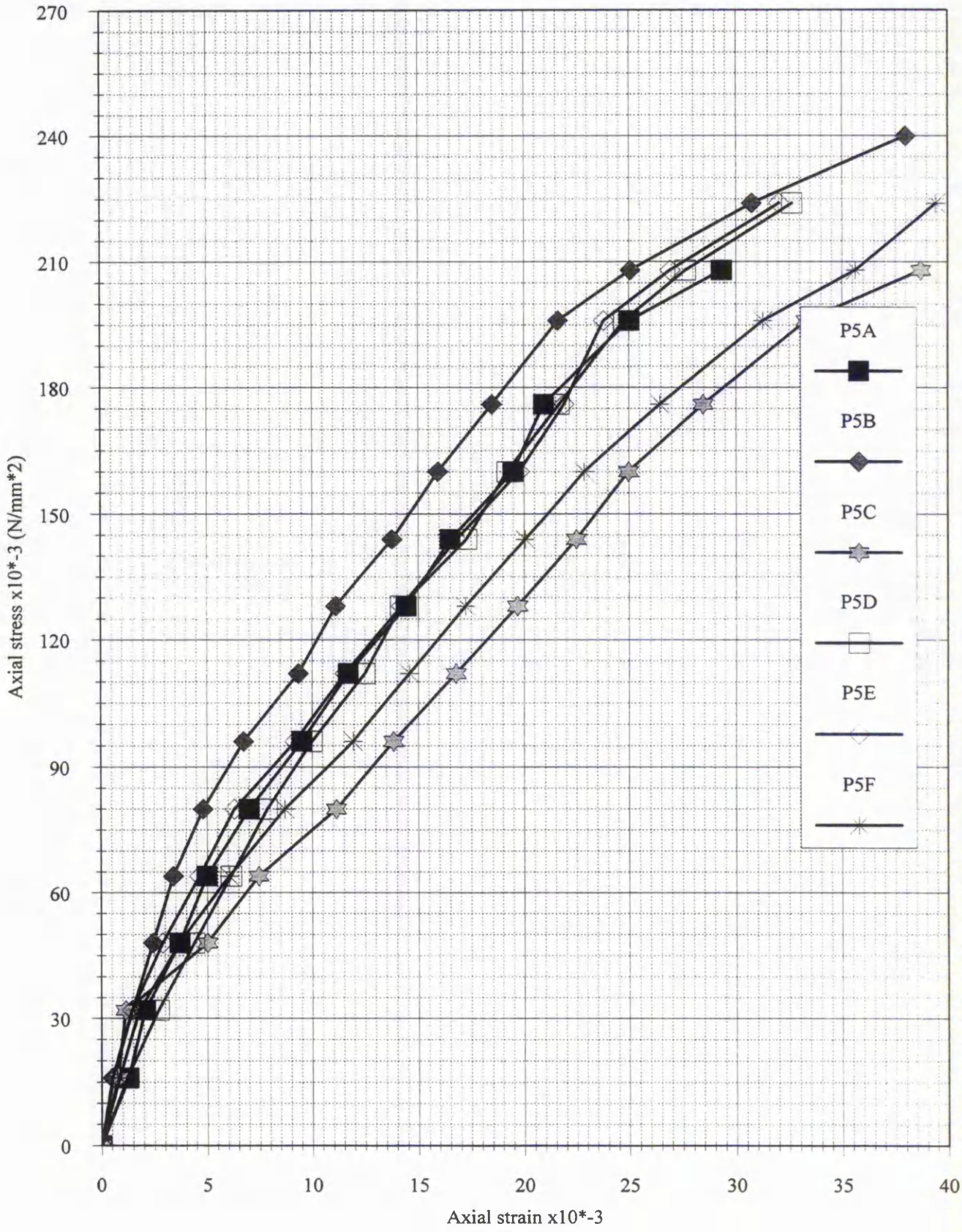

Figure A4.13 Uniaxial tension tests results of load versus displacement for panel P5

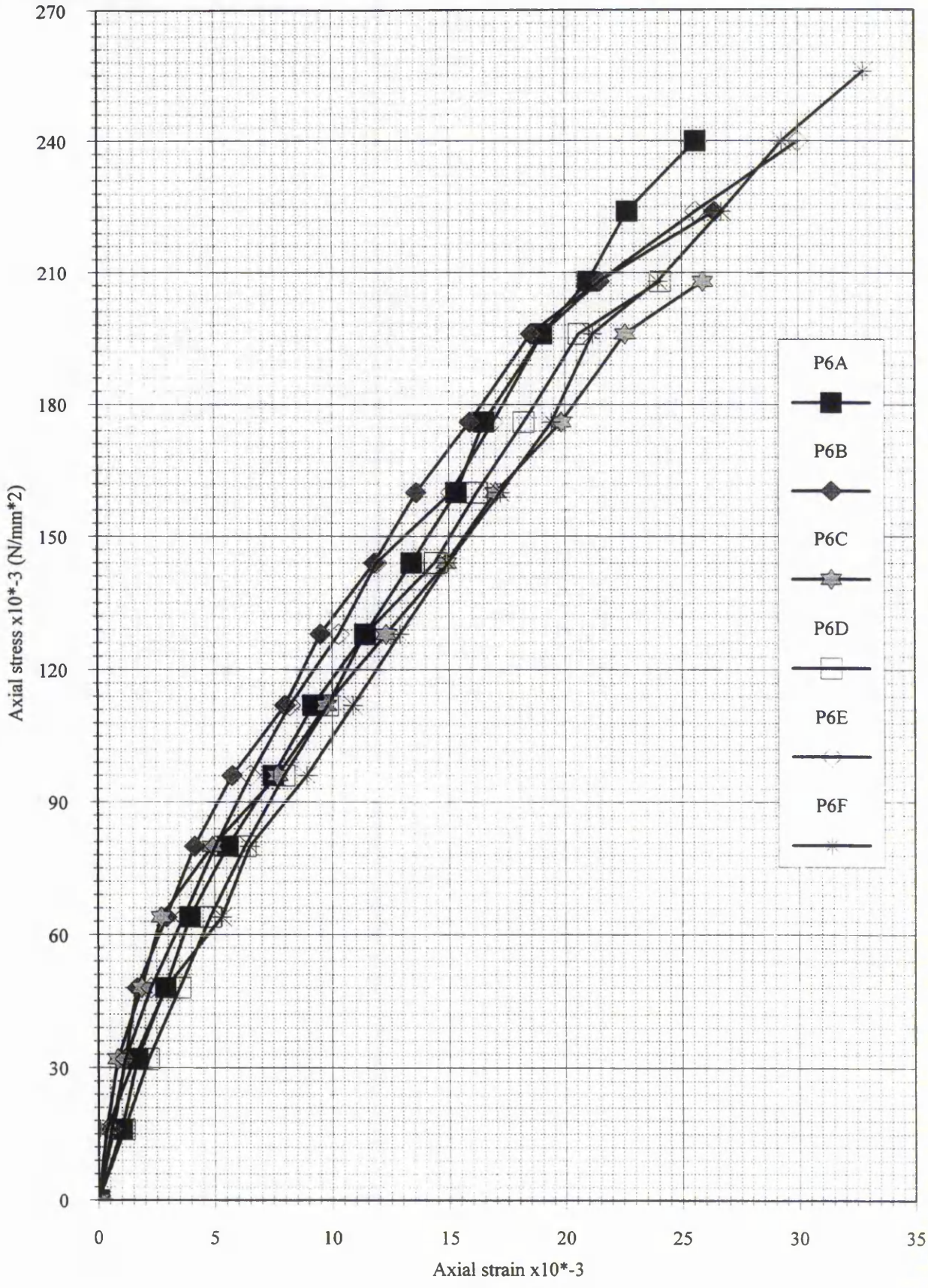

Figure A4.14 Uniaxial tension tests results of load versus displacement for panel P6

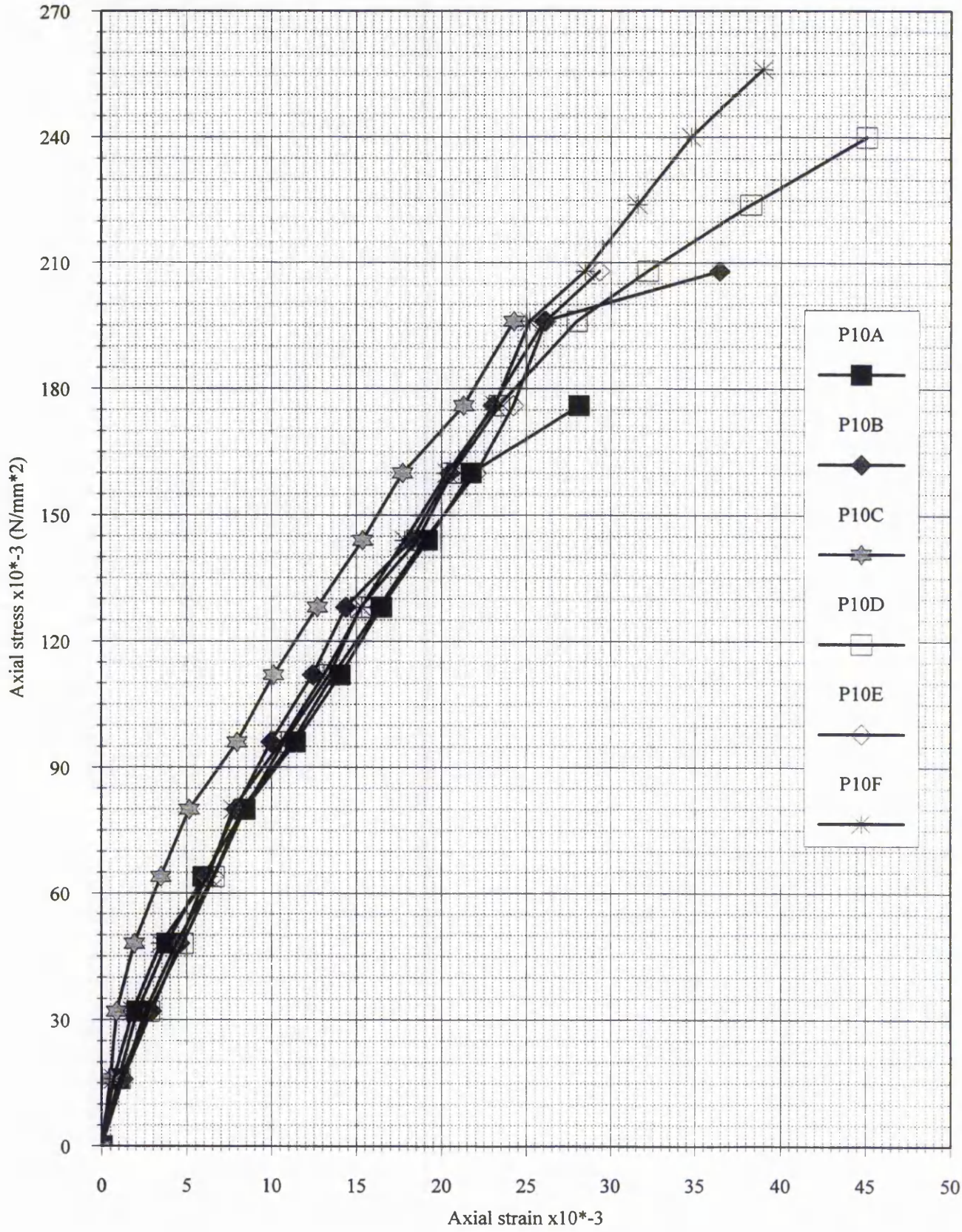

Figure A4.15 Uniaxial tension tests results of load versus displacement for panel P10

Appendix B

CHAPTER 5

SHEAR TESTING AND ANALYSIS

Panel No.	Temp °C	Rel Hum %	X-head speed	Chart speed	Full range (kg)	X-head disp. (mm)	X-head G (N/mm^2)	X-plate disp. (mm)	X-plate G (N/mm^2)	Average values
P1a	21.6	62	1.00	20	500	5.30	1.85	4.62	2.12	
P1b	21.9	58	1.00	20	500	4.90	2.00	4.03	2.43	**T = 21.8 °C**
P1c	21.4	61	1.00	20	500	7.15	1.37	6.24	1.57	**RH = 59 %**
P1d	21.8	59	1.00	20	500	6.91	1.36	4.23	1.42	**XH = 1.87 N/mm^2**
P1e	22.3	57	1.00	20	500	3.65	2.69	2.88	3.41	**XP = 2.37 N/mm^2**
P2a	21.8	63	1.00	20	500	8.23	1.19	6.68	1.47	
P2b	21.7	61	1.00	20	500	7.75	1.27	7.52	1.30	**T = 21.6 °C**
P2c	21.7	59	1.00	20	500	6.65	1.47	6.01	1.63	**RH = 60 %**
P2d	21.3	60	1.00	20	500	8.30	1.18	7.74	1.27	**XH = 1.30 N/mm^2**
P2e	21.5	60	1.00	20	500	6.98	1.41	6.13	1.60	**XP = 1.45 N/mm^2**
P3a	21.3	65	1.00	20	500	1.88	4.39	1.48	5.57	
P3b	21.6	67	1.00	20	500	3.70	2.23	3.20	2.57	**T = 21.8 °C**
P3c	22.3	61	1.00	20	500	2.93	2.82	2.44	3.38	**RH = 64 %**
P3d	22.4	64	1.00	20	500	3.50	2.35	2.84	2.90	**XH = 2.72 N/mm^2**
P3e	21.5	63	1.00	20	500	4.53	1.82	4.04	2.04	**XP = 3.29 N/mm^2**
P4a	22.1	63	1.00	20	500	3.95	2.48	3.12	3.14	
P4b	22.0	62	1.00	20	500	4.08	2.41	3.13	3.13	**T = 21.9 °C**
P4c	21.5	67	1.00	20	500	4.15	2.36	3.21	3.06	**RH = 64 %**
P4d	22.1	64	1.00	20	500	4.33	2.27	3.32	2.95	**XH = 2.39 N/mm^2**
P4e	21.6	63	1.00	20	500	4.00	2.45	2.91	3.37	**XP = 3.13 N/mm^2**
P5a	22.7	59	1.00	20	500	4.23	2.32	3.34	2.93	
P5b	22.8	60	1.00	20	500	4.04	2.43	3.10	3.16	**T = 22.7 °C**
P5c	23.0	56	1.00	20	500	4.68	2.10	3.62	2.71	**RH = 58 %**
P5d	23.0	55	1.00	20	500	4.25	2.31	3.26	3.01	**XH = 2.29 N/mm^2**
P5e	22.0	59	1.00	20	500	4.30	2.28	3.12	3.14	**XP = 2.99 N/mm^2**
P6a	22.0	60	1.00	20	500	4.40	2.23	3.52	2.78	
P6b	21.8	59	1.00	20	500	4.18	2.35	3.15	3.11	**T = 22.3 °C**
P6c	22.4	61	1.00	20	500	4.50	2.18	3.52	2.79	**RH = 59 %**
P6d	23.1	57	1.00	20	500	4.05	2.42	3.40	2.88	**XH = 2.24 N/mm^2**
P6e	22.1	60	1.00	20	500	4.90	2.00	4.02	2.44	**XP = 2.80 N/mm^2**
P8a	22.0	61	1.00	20	500	3.65	2.69	3.23	3.04	
P8b	22.7	64	1.00	20	500	3.73	2.63	3.13	3.13	**T = 22.4 °C**
P8c	22.7	63	1.00	20	500	3.63	2.71	2.90	3.38	**RH = 63 %**
P8d	22.5	62	1.00	20	500	3.55	2.78	3.14	3.13	**XH = 2.72 N/mm^2**
P8e	22.0	64	1.00	20	500	3.53	2.78	2.95	3.32	**XP = 3.20 N/mm^2**
P9a	21.7	63	1.00	20	500	5.45	1.80	4.59	2.14	
P9b	21.6	62	1.00	20	500	4.83	2.03	4.08	2.40	**T = 21.9 °C**
P9c	22.0	64	1.00	20	500	4.20	2.33	3.54	2.77	**RH = 62 %**
P9d	22.4	57	1.00	20	500	6.75	1.45	6.13	1.60	**XH = 1.90 N/mm^2**
P9e	21.7	58	1.00	20	500	5.41	1.84	4.71	2.20	**XP = 2.23 N/mm^2**
P10a	22.0	60	1.00	50	500	1.94	2.02	1.69	2.31	
P10b	21.9	62	1.00	50	500	1.88	2.09	1.61	2.43	**T = 22.0 °C**
P10c	22.0	61	1.00	50	500	1.77	2.22	1.42	2.76	**RH = 61 %**
P10d	22.0	62	1.00	50	500	2.08	1.88	1.72	2.28	**XH = 2.04 N/mm^2**
P10e	22.0	62	1.00	50	500	1.95	2.01	1.71	2.29	**XP = 2.41 N/mm^2**

Table B5.1 BS 4370 crosshead and crossplate shear test results

Panel No.	Temp °C	Rel Hum %	X-head speed	Chart speed	Full range (kg)	X-head disp. (mm)	X-head G (N/mm^2)	X-plate disp. (mm)	X-plate G (N/mm^2)	Average values
P1a	20.6	62	1.00	50	500	2.06	1.90	1.53	2.57	
P1b	21.3	61	1.00	50	500	1.80	2.18	1.44	2.72	**T = 21.2 °C**
P1c	21.2	57	1.00	50	500	2.58	1.52	2.12	1.85	**RH = 60 %**
P1d	21.2	62	1.00	50	500	2.64	1.48	2.25	1.74	**XH = 1.89 N/mm^2**
P1e	22.5	57	1.00	50	500	1.64	2.39	1.31	2.99	**XP = 2.37 N/mm^2**
P2a	20.0	63	1.00	50	500	3.35	1.17	3.15	1.25	
P2b	20.7	65	1.00	50	500	2.81	1.40	2.54	1.55	**T = 20.9 °C**
P2c	21.0	63	1.00	50	500	2.54	1.54	2.31	1.70	**RH = 63 %**
P2d	21.2	62	1.00	50	500	2.92	1.34	2.73	1.44	**XH = 1.39 N/mm^2**
P2e	21.7	61	1.00	50	500	2.65	1.48	2.39	1.64	**XP = 1.52 N/mm^2**
P3a	21.7	65	1.00	50	500	0.75	4.39	0.54	6.23	
P3b	21.8	67	1.00	50	500	1.36	2.42	0.96	3.44	**T = 22.1 °C**
P3c	22.4	64	1.00	50	500	1.10	3.00	0.80	4.11	**RH = 64 %**
P3d	22.3	62	1.00	50	500	1.22	2.70	096	3.45	**XH = 2.94 N/mm^2**
P3e	22.4	63	1.00	50	500	1.52	2.17	1.36	2.43	**XP = 3.92 N/mm^2**
P4a	21.7	63	1.00	50	500	1.48	2.65	1.16	3.40	
P4b	21.7	60	1.00	50	500	1.46	2.69	1.16	3.39	**T = 22.0 °C**
P4c	22.5	59	1.00	50	500	1.56	2.51	1.24	3.16	**RH = 60 %**
P4d	22.0	59	1.00	50	500	1.54	2.55	1.29	3.03	**XH = 2.61 N/mm^2**
P4e	22.0	57	1.00	50	500	1.47	2.67	1.09	3.59	**XP = 3.31 N/mm^2**
P5a	21.5	59	1.00	50	500	1.54	2.55	1.15	3.41	
P5b	22.8	58	1.00	50	500	1.56	2.52	1.20	3.26	**T = 22.0 °C**
P5c	21.8	57	1.00	50	500	1.47	2.68	1.17	3.35	**RH = 58 %**
P5d	22.0	58	1.00	50	500	1.53	2.56	1.13	3.47	**XH = 2.55 N/mm^2**
P5e	21.9	58	1.00	50	500	1.60	2.45	1.30	3.01	**XP = 3.31 N/mm^2**
P6a	22.3	57	1.00	50	500	1.58	2.48	1.22	3.23	
P6b	22.8	59	1.00	50	500	1.52	2.58	1.13	3.47	**T = 22.6 °C**
P6c	22.9	53	1.00	50	500	1.75	2.24	1.32	2.97	**RH = 57 %**
P6d	22.9	59	1.00	50	500	1.60	2.45	1.26	3.11	**XH = 2.41 N/mm^2**
P6e	22.2	56	1.00	50	500	1.72	2.28	1.32	2.96	**XP = 3.15 N/mm^2**
P8a	21.4	64	1.00	50	500	1.08	3.63	0.88	4.45	
P8b	21.9	64	1.00	50	500	1.28	3.06	1.05	3.75	**T = 21.8 °C**
P8c	21.7	63	1.00	50	500	1.21	3.24	0.99	3.97	**RH = 63 %**
P8d	21.9	61	1.00	50	500	1.34	2.93	1.06	3.69	**XH = 3.10 N/mm^2**
P8e	22.1	62	1.00	50	500	1.48	2.65	1.21	3.25	**XP = 3.82 N/mm^2**
P9a	21.1	65	1.00	50	500	1.74	2.25	1.50	2.62	
P9b	21.5	67	1.00	50	500	1.63	2.42	1.47	2.67	**T = 21.6 °C**
P9c	21.7	67	1.00	50	500	1.42	2.76	1.30	3.02	**RH = 64 %**
P9d	22.0	61	1.00	50	500	2.44	1.61	1.59	2.46	**XH = 2.13 N/mm^2**
P9e	21.8	62	1.00	50	500	2.44	1.61	1.63	2.41	**XP = 2.64 N/mm^2**
P10a	22.0	56	1.00	50	500	1.93	2.03	1.74	2.26	
P10b	22.0	55	1.00	50	500	1.98	1.98	1.70	2.31	**T = 22.2 °C**
P10c	22.5	55	1.00	50	500	1.76	2.23	1.46	2.69	**RH = 56 %**
P10d	22.2	57	1.00	50	500	2.20	1.78	1.84	2.13	**XH = 1.94 N/mm^2**
P10e	22.1	59	1.00	50	500	2.32	1.69	1.84	2.13	**XP = 2.30 N/mm^2**

Table B5.2 ASTM C273 crosshead and crossplate shear test results

Actual υ	Actual E N/mm^2	Actual G N/mm^2	BS G_{XH}	BS G_{XP}	BS G_{XH} %	BS G_{XP} %	ASTM G_{XH}	ASTM G_{XP}	ASTM G_{XH} %	ASTM G_{XP} %
0.10	2.00	0.9091	0.8637	0.8684	4.99	4.07	0.8854	0.8901	2.61	2.09
0.10	4.00	1.8181	1.7125	1.7276	5.81	4.98	1.7578	1.7698	3.32	2.66
0.10	6.00	2.7272	2.5296	2.5600	7.25	6.13	2.6279	2.6500	3.64	2.84
0.10	8.00	3.6363	3.3338	3.3850	8.32	6.91	3.4856	3.5181	4.15	3.25
0.10	10.00	4.5454	4.1205	4.1968	9.35	7.67	4.3345	4.3836	4.64	3.56
0.15	2.00	0.8696	0.8275	0.8319	4.84	3.77	0.8483	0.8529	2.43	1.92
0.15	4.00	1.7391	1.6359	1.6498	5.94	5.14	1.6878	1.6994	2.95	2.29
0.15	6.00	2.6087	2.4260	2.4543	7.00	5.92	2.5188	2.5390	3.45	2.67
0.15	8.00	3.4783	3.1987	3.2361	8.04	6.96	3.3415	3.3739	3.93	3.00
0.15	10.00	4.3478	3.9555	4.0260	9.02	7.40	4.1563	4.2025	4.41	3.34
0.20	2.00	0.8333	0.7943	0.7984	4.68	4.19	0.8142	0.8186	2.29	1.77
0.20	4.00	1.6667	1.5709	1.5838	5.75	4.97	1.6203	1.6314	2.78	2.12
0.20	6.00	2.5000	2.3307	2.3600	6.77	5.60	2.4185	2.4384	3.26	2.47
0.20	8.00	3.3333	3.0746	3.1186	7.76	6.44	3.2092	3.2399	3.72	2.80
0.20	10.00	4.1667	3.8034	3.8688	8.72	7.15	3.9924	4.0336	4.18	3.19
0.25	2.00	0.8000	0.7637	0.7675	4.54	4.06	0.7827	0.7871	2.16	1.62
0.25	4.00	1.6000	1.5110	1.5230	5.56	4.81	1.5580	1.5625	2.62	1.97
0.25	6.00	2.4000	2.2427	2.2672	6.55	5.53	2.3261	2.3445	3.08	2.31
0.25	8.00	3.2000	2.9597	3.0005	7.51	6.23	3.0870	3.1151	3.53	2.65
0.25	10.00	4.0000	3.6699	3.7309	8.25	6.73	3.8412	3.8809	3.97	2.98
0.30	2.00	0.7692	0.7353	0.7389	4.41	3.94	0.7537	0.7579	2.02	1.48
0.30	4.00	1.5385	1.4555	1.4668	5.39	4.66	1.5005	1.5108	2.47	1.80
0.30	6.00	2.3077	2.1612	2.1841	6.35	5.36	2.2406	2.2583	2.91	2.14
0.30	8.00	3.0769	2.8533	2.8914	7.27	6.03	2.9741	3.0009	3.34	2.47
0.30	10.00	3.8462	3.5323	3.5891	8.16	6.68	3.7013	3.7386	3.77	2.80

Table B5.3 Comparison of theoretical and computer simulated shear test results.

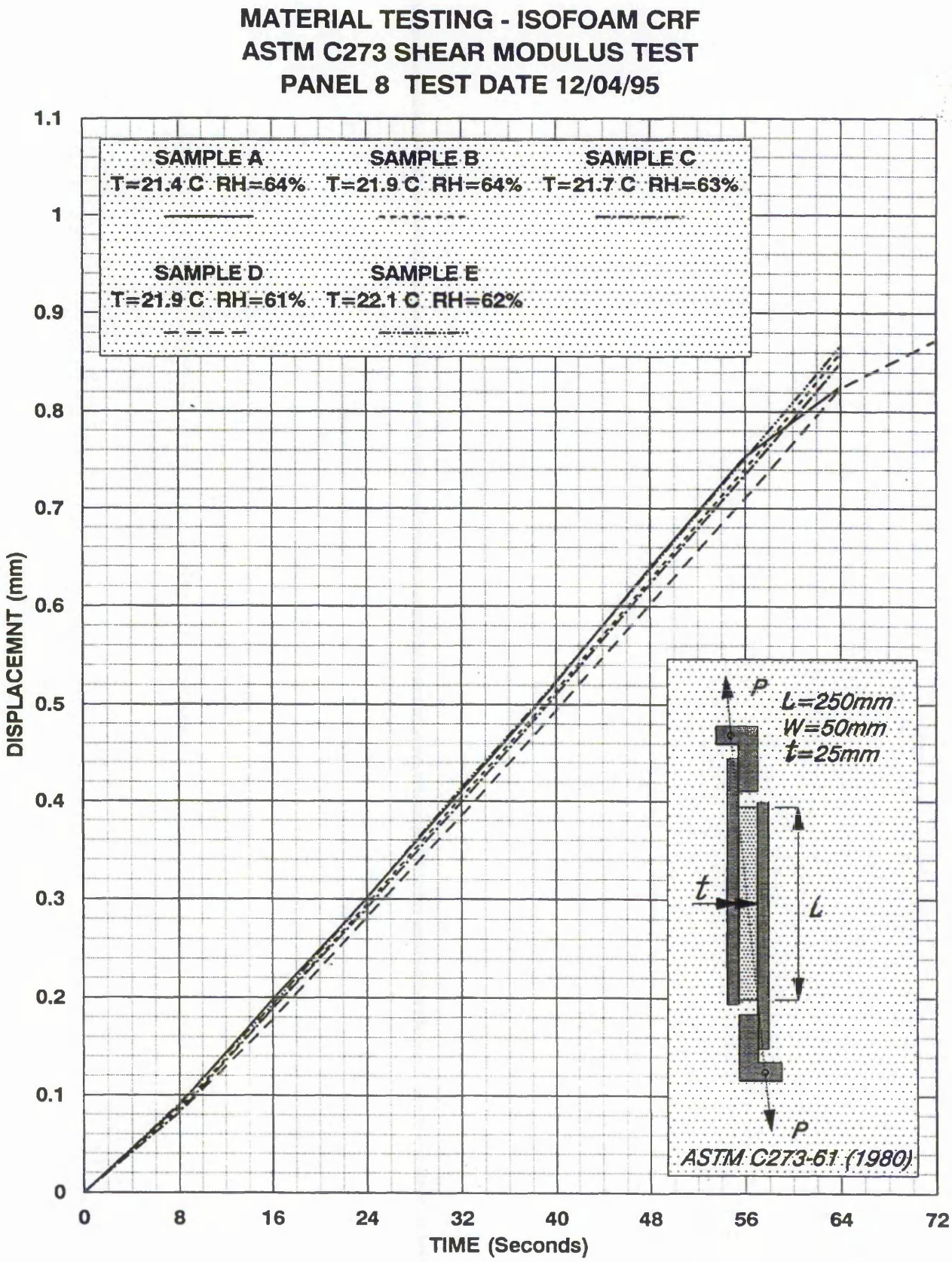

Figure B5.1 A typical experimental American Standard crossplate displacement shear test plot of load versus displacement for a specimen from panel P8

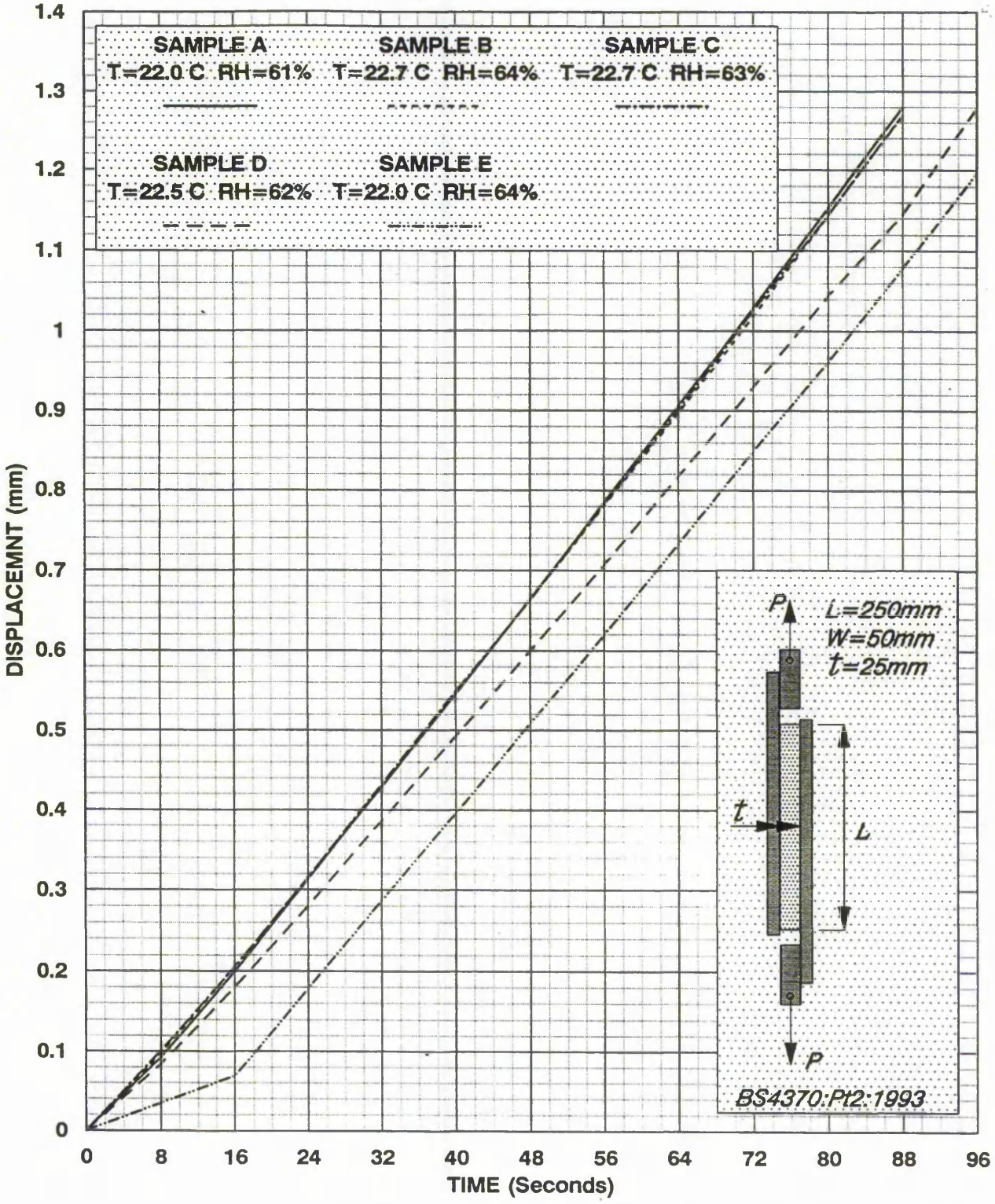

Figure B5.2 A typical experimental British Standard crossplate displacement shear test plot of load versus displacement for a specimen from panel P8

Elastic modulus = 6.0 N/mm^2, Poisson's ratio = 0.20

Figure B5.3a American Standard test configuration y-displacement contour plot showing plate bending

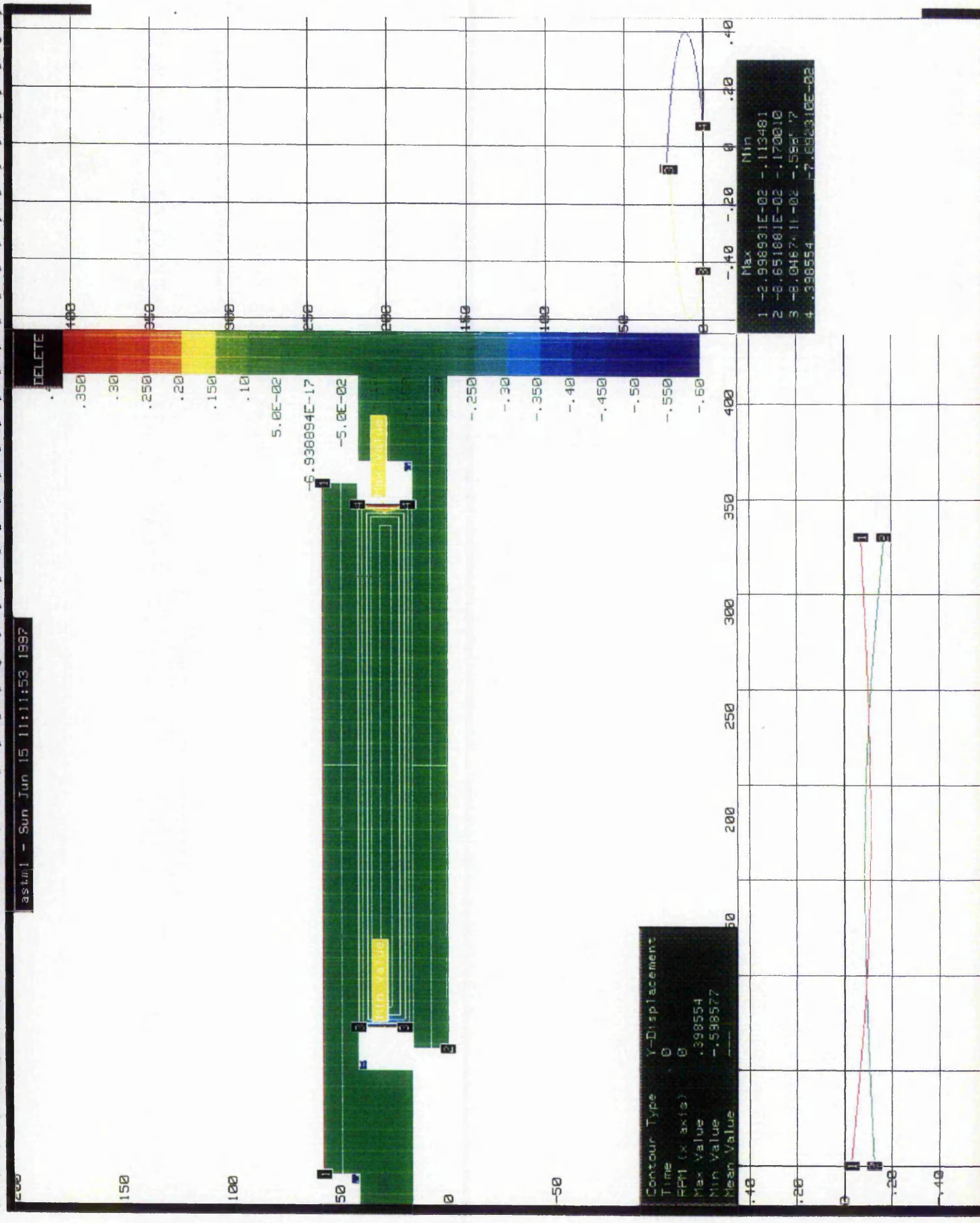

Elastic modulus = 2.0 N/mm^2, Poisson's ratio = 0.20

Figure B5.3b British Standard test configuration y-displacement contour plot showing plate bending

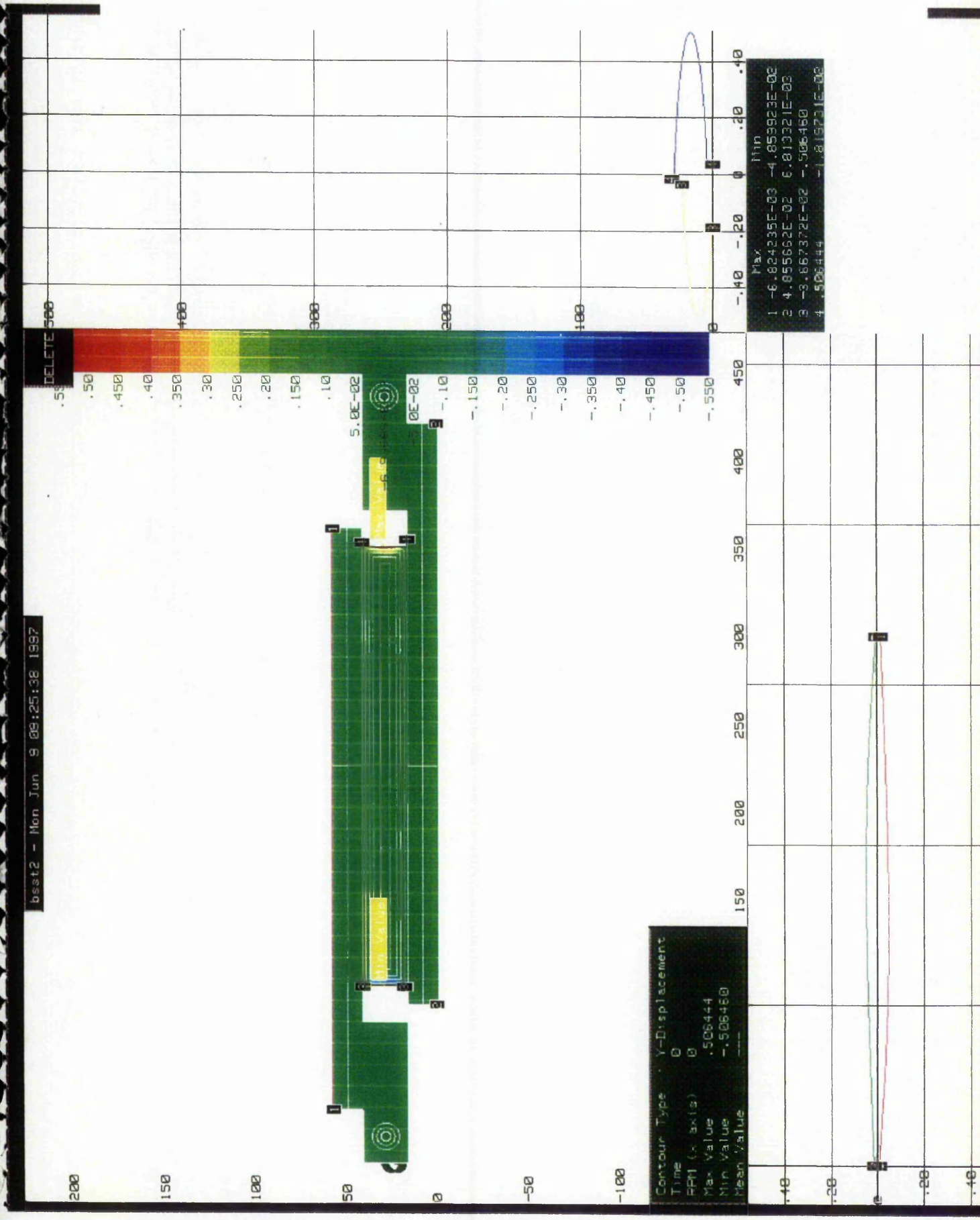

Elastic modulus = 6.0 N/mm^2, Poisson's ratio = 0.20

Figure B5.3c British Standard test configuration y-displacement contour plot showing plate bending

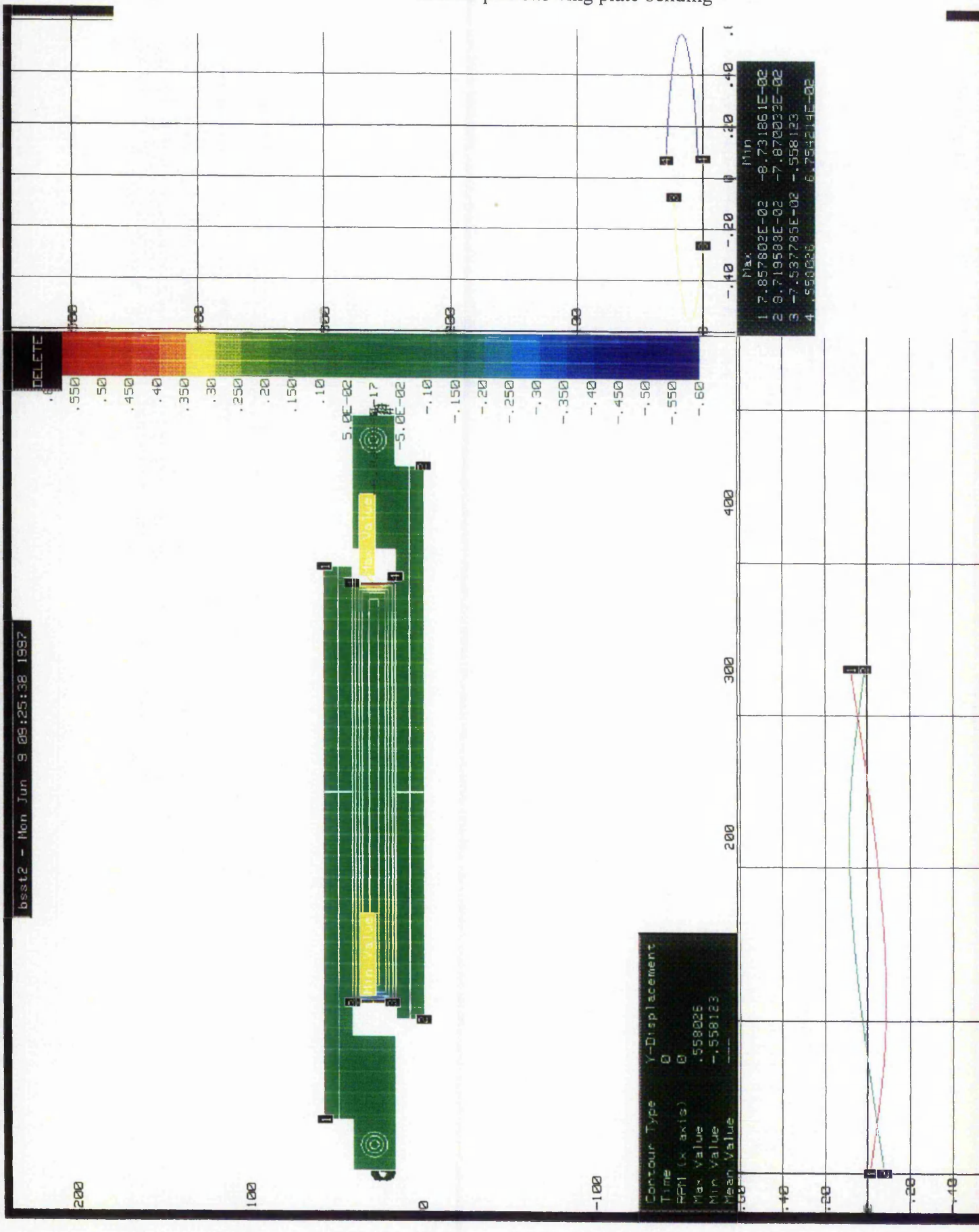

Elastic modulus = 10.0 N/mm^2, Poisson's ratio = 0.20

Figure B5.3d British Standard test configuration y-displacement contour plot showing plate bending

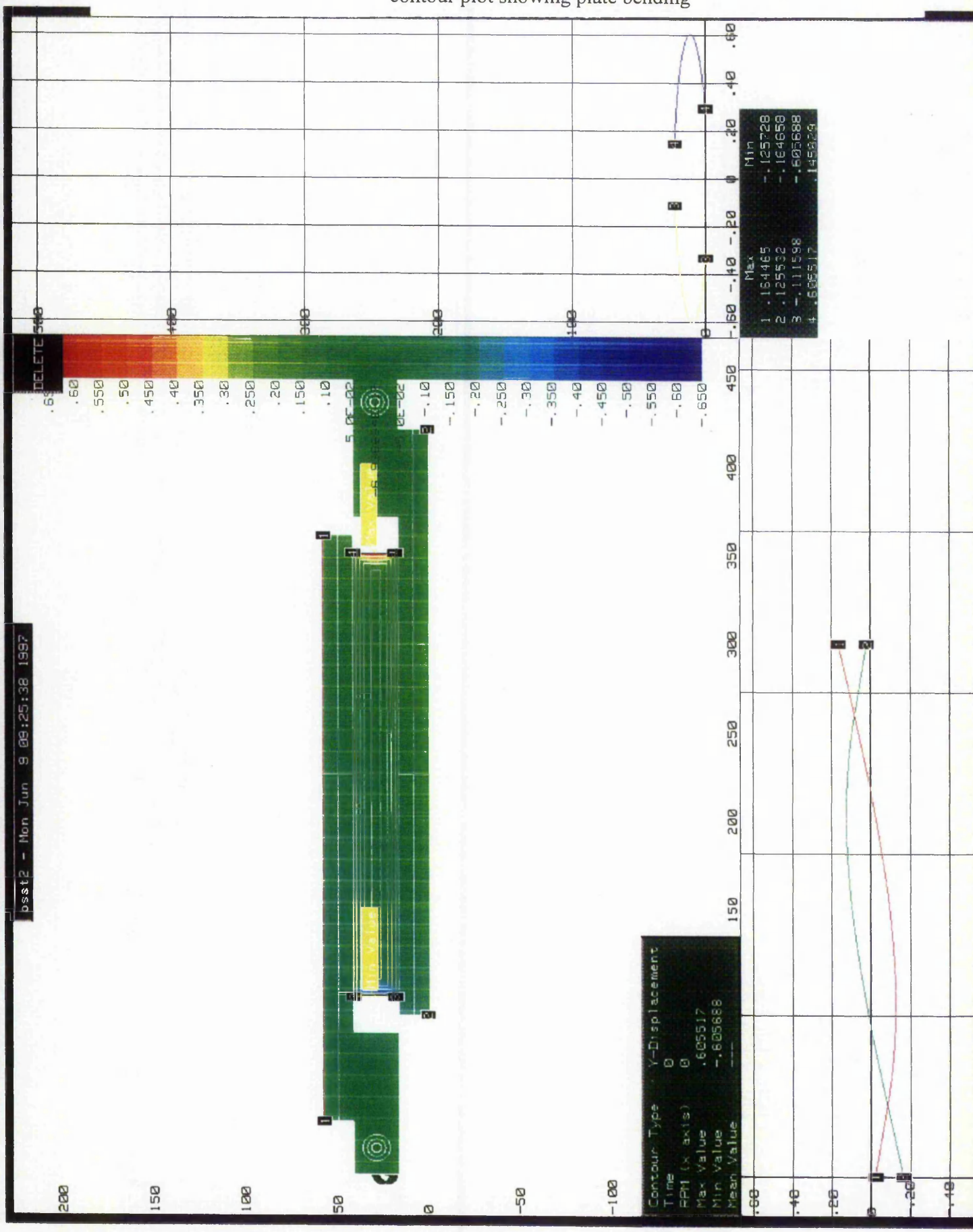

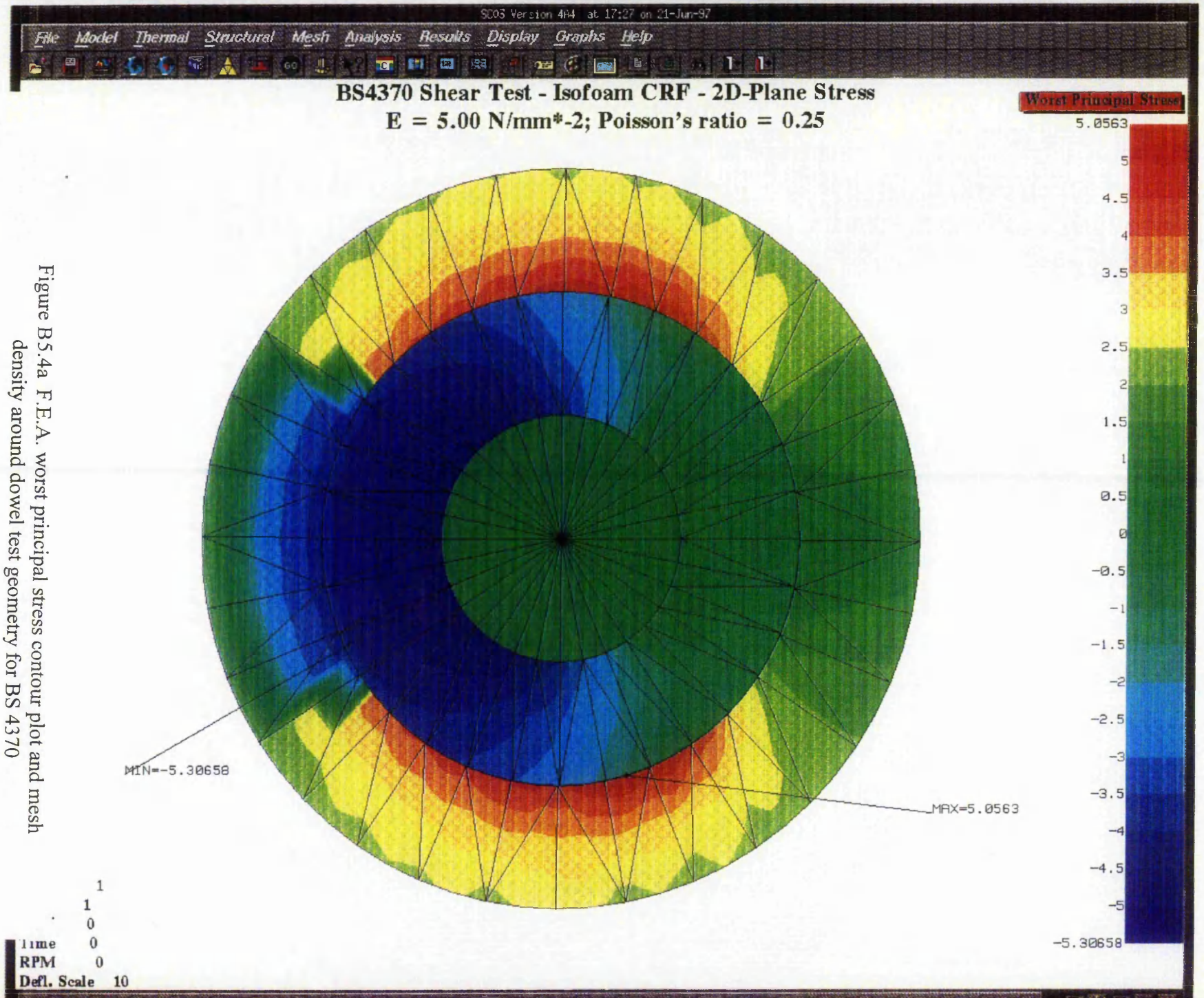

Figure B5.4a F.E.A. worst principal stress contour plot and mesh density around dowel test geometry for BS 4370

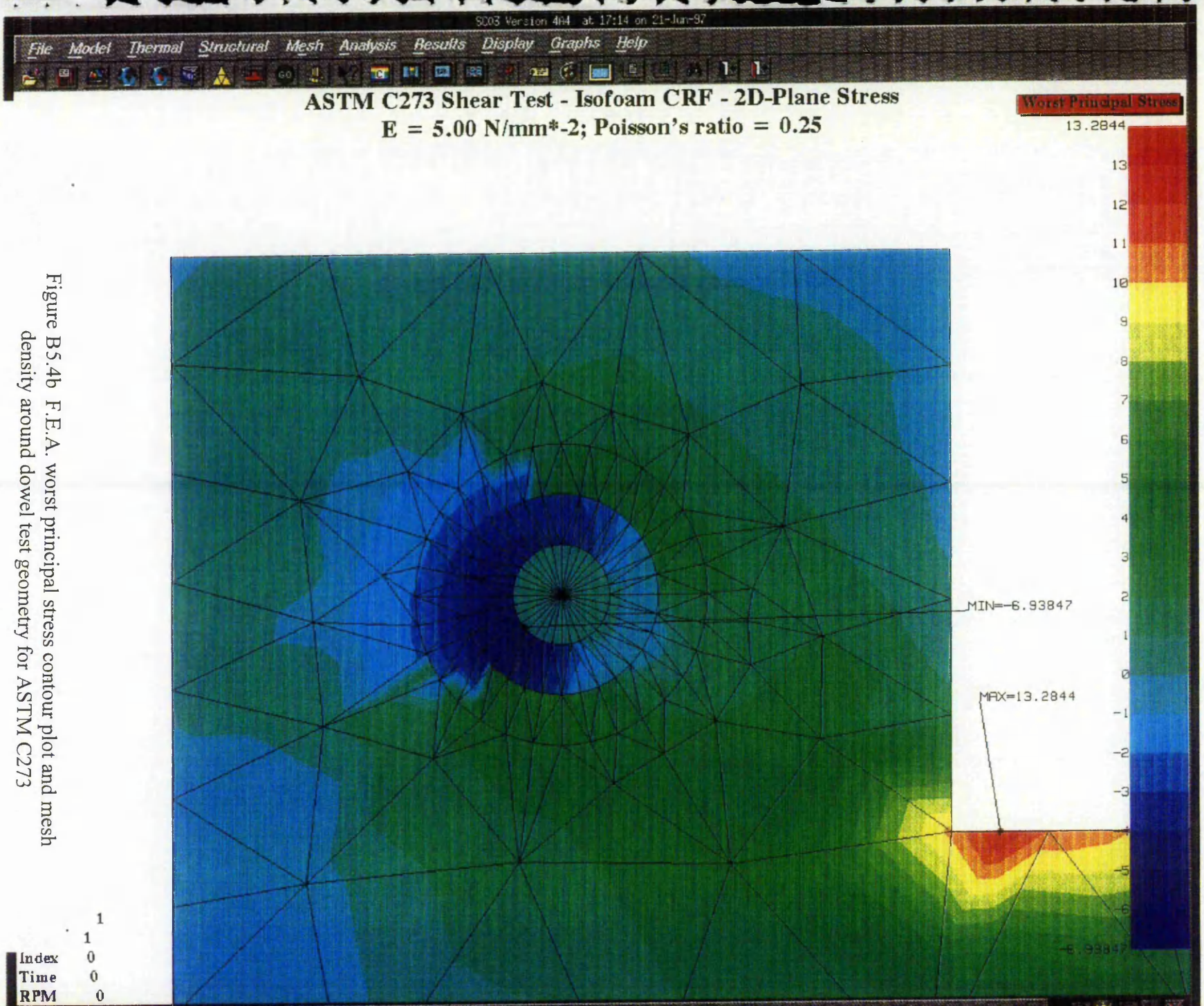

Figure B5.4b F.E.A. worst principal stress contour plot and mesh density around dowel test geometry for ASTM C273

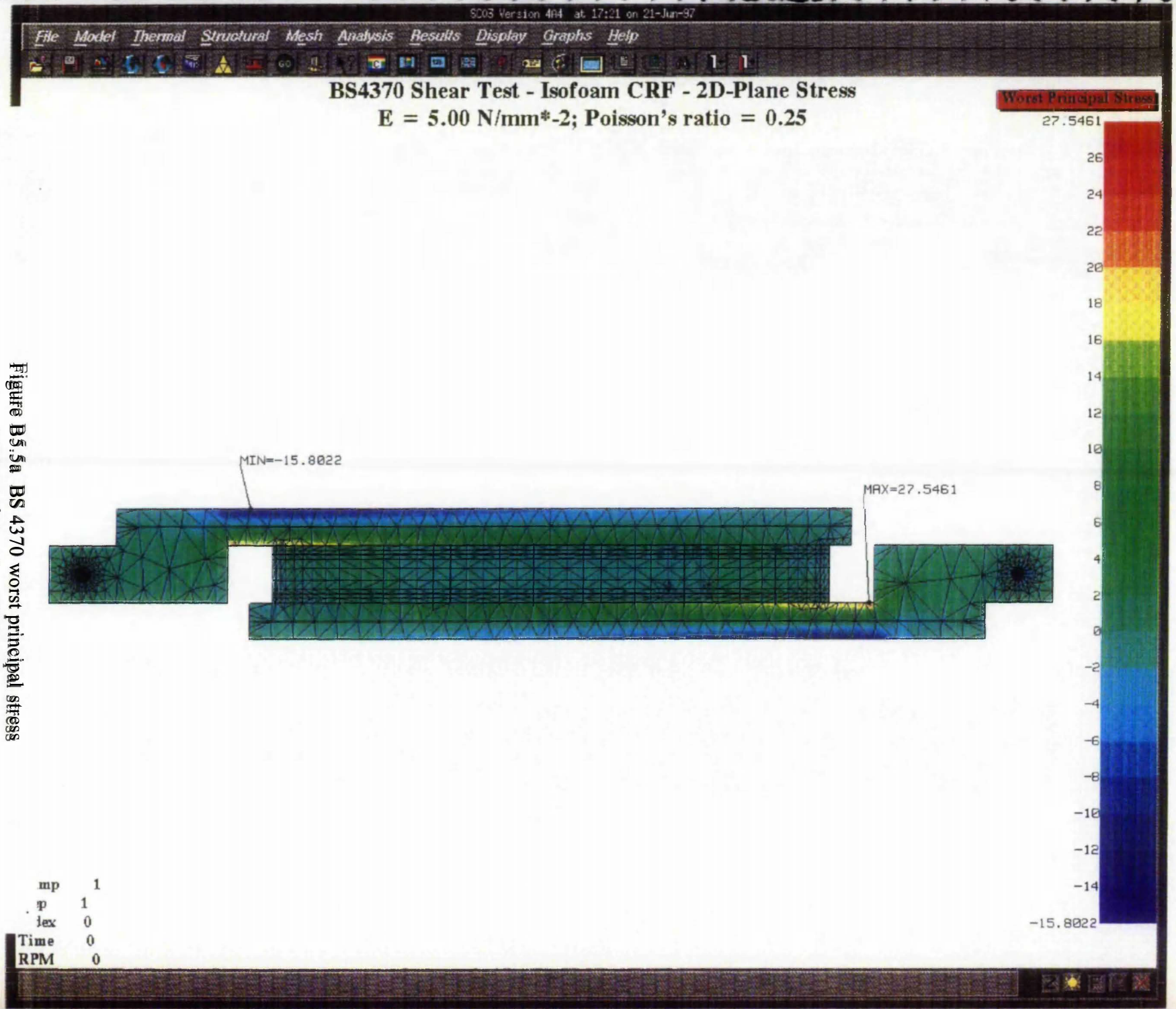

Figure B5.5a BS 4370 worst principal stress contour plot and mesh density

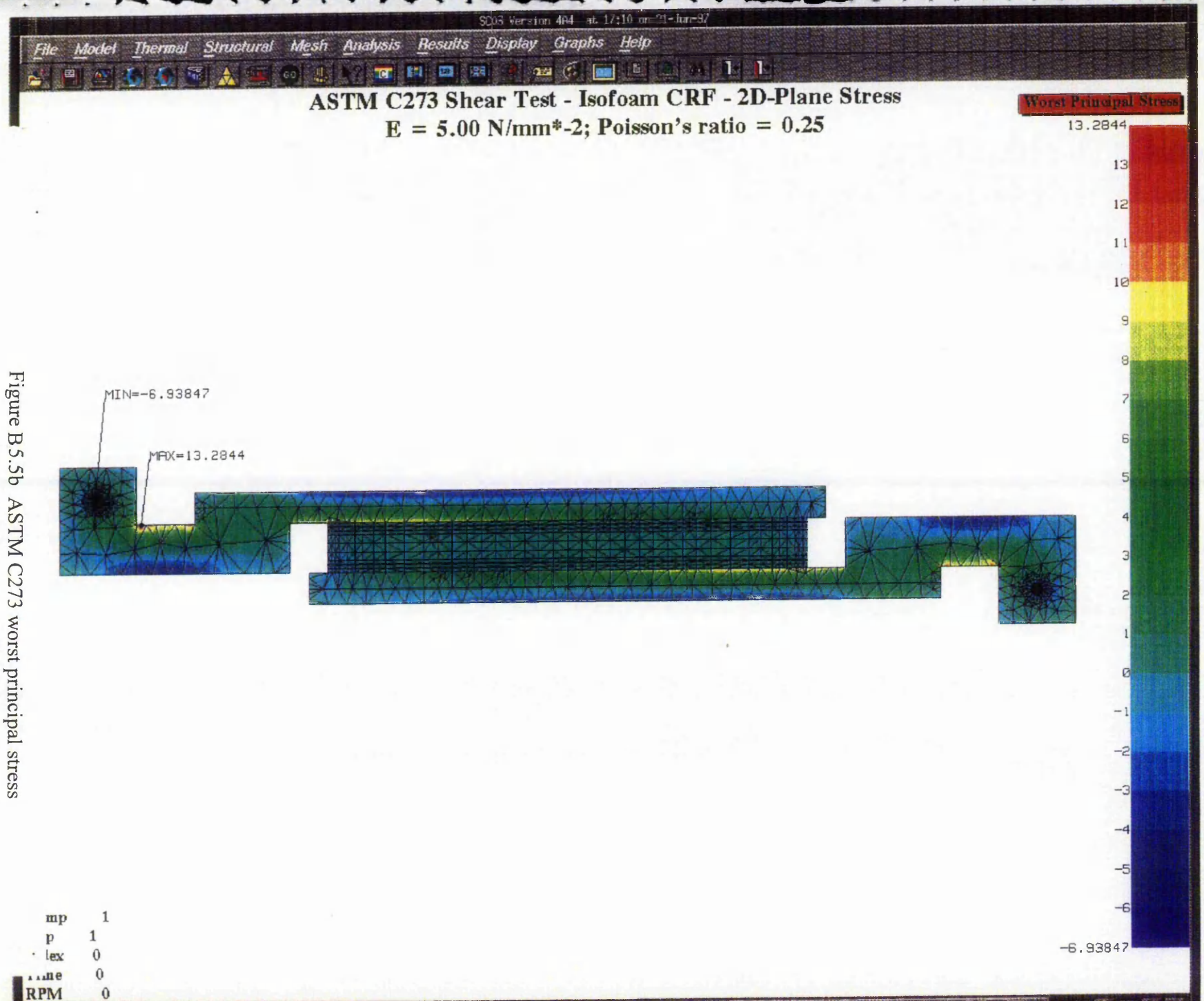

Figure B.5.5b ASTM C273 worst principal stress contour plot and mesh density

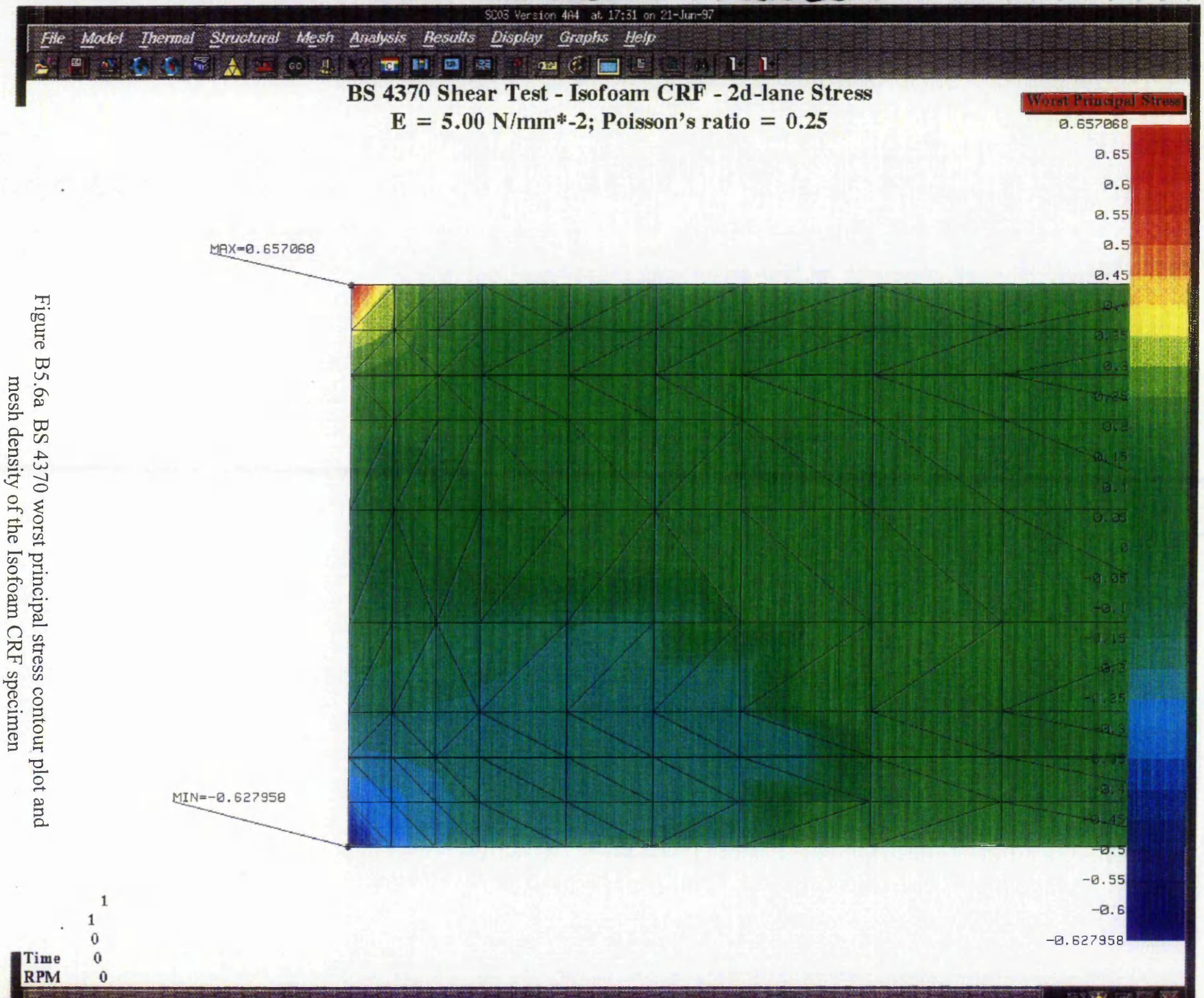

Figure B5.6a BS 4370 worst principal stress contour plot and mesh density of the Isofoam CRF specimen

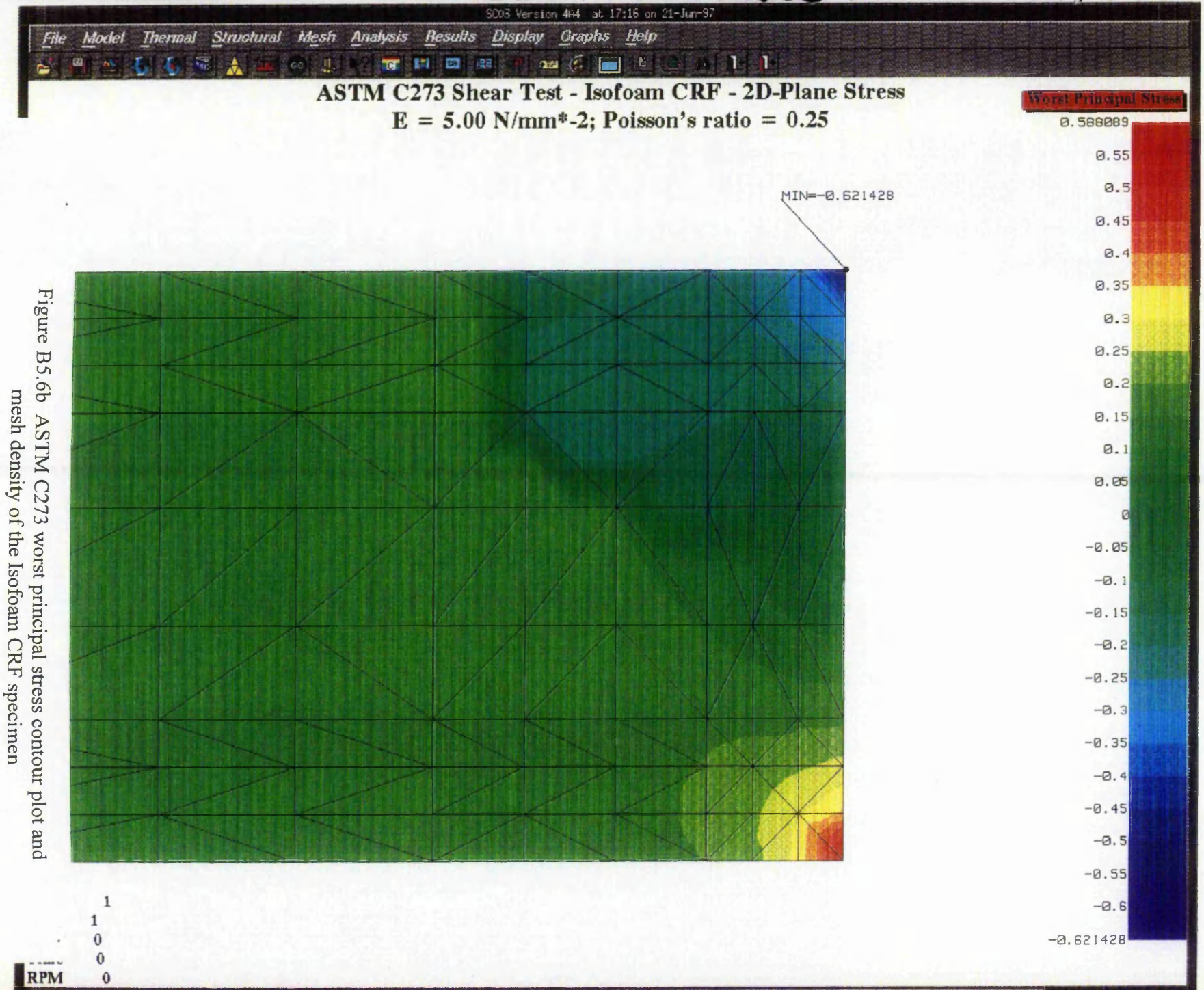

Figure B5.6b ASTM C273 worst principal stress contour plot and mesh density of the Isofoam CRF specimen

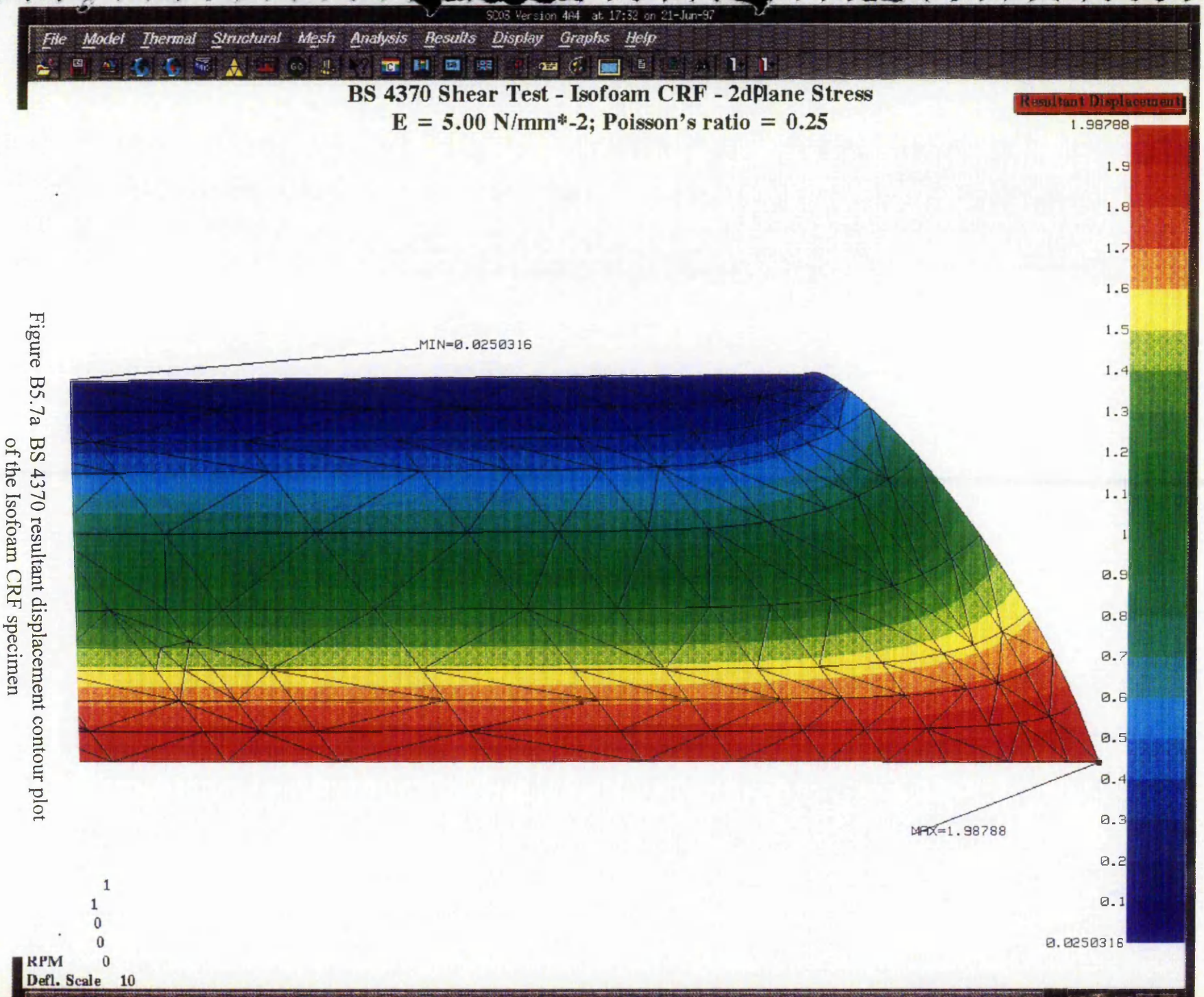

Figure B5.7a BS 4370 resultant displacement contour plot of the Isofoam CRF specimen

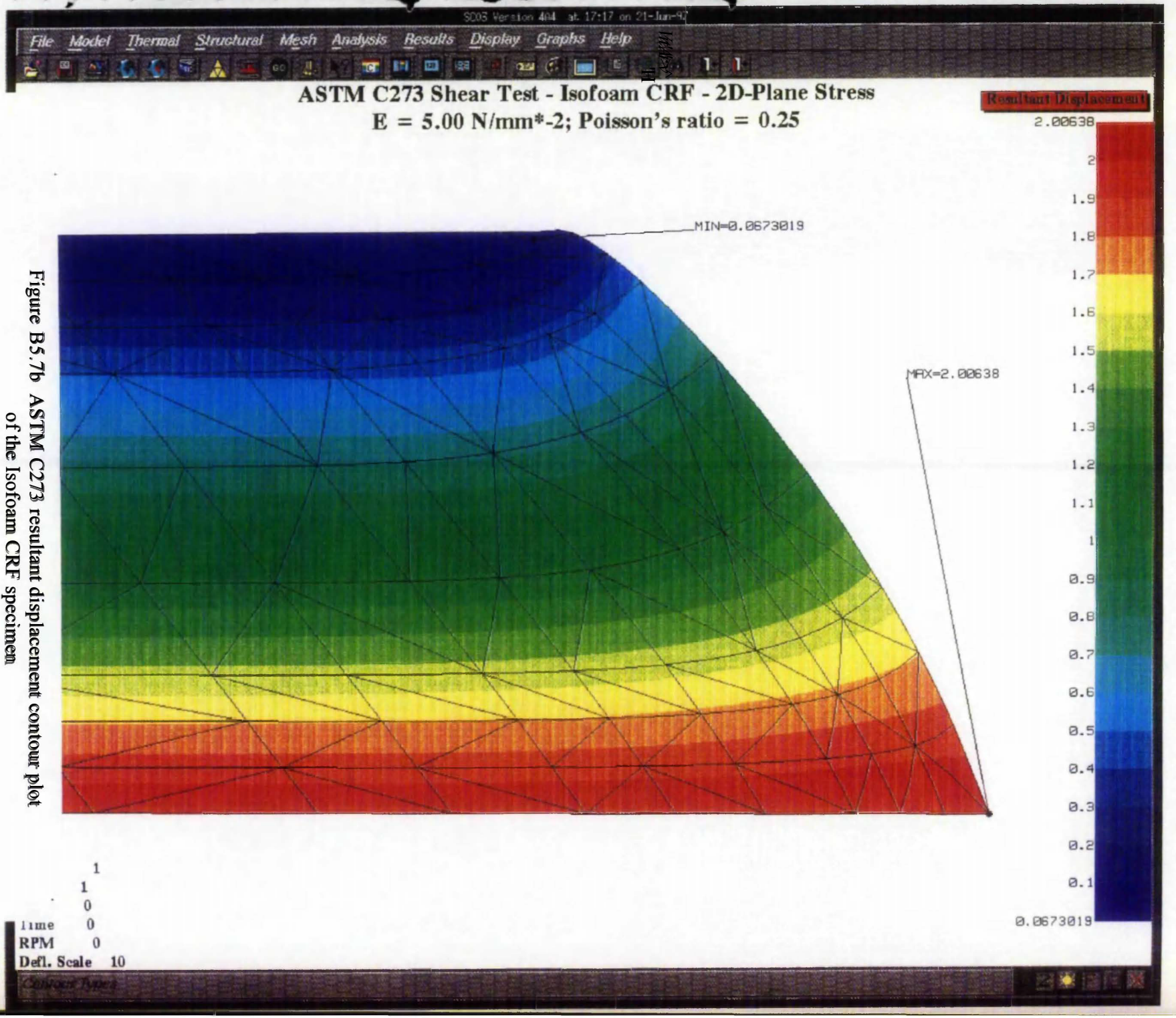

Figure B5.7b ASTM C273 resultant displacement contour plot of the Isofoam CRF specimen

Appendix C

CHAPTER 6

MULTIPLE SPAN BEAM TESTING AND ANALYSIS

Beam	Graph	Elastic modulus, E_f N/mm^2	Shear modulus, G N/mm^2	Graph	Elastic modulus, E_f N/mm^2	Shear modulus, G N/mm^2
P1B3	A5.2	5300	2.3	A5.3	9400	2.1
P1B4	A5.2	5400	2.4	A5.3	9400	2.2
P1B5	A5.2	9400	2.3	A5.3	9400	2.3
P1B6	A5.2	9100	2.2	A5.3	9400	2.1
P1B7	(A5.2)	6400	2.2	(A5.3)	9400	2.3
P1B8	(A5.2)	6900	2.1	(A5.3)	9400	2.2
P1B9	(A5.2)	8100	2.4	(A5.3)	9400	2.1
P1B10	(A5.2)	7800	2.4	(A5.3)	9400	2.2
	Average	7300	2.3	Average		2.2
P1B3	A5.4	7500	2.2	A5.5	9400	2.1
P1B4	A5.4	7500	2.2	A5.5	9400	2.2
P1B5	A5.4	9400	2.3	A5.5	9400	2.4
P1B6	A5.4	5200	2.3	A5.5	9400	2.1
P1B7	(A5.4)	8900	2.4	(A5.5)	9400	2.2
P1B8	(A5.4)	8100	2.3	(A5.5)	9400	2.3
P1B9	(A5.4)	5900	2.3	(A5.5)	9400	2.2
P1B10	(A5.4)	6700	2.1	(A5.5)	9400	2.2
	Average	7400	2.3	Average		2.2

Table C6.1 MSBT - Doherty et al / Allen method, Panel P1 specimens

Beam	Graph	Elastic modulus, E_f N/mm^2	Shear modulus, G N/mm^2	Graph	Elastic modulus, E_f N/mm^2	Shear modulus, G N/mm^2
P2B3	(A5.2)	7600	2.8	(A5.3)	9400	2.6
P2B4	(A5.2)	5900	3.7	(A5.3)	9400	2.8
P2B5	(A5.2)	6200	2.4	(A5.3)	9400	2.1
P2B6	(A5.2)	5900	3.6	(A5.3)	9400	2.8
P2B7	(A5.2)	6400	2.6	(A5.3)	9400	2.5
P2B8	(A5.2)	5900	3.1	(A5.3)	9400	2.6
P2B9	(A5.2)	7100	3.4	(A5.3)	9400	2.6
P2B10	(A5.2)	6200	3.2	(A5.3)	9400	2.3
	Average	6400	2.3	Average		2.5
P2B3	(A5.4)	10400	2.2	(A5.5)	9400	2.5
P2B4	(A5.4)	11000	2.2	(A5.5)	9400	2.4
P2B5	(A5.4)	9400	2.3	(A5.5)	9400	2.6
P2B6	(A5.4)	11000	2.3	(A5.5)	9400	2.6
P2B7	(A5.4)	9900	2.4	(A5.5)	9400	2.8
P2B8	(A5.4)	10800	2.3	(A5.5)	9400	2.5
P2B9	(A5.4)	10400	2.3	(A5.5)	9400	2.6
P2B10	(A5.4)	10300	2.1	(A5.5)	9400	2.2
	Average	10400	2.3	Average		2.6

Table C6.2 MSBT - Doherty et al / Allen method, Panel P2 specimens

	Total load N	Canti-lever load P, N	A mm^2	$(1-I_f/I)^2$	Inter-cept $x10^{-9}$ mm^{-2}	δ / l_1^3 $x10^{-9}$ mm^{-2}	$1/l_1^2$ $x10^{-6}$ mm^{-2}	Slope, S_{84} $x10^{-3}$	G_{84} N/mm^2	Ave. G_{84} N/mm^2
P3A	196.1	98.07	3960	0.9149	4.53	28.1	6.0	3.928	2.42	
P3B	196.1	98.07	3960	0.9149	4.53	27.3	6.0	3.795	2.99	
P3C	196.1	98.07	3960	0.9149	4.53	27.8	6.0	3.878	2.92	
P3D	196.1	98.07	3960	0.9149	4.53	30.0	5.95	4.381	2.65	
P3E	196.1	98.07	3960	0.9149	4.53	25.8	6.0	3.545	3.20	2.8
P4A	392.3	196.1	5892	0.9509	2.58	36.2	6.0	5.603	2.82	
P4B	392.3	196.1	5892	0.9509	2.58	34.2	6.0	5.270	3.00	
P4C	392.3	196.1	5892	0.9509	2.58	35.2	6.0	5.437	2.91	
P4D	392.3	196.1	5892	0.9509	2.58	35.0	6.0	5.403	2.93	
P4E	392.3	196.1	5892	0.9509	2.58	33.2	6.0	5.103	3.10	3.0
P5A	392.3	196.1	7403	0.9859	1.46	25.8	6.0	4.057	3.22	
P5B	392.3	196.1	7403	0.9859	1.46	26.9	6.0	4.240	3.08	
P5C	392.3	196.1	7403	0.9859	1.46	26.0	6.0	4.090	3.19	
P5D	392.3	196.1	7403	0.9859	1.46	25.6	6.0	4.023	3.25	
P5E	392.3	196.1	7403	0.9859	1.46	25.5	6.0	4.007	3.26	3.2
P6A	392.3	196.1	9754	0.9946	0.644	20.0	6.45	3.001	3.33	
P6B	392.3	196.1	9754	0.9946	0.644	20.0	6.45	3.001	3.33	
P6C	392.3	196.1	9754	0.9946	0.644	20.0	5.60	3.456	2.89	
P6D	392.3	196.1	9754	0.9946	0.644	19.6	6.5	2.916	3.43	
P6E	392.3	196.1	9754	0.9946	0.644	18.8	6.5	2.793	3.58	3.3
P10A	196.1	98.07	4358	0.9966	3.63	34.6	6.0	5.162	2.17	
P10B	196.1	98.07	4358	0.9966	3.63	35.8	6.0	5.362	2.09	
P10C	196.1	98.07	4358	0.9966	3.63	39.6	6.0	5.995	1.87	
P10D	196.1	98.07	4358	0.9966	3.63	36.0	6.0	5.395	2.08	
P10E	196.1	98.07	4358	0.9966	3.63	38.7	6.0	5.845	1.92	2.0

$$\text{Intercept } B_{40} = \frac{88P}{384EI}, \text{ Shear modulus } G_{40} = \frac{P(1-I_f/I)^2}{2AS_{40}}$$

Table C6.3 MSBT - O'Connor, Conjugate Point Method, quarter span / support

	Total load N	Canti-lever load P, N	A mm^2	$(1-I_f/I)^2$	Inter-cept $x10^{-9}$ mm^{-2}	δ / l_1^3 $x10^{-9}$ mm^{-2}	$1/l_1^2$ $x10^{-6}$ mm^{-2}	Slope, S_{84} $x10^{-3}$	G_{84} N/mm^2	Ave. G_{84} N/mm^2
P3A	196.1	98.07	3960	0.9149	2.42	15.3	6.0	2.147	2.64	
P3B	196.1	98.07	3960	0.9149	2.42	15.6	6.0	2.197	2.58	
P3C	196.1	98.07	3960	0.9149	2.42	13.3	6.0	1.813	3.12	
P3D	196.1	98.07	3960	0.9149	2.42	16.6	6.0	2.363	2.40	
P3E	196.1	98.07	3960	0.9149	2.42	14.8	6.0	2.063	2.75	2.7
P4A	392.3	196.1	5892	0.9509	1.38	18.8	6.0	2.903	2.73	
P4B	392.3	196.1	5892	0.9509	1.38	18.8	6.0	2.903	2.73	
P4C	392.3	196.1	5892	0.9509	1.38	18.0	6.0	2.770	2.86	
P4D	392.3	196.1	5892	0.9509	1.38	19.0	6.0	2.938	2.69	
P4E	392.3	196.1	5892	0.9509	1.38	18.3	6.0	2.820	2.81	2.8
P5A	392.3	196.1	7403	0.9859	0.782	13.5	6.0	2.120	3.08	
P5B	392.3	196.1	7403	0.9859	0.782	14.2	6.0	2.236	2.92	
P5C	392.3	196.1	7403	0.9859	0.782	14.1	6.0	2.220	2.94	
P5D	392.3	196.1	7403	0.9859	0.782	13.7	6.0	2.153	3.03	
P5E	392.3	196.1	7403	0.9859	0.782	13.3	6.0	2.086	3.13	3.0
P6A	392.3	196.1	9754	0.9946	0.344	10.2	6.5	1.520	3.30	
P6B	392.3	196.1	9754	0.9946	0.344	10.3	6.5	1.532	3.26	
P6C	392.3	196.1	9754	0.9946	0.344	10.9	6.5	1.624	3.08	
P6D	392.3	196.1	9754	0.9946	0.344	10.6	6.5	1.578	3.17	
P6E	392.3	196.1	9754	0.9946	0.344	10.0	6.5	1.486	3.36	3.2
P10A	196.1	98.07	4358	0.9966	1.94	17.4	6.0	2.577	2.17	
P10B	196.1	98.07	4358	0.9966	1.94	19.4	6.0	2.910	1.93	
P10C	196.1	98.07	4358	0.9966	1.94	22.2	6.0	3.377	1.66	
P10D	196.1	98.07	4358	0.9966	1.94	22.8	6.0	3.477	1.61	
P10E	196.1	98.07	4358	0.9966	1.94	25.4	6.0	3.910	1.43	1.8

$$\text{Intercept } B_{80} = \frac{47P}{384EI}, \text{ Shear modulus } G_{80} = \frac{P(1-I_f/I)^2}{4AS_{80}}$$

Table C6.4 MSBT - O'Connor, Conjugate Point Method, eighth span / support

	Total load N	Canti-lever load P, N	A mm^2	$(1-I_f/I)^2$	Inter-cept $x10^{-9}$ mm^{-2}	δ/l_1^3 $x10^{-9}$ mm^{-2}	$1/l_1^2$ $x10^{-6}$ mm^{-2}	Slope, S_{84} $x10^{-3}$	G_{84} N/mm^2	Ave. G_{84} N/mm^2
P3A	196.1	98.07	3960	0.9149	2.11	14.3	6.0	2.030	2.79	
P3B	196.1	98.07	3960	0.9149	2.11	13.2	6.0	1.850	3.06	
P3C	196.1	98.07	3960	0.9149	2.11	12.3	6.0	1.698	3.34	
P3D	196.1	98.07	3960	0.9149	2.11	14.2	6.0	2.015	2.81	
P3E	196.1	98.07	3960	0.9149	2.11	14.7	6.0	2.098	2.70	2.9
P4A	392.3	196.1	5892	0.9509	1.20	17.7	6.0	2.750	2.88	
P4B	392.3	196.1	5892	0.9509	1.20	16.9	6.0	2.617	3.02	
P4C	392.3	196.1	5892	0.9509	1.20	17.3	6.0	2.683	2.95	
P4D	392.3	196.1	5892	0.9509	1.20	17.4	6.0	2.700	2.93	
P4E	392.3	196.1	5892	0.9509	1.20	16.2	6.0	2.250	3.52	3.1
P5A	392.3	196.1	7403	0.9859	1.18	12.9	6.0	1.953	3.34	
P5B	392.3	196.1	7403	0.9859	1.18	12.3	6.0	1.853	3.52	
P5C	392.3	196.1	7403	0.9859	1.18	12.2	6.0	1.837	3.55	
P5D	392.3	196.1	7403	0.9859	1.18	12.0	6.0	1.803	3.62	
P5E	392.3	196.1	7403	0.9859	1.18	11.2	6.0	1.607	4.06	3.6
P6A	392.3	196.1	9754	0.9946	0.300	9.1	6.5	1.354	3.69	
P6B	392.3	196.1	9754	0.9946	0.300	9.7	6.5	1.446	3.46	
P6C	392.3	196.1	9754	0.9946	0.300	9.8	6.5	1.462	3.42	
P6D	392.3	196.1	9754	0.9946	0.300	10.4	6.5	1.554	3.22	
P6E	392.3	196.1	9754	0.9946	0.300	8.6	6.5	1.277	3.91	3.5
P10A	196.1	98.07	4358	0.9966	1.69	16.1	6.0	2.402	2.33	
P10B	196.1	98.07	4358	0.9966	1.69	17.6	6.0	2.652	2.11	
P10C	196.1	98.07	4358	0.9966	1.69	20.5	6.0	3.155	1.79	
P10D	196.1	98.07	4358	0.9966	1.69	19.3	6.0	2.935	1.91	
P10E	196.1	98.07	4358	0.9966	1.69	20.5	6.0	3.135	1.79	2.0

$$\text{Intercept } B_{84} = \frac{41P}{384EI}, \text{ Shear modulus } G_{84} = \frac{P(1-I_f/I)^2}{4AS_{84}}$$

Table C6.5 MSBT - O'Connor, Conjugate Point Method, eighth span / quarter

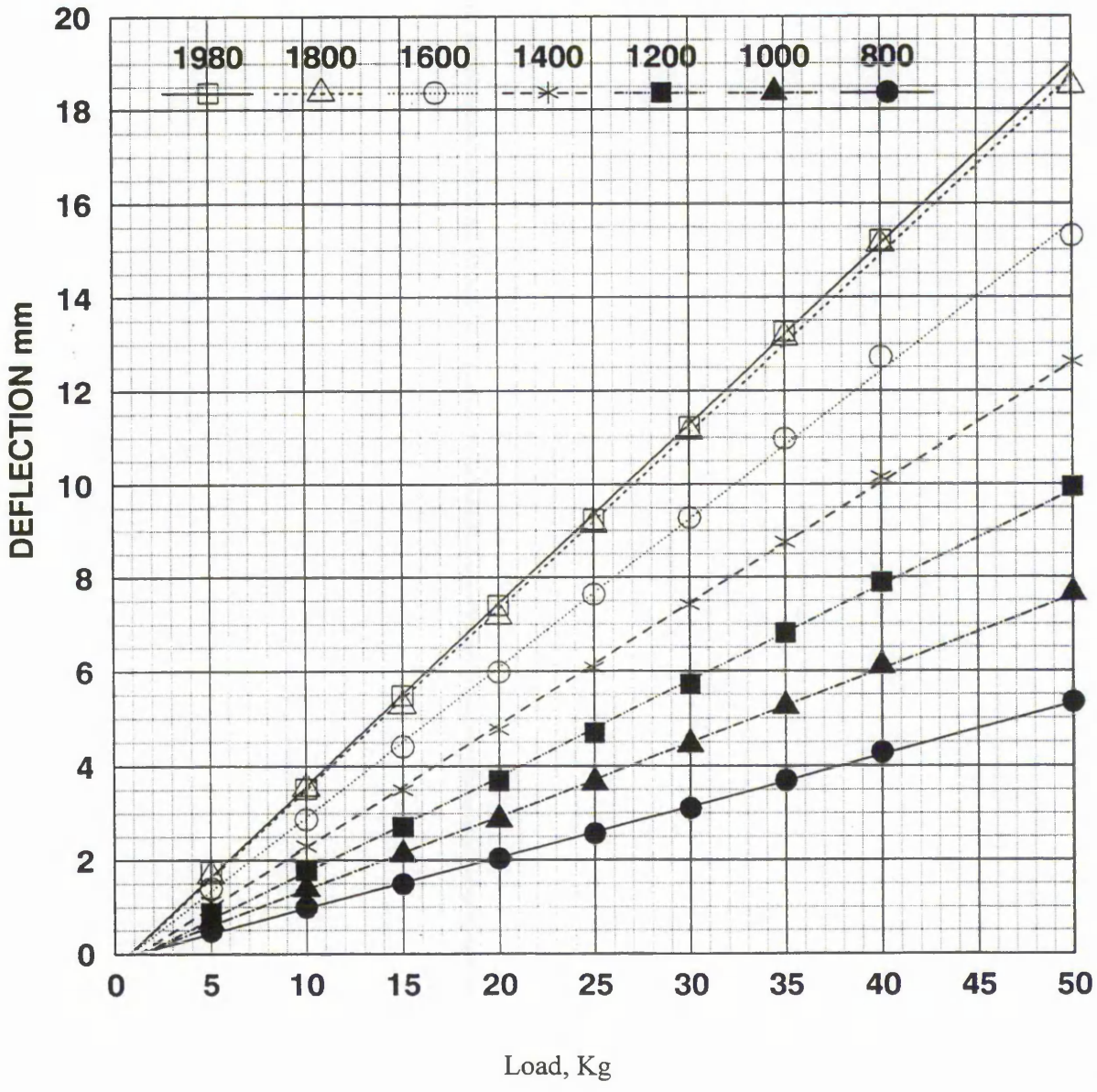

Figure C6.1 shows a typical plot of load versus deflection at centre span for varying lengths of span of panel P1 beam 3.

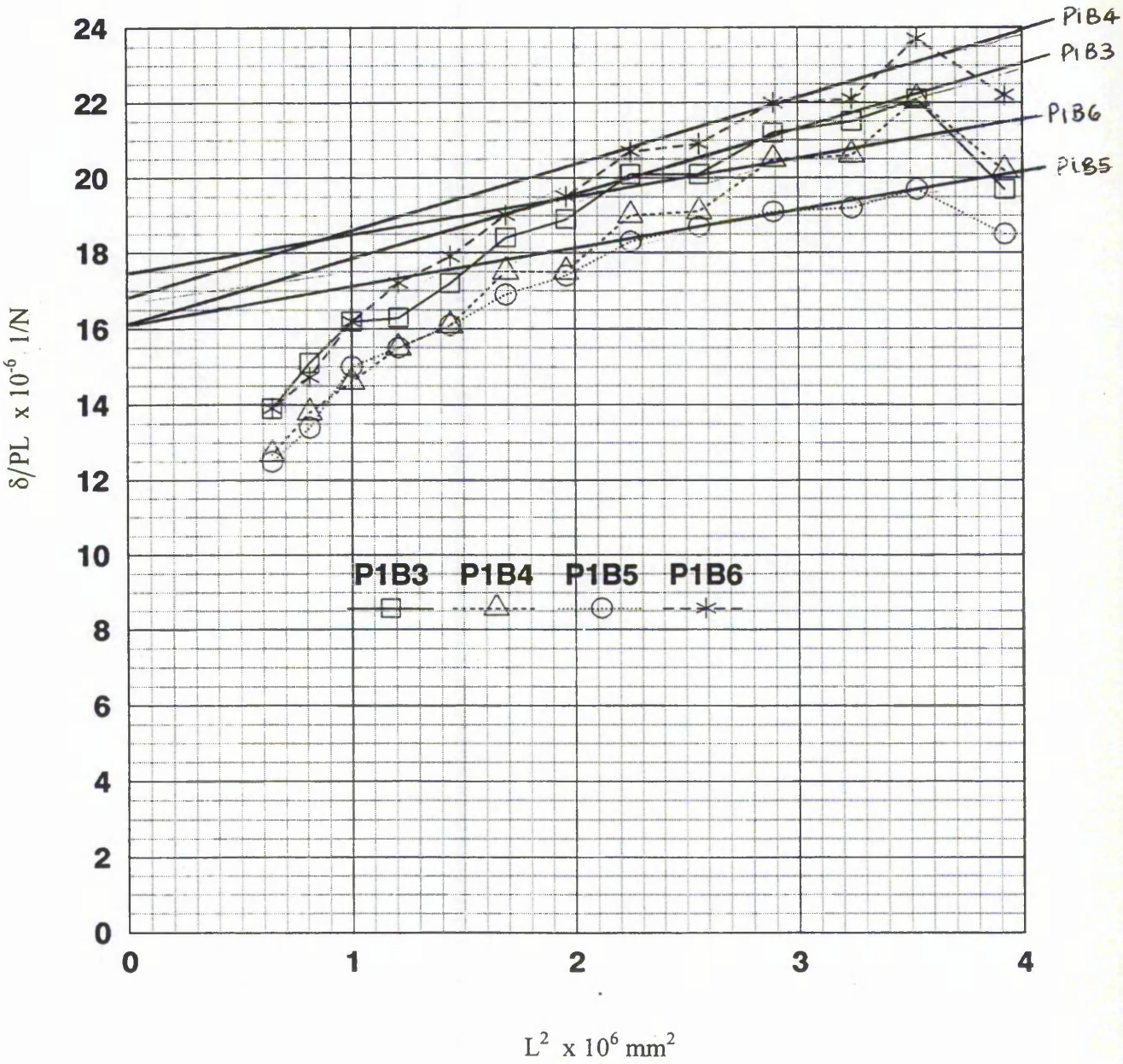

Figure C6.2 Type 1 plot of δ/PL versus L^2 for beams 3, 4, 5, 6 from panel P1. E_{ply} and G_c are evaluated.

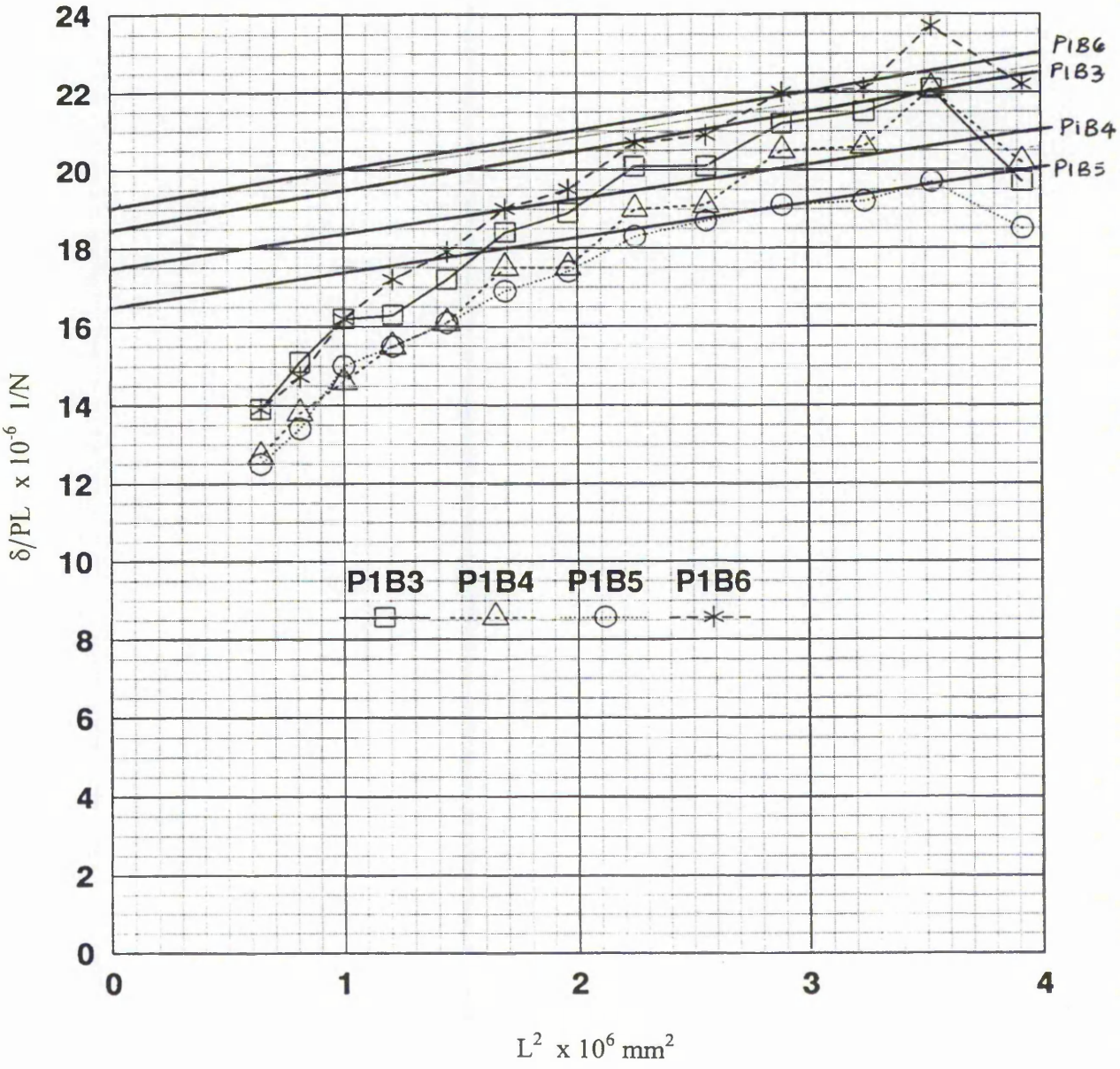

Figure C6.3 Type 1 plot of δ/PL versus L^2 for beams 3, 4, 5, 6 from panel P1. E_{ply} predetermined , G_c evaluated.

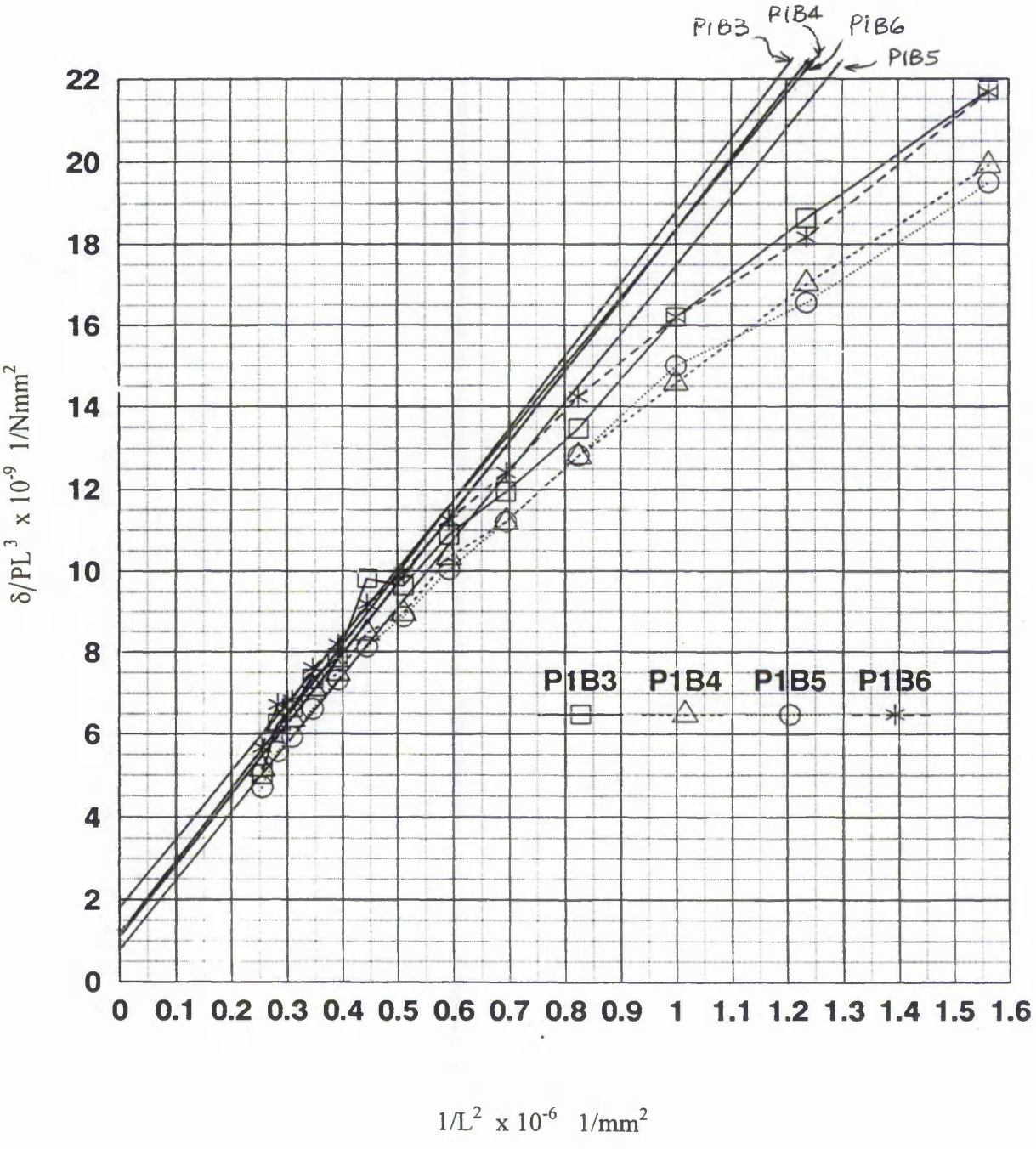

Figures C6.4 Type 2 plot of δ/PL^3 versus $1/L^2$ for beams 3, 4, 5, 6 from panel P1. E_{ply} and G_c are evaluated.

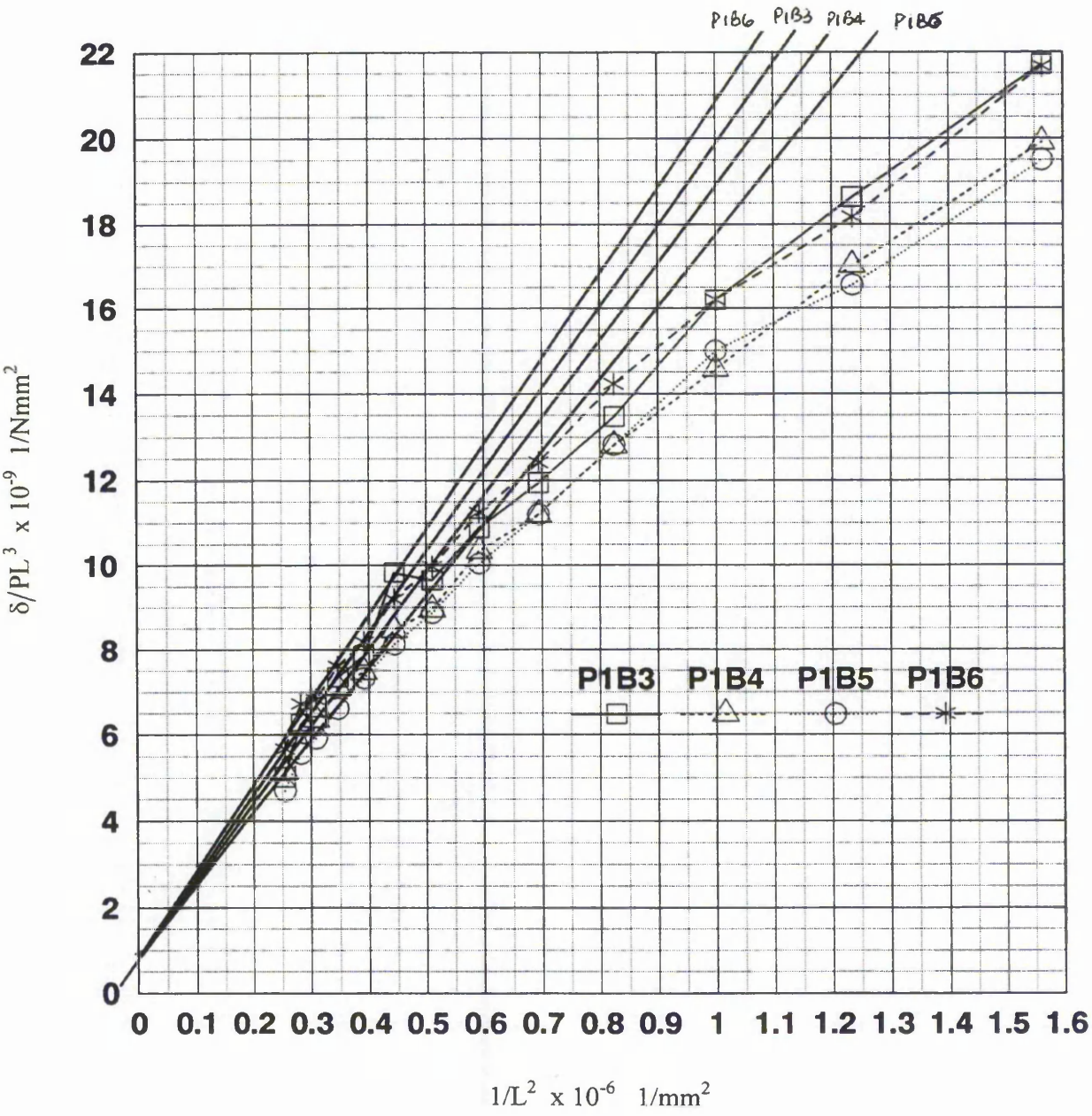

Figures C6.5 Type 2 plot of δ/PL^3 versus $1/L^2$ for beams 3, 4, 5, 6 from panel P1. E_{ply} predetermined , G_c evaluated.

MULTIPLE SPAN TESTING

Conjugate point method - 3-point load config.

P5A - Isofoam CRF core shear modulus evaluation

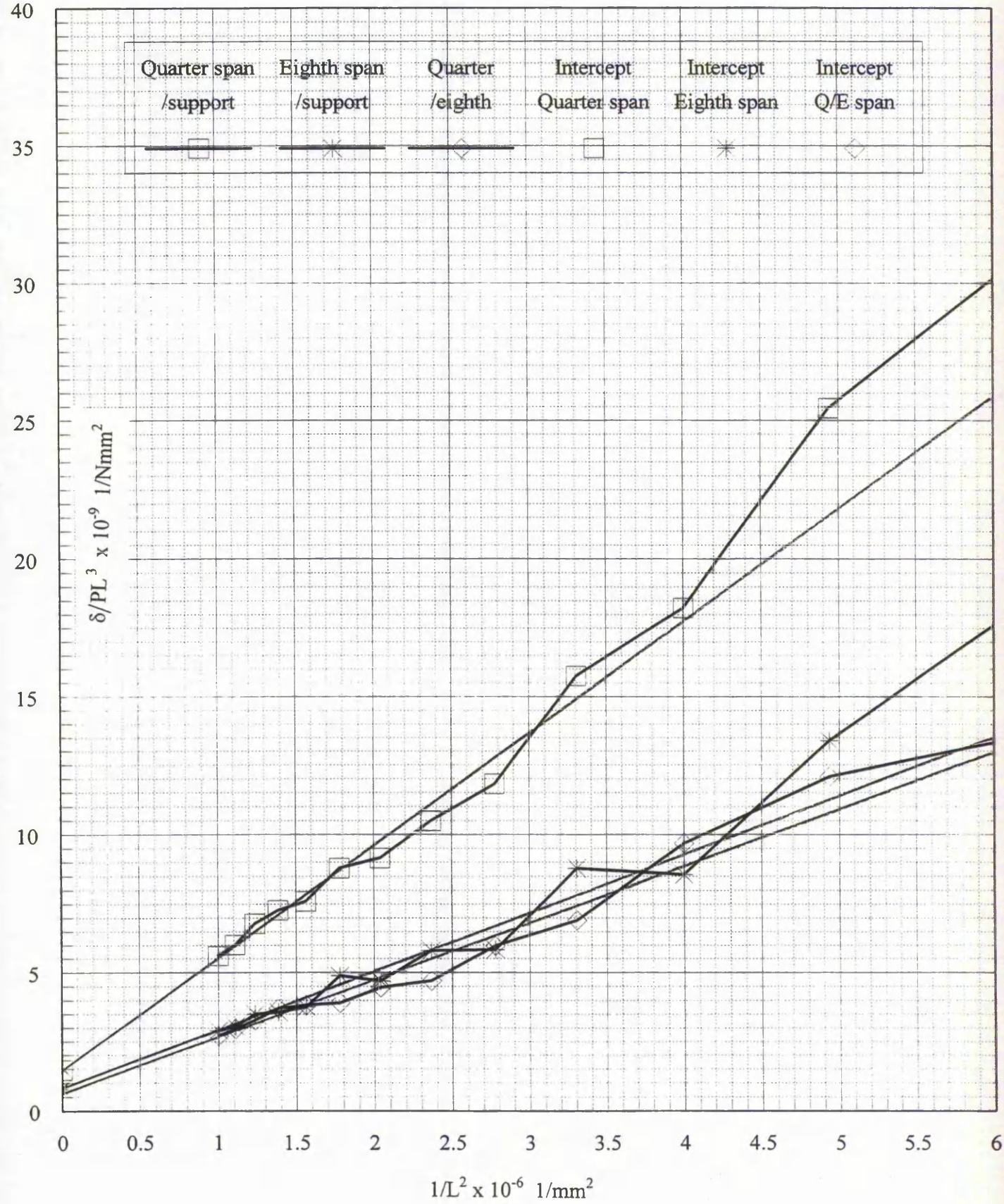

Figure C6.6 Type 2 plot using conjugate points.
E_{ply} is predetermined and G_c is evaluated from the gradient.

Appendix D

CHAPTER 7

SANDWICH PANEL TESTING AND ANALYSIS

P1	b = 1000 mm		c = 52 mm		t = 12.2 mm		x = 640 mm		
Load = 10.0 kN	E_f N/mm^2	υ	G_c N/mm^2	E_c N/mm^2	δ_0	δ_4	δ_{40}	δ_8	δ_{80}
Experimental	N/A	N/A	N/A	N/A	N/A	N/A	21.6	N/A	11.2
UC	11100	0.2	N/A	N/A	N/A	N/A	N/A	N/A	N/A
UT	11100	0.2	N/A	N/A	N/A	N/A	N/A	N/A	N/A
ST BS XH	11100	0.2	1.98	4.8	29.58	12.22	17.4	21.02	8.6
ST BS XP	11100	0.2	2.26	5.4	26.74	11.12	15.6	19.04	7.7
ST ASTM XH	11100	0.2	2.12	5.1	28.05	11.63	16.4	19.96	8.1
ST ASTM XP	11100	0.2	2.35	5.6	25.94	10.80	15.1	18.48	7.5
MSBT Type 1	7300	0.2	2.3	5.5	31.55	13.38	18.2	22.58	9.0
MSBT Type 1	11100	0.2	2.2	5.3	27.28	11.33	16.0	19.42	7.9
MSBT Type 2	7400	0.2	2.3	5.5	31.42	13.32	18.1	22.48	8.9
MSBT Type 2	11100	0.2	2.2	5.3	27.28	11.33	16.0	19.42	7.9

Table D7.1a Material properties used in the F.E.A. and the calculated displacements.

P2	b = 1000 mm		c = 52 mm		t = 12.2 mm		x = 640 mm		
Load = 10.0 kN	E_f N/mm^2	υ	G_c N/mm^2	E_c N/mm^2	δ_0	δ_4	δ_{40}	δ_8	δ_{80}
Experimental	N/A	N/A	N/A	N/A	N/A	N/A	17.6	N/A	8.7
UC	N/A	N/A	N/A	N/A	N/A	N/A	N/A	N/A	N/A
UT	N/A	N/A	N/A	N/A	N/A	N/A	N/A	N/A	N/A
ST BS XH	11100	0.2	1.33	3.2	40.30	16.23	24.1	28.39	11.9
ST BS XP	11100	0.2	1.39	3.3	38.88	15.77	23.1	27.43	11.5
ST ASTM XH	11100	0.2	1.50	3.6	36.67	14.90	21.8	25.91	10.8
ST ASTM XP	11100	0.2	1.51	3.6	36.52	14.84	21.7	25.81	10.7
MSBT Type 1	6400	0.2	3.1	7.4	27.09	11.41	15.7	19.30	7.8
MSBT Type 1	11100	0.2	2.5	6.0	24.75	10.34	14.4	17.65	7.1
MSBT Type 2	10400	0.2	2.8	6.7	24.67	10.43	14.2	17.65	7.0
MSBT Type 2	11100	0.2	2.6	6.2	24.03	10.05	14.0	17.15	6.9

Table D7.1b Material properties used in the F.E.A. and the calculated displacements.

P3	b = 1000 mm		c = 21 mm		t = 12.3 mm		x = 640 mm		
Load = 6.9 kN	E_f N/mm^2	υ	G_c N/mm^2	E_c N/mm^2	δ_0	δ_4	δ_{40}	δ_8	δ_{80}
Experimental	N/A	N/A	N/A	N/A	N/A	N/A	25.8	N/A	13.2
UC	9400	0.15	N/A	2.2	64.96	24.88	40.09	44.82	20.15
UT	9400	0.15	N/A	N/A	N/A	N/A	N/A	N/A	N/A
ST BS XH	9400	0.15	3.0	6.9	37.78	13.05	20.7	23.32	10.5
ST BS XP	9400	0.15	3.11	7.2	33.11	12.78	20.36	22.84	10.3
ST ASTM XH	9400	0.15	3.61	8.3	31.04	11.92	19.1	21.37	9.7
ST ASTM XP	9400	0.15	3.88	8.9	30.12	11.54	18.6	20.71	9.4
MSBT G_{84}	9400	0.15	2.9	6.7	34.25	13.25	21.0	23.65	10.6
MSBT G_{40}	9400	0.15	2.8	6.4	35.02	13.56	21.5	24.20	10.8
MSBT G_{80}	9400	0.15	2.7	6.2	35.58	13.94	21.7	24.59	11.0

Table D7.1c Material properties used in the F.E.A. and the calculated displacements.

P4	b = 1000 mm		c = 51 mm		t = 12.3 mm		x = 640 mm		
Load = 10.0 kN	E_f N/mm^2	υ	G_c N/mm^2	E_c N/mm^2	δ_0	δ_4	δ_{40}	δ_8	δ_{80}
Experimental	N/A	N/A	N/A	N/A	N/A	N/A	16.7	N/A	8.7
UC	9400	0.18	N/A	4.2	37.25	15.51	21.7	26.34	10.9
UT	9400	0.18	N/A	5.0	32.72	13.69	19.0	23.16	9.6
ST BS XH	9400	0.18	2.58	6.1	28.35	11.89	16.5	20.07	8.3
ST BS XP	9400	0.18	2.94	6.9	26.01	10.90	15.1	18.40	7.6
ST ASTM XH	9400	0.18	3.11	7.3	25.02	10.49	14.5	17.70	7.3
ST ASTM XP	9400	0.18	3.30	7.8	23.92	10.02	13.9	16.91	7.0
MSBT G_{84}	9400	0.18	3.1	7.3	25.02	10.48	14.5	17.70	7.3
MSBT G_{40}	9400	0.18	3.0	7.1	25.49	10.69	14.8	18.04	7.5
MSBT G_{80}	9400	0.18	2.8	6.6	26.82	11.25	15.6	18.98	7.8

Table D7.1d Material properties used in the F.E.A. and the calculated displacements.

P5	b = 1000 mm		c = 78 mm		t = 12.3 mm		x = 640 mm		
Load = 10.0 kN	E_f N/mm^2	υ	G_c N/mm^2	E_c N/mm^2	δ_0	δ_4	δ_{40}	δ_8	δ_{80}
Experimental	N/A	N/A	N/A	N/A	N/A	N/A	11.6	N/A	5.9
UC	9400	0.18	N/A	6.2	21.18	9.19	12.0	15.23	6.0
UT	9400	0.18	N/A	6.2	21.18	9.19	12.0	15.23	6.0
ST BS XH	9400	0.18	2.47	5.8	22.30	9.72	12.6	16.03	6.3
ST BS XP	9400	0.18	2.81	6.6	20.19	8.81	11.4	14.52	5.7
ST ASTM XH	9400	0.18	3.03	7.2	18.90	8.25	10.7	13.59	5.3
ST ASTM XP	9400	0.18	3.31	7.8	17.80	7.77	10.0	12.79	6.1
MSBT G_{84}	9400	0.18	3.6	8.5	16.71	7.29	9.4	12.00	4.7
MSBT G_{40}	9400	0.18	3.2	7.6	18.26	7.97	10.3	13.12	5.1
MSBT G_{80}	9400	0.18	3.0	7.1	19.10	8.34	10.8	13.73	5.4

Table D7.1e Material properties used in the F.E.A. and the calculated displacements.

P6	b = 1000 mm		c = 102 mm		t = 12.3 mm		x = 640 mm		
Load = 10.0 kN	E_f N/mm^2	υ	G_c N/mm^2	E_c N/mm^2	δ_0	δ_4	δ_{40}	δ_8	δ_{80}
Experimental	N/A	N/A	N/A	N/A	N/A	N/A	7.5	N/A	3.8
UC	9400	0.19	N/A	5.8	16.35	7.46	8.9	11.98	4.4
UT	9400	0.19	N/A	6.7	14.51	6.60	7.9	10.57	3.9
ST BS XH	9400	0.19	2.40	5.7	16.59	7.63	9.0	12.15	4.4
ST BS XP	9400	0.19	2.66	6.3	15.26	6.97	8.3	11.19	4.1
ST ASTM XH	9400	0.19	2.83	6.7	14.51	6.60	7.9	10.57	3.9
ST ASTM XP	9400	0.19	3.14	7.5	13.23	6.06	7.2	9.70	3.5
MSBT G_{84}	9400	0.19	3.5	8.3	12.19	5.59	6.6	8.94	3.3
MSBT G_{40}	9400	0.19	3.3	7.9	12.69	5.81	6.9	9.30	3.4
MSBT G_{80}	9400	0.19	3.2	7.6	13.09	5.99	7.1	9.60	3.5

Table D7.1f Material properties used in the F.E.A. and the calculated displacements.

P10	b = 1000 mm		c = 50 mm		t = 3.9 mm		x = 640 mm		
Load = 4.0 kN	E_f N/mm^2	υ	G_c N/mm^2	E_c N/mm^2	δ_0	δ_4	δ_{40}	δ_8	δ_{80}
Experimental	**N/A**	**N/A**	**N/A**	**N/A**	**N/A**	**N/A**	**17.7**	**N/A**	**9.2**
UC	9400	0.13	N/A	6.3	20.55	9.09	11.4	14.83	5.7
UT	9400	0.13	N/A	6.2	20.96	9.39	11.6	15.15	5.8
ST BS XH	**9400**	**0.13**	**2.17**	**4.9**	**24.32**	**11.07**	**13.2**	**17.74**	**6.6**
ST BS XP	**9400**	**0.13**	**2.36**	**5.3**	**23.02**	**26.36**	**12.6**	**16.74**	**6.3**
ST ASTM XH	**9400**	**0.13**	**2.32**	**5.2**	**23.33**	**10.54**	**12.8**	**16.97**	**6.4**
ST ASTM XP	**9400**	**0.13**	**2.39**	**5.4**	**22.72**	**10.23**	**12.5**	**16.51**	**6.2**
MSBT G_{84}	9400	0.13	2.0	4.5	25.88	11.89	14.0	18.94	6.9
MSBT G_{40}	9400	0.13	2.0	4.5	25.88	11.89	14.0	18.94	6.9
MSBT G_{80}	9400	0.13	1.8	4.1	27.79	12.91	14.9	20.42	7.4

Table D7.1g Material properties used in the F.E.A. and the calculated displacements.

Panel P3	Upper facing		Lower facing	
Load = 3 kN	Support point	Load point	Support point	Load point
O'Connor		580		
Allen	400	50	400	50
F.E.A.	220	240	200	200
Experimental	190	190	190	190

Table D7.2a Panel P3 (Diagram D7.4) local distortion lengths

Panel P4	Upper facing		Lower facing	
Load = 5 kN	Support point	Load point	Support point	Load point
O'Connor		520		
Allen	400	75	400	75
F.E.A.	180	200	280	240
Experimental	190	180	260	220

Table D7.2b Panel P4 (Diagram D7.5) local distortion lengths

Panel P5	Upper facing		Lower facing	
Load = 5 kN	Support point	Load point	Support point	Load point
O'Connor		470		
Allen	400	100	400	100
F.E.A.	180	200	260	240
Experimental	190	200	280	200

Table D7.2c Panel P5 (Diagram D7.6) local distortion lengths

Panel P6	Upper facing		Lower facing	
Load = 5 kN	Support point	Load point	Support point	Load point
O'Connor		380		
Allen	400	200	400	200
F.E.A.	190	200	320	220
Experimental	190	190	280	200

Table D7.2d Panel P6 (Diagram D7.7) local distortion lengths

Panel P10	Upper facing		Lower facing	
Load = 3 kN	Support point	Load point	Support point	Load point
O'Connor		160		
Allen	110	110	110	110
F.E.A.	80	80	170	105
Experimental	90	90	190	90

Table D7.2e Panel P10 (Diagram D7.8) local distortion lengths

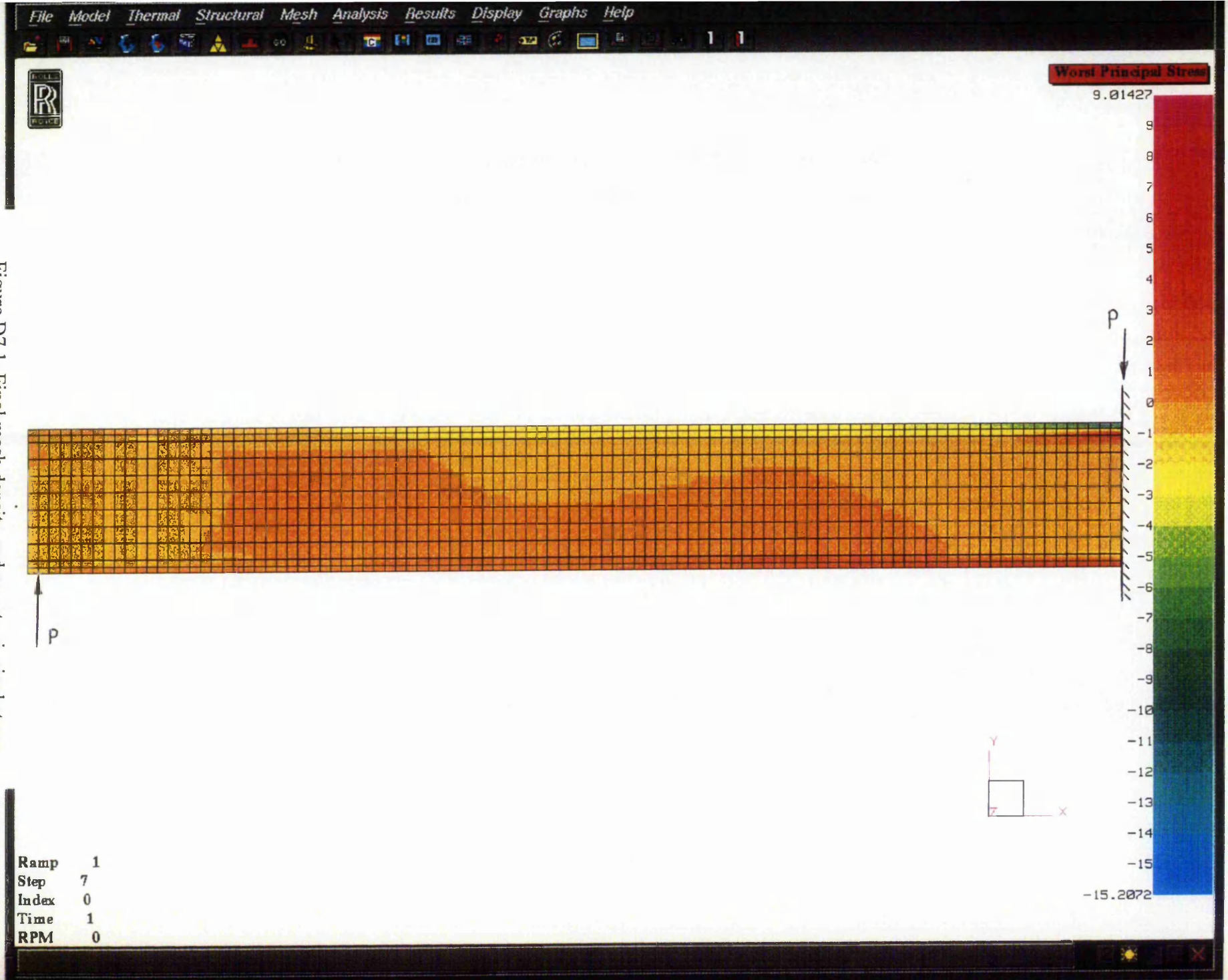

Figure D7.1 Final mesh density and worst principal stress contour plot for panel P6

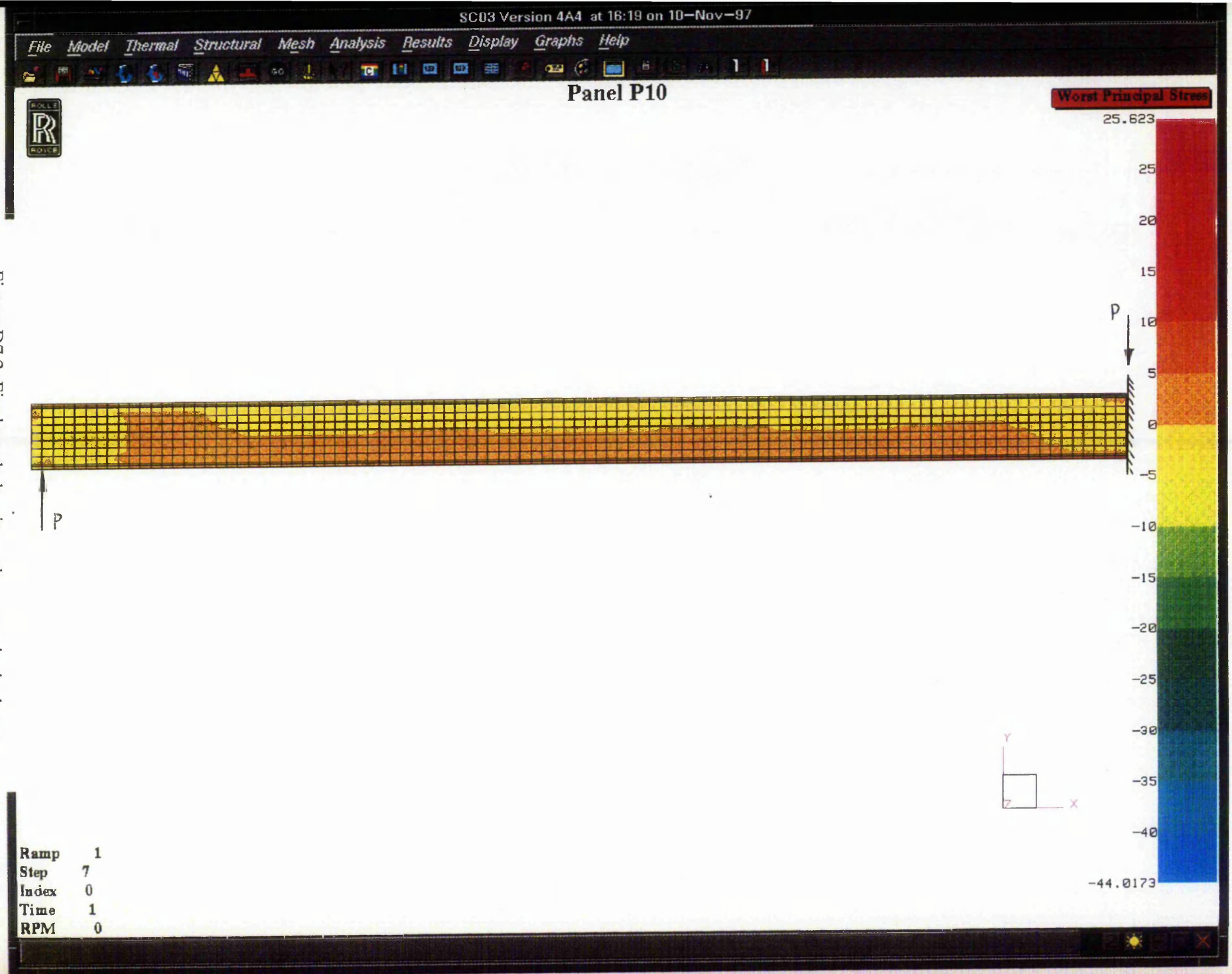

Figure D7.2 Final mesh density and worst principal stress contour plot for panel P10

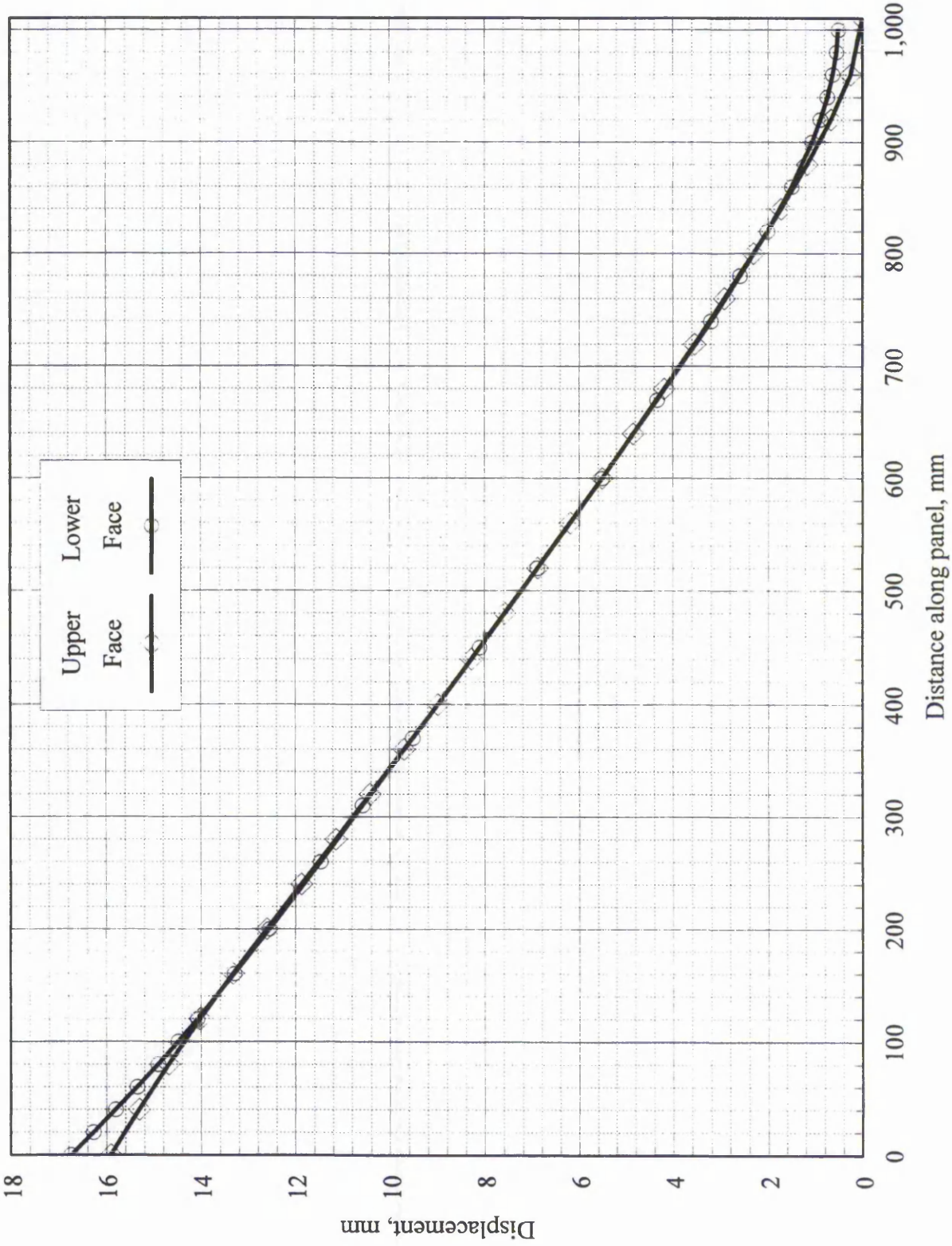

Figure D7.3 Displacement profile for the upper and lower facings of panel P6

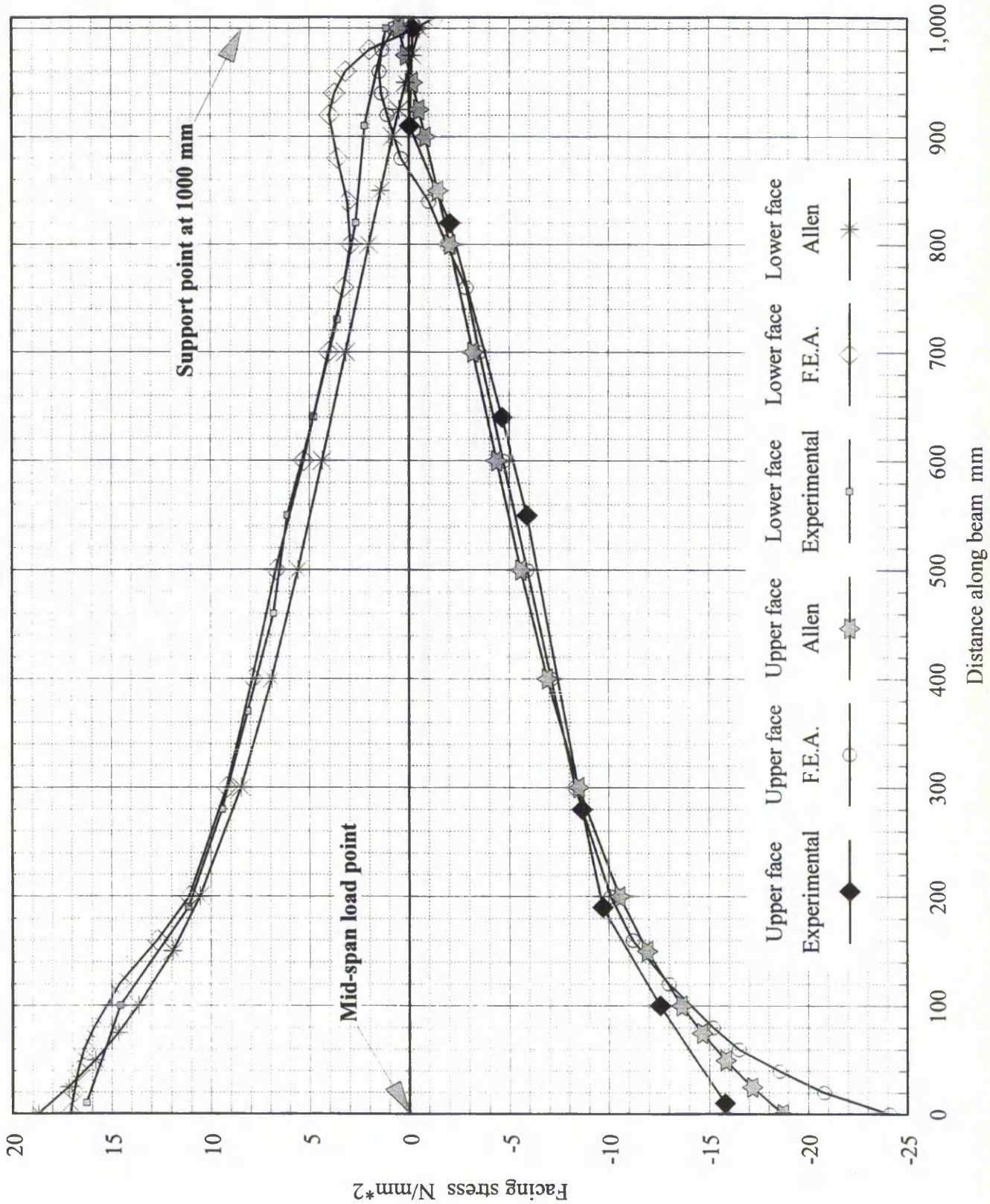

Figure D7.4 Stress profiles along upper and lower facings for panel P3

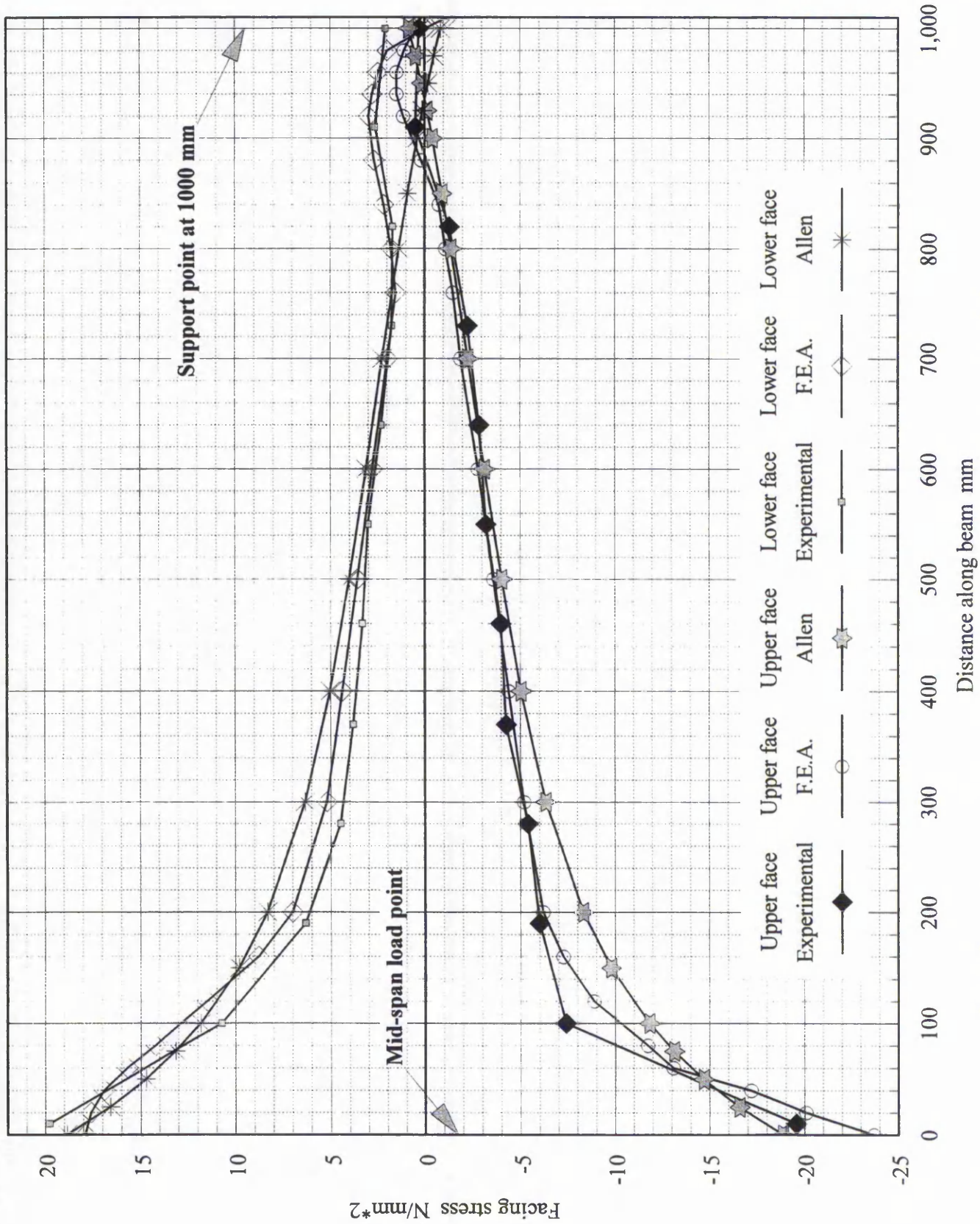

Figure D7.5 Stress profiles along upper and lower facings for panel P4

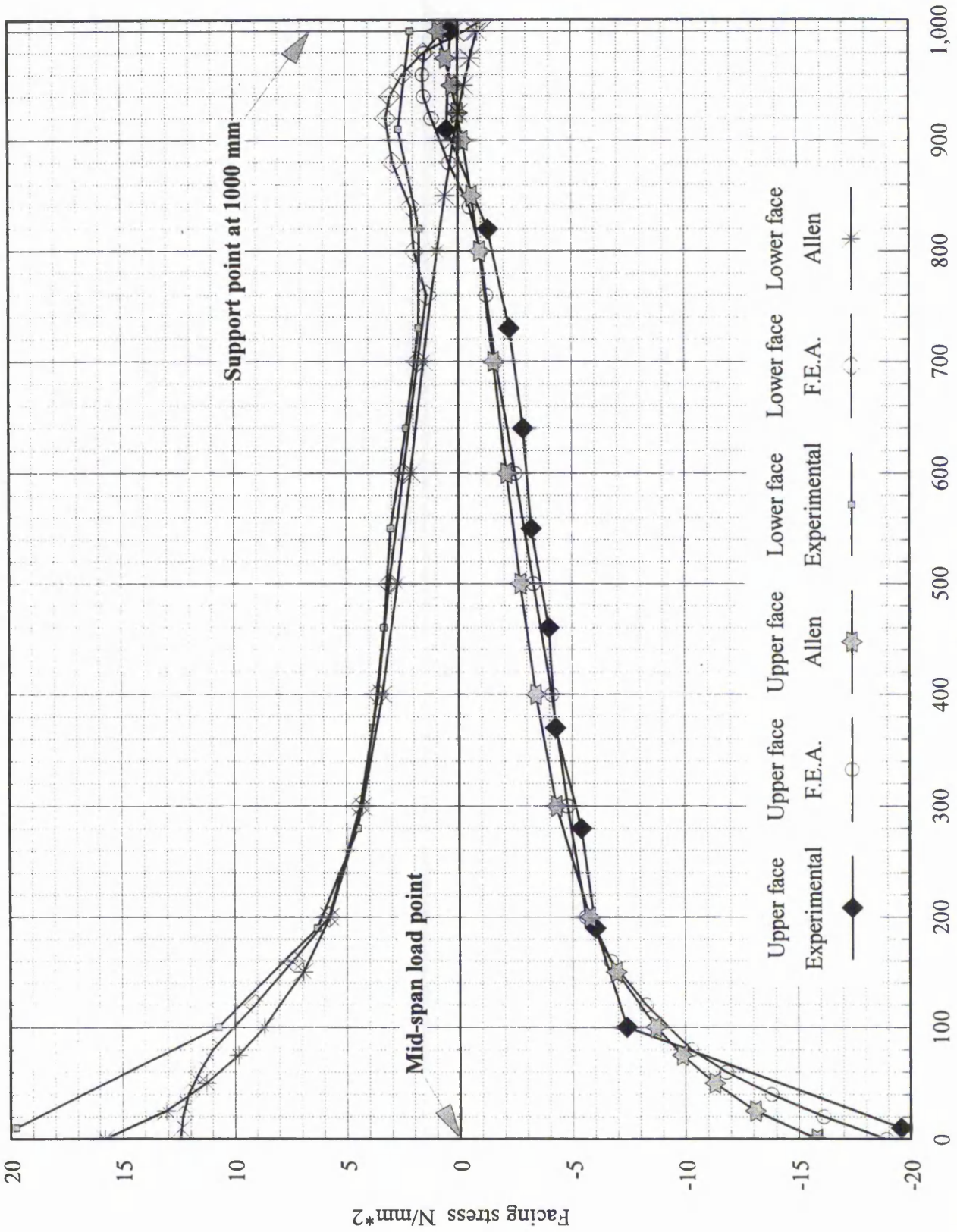

Figure D7.6 Stress profiles along upper and lower facings for panel P5

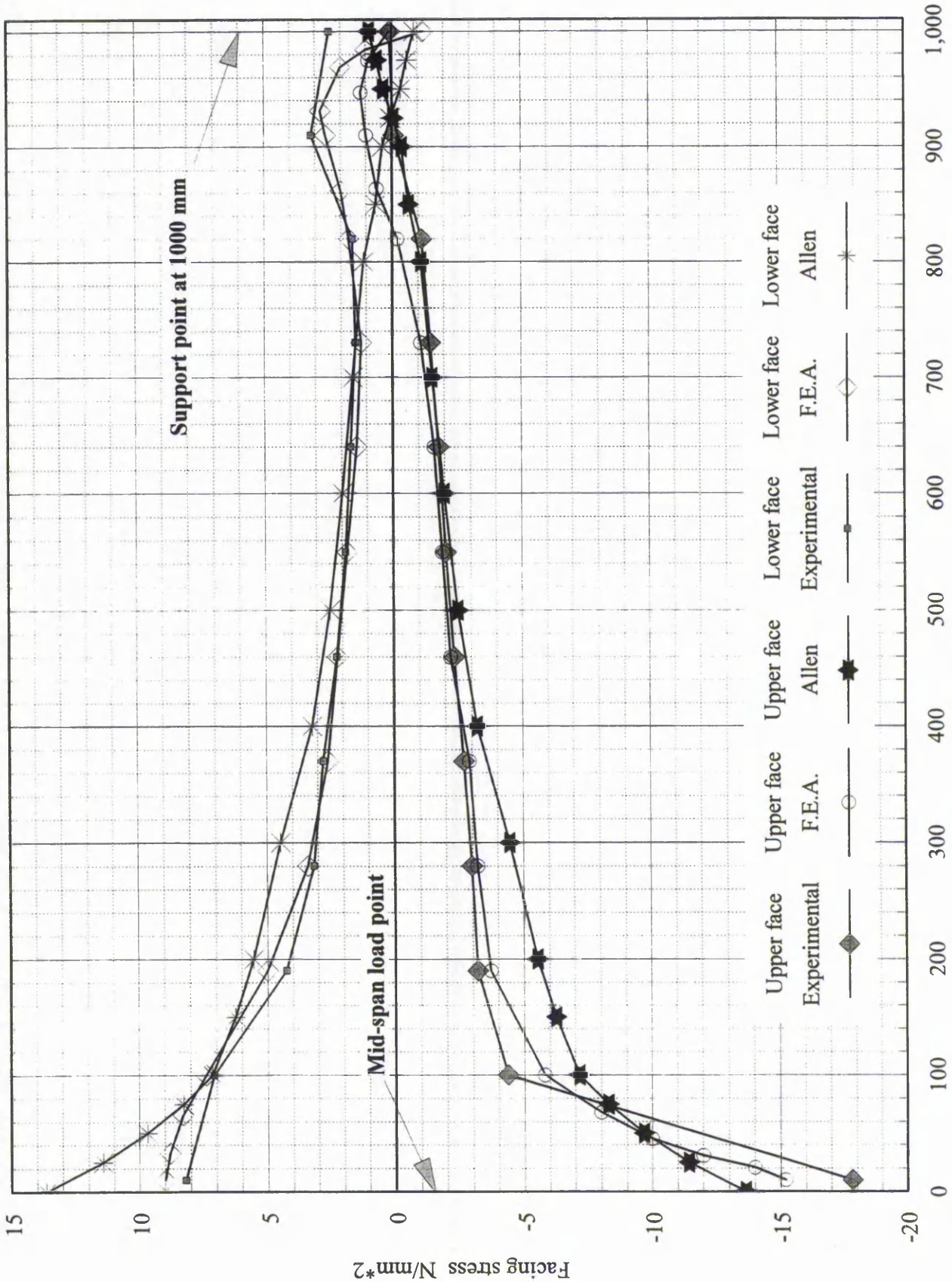

Figure D7.7 Stress profiles along upper and lower facings for panel P6

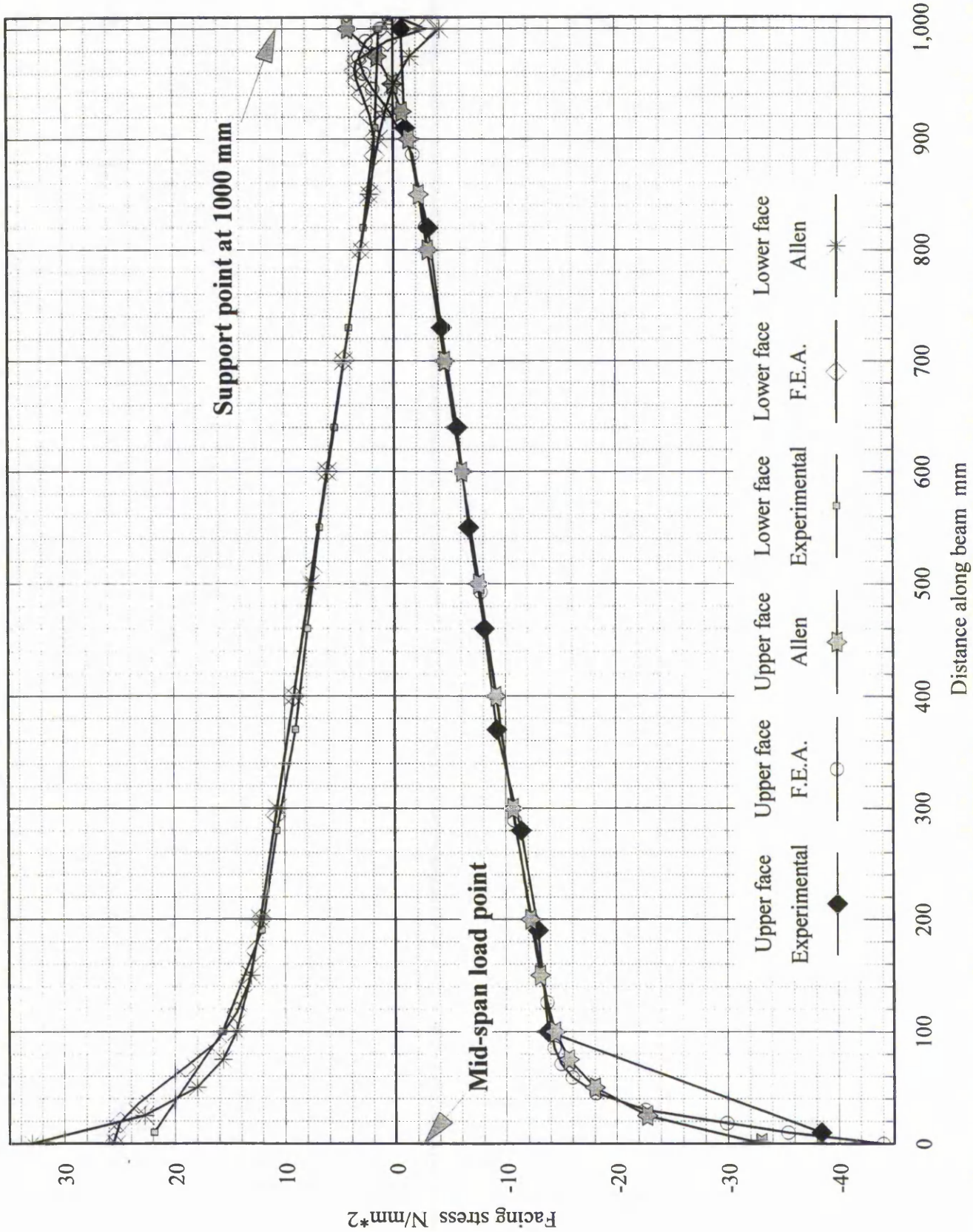

Figure D7.8 Stress profiles along upper and lower facings for panel P10

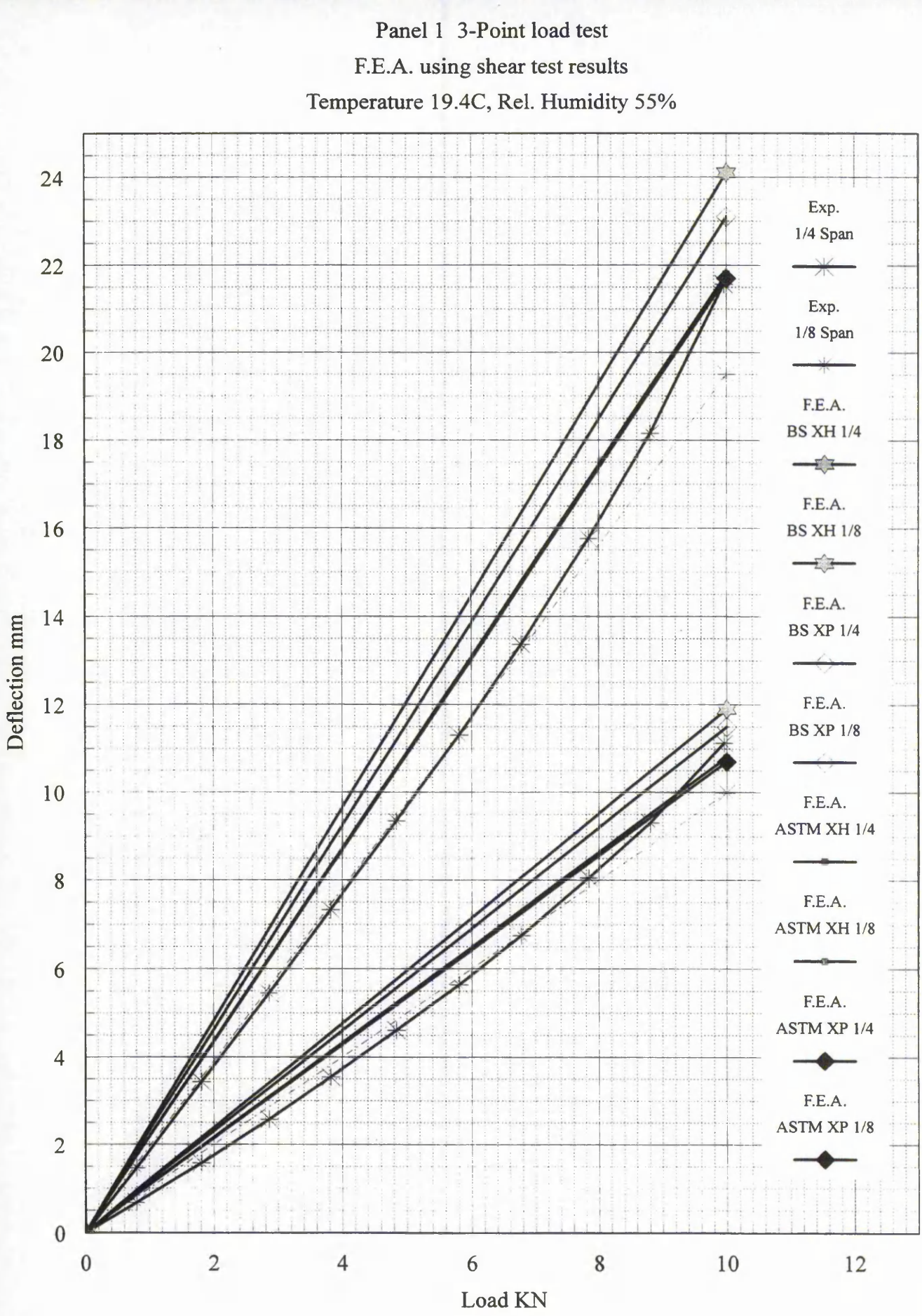

Figure D7.9a Finite element analysis and experimental load versus displacement plots for panel P1

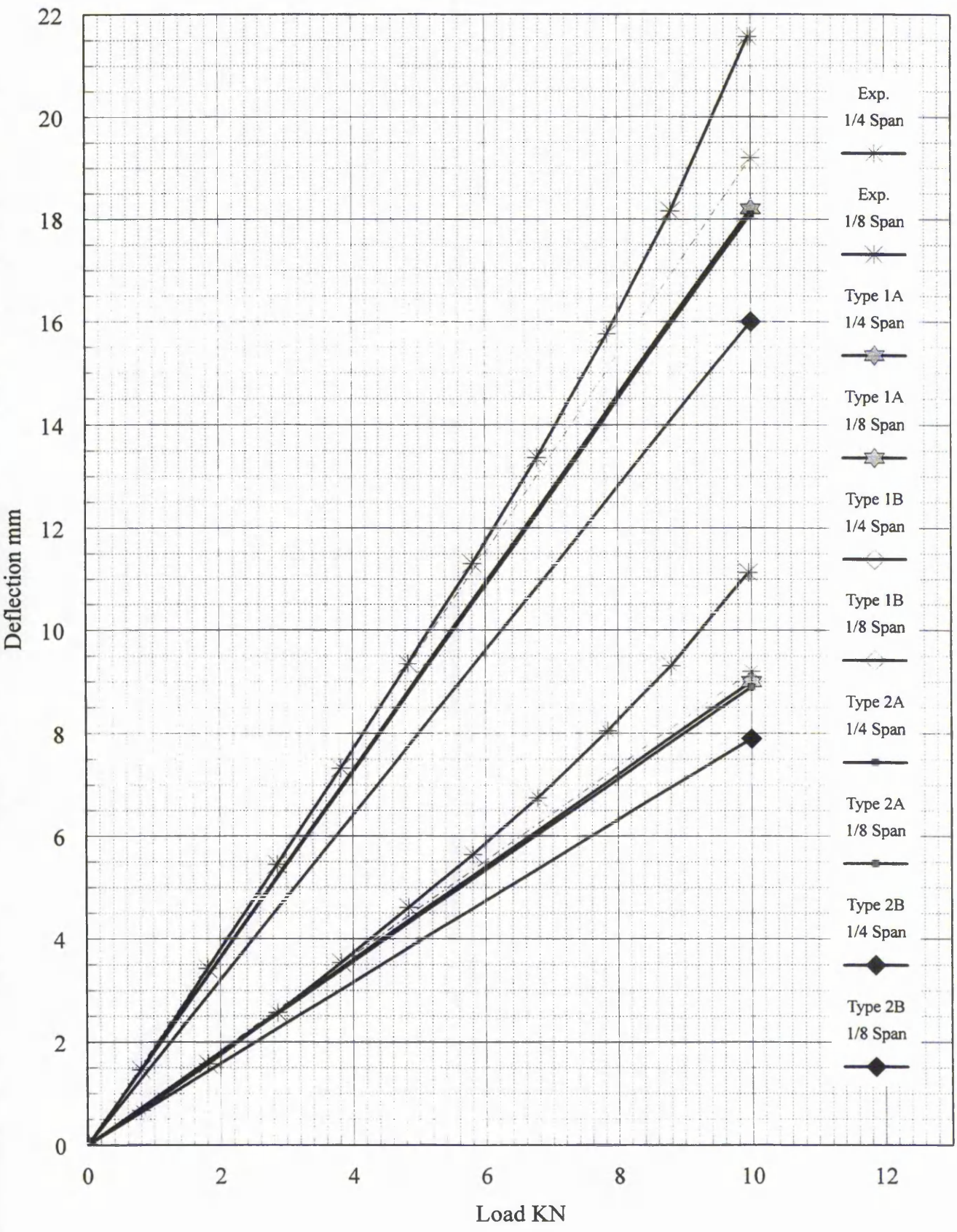

Figure D7.9b Finite element analysis and experimental load versus displacement plots for panel P1

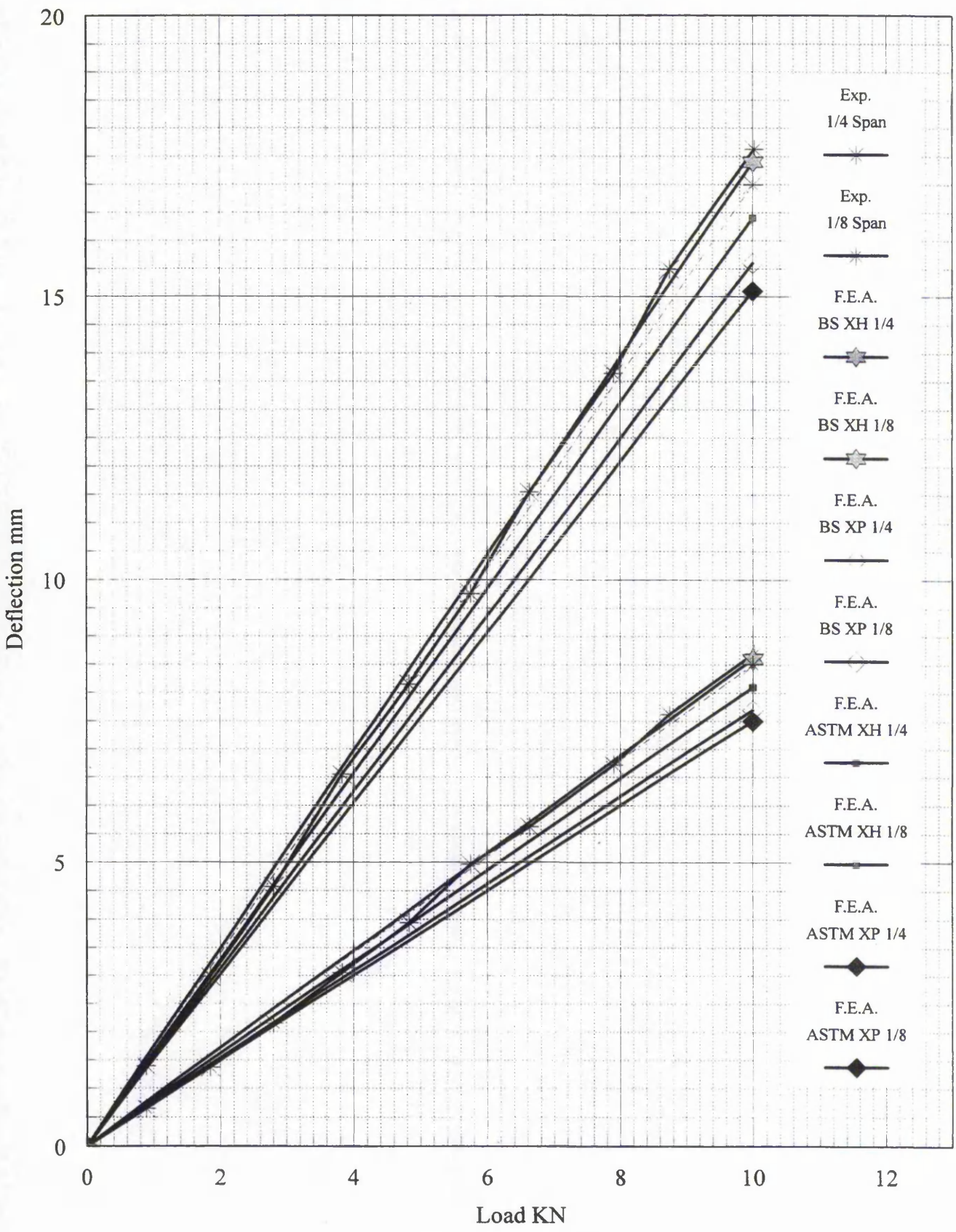

Figure D7.10a Finite element analysis and experimental load versus displacement plots for panel P2

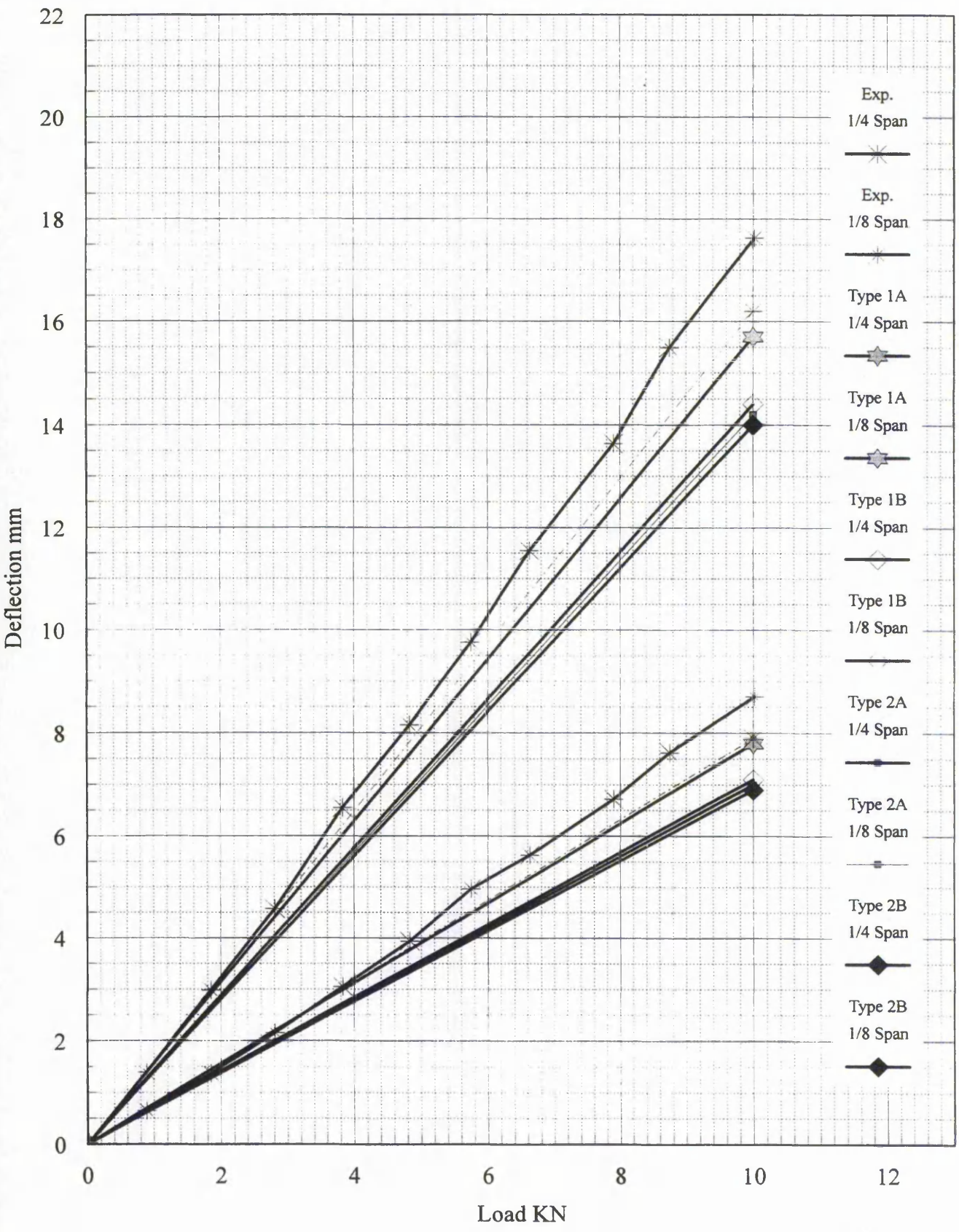

Figure D7.10b Finite element analysis and experimental load versus displacement plots for panel P2

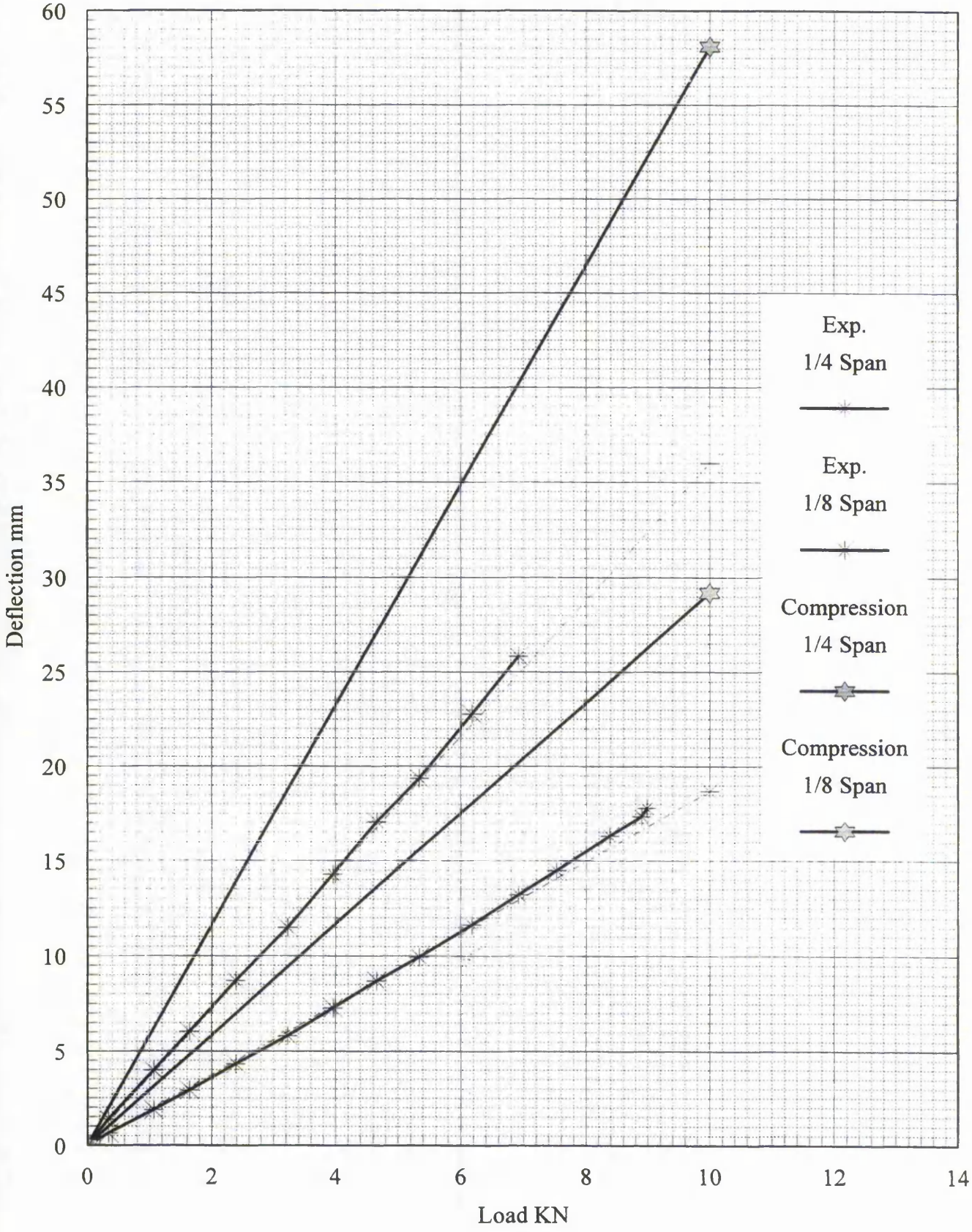

Figure D7.11a Finite element analysis and experimental load versus displacement plots for panel P3

Panel 3 3-Point load test

F.E.A. using shear test results

Temperature 20.1C, Rel. Humidity 52%

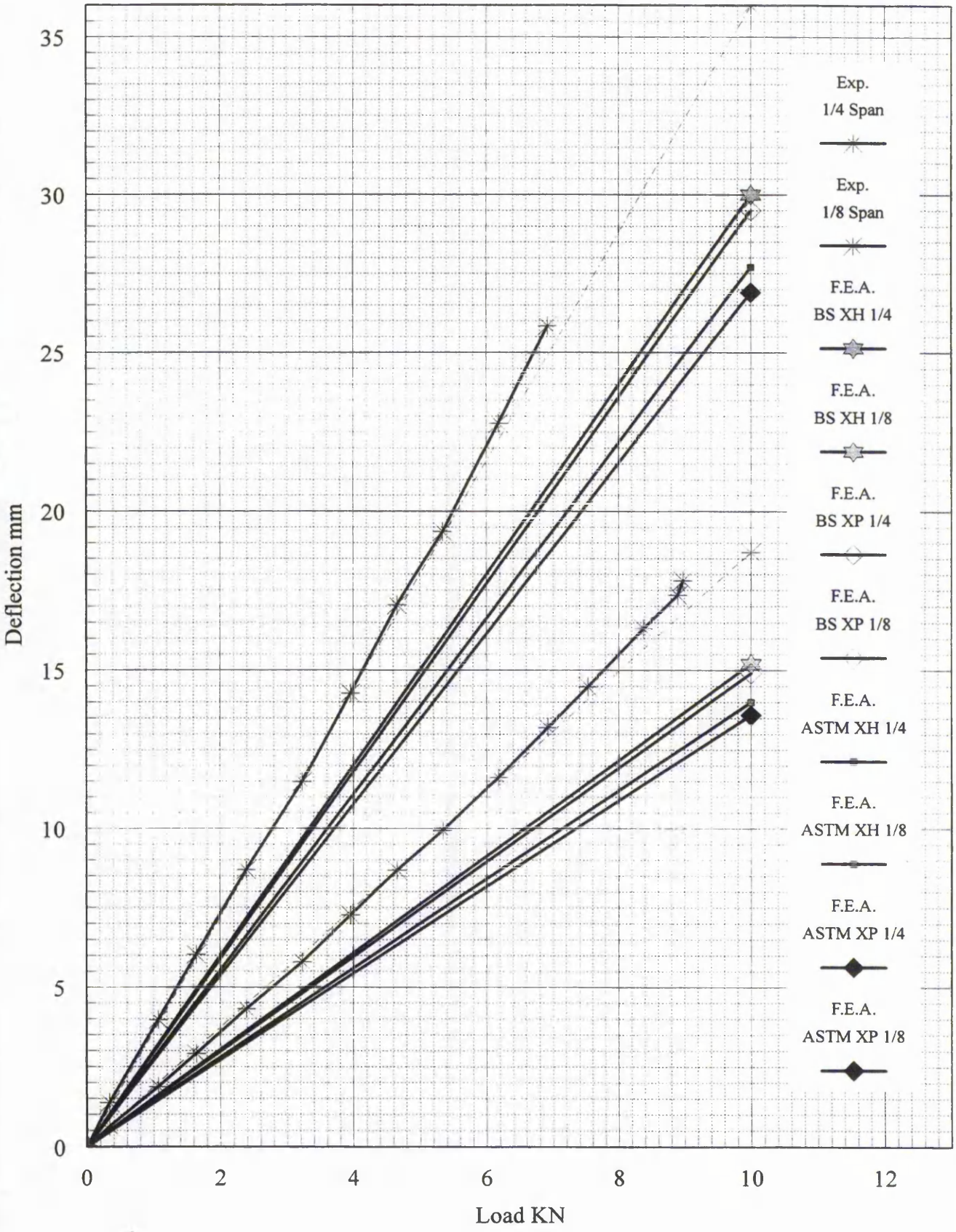

Figure D7.11b Finite element analysis and experimental load versus displacement plots for panel P3

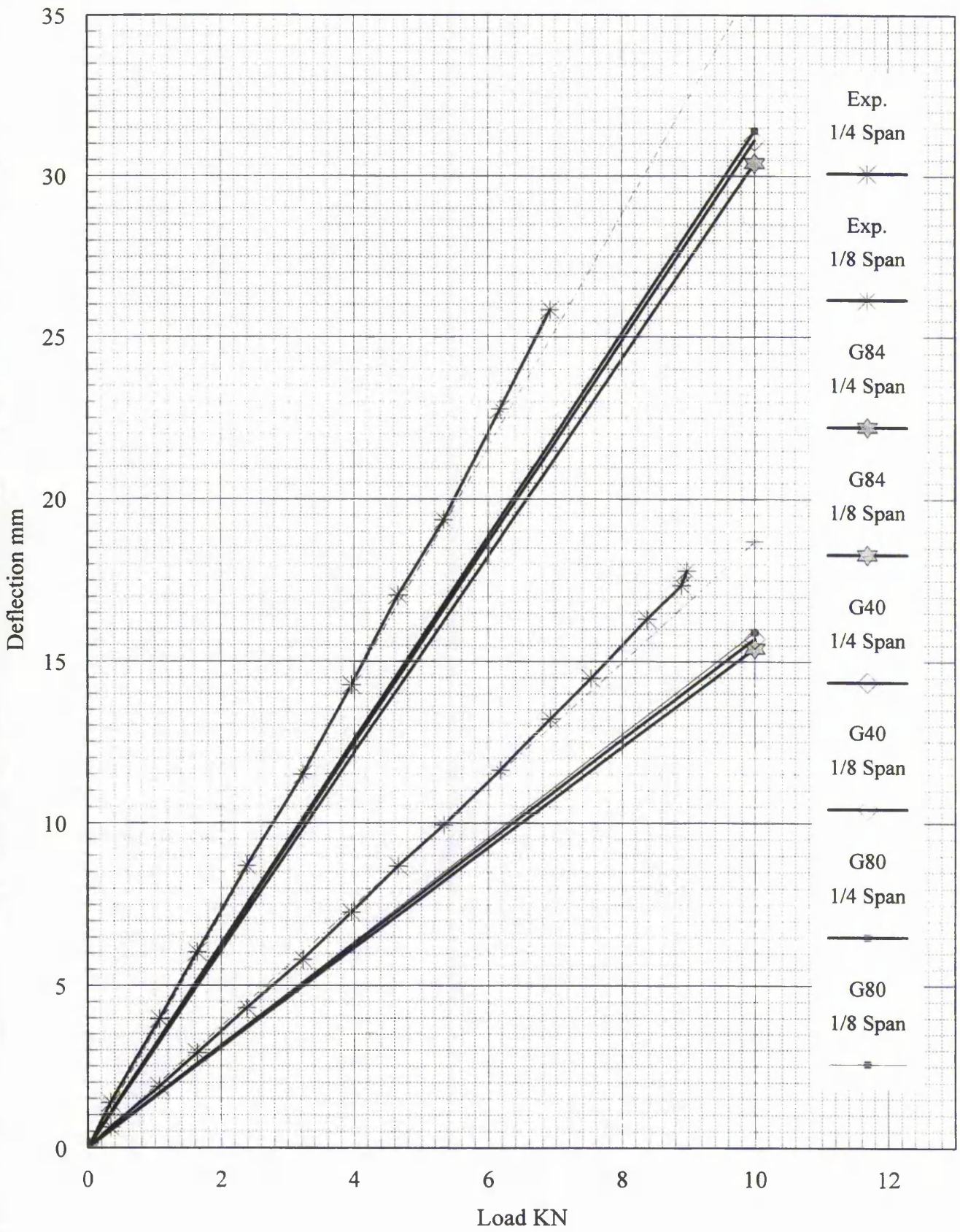

Figure D7.11c Finite element analysis and experimental load versus displacement plots for panel P3

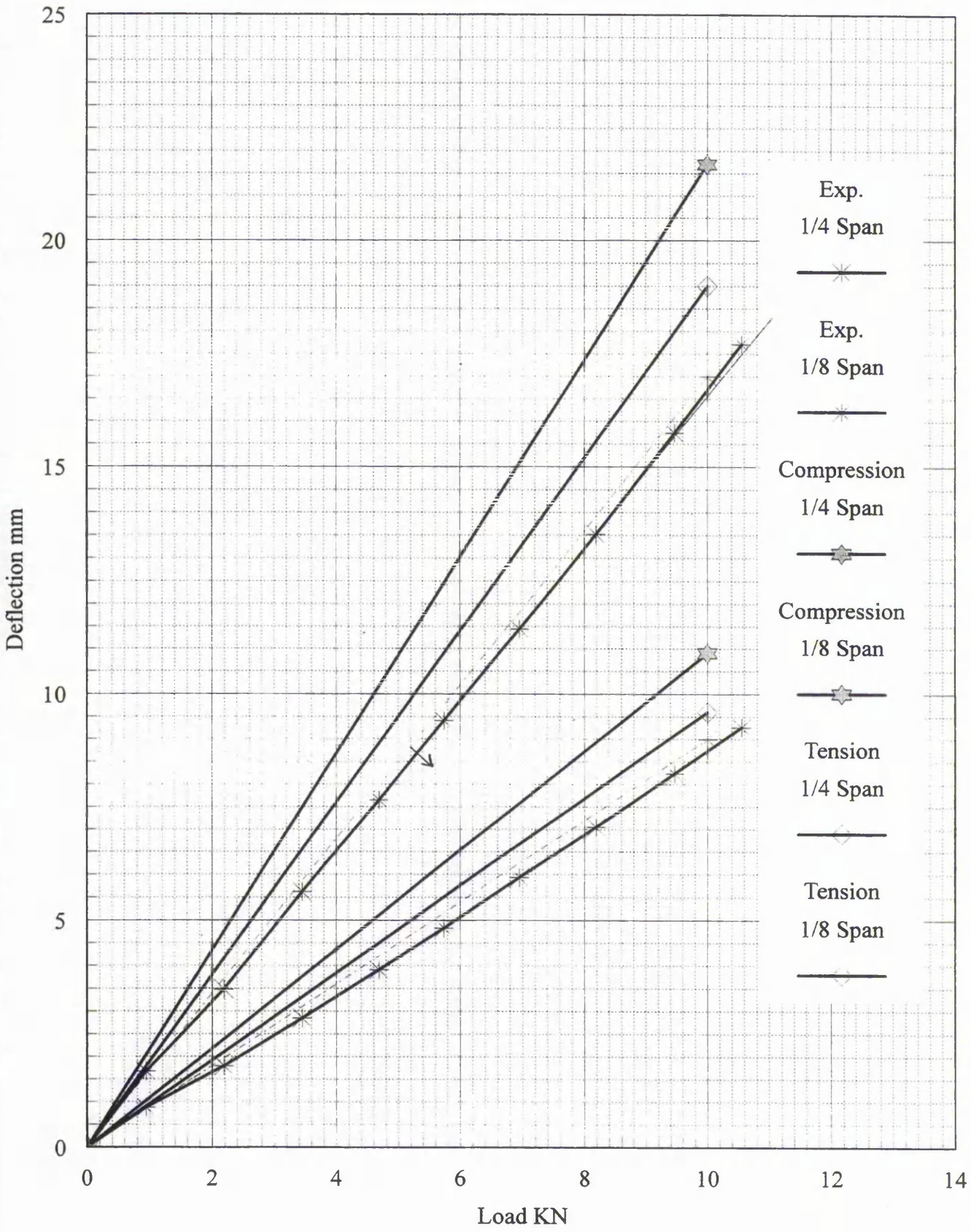

Figure D7.12a Finite element analysis and experimental load versus displacement plots for panel P4

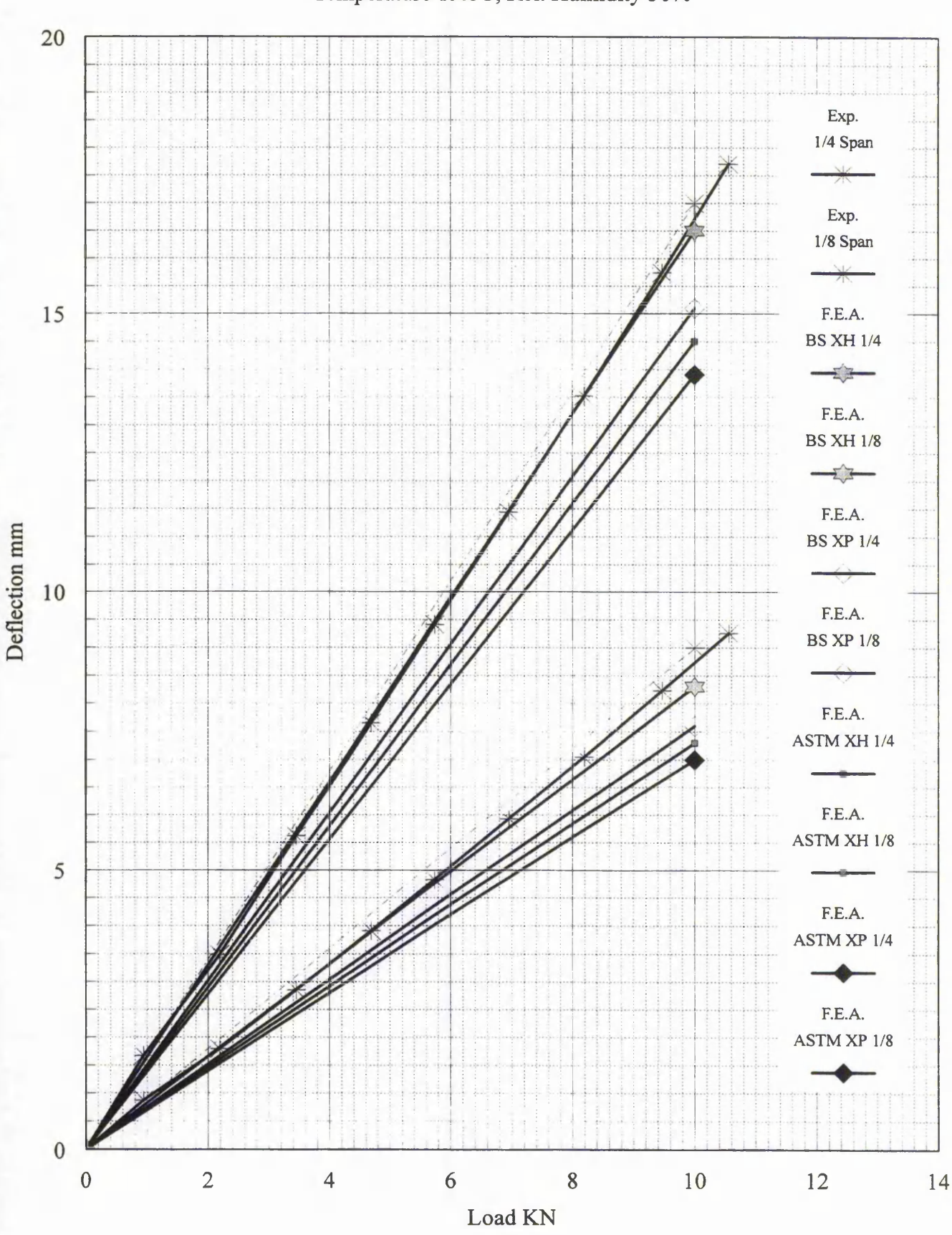

Figure D7.12b Finite element analysis and experimental load versus displacement plots for panel P4

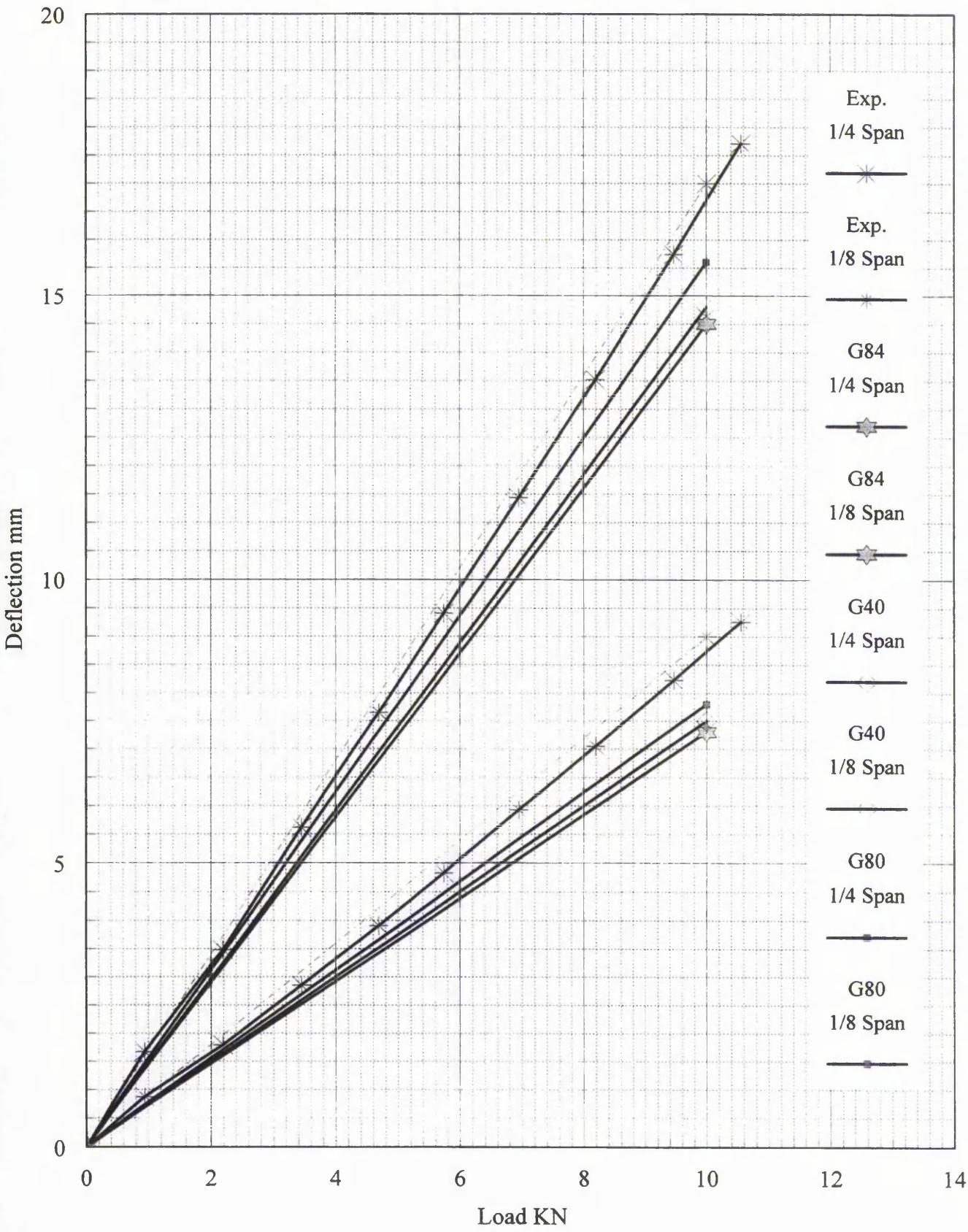

Figure D7.12c Finite element analysis and experimental load versus displacement plots for panel P4

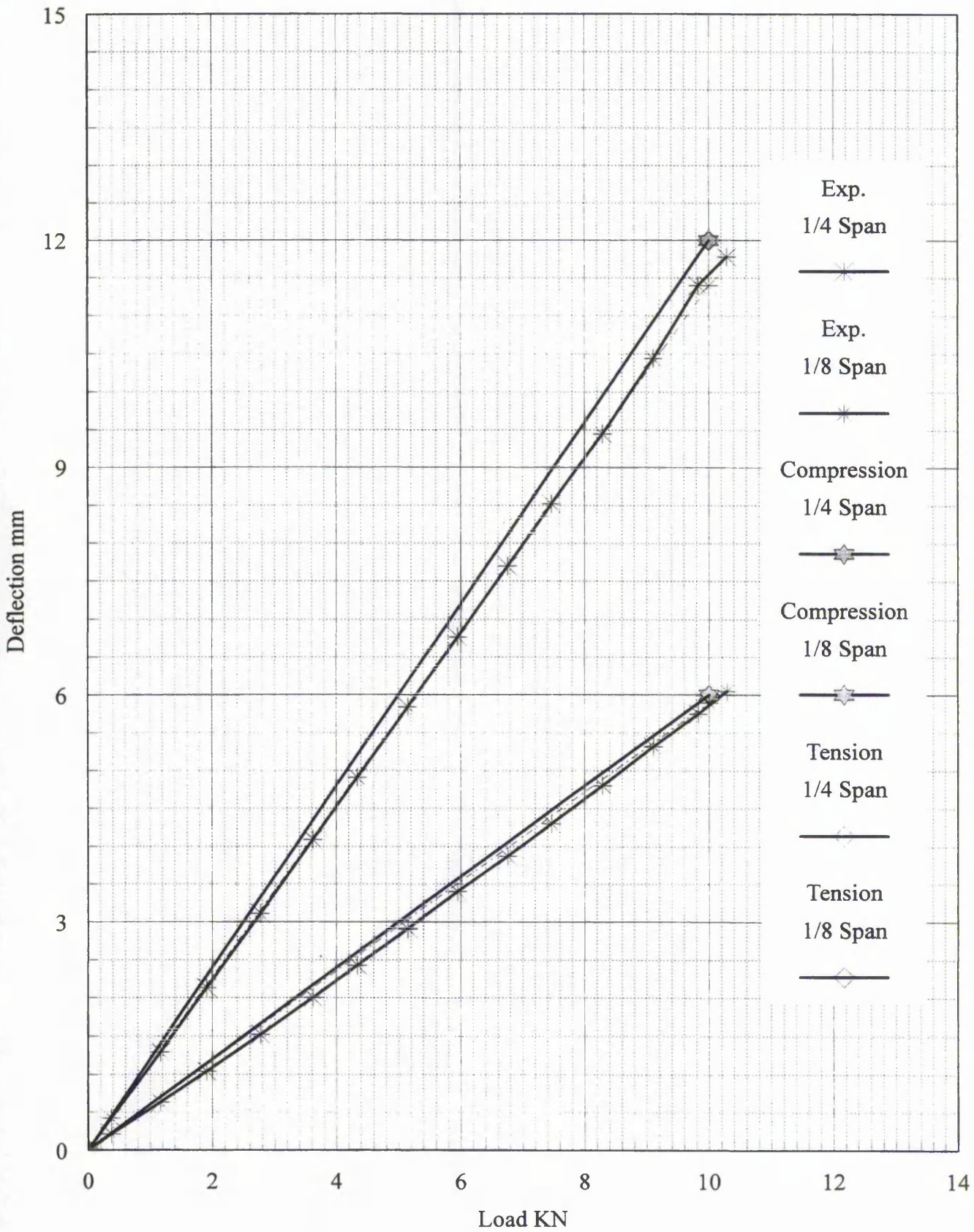

Figure D7.13a Finite element analysis and experimental load versus displacement plots for panel P5

Panel 5 3-Point load test

F.E.A. using shear test results

Temperature 19.1C, Rel. Humidity 49%

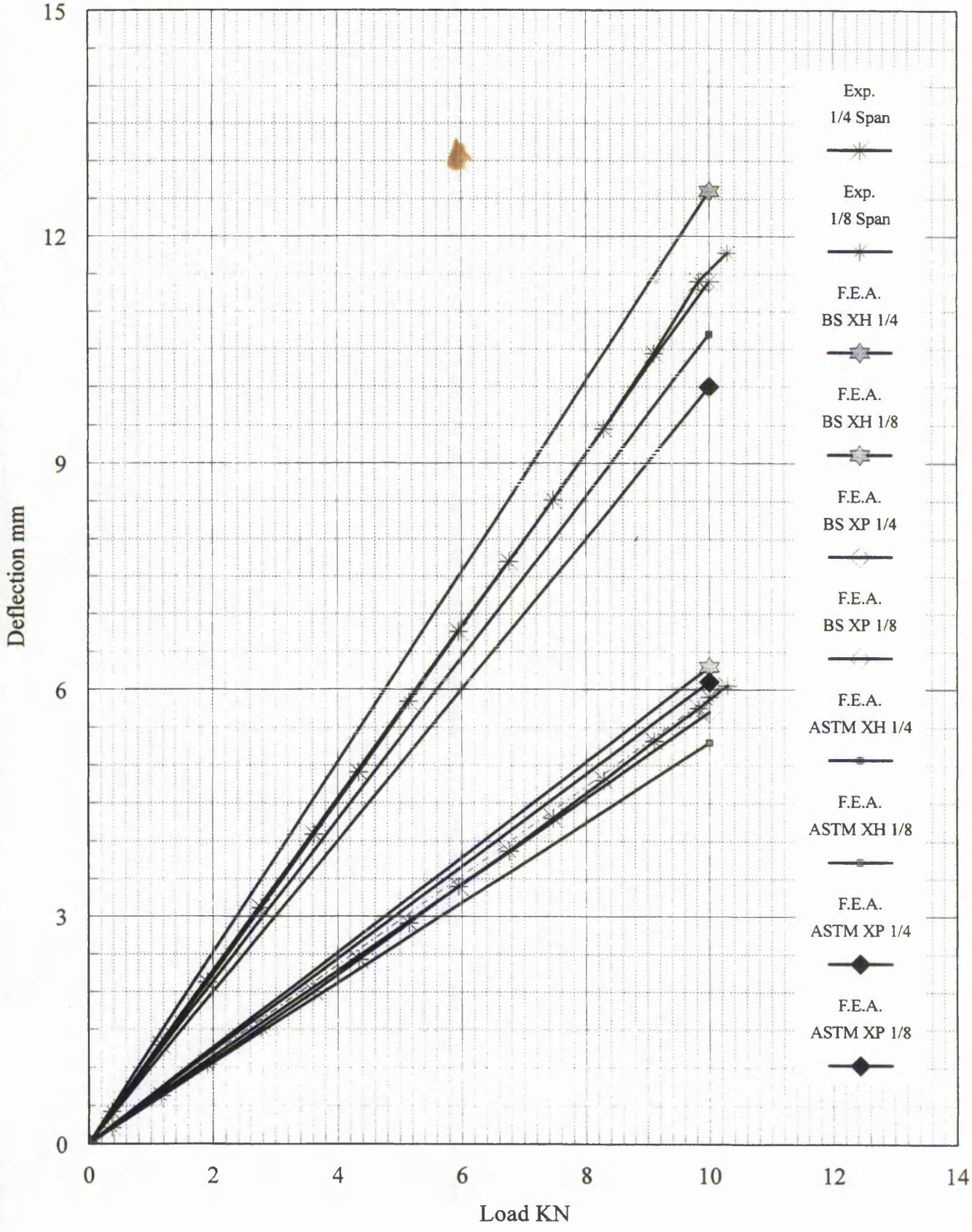

Figure D7.13b Finite element analysis and experimental load versus displacement plots for panel P5

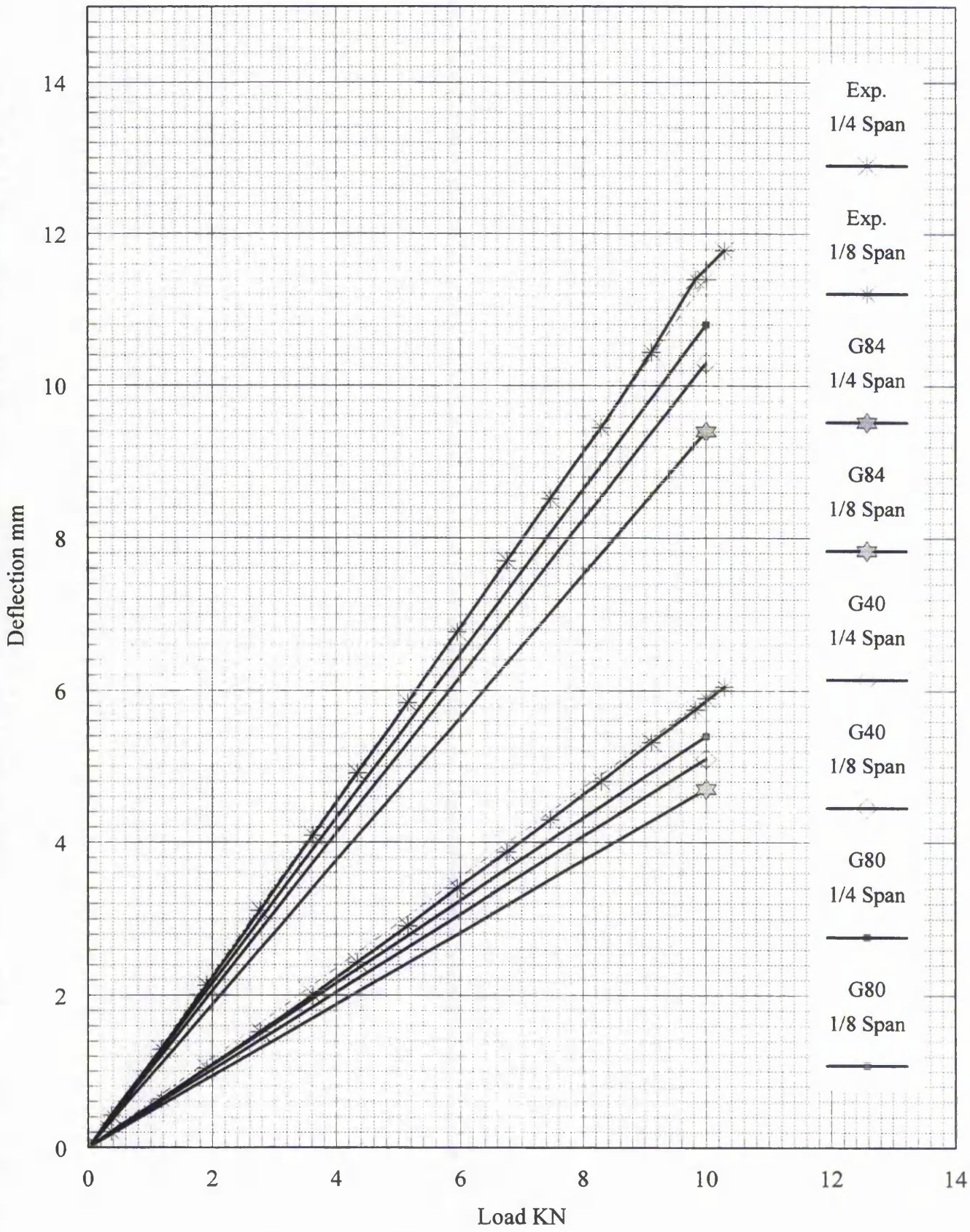

Figure D7.13c Finite element analysis and experimental load versus displacement plots for panel P5

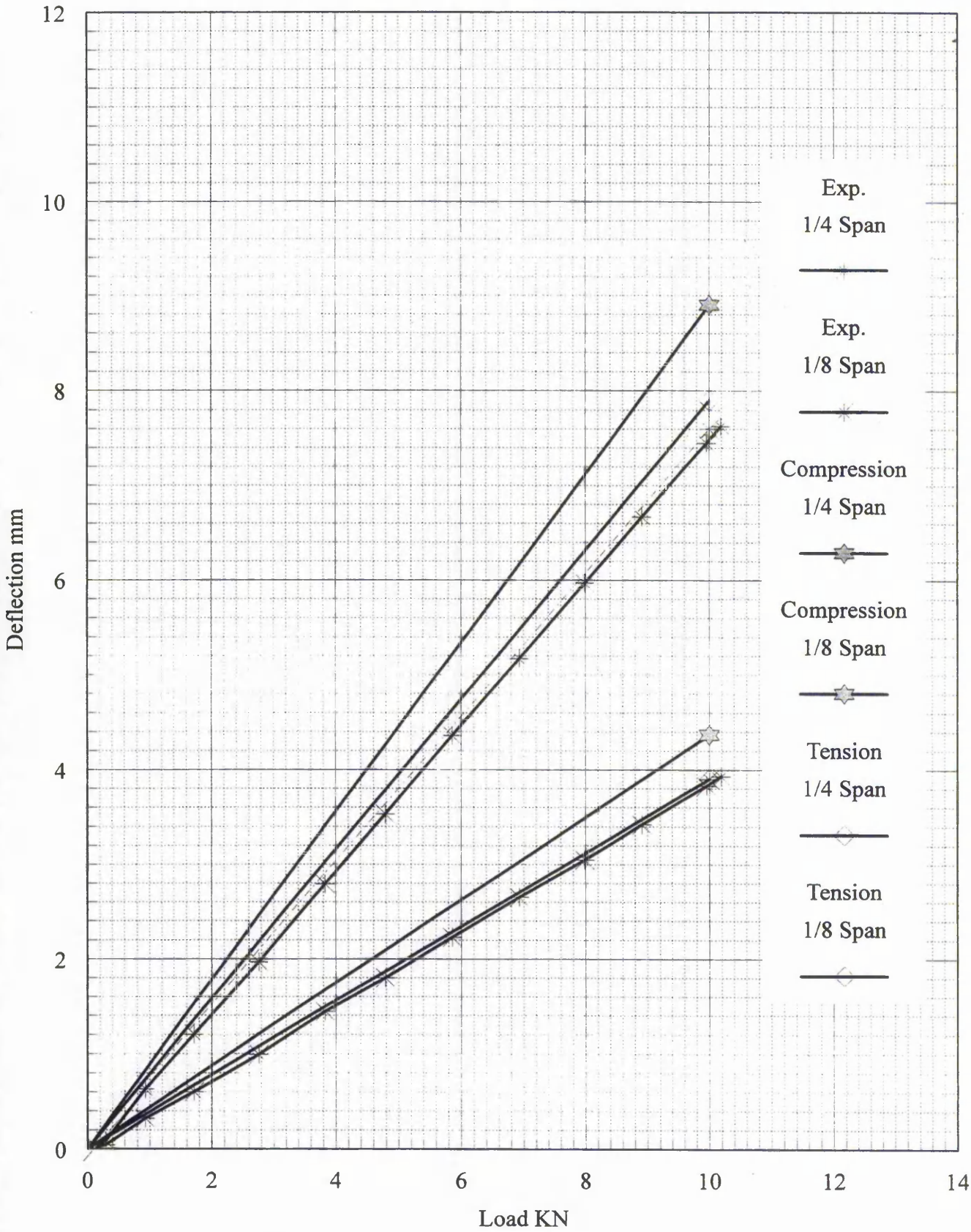

Figure D7.14a Finite element analysis and experimental load versus displacement plots for panel P6

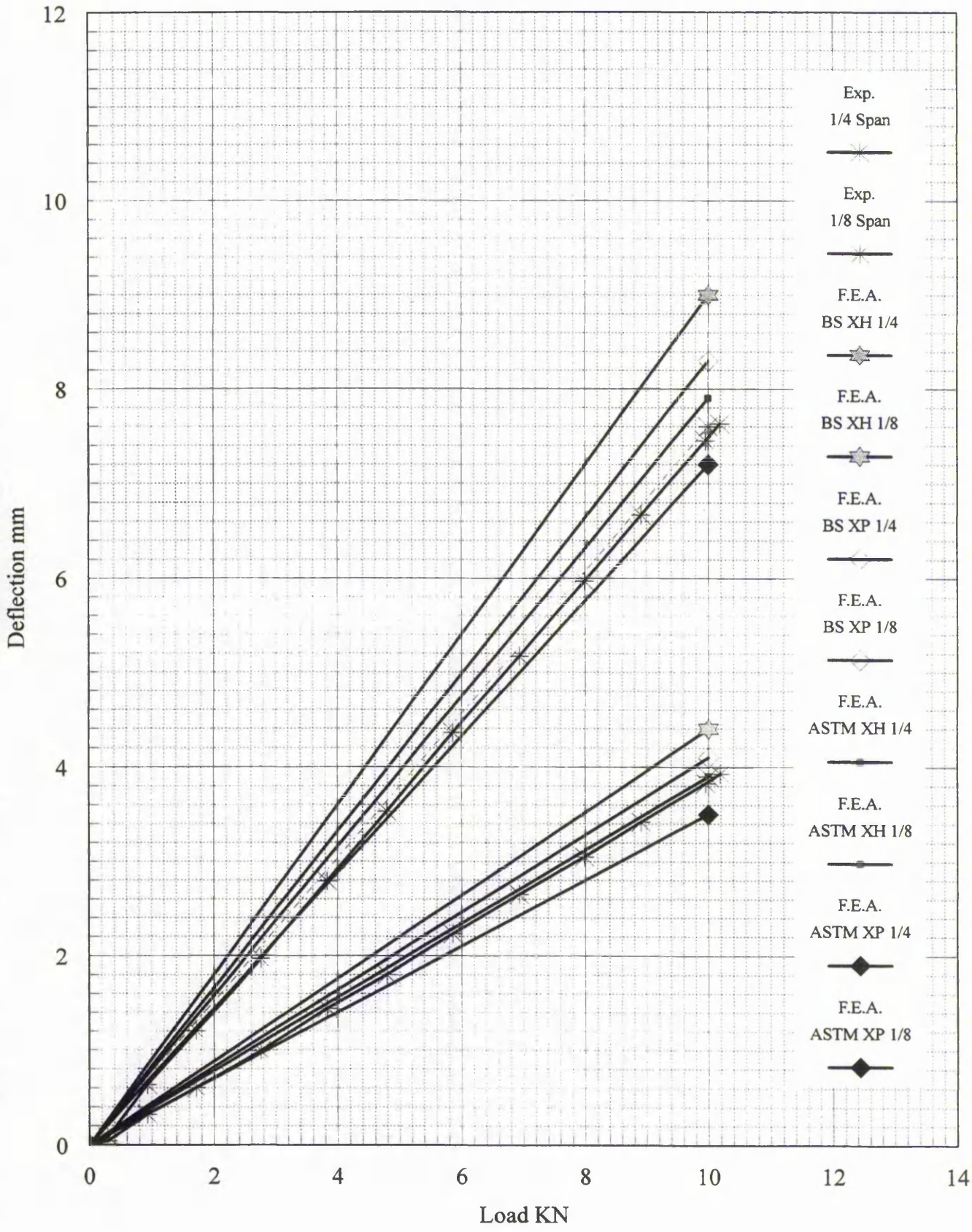

Figure D7.14b Finite element analysis and experimental load versus displacement plots for panel P6

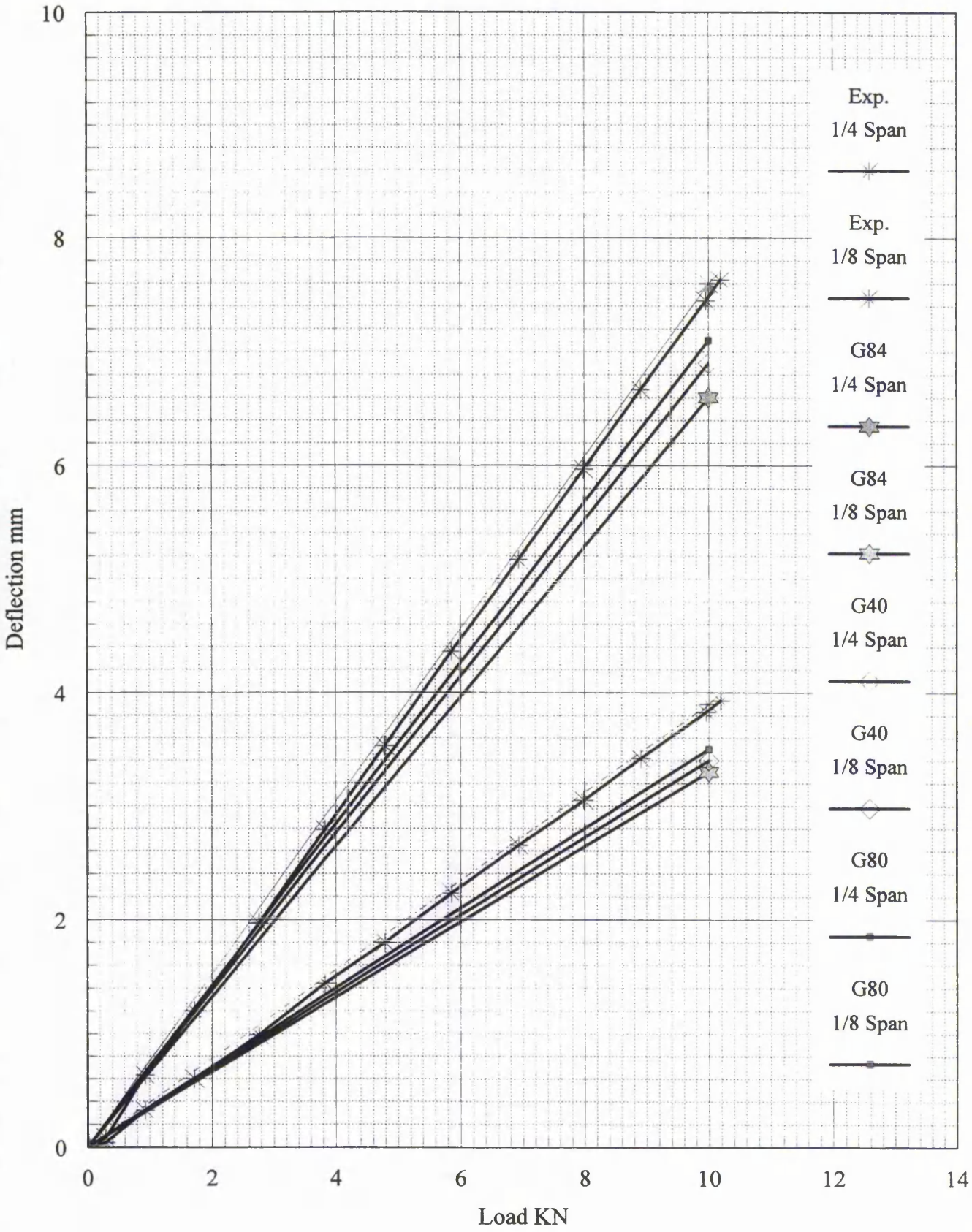

Figure D7.14c Finite element analysis and experimental load versus displacement plots for panel P6

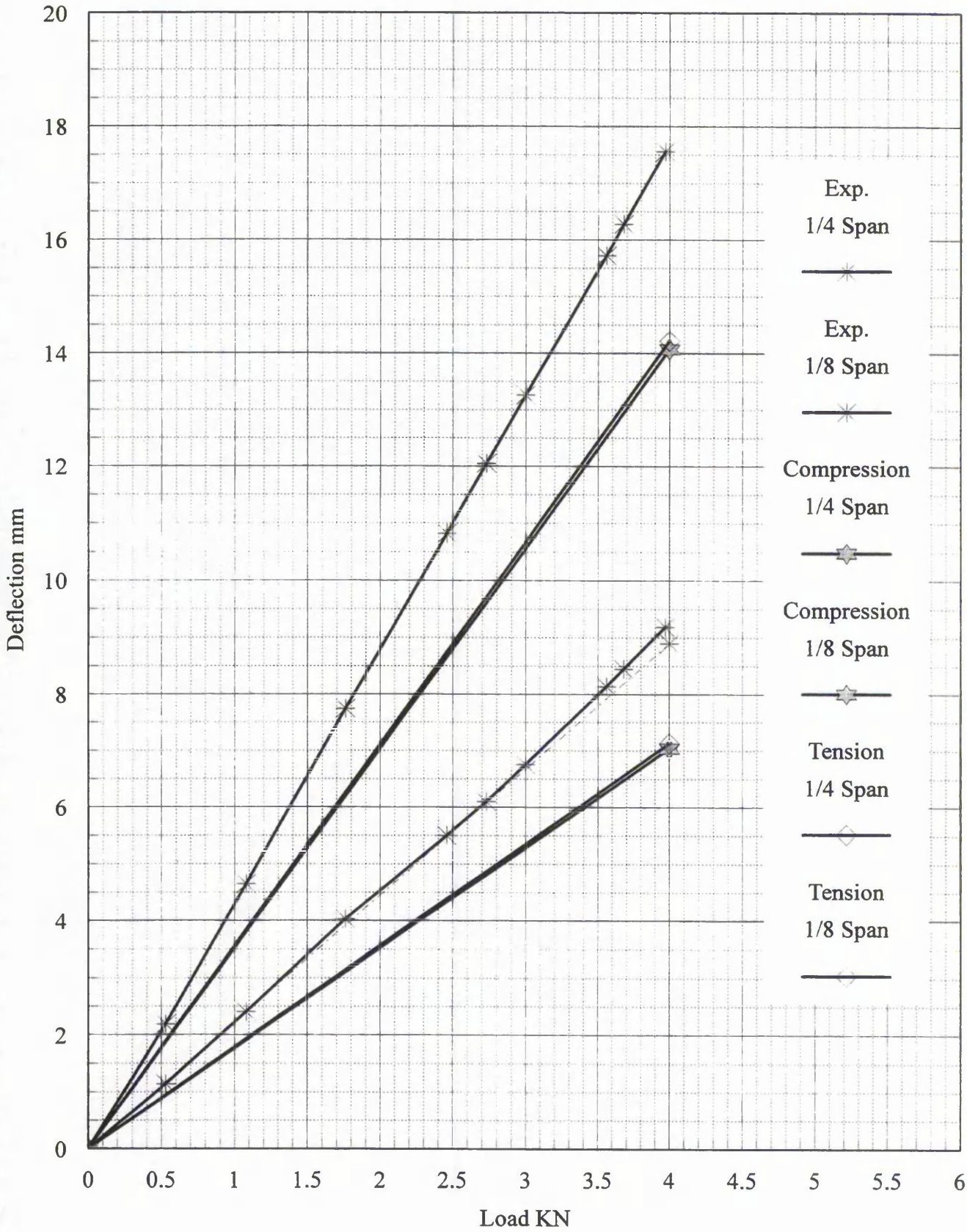

Figure D7.15a Finite element analysis and experimental load versus displacement plots for panel P10

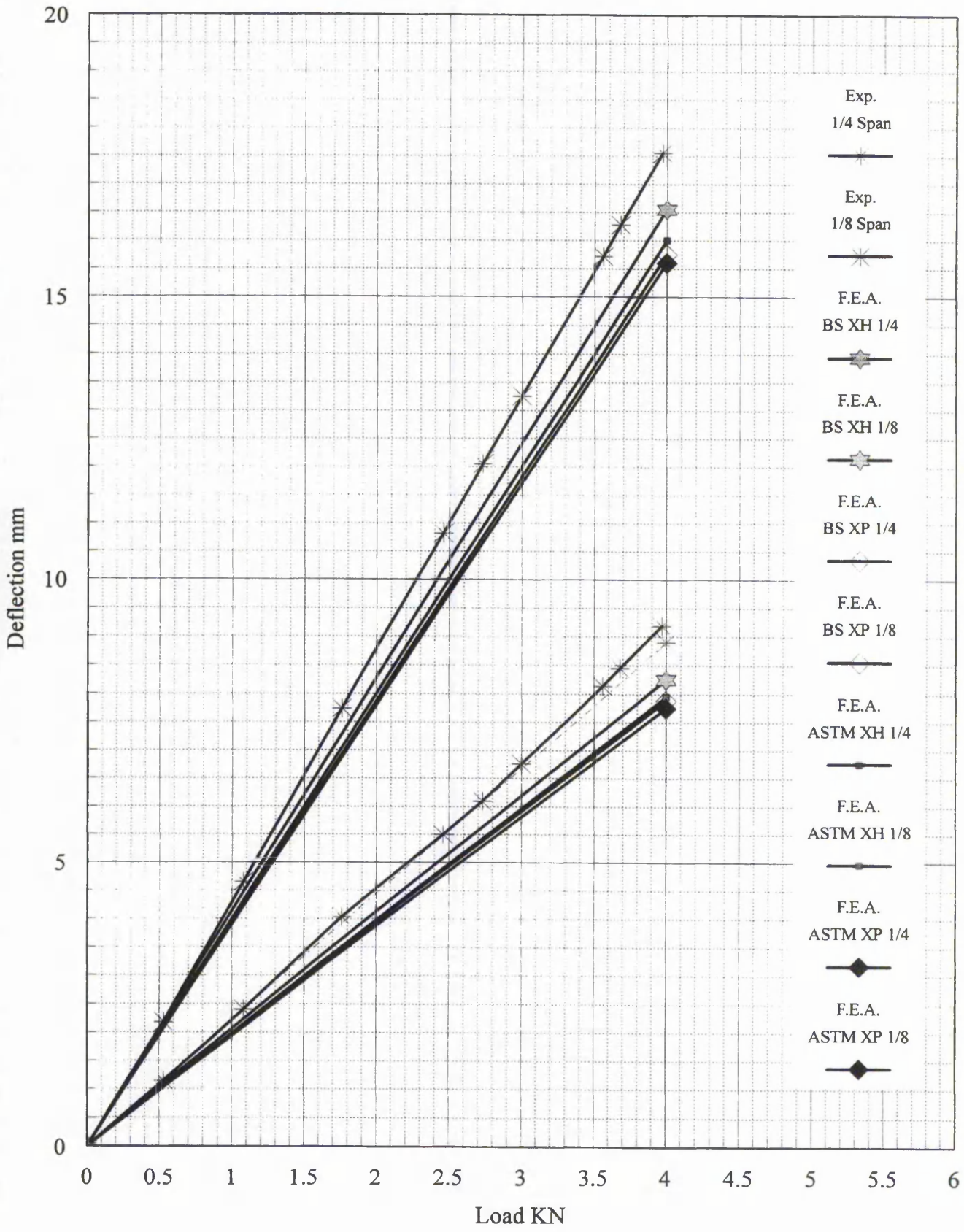

Figure D7.15b Finite element analysis and experimental load versus displacement plots for panel P10

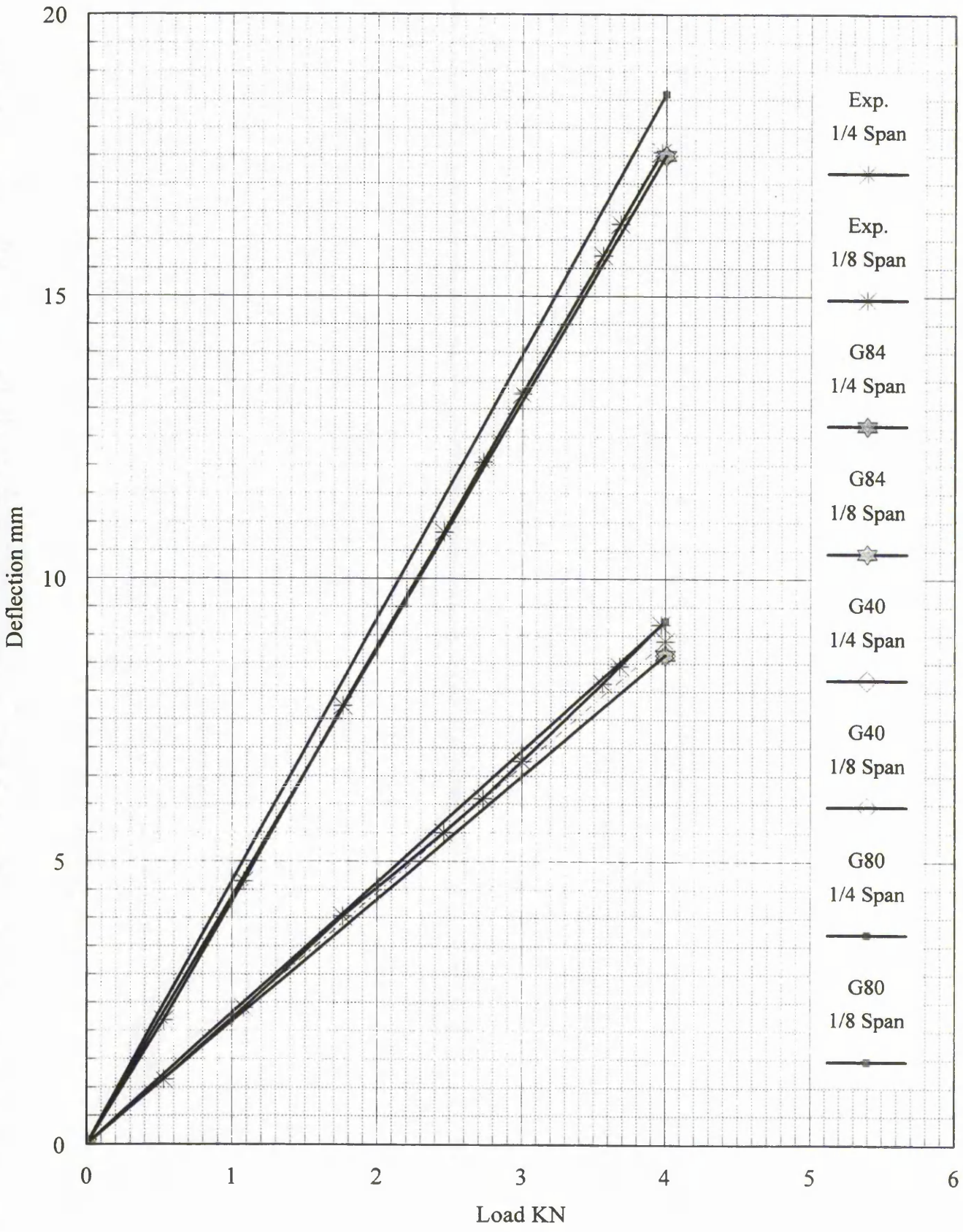

Figure D7.15c Finite element analysis and experimental load versus displacement plots for panel P10

Appendix E

CHAPTER 8

MASONRY WALLETTE AND CONSTITUENT TESTING AND ANALYSIS

Cube desig.	Date made	Date tested	Age at test, days	Ult. load kN	Ultimate strength N/mm2	Elastic modulus N/mm2	Poisson's ratio, X-dir	Poisson's ratio, Y-dir
CW1AL 1	31.07.95	19.11.95	111	141		2870	0.15	0.19
2	31.07.95	19.11.95	111	146				
3	31.07.95	19.11.95	111	150				
4	31.07.95	19.11.95	111	139				
5	31.07.95	19.11.95	111	146				
6	31.07.95	19.11.95	111	142	14.4			
CW1BL 1	01.08.95	19.11.95	110	139				
2	01.08.95	19.11.95	110	139		2626	0.20	0.32
3	01.08.95	19.11.95	110	148				
4	01.08.95	19.11.95	110	147				
5	01.08.95	19.11.95	110	142				
6	01.08.95	19.11.95	110	143	14.3			
CW1AU 1	07.08.95	19.11.95	104	136				
2	07.08.95	19.11.95	104	137				
3	07.08.95	19.11.95	104	145		2665	0.19	0.29
4	07.08.95	19.11.95	104	147				
5	07.08.95	19.11.95	104	128				
6	07.08.95	19.11.95	104	128	13.7			
CW1BU 1	08.08.95	19.11.95	103	146				
2	08.08.95	19.11.95	103	155				
3	08.08.95	19.11.95	103	129				
4	08.08.95	19.11.95	103	147		2400	0.22	0.34
5	08.08.95	19.11.95	103	130				
6	08.08.95	19.11.95	103	134				
CW2AL 1	02.08.95	19.11.95	109	137	14.0			
2	02.08.95	19.11.95	109	157				
3	02.08.95	19.11.95	109	154				
4	02.08.95	19.11.95	109	137				
5	02.08.95	19.11.95	109	155		2300	0.17	0.22
6	02.08.95	19.11.95	109	161	15.0			
CW2BL 1	03.08.95	19.11.95	108	129				
2	03.08.95	19.11.95	108	129				
3	03.08.95	19.11.95	108	134				
4	03.08.95	19.11.95	108	143				
5	03.08.95	19.11.95	108	118				
6	03.08.95	19.11.95	108	140	13.2	2609	0.19	0.27

Table E8.1a Mortar cube uniaxial compression test and analysis data

Cube desig.	Date made	Date tested	Age at test, days	Ult load kN	Ultimate strength N/mm^2	Elastic modulus N/mm^2	Poisson's ratio, X-dir	Poisson's ratio, Y-dir
CW2AU 1	09.08.95	24.11.95	107	141		2450	0.16	0.26
2	09.08.95	24.11.95	107	127				
3	09.08.95	24.11.95	107	135				
4	09.08.95	24.11.95	107	132				
5	09.08.95	24.11.95	107	138				
6	09.08.95	24.11.95	107	136	13.5			
CW2BU 1	10.08.95	24.11.95	106	136		2271	0.15	0.29
2	10.08.95	24.11.95	106	145				
3	10.08.95	24.11.95	106	141				
4	10.08.95	24.11.95	106	138				
5	10.08.95	24.11.95	106	140				
6	10.08.95	24.11.95	106	142	14.0			
CW3AL 1	03.08.95	24.11.95	114	136				
2	03.08.95	24.11.95	114	149				
3	03.08.95	24.11.95	114	151		2374	0.18	0.24
4	03.08.95	24.11.95	114	150				
5	03.08.95	24.11.95	114	145				
6	03.08.95	24.11.95	114	151	14.7			
CW3BL 1	04.08.95	24.11.95	113	124				
2	04.08.95	24.11.95	113	133				
3	04.08.95	24.11.95	113	147				
4	04.08.95	24.11.95	113	130		2655	0.29	0.40
5	04.08.95	24.11.95	113	134				
6	04.08.95	24.11.95	113	136	13.4			
CW3AU 1	16.08.95	24.11.95	100	130				
2	16.08.95	24.11.95	100	148				
3	16.08.95	24.11.95	100	147				
4	16.08.95	24.11.95	100	136				
5	16.08.95	24.11.95	100	145		2319	0.16	0.21
6	16.08.95	24.11.95	100	138	14.1			
CW3BU 1	18.08.95	24.11.95	98	129				
2	18.08.95	24.11.95	98	133				
3	18.08.95	24.11.95	98	132				
4	18.08.95	24.11.95	98	134				
5	18.08.95	24.11.95	98	129				
6	18.08.95	24.11.95	98	136	13.2	2483	0.22	0.32

Table E8.1b Mortar cube uniaxial compression test and analysis data

Wallette	Failure joint	Failure load kN	Max. disp. mm	E_R N/mm^2	Compressive strain at failure joint με	Tensile strain at failure joint με
1	5	3.0	0.114	5100	-91	600
2	6	8.8	0.138	6600	-62	110
3	3	4.7	0.246	1200	-125	330
4	5	9.2	0.135	5500	-60	114
5	4	4.0	0.162	3100	-74	895
6	5/6	6.5	0.101	8300	-90	589
7	5	8.0	0.104	7900	-46	127
8	5	6.9	0.093	9400	-83	310
9	4/5	7.7	0.195	5100	-146	791
10	4	6.4	0.163	3500	-76	253
11	5	7.2	0.154	4700	-67	143
12	4	6.3	0.075	5200	N/A	38
Mean		6.6		5500		
S.D.*		1.8		2000		

* Standard deviation

Table E8.2 Wallette test data

Wallette	Date built	Test date	Span, L mm	Ixx x 10^6 mm^4	P/δ x10^3 N/mm	E_R N/mm^2	Failure load kN
1	31.07.95	21.02.96	675	79.9	63	5100	3.0
2	07.08.95	21.02.96	675	79.9	83	6600	8.8
3	01.08.95	23.02.96	675	79.9	16	1200	4.7
4	08.08.95	23.02.96	675	79.9	68	5500	9.2
5	02.08.95	04.12.95	675	79.9	39	3100	4.0
6	09.08.95	04.12.95	675	79.9	104	8300	6.5
7	03.08.95	06.12.95	675	79.9	98	7900	8.0
8	10.08.95	06.12.95	675	79.9	118	9400	6.9
9	03.08.95	12.12.95	675	79.9	64	5100	7.7
10	16.08.95	12.12.95	675	79.9	44	3500	6.4
11	04.08.95	13.12.95	675	79.9	59	4700	7.2
12	18.08.95	13.12.95	675	79.9	65	5200	6.3
					Average	5500	

Table E8.3 Wallette test and analysis data

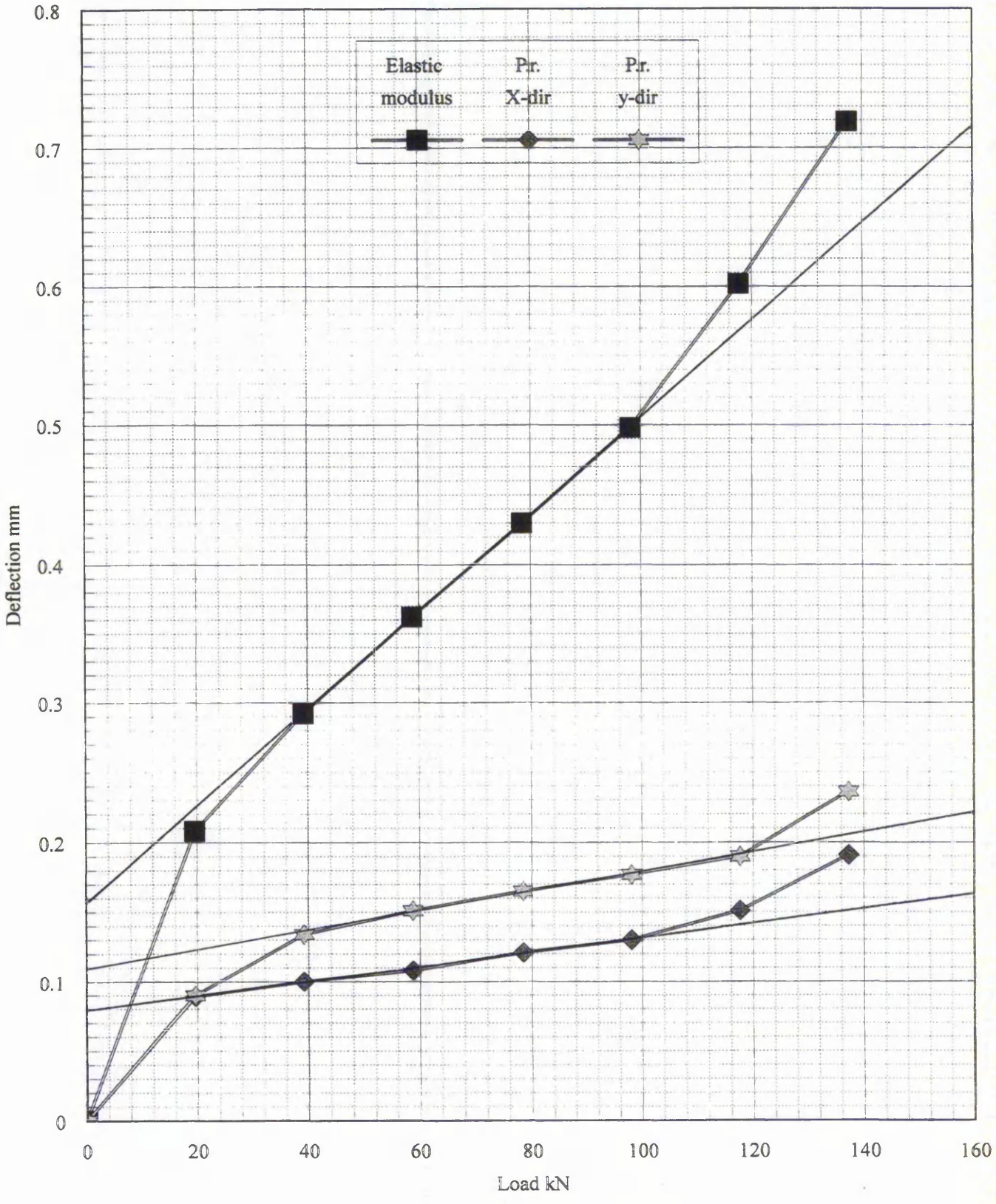

Figure E8.1 Load versus displacement relationship for a mortar compression cube

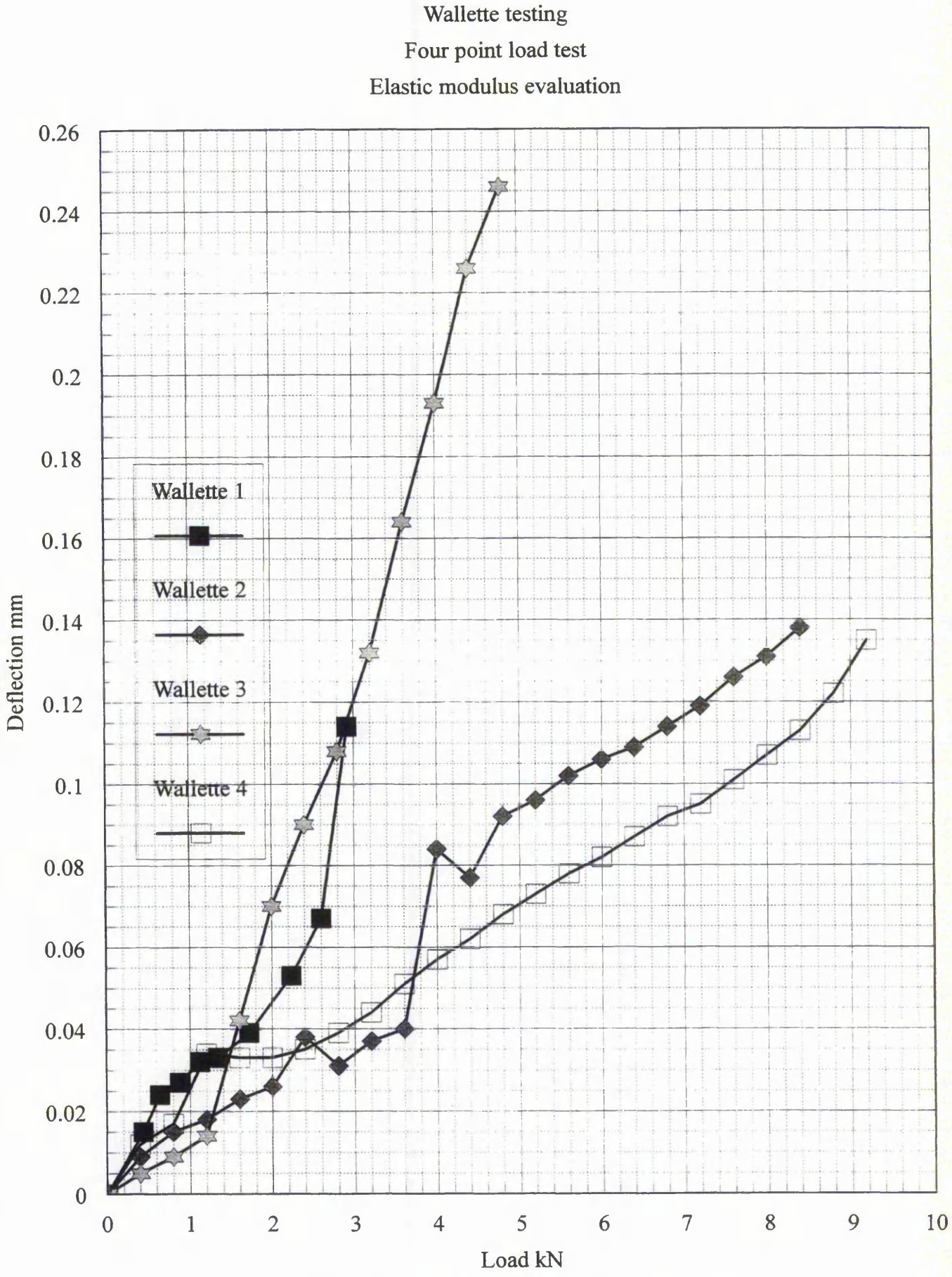

Figure E8.2 Total lateral load versus mid height displacement for wallettes 1 to 4

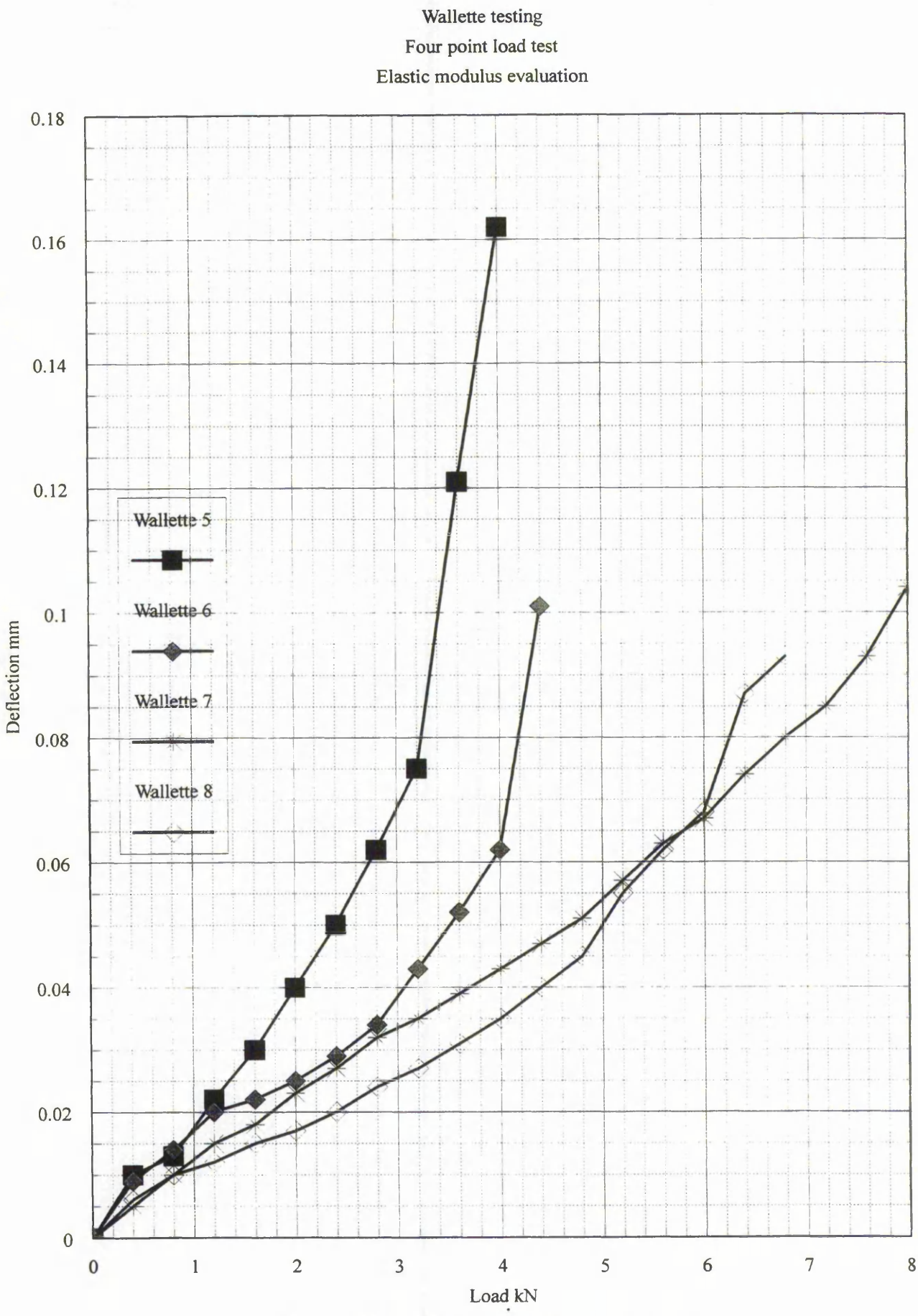

Figure E8.3 Total lateral load versus mid height displacement for wallettes 5 to 8

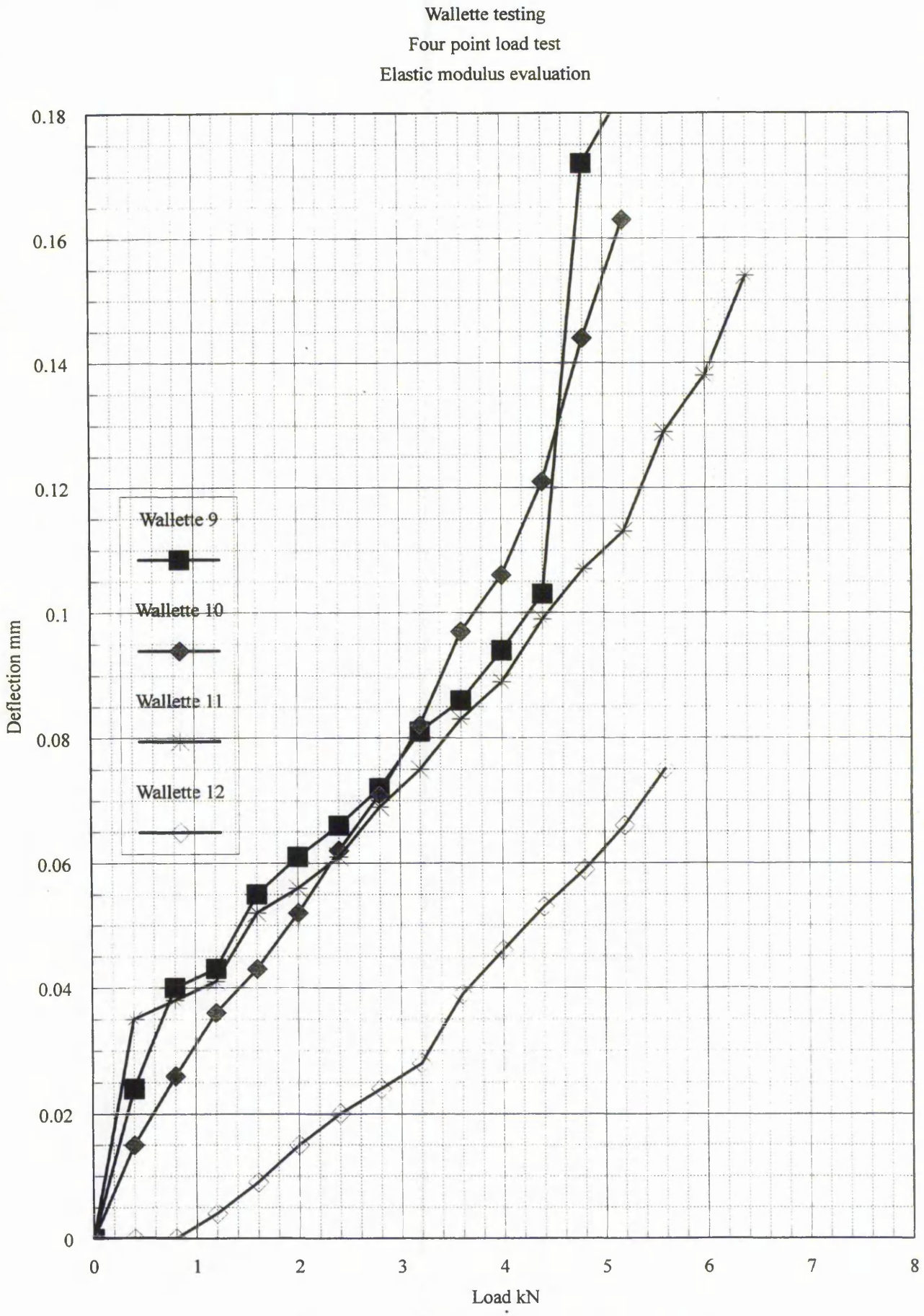

Figure E8.4 Total lateral load versus mid height displacement for wallettes 9 to 12

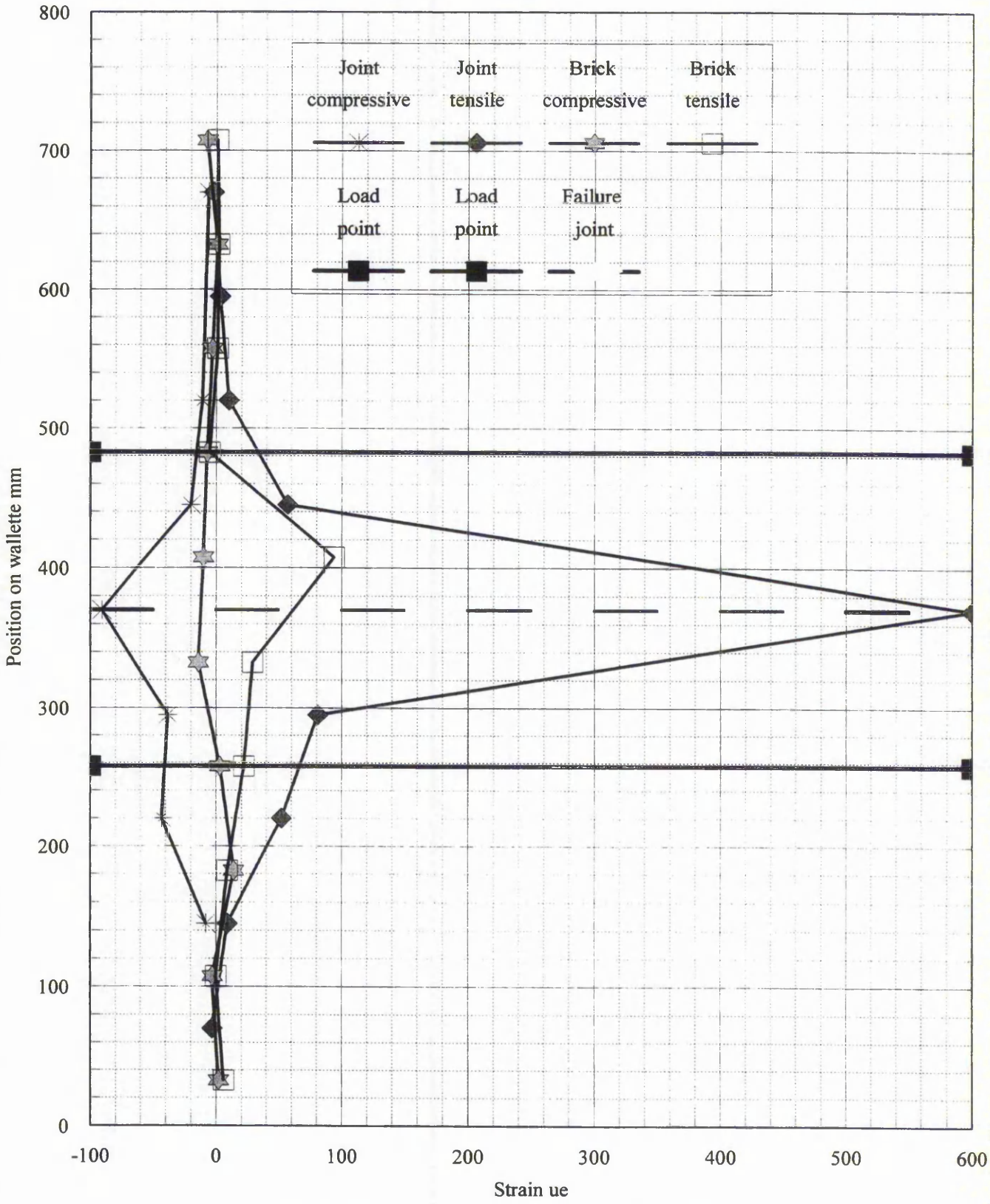

Figure E8.5 Strain profiles on loaded and support faces across joint just prior to failure for wallette 1

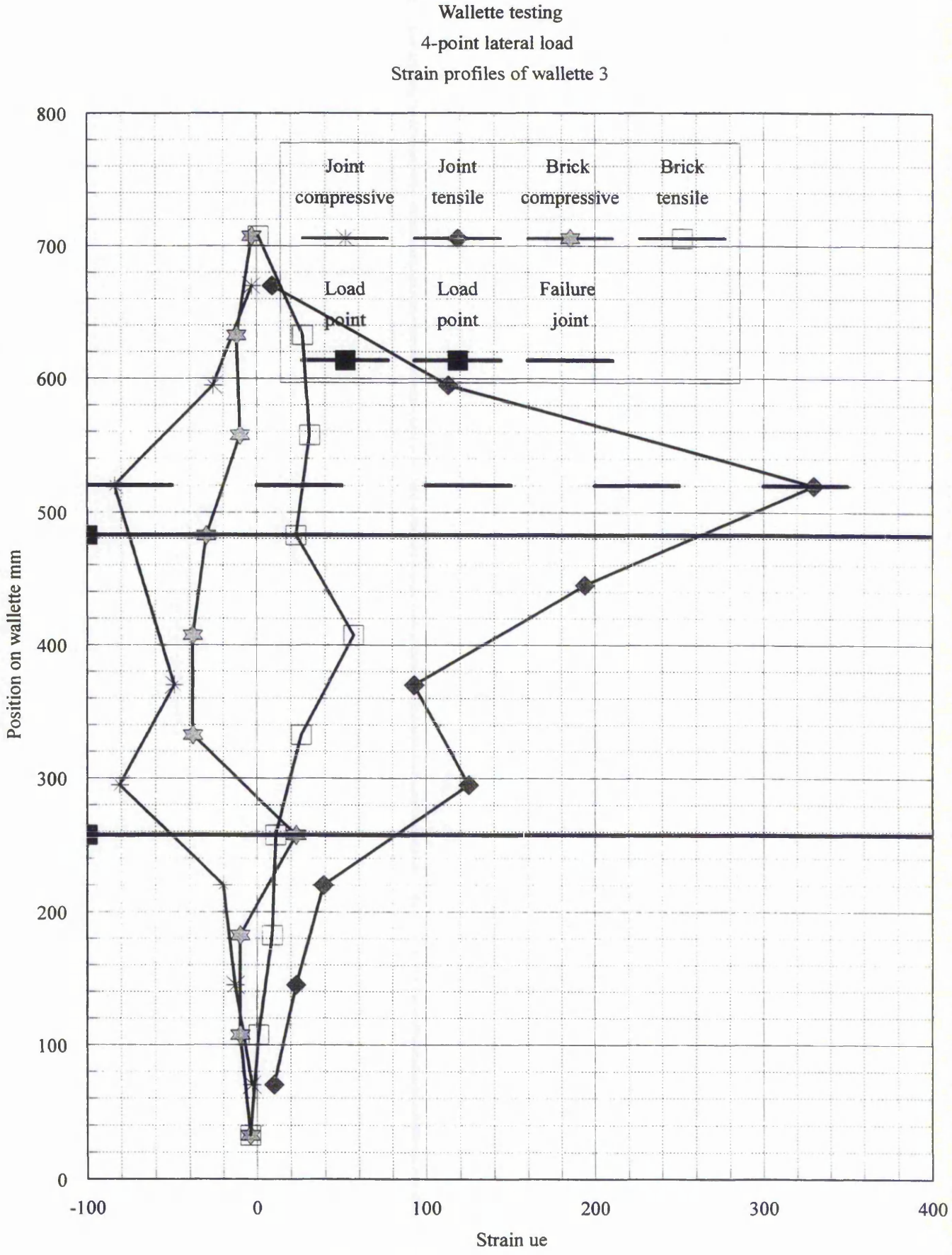

Figure E8.6 Strain profiles on loaded and support faces across joint just prior to failure for wallette 3

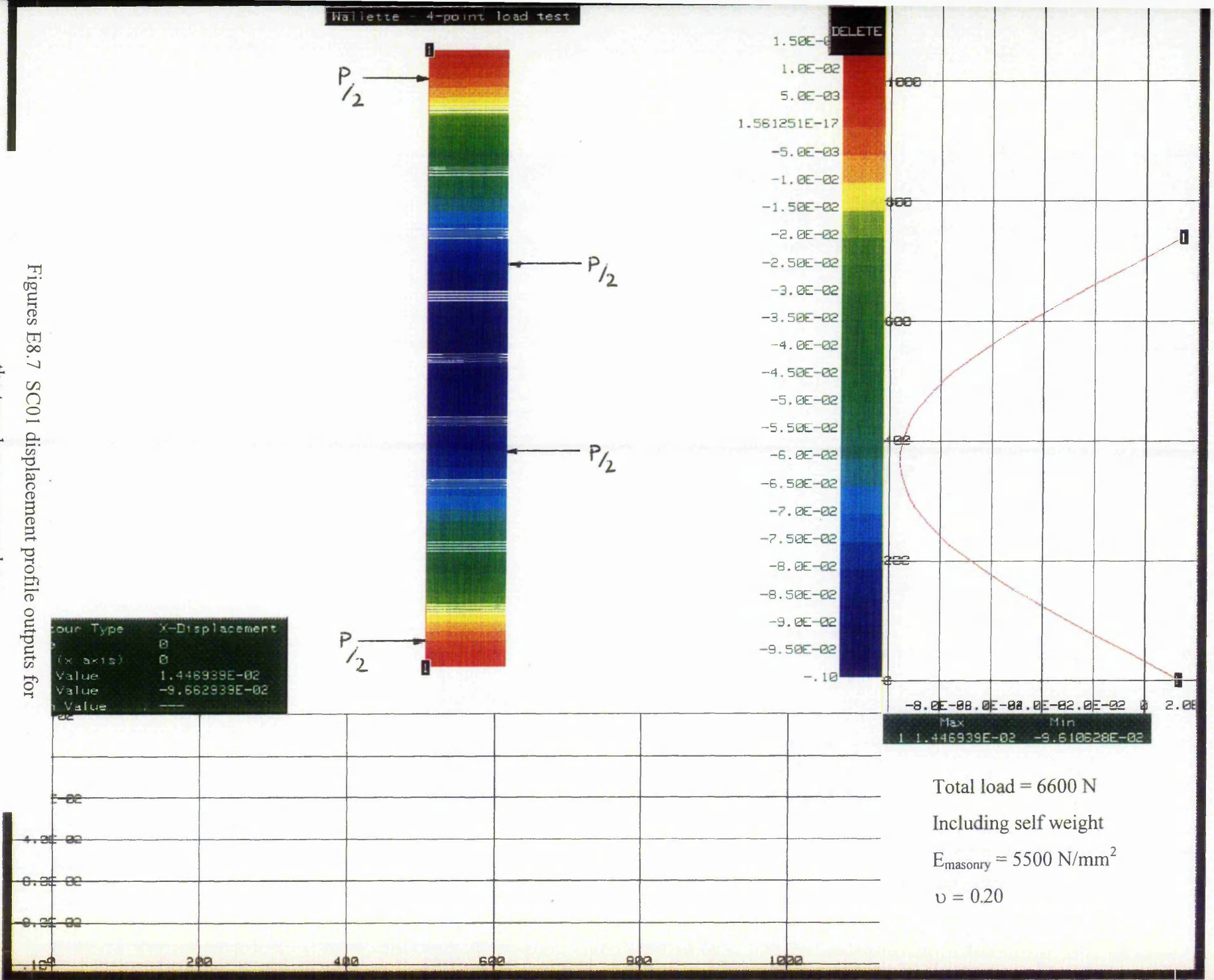

Figures E8.7 SC01 displacement profile outputs for the type 1 masonry analyses

Total load = 6600 N

Including self weight

$E_{masonry}$ = 5500 N/mm^2

υ = 0.20

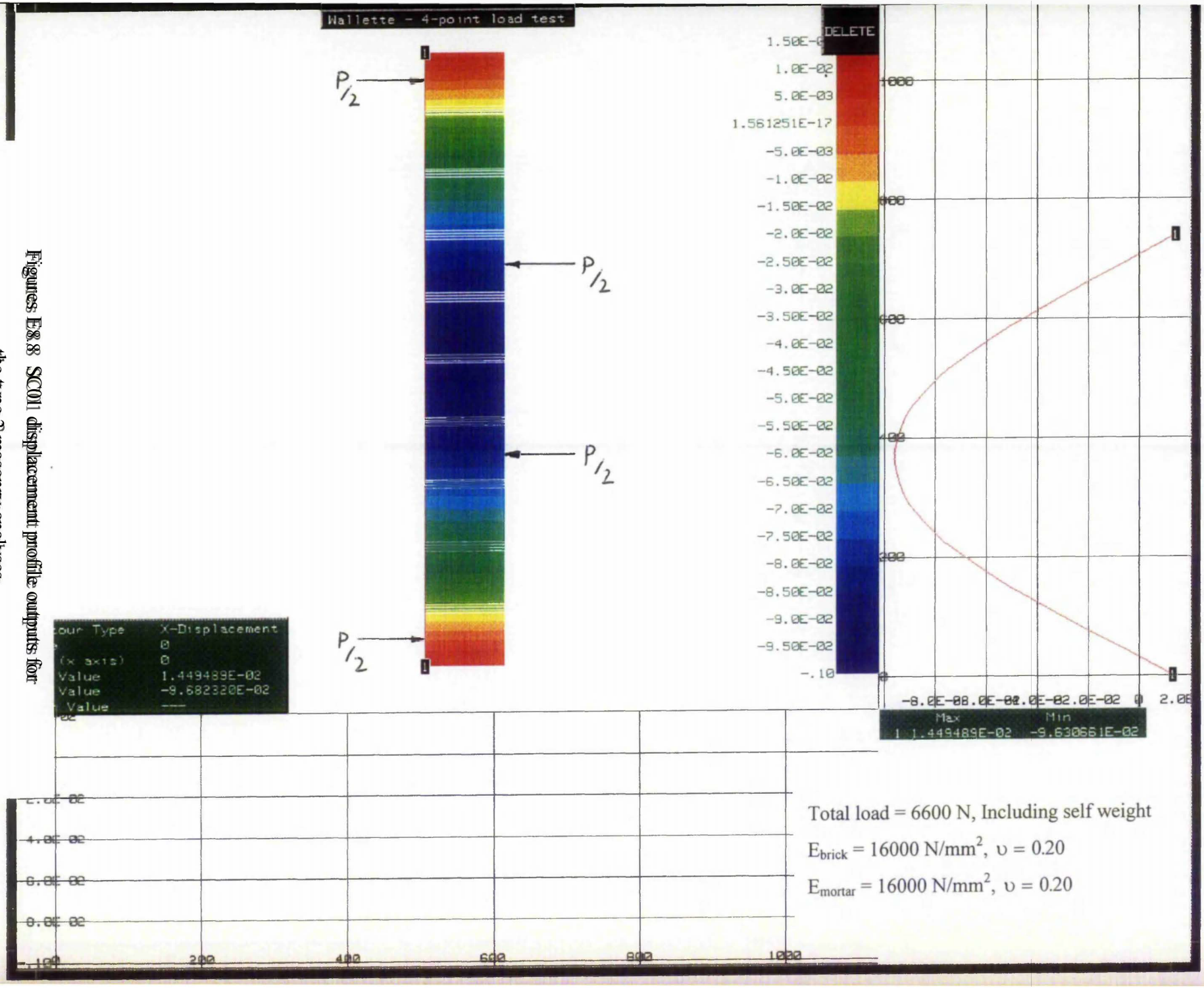

Figures E8.8 SC01 displacement profile outputs for the type 2 masonry analyses

Appendix F

CHAPTER 9

MASONRY CAVITY WALL TESTING AND ANALYSIS

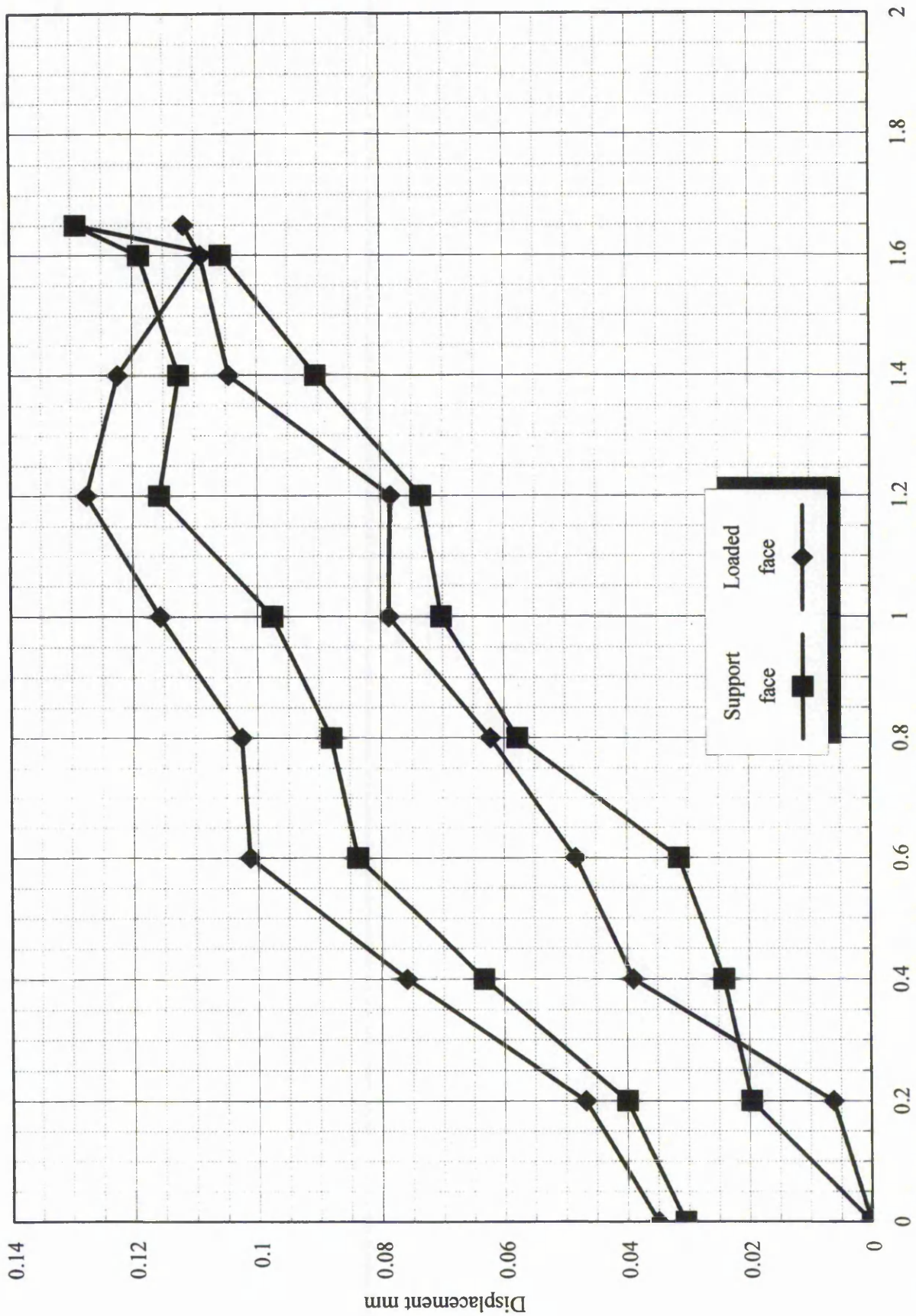

Figure F9.1a Load versus displacement relationship for cavity wall CW1 upto maximum equivalent wind load

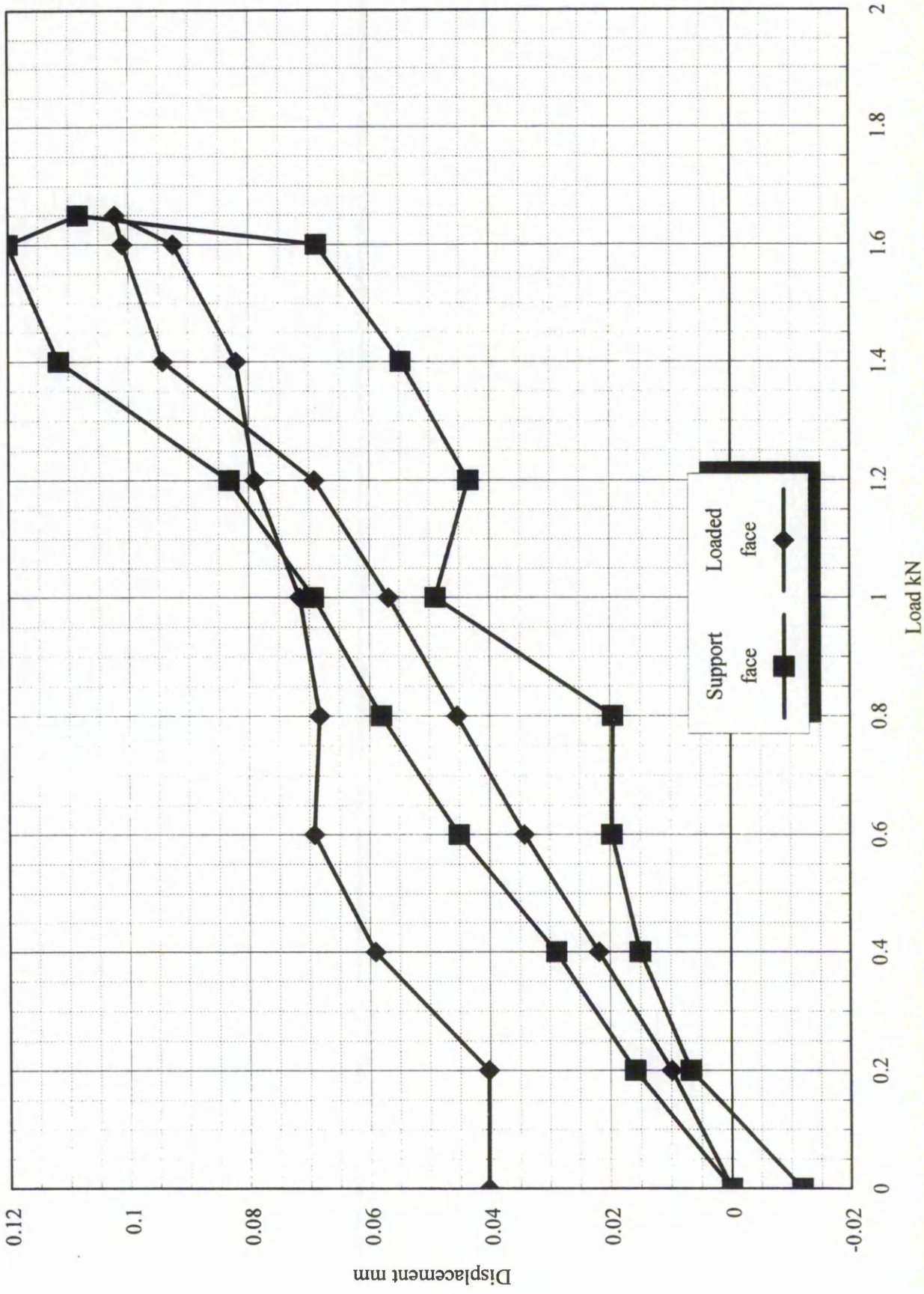

Figure F9.1b Load versus displacement relationship for cavity wall CW2 upto maximum equivalent wind load

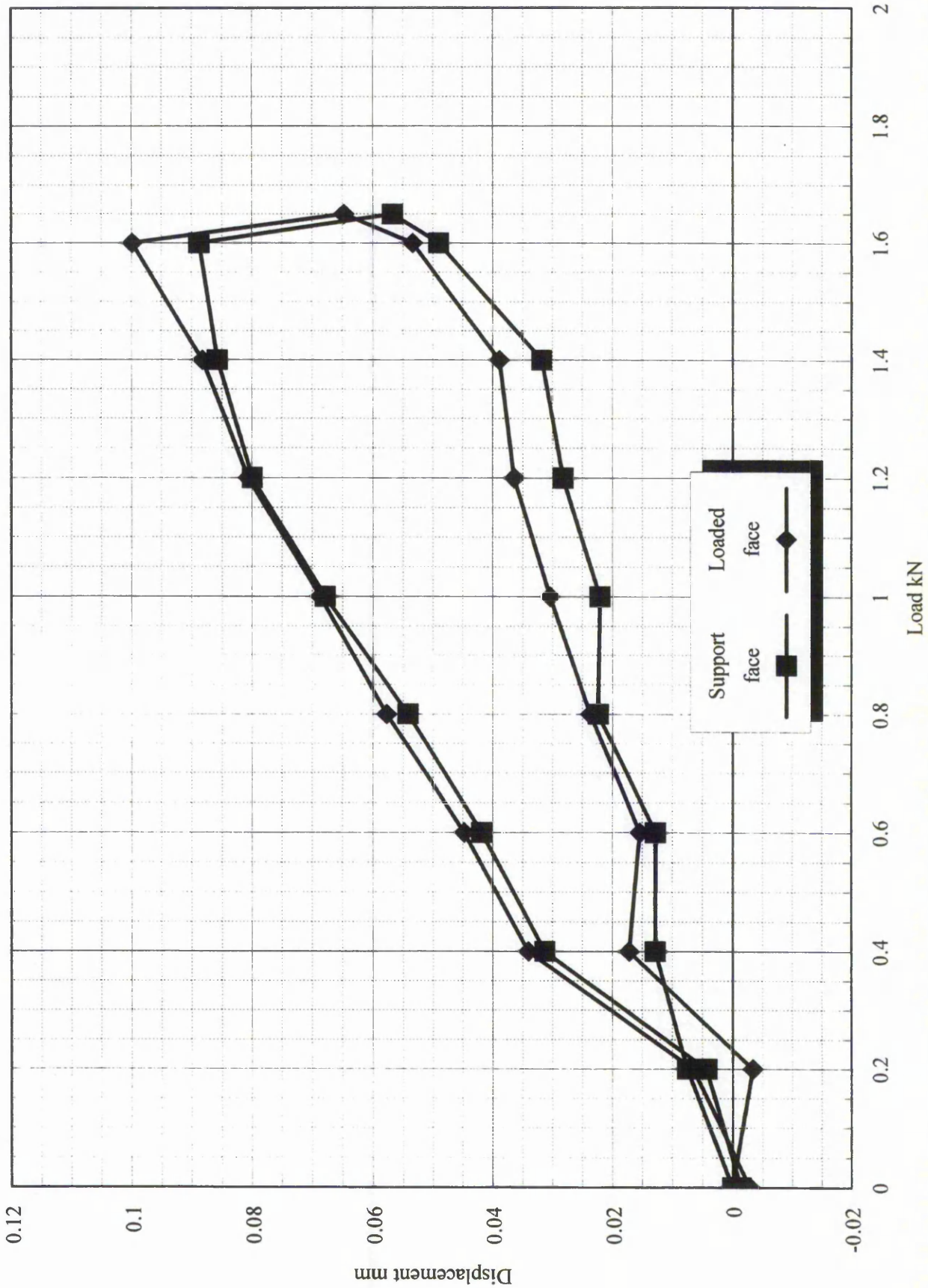

Figure F9.1c Load versus displacement relationship for cavity wall CW3 upto maximum equivalent wind load

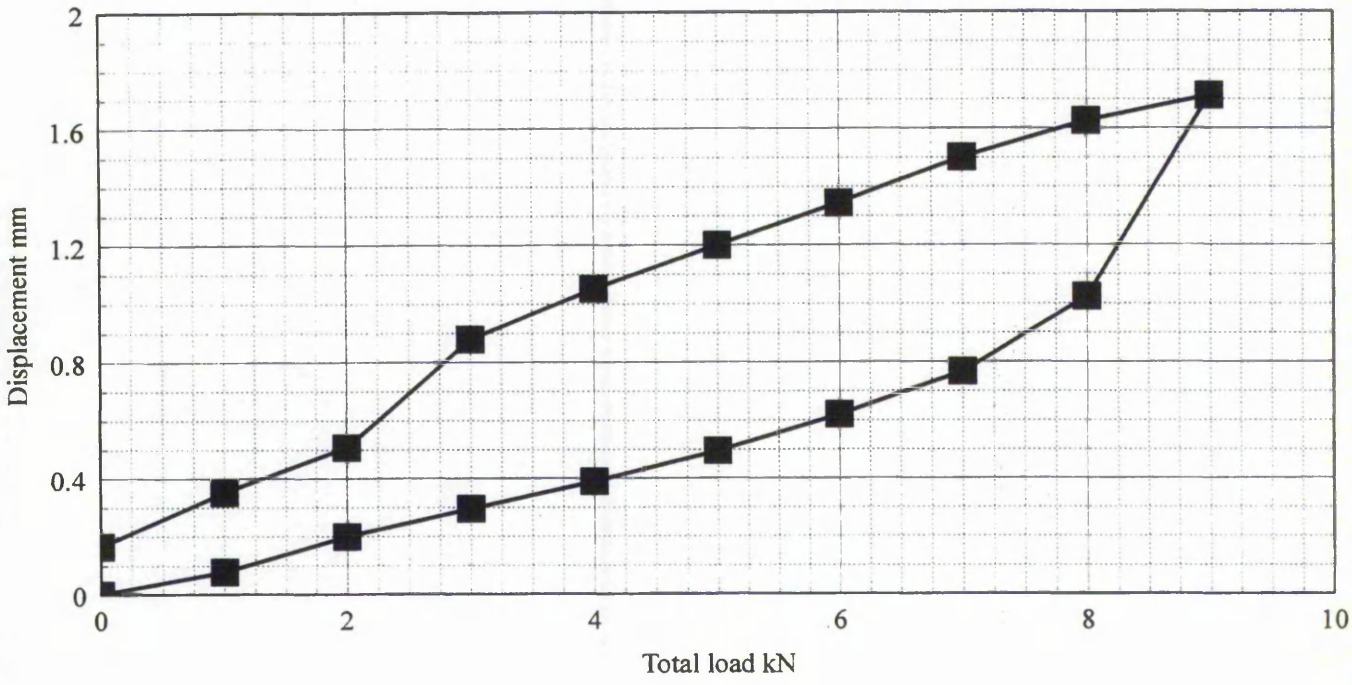

Figure F9.2a Hysteresis plot of load versus displacement
for cavity wall CW2

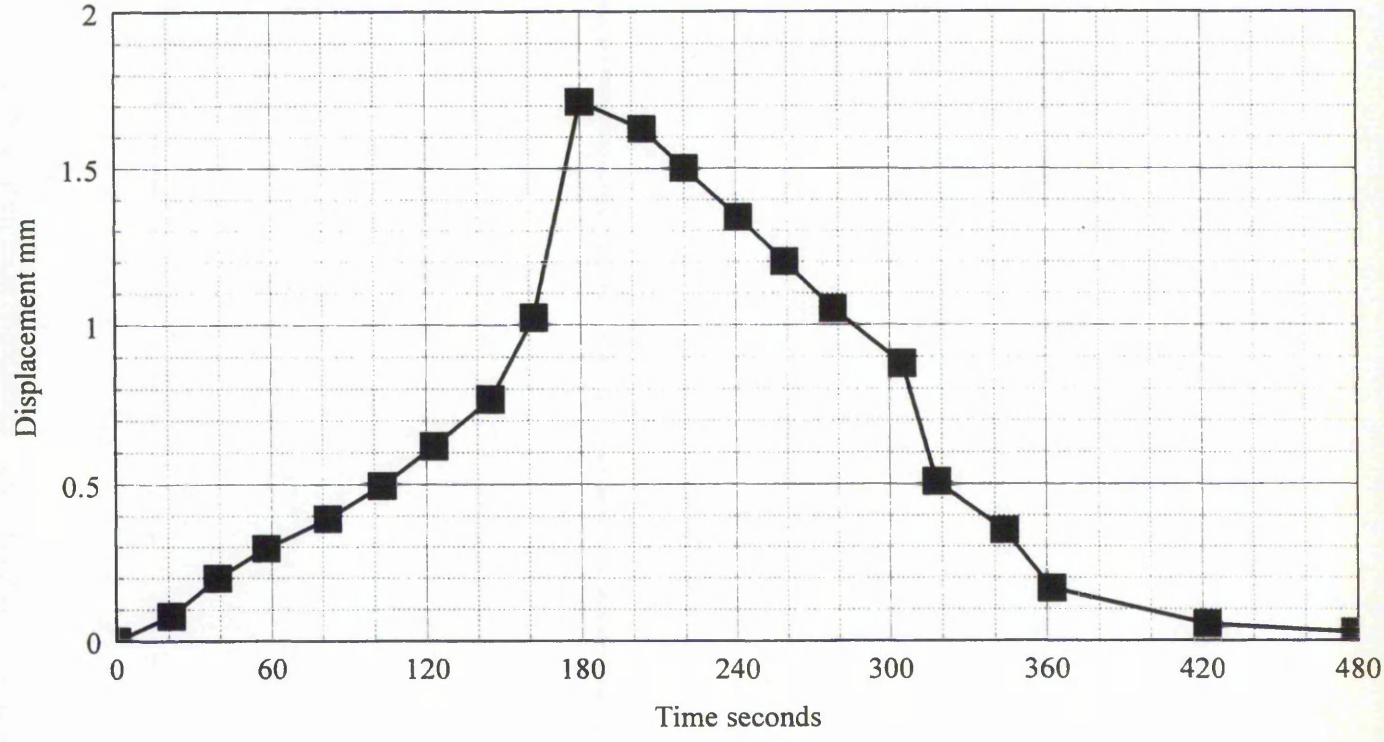

Figure F9. 2b Hysteresis plot of time versus displacement
for cavity wall CW2

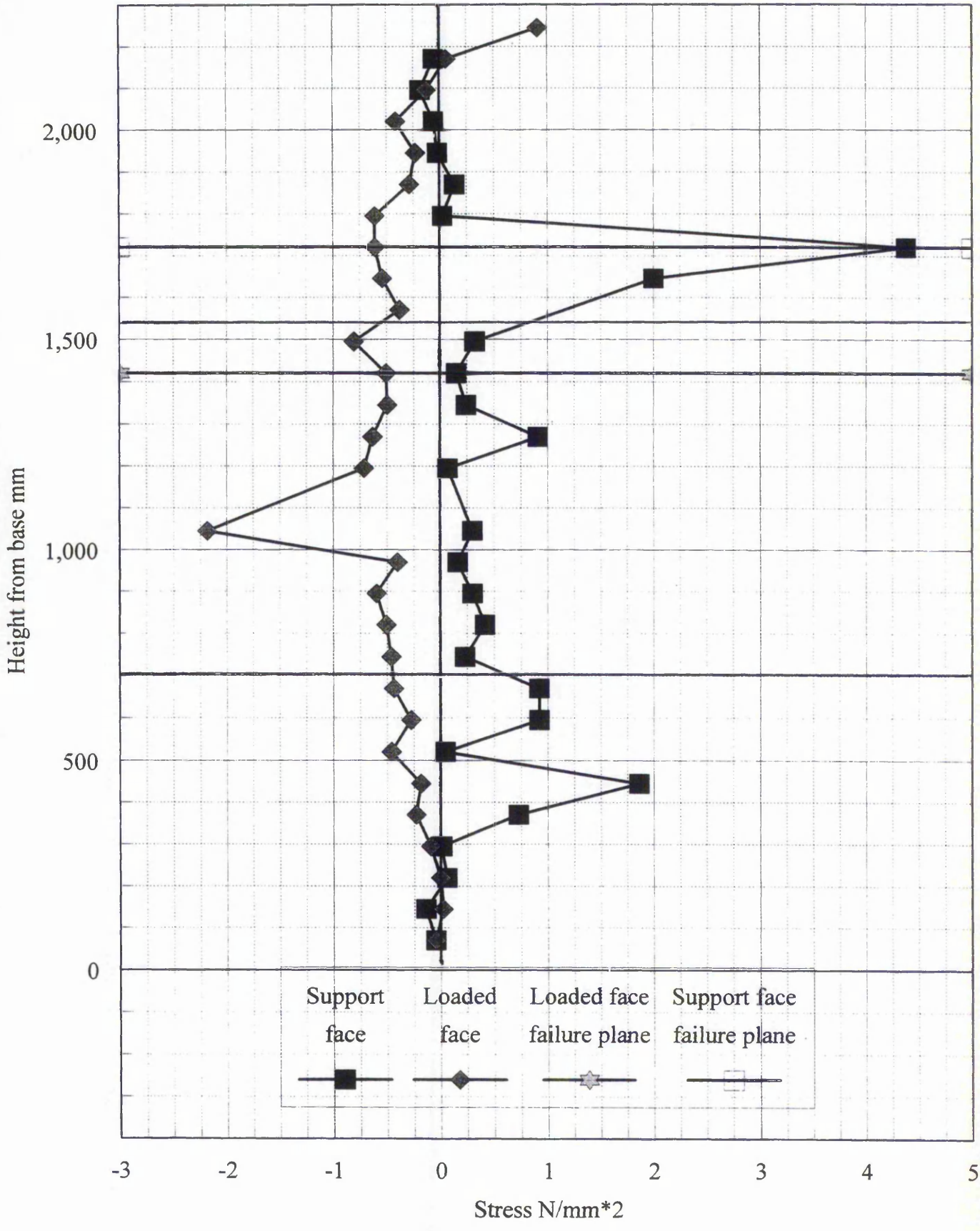

Figure F9.3a Experimental stress profile for cavity wall CW1

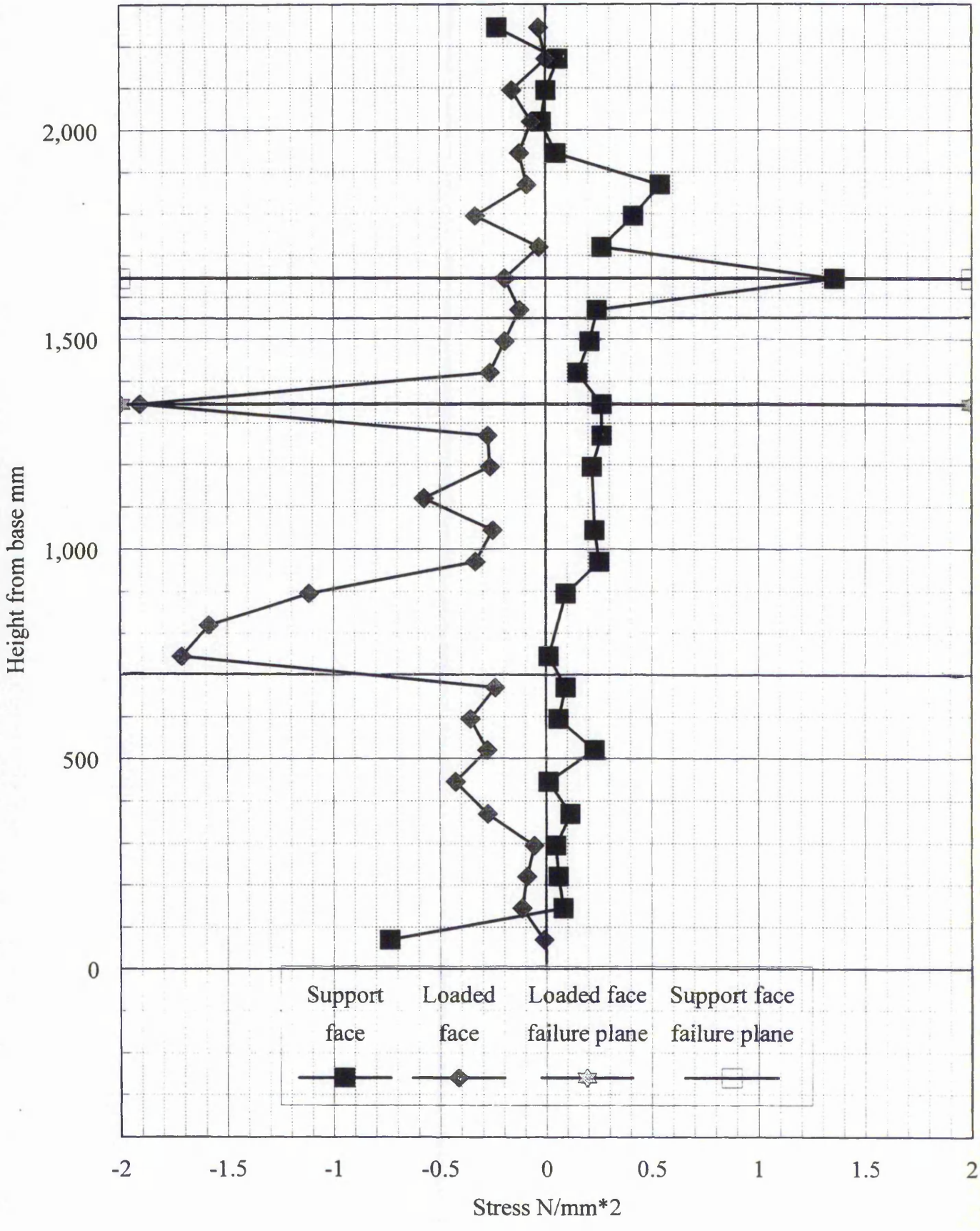

Figure F9.3b Experimental stress profile for cavity wall CW2

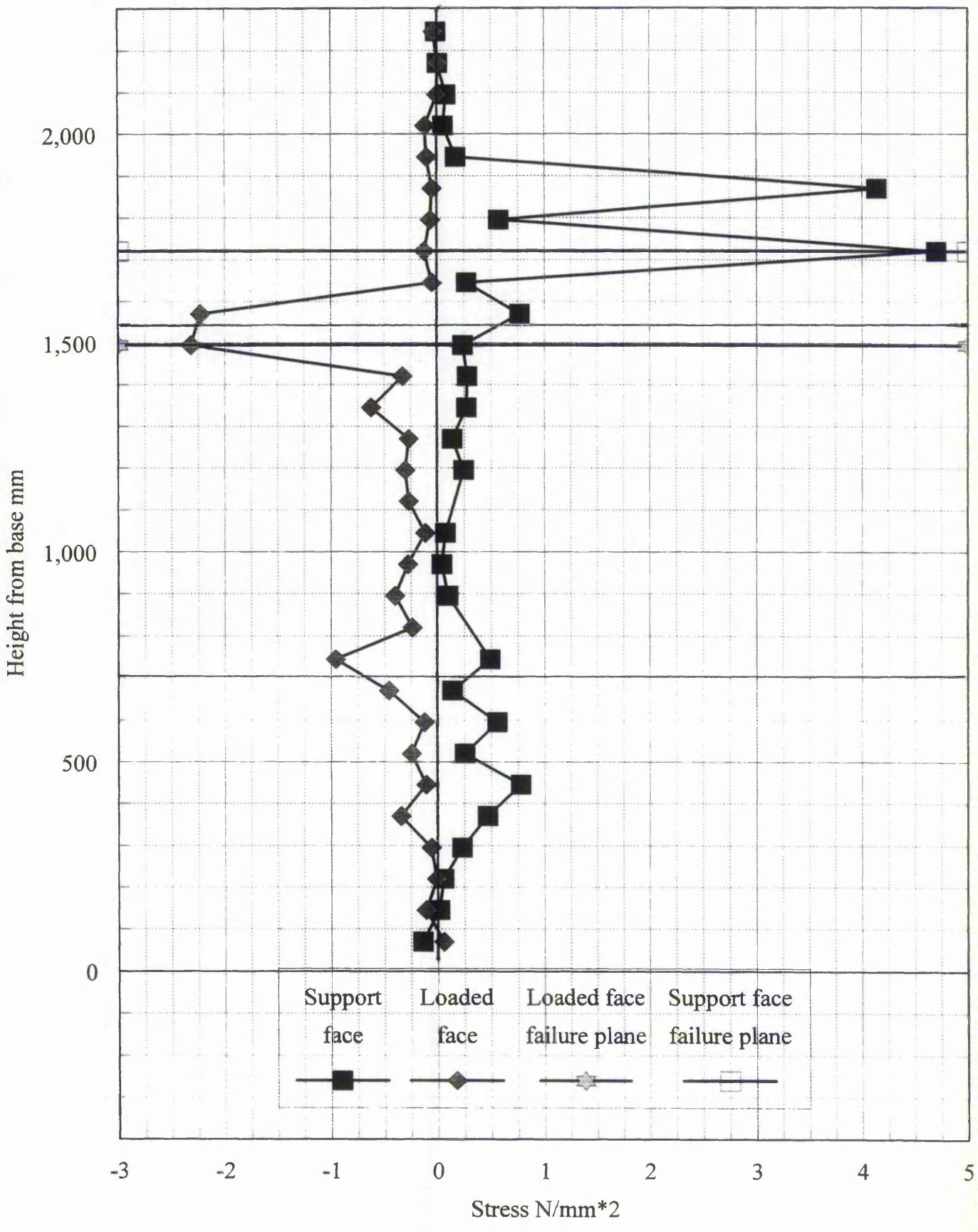

Figure F9.3c Experimental stress profile for cavity wall CW3

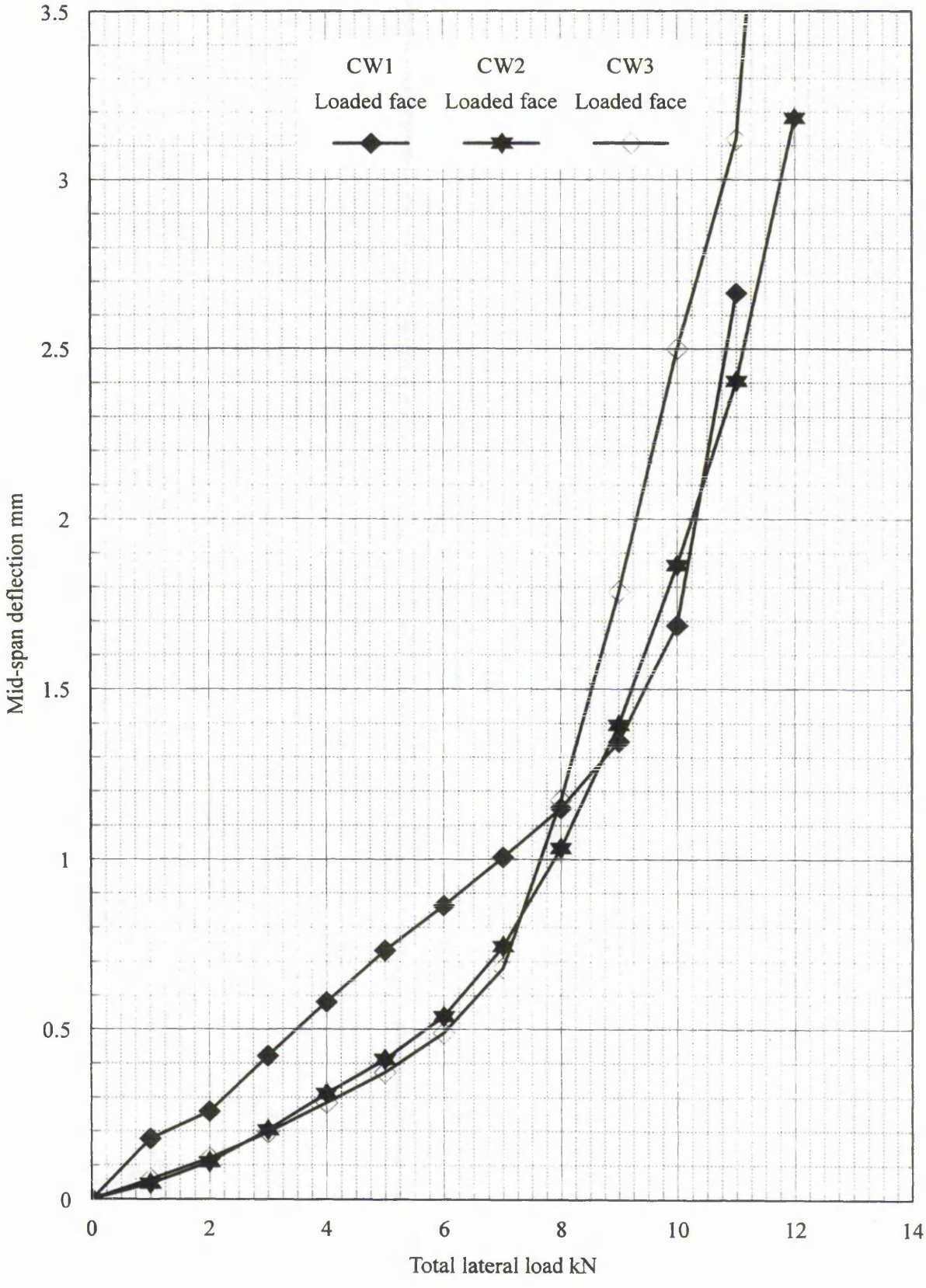

Figure F9.4 Experimental load versus mid span displacements to failure for all cavity walls

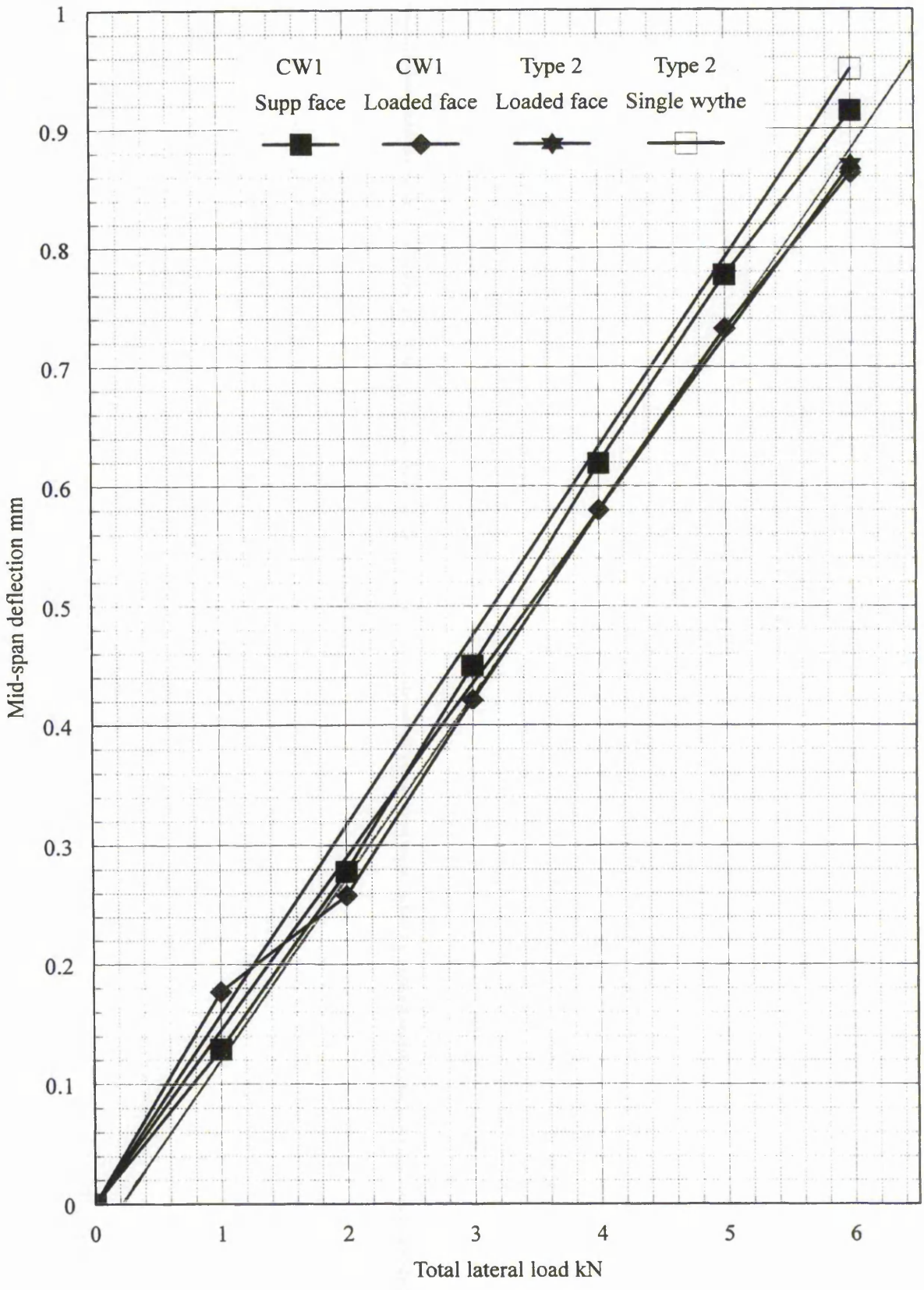

Figure F9.5a Comparison of experimental and F.E.A. load versus deflection limited to linear elastic response below a total lateral load of 6.0 kN for cavity wall CW1

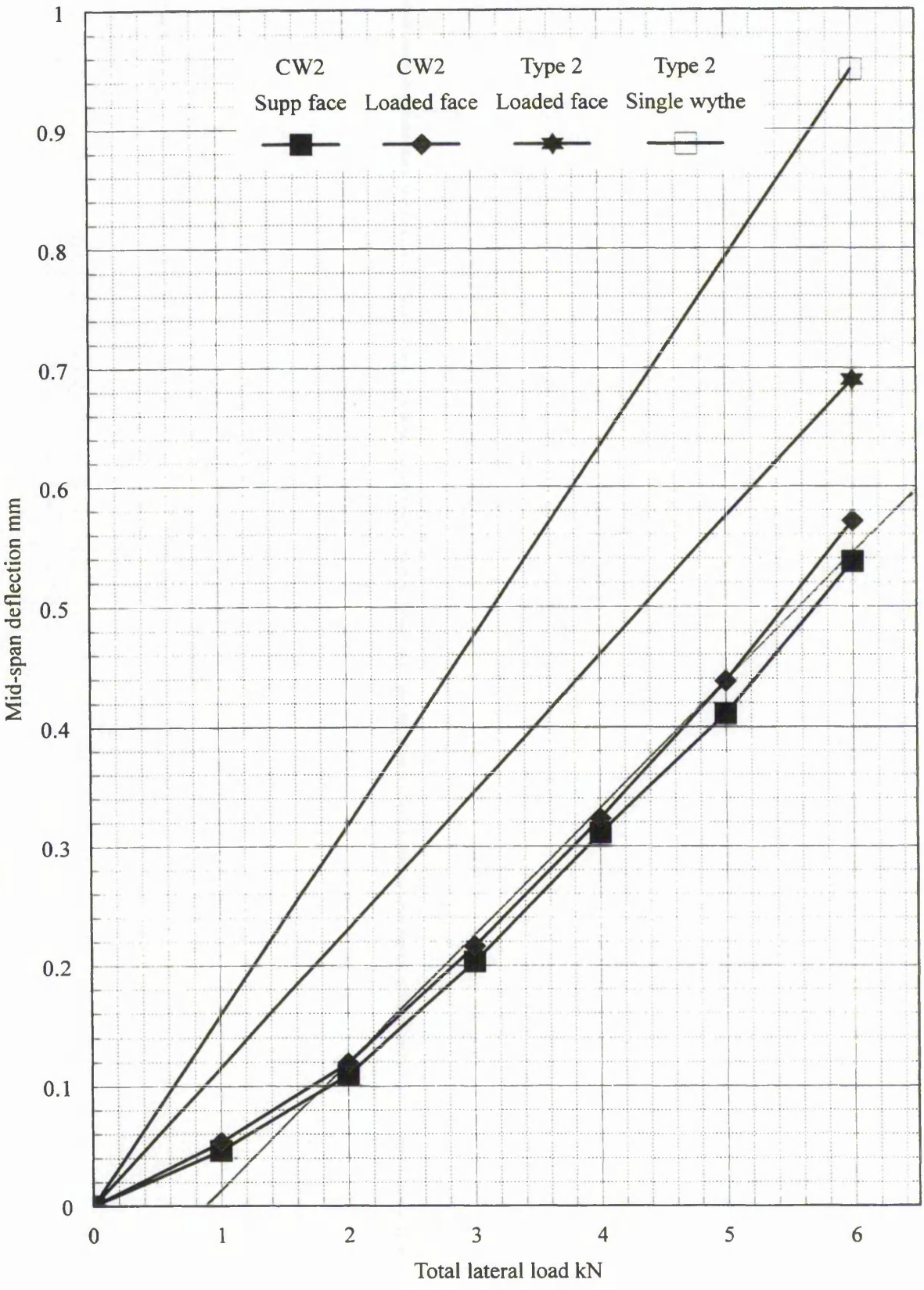

Figure F9.5b Comparison of experimental and F.E.A. load versus deflection limited to linear elastic response below a total lateral load of 6.0 kN for cavity wall CW2

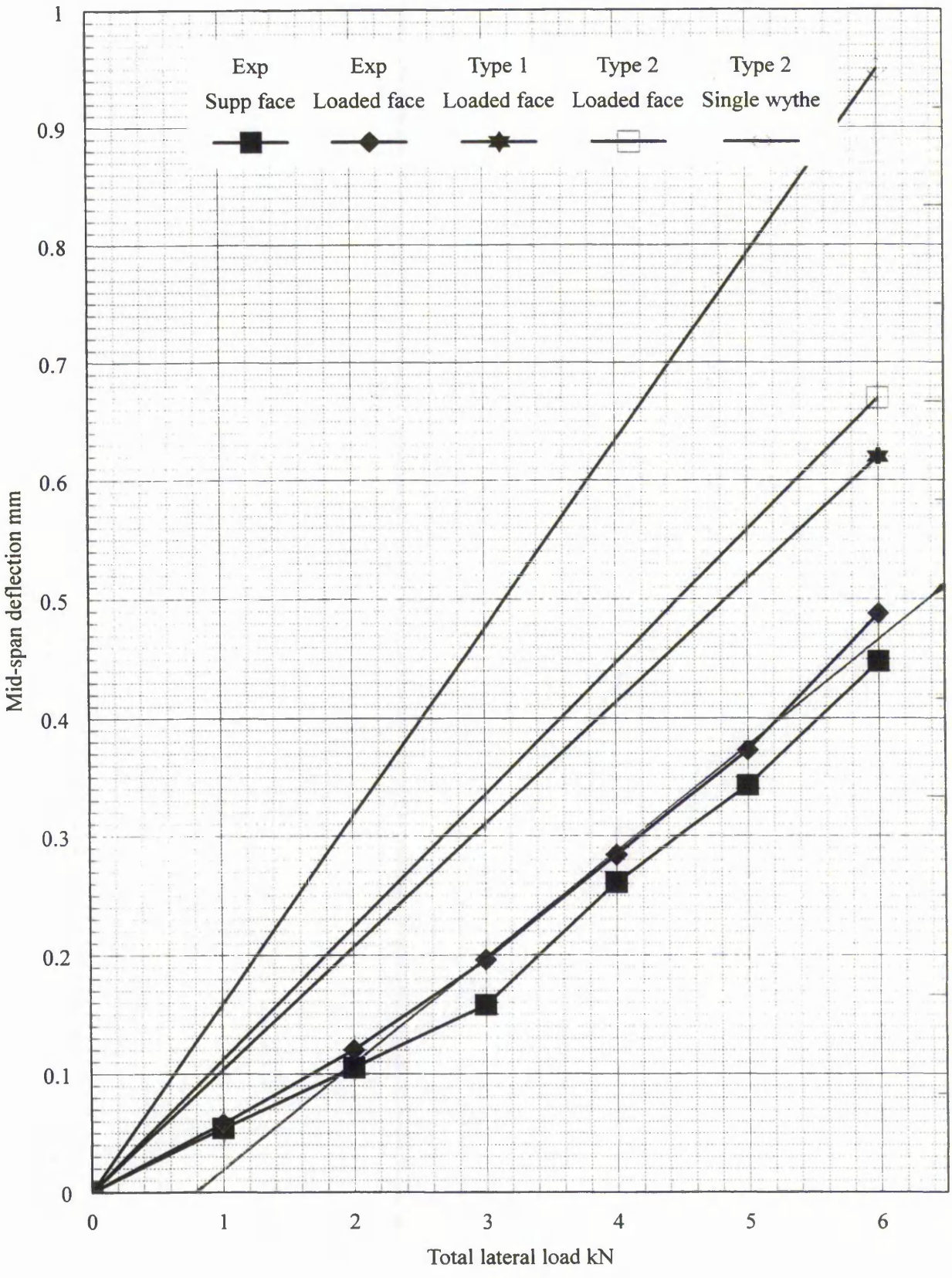

Figure F9.5c Comparison of experimental and F.E.A. load versus deflection limited to linear elastic response below a total lateral load of 6.0 kN for cavity wall CW3

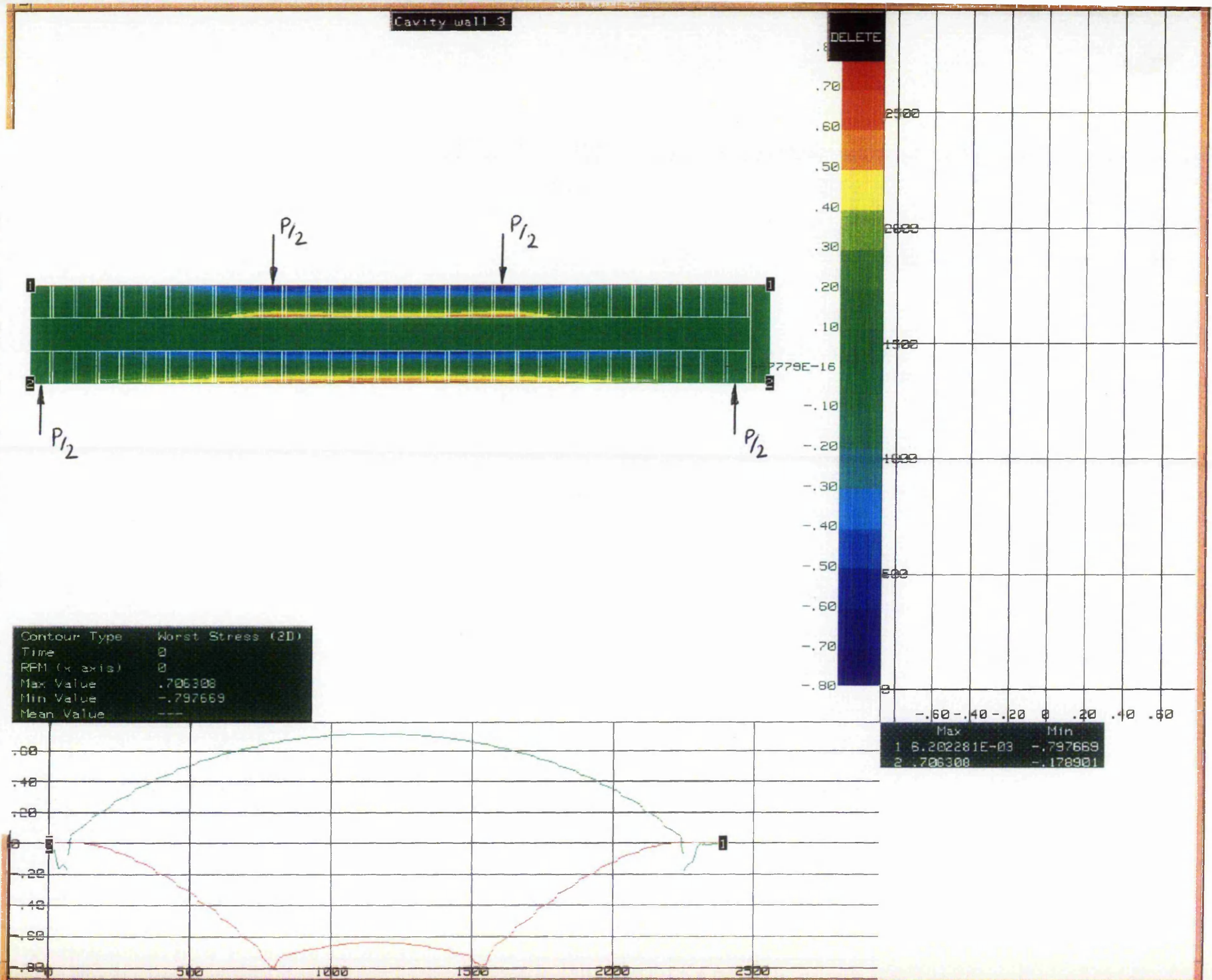

Figure F9.6 F.E.A. Type 1 analysis worst 2D stress colour contour plot for cavity wall CW3

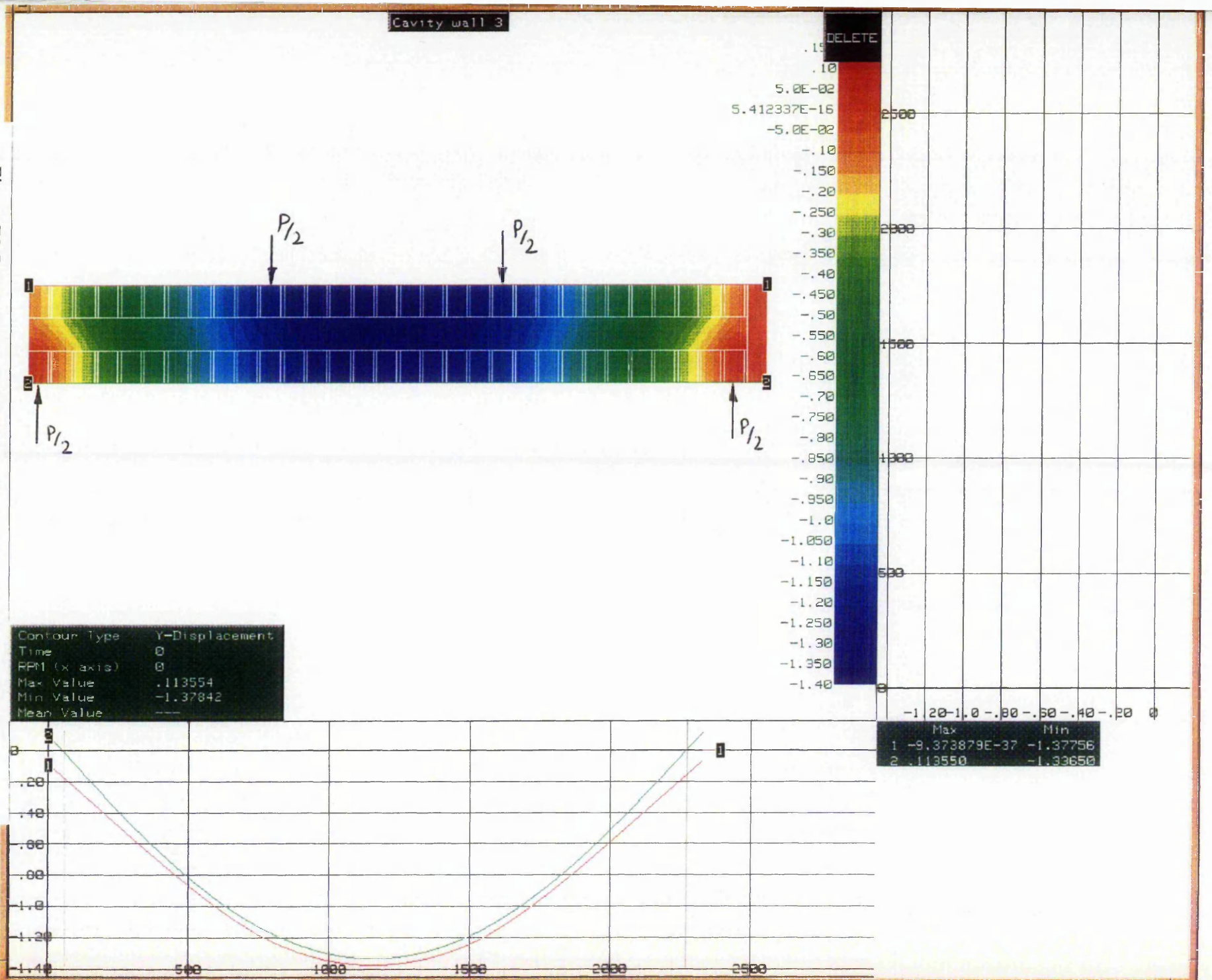

Figure F9.7 F.E.A. Type 1 analysis load versus displacement colour contour plot for cavity wall CW3

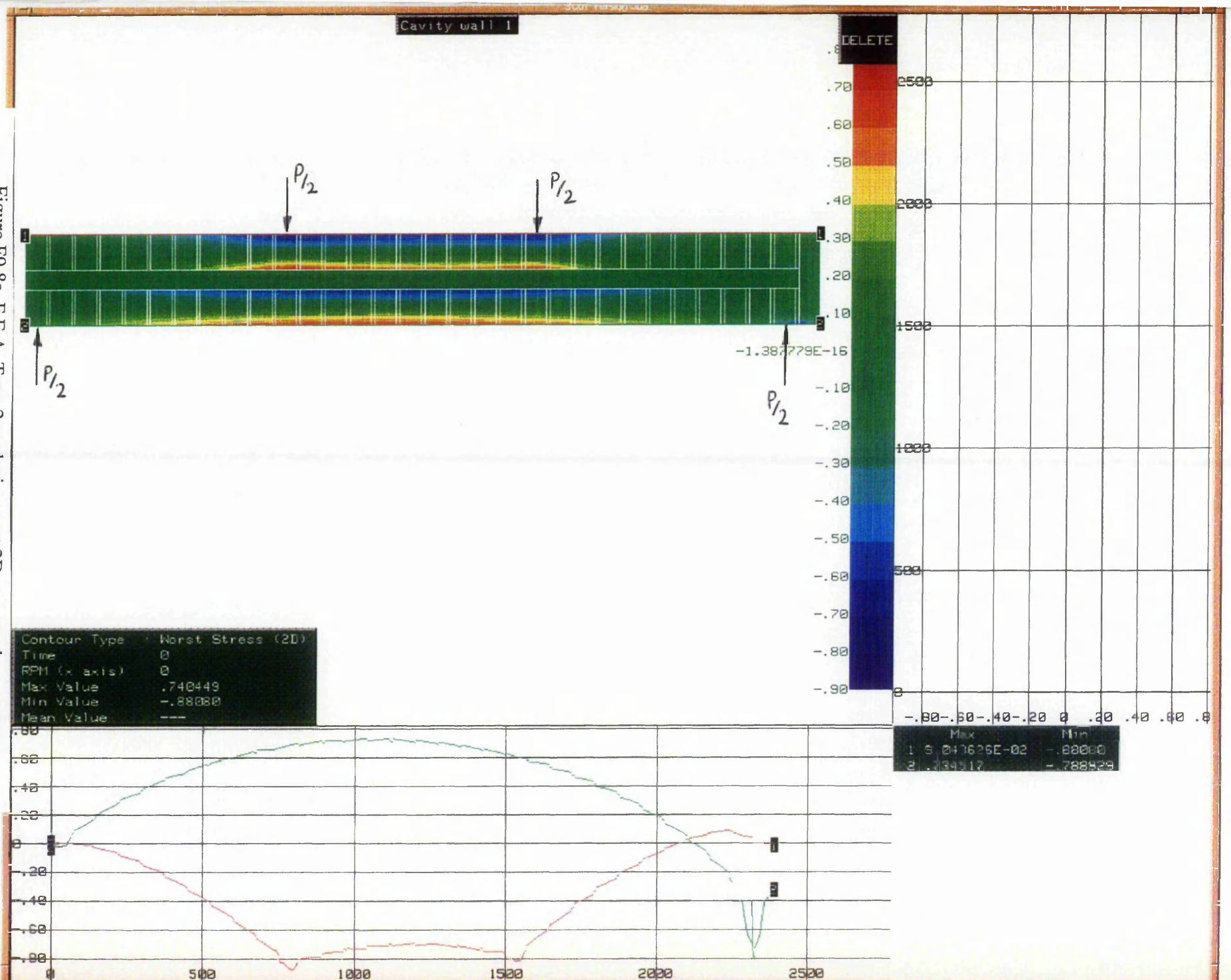

Figure F9.8a F.E.A. Type 2 analysis worst 2D stress colour contour plot for cavity wall CW1

Figure F9. 8b F.E.A. Type 2 analysis worst 2D stress colour contour plot for cavity wall CW2

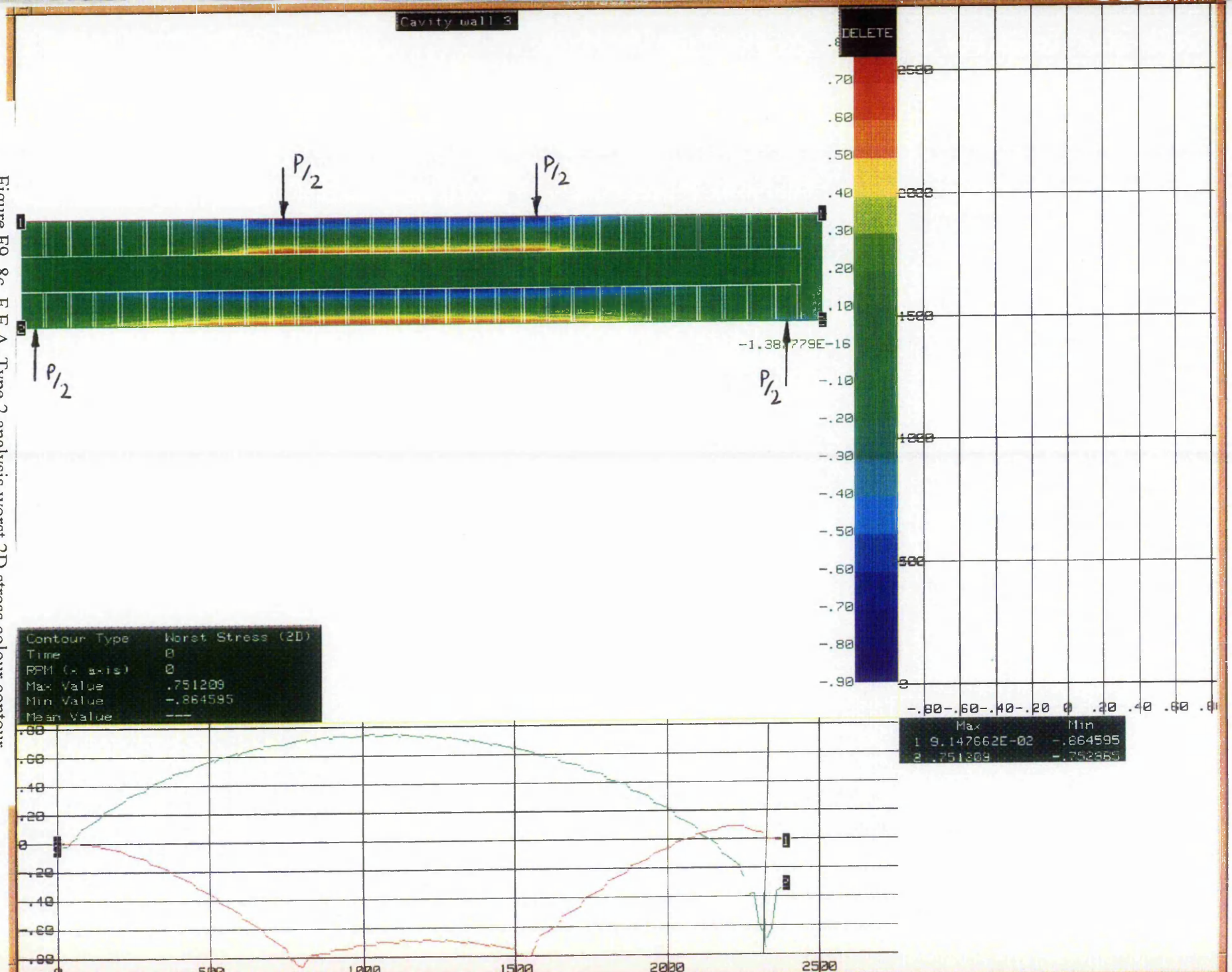

Figure F9. 8c F.E.A. Type 2 analysis worst 2D stress colour contour plot for cavity wall CW3

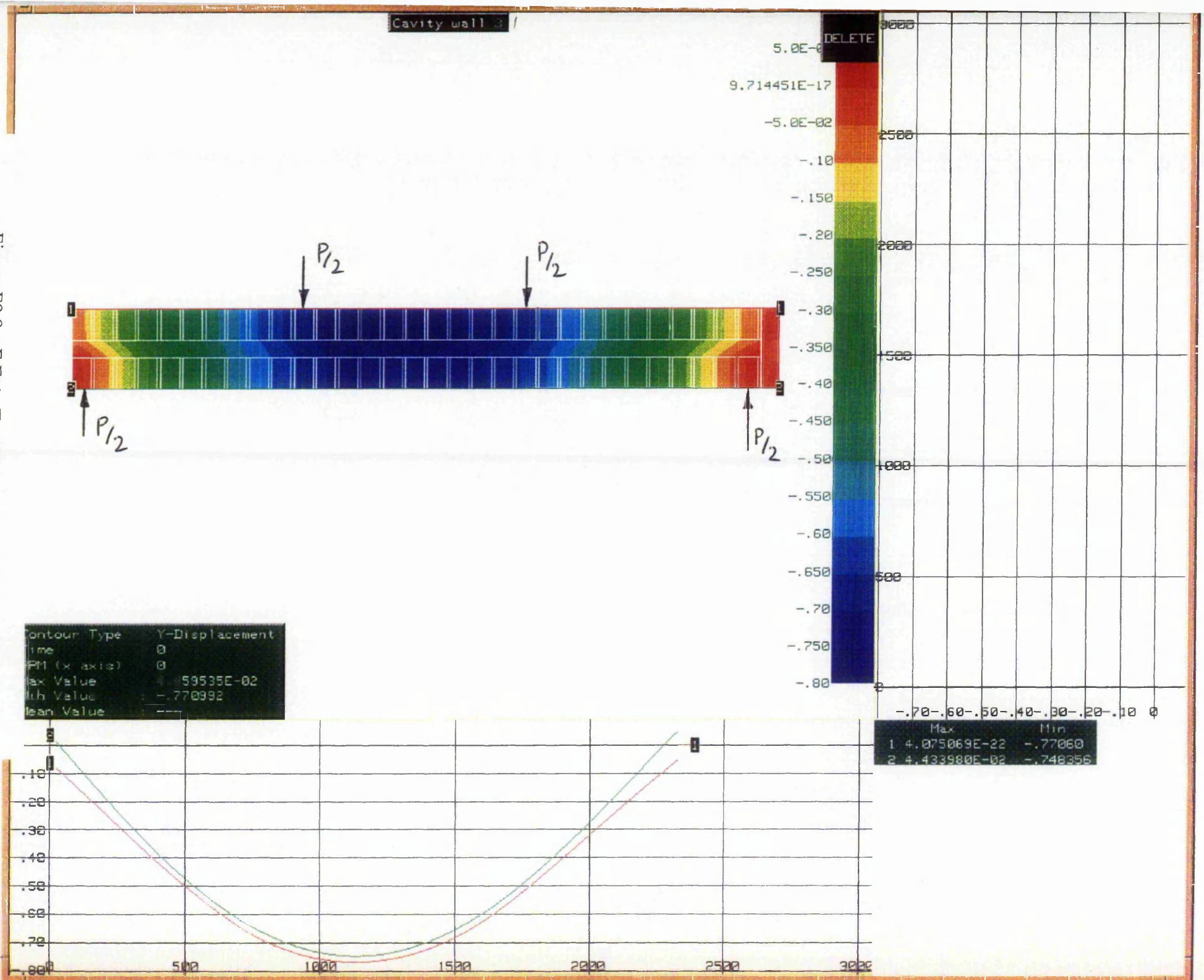

Figure F9.9a F.E.A. Type 2 analysis load versus displacement colour contour plot for cavity wall CW1

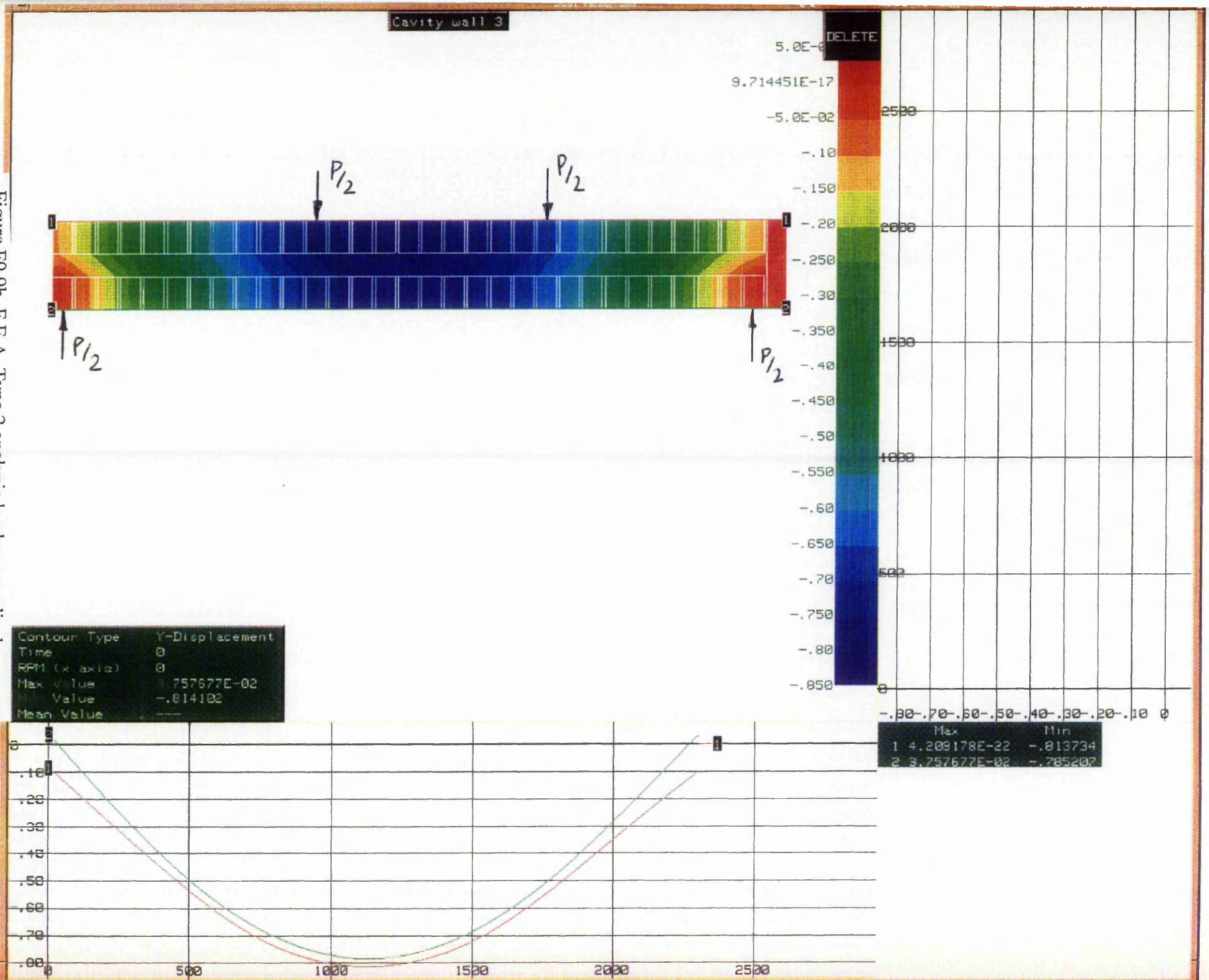

Figure F9.9b F.E.A. Type 2 analysis load versus displacement colour contour plot for cavity wall CW2

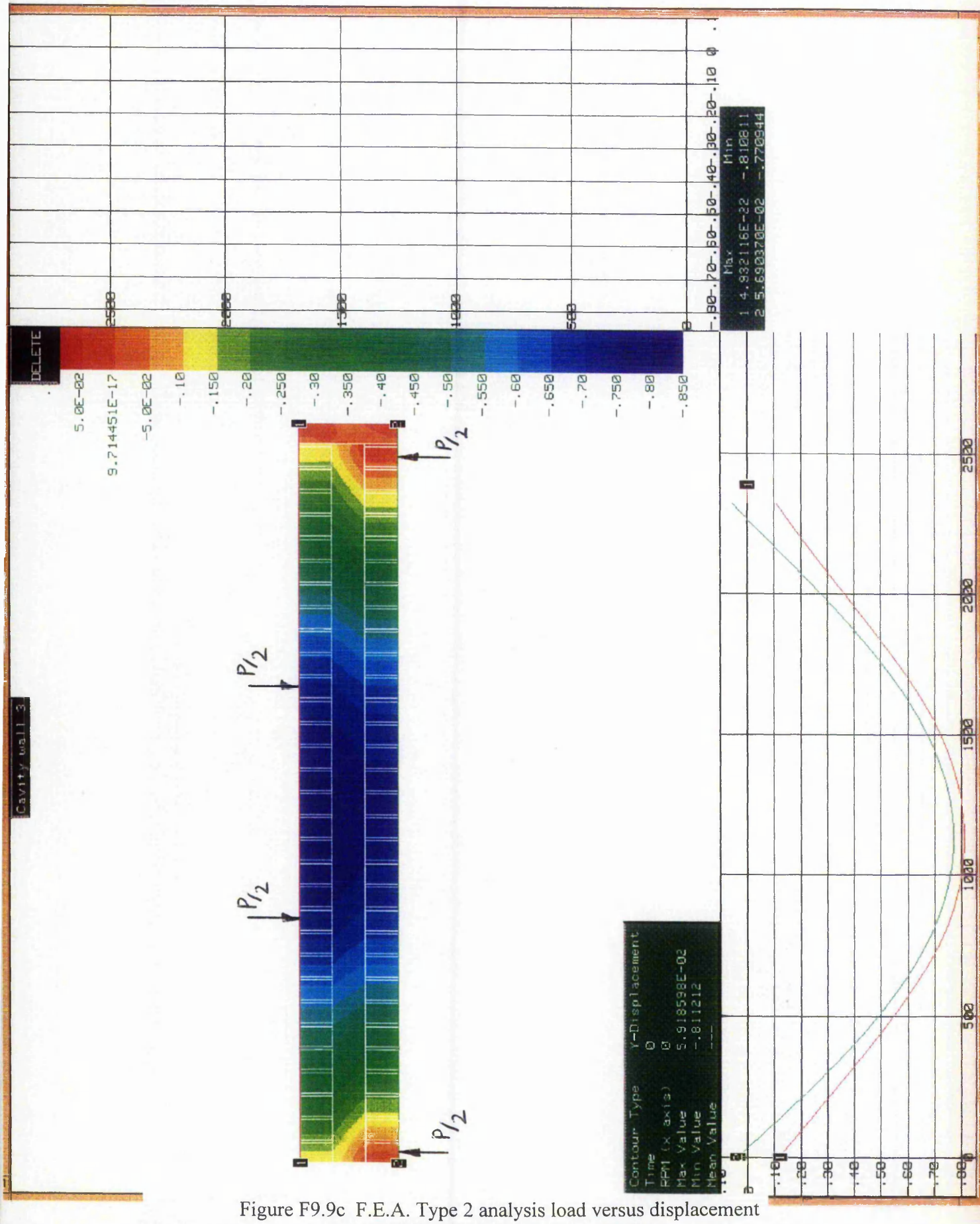

Figure F9.9c F.E.A. Type 2 analysis load versus displacement colour contour plot for cavity wall CW3

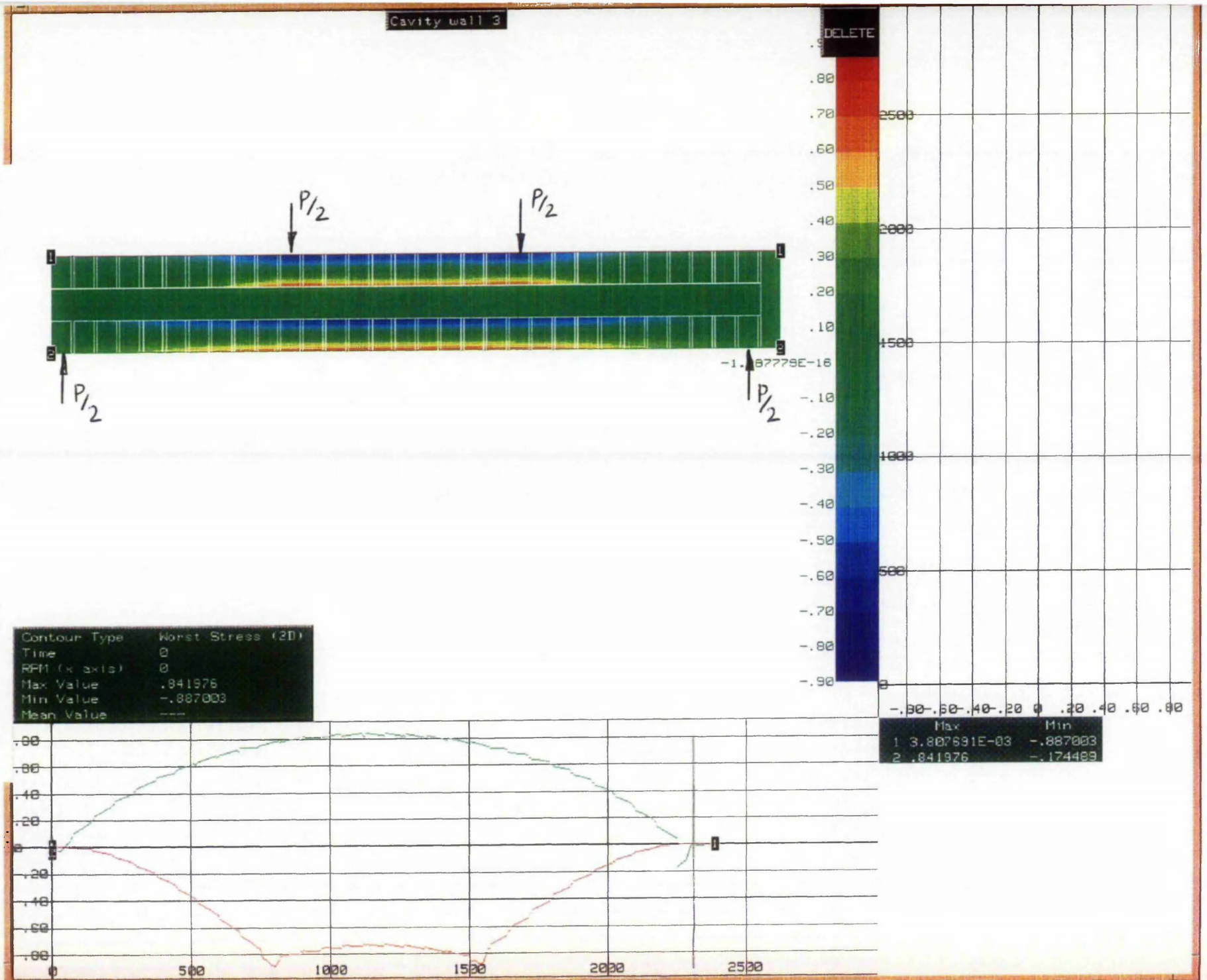

Figure F9.10 F.E.A. Type 2 analysis worst 2D stress colour contour plot for cavity wall CW3 with no self weight

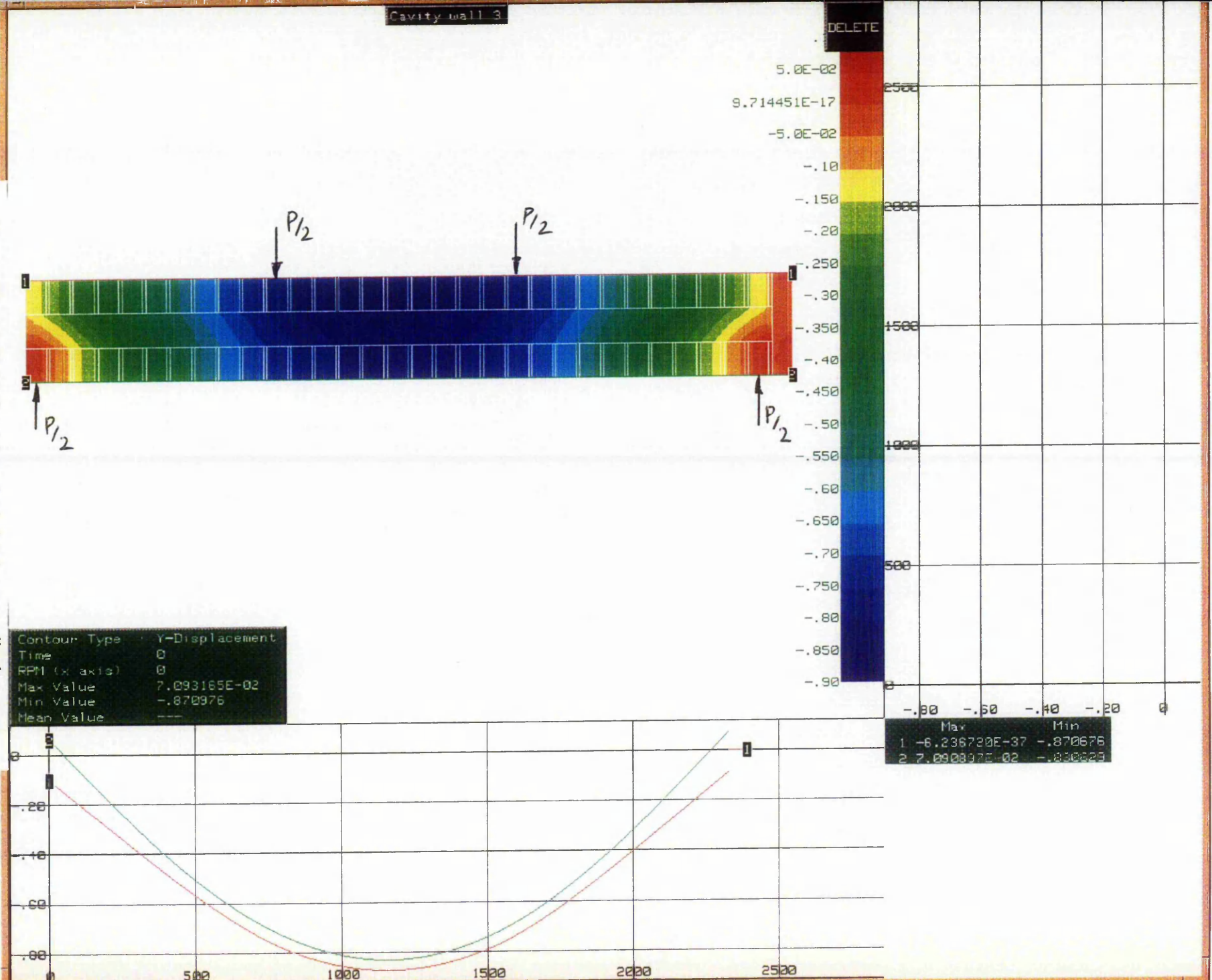

Figure F9.11 F.E.A. Type 2 analysis load versus displacement colour contour plot for cavity wall CW3 with no self weight

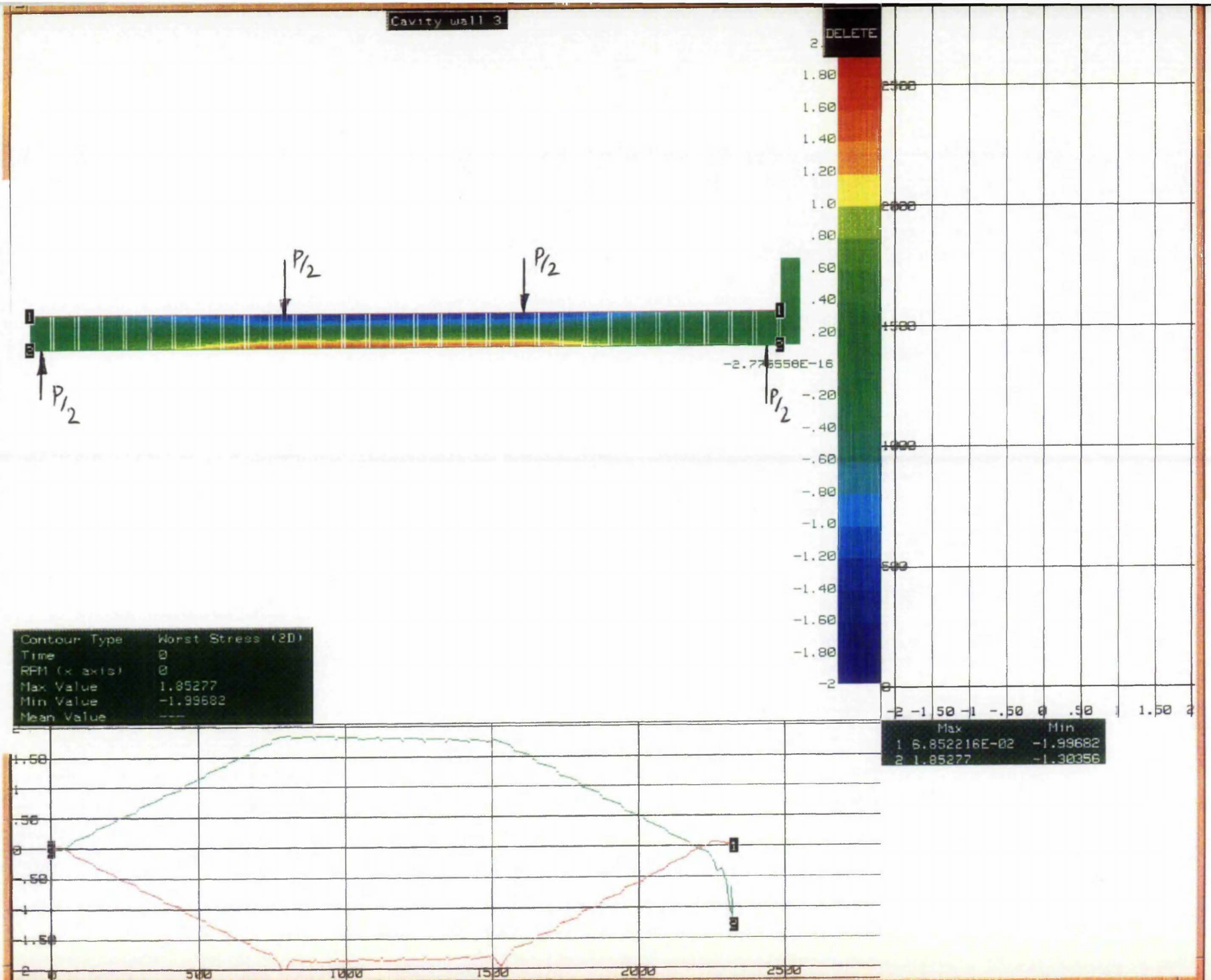

Figure F9.12 F.E.A. Type 2 analysis worst 2D stress colour contour plot for a single wythe with self weight

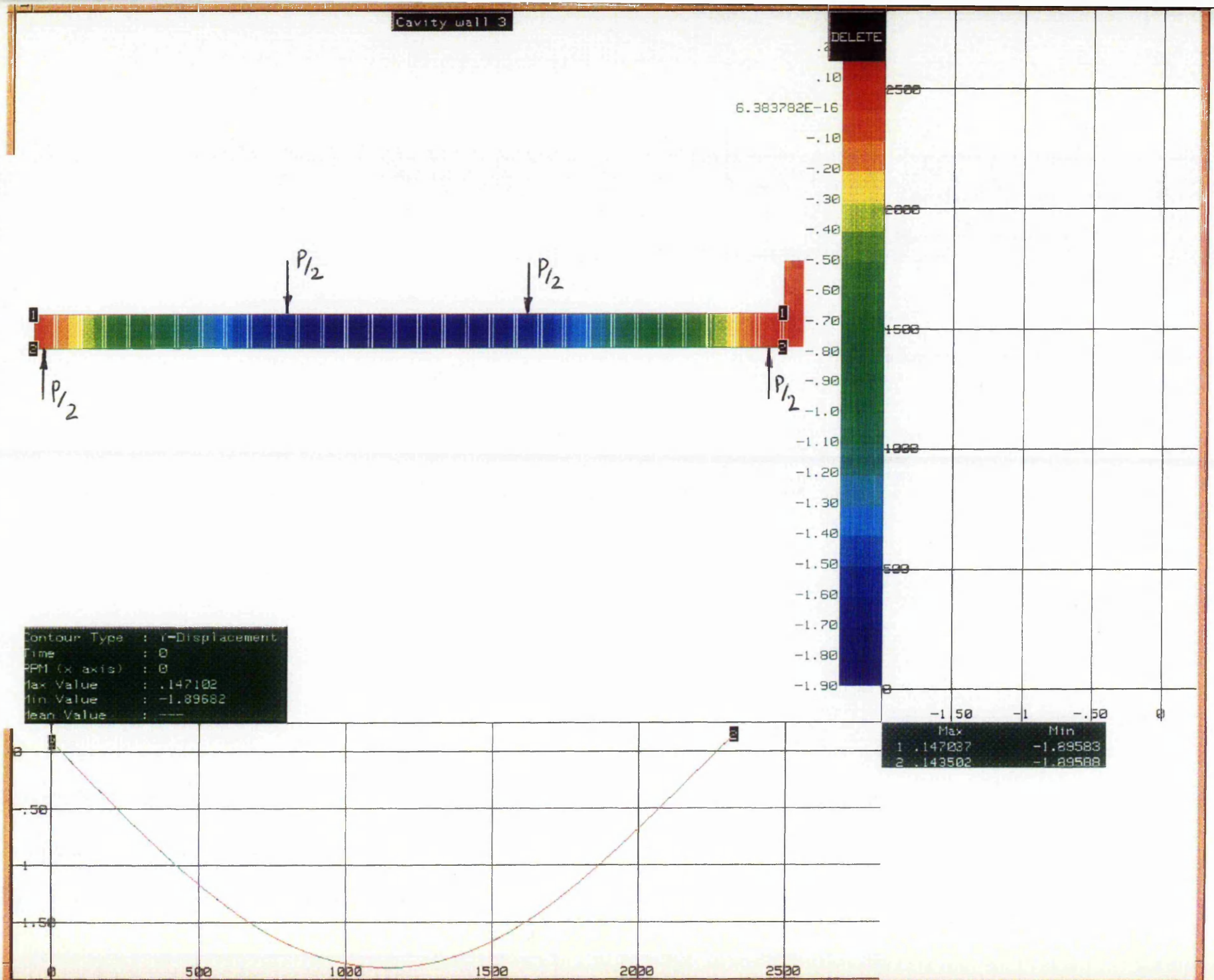

Figure F9.13 F.E.A. Type 2 analysis load versus displacement colour contour plot for a single wythe with self weight

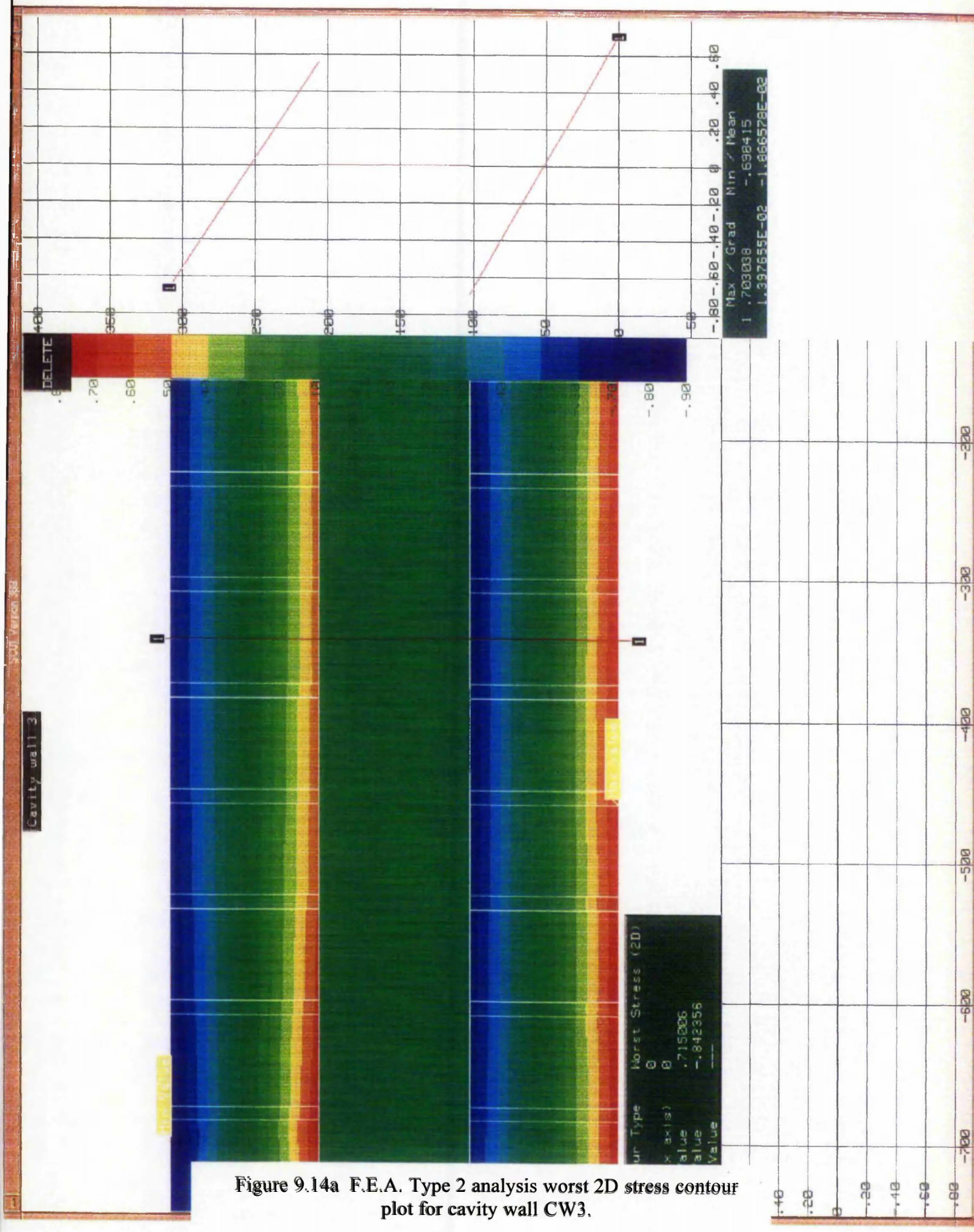

Figure 9.14a F.E.A. Type 2 analysis worst 2D stress contour plot for cavity wall CW3.

Isofoam CRF ρ = 32 kg/m^3, μ = 0.2

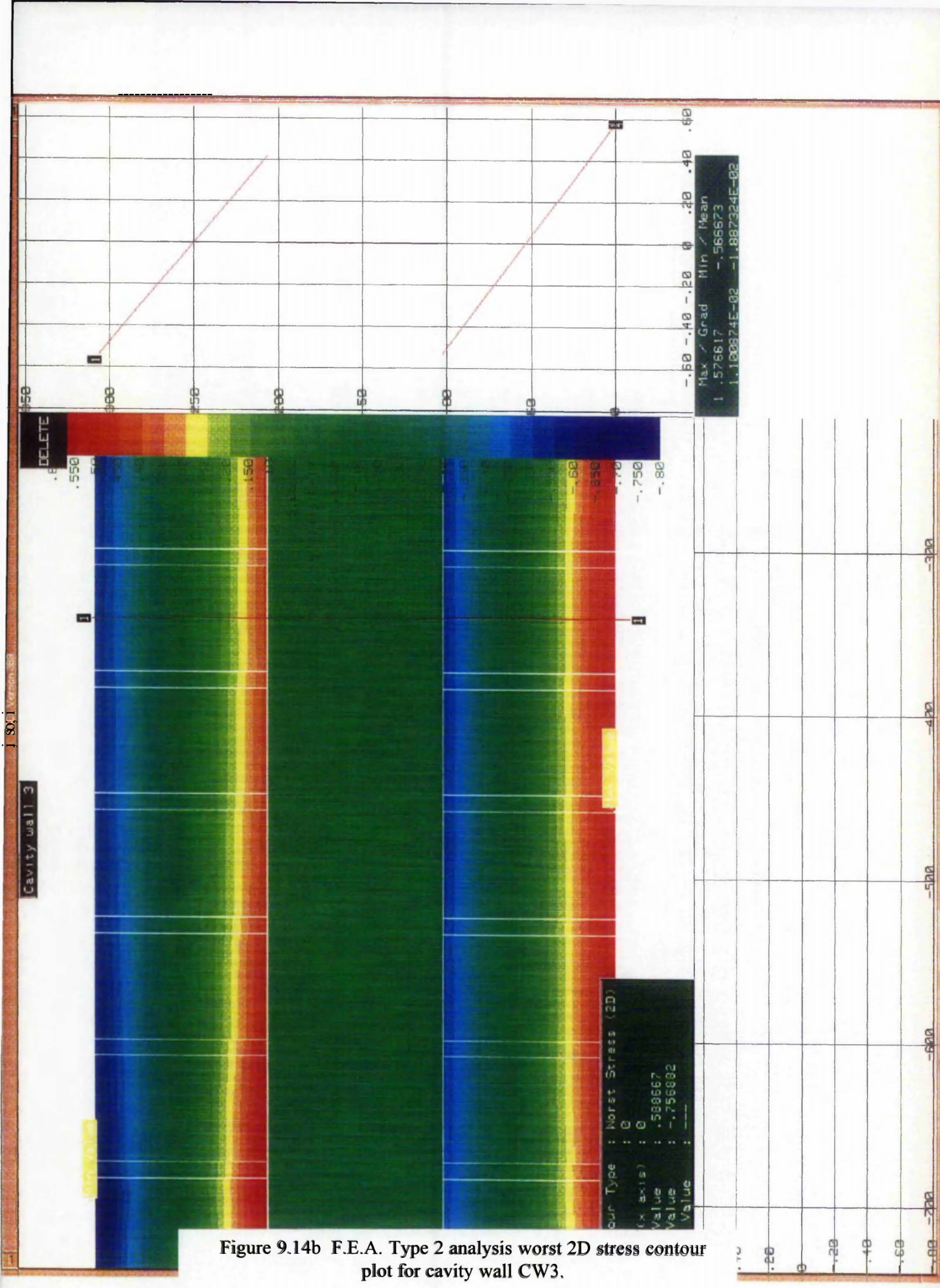

Figure 9.14b F.E.A. Type 2 analysis worst 2D stress contour plot for cavity wall CW3.

Isofoam CRF $\rho = 64$ kg/m^3, $\mu = 0.2$

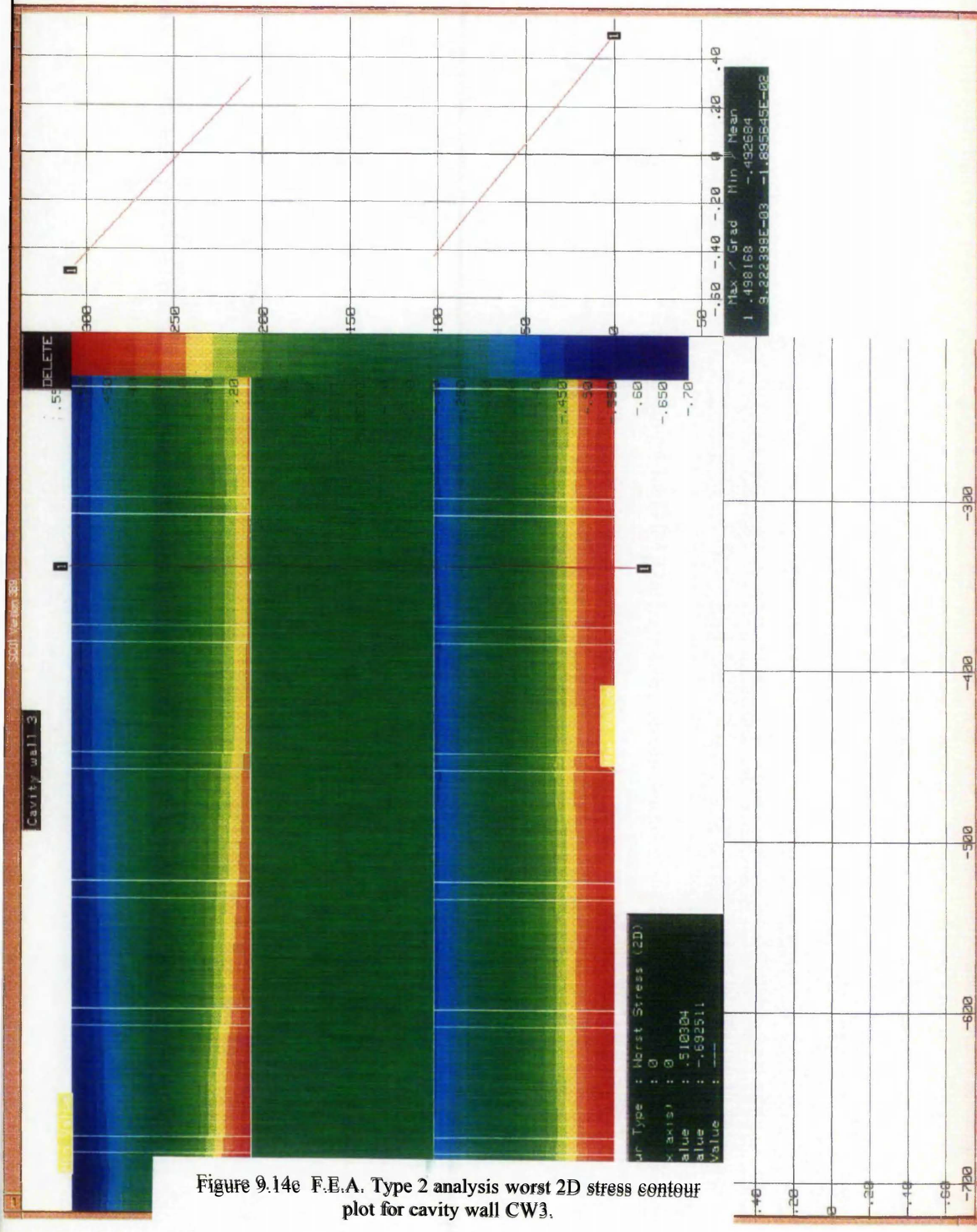

Figure 9.14c F.E.A. Type 2 analysis worst 2D stress contour plot for cavity wall CW3.

Isofoam CRF $\rho = 96$ kg/m^3, $\mu = 0.2$

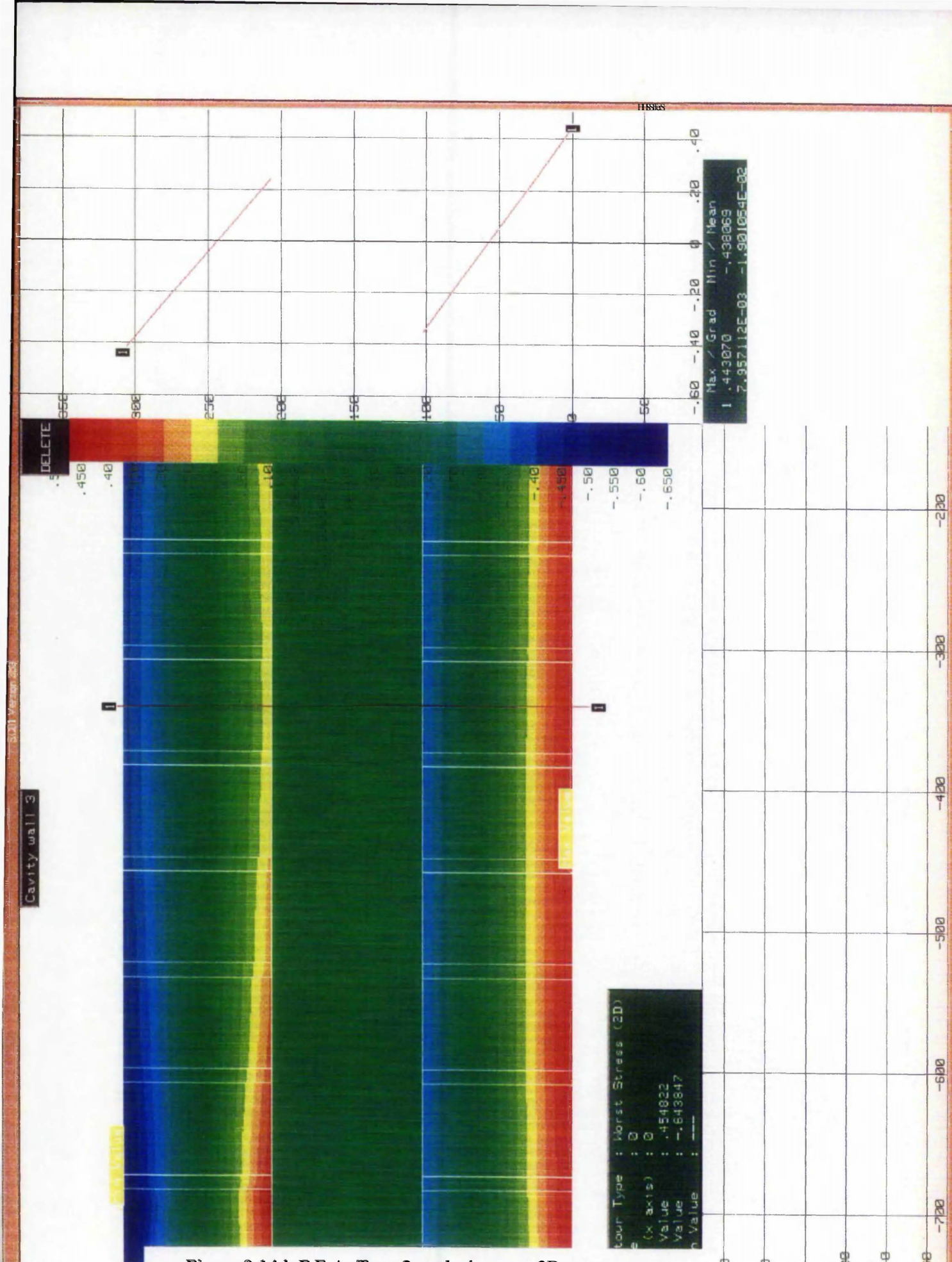

Figure 9.14d F.E.A. Type 2 analysis worst 2D stress contour plot for cavity wall CW3.

Isofoam CRF ρ = 128 kg/m^3, μ = 0.2

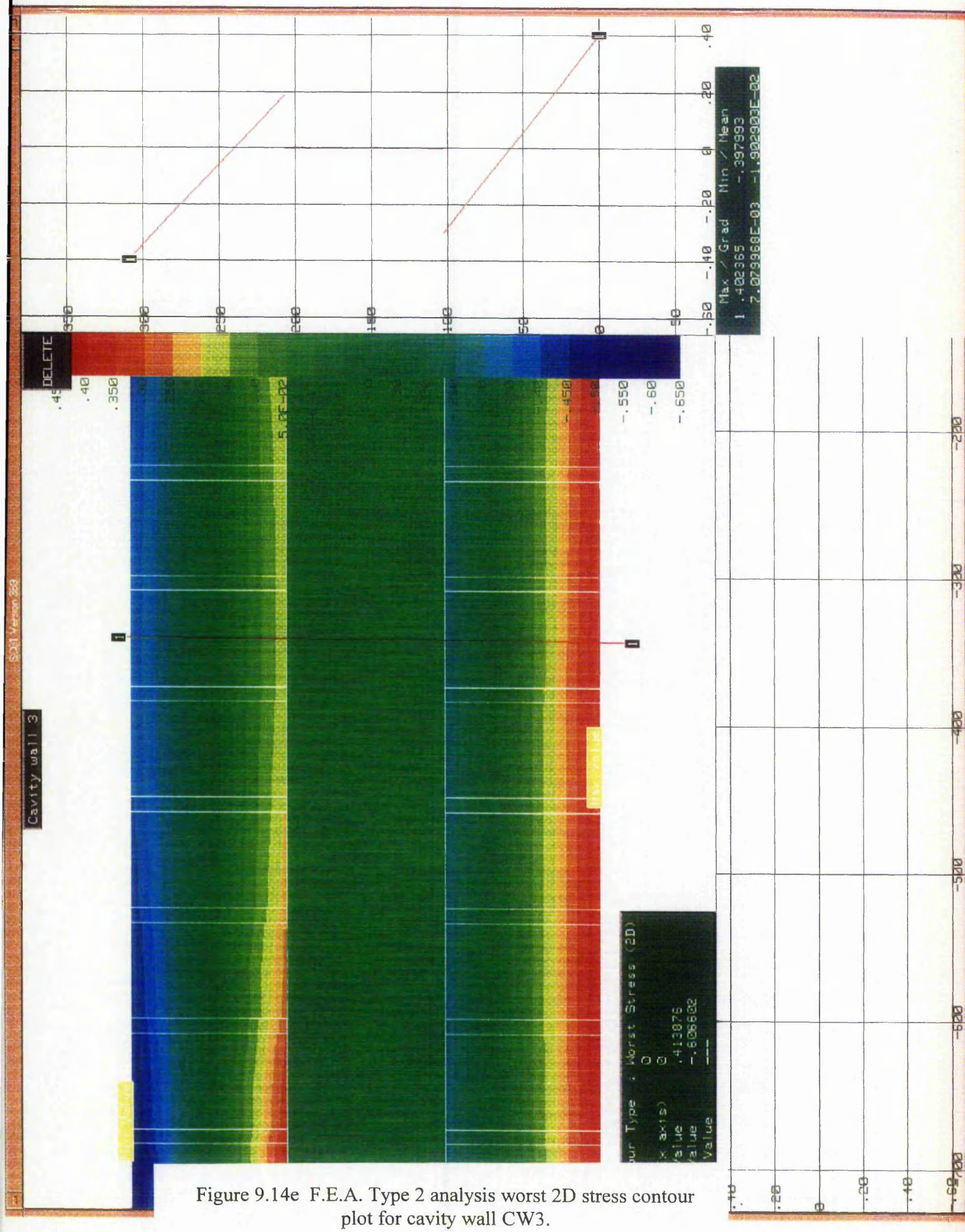

Figure 9.14e F.E.A. Type 2 analysis worst 2D stress contour plot for cavity wall CW3.

Isofoam CRF $\rho = 160$ kg/m^3, $\mu = 0.2$

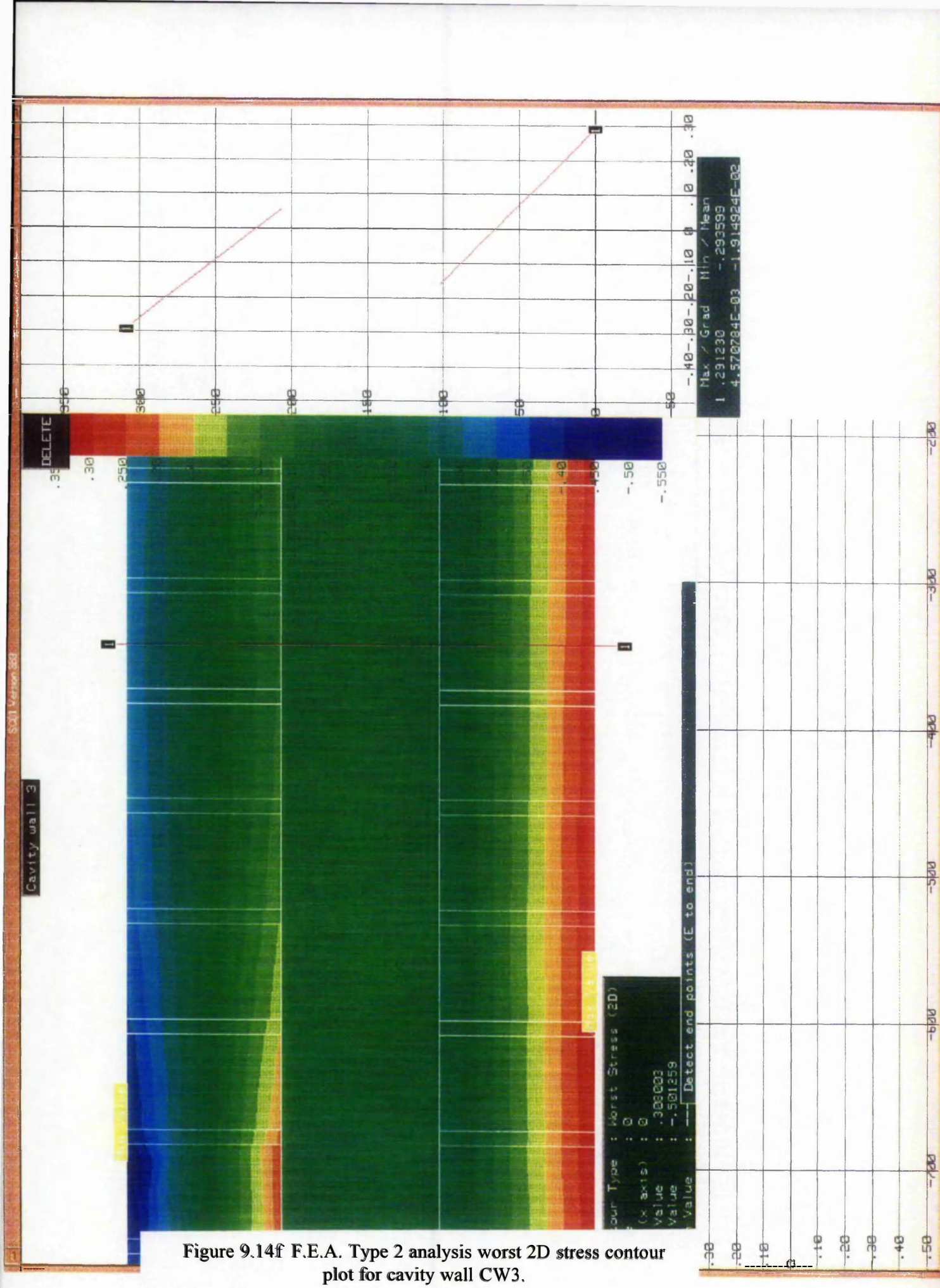

Figure 9.14f F.E.A. Type 2 analysis worst 2D stress contour plot for cavity wall CW3.

Isofoam CRF ρ = 320 kg/m^3, μ = 0.2

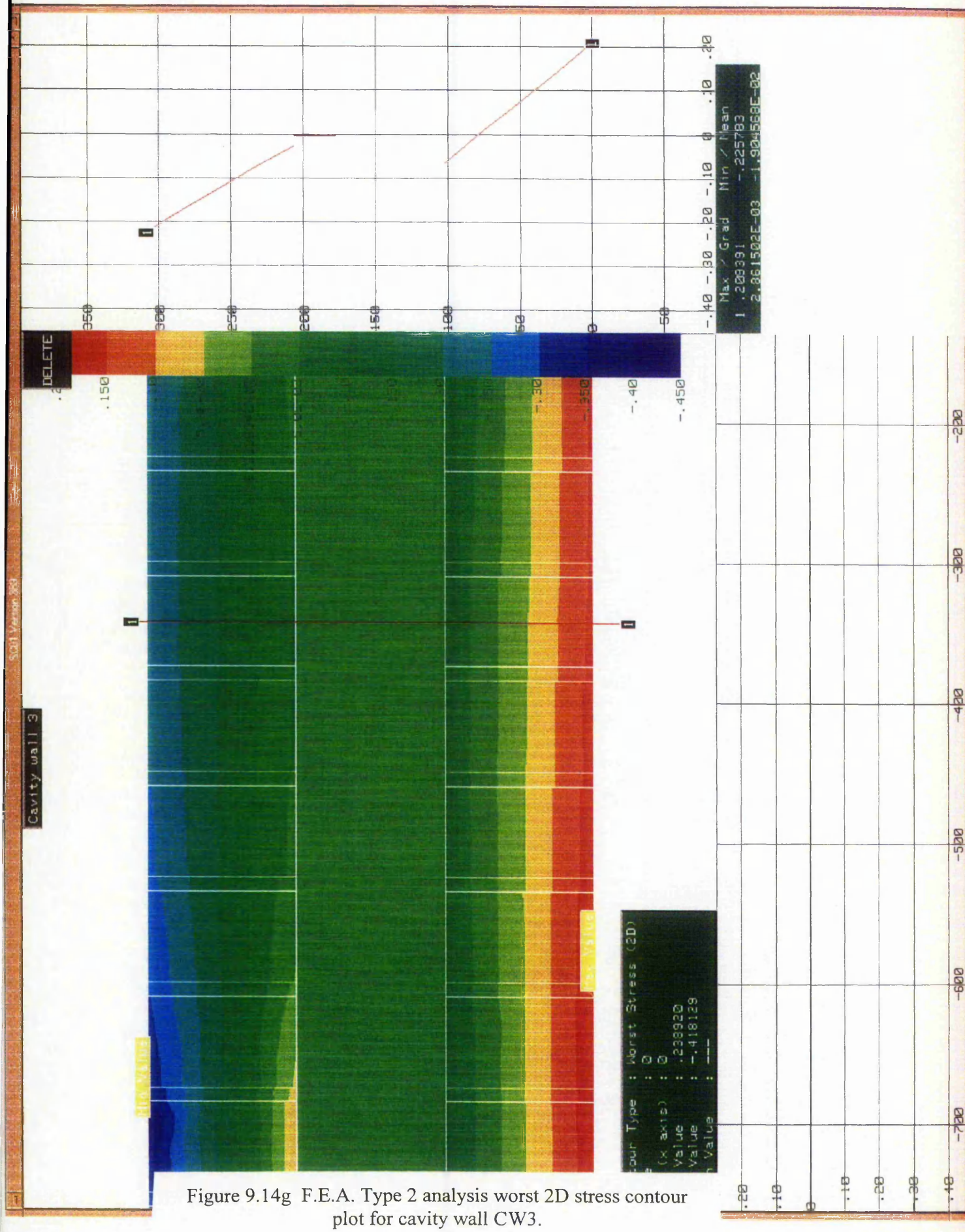

Figure 9.14g F.E.A. Type 2 analysis worst 2D stress contour plot for cavity wall CW3.

Isofoam CRF $\rho = 640$ kg/m^3, $\mu = 0.2$

References

ABAQUS, 1995.
Finite element analysis program.
Hibbitt, Karlsson and Sorensen (UK) Ltd., The Genesis Centre, Science Park South, Birchwood, Warrington, Cheshire, WA3 7BH.

Allen, H.G., 1967.
Measurement of shear stiffness of sandwich beams.
Trans. Journal of the Plastics Institute, 10-15pp, 1967.

Allen, H.G., 1969.
Analysis and design of structural sandwich panels.
Pergamon Press, London, First Edition, 283pp

American Society for Testing Materials, 1957.
Flatwise compressive strength of sandwich cores.
ASTM C365

American Society for Testing Materials, 1980.
Flexural test of flat sandwich construction.
ASTM C393-62, 1980, U.S.A.

American Society for Testing Materials, 1988.
Standard Test Method for Shear Properties in Flatwise Plane of Flat Sandwich Cores.
ASTM C273-61, reapproved 1988, U.S.A.

Anderson, C., 1982.
Some observations on masonry wallette testing.
International Journal of Masonry Construction, 2, 4, 146-154, 1982.

Anderson, C. 1985.
Test on walls subjected to uniform lateral loading and edge loading.
Proceedings of the 7th International Brick Masonry Conference, 2, 889-899, Melbourne, Australia.

Baker, L.R. 1979.
Some factors affecting the bond strength of brickwork.
Proceedings of the 5th Brick Masonry Conference, Session 2, Paper 9, 1979

Baxenden Chemicals Ltd., 1993.
Isofoam Cavity Reinforcement Foam Specification.
Baxenden Chemicals Ltd. Provisional Data Sheet, 1993.

British Board of Agrement, 1986.
Isofoam CRF cavity wall stabilisation and insulation system.
Agrement certificate No. 85/1567, 1986.

British Standards, 1976.
Methods of test for clear plywood.
BS 4512, BSI, London.

British Standard, 1991.
Polyurethane (PUR) foam systems suitable for stabilization and thermal insulation of cavity walls with masonry or concrete inner and outer leaves.
BS 7457, 1991, BSI, London.

British Standard, 1991.
Stabilization and thermal insulation of cavity walls (with masonry or concrete inner and outer leaves) by filling with polyurethane (PUR) foam systems.
BS 7456, 1991, BSI, London.

British Standard, 1992.
Rigid cellular materials.
BS 4370, 1992, BSI, London.

British Standard, 1992.
Code of Practice for structural use of masonry.
BS 5628:Part 1: Unreinforced Masonry, BSI, London

British Standard, 1997.
Code of practice for wind loads.
BS 6399, Part 2, Loading for buildings 1997.

Brown, R.H. and Elling, E.R., 1979.
Lateral load distribution in cavity walls.
Proceedings of the 5th International Brick Masonry Conference, Washington, Session 4, Paper 19, 351-359,1979.

Butterley Brick Ltd, 1993.
A complete guide to Butterley Brick products.
Butterly Brick Ltd., Derby, 57pp, 1993.

Clough, R.W. 1960.
The finite element method in plane stress analysis.
Proceedings of the 2nd American Society of Civil Engineering, Conference on Electronic Computations, 345-378, Sept, 1960.

Davies, J.M., 1986.
The analysis of sandwich panels with profiled faces.
Eighth International Speciality Conference on Cold-formed Steel Structures, St. Louis, Missouri, U.S.A., 351-369.

Davies, J.M., 1987.
Design criteria for structural sandwich panels.
The Structural Engineer, 65A, 435-441, 1987.

Dhanasekar, M., Page, A.W., and Kleeman, P.W., 1982.
The elastic properties of brick masonry.
International Journal of Masonry Construction, 2, 4, 155-160, 1982.

Dodia, J.T., Anderson, C., Smith, D.N. and de Vekey, R.C., 1988.
Laterally loaded cavity walls - a parametric study based on elastic theory.
Proceedings of the 8th International Brick/Block Masonry Conference, Berlin, 3, 1270-1281, 1988.

de Vekey, R.C., Anderson, C., Beard, R. and Hodgkinson, H.R., 1982.
A collaborative evaluation of the BS 5628 "Wallette" test for measuring the flexural strength of brickwork.
6th International Brick Masonry Conference, 131-141, Rome, 1982.

de Vekey, R.C. and Jun, M., 1993.
The effect of joint finishes on the flexural strength of masonry.
The Sixth North American Masonry Conference, 149-158, June 6-9, 1993.

Doherty, D.J., Ball, G.W. and Walker, M.G., 1965.
The physical properties of rigid urethane foam sandwich panels.
Paper 33, Conference, Plastics in Building Structures, London.

Drysdale, R.G. and Gazzola, E., 1985.
Influence of mortar properties on the tensile bond strength of brick masonry.
Proceedings of the 5th Brick/Block Masonry Conference, Melbourne, Australia, 927-936, 1985.

Evison, N.T.R., 1991.
Flexural behaviour of composite panels.
Unpublished Thesis, Nottingham Trent University.

Fairbairn, W., 1849.
An account of the construction of the Britannia and Conway tubular bridges.
John Weale et al, London, 1849.

Handbook of Finish Plywood, 1991.
Finnish Plywood International, Herts, England, 48pp, 1991.

Fried, A., Anderson, C. and Smith, D., 1988.
Predicting the transverse lateral strength of masonry walls.
Proceedings of the 8th Brick/Block Masonry Conference, 2, 1171-1183, 1988.

Ghosh, S.K., 1990.
Flexural bond strength of masonry: an experimental review.
Fifth North American Masonry Conference, University of Illinois at Urbbana-Champaign, June 3-6, 701-711, 1990.

Handbook to BS 5628, 1981.
Structural use of masonry, Part 1: Unreinforced masonry.
The Brick Development Association.
Ronald Adams Associates, 118pp, 1981.

Hartsock, J.A., 1966.
Experiments on shear and buckling in foam-filled panels.
Journal of Cellular Plastics, Vol 2, No. 6, 332-339.

Hartsock, J.A., 1969.
Design of foam-filled structures
Technomic Publishing Co. Inc., Stamford, Connecticut, U.S.A, 54pp.

Hatzinikolas, M.A. and Warwaruk, J., 1991.
Connecting cavity walls.
Proceedings of the 9th International Brick/Block Masonry Conference, Berlin, 996-1003, 1991.

Hinton, E. and Owen, D.R.J., 1990.
An introduction to finite element computations.
Pineridge Press Ltd., Swansea, U.K., 385pp.

Hodgkinson, H.R., 1977.
Experiments on the resistance of brickwork to lateral loading.
Journal of the Institute of Structural Engineering, 55, 11, Oct. 1977.

Hoff, N.J. and Maunter, S.E., 1948.
Bending and buckling of sandwich beams.
Journal of the Aeronautical Society, 69, 651, 193-197.

Huang, J.S. and Gibson, L.J. 1990.
Creep of sandwich beams with polymer foam cores.
Journal of Materials in Civil Engineering, 2, 3, 171-182, Aug 1990.

Huang, J.S. and Gibson, L.J. 1991.
Creep of polymer foams.
Journal of Materials Science, 26, 637-647, 1991.

Institute of Civil Engineers, 1994.
Subsidence of low rise buildings.
S.E.T.O. Ltd., London, First edition.

Just, M. 1983.
Results of experimental tests regarding the long term behaviour of supporting building components made of PUR-hardfoam and the conclusions for their use.
Ifl-Mitt, 22, 3, 95-104, 1983.

Knutsson, H.H. and Nielson, J., 1995.
On the modulus of elasticity for masonry.
Masonry International, Journal of the British Masonry Society, 9, 2, 57-61, 1995.

Krajcinovic, D. 1971.
Sandwich beam analysis.
Journal of Applied Mechanics, ASME, 33, 3, 773-778.

Krajcinovic, D. 1974.
Sandwich beam with arbitrary boundary conditions.
Journal of Engineering for Industry, ASME, 74-WA/DE-11,1-8.

Lawrence, S.J. 1979.
Full-scale tests of brickwork panels under simulated wind load.
5th International Brick Masonry Conference, Session 4, Paper 31, 419-423.

Lawrence, S.J. and Cao, H.T., 1988.
Cracking of non-loadbearing masonry under lateral forces.
Proceedings of the 8th Brick/Block Masonry Conference, 2, 1184-1194, 1988.

Lock, T.J., 1990.
Structural defects - a case study.
Unpublished Thesis, Nottingham Trent University.

Lovegrove, R., 1988.
The effect of thickness and bond pattern on the lateral strength of brickwork.
Proceedings of the British Masonry Society, 2, 95-97, Apr 1988.

LUSAS, 1991
Finite Element Analysis Package, Version 11.
FEA Ltd., Forge House, 66 High Street, Kingston Upon Thames, Surrey.

March, H.W., 1944.
Flexural rigidity of a rectangular strip of sandwich construction.
United States Forest Products Laboratory Report No. 1505.

Microsoft Excel, 1994.
Spreadsheet.
Microsoft Corporation, 5.0c, 1994.

Mullins, P. J. and O'Connor, C., 1991.
Brick walls spanning vertically - a theoretical investigation of the capacity to resist out-of-plane loads.
Proceedings of the 9th International Brick/Block Masonry Conference, Berlin, 800-807, 1991.

Norris, C.B., Ericksen, W.S., and Kommers, W.J., 1944.
Supplement to flexural rigidity of a rectangular strip of sandwich construction - comparison between mathematical analysis and results of tests.
United States Forest Products Laboratory Report No. 1505A.

Norris, C.B., Ericksen, W.S., and Kommers, W.J., 1962.
Supplement to 'The flexural rigidity of a rectangular strip of sandwich construction
United States Forest Products Laboratory Report No. 1505A.

O'Connor, D.J., 1984.
An evaluation of test methods for shear modulus of sandwich cores.
The International Journal of Cement Composites and Lightweight Concrete, 6, 1, 1984.

O'Connor, D.J. 1985.
The flexural behaviour of sandwich beams with thick facings and rigid plastic foam cores.
Unpublished PhD Thesis, University of Ulster, Dublin, 377pp.

O'Connor, D.J. 1987.
A finite element package for the analysis of sandwich constructions.
Composite Structures, 8, 143-161, 1987.

O'Connor, D.J., 1988.
Point concentrations in thick-faced sandwich beams.
Journal of Engineering Mechanics, 114, 5, 733-752p, May, 1988.

Powell, B. and Hodgkinson, H.R.
The determination of stress-strain relationship of brickwork.
Proceedings of Fourth International Brick Masonry Conference, Brugge, 2.a.5.0-2.a.5.5.

Rao, S.S., 1992.
The finite element method in engineering.
Pergammon Press, Oxford, U.K., 3rd Edition, 643pp.

Rashwan, M., 1991.
Analytical modelling of shear connected masonry cavity walls.
Proceedings of the 9th International Brick/Block Masonry Conference, Berlin, 1012-1019, 1991.

SC01, 1997.
Two dimensional automatic finite element mesh generation program.
Rolls-Royce Plc., Mechanical Sciences, Bristol, v5.5, 1997.

SC03, 1997.
Three dimensional automatic finite element mesh generation program.
Rolls-Royce Plc., Technology Department, Bristol, v4.2, 1997.

Stamme, K. and Witte, H. 1974.
Sandwichkonstruktionen - Berechnung, Fertigung, Ausfuhrung (Sandwich construction - calculation, manufacture and use).
Springer-Verlag, Wien and New York. (In German).

Stengard, R.A. 1963.
Properties of rigid urethane foam.
E.I. DuPont de Nemours and Company, Foam bulletin, 31pp.

West, H.W.H., Hodgkinson, H.R., Haseltine, B.A. and Tutt, J.N., 1977.
The resistance of brickwork to lateral loading.
Journal of the Institute of Structural Engineering, 55, 10, 411-430, Oct. 1977.

West, H.W.H., Hodgkinson, H.R. and de Vekey, R.C., 1979.
The lateral resistance of cavity walls with different types of wall ties.
Proceedings of the 5th International Brick Masonry Conference, Washington, Session 4, Paper 25, 387-390, 1979.

West, H.W.H., Hodgkinson, H.R., Haseltine, B.A. and Tutt, J.N., 1982.
The lateral resistance of cavity walls with dissimilar leaves.
Proceedings of the 6th International Brick Masonry Conference, 781-792, 1982.

Zienkiewicz, O.C., 1992.
The finite element method.
McGraw-Hill Book Company (U.K.) Ltd., Maidenhead, U.K., 787pp.